Durham E-Theses

Analytical methods for the study of membranes and peptide-membrane interactions

CATHERINE JANE PRIDMORE

How to cite:

PRIDMORE, CATHERINE JANE (2010) Analytical methods for the study of membranes and peptide-membrane interactions. Doctoral thesis, Durham University.

Use policy

Analytical methods for the study of membranes and peptide-membrane interactions

Catherine Jane Pridmore

This thesis describes analytical work carried out to determine the stability and properties of lipid and peptide-lipid systems.

Matrix-assisted laser desorption/ionisation mass spectrometry (MALDI-MS) and tandem mass spectrometry (MSMS) analyses were carried out to establish a validated protocol for the complete identification of phospholipids, including the nature of the headgroup and acyl chains and the positions of the acyl chains on the glycerol backbone. Statistical differences were observed in the relative intensities of peaks corresponding to the neutral loss of the acyl chain from the *sn*-1 and *sn*-2 positions of POPE, POPC and OPPC, with a preferential cleavage of the chain from the *sn*-2 position of all three in the absence of added salt and a preferential cleavage at the *sn*-1 position in the presence of sodium or lithium ions. This knowledge was applied to the identification of unknown lipid mixtures both of the standard MALDI target plate and directly onto thin layer chromatography plates after separation.

The above techniques, together with other analytical methods including thin layer chromatography and dynamic light scattering, were applied to the study and identification of lipids modified by actions such as hydrolysis and oxidation under conditions used for binding analyses of peptides and small molecules. Long-term analyses of samples containing synthetic melittin and liposomes showed that over time melittin both promotes the hydrolysis of liposomal lipids and is itself acylated.

Analyses of the binding of a prototypical peptide (human neutrophil defensin HNP-2) to membranes, using methods that included dichroism and fluorescence spectroscopy, demonstrated that HNP-2 dimers act on lipid membranes via a carpet-type mechanism and allowed the rate of the formation of bound HNP-2 states to be determined. HNP-2 was modeled as a consecutive two-step process following pseudo-first order kinetics. The first step (membrane association) was rapid, with a half-life of around 0.5 minutes, while the second step (reorientation and partial insertion into the membrane) was slower by an order of magnitude.

Analytical methods for the study of membranes and peptide-membrane interactions

Catherine Jane Pridmore

Submitted in partial fulfilment of the requirements of Durham University for the degree of Doctor of Philosophy

Centre for Bioactive Chemistry
Department of Chemistry
2010

TABLE OF CONTENTS

List of figures

List of Tables

List of schemes

List of abbreviations

%Pd	% Polydispersity
α-CHCA	α-cyano-4-hydroxycinnamic acid
AMP	Antimicrobial peptide
ANTS	8-aminonaphthalene-1,3,6 trisulfonic acid
Bis-tris propane	1,3-Bis(tris(hydroxymethyl)methylamino)propane
CAD	Collisionally activated decay
CD	Circular dichroism
CID	Collision induced dissociation
DHB	2,5-dihydroxybenzoic acid
DLPC	1,2-dilinoleoyl-*sn*-glycero-3-phosphocholine
DLS	Dynamic light scattering
DMPC	1,2-myristoyl-*sn*-glycero-3-phosphocholine
DNA	Deoxyribonucleic acid
DOPC	1,2-dioleoyl-*sn*-glycero-3-phosphocholine
DOPS	1,2-dioleoyl-*sn*-glycero-3-phosphoserine
DoxnoPC	1,2-di(9'-oxo-nonanoyl)-*sn*-glycero-3-phosphocholine
DPPA	1,2-dipalmitoyl-*sn*-glycero-3-phosphate
DPPC	1,2-dipalmitoyl-*sn*-glycero-3-phosphocholine
DPPE	1,2-dipalmitoyl-*sn*-glycero-3-phosphoethanolamine
DPX	*p*-xylene-bis-pyridinium bromide
DSC	Differential scanning calorimetry
DSPC	1,2-distearoyl-*sn*-glycero-3-phosphocholine
ECD	Electron capture dissociation
EDTA	Ethylene diaminetetracetic acid
ESI	Electrospray ionisation
FAB	Fast atom bombardment
FD	Fluorescent dextran
FRET	Fluorescence resonance energy transfer
HBD	Human beta defensin
HD	Human defensin
HFIP	1,1,1,3,3,3-hexafluoroisopropanol
HNP	Human neutrophil peptide
HPTLC	High performance thin layer chromatography
HT	High tension
LIFT	Tandem mass spectrometry technology available on Bruker Daltonics MALDI instruments (not an abbreviation)
LCMS	Liquid chromatography mass spectrometry
LD	Linear dichroism
Lyso-PPC	1-palmitoyl-2-hydroxy-*sn*-glycero-3-phosphocholine
Lyso-OPC	1-oleoyl-2-hydroxy-*sn*-glycero-3-phosphocholine
m/z	Mass-to-charge ratio
MALDI	Matrix-assisted laser desorption/ionisation
MIC	Minimum inhibitory concentration
MS	Mass spectrometry

MSMS	Tandem mass spectrometry ("mass spectrometry mass spectrometry")
NBD	4-fluoro-7-nitrobenz-2-oxa-1,-3-diazole
NBD-PE	N-(7-nitrobenz-2-oxa-1,3-benzoxadiazol-4-yl)-phosphatidylethanolamine
NMR	Nuclear magnetic resonance
NP	Neutrophil peptide
NR	Neutron reflectivity
OCD	Oriented circular dichroism
OoxnoPC	1-(9'-oxo-nonanoyl)-2-oleoyl-*sn*-glycero-3-phosphocholine or 1-oleoyl-2-(9'-oxo-nonanoyl)-*sn*-glycero-3-phosphocholine
OPPC	1-oleoyl-2-palmitoyl-*sn*-glycero-3-phosphocholine
PazePC	1-palmitoyl-2-azelaolyl-*sn*-glycero-3-phosphocholine
PA	Phosphate
PC	Phosphocholine
PDB	Protein data bank
PdI	Polydispersity index
PE	Phosphoethanolamine
PEG	Poly(ethylene glycol)
PG	Phosphoglycerol
PI	Phosphoinositol
PICUP	Photo-induced cross-linking of unmodified proteins
PLA$_2$	Phospholipase A$_2$
PLPC	1-palmitoyl-2-linoleoyl-*sn*-glycero-3-phosphocholine
PMA	Phosphomolybdic acid
PMT	Photomultiplier tube
POPC	1-palmitoyl-2-oleoyl-*sn*-glycero-3-phosphocholine
POPE	1-palmitoyl-2-oleoyl-*sn*-glycero-3-phosphoethanolamine
POPG	1-palmitoyl-2-oleoyl-*sn*-glycero-3-phosphoglycerol
PoxnoPC	1-palmitoyl-2-(9'-oxo-nonanoyl)-*sn*-glycero-3-phosphocholine
PS	Phosphoserine
PSD	Post source decay
REES	Red-edge excitation shift
RET	Resonance energy transfer
Rh-PE	N-(Lissamine Rhodamine B sulfonyl)-phosphatidylethanolamine
SAXS	Small-angle X-ray scattering
SDS-PAGE	Sodium dodecyl sulfate polyacrylamide gel electrophoresis
sn	Stereospecifically numbered
sPSD	Seamless post source decay
TEM	Transmission electron microscope
TFA	Trifluoroacetic acid
TLC	Thin layer chromatography
TOF	Time of flight
Tris	Tris(hydroxymethyl)aminoethane
v/v	Volume to volume

Units

°	Degrees of arc
°C	Degrees Celcius
a.u.	Arbitrary units
Da	Daltons
MHz	Megahertz
keV	Kilo-electron volts
M	Molarity in moles per litre (= mol/dm^3)
mM	Molarity in millimoles (10^{-3} moles) per litre
μM	Molarity in micromoles (10^{-6} moles) per litre
g	Grams
mg	Milligrams (10^{-3} grams)
m	Metres
mm	Millimetres (10^{-3} metres)
μm	Micrometres (10^{-6} metres)
nm	Nanometres (10^{-9} metres)
Å	Ångstroms (10^{-10} metres)
mL	Millilitres (10^{-3} litres)
μL	Microlitres (10^{-6} litres)
s	Seconds

Lipids
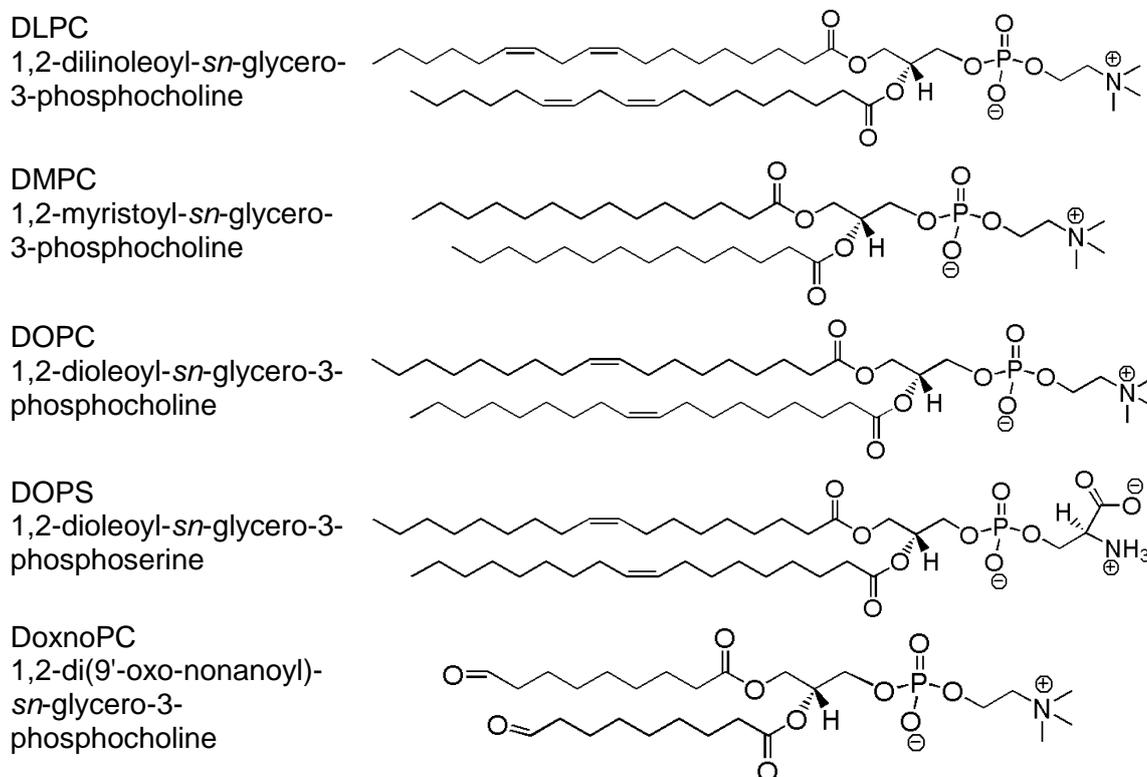
DLPC
1,2-dilinoleoyl-*sn*-glycero-3-phosphocholine
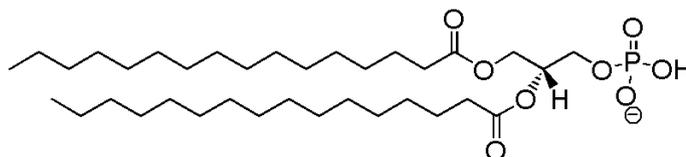
DMPC
1,2-myristoyl-*sn*-glycero-3-phosphocholine

DOPC
1,2-dioleoyl-*sn*-glycero-3-phosphocholine

DOPS
1,2-dioleoyl-*sn*-glycero-3-phosphoserine

DoxnoPC
1,2-di(9'-oxo-nonanoyl)-*sn*-glycero-3-phosphocholine

DPPA
1,2-dipalmitoyl-*sn*-glycero-3-phosphate

DPPC
1,2-dipalmitoyl-*sn*-glycero-3-phosphocholine
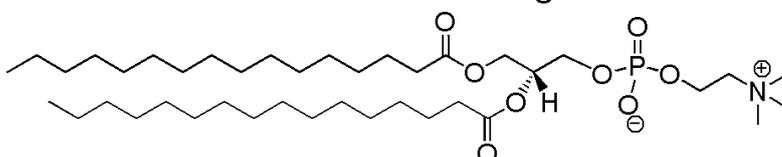
DPPE
1,2-dipalmitoyl-*sn*-glycero-3-phosphoethanolamine
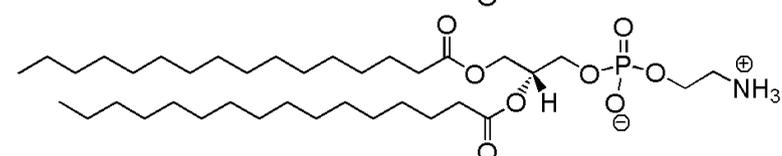
NBD-PE
N-(7-nitro-2,1,3-benzoxadiazol-4-yl)-phosphatidylethanolamine
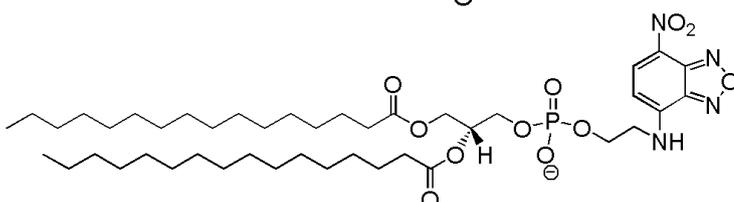
OoxnoPC
1-(9'-oxo-nonanoyl)-2-oleoyl-*sn*-glycero-3-phosphocholine or 1-oleoyl-2-(9'-oxo-nonanoyl)-*sn*-glycero-3-phosphocholine

*
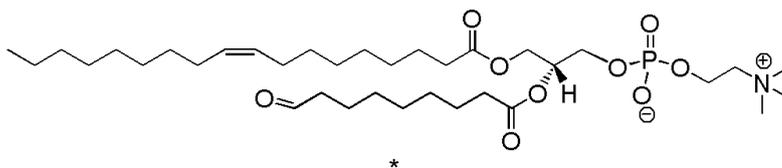
OPPC
1-oleoyl-2-palmitoyl-*sn*-glycero-3-phosphocholine
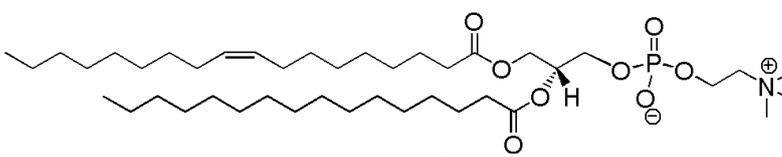
PazePC
1-palmitoyl-2-azelaolyl-*sn*-glycero-3-phosphocholine
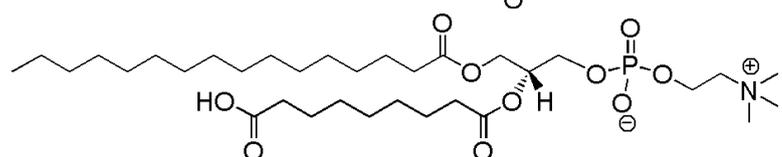
PLPC
1-palmitoyl-2-linoleoyl-*sn*-glycero-3-phosphocholine
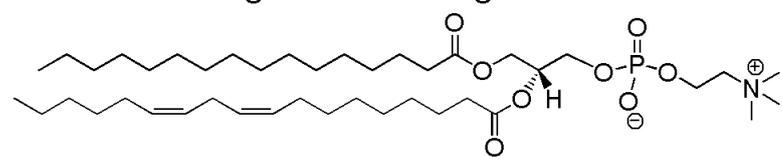
POPC
1-palmitoyl-2-oleoyl-*sn*-glycero-3-phosphocholine
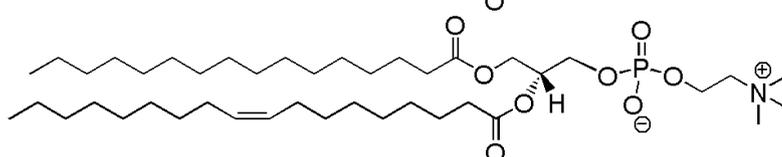
POPE
1-palmitoyl-2-oleoyl-*sn*-glycero-3-phosphoethanolamine

---
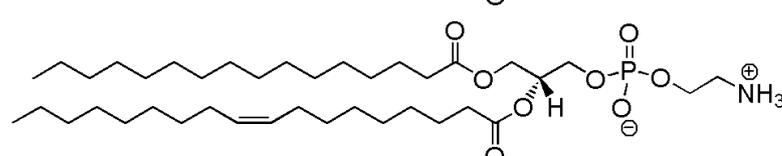
* 9'-oxo-nonanoyl chain could be at *sn*-1 or *sn*-2 position

POPG
1-palmitoyl-2-oleoyl-*sn*-
glycero-3-phosphoglycerol

PoxnoPC
1-palmitoyl-2-(9'-oxo-
nonanoyl)-*sn*-glycero-3-
phosphocholine

Rh-PE
N-(Lissamine Rhodamine
B sulfonyl)-
phosphatidylethanolamine
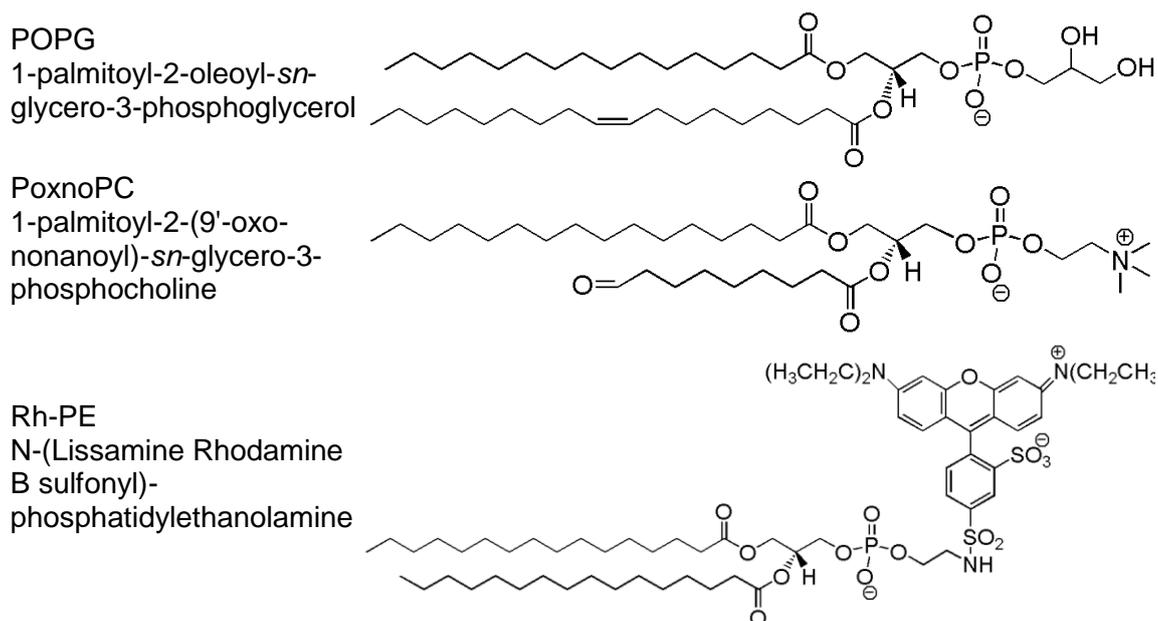
The amino acids

Name	3-Letter Code	1-Letter Code
Alanine	Ala	A
Arginine	Arg	R
Asparagine	Asn	N
Aspartic Acid	Asp	D
Cysteine	Cys	E
Glutamic Acid	Glu	E
Glutamine	Gln	Q
Glycine	Gly	G
Histidine	His	H
Isoleucine	Ile	I
Leucine	Leu	L
Lysine	Lys	K
Methionine	Met	M
Phenylalanine	Phe	F
Proline	Pro	P
Serine	Ser	S
Threonine	Thr	T
Tryptophan	Trp	W
Tyrosine	Tyr	Y
Valine	Val	V

Statement of copyright

The copyright of this thesis rests with the author. No quotation from it should be published without prior written consent and information from it should be acknowledged.

Acknowledgements

This work would not have been possible without the help, support and advice of my supervisors Dr John Sanderson, Dr Jackie Mosely and Prof. Alison Rodger. I would also like to thank the past and present members of the Sanderson group, Dr Liz Grayson, Mike and Aruna, for their friendship and support, and Mike, Lara, Dave and Pete for their help and advice. I am especially grateful to Matt and Angeliki, and everyone else at Warwick University who made me so welcome and helped me to make the most of my visits. Finally, I would like to thank my family and friends for all of their support and encouragement, climbing trips, fruitcake and tea.

1 INTRODUCTION

1.1 The cell

Every living species in composed of cells, from single-celled yeast to complex multicellular humans. Cells can be classed as prokaryotic or eukaryotic by the presence (eukaryote) or absence (prokaryote) of a nucleus. Bacteria are prokaryotic, whether single-celled or multicellular, and animals, fungi and plants are eukaryotic.[1] Both types of cell contain one or more lipid cell membranes. The outermost of these is the plasma membrane. In eukaryotic cells this is the outer membrane of the cell, while in prokaryotic cells it sits beneath the capsule and cell wall (Figure 1.1). Prokaryotic cells are further divided into Gram positive, which have a thick peptidoglycan cell wall outside the plasma membrane, and Gram negative, which have a thinner peptidoglycan layer underneath an outer membrane of lipopolysaccharides and membrane proteins. Some bacterial cells also have flagellae, filamentous protein appendages which aid the motion of the cells.[2]
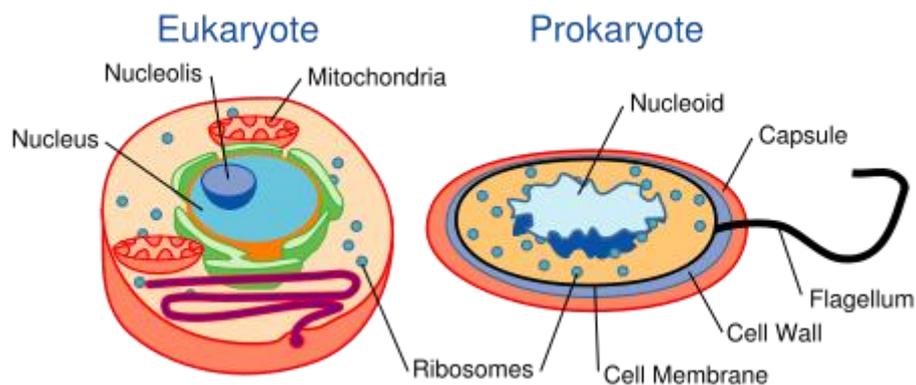
Figure 1.1. Prokaryotic and eukaryotic cells.[*]

In 1972, Singer and Nicholson proposed the 'fluid mosaic model' to elucidate the structure of biological membranes.[3] The model described two layers of lipids arranged tail to tail, interspersed with proteins and carbohydrates (Figure 1.2). The lipids are free to diffuse laterally within each layer, but not to swap between them. The proteins are either 'integral', spanning the membrane, or 'extrinsic', bound to the surface. They perform a number of functions, including acting as pumps, gates and enzymes.[4]

---

[*] http://schools-wikipedia.org/images/915/91506.png.htm (A non-copyright public domain image from the Science Primer (US Federal Government National Centre for Biotechnology Information))
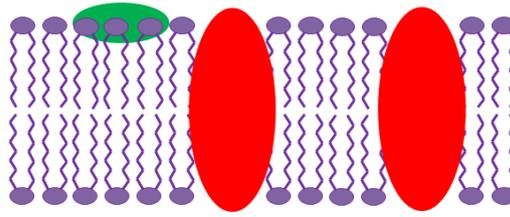
Figure 1.2. The cell membrane. Phospholipid bilayer shown in purple and integral and extrinsic membrane proteins in red and green respectively.

1.2 Lipids

Lipids are amphiphilic species with hydrophilic headgroups and hydrophobic tailgroups separated by a cyclopenta[*a*]phenanthrene, sphinganine or glycerol group. They can be classed by their central group, with sterols built around cyclopenta[*a*]phenanthrene, sphingolipids built around sphinganine and glycerophospholipids based around glycerol.

1.2.1 Sterols

Sterols are a minor component of cell membranes. They are neutral lipids, based on a cyclopenta[*a*]phenanthrene skeleton with a hydroxyl group at the C-3 position. Cholesterol (Figure 1.3) is the most commonly occurring sterol, and is present in all erythrocyte (red blood cell) membranes but rarely in prokaryotic cell membranes.[4] It comprises approximately 30 % of the lipid mass of mammalian cell membranes.[5]
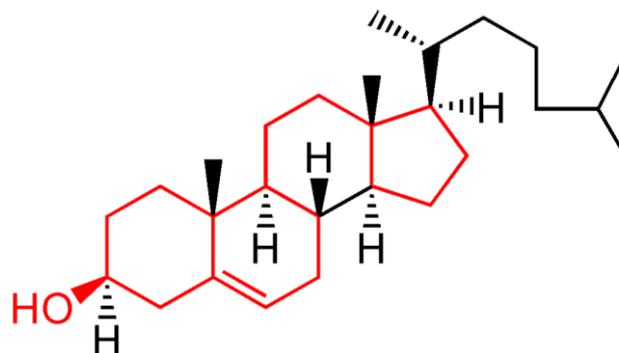
Figure 1.3. Structure of cholesterol. The common sterol cyclopenta[*a*]phenanthrene skeleton and hydroxyl group are shown in red.

1.2.2 Sphingolipids

Sphingolipids are based around a sphingosine skeleton attached to an amide and either a sugar (glycosphingolipids, Figure 1.4A) or a phosphate group (sphingomyelins,

Figure 1.4B). The phosphate group of sphingomyelin lipids is in turn linked to one of a number of groups, usually choline ($(CH_2)_2NMe_3$).
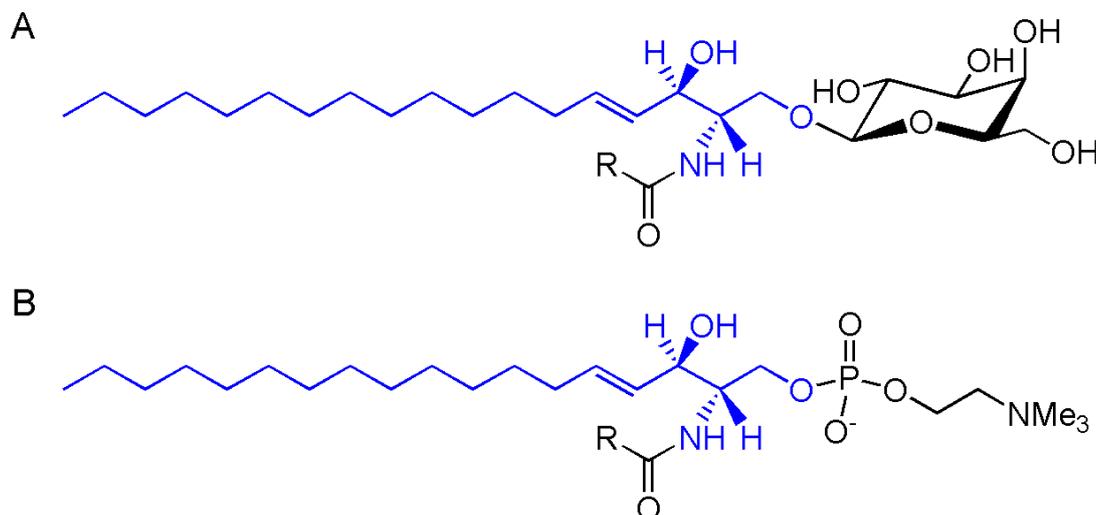
Figure 1.4. Structure of A) glycosphingolipids and B) sphingomyelin. R corresponds to a hydrocarbon chain. Sphingosine is shown in blue.

1.2.3 Glycerophospholipids

Glycerophospholipids are composed of two acyl chains attached through a glycerol linker to a phosphate, which is in turn linked to one of a number of groups (Table 1.1).
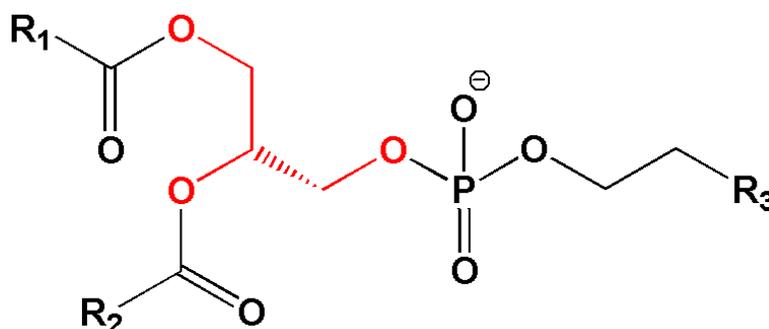
Figure 1.5. Structure of glycerophospholipids. R_1 and R_2 correspond to hydrocarbon chains and R_3 corresponds to one of a number of groups, as described in Table 1.1. Glycerol is shown in red.

Glycerophospholipids are the major lipid component of cell membranes, and all further discussion of 'phospholipids' refers to glycerophospholipids. Table 1.1 shows the common phospholipid headgroups. These headgroups can be zwitterionic (neutral with balanced positive and negative charges), positive or negatively charged. Prokaryotic and eukaryotic plasma membranes differ in their phospholipid compositions, with prokaryotic membranes containing a higher percentage of negatively charged lipids than those of

eukaryotes. For example, the major phospholipid components of the plasma membrane of the Gram-negative bacteria *E. coli* are phosphoethanolamine (74%) and phosphoglycerol (19%), while the main phospholipid components of human liver plasma membranes are phosphocholine (44%), phosphoethanolamine (28%), phosphoinositol (9%) and phosphoserine (3%) (as % of total lipid composition).[6]

Table 1.1. Phospholipid headgroups.

Name	Abbreviation	Net Charge (pH 7)	Structure
Phosphate	PA	-1	
Phosphocholine	PC	Neutral	
Phosphoethanolamine	PE	Neutral	
Phosphoglycerol	PG	-1	
Phospho-L-serine	PS	-1	
Phosphoinositol	PI	-1	

The acyl chains of naturally occurring lipid membranes can be saturated or contain one or more double bonds. These double bonds are normally the *cis* isomers.[7] The structures, systemic, trivial and shorthand names of some commonly occurring lipid acyl chains are shown in Table 1.2. The shorthand name corresponds to the length of the carbon chain followed by the number, position and configuration of the double bonds.

Table 1.2. Some commonly occurring acyl chains of phospholipids.

Structure	Systemic Name	Trivial Name	Shorthand Name
$CH_3(CH_2)_{14}COO$	Hexadecanoic	Palmitic	16:0
$CH_3(CH_2)_7CH=CH(CH_2)_7COO$	*Z*-9-octadecanoic	Oleic	18:1 9*c*
$CH_3(CH_2)_3(CH_2CH=CH)_2(CH_2)_7COO$	*Z,Z*-9,12-octadecanoic	Linoleic	18:2 9*c*,12*c*

Phospholipid bilayers exhibit liquid crystalline properties. With increasing temperature or decreasing pressure, bilayers composed of a single phospholipid types undergo transitions between gel ($L_{\beta'}$), rippled gel ($P_{\beta'}$) and liquid crystalline (L_α) phases (Figure 1.6). The first transition is termed pre-transition (T_p) and the second the main transition (T_m).[8] The phase transition temperatures of lipids increase with increasing chain length, due to the increased van der Waals forces between the chains, and decrease with increasing unsaturation due to the disruption to the ordered chain packing this causes.[9] Lipids with unsaturated acyl chains generally have T_m values below 0 ℃, while those of saturated lipids can be much higher (80 °C for 24:0/24:0-PC).[10] The phase transition temperatures of mixed phospholipid bilayers depend on the mixing of the different lipid types; if the lipids mix ideally then T_m will be the average of those of the constituent lipids, whereas if they do not mix ideally the separate lipid components will undergo individual transitions. The binding of antimicrobial peptides to lipid bilayers has been shown to be affected by the phase of the lipids, for example the peptide gramicidin S does not bind to zwitterionic neutral bilayers below the main phase transition temperature, binding only when the bilayer is in a liquid-crystalline state.[11]

$L_{\beta'}$ $P_{\beta'}$ L_α
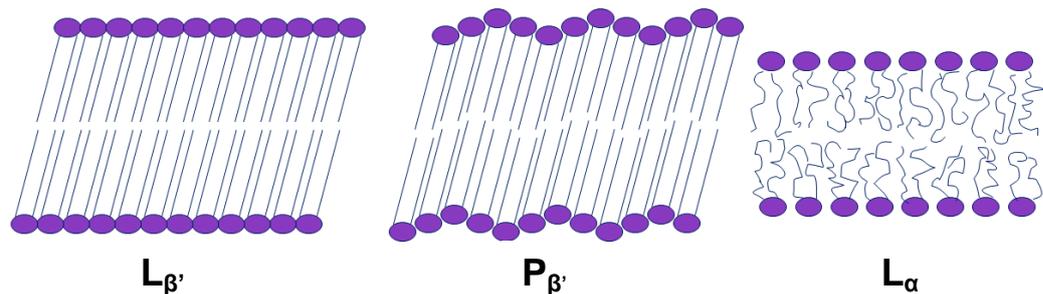
Figure 1.6. Gel ($L_{\beta'}$), rippled gel ($P_{\beta'}$) and liquid crystalline (L_α) phospholipid phases.

1.3 Antimicrobial peptides

Antimicrobial peptides (AMPs) are a form of innate immunity found in virtually all living species as a protection against microbes.[12] Many are cationic, with a net charge between + 2 and + 9, and they usually form amphipathic secondary structures.[12] AMPs can be classed according to their secondary structures, for example α-helical, β-sheet, linear and loop structures (Figure 1.7).[14, 15] They are also grouped into families which share similarities such as structure, sections of sequence, disulphide bridges and action, along with evolutionary relationships determinable from the location of their genes within the genome.[16] Table 1.3 contains descriptions and structures of a number of different AMPs.
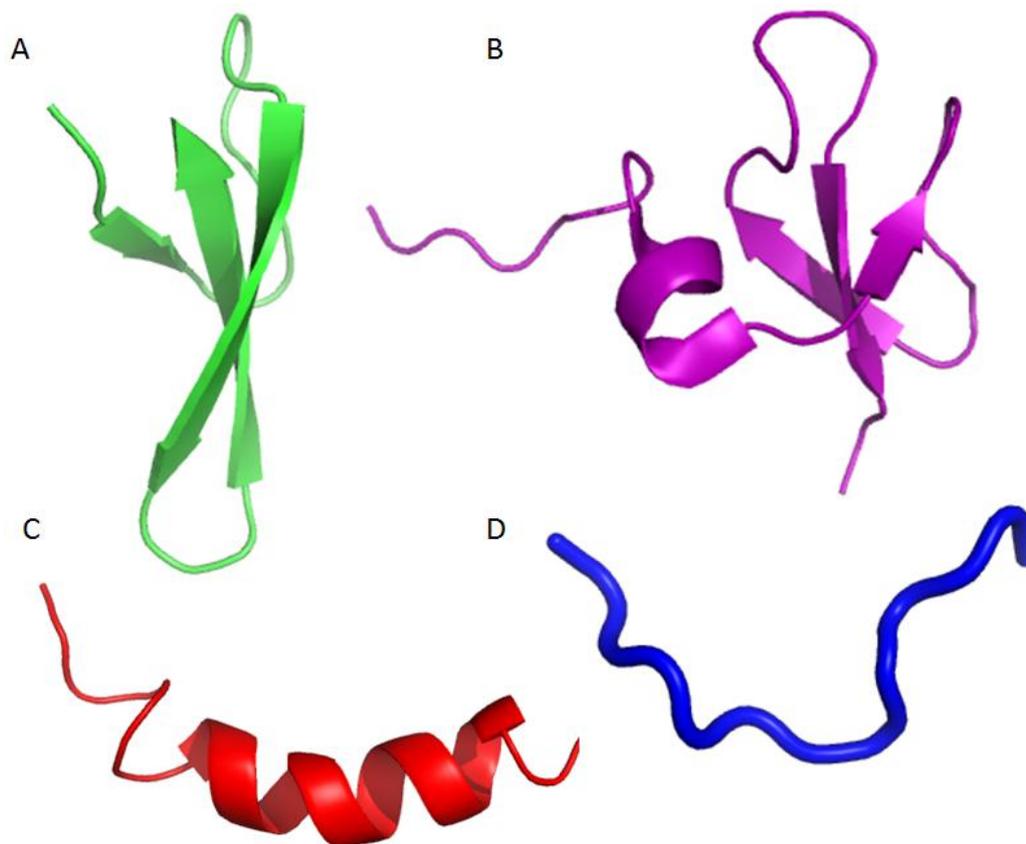
Figure 1.7. Secondary structures of A) defensin HNP-3 monomer (56% β-sheet); B) defensin HBD-3 monomer (11% α-helix, 28% β-sheet); C) magainin-2 monomer (52% α-helix) and D) indolicidin (linear). Entries 1DFN, 1KJ6, 1DUM and 1G89 respectively in the Protein Data Bank (http://www.rscb.org/pdb).[17–20] Structures displayed using The PyMOL Molecular Graphics System, Version 1.2r1, Schrödinger, LLC (www.pymol.org).

1.3.1   AMP action against different cell types

AMPs can act against a number of cell types including Gram positive and Gram negative bacteria, erythrocytes, fungi, protozoa and viruses. The examples described in Table 1.3 show that not all AMPs have the same activity. Research using peptides where residues have been replaced to alter the structure, hydrophobicity and amphipathicity has given an insight into the features which determine the hemolytic, antibacterial and antifungal properties of AMPs. High amphipathicity,[21] high hydrophobicity,[22] and high proportions of either α-helix or β-sheet in the secondary structure have all been observed to promote hemolysis while suppressing antimicrobial activity.[23, 24] An optimum hydrophobicity for antibacterial activity was determined, above and below which activity decreased strongly.[25] It was also found that positioning a polar lysine residue in the centre of the hydrophobic region caused a dramatic improvement in antibacterial activity and reduction in hemolytic activity. Fungal cells are eukaryotic, with a high percentage of

PC and PE lipids, but also contain a small percentage of each of PI, PS and diphosphatidyl PG lipids, which increases their susceptibility to AMPs above mammalian cells.[2] Fungal cell plasma membranes are surrounded by a cell wall of cross-linked chitin, mannoproteins (mannose-containing proteins), glucans and glycoproteins, which can act as a barrier to antimicrobial peptide attack on the membrane.[26] It has been proposed that if peptides form strong dimers in solution their activity against fungal cells is reduced, possibly due to a need to dissociate to pass through the cell wall.[27]

The different activities of antimicrobial peptide species toward erythrocytes and prokaryotes depending on their hydrophobicity has been explained by reference to the mechanism of action of the peptides and the different modes of interaction between the peptides and lipid membranes. Peptide-membrane interactions can either be electrostatic (enthalpic) or hydrophobic (entropic). It has been proposed that when cationic peptides interact with anionic membranes the attraction is primarily electrostatic, while interactions between peptides, cationic or otherwise, with neutral membranes are dominated by hydrophobic effects between the hydrophobic regions of the peptides and the hydrocarbon chain region of the bilayer.[24] It has also been suggested that more hydrophobic peptides penetrate deep into the hydrocarbon region of the bilayer of red blood cells during hemolysis, forming pores or channels.[25] As described below, when interacting with anionic membranes antimicrobial peptides can cause lysis without penetrating deeply into the membrane through carpet-like mechanisms (as described in Section 1.3.2.3).

AMPs do not cause the death of viral particles through permeabilization of the cell membrane in the same manner as they do with bacterial cells. The antiviral activity of AMPs has been found to be a combination of direct action on the viral particle and indirect action via interaction with the viral target cell, depending on the virus and the peptide.[28] Lactoferrin has been found to interact directly with viral particles, including those of feline calcivirus, poliovirus and human immunodeficiency virus, through binding to their surface, which hinders the interaction of the viral particle with target cells.[29–31] Defensin HNP-1 has been shown to have a dual effect on the viral haemorrhagic septicaemia virus. The peptide binds directly to viral particles to alter their ability to interact with target cells in the same manner as lactoferrin, but also hinders the virus through inducing an antiviral response in host cells.[32]

Family	Peptide	Species	Target	Structure	sequence	Net Charge (Ph7)	Notes	Ref
Magainins	Magainin 1	African Clawed Frog *(Xenopus laevis)*	Gram -ve and Gram +ve bacteria; fungi; protozoa; anti-tumour	α- helical	GIGKFLHSAGKFGKAFVGEIMKS	+ 3		[33]
	Magainin 2	African Clawed Frog *(Xenopus laevis)*	Gram -ve and Gram +ve bacteria; fungi; protozoa; anti-tumour	α- helical	GIGKFLHSAKKFGKAFVGEIMNS	+ 3		[33]
Tachyplesins	Tachyplesin 1	Chinese Horseshoe Crab *(Tachypleus tridentatus)*	Gram -ve and Gram +ve bacteria; fungi	β-sheet	KWCFRVCYRGICYRRCR	+ 7	Two disulphide bridges	[34]
	Tachyplesin 2	Chinese Horseshoe Crab *(Tachypleus tridentatus)*	Gram -ve and gram +ve bacteria; fungi	β-sheet	RWCFRVCYRGICYRKCR	+ 7		[35]
Cathelicidins	Indolicidin	Cattle	Gram -ve and Gram +ve bacteria; fungi; protozoa	Linear	ILPWKWPWWPWRR	+ 3		[20]
	LL-37	Human	Gram -ve and Gram +ve bacteria; fungi; protozoa	α- helical	LLGDFFRKSKEKIGKEFKRIVQRIKD FLRNLVPRTES	+ 6		[36]
Defensins	HNP-1	Human	Gram -ve and Gram +ve bacteria; fungi; enveloped viruses	β-sheet	ACYCRIPACIAGERRYGTCIYQGRL WAFCC	+ 3	Three disulphide bridges; an α defensin	[37]
	TAP	Cattle	Gram -ve and Gram +ve bacteria; fungi	β-sheet	NPVSCVRNKGICVPIRCPGSMKQIG TCVGRAVKCCRKK	+ 9	Three disulphide bridges; an insect defensin	[37]
	Phormia A	Flies	Primarily Gram +ve bacteria	β-sheet	ATCDLLSGTGINHSACAAHCLLRGN RGGYCNGKGVCVCRN	+ 3	Three disulphide bridges; a β defensin	[37]
Melittin	Melittin *(Apis mellifera)*	Honeybee *(Apis mellifera)*	Erythrocytes; Gram -ve and Gram +ve bacteria; fungi	α- helical	GIGAVLKVLTTGLPALISWIKRKRQQ	+ 5		[40, 41, 42]

Table 1.3. Descriptions of a number of antimicrobial peptides.

1.3.2 Modes of action

Three general models have been proposed for the mode of action of AMPs on microbe cells.[12] It must be noted that these mechanisms are not universally accepted by all researchers in the field of antimicrobial peptide analysis; other mechanisms have been proposed, including detergent-type micellization, and some peptides are known to bind via different mechanisms depending on the lipid type and buffer conditions.[12,13] All of the general models initially require the ratio of bound peptide:lipid to reach a threshold value (P:L), often termed the 'threshold concentration'.

1.3.2.1 The barrel stave mechanism

During this mechanism, the AMPs initially bind to the surface of the cell, weakening it, before the hydrophobic portion of the peptide inserts into the outer lipid monolayer. When enough peptides are bound to this degree, they aggregate and push through the membrane, forming a 'barrel'-like structure spanning the cell with the peptide hydrophobic regions facing the hydrophobic portions of the membrane and hydrophobic regions facing inwards, forming a pore through which cell contents can leak, causing cell death.

1.3.2.2 The toroidal pore mechanism

This mechanism describes the action of peptides which bind to the surface of the cell, causing the outer lipid layer to bend in on itself and join up with the inner leaflet, giving a pore lined with lipid headgroups interspersed with peptides.

1.3.2.3 The carpet mechanism

AMPs employing the carpet mechanism never actually form a pore through the membrane. They initially bind to the surface through electrostatic interactions, then once a sufficient number are bound, the interactions of the peptides with the membrane disrupt the ordered lipid bilayer to such an extent that it becomes permeable.
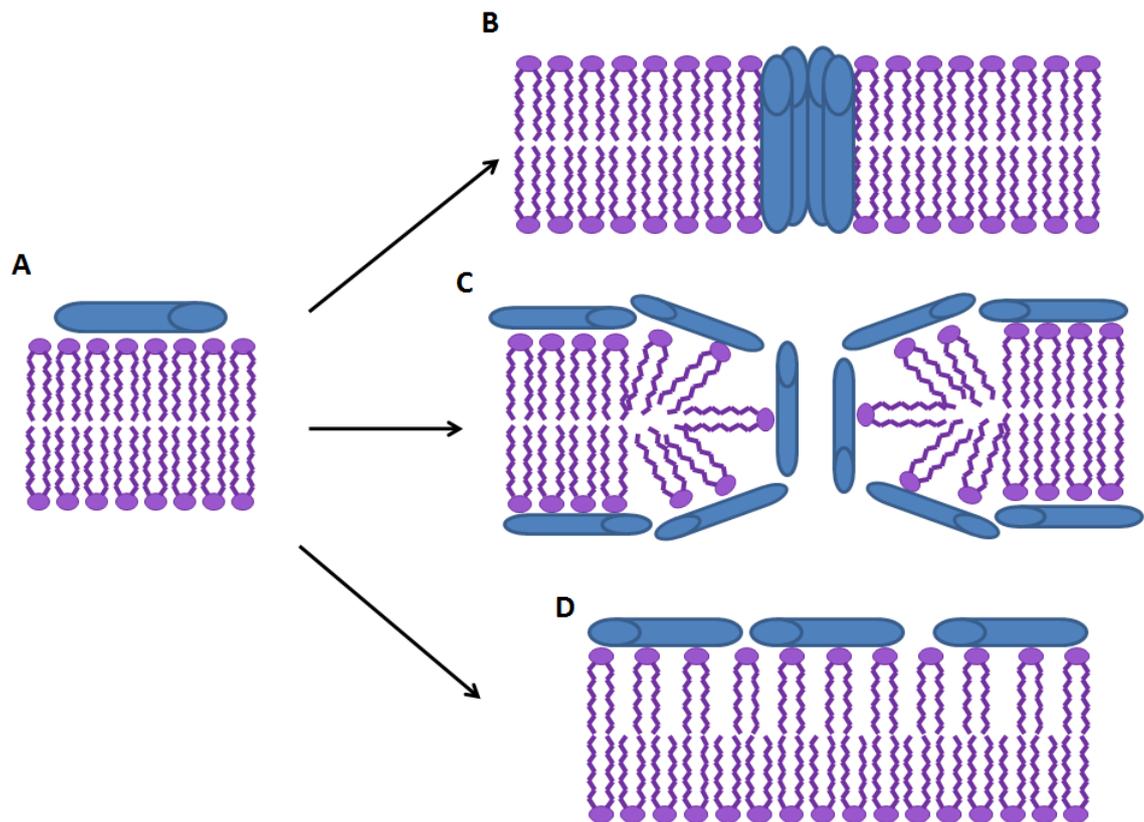
Figure 1.8. Binding mechanisms of antimicrobial peptides. A) Electrostatic binding of peptide to bilayer surface below threshold peptide concentration; B) barrel stave mechanism; C) toroidal pore mechanism; D) carpet binding mechanism.

All of these mechanisms cause permeabilization of the cell membrane, followed by the leakage of cell contents and/or the introduction of water by osmosis. This was initially thought to be the cause of cell death by AMPs, but there is evidence that in some cases the permeabilization of the cell membrane, though present, is not the actual cause of cell death. In some cases cell death is caused by the inhibition of intracellular processes. Defensin human neutrophil peptides have been suggested to attack the plasma membrane of bacterial cells and then to cause inhibition of DNA biosynthesis, both of which contribute to cell death.[43, 44] It has also been observed that 30 minutes after addition of defensin peptides to microbial cells, after evidence of widespread cell permeabilization has been observed, the cells could recover after re-suspending in peptide-free media, therefore cell permeabilization may not be sufficient to cause cell death.[45]

1.3.3 The study of antimicrobial peptide binding

There are a number of methods by which the binding of AMPs has been studied and from which the binding models were initially suggested. Analyses of pore formation

were initially carried out using electrical measurements and the observation of the leakage of fluorescence markers after the addition of peptides to marker-containing vesicles.[46, 47] The release of fluorescent markers due to pore formation and release due to membrane disruption can be distinguished by determining whether the release is graded or an all-or-none occurrence.[48, 49, 50] If the release is graded, all of the vesicles lose some of their contents, suggesting membrane disruption due to a carpet-like model. If the release is all-or-none, some of the vesicles release all of their contents and some are unaffected. This can be caused either by pore formation, which requires a certain number of peptide molecules to be present on one vesicle and aggregate to form the pore and therefore does not occur on every vesicle, or the complete disruption of some vesicles in a detergent-like manner (gross vesicle destabilization). The release of different sized markers after the addition of peptides can be used to give an indication of pore sizes.[49] Fluorescence labelling can be used to follow the insertion of peptides into the lipid membrane, by following the blue-shift of, for example, 4-fluoro-7-nitrobenz-2-oxa-1,-3-diazole (NBD) as it moves from being surrounded by aqueous solution to the more hydrophobic environment inside the lipid bilayer. The shape of binding isotherms can then be used to give an idea of whether the peptide monomers aggregate within the bilayer. Straight line isotherms indicate simple adhesion processes, while an increase in the slope as the peptide/lipid molar ratio is increased suggests slight aggregation within the lipid bilayers.[47] Initially the only pore-forming mechanism suggested was the barrel stave mechanism. The toroidal pore mechanism was first proposed to explain the binding of the peptide magainin. Oriented circular dichroism (OCD) had shown the magainin helices to be oriented perpendicular to the membrane surface, and neutron scattering data showed a pore was being formed.[51, 52] The neutron scattering data did not fit a barrel stave model however. Two measurements can be produced from neutron scattering analysis to describe an AMP pore, the core radius (the radius of the aqueous solution at the centre of the pore, which is treated as a cylinder) and the contact radius (the radius from the outer edge of a peptide monomer to the centre of the pore). For the helical AMP alamethicin, the core radius had been calculated as 9 Å and the contact radius 20 Å, which correlates with the helix diameter, known from the crystal structure, of 11 Å. Alamethicin was clearly forming barrel stave pores. The core radius of magainin pores was calculated as 14 Å from the neutron scattering data, while the contact radius was found to be 35.5 Å. The difference, 20 Å, was much greater than the diameter of the magainin helix (11 Å). Using measurements of the fraction of the membrane surface covered by peptide and the contact radius, and calculating the number of bound peptide monomers, it was determined that each pore must be composed of 4–7 monomers, which was not enough to create a pore of the size calculated from the neutron data. A toroidal

or wormhole-like structure was therefore suggested to explain this, lined with lipid head groups interspersed with peptide monomers. The difference between the core and contact radii correlated well with the thickness of a lipid monolayer (approximately 20 Å), and, since the peptides would be interspersed with lipids and not in direct contact with each other, the presence of only 4–7 peptide monomers in each pore was also explained.[52] The toroidal pore model has since been proposed to describe the binding of other AMPs including protegrin and melittin.[53, 54]

The development of analytical techniques over recent years is allowing a much greater understanding of the nature of antimicrobial peptide binding. AMPs are very hard to crystallise, due mainly to their amphiphilic nature and tendency to be partially disordered in solution, which has caused a major hurdle in understanding their structure and binding. In 2003 the Protein Data Bank (PDB) contained the 3D structures of only 54 of the 525 AMPs which were thought to be known, according to the authors of the Antimicrobial Peptide Database, though 68 had been studied by nuclear magnetic resonance (NMR) in membrane-mimetic environments or lipid bilayers.[55] High-resolution solution state NMR in membrane-mimetic environments has become the most widely-used method for structure determination of AMPs.[56] Other analytical techniques provide complimentary information about peptide binding, especially the orientation of peptides within the lipid bilayer, which can be determined by, for example, linear dichroism, and solid-state NMR of peptides binding to magnetically-oriented lipid bilayers.[57] The addition of secondary structural information, obtained from solution or crystal structures or by circular dichroism, membrane penetration information from, for example, fluorescence spectra, and liposome stability effects analysed by dynamic light scattering or fluorescence of labelled peptides, provides pictures of the nature of antimicrobial peptide binding.

1.3.4 Linear dichroism as a tool for studying antimicrobial peptides

Linear dichroism is the difference in absorbance of parallel and perpendicular linearly polarised light by an oriented sample (Equation 1.1), and is used to study the orientation of species including membrane-bound peptides and proteins.

$$LD = A_{\parallel} - A_{\perp} \tag{1.1}$$

In linearly polarised light, the electric field vector oscillates in the same plane (Figure 1.9)
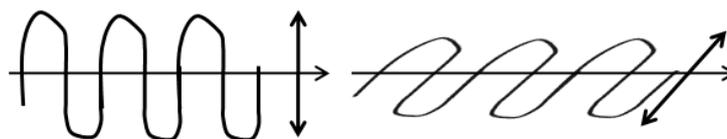
Figure 1.9. Parallel and perpendicular linearly polarised electromagnetic radiation.

Peptides and proteins can contain a number of chromophores, including the peptide amide bond, the side chains of aromatic residues and disulphide bonds. The main transitions of the amide bond are the weak, but not strictly forbidden, n–π^* transition, and two allowed π–π^* transitions (Figure 1.10).[58]
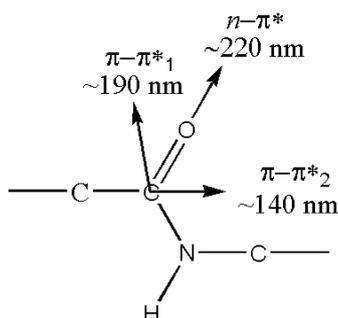
Figure 1.10. The electronic transitions of the peptide amide bond.

These transitions all have transition moments, as do the aromatic amino acids tryptophan, tyrosine and phenylalanine.[59] Transition moments are vector properties describing the intensity and polarization of the transition. The transition moments of α-helices, β-sheets, phenylalanine, tryptophan and tyrosine are shown in Figure 1.11.
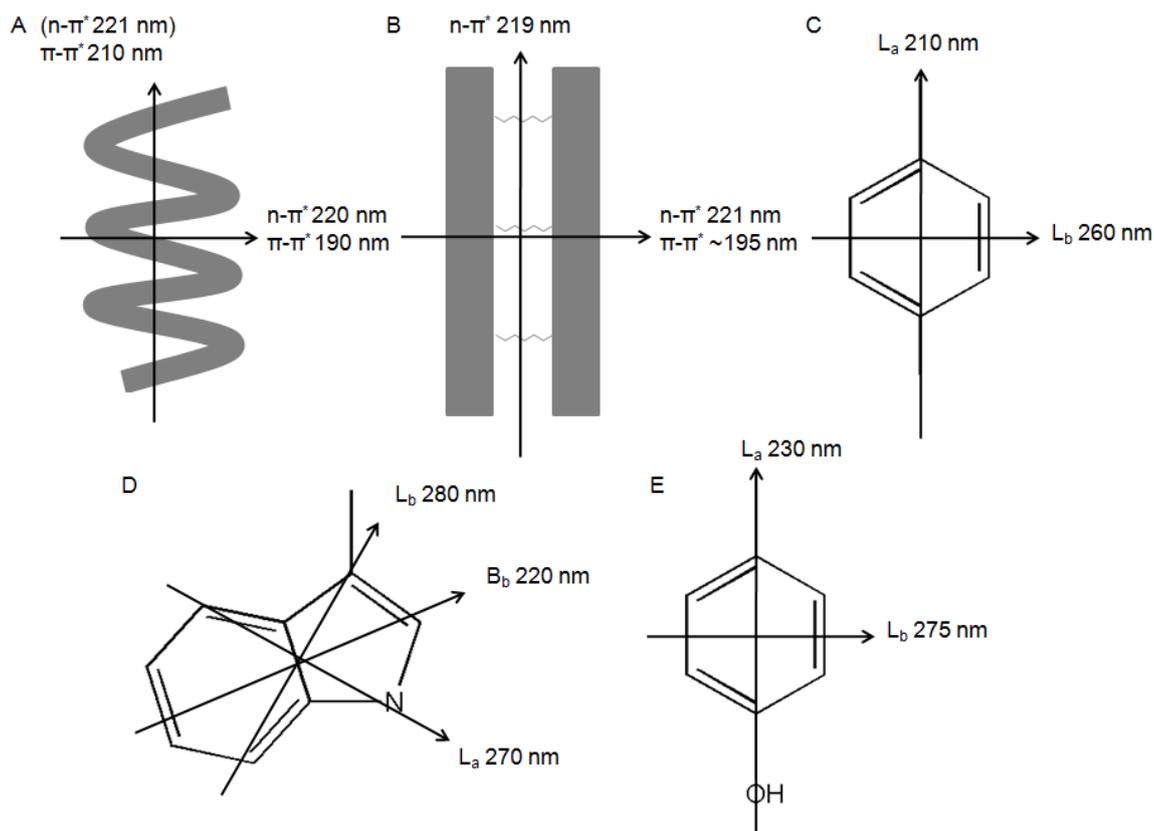
Figure 1.11. The transition moments of A) an α-helix; B) a β-sheet; C) phenylalanine; D) tryptophan and E) tyrosine.[58, 59] Transition shown in parentheses is weak in intensity.

If the transition moment is oriented parallel to the surface of the membrane a positive signal is recorded at the wavelength of the transition on the LD spectrum. If the orientation is perpendicular to the surface of the membrane then the signal will be negative. If the sample is not oriented then no net signal will be observed, as the signals will cancel out from the interactions of the polarised light with the randomly oriented sample molecules. For the study of membrane peptides and proteins, orientation can be achieved through orienting the liposomes to which binding occurs. The liposomes are distorted into ellipses though shear flow in a Couette cell (Figure 1.12).[60] The Couette cell is composed of two concentric cylinders, between which the sample is placed. The central cylinder is rotated at 3000 rpm during LD experiments, which causes the distortion of the liposomes.
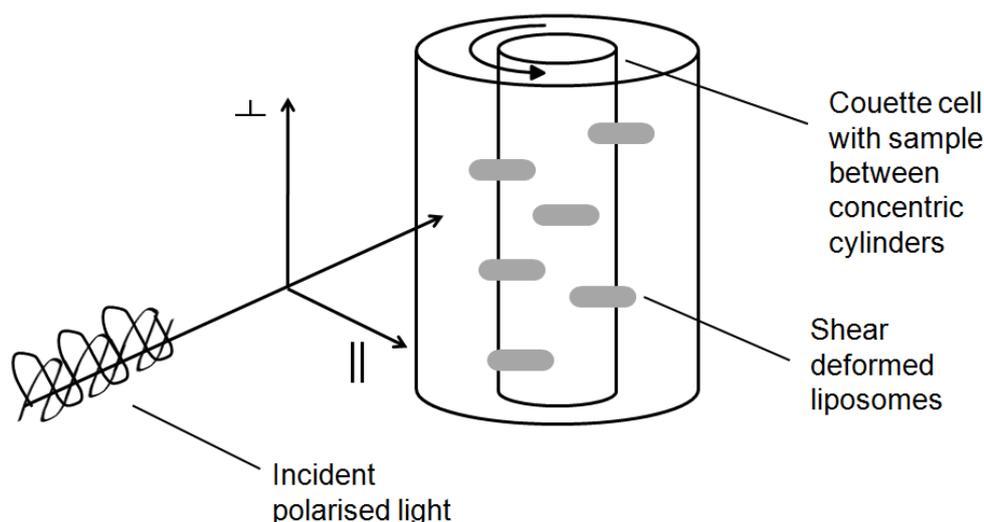
Figure 1.12. Design of LD experiment for the analysis of the binding of membrane proteins to liposomes.

In order to calculate the linear dichroism of peptides binding to shear deformed liposomes, the distorted liposomes are modelled as in Figure 1.13, where all peptides bound to the cylindrical section will be oriented in the same way relative to the polarised light.[59] By definition the long axis of the liposome is the 'parallel' orientation and the short axis is the 'perpendicular' orientation.
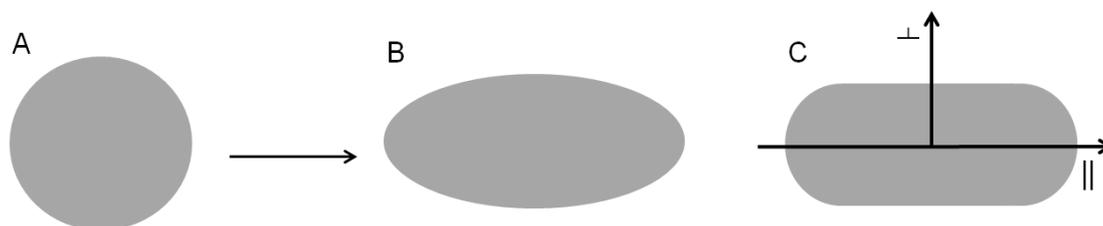
Figure 1.13. Illustrations of A) a liposome; B) a shear deformed liposome; C) model of a shear deformed liposome with defined perpendicular and parallel axes.

Equation 1.2 describes the linear dichroism of peptides bound to liposomes, where μ is the transition dipole, α is the angle between the transition moment and the membrane normal and S is the scaling factor. The equation is often described in terms of the reduced *LD*, *LD^r*, which is independent of the concentration of the sample and the strength of the transition dipole. Equation 1.3 is achieved by dividing Equation 1.2 by the isotropic absorbance, which is equal to $\mu^2/3$

$$LD = \frac{S\mu^2(1-3\cos^2\alpha)}{4}$$
(1.2)

$$LD^r = \frac{3LD}{\mu^2} = \frac{3S(1-3\cos^2\alpha)}{4}$$
(1.3)

Whilst there are uncertainties concerning the mechanisms of peptide binding to membranes, circular and in particular linear dichroism spectroscopies (discussed above), allied to other methods such as mass spectrometry and fluorescence spectroscopy, have the potential to reveal key features of the binding process. The following chapters describe experiments conducted to examine the scope of these analytical techniques for this purpose. Initially, the challenge of identifying lipids by mass spectrometric techniques is explored. This is followed by studies of liposome stability in the presence and absence of both natural and synthetic samples of a membrane-active peptide (melittin). The final chapter describes investigations into the membrane binding, including characterisation of membrane alignment and binding kinetics, of the antimicrobial peptide defensin HNP-2.

1.4 References

1. R. Y. Stanier and C. B. van Niel, *J. Bacteriol.*, 1994, **42**, 437– 466.

2. R. Prasad and M.A. Ghannoum, *Lipids of Pathogenic Fungi*, CRC Press, Boca Raton, FL, USA, 1996.

3. S. J. Singer and G. L. Nicholson, *Science*, 1972, **175**, 720–731.

4. J.M. Berg, J.L. Tymoczko and L. Stryer, *Biochemistry*, W.H. Freeman and Company, New York, USA, 5th edn., 2002.

5. H Hauser and G. Poupart in *The Structure of Biological Membranes*, ed. P. L. Yeagle, CRC Press, Boca Raton, FL, USA, 2nd edn., 2005.

6. J.L. Harwood in *The Lipid Handbook*, ed. F.D. Gunstone, J.L. Harwood and A.J. Dijkstra, CRC Press, Boca Ranton, Fl, USA, 3rd edn., 2007, pp 119–120.

7. C.M. Scrimgeour in *The Lipid Handbook*, ed. F.D. Gunstone, J.L. Harwood and A.J. Dijkstra, CRC Press, Boca Ranton, Fl, USA, 3rd edn., 2007, pp. 1–3.

8. J.M. Sanderson, *Org. Biomol. Chem.*, 2005, **3**, 201–212.

9. G. Cevc, *Biochemistry*, 1991, **30**, 7186–7193.

10. J.R. Silvius in *Lipid Protein Interactions*, ed. P.C. Jost and O.H. Griffth, John Wiley and Sons, New York, USA, 1982, Vol. 2, pp. 240–281.

11. R.N.A.H. Lewis, E.J. Prenner, L. H. Kondejewski, C.R. Flach, R. Mendelsohn, R.S. Hodges and R.N. McElhaney, *Biochemistry*, 1999, **38**, 15193–15203.

12. M.R. Yeaman and N.Y. Yount, *Pharmacol. Rev.*, 2003, **55**, 27–55.

13. A. Giuliani, G. Pirri, A. Bozzi, A. Di Giulio, M. Aschi and A. C. Rinaldi, *Cell. Mol. Life Sci.*, 2008, **65**, 2450–2460.

14. R.E.W. Hancock, *Lancet*, 1997, **349**, 418–422.

15. M. Zasloff, *Nature*, 2002, **415**, 389–395.

16. J.M. Conlon, *Peptides*, 2008, **29**, 1815–1819.

17. PDB ID: 1DFN, C.P. Hill, J. Yee, M.E. Selsted and D. Eisenberg, *Science*, 1991, **251**, 1481–1485.

18. PDB ID: 1KJ6, D.J. Schibli, H.N. Hunter, V. Aseyev, T.D. Starner, J.M. Wiencek, P.B. McCray Jr., B.F. Tack and H.L. Vogel, *J. Biol. Chem.* 2002, **277**, 8279–8289.

19. PDB ID: 1DUM, T. Hara, H. Kodama, M. Kondo, K. Wakamatsu, A. Takeda, T. Tachi and K. Matsuzaki, *Biopolymers*, 2001, **58**, 437–446.

20. PDB ID: 1G89, A. Rozek, C.L. Friedrich and R.E. Hancock, *Biochemistry*, 2000, **39**, 15765–15774.

21. L.H. Kondejewski, M. Jelokhani-Niaraki, S.W. Farmer, B. Lix, C.M. Kay, B.D. Sykes, R.E.W. Hancock and R.S. Hodges, *J. Biol. Chem.*, 1999, **274**, 13181–13192.

22. M. Dathe, T. Wieprecht, H. Nikolenko, L. Handel, W.L. Maloy, D.L. MacDonald, M. Beyermann and M. Bienert, *FEBS Letts.*, 1997, **403**, 208–212.

23. H.-C. Chen, J.H. Brown, J.L. Morel and C.M. Huang, *FEBS Letts.*, 1988, **236**, 462–466.

24. M. Dathe, M. Schümann, T. Wieprecht, A. Winkler, M. Beyermann, E. Krause, K. Matsuzaki, O. Murase and M. Bienert, *Biochemistry*, 1996, **35**, 12612–12622.

25. Y. Chen, M. T. Guarnieri, A.I. Vasil, M.L. Vasil, C.T. Mant and R.S. Hodges, *Antimicrob. Agents Chemother.*, 2007, **51**, 1398–1406.

26. S.M. Bowman and S.J. Free, *Bioessays*, 2006, **28**, 799–808.

27. Z. Jiang, B.J. Kullberg, H. van der Lee, A.I. Vasil, J. D. Hale, C. T. Mant, R. E. W. Hancock, M. L. Vasil, M. G. Netea and R. S. Hodges, *Chem. Biol. Drug Des.*, 2008, **72**, 483–495.

28. M.E. Klotman and T.L. Chang, *Nature Rev. Immunology*, 2006, **6**, 447–456.

29. D.M. Mann, E. Romm and M. Migliorini, *J. Biol. Chem.* Vol., 1994, **269**, 23661–23667.

30. K.B. McCann, A. Lee, J. Wan, H. Roginski and M.J. Coventry, *J. Appl. Microbiol.*, 2003, **95**, 1026–1033.

31. B. Berkhout, J.L.B. van Wamel, L. Beljaars, D.K.F. Meijer, S. Visser and R. Floris, *Antiviral Res.*, 2002, **55**, 341–355.

32. A. Falco, V. Masa, C. Tafalla, L. Perez, J.M. Coll and A. Estepa, *Antiviral Res.*, 2007, **76**, 111–123.

33. K. Matsuzaki, *Biochim. Biophys. Acta*, 1998, **1376**, 391–400.

34. K. Matsuzaki, M. Fukui, N. Fujii and K. Miyajima, *Biochim. Biophys. Acta*, 1991, **1070**, 259–264.

35. T. Miyata, F. Tokunaga, T. Yoneya, K. Yoshikawa, S. Iwanaga, M. Niwa, T. Takao, and Y. Shimonishi, *J. Biochem.*, **106**, 663–668.

36. Z. Oren, J. C. Lerman, G.H. Gudmundsson, B. Agerberth and Y. Shai, *Biochem. J.,* 1999, **341**, 501–513.

37. S.H. White, W.C Wimley and M.E Selsted, *Curr. Opin. Struct. Biol.*, 1995, **5**, 521–527.

38. N. Sitaram, K.P. Sai, S. Singh, K. Sankaran and R. Nagaraj, *Antimicrob. Agents Chemother.*, 2002, **46**, 2279–2283.

39. K.P. Sai, M.V. Jagannadham, M. Vairamani, N.P. Raju, A.S. Devi, R. Nagaraj and N. Sitaram, *J. Biol. Chem.*, 2001, **276**, 2701–2707.

40. S.E. Blondelle and R.A. Houghten, *Biochemistry*, 1991, **30**, 4671–4678.

41. Z. Oren and Y. Shai, *Biochemistry*, 1997, **36**, 1826–1835.

42. H.J. Jung, Y. Park, W.S. Sung, B.K. Suh, J. Lee, K.-S. Hahm and D.G. Lee, *Biochim. Biophys. Acta*, 2007, **1768**, 1400–1405.

43. S. Sharma, I. Verma and G.K. Khuller, *Arch. Microbiol.,* 1999, **171**, 338–342.

44. J.F. Gera and A. Lichtenstein, *Cellular Immunology*, 1991, **138**, 108–120.

45. A. Lichtenstein, *J. Clin. Invest.*, 1991, **88**, 93–100.

46. B.J. Christensen, J. Fink, R.B. Merrifield and D. Mauzerall, *Proc. Natl. Acad. Sci. USA.*, 1988, **85**, 5072–5076.

47. Y. Pouny, D. Rapaport, A. More, P. Nicolas and Y. Shai, *Biochemistry*, 1992, **31**, 12416–12423.

48. A.S. Ladokhin, W.C. Wimley and S.H. White, *Biophys. J.*, 1995, **69**, 1964–1971.

49. W.C. Wimley, M.E. Selsted and S.H. White, *Protein Sci.*, 1994, **3**, 1362–1373.

50. R.A. Parente, S. Nir and F.C. Szoka, Jr., *Biochemistry*, 1990, **29,** 8720–8728.

51. S.J. Ludtke, K. He, Y. Wu and H.W. Huang, *Biochim. Biophys. Acta,* 1994, **1190**, 181–184.

52. S.J. Ludtke, K. He, W.T. Heller, T.A. Harroun, L. Yang and H.W. Huang, *Biochemistry*, 1996, **35**, 13723-13728.

53. L. Yang, T.M. Weiss, R.I. Lehrer and H.W. Huang, *Biophys. J.*, 2000, **79**, 2002–2009.

54. L. Yang, T.A. Harroun, T.M. Weiss, L. Ding and H.W. Huang, *Biophys. J.*, 2001, **81**, 1475–1485.

55. Z. Wang and G. Wang, *Nucleic Acids Res.*, 2004, **32**, D590–D592.

56. E.F. Haney, H.N. Hunter, K. Matsuzaki and H.J. Vogel, *Biochim. Biophys. Acta*, 2009, **1788**, 1639–1655.

57. K. Nomura, G. Corzo, T. Nakajima and T. Iwashita, *Biophys. J.*, 2004, **87**, 2497–2507.

58. N. Sreerama and R.W. Woody in *Circular Dichroism : Principles and Applications*, ed. N. Berova, K. Nakanishi and R.W. Woody, Wiley-VCH, Berlin, DE, 2nd edn., 2000, pp. 602.

59. T.R. Dafforn and A. Rodger, *Curr. Opin. Struct. Biol.*, 2004, **14**, 541–546.

60. R. Marrington, T.R. Dafforn, D.J. Halsall, J.I. MacDonald, M. Hicks and A. Rodger, *Analyst*, 2005, **130**, 1608–1616.

2   THE IDENTIFICATION OF PHOSPHOLIPIDS BY MASS SPECTROMETRY

2.1   Introduction

2.1.1   Lipid and bilayer properties

The properties of cell membranes are influenced by certain features of the lipids from which they are composed. Headgroup composition determines the charge of the membrane, which in turn affects the membrane's physiological behaviour and interactions with other molecules such as peptides and proteins.[1] The major phospholipid components of the plasma membrane of the gram-negative bacteria *E. coli* are phosphoethanolamine (74% of total lipid composition) and phosphoglycerol (19%), which are neutral and negatively charged, respectively, at pH 7 (Table 2.1). The majority of the phospholipid components of human liver plasma membranes are neutral at pH 7, including phosphocholine (44%) and phosphoethanolamine (28%), with just a small amount of the negative phosphoinositol (9%) and phosphoserine (3%).[2]

The bilayer thickness, phase transition and mixing behaviour are features of the length and degree of unsaturation of the lipid hydrocarbon chains.[3] As can be seen from Table 2.1, the bilayer thickness increases by approximately 4 Å for every addition of $(CH_2)_2$ to the unsaturated acyl chains. The addition of a double bond reduces the bilayer thickness. The phase transition temperature increases with increasing chain length and drops dramatically with increasing unsaturation.

Table 2.1. Bilayer properties of saturated phosphocholine lipids.

Lipid	Bilayer Thickness (hydrocarbon region) (Å) (± 1)[4,a]	T_m (°C)[5]
10:0	15.5	-
12:0	19.5	-1
14:0	23	23
16:0	26	41
18:0	29.5	55
18:1	27	-20
18:2	-	-53
18:3	-	-60

a) Bilayer thickness measurements were obtained by X-ray scattering above the lipid phase transition temperature.

The position of the double bond of unsaturated lipids is also important, affecting the bilayer thickness, the surface area occupied by each lipid molecule and the

arrangement of hydrocarbon chains within the bilayer (Table 2.2).[6] The surface area per molecule increases slowly with the distance of the double bond from the headgroup until the double bond is at the middle of the chain (C_9 in Table 2.2), then decreases rapidly. The bilayer thickness remains stable until the double bond is in the centre of the chain, then increases. These measurements correlate with measurements of the chain order, which decreases as the double bond is moved away from the headgroup towards the middle of the chain and then increases again as the bond is moved further towards the end of the chain. In lipids with two different acyl chains, the phase transition temperature has been shown to decrease as the difference in chain lengths increases, due to the decreased attraction between the chains and therefore lower stability of the bilayer.[7]

Table 2.2. Bilayer properties of phosphocholine lipids with C_{18} chains with no or one double bond.[6]

Double bond position	Area per molecule (nm^2)	Bilayer thickness (P–P) (nm)
3	0.724	3.72
5	0.726	3.72
7	0.728	3.72
9 (DOPC)	0.731	3.71
11	0.719	3.77
13	0.706	3.83
15	0.686	3.93
none	0.669	4.02

Due to the strong effects of these different features, it is important to be able to fully identify unknown lipids, down to the position of each acyl chain on the central lipid glycerol.

2.1.2 Lipid identification by mass spectrometry

A number of different mass spectrometers and mass spectrometry techniques have been explored in relation to lipid analysis, with the aim of obtaining the maximum possible information for lipid identification, especially from samples at low concentrations. Different types of matrices have been studied for their suitability for the analysis of lipids by matrix-assisted laser desorption/ionisation-mass spectrometry (MALDI-MS). A solid ionic crystal matrix composed of *p*-nitroaniline and butyric acid was found to be particularly suited to the analysis of lipids present in only small quantities, by producing strong molecular ion peaks ([M + H]$^+$ for PC and PE lipids, [M + Na]$^+$ for PA, PG and PS lipids) in full-scan spectra, with the formation of virtually no other salt adducts and causing very little fragmentation. This gave less complex MS spectra, which is especially important when analysing lipid mixtures, and improved tandem mass spectrometry

through giving the maximum intensity of parent ions.[8]   Different isomers of dihydroxybenzoic acid (DHB) have also been explored in relation to their suitability for phospholipid analysis, though the commonly used 2,5 isomer was found to be best for lipid analysis in both positive and negative mode due to it having the optimum acidity compared to the other isomers and forming of the smallest crystals and thinnest crystal layers.[9]   The addition of metal salts has been shown to have effects on the product ion spectra of lipids analysed using a range of mass spectrometric techniques.   The dissociation of PE and PC [lipid + Na]$^+$ product ions by electrospray ionisation-tandem mass spectrometry (ESI-MSMS) was demonstrated to achieve greater sensitivity than the dissociation of protonated lipids, allowing the characterisation of species present in only picomole quantities.[10]   The analysis of PC lipids by MALDI-post-source decay (MALDI-PSD) was greatly improved by the addition of NaCl to the sample. Dissociation of the [M + H]$^+$ parent under these conditions produced a spectrum with only one peak, corresponding to [OP(O)$_2$OCH$_2$CH$_2$NMe$_3$]$^+$, therefore not allowing identification of the acyl chains, whereas dissociation of [M + Na]$^+$ produced a product ion spectrum from which the acyl chains could be identified.[11]   MALDI-MSMS analysis of lithium adducts of phospholipids has been shown to produce spectra which are more useful for lipid identification than those of [M + H]$^+$ and [M + Na]$^+$, with more abundant product ion peaks and the presence of pairs of peaks separated by 6 Da corresponding to protonated and lithium adducts of fragments.[12]   It has also been suggested that the addition of a salt to lipid mixtures before analysis can improve the identification of the individual lipids by separating out overlapping proton and sodium adducts of lipids which may have the same mass, such as [18:1/18:2-PC + H]$^+$ and [16:0/18:0-PC + Na]$^+$ (1-oleoyl-2-linoleoyl-*sn*-3-phosphocholine and 1-palmitoyl-2-stearolyl-*sn*-glycero-3-phosphocholine respectively), which both have *m/z* values of 784.58 Da.[13]   This method works better with metals of higher *m/z* values however, such as Cs$^+$ (132.97 Da), as the lithium adducts of some lipids can overlap with the proton adducts of others.[13]
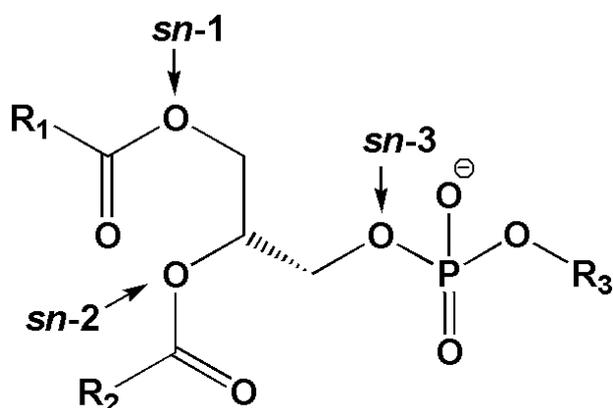
Figure 2.1. The *sn*-1, *sn*-2 and *sn*-3 positions on the glycerol backbone of phospholipids, along with the hydrocarbon chain sections referred to as R$_1$ and R$_2$.

It has been demonstrated that under certain conditions tandem mass spectrometry can allow the identification of the arrangement of the two acyl chains at the *sn*-1 (stereospecifically numbered-1) and *sn*-2 positions of the central lipid glycerol (Figure 2.1). This can be achieved by comparing the intensity of peaks corresponding to the loss of the chain from the *sn*-1 position with the intensity of those corresponding to the loss of the chain from the *sn*-2 position for analogous fragments. Under certain conditions a difference in intensities has been shown to be diagnostic of the position of the chain. A number of inconsistencies can be observed in the literature referring to the analysis of PC and PE lipids in the presence and absence of salts and fragmented by different techniques however.[10–12, 14–32] Differences can be observed in both the degree of fragmentation reported and the relative intensities associated with the fragments. Reports of collision induced dissociation (CID) describe the observation of peaks corresponding to the loss of each acyl chain in every case where fragmentation occurred in a sector instrument,[15, 16, 25, 27, 31, 32] a linear ion trap,[21, 23] or a MALDI-TOF/TOF.[12, 14, 22] CID in a triple quadrupole caused a range of results however: a) no peaks corresponding to the cleavage of either acyl chain were observed;[18] b) peaks were observed which corresponded to the loss of each acyl chain and there were statistical differences in intensities of those corresponding to analogous fragmentations at the *sn*-1 and *sn*-2 positions;[17, 18, 20, 29] c) peaks were observed which corresponded to the loss of each acyl chain but there were no statistical differences in the intensities of those corresponding to analogous fragmentations at the *sn*-1 and *sn*-2 positions;[26] d) a number of peaks corresponding to different types of fragmentations at the *sn*-1 and *sn*-2 positions were observed, and the differences in relative intensities varied between the different fragment types.[19] Inconsistencies were also observed in the data reported from post source decay (PSD) or seamless post source decay (sPSD), where in 50 % of cases peaks corresponding to cleavage of the acyl chains were not observed.[11, 15, 24] Results reported for the fragmentation of [PC + Na]$^+$ lipids highlight the differences observed. sPSD was reported to produce no product ions corresponding to the cleavage at either the *sn*-1 or *sn*-2 positions,[15] yet PSD or CID of [PC + Na]$^+$ in a linear ion trap instrument was shown to produce dissociation at the *sn*-1 and *sn*-2 positions, with a preferential loss of the chain from the *sn*-1 position observed.[11, 23] When the same ion was fragmented by high energy CID in a sector instrument however preferential loss of the chain from the *sn*-2 position was observed.[27]

2.1.3   MALDI imaging of lipids and thin layer chromatography plates

MALDI imaging of lipids is a growing field. Direct analysis of thin slices of biological tissue allows the identification of not only which lipids are present, but also their distribution. This can be used to study diseases which affect lipid production and distribution, such as Duchenne muscular dystrophy, which was shown by MALDI imaging of mouse muscle tissue to cause differences in certain phosphocholine lipids between diseased and healthy muscle.[33] MALDI imaging of thin layer chromatography (TLC) plates on which lipids have been separated is a more recent development for identifying individual lipids from mixtures, and offers advantages over the traditional method of using stains to give broad indications of the species which are present on the TLC plate. The separation of lipid mixtures by TLC prior to MALDI analysis also offers advantages for lipid identification compared to the direct analysis of the mixture. The presence of PC lipids in samples analysed by MALDI-MS is known to suppress the detection of other lipid species, therefore if equal concentrations of different lipid types are present in an analysed mixture, peaks corresponding to PC lipids will dominate the mass spectrum. This is thought to be due to the increased detection sensitivity of neutral phospholipids, such as PC lipids, compared to acidic lipids, with PC lipids having the lowest detection limit due to the positive charge of the quaternary ammonium salt. This means that separation of different lipid types before analysis will enhance the detection of non-PC lipids.[34] A number of different methods have been proposed for the analysis of lipids, and non-lipids, separated on TLC plates, from different ways to apply the matrix to the TLC plate for direct analysis, to methods of extracting the separated species either to the surface of the TLC plate or into a different substrate.[35, 36]

2.1.4   MALDI-TOF/TOF MS

During MALDI, a laser is fired at a dried mixture of sample and matrix, causing both to ablate from a flat conductive surface. The matrix molecules have a strong absorbance at the wavelength of the laser (337 nm), hence will absorb energy from the laser radiation and become electronically excited. Ionised matrix molecules then collide with sample molecules and causing the sample molecules to be ionised. In full scan mode, the ions are then accelerated through a potential of 19 kV through the ion optics before entering a field-free region. The polarity of the ion optics determines whether positive or negatively charged ions will be extracted and accelerated. All of the ions with the same charge have the same kinetic energy after acceleration (E_k), 19 keV, which means that their velocity is dependent on their mass, as shown in Equation 2.1.   Ions

with lower masses (m) have greater velocities (v), therefore ions of different mass to charge ratio are separated in time.

$$E_k = \frac{1}{2}mv^2 \hspace{6cm} (2.1)$$

In the field free region the ions can undergo metastable decay to produce product ions. The product ions travel with the same velocity as the precursor ions from which they were formed, but have a lower mass and less kinetic energy.
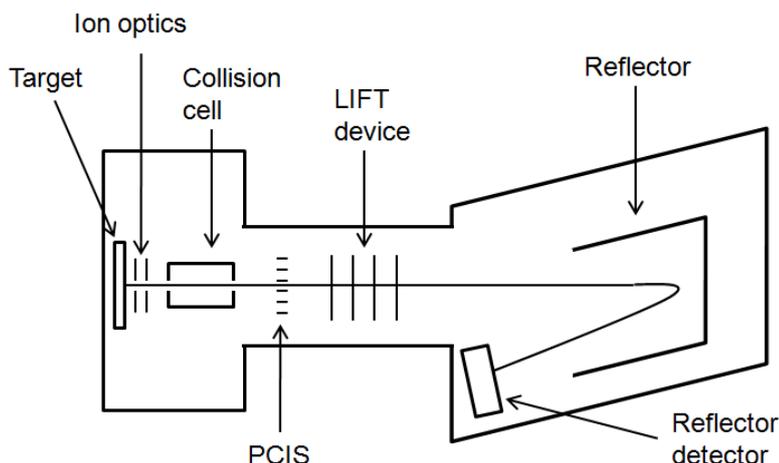
Figure 2.2. Schematic diagram of the Bruker Daltonics Autoflex MALDI TOF-TOF mass spectrometer.

At the end of the field free region the ions enter the electric field of the reflector. The reflector separates the ions, as ions with more kinetic energy will travel further into the reflector electric field, taking longer to turn around and exit thus emerging at different times relative to the product ions. The reflector detector can only focus within approximately a 30% difference in kinetic energy, therefore only fragments with at least 70% of the mass of the precursor will be detected.

Two types of tandem mass spectrometry can be carried out on the MALDI mass spectrometer used for the research described herein. One is collision induced dissociation and the other is LIFT, although both use the LIFT device. If the LIFT device is used the ions are initially only accelerated through 8 kV by the ion optics. This slows the ions down, thus allowing more time for dissociation to occur. Collision induced dissociation occurs if an inert collision gas such as argon is introduced into the collision cell situated before the LIFT device (Figure 2.2). Interactions with the collision gas cause the parent ions to undergo different fragmentation than when they fragment through metastable decay. Comparison of the product ion spectra of peptides analysed by LIFT and by CID found that a greater proportion of the product ions produced by CID were in the lower mass region of the spectrum, and that more internal fragment ions were produced by CID.[37] A precursor ion selector (PCIS) situated before the LIFT device is

used to separate out the required precursor ion and related product ions formed through collisions or, in the absence of a collision gas, through metastable decay. The LIFT device is a series of electrodes which raise the kinetic energy of the both the parent and daughter ions by 19 keV so that more of the daughter ions have at least 70% of the kinetic energy of the parent to enable them to be detected after separation in the reflector. As an example, if a precursor ion has 8 keV of kinetic energy, a fragment with 5% of the parent mass will have 5% of the kinetic energy of the parent (0.4 keV). After acceleration by 19 keV in the LIFT device the parent will have 27 keV of kinetic energy and the daughter will have 19.4 keV, which is now 72% of the kinetic energy of the parent, therefore it will be detected after separation in the reflector.[38]

2.1.5 The limitations of current methods and scope of this research

It has been established that product ion spectra of phospholipids can, in some cases, reveal the positions of the two acyl chains on the backbone glycerol, although a number of discrepancies are apparent within the literature on the topic. These discrepancies mean that the relative intensities of peaks corresponding to the loss of each acyl chain reported in one paper may not be extrapolated to interpret data obtained under different experimental conditions. The aim of this work is to establish a validated method that could be used for identifying unknown lipids from mixtures, and ultimately to the MALDI imaging of lipid bilayers and lipid mixtures separated on TLC plates. The methodology was developed on the basis that the same bilayer or TLC surface could not be analysed multiple times, due to the fact that lipid bilayers are very thin and that the quantity of lipid brought to the surface of the TLC plate by the addition of the matrix may be low. The method must, if possible, allow all of the molecular ions to be observed in one 'pass' over the surface, and then MSMS analysis could be used on specific areas of interest to provide full identification of the lipids. Determination of the optimum conditions depends on a number of factors relating to the analysis, both in terms of the instrument used and the systematic protocols deployed. Key issues are summarised in a–d below:

a)   Whether all of the phospholipid classes can be analysed and whether particular lipids preferentially produce positive or negative ions.

b)   Establishing the effect of metal salts on MS and MSMS spectra and whether the addition of such enhances the spectra in relation to lipid identification.

c)   Determining whether a statistical difference can be observed in the intensities of any peaks corresponding to the loss of the acyl chains from the *sn*-1 and *sn*-2 positions under the conditions established through a) and b).

d)   The development of a method of carrying out MALDI imaging of TLC plates, and the application of the analysis method developed through a) to c) in order to identify unknown lipids.

2.2   Results and discussion

2.2.1   Lipid analysis by MALDI-MS

Initially, positive ions of the lipids DOPC, DPPC, POPC, DPPE, POPE, DPPA, DOPS and POPG were analysed by MALDI-MS to determine to what degree they could be identified.   The MS analysis of each lipid produced peaks corresponding to the molecular ion and, in some cases, decomposition fragments (Table 2.3).   The lipids and references to 'R' when discussing fragmentation are described in Figure 2.3.

POPE/POPC/POPG
$R_1 = (CH_2)_{14}CH_3$
$R_2 = (CH_2)_7CH=CH(CH_2)_7CH_3$

DOPC/DOPS
R_1 and $R_2 = (CH_2)_7CH=CH(CH_2)_7CH_3$

DPPC/DPPA/DPPE
R_1 and $R_2 = (CH_2)_{14}CH_3$

DOPC/POPC/DPPC
$R_3 = CH_2CH_2^+NMe_3$

POPG
$R_3 = CH_2CH(OH)CH_2(OH)$

DOPS
$R_3 = CH_2CH(^+NH_3)CO_2$

POPE/DPPE
$R_3 = CH_2CH_2^+NH_3$

DPPA
$R_3 = OH$
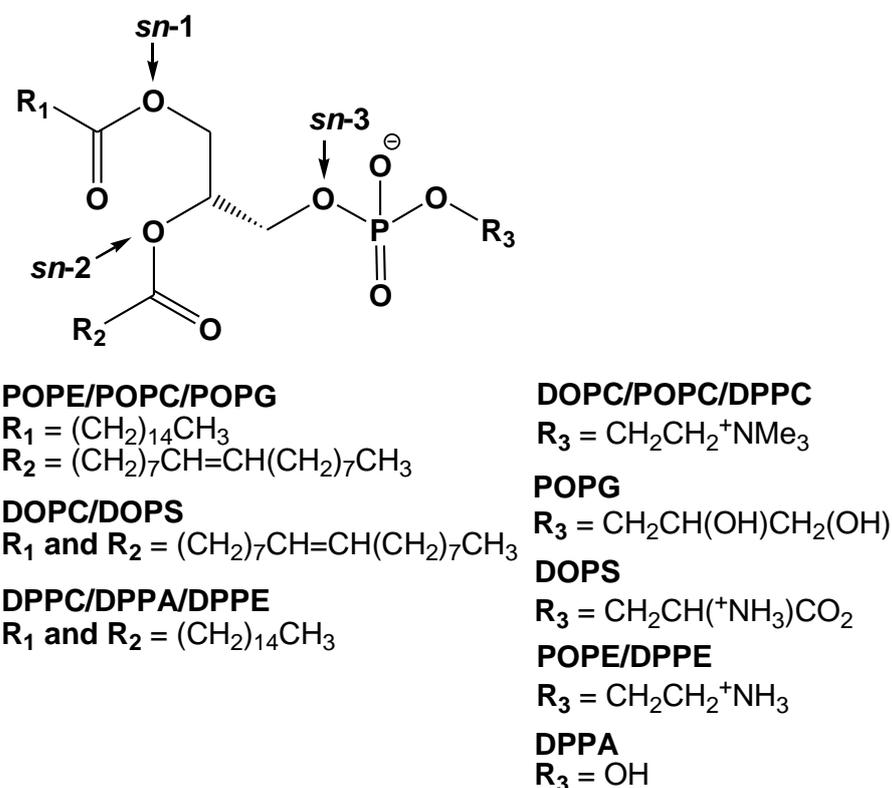
Figure 2.3. Nomenclature used in descriptions of lipids and lipid fragmentation.

All of the spectra revealed peaks which allowed the identification of the lipid headgroup, either through its neutral loss or through peaks corresponding to the headgroup itself.   Two peaks were observed in the spectrum of POPG from which the oleoyl chain could be identified (Figure 2.4A), one at *m/z* 467.3, corresponding to the neutral loss of $OC(O)CH=CH(CH_2)_7CH_3$ from the *sn*-2 position, and one at *m/z* 282.3, corresponding to $[R_2COO + H]^+$.   Peaks corresponding to the equivalent fragmentation involving the palmitoyl chain were not observed.   Neither acyl chain could be identified in

the full-scan spectra of the other lipids analysed in positive ion mode, and any decomposition species which were used to identify headgoups or acyl chains could not be assumed to have been formed during ionisation; the sample may have degraded during storage, or the peaks may have been caused by the matrix or contaminants and then misidentified. A matrix-only MS spectrum is shown in Figure 2.4D, and it is apparent from this spectrum that a large number of peaks are observed in MS spectra which are not related to the sample being analysed, due to the matrix, matrix clusters and any contaminants present in the matrix solution or on the target plate. An example of possible misidentification is the peak at m/z 154.0 in all of the spectra. This is the molecular weight of the matrix, 2,5-dihydroxybenzoic acid (DHB), but also corresponds to the $P(O)_2OCH_2CH_2(OH)CH_2OH$ portion of the headgroup of PG lipids. Without a matrix blank for comparison this peak could be wrongly assigned, and the matrix peak may be masking a peak corresponding to this lipid fragment. For these reasons, MS analysis in positive mode with this matrix is not adequate for the complete identification of phospholipids.
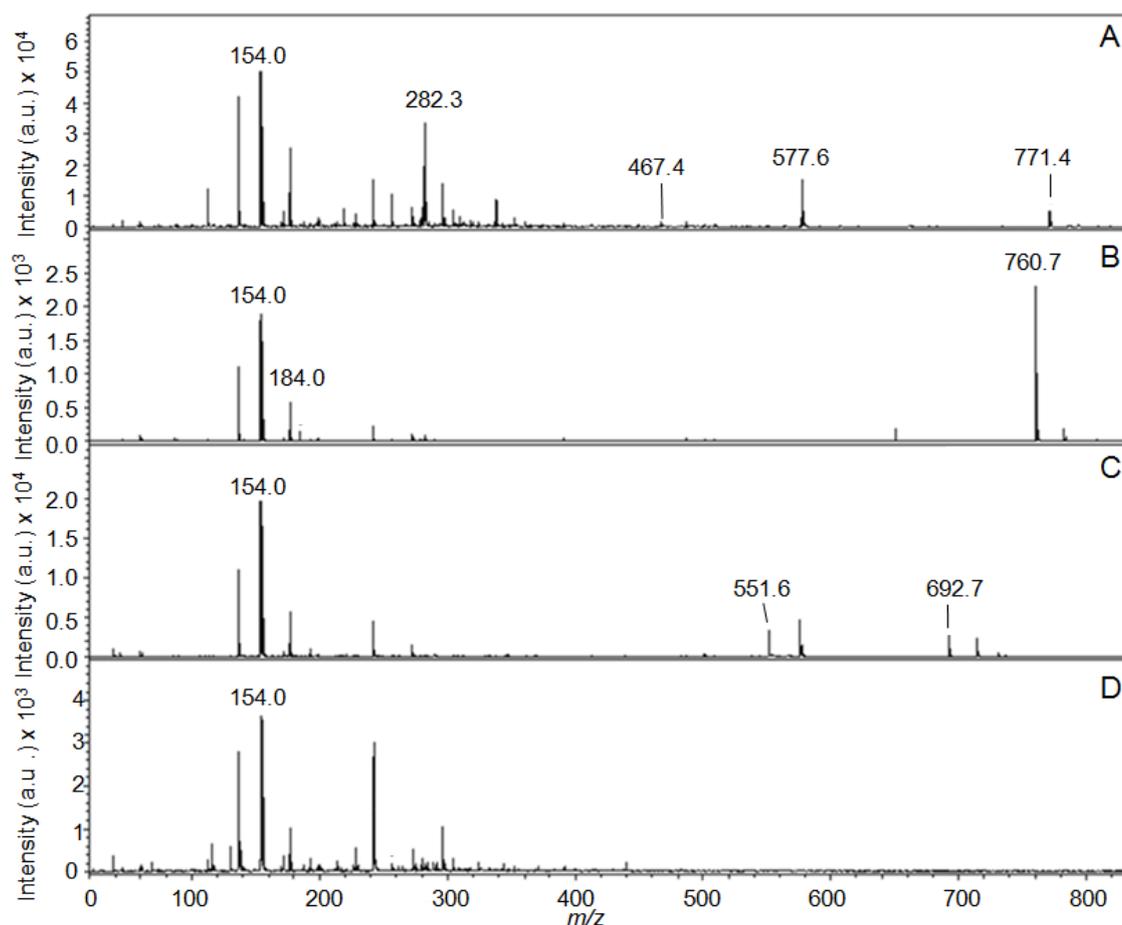
Figure 2.4. Full scan MALDI-MS spectra of A) POPG; B) POPC and C) DPPE, and D) a matrix-only spectrum. The samples were prepared by mixing a solution of the lipid in $CHCl_3$ (1 mg/mL) 1:9 (v/v) with solutions of DHB (30 mg/mL) in $EtOH/H_2O$ (50:50 (v/v)) or by spotting just DHB (30 mg/mL) in $EtOH/H_2O$ (50:50 (v/v)).

Table 2.3. Decomposition products observed in the positive ion MALDI-MS spectra of DOPC, DPPC, DPPE, POPE, POPG, DPPA, POPC and DOPS.

DOPC		DPPC	
m/z	**Assignment**	*m/z*	**Assignment**
184.1	$[OP(O)_2OCH_2CH_2NMe_3]^+$	184.3	$[OP(O)_2OCH_2CH_2NMe_3]^+$
786.6	$[M + H]^+$	735.4	$[M + H]^+$
POPC		**DPPE**	
m/z	**Assignment**	*m/z*	**Assignment**
184.0	$[OP(O)_2OCH_2CH_2NMe_3]^+$	551.6	$[M - OP(O)_2OCH_2CH_2NH_3]^+$
760.7	$[M + H]^+$	692.7	$[M + H]^+$
DOPS		**DPPA**	
m/z	**Assignment**	*m/z*	**Assignment**
603.7	$[M - OP(O)_2OCH_2CH(NH_3)CO_2]^+$	551.6	$[M - OP(O)_2OH + Na]^+$
788.6	$[M + 2H]^+$	671.6	$[M + Na + H]^+$
POPG		**POPE**	
m/z	**Assignment**	*m/z*	**Assignment**
282.3	$[R_2COO + H]+$	577.6	$[M - OP(O)_2OCH_2CH_2NH_3]^+$
467.4	$[M - R_2COO + H]^+$	592.4	$[M - P(O)_2OCH_2CH_2NH_3]^+$
577.6	$[M - OP(O)_2OCH_2CH_2(OH)CH_2OH]^+$	718.5	$[M + H]^+$
771.4	$[M + Na + H]^+$		

Table 2.4. Decomposition products observed in the negative ion MALDI-MS spectra of DPPE, POPE, DOPS, POPG and DPPA.

DPPE		POPE	
m/z	**Assignment**	*m/z*	**Assignment**
675.1	$[M - NH_3]^-$	437.1	$[M - R_2COO + H]^-$
690.6	$[M - H]^-$	716.7	$[M - H]^-$
POPG		**DOPS**	
m/z	**Assignment**	*m/z*	**Assignment**
168.9	$[OP(O)_2OCH_2CH(OH)CH_2OH - H]^-$	681.7	$[M - OCH_2CH(NH_3)CO_2 - H]^-$
464.8	$[M - R_2COO - H]^-$	787.3	$[M - H]^-$
491.3	$[M - R_1COO - H]^-$		
747.2	$[M]^-$		
DPPA			
m/z	**Assignment**		
647.1	$[M]^-$		

a) R_1 and R_2 correspond to the acyl chains at the *sn*-1 and *sn*-2 positions respectively

The negative ions of DOPC, DPPC, POPC, DPPE, POPE, DPPA, DOPS and POPG were also analysed by MALDI-MS to determine what structural information could be determined. As shown in Table 2.4, by this method peaks were observed which corresponded to the loss of each chain and to the headgroup in the spectrum of POPG. A peak corresponding to the loss of the headgroup was observed in the spectrum of DOPS, and one corresponding to the neutral loss of the oleoyl chain in the spectrum of POPE. No decomposition products were observed in the spectrum of DPPA, and only the neutral loss of NH_3 was observed in the spectrum of DPPE. None of the phosphocholine lipids could be ionised in negative mode, which is to be expected given the structure and neutral charge of the PC headgroup (Figure 2.3). Overall, full scan analysis in negative

mode was found to be a less informative method of identifying lipids than full scan analysis in positive mode, and the lack of ionisation of phosphocholine lipids implied that MALDI-MSMS analysis in negative mode would also be unsuitable for the analysis of unknown lipids, particularly mixtures.

2.2.2   MALDI-MS in the absence of a matrix

Small molecules can in some cases be analysed without the addition of a matrix, giving spectra without interfering matrix peaks.[39]   This would provide more reliable identification of any peaks observed in the MS spectra of lipids and could allow weak peaks to be observed which may have been suppressed or overlapped by matrix peaks. For this reason, POPG and DPPC were analysed in the absence of a matrix: 1 µL lipid (1 mg/mL in $CHCl_3$) was spotted onto the target plate and allowed to dry, then initially irradiated with a very low laser power. The laser power was slowly increased to try to find the level at which peaks corresponding to the molecular ion or decomposition products could be observed, however no peaks corresponding to molecular ions or decomposition products were observed even at high laser power.

2.2.3   Lipid analysis by MALDI-MSMS

Having concluded that the neither positive nor negative mode MALDI-MS analysis provided sufficient information for the identification of all of the lipids, and that, due to the lack of ionisation of PC lipids in negative mode, MALDI-MSMS in negative mode would be unsuitable, MALDI-MSMS in positive ionisation mode was considered. This method provides more information than MALDI-MS, as product ion spectra of a specific parent ion are produced, so all of the peaks observed in the spectrum can be relied upon to have originated from the selected ion, without the interference of matrix or contaminants. MALDI-MSMS spectra were obtained from $[DOPC + H]^+$, $[DPPC + H]^+$, $[DPPA + Na + H]^+$, $[DOPS + 2H]^+$, $[POPE + H]^+$, $[POPG + Na + H]^+$ and $[POPC + H]^+$. DPPA and POPG were supplied as sodium salts due to their inherent negative charges, and non-sodiated parent ions were not observed in the MALDI-MS spectra of either. The product ions observed in the spectra are shown in Table 2.5.

Table 2.5. Product ions observed in the MALDI-MSMS spectra of [DOPC + H]⁺, [POPC + H]⁺, [DPPC + H]⁺, [DOPS + 2H]⁺, [POPE + H]⁺, [POPG + Na + H]⁺ and [DPPA + Na + H]⁺.

[DPPA + Na + H]⁺		[POPC + H]⁺	
m/z	**Product ion**	*m/z*	**Product ion**
121.0	[OP(O)₂OH + Na + 2H]⁺	184.0	[OP(O)₂OCH₂CH₂NMe₃]⁺
239.3	[RCO]⁺	478.2	[M – R₂COO]⁺
415.4	[M + Na – RCOO]⁺	496.2	[M – R₂CO + 2H]⁺
433.4	[M – RCO + Na + 2H]⁺	504.2	[M – R₂COO]⁺
551.7	[M – OP(O)₂OH]⁺	522.2	[M – R₁CO + 2H]⁺
573.7	[M + Na – OP(O)₂OH –H]⁺	577.4	[M – OP(O)₂OCH₂CH₂NMe₃]⁺
[DOPS + 2H]+		**[DOPC + H]⁺**	
m/z	**Product ion**	*m/z*	**Product ion**ᵃ
184.1	[OP(O)₂OCH₂CH(NH₃)CO₂]⁺	184.0	[OP(O)₂OCH₂CH₂NMe₃]⁺
265.3	[RCO]⁺	504.3	[M – RCOO]⁺
339.4	[M – RCOO – P(O)₂OCH₂CH(NH₃)CO₂]⁺	522.2	[M – RCO + 2H]⁺
506.4	[M – RCOO + H]+	603.2	[M – OP(O)₂OCH₂CH₂NMe₃]⁺
603.7	[M – OP(O)₂OCH₂CH(NH₃)CO₂]⁺		
[POPG + Na + H]⁺		**[POPE + H]⁺**	
m/z	**Product ion**	*m/z*	**Product ion**
194.9	[OP(O)₂OCH₂CH(OH)CH₂(OH) + Na + 2H]⁺	282.3	[R₂COO + H]⁺
239.1	[R₁CO]⁺	308.3	[R₂COOCH₂CH₂ + H]⁺
265.1	[R₂CO]⁺	436.6	[M – R₂COO]+]⁺
415.1	[M– R₂CO – OCH₂CH(OH)CH₂OH +Na + H]⁺	454.3	[M – R₂CO + 2H]⁺
441.1	[M– R₁CO – OCH₂CH(OH)CH₂OH +Na + H]⁺	462.3	[M – R₁COO]⁺
489.1	[M +Na – R₂COO]⁺	480.3	[M – R₁CO + 2H]⁺
515.2	[M +Na – R₁COO]⁺	577.5	[M – OP(O)₂OCH₂CH₂NH₃]⁺
577.4	[M – OP(O)₂OCH₂CH(OH)CH₂(OH)]⁺	591.9	[M – P(O)₂OCH₂CH₂NH₃]⁺
599.4	[M – OP(O)₂OCH₂CH(OH)CH₂(OH) + Na – H]⁺		
[DPPC + H]⁺			
m/z	**Product ion**		
183.8	[OP(O)₂OCH₂CH₂NMe₃]⁺		
477.8	[M – RCOO]⁺		
495.8	[M – RCO + 2H]⁺		

a) R₁ and R₂ correspond to the acyl chains and the *sn*-1 and *sn*-2 positions respectively

Each product ion spectrum provided enough information to fully identify the lipids analysed, with peaks corresponding to the neutral loss of the headgroup and to the neutral loss of each acyl chain observed in the spectrum of each lipid. Some lipids were fragmented more than others. Only three peaks were observed in the product ion spectrum of [DPPC + H]⁺ from which the lipid could be identified, whereas peaks corresponding to five fragments of DOPS were observed. Some peaks, especially those from which the acyl chains could be identified, were very weak. The effects of the addition of metal ions on MSMS spectra were therefore explored, to determine whether fragmentation and/or peak intensities could be increased.

2.2.4 MALDI-MSMS of lipids in presence of metal salts

2.2.4.1 Analysis of POPE with CaCl₂, CuCl₂, MgCl₂, ZnCl₂, LiCl and NaCl

Initially, the effect of a number of different metal salts on the MS analysis of POPE was explored. Spectra were obtained for POPE with each of CaCl₂, CuCl₂, MgCl₂, ZnCl₂, LiCl and NaCl and compared to a spectrum obtained in the absence of added salt (Figure

2.5 and Table 2.6). Peaks corresponding to the protonated molecular ion were observed at m/z 718.6 in the all of the spectra, however the peak could only be observed weakly in the spectra of POPE with magnesium and zinc. Peaks corresponding to [POPE + Na]$^+$ (m/z 740.6), due to Na$^+$ naturally present in the samples, were observed in the spectra obtained in the absence of added salt, in the presence of Ca^{2+}, Cu^{2+} and, to a far lesser extent, Zn^{2+}. Additions of both ^{63}Cu and ^{65}Cu (relative abundance 69:31) to POPE were observed in the MS spectrum obtained with CuCl$_2$ at m/z 780.5 and m/z 782.6, corresponding to [POPE + ^{63}Cu – H]$^+$ and [POPE + ^{65}Cu – H]$^+$ respectively (Figure 2.5E).[40] The addition of Li$^+$ to POPE generated molecular ion peaks corresponding to [POPE + ^{6}Li]$^+$, [POPE + ^{7}Li]$^+$ [POPE – H + ^{6}Li + ^{7}Li]$^+$, and [POPE – H + 2^{7}Li]$^+$, though [POPE + ^{6}Li]$^+$ and [POPE – H + ^{6}Li + ^{7}Li]$^+$ were present as minor peaks due to the relative isotopic abundances of 7.5 and 92.5 for ^{6}Li and ^{7}Li respectively (Figure 2.5B).[40] Calcium also has a number of isotopes, but the relative abundances of ^{42}Ca, ^{43}Ca, ^{44}Ca, ^{46}Ca and ^{48}Ca are very low (0.647:0.135:2.07:0.004:0.187) compared to ^{40}Ca (96.9%) and only the addition of the most abundant isotope was observed in the MS spectrum of POPE in the presence of CaCl$_2$, with a peak at m/z 756.5 corresponding to [POPE + ^{40}Ca – H]$^+$ (Figure 2.5D).[40] Peaks corresponding to [POPE + Na]$^+$ and [POPE + 2Na – H]$^+$ were observed in the spectrum of POPE with NaCl (Figure 2.5C). The addition of two singly charged metal ions to POPE can be attributed to the pKa of the ammonium and phosphate groups, which are 9.8 and 1.7 respectively.[41] Though POPE has a neutral charge between approximately pH 4 and pH 8, the presence of a small population of the negatively charged species allows the addition of two singly charged metal ions. No magnesium or zinc adducts of POPE were observed (Figure 2.5F and G respectively). All of the MS spectra revealed peaks corresponding to [M – OP(O)$_2$OCH$_2$CH$_2$NMe$_3$]$^+$ i.e. loss of the metal ion and the headgroup, but there was no evidence of any other decomposition.
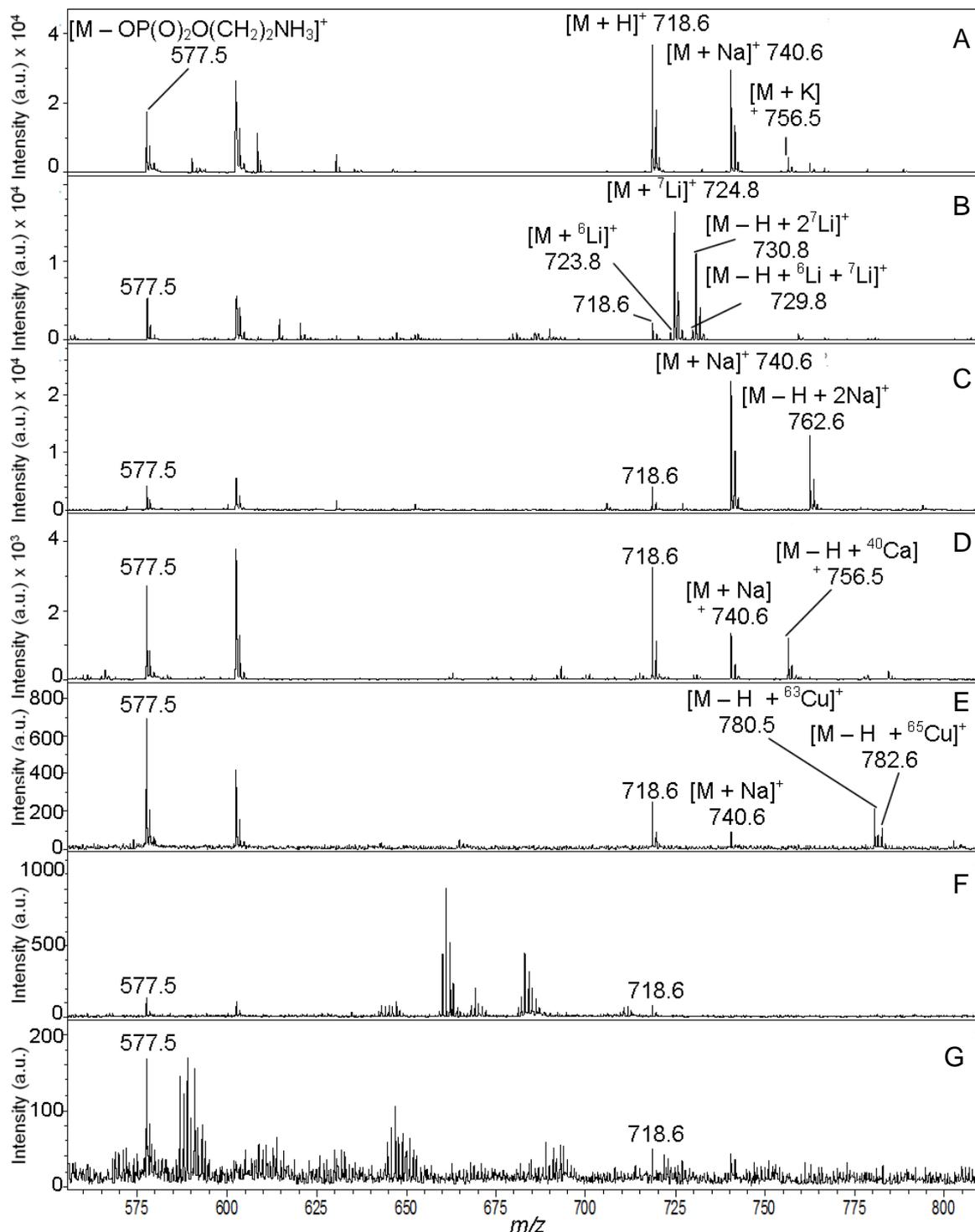
Figure 2.5. MALDI-MS spectra of POPE A) in the absence of added salt, and with B) LiCl; C) NaCl; D) CaCl₂; E) CuCl₂; F) MgCl₂; and G) ZnCl₂. The samples were prepared by mixing a solution of the lipid in CHCl₃ (1 mg/mL) 1:9 (v/v) with solutions of DHB (30 mg/mL) in EtOH/H₂O (50:50 (v/v)) or CaCl₂ (4.5 mM), CuCl₂ (100 mM), MgCl₂ (100 mM), ZnCl₂ (100 mM), LiCl (100 mM) or NaCl (100 mM) in EtOH/H₂O (50:50 (v/v)) for each of the salt adducts respectively.

MALDI-MSMS analysis was then carried out on [POPE – H + Ca]⁺, [POPE – H + Cu]⁺, [POPE + Li]⁺ and [POPE + Na]⁺, and the resulting product ion spectra compared to

that of $[POPE + H]^+$. It was not possible to isolate the ^6Li and ^7Li isotope adducts of POPE separately for MSMS analysis; discussion of fragments refers only to those involving more abundant ^7Li isotope. The main product ions observed in the MSMS spectra of $[POPE + H]^+$, $[POPE + Li]^+$, $[POPE + Na]^+$, and $[POPE - H + Ca]^+$ (Figure 2.6) are recorded in Table 2.6; the product ion peaks of $[POPE - H + Cu]^+$ were too weak to record. It is possible that the low intensity of the product ions of $[POPE - H + Cu]^+$ was due to the two copper isotopes, ^{63}Cu and ^{65}Cu, with relative abundance 69:31, causing the signal-to-noise ratio of each fragment to be reduced according to the isotopic abundance.[40]

Table 2.6. Product ions observed in the MALDI-MSMS spectra of $[POPE + H]^+$, $[POPE + Li]^+$, $[POPE - H + Ca]^+$ and $[POPE + Na]^+$.

[POPE + H]⁺		**[POPE + Li]⁺**	
m/z	**Product ion**[a]	*m/z*	**Product ion**
282.3	$[R_2COOH]^+$	148.0	$[OP(O)_2O(CH_2)_2NH_3 + {}^7Li + H]^+$
308.3	$[R_2COOCH_2CH_2]^+$	399.2	$[M - R_2COO - (CH_2)_2NH_3 + H + {}^7Li]^+$
436.3	$[M - R_2COO]^+$	425.2	$[M - R_1COO - (CH_2)_2NH_3 + H + {}^7Li]^+$
454.3	$[M - R_2CO + 2H]^+$	577.2	$[M - OP(O)_2O(CH_2)_2NH_3]^+$
462.3	$[M - R_1COO]^+$	601.7	$[M - P(O)_2O(CH_2)_2NH_3 + H + {}^7Li]^+$
480.3	$[M - R_1CO + 2H]^+$	681.5	$[M - (CH_2)_2NH_3 + 2H + {}^7Li]^+$
577.5	$[M - OP(O)_2O(CH_2)_2NH_3]^+$		
591.9	$[M - P(O)_2O(CH_2)_2NH_3 - 2H]^+$		
[POPE + Na]⁺		**[POPE + Ca]+**	
m/z	**Product ion**	*m/z*	**Product ion**
145.9	$[P(O)_2(CH_2)_2NH_3 - H + Na]^+$	163.9	$[P(O)_2O(CH_2)_2NH_3 + Ca]^+$
164.0	$[OP(O)_2O(CH_2)_2NH_3 + H + Na]^+$	180.0	$[OP(O)_2O(CH_2)_2NH_3 + Ca]^+$
239.0	$[R_1CO]^+$	431.2	$[M - R_2COO - CH_2CH_2NH_3 + Ca]^+$
265.0	$[R_2CO]^+$	457.2	$[M - R_1COO - CH_2CH_2NH_3 + Ca]^+$
415.0	$[M - R_2CO - O(CH_2)_2NH_3 + H + Na]^+$	474.3	$[M - R_2COO - 2H + Ca]^+$
420.4	$[M - R_2COO - NH_3 + 2H]^+$	500.3	$[M - R_1COO - 2H + Ca]^+$
441.1	$[M - R_2COO NH_3 - H + Na]^+$	577.5	$[M - OP(O)_2O(CH_2)_2NH_3]^+$
446.3	$[M - R_1COO - NH_3 + 2H]^+$		
458.0	$[M - R_2COO - H + Na]^+$		
466.8	$[M - R_1COO NH_3 - H + Na]^+$		
484.1	$[M - R_1COO - H + Na]^+$		
577.5	$[M - OP(O)_2O(CH_2)_2NH_3]^+$		
599.4	$[M - OP(O)_2O(CH_2)_2NH_3 - H + Na]^+$		

a) R_1 and R_2 correspond to the acyl chains and the *sn*-1 and *sn*-2 positions respectively
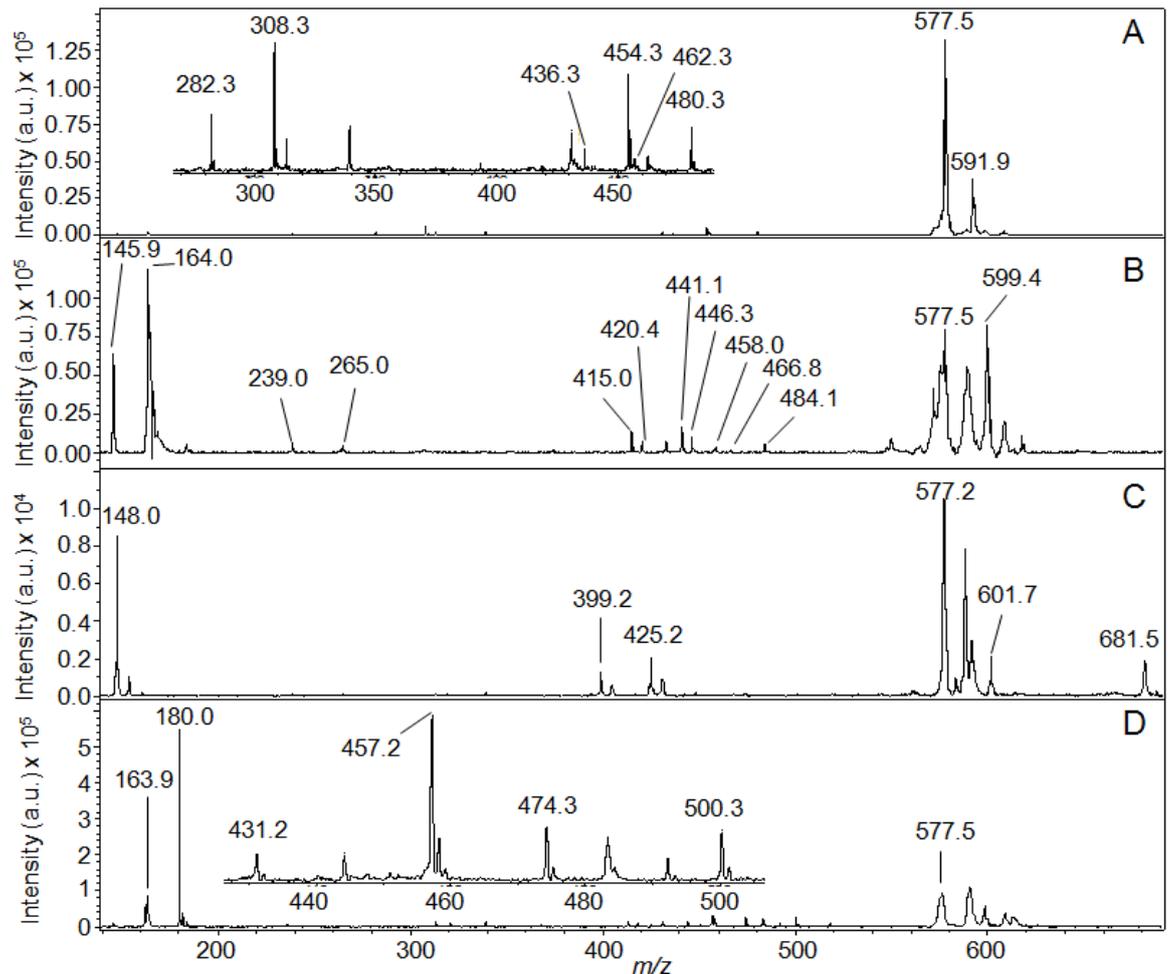
Figure 2.6. MALDI-MSMS spectra of A) [POPE + H]$^+$; B) [POPE + Na]$^+$; C) [POPE + Li]$^+$ and D) [POPE – H + Ca]$^+$. The samples were prepared by mixing a solution of the lipid in CHCl$_3$ (1 mg/mL) 1:9 (v/v) with solutions of DHB (30 mg/mL) in EtOH/H$_2$O (50:50 (v/v)) or NaCl (100 mM), LiCl (100 mM) or CaCl2 (4.5 mM) in EtOH/H$_2$O (50:50 (v/v)) for each of the salt adducts respectively.

[POPE + Li]$^+$, [POPE – H + Ca]$^+$ and [POPE + Na]$^+$ were all shown to give more clear product ion spectra than the protonated species. The peaks corresponding to the neutral loss of the acyl chains from the Na$^+$ and Li$^+$ adducts (Figures 2.6B and C respectively) had the greatest intensity relative to the peaks corresponding to the headgroup or neutral loss of the headgroup, compared to the spectra of the Ca^{2+} adduct (Figure 2.6D) and the protonated lipid (Figure 2.6A). Further comparisons were therefore carried out between POPC and POPE MSMS spectra obtained in the presence and absence of LiCl and NaCl to determine which gave the most useful spectrum for lipid identification in terms of the amount of fragmentation, the nature of the fragmentations and the signal-to-noise ratio.

2.2.4.2 MALDI-MS analysis of POPC and POPE in the presence of LiCl and NaCl and in the absence of added salt

The MALDI-MS spectrum of POPE in the absence of added metal salts showed three molecular ions, corresponding to $[M + H]^+$, $[M + Na]^+$ and $[M + K]^+$, in order of increasing mass and decreasing intensity (Figure 2.5A). The spectrum obtained in the presence of added Na^+ (Figure 2.5C) also contained three molecular ions, corresponding to $[M + H]^+$, $[M + Na]^+$ and $[M + 2Na – H]^+$, with the peak corresponding to $[M + Na]^+$ the most intense and that corresponding to $[M + H]^+$ the weakest. In the presence of added Li^+ (Figure 2.5B), a peak corresponding to $[M + H]^+$ was weak, one corresponding to $[M + {}^7Li]^+$ more intense, and one corresponding to $[M + 2{}^7Li – H]^+$ more intense again. This trio of peaks was separated by 6 Da each. The observation of molecular ion peaks separated by 6 Da in the presence of lithium may provide a useful visual indication of the masses of molecular ions in full scan MS spectra of lipid mixtures. Minor peaks corresponding to $[M + {}^6Li]^+$ and $[M + 2{}^6Li – H]^+$ were also observed.

Hydrogen, sodium and potassium adducted molecular ion peaks were also observed in the MALDI-MS spectrum of POPC (Figure 2.7A), again with $[M + H]^+$ the most intense and $[M + K]^+$ the weakest. In the presence of the sodium salt (Figure 2.7C), only protonated and singly sodiated molecular ions were observed, with $[M + H]^+$ more intense than $[M + Na]^+$. Similarly, in the spectrum obtained in the presence of the lithium salt (Figure 2.7B) only peaks corresponding to $[M + H]^+$, $[M + {}^6Li]^+$ and $[M + {}^7Li]^+$ were observed, with the peak corresponding to $[M + H]^+$ slightly more intense than that of $[M + {}^7Li]^+$ and $[M + {}^6Li]^+$ present as a minor peak. The H and ^7Li adducts were again separated by only 6 Da, making them clearly identifiable. The observation of only single sodium and lithium adducts of POPC, compared to the addition of two metal ions to POPE, is due to the phosphocholine headgroup having only one ionisable group at physiological pH, allowing only the single metal adducts.
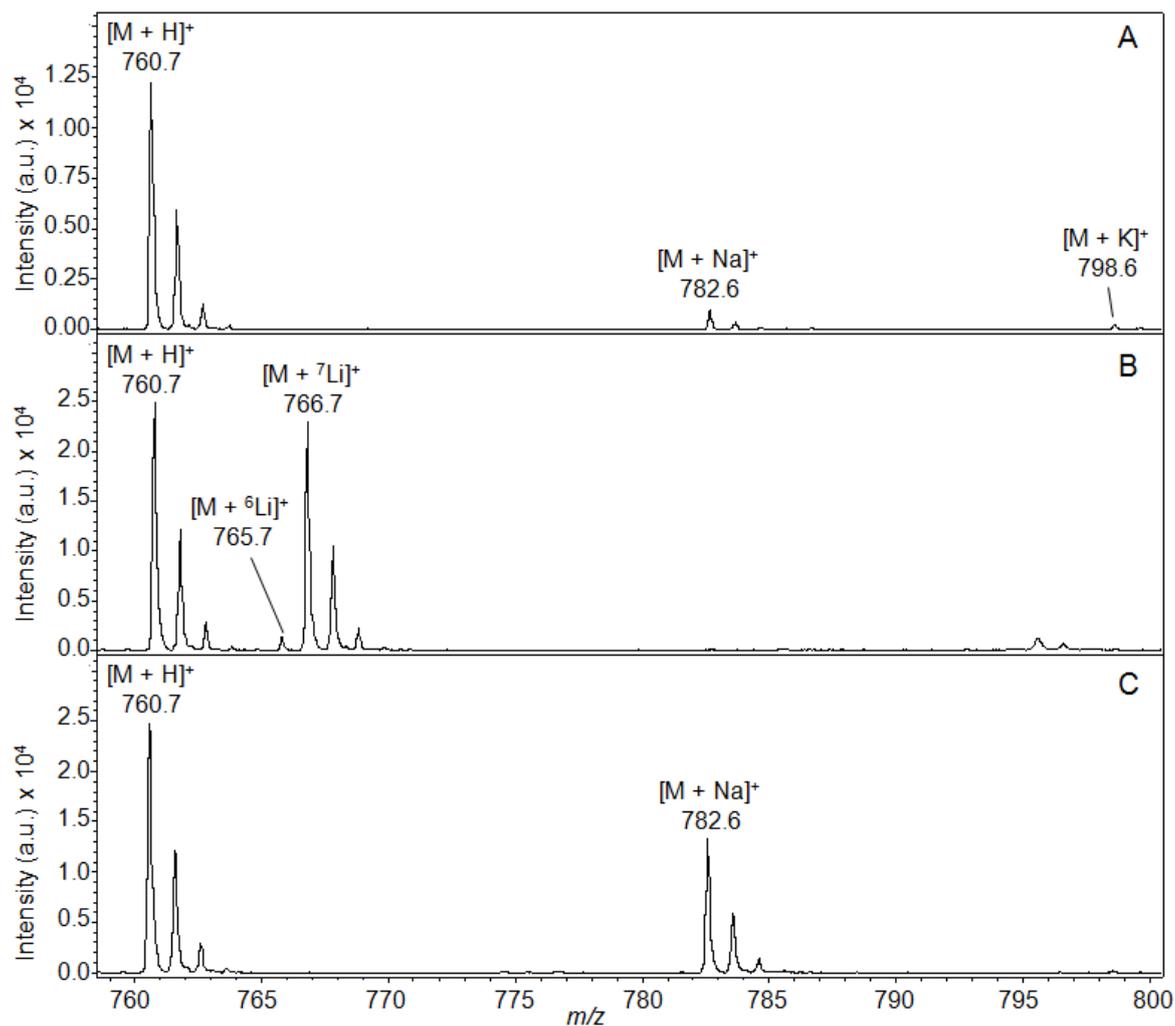
Figure 2.7. MALDI-MS spectra of POPC A) in the absence of added salt, and with B) LiCl and C) NaCl. The samples were prepared by mixing a solution of the lipid in $CHCl_3$ (1 mg/mL) 1:9 (v/v) with solutions of DHB (30 mg/mL) in $EtOH/H_2O$ (50:50 (v/v)) or LiCl (100 mM) or NaCl (100 mM) in $EtOH/H_2O$ (50:50 (v/v)).

2.2.4.3 MALDI-MSMS of POPE in the presence of LiCl and NaCl and in the absence of added salt

The dominant peak in the product ion spectrum of [POPE + H]$^+$ (Figure 2.6A, Table 2.6) corresponds to the neutral loss of the headgroup, [M – OP(O)$_2$O(CH$_2$)$_2$NH$_3$]$^+$, at *m/z* 577.5, and the next most intense corresponds to the neutral loss of P(O)$_2$O(CH$_2$)$_2$NH$_3$ at *m/z* 591.9. Two pairs of peaks were observed which correspond to the loss of the palmitoyl or oleoyl chain, [M – R$_x$COO]+ and [M – R$_x$CO + 2H]$^+$, and two more peaks were observed which correspond to fragments involving the chain from the *sn*-2 position, [R$_2$COOH]$^+$ and [R$_2$COOCH$_2$CH$_2$]$^+$, though peaks corresponding to their analogous *sn*-1 fragments were not observed. All of these peaks were very weak in relation to those corresponding to fragments involving the loss of the headgroup. The product ion spectrum of the sodium adduct of POPE (Figure 2.6B, Table 2.6) contained a number of intense peaks corresponding to the headgroup or to the neutral loss of the headgroup,

60

with and without the sodium ion. These were observed at *m/z* 145.9, *m/z* 164.0, *m/z* 577.5 and *m/z* 599.4, corresponding to $[P(O)_2(CH_2)_2NH_3 - H + Na]^+$, $[OP(O)_2(CH_2)_2NH_3 + H + Na]^+$, $[M - OP(O)_2(CH_2)_2NH_3]^+$ and $[M - OP(O)_2O(CH_2)_2NH_3 - H + Na]^+$ respectively. Four pairs of peaks were observed from which the acyl chains could be identified. The most intense of these pairs corresponds to $[M - R_xCO - OCH_2CH_2NH_3 + H + Na]^+$, at *m/z* 415.0 and *m/z* 441.1 for fragmentation at the *sn*-2 and *sn*-1 positions respectively. The other pairs of peaks, corresponding to $[R_xCO]^+$, $[M - R_xCOO - NH_3 + 2H]^+$ and $[M - R_xCOO - H + Na]^+$, were also relatively intense in relation to the peaks corresponding to the presence or loss of the headgroup and when compared with the acyl chain fragment peaks in the product ion spectrum of $[POPE + H]^+$. As with the spectrum of $[POPE + Na]^+$, the product ion spectrum of $[POPE + Li]^+$ (Figure 2.6C, Table 2.6) was dominated by four peaks corresponding to fragments involving the cleavage of the headgroup, namely $[OP(O)_2O(CH_2)_2NH_3 + Li + H]^+$, $[M - OP(O)_2O(CH_2)_2NH_3]^+$, $[M - P(O)_2O(CH_2)_2NH_3 + H + Li]^+$ and $[M - (CH_2)_2NH_3 + 2H + Li]^+$ at *m/z* 147.9, *m/z* 577.2, *m/z* 601.7 and *m/z* 681.5 respectively. Only one pair of peaks was observed from which the acyl chains could be identified, corresponding to $[M - R_1COO - (CH_2)_2NH_3 + H + Li]^+$ and $[M - R_2COO - (CH_2)_2NH_3 + H + Li]^+$ at *m/z* 425.2 and *m/z* 399.2 respectively, however these peaks were both intense. Weak peaks could also be observed at *m/z* 405 and *m/z* 431. These are double lithium adducts of the $[M - R_xCOO - (CH_2)_2NH_3 + H + Li]^+$ fragments due to incomplete isolation of the $[POPE + Li]^+$ parent, despite an isolation window of ± 5 Da.

2.2.4.4 MALDI-MSMS of POPC in the presence of LiCl and NaCl and in the absence of added salt.

Table 2.7 and Figure 2.8 show the product ion spectra and peak assignments for $[POPC + H]^+$, $[POPC + Na]^+$ and $[POPC + Li]^+$. All of these spectra revealed peaks from which the identity of the headgroup and both chains could be determined. As with the analysis of POPE, it was not possible to isolate the [6]Li and [7]Li isotope adducts of POPC separately for MSMS analysis and discussion of fragments refers only to those involving more abundant [7]Li isotope. The dominant peak in each spectrum corresponded to $[OP(O)_2(CH_2)_2NMe_3 + 2H]^+$, and all spectra also showed peaks corresponding to $[M - OP(O)_2(CH_2)_2NMe_3]^+$, which were intense in the spectra of the salt adducts but weak in the spectrum obtained in the absence of salt. In the product ion spectra of $[POPC + Na]^+$ and $[POPC + Li]^+$ (Figure 2.8B and C) peaks corresponding to $[M - OP(O)_2(CH_2)_2NMe_3 - H + Na]^+$ and $[M - OP(O)_2(CH_2)_2NMe_3 - H + Li]^+$ were also observed. Determination of both lipid chains is also essential for lipid identification. Two pairs of peaks were observed in the spectrum of $[POPC + H]^+$ (Figure 2.8A) from which both lipid chains could be identified. The peaks corresponding to $[M - R_1CO + 2H]^+$ and $[M - R_2CO + 2H]^+$ were

both relatively intense in comparison to the other peaks in the spectrum. The spectrum of $[POPC + Na]^+$ revealed four pairs of peaks involving the loss of an acyl chain. Of these, $[M - R_1COO - NMe_3 - H + Na]^+$ and $[M - R_2COO - NMe_3 - H + Na]^+$ were the most intense, but were still relatively weak compared to the rest of the spectrum. The peaks corresponding to $[R_xCO]^+$ were particularly weak. Four pairs of peaks corresponding to the loss of an acyl chain were also observed in the spectrum of $[POPC + Li]^+$. Of these, the pairs of peaks corresponding to $[M - R_xCOO - NMe_3 - H + Li]^+$, $[M - R_xCOO]^+$ and $[M - R_xCOO - H + Li]^+$ were all relatively strong in comparison to the other peaks in the spectrum, especially when compared to the peaks corresponding to the loss of an acyl chain in the MSMS spectra of POPC obtained with sodium and in the absence of an added salt. Pairs of peaks separated by 6 mass units, corresponding to protonated and lithiated fragments, could be observed in the spectrum of $[POPC + Li]^+$ in the same way as the molecular ions in the full-scan mass spectra of both lipids. Examples were observed at m/z 478.1 and m/z 484.3, corresponding to $[M - R_2COO]^+$ and $[M - R_2COO - H + Li]^+$ and m/z 504.4 and m/z 510.3, corresponding to $[M - R_1COO]^+$ and $[M - R_1COO - H + Li]^+$ respectively. Peaks could also be observed at m/z 432 and m/z 458 in the product ion spectrum of $[POPC + Li]^+$. These are assigned as metastable due to their peak shapes.

Table 2.7. Product ions observed in the MALDI-MSMS spectra of $[POPC + Li]^+$, $[POPC + Na]^+$, and $[POPC + H]^+$.

$[POPC + Li]^+$		$[POPC + Na]^+$	
m/z	**Product ion**	*m/z*	**Product ion**
184.1	$[OP(O)_2(CH_2)_2NMe_3 + 2H]^+$	183.7	$[OP(O)_2(CH_2)_2NMe_3 + 2H]^+$
239.3	$[R_1CO]^+$	239.3	$[R_1CO]^+$
265.1	$[R_2CO]^+$	265.3	$[R_2CO]^+$
425.2	$[M - R_2COO - NMe_3 - H + Li]^+$	441.2	$[M - R_2COO - NMe_3 - H + Na]^+$
451.2	$[M - R_1COO - NMe_3 - H + Li]^+$	467.2	$[M - R_1COO - NMe_3 - H + Na]^+$
478.1	$[M - R_2COO]^+$	478.3	$[M - R_2COO]^+$
484.3	$[M - R_2COO - H + Li]^+$	500.3	$[M - R_2COO - H + Na]^+$
504.4	$[M - R_1COO]^+$	504.3	$[M - R_1COO]^+$
510.3	$[M - R_1COO - H + Li]^+$	526.3	$[M - R_1COO - H + Na]^+$
577.0	$[M - OP(O)_2(CH_2)_2NMe_3]^+$	577.5	$[M - OP(O)_2(CH_2)_2NMe_3]^+$
583.5	$[M - OP(O)_2(CH_2)_2NMe_3 - H + Li]^+$	599.7	$[M - OP(O)_2(CH_2)_2NMe_3 - H + Na]^+$

$[POPC + H]^+$	
m/z	**Product ion**
184.1	$[OP(O)_2(CH_2)_2NMe_3 + 2H]^+$
478.2	$[M - R_2COO]^+$
496.2	$[M - R_2CO + 2H]^+$
504.4	$[M - R_1COO]^+$
522.2	$[M - R_1CO + 2H]^+$
577.0	$[M - OP(O)_2(CH_2)_2NMe_3]^+$

a) R_1 and R_2 correspond to the acyl chains and the *sn*-1 and *sn*-2 positions respectively
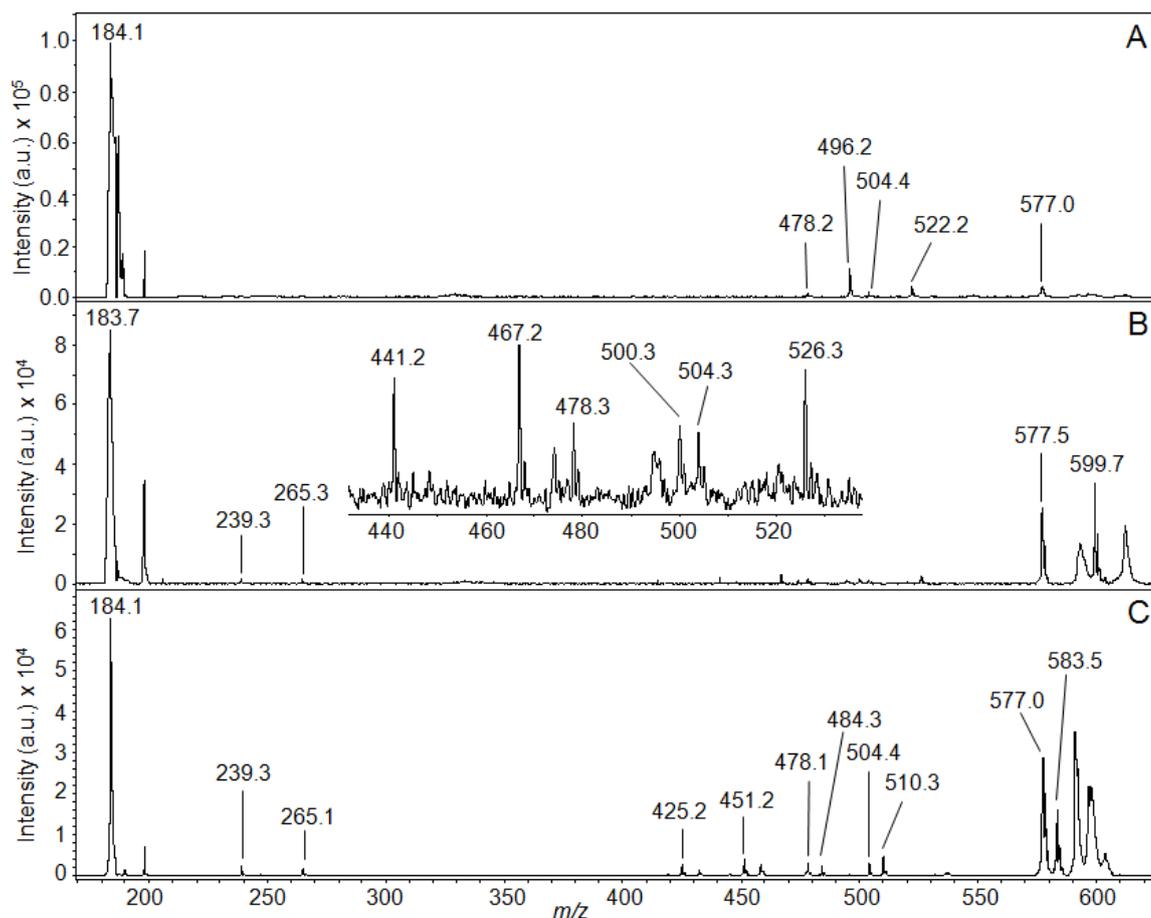
Figure 2.8. MALDI-MSMS spectra of A) [POPC + H]⁺; B) [POPC + Na]⁺; and C) [POPC + Li]⁺. The samples were prepared by mixing a solution of the lipid in $CHCl_3$ (1 mg/mL) 1:9 (v/v) with solutions of DHB (30 mg/mL) in EtOH/H_2O (50:50 (v/v)), or NaCl (100 mM) or LiCl (100 mM) in EtOH/H_2O (50:50 (v/v)) respectively.

2.2.4.5 Comparison of POPE and POPC fragmentation in the presence of LiCl, NaCl and in the absence of added salt

For both of the lipids, lithium and sodium adducts gave more useful product ion spectra for lipid identification than the spectra of [M + H]⁺. This was particularly noticeable for the fragments involving the loss of the acyl chains. Although the presence of salt ions did not always cause a greater number of these fragments, they were more intense compared to the other peaks in the spectra, in both cases. The product ion spectrum obtained in the presence of Li⁺ was the most useful of the three obtained for POPC in terms of the ease of lipid identification. Although the same number of fragments involving the acyl chains were observed in the spectrum of [POPC + Na]⁺, the signal-to-noise ratio was much better in the spectrum of the lithium adduct. In the case of POPE, the product ion spectrum of [POPE + Na]⁺ contained more fragments from which the lipid could be identified, especially the acyl chains, but they were of no greater intensity than those in the spectrum of [POPE + Li]⁺. Overall, using the results from both lipids, the addition of lithium is more useful than the addition of sodium for the MSMS analysis of lipids.

2.2.4.6 The effect of LiCl concentration

An investigation was carried out into the effects of LiCl concentration on MALDI-MSMS spectra to determine if there was an optimum concentration for the analysis for POPE and POPC. The normalised intensities of a number of lipid fragments were averaged for eight repeat analyses at each of six LiCl concentrations from 5 mM to 100 mM. As figures 2.9 and 2.10 show, no statistical differences were observed in the spectra of POPE or POPC over the range of concentrations analysed.
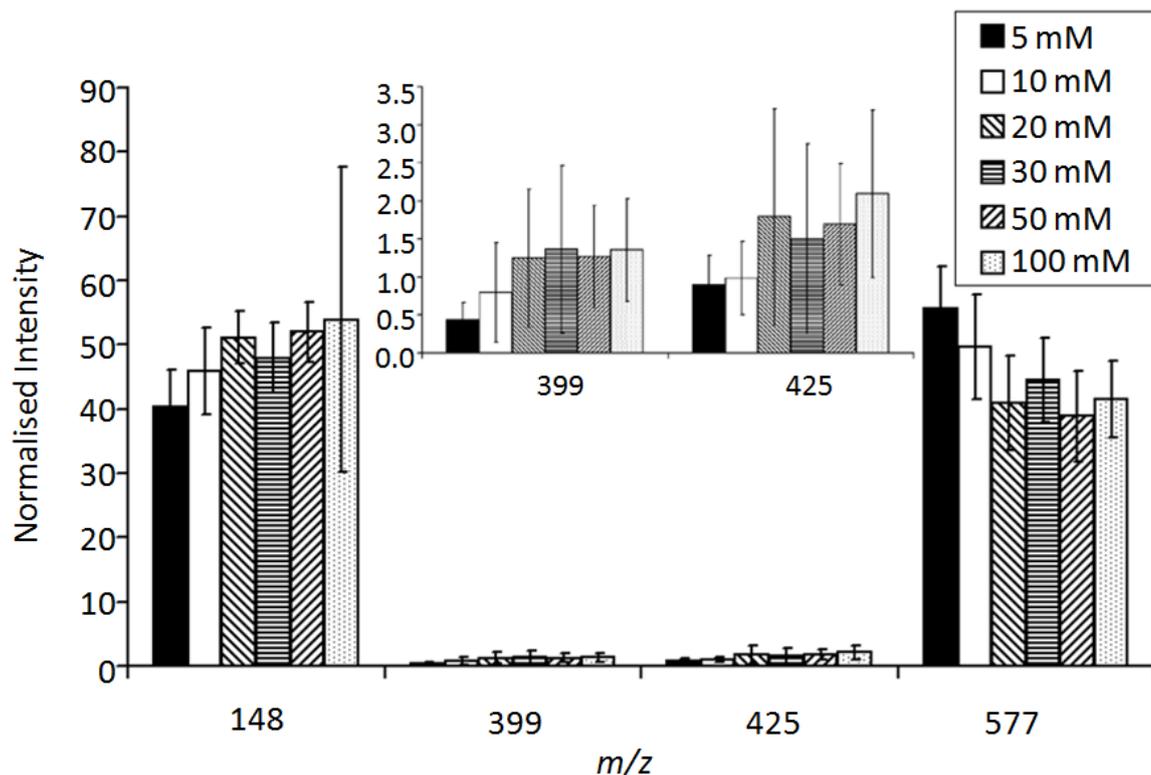
Figure 2.9. Normalized intensities of [POPE + Li]$^+$ fragment peaks with varying [LiCl] (5, 10, 20, 30, 50, 100 mM). The peaks with m/z 148, m/z 399 , m/z 425 and m/z 577 refer to the fragments [OP(O)$_2$O(CH$_2$)$_2$NH$_3$ + Li + H]$^+$, [M − R$_2$COO − (CH$_2$)$_2$NH$_3$ + H + Li]$^+$, [M − R$_1$COO − (CH$_2$)$_2$NH$_3$ + H + Li]$^+$, and [M − OP(O)$_2$O(CH$_2$)$_2$NH$_3$]$^+$ respectively. Error bars represent two times the standard deviation from 8 repeat scans in each case.
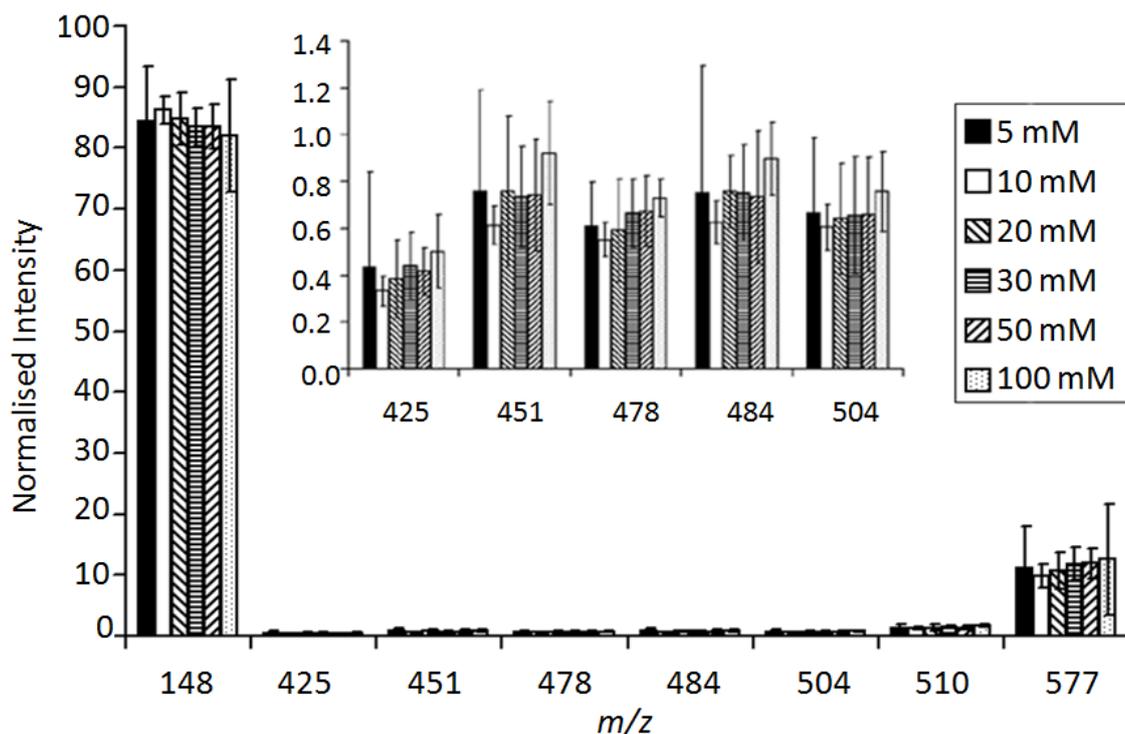
Figure 2.10. Normalized intensities of $[POPC + Li]^+$ fragment peaks with varying [LiCl] (5, 10, 20, 30, 50, 100 mM). The peaks with m/z 184, m/z 425, m/z 451, m/z 478, m/z 484, m/z 504, m/z 510 and m/z 577 refer to the fragments $[OP(O)_2(CH_2)_2NMe_3+ 2H]^+$, $[M - R_2COO - NMe_3 - H + Li]^+$, $[M - R_1COO - NMe_3 - H + Li]^+$, $[M - R_2COO]^+$, $[M - R_2COO - H + Li]^+$, $[M - R_1COO]^+$, $[M - R_1COO - H + Li]^+$ and $[M - OP(O)_2(CH_2)_2NMe_3]^+$ respectively. Error bars represent two times the standard deviation from 8 repeat scans in each case. R_1 and R_2 are described in Figure 2.3.

2.2.5 Acyl chain identification

It has been stated in the literature that in some cases a comparison of the relative intensities of peaks corresponding to fragmentations at the *sn*-1 and *sn*-2 positions can be used to identify which acyl chain is situated at which position on the lipid glycerol backbone.[10–12, 14–32] In order to determine whether this could be used to identify lipids under the conditions found to give the clearest product ion spectra for lipid identification, as described in Sections 2.2.3 and 2.2.4, POPC and POPE were each fragmented 24 times in the presence of LiCl, NaCl and in the absence of added salt to see if statistical differences could be observed in the relative intensities of any product ion peaks corresponding to losses of the acyl chains. Although LiCl had been shown to give more useful product ion spectra for lipid identification than NaCl, this did not rule out NaCl giving as good or better relative intensity data from which the position of the lipid acyl chains could be determined.

POPC/POPE
$R_1 = (CH_2)_{14}CH_3$
$R_2 = (CH_2)_7CH=CH(CH_2)_7CH_3$

OPPC
$R_1 = (CH_2)_7CH=CH(CH_2)_7CH_3$
$R_2 = (CH_2)_{14}CH_3$

POPC/OPPC
$R_3 = {}^+NMe_3$
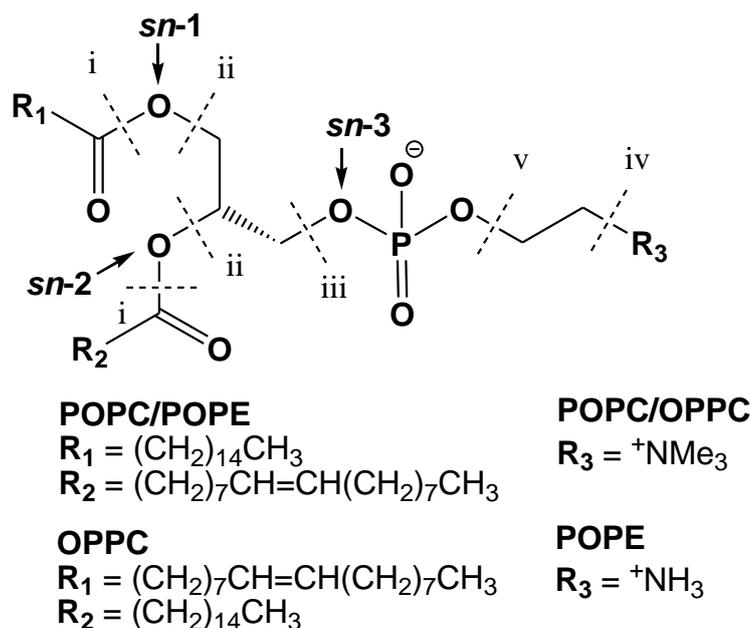
POPE
$R_3 = {}^+NH_3$

Figure 2.11. Identities of fragmentations of POPC, OPPC and POPE used for the comparison of relative intensities of cleavages at the *sn*-1 and *sn*-2 position.

2.2.5.1 POPE

Table 2.8 shows all of the fragment types involving the loss of the palmitoyl or oleoyl chain from POPE observed in the spectra obtained in the absence of added salt and in the presence of either lithium or sodium ions. For each fragment type, the intensity of the peak corresponding to a loss from the *sn*-1 position has been normalised relative to the intensity of the peak corresponding to a loss from the *sn*-2 position, with the data in Table 2.8 and Figure 2.12 showing results averaged from 24 spectra. Two pairs of fragments of $[POPE + H]^+$ were identified, both of which showed a preferential loss from the *sn*-2 position. For the $[i]^+$ fragments of $[POPE + Li]^+$, a preferential loss of the acyl chain from the *sn*-1 position was observed. Of the four pairs of peaks corresponding to the loss of an acyl chain from $[POPE + Na]^+$, in two cases no difference in relative intensities was observed within an error of two times the standard deviation. For the $[i]^+$ fragments, a slight preference for $[R_1CO]^+$ was observed, but this was only just outside error. A clear preference for the loss of the chain from the *sn*-1 position was observed for the $[M – ii – iv + 2H]^+$ fragments however. A number of points can be made from this data. Firstly, different product ions involving the acyl chains were shown to be formed depending on the presence or absence of salt ions, with many more fragments of $[POPE + Na]^+$ observed than of the other two parent ions. Secondly, the relative intensities were different for each type of fragment from each parent ion. The two pairs of fragments of $[POPE + H]^+$ had different relative intensities, as did the four pairs of fragments of $[POPE + Na]^+$, and different relative intensities were observed for the analogous fragments of $[POPE + Li]^+$ and $[POPE + Na]^+$, $[M – ii – v + H + Li]^+$ and $[M – ii – v + H + Na]^+$. Thirdly, in

the absence of added salt, preferential losses of the chain from the *sn*-2 position were observed, while in the presence of Na or Li the chain was preferentially lost from the *sn*-1 position. The greatest difference in relative intensity was observed for the $[M - i + 2H]^+$ fragment of $[POPE + H]^+$, but at least one fragment type was observed for each parent where the acyl chain position could be determined from relative intensities.

Table 2.8. Product ions corresponding to the loss of the acyl chain from the *sn*-1 or *sn*-2 positions of POPE observed in the MALDI-MSMS spectra of $[POPE + H]^+$ and $[POPE + Li]^+$. The relative intensities of peaks corresponding to the loss of the acyl chains from the *sn*-1 and *sn*-2 positions have been normalized with respect to one another for each type of fragment.

	Parent ion	Fragment[a]	Relative intensity x = 1	Relative intensity x = 2
a	$[POPE + H]^+$	$[M - ii]^+$	0.43 ± 0.05^b	0.57 ± 0.05
b	$[POPE + H]^+$	$[M - i + 2H]^+$	0.28 ± 0.03	0.72 ± 0.03
c	$[POPE + Li]^+$	$[M - ii - v + H + Li]^+$	0.60 ± 0.05	0.40 ± 0.05
d	$[POPE + Na]^+$	$[i]^+$	0.57 ± 0.06	0.43 ± 0.06
e	$[POPE + Na]^+$	$[M - ii - H + Na]^+$	0.56 ± 0.10	0.44 ± 0.10
f	$[POPE + Na]^+$	$[M - ii - v + H + Na]^+$	0.55 ± 0.05	0.45 ± 0.05
g	$[POPE + Na]^+$	$[M - ii - iv + 2H]^+$	0.63 ± 0.06	0.37 ± 0.06

a) x = 1 and x = 2 correspond to *sn*-1 and *sn*-2 positions of lipid respectively.

b) The error corresponds to two times the standard deviation.
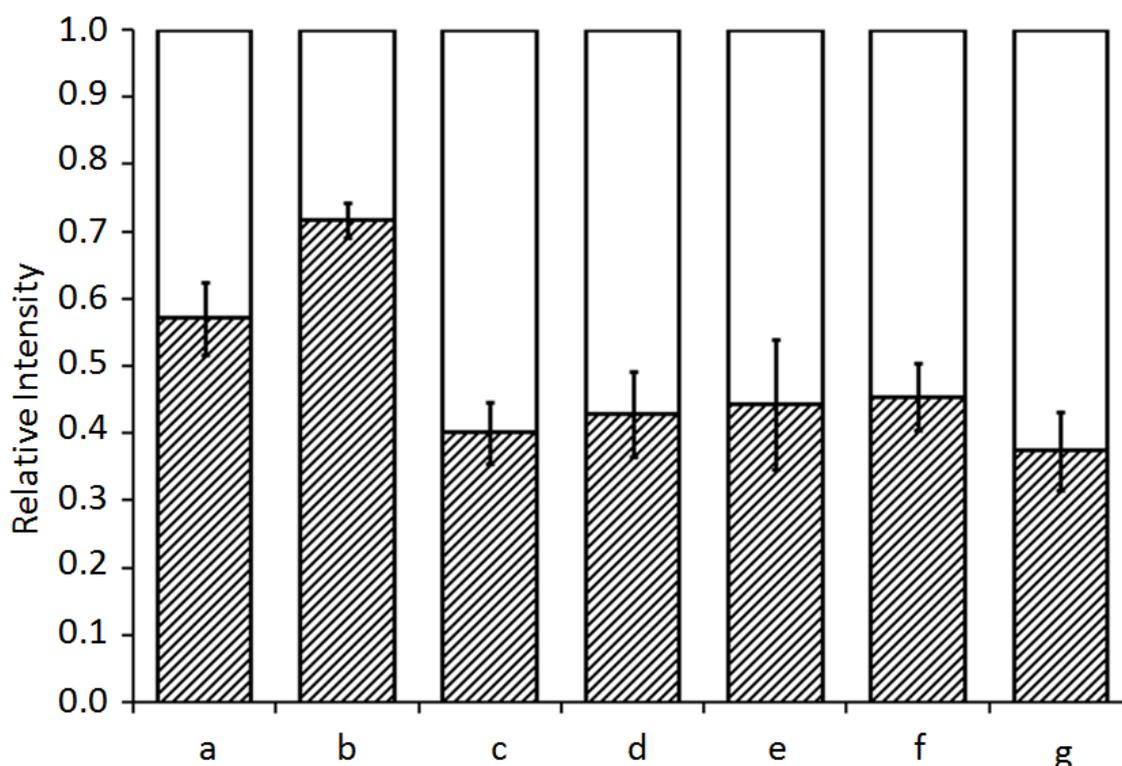
Figure 2.12. The relative intensities of peaks corresponding to loss of the acyl chain from the *sn*-1 and *sn*-2 positions of different types of fragments of POPE from MSMS spectra of $[POPE + H]^+$, $[POPE + Li]^+$ and $[POPE + Na]^+$. The white sections correspond to a loss from *sn*-1 position, shaded to the *sn*-2 position. Refer to Table 2.8 for identification of a–g. The error bars correspond to two times the standard deviation of the data.

2.2.5.2 POPC

The data from POPC were analysed in the same way as those of POPE, and the relative intensities of all of the peaks corresponding to the loss of an acyl chain from [POPC + H]$^+$, [POPC + Li]$^+$ and [POPC + Na]$^+$ are shown in Table 2.9 and Figure 2.13. Two types of fragmentation of [POPC + H]$^+$ were observed which involved the loss of an acyl chain, [M – ii]$^+$ and [M – i + 2H]$^+$. No difference in relative intensity was observed between the peaks corresponding to [M – R$_1$COO]$^+$ and [M – R$_2$COO]$^+$ within the margin of error, but a preferential loss from the *sn*-2 position was observed for the [M – i + 2H]$^+$ fragments. Of the four different types of [POPC + Li]$^+$ fragmentation involving the loss of an acyl chain, no difference in intensity within the margin of error was observed between the peaks corresponding to [M – ii]$^+$ but the other three fragmentations all showed preferential cleavage at the *sn*-1 position. Three of the four fragmentations of [POPC + Na]$^+$ showed no preferential cleavage at the *sn*-1 or *sn*-2 position, and the fourth fragmentation showed only a slight preference for the loss of the acyl chain from the *sn*-1 position, with a relative intensities of 0.59 ± 0.08 and 0.41 ± 0.08 for [M – R$_1$COO – H + Na]$^+$ and [M – R$_2$COO – H + Na]$^+$ respectively. As with POPE, differences were observed between the fragmentation of the three parents, though the product ions of the sodium and lithium adducts were analogous. The protonated parent ion showed a preferential loss from the *sn*-2 position, while the salt adducts were preferentially cleaved at the *sn*-1 position, the same results as observed for the fragmentation of POPE. Similarly to POPE, differences could be observed in the relative intensities of the fragments of the three POPC parent ions, but some similarities could also be noted.

The four fragmentations of [POPC + Li]$^+$ and [POPC + Na]$^+$ were analogous, but the same relative intensity results were only observed for two pairs of peaks. The [M – ii – H + salt]$^+$ fragmentations showed preferential cleavage at the *sn*-1 position, though the preference was only slight for the fragments of [POPC + Na]$^+$. There was no preferential loss of either acyl chain from either parent ion within the margin of error for the peaks corresponding to [M – ii]$^+$. A preferential loss of the chain from the *sn*-1 position was observed for the other two fragments of [POPC + Li]$^+$, [i]$^+$ and [M – ii – iv – H + Li]$^+$, while no preferential loss of either chain was observed for the same two fragmentations of [POPC + Na]$^+$. Peaks corresponding to [M – ii]$^+$ could be observed in all three spectra, with no preferential cleavage at the *sn*-1 or *sn*-2 positions of any of the parent ions. The greatest difference in relative intensities was observed between the [M – R$_1$CO + 2H]$^+$ and [M – R$_2$CO + 2H]$^+$ fragments of [POPC + H]$^+$, but the most information was provided by the fragmentation of the [POPC + Li]$^+$ parent ion, which produced three pairs of peaks where a clear difference in intensity could be observed. Fragmentation of the [POPC +

Na]$^+$ parent ion gave little information from which the positions of the acyl chains on the glycerol backbone could be determined.

Table 2.9. Product ions corresponding to the loss of the acyl chain from the *sn*-1 or *sn*-2 positions of POPC observed in the MALDI-MSMS spectra of [POPC + H]$^+$ and [POPC + Li]$^+$. The relative intensities of peaks corresponding to the loss of the acyl chains from the *sn*-1 and *sn*-2 positions have been normalized with respect to one another for each type of fragmentation.

	Parent ion	Fragment[a]	Relative intensity x = 1	Relative intensity x = 2
a	[POPC + H]$^+$	[M − ii]$^+$	0.55 ± 0.06[b]	0.45 ± 0.06
b	[POPC + H]$^+$	[M − i + 2H]$^+$	0.28 ± 0.03	0.72 ± 0.03
c	[POPC + Li]$^+$	[i]$^+$	0.61 ± 0.04	0.39 ± 0.04
d	[POPC + Li]$^+$	[M − ii]$^+$	0.53 ± 0.03	0.47 ± 0.03
e	[POPC + Li]$^+$	[M − ii − H + Li]$^+$	0.64 ± 0.04	0.36 ± 0.04
f	[POPC + Li]$^+$	[M − ii − iv − H + Li]$^+$	0.64 ± 0.03	0.36 ± 0.03
g	[POPC + Na]$^+$	[i]$^+$	0.57 ± 0.11	0.43 ± 0.11
h	[POPC + Na]$^+$	[M − ii]$^+$	0.45 ± 0.10	0.55 ± 0.10
i	[POPC + Na]$^+$	[M − ii − H + Na]$^+$	0.59 ± 0.08	0.41 ± 0.08
j	[POPC + Na]$^+$	[M − ii − iv − H + Na]$^+$	0.56 ± 0.10	0.44 ± 0.10

a)   x = 1 and x = 2 correspond to *sn*-1 and *sn*-2 positions of lipid respectively.
b)   The error corresponds to two times the standard deviation.
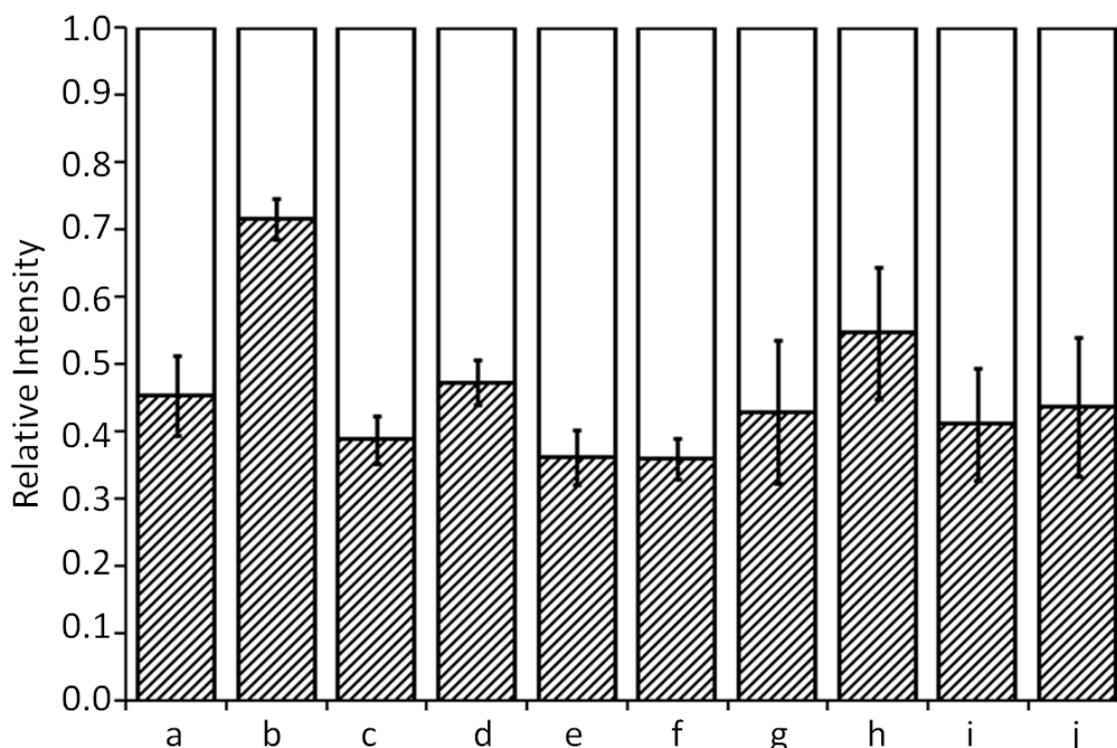
Figure 2.13. The relative intensities of peaks corresponding to loss of the acyl chain from the *sn*-1 and *sn*-2 positions of different types of fragments of POPC from MSMS spectra of [POPC + H]$^+$, [POPC + Li]$^+$ and [POPC + Na]$^+$. The white sections correspond to a loss from *sn*-1 position, shaded to the *sn*-2 position. Refer to Table 2.9 for identification of a–j. The error bars correspond to two times the standard deviation of the data.

2.2.5.3 Comparison of POPE and POPC acyl chain fragmentation

Some similarities could be observed between the results of the fragmentation of the two lipids. [POPE + H]$^+$ and [POPC + H]$^+$ fragmented in analogous ways, producing [M − ii]$^+$ and [M − i + 2H]$^+$ ions with comparable relative intensities. [POPE + Li]$^+$ and [POPC + Li]$^+$ produced similar fragments involving the loss of a portion of the headgroups, [POPE − ii − v + H + Li]$^+$ and [POPC − ii − iv − H + Li]$^+$, and the relative intensities of the peaks were similar for the two parents. The product ion spectra of [POPE + Na]$^+$ and [POPC + Na]$^+$ also showed some similarities, with pairs of peaks corresponding to [i]$^+$ and [M − ii − H + Na]$^+$ observed in both spectra.

Overall, the positions of the acyl chains could be determined from the product ion spectra of POPE in the presence of Li$^+$, Na$^+$ or in the absence of a salt, and for POPC they could be clearly determined in the presence or absence of Li$^+$.

2.2.5.4 Comparison of analysis of POPC by LIFT and CID

In order to test whether fragmentation by CID produced different relative intensities of peaks corresponding to fragmentation at the *sn*-1 or *sn*-2 positions from those obtained by LIFT, 25 CID spectra were collected of [POPC + H]$^+$ and [POPC + Li]$^+$. Figure 2.14 shows CID and LIFT spectra of [POPC + Li]$^+$. The relative intensities of the fragments which involved the loss of an acyl chain are shown in Table 2.10 and Figure 2.15, with the relative intensities of the LIFT data for comparison.
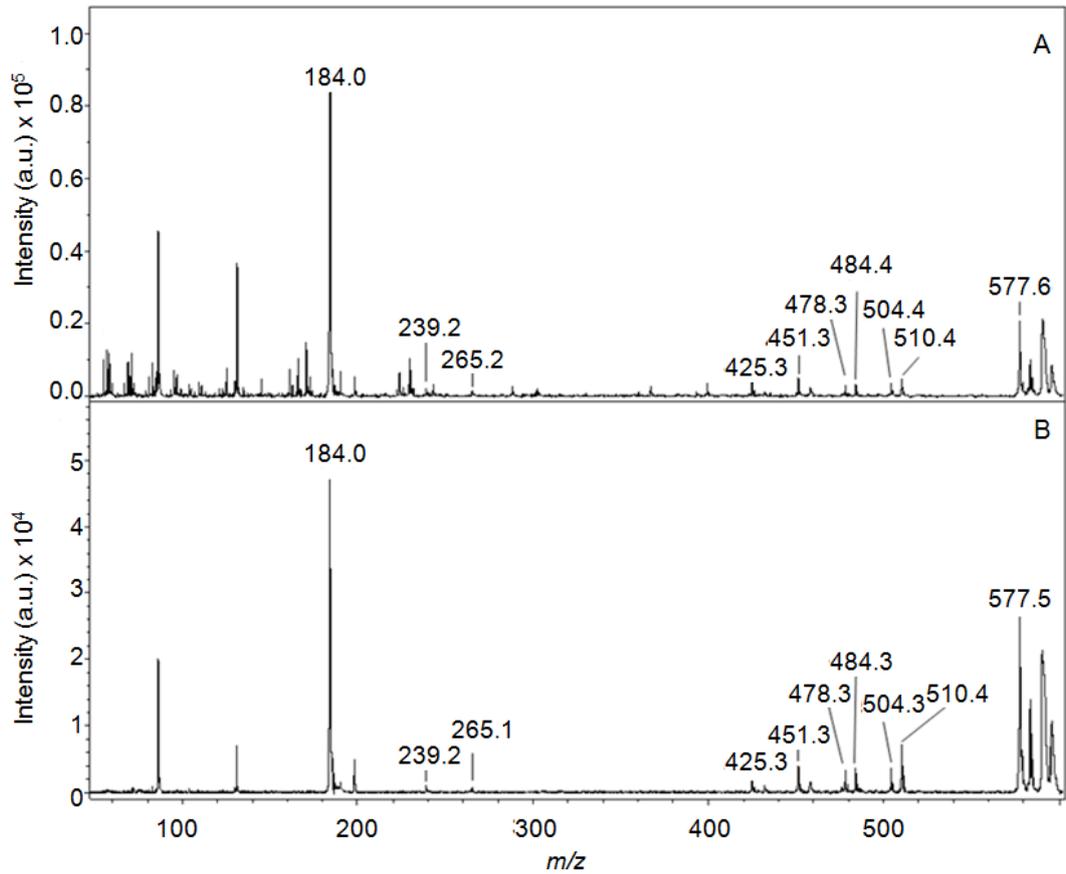
Figure 2.14. A) CID and B) LIFT MALDI-MSMS spectra of POPC with lithium. The samples were prepared by mixing a solution of the lipid in $CHCl_3$ (1 mg/mL) 1:9 (v/v) with a solution of LiCl (100 mM) and DHB (30 mg/mL) in $EtOH/H_2O$ (50:50 (v/v)).

Table 2.10. Product ions corresponding to the loss of the acyl chain from the *sn*-1 or *sn*-2 positions of POPC observed in CID and LIFT spectra of [POPC + H]$^+$ and [POPC + Li]$^+$. The relative intensities of peaks corresponding to the loss of the acyl chains from the *sn*-1 and *sn*-2 positions have been normalized with respect to one another for each type of fragmentation.

	Parent ion	Fragmentation method	Fragment[a]	Relative intensity x = 1	Relative intensity x = 2
	[POPC + H]$^+$	LIFT	[M − ii]$^+$	0.55 ± 0.06[b]	0.45 ± 0.06
a	[POPC + H]$^+$	CID	[M − ii]$^+$	0.45 ± 0.16	0.55 ± 0.16
	[POPC + H]$^+$	LIFT	[M − i + 2H]$^+$	0.28 ± 0.03	0.72 ± 0.03
b	[POPC + H]$^+$	CID	[M − i + 2H]$^+$	0.29 ± 0.08	0.71 ± 0.08
	[POPC + Li]$^+$	LIFT	[i]$^+$	0.61 ± 0.04	0.39 ± 0.04
c	[POPC + Li]$^+$	CID	[i]$^+$	0.61 ± 0.11	0.39 ± 0.11
	[POPC + Li]$^+$	LIFT	[M − ii]$^+$	0.53 ± 0.03	0.47 ± 0.03
d	[POPC + Li]$^+$	CID	[M − ii]$^+$	0.53 ± 0.06	0.47 ± 0.06
	[POPC + Li]$^+$	LIFT	[M − ii − H + Li]$^+$	0.64 ± 0.03	0.36 ± 0.03
e	[POPC + Li]$^+$	CID	[M − ii − H + Li]$^+$	0.59 ± 0.08	0.41 ± 0.08
	[POPC + Li]$^+$	LIFT	[M − ii − iv − H + Li]$^+$	0.64 ± 0.04	0.36 ± 0.04
f	[POPC + Li]$^+$	CID	[M − ii − iv − H + Li]$^+$	0.50 ± 0.08	0.50 ± 0.08

a)   x = 1 and x = 2 correspond to *sn*-1 and *sn*-2 positions of lipid respectively.
b)   The error corresponds to two times the standard deviation.

Three observations were made from comparison of the LIFT and CID data. Firstly, the same fragments involving the loss an acyl chain were produced by each fragmentation method, in both of the presence and absence of Li^+. This is despite the fact that, as can be observed in the CID and LIFT spectra of $[POPC + Li]^+$ in Figure 2.14, CID caused more fragmentation of the lipid than LIFT. Secondly, for all but one fragment type the average relative intensities were very similar (ignoring the case of the $[M - ii]^+$ fragments of $[POPC + H]^+$ where, although a difference in average relative intensities could be observed within an error of two times standard deviation, neither the LIFT or the CID data showed statistical differences in relative intensities). A difference was observed between the LIFT and CID results for the $[M - ii - iv - H + Li]^+$ fragments of $[POPC + Li]^+$, where a clear preferential loss from the *sn*-1 position was observed when LIFT was carried out but the relative intensities were 0.5:0.5 within the margin of error for fragments produced by CID. The final observation referred to the reproducibility of the relative intensities. The errors of two times the standard deviation were at least twice as great for the CID data than for the LIFT data. This was notable for the $[i]^+$ fragmentation of $[POPC + Li]^+$, where the average relative intensities were the same for fragmentation by LIFT and CID, but the variation in the CID data meant that the relative intensities were 0.5:0.5 within error, while for fragmentation by LIFT the error was smaller and a statistical difference could be observed in the relative intensities.
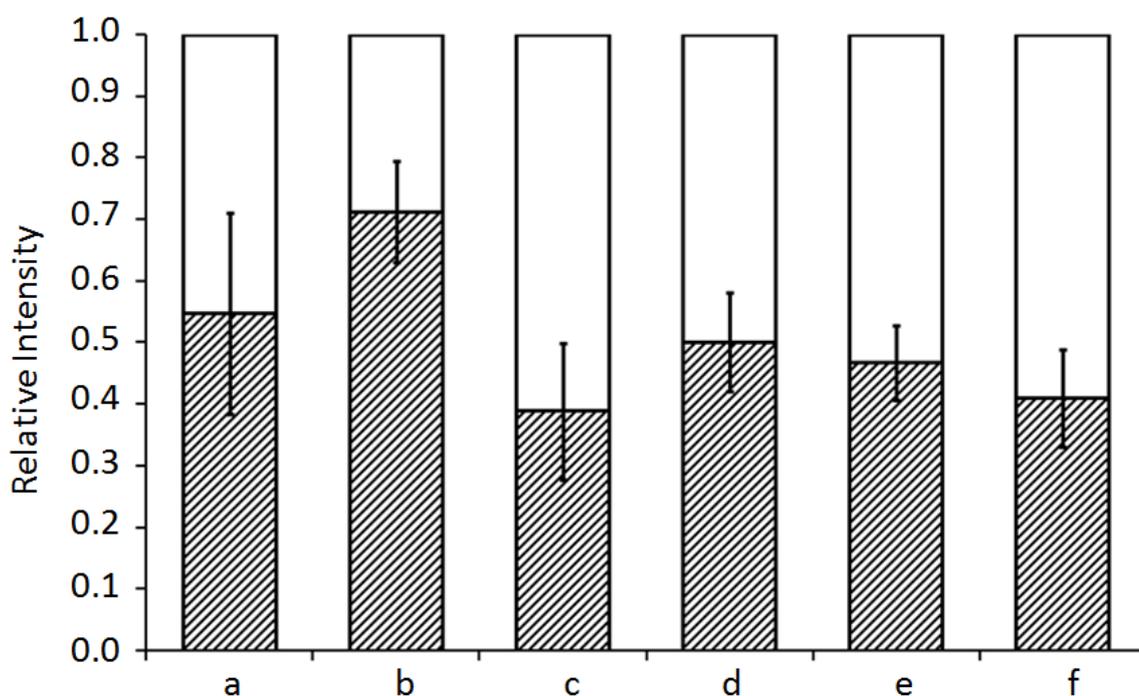
Figure 2.15. The relative intensities of peaks corresponding to loss of the acyl chain from the *sn*-1 and *sn*-2 positions of different types of fragments of POPC from CID spectra of $[POPC + H]^+$ and $[POPC + Li]^+$. The white sections correspond to a loss from *sn*-1 position, shaded to the *sn*-2 position. Refer to Table 2.10 for identification of a–f. The error bars correspond to two times the standard deviation of the data.

2.2.5.5 Comparison of POPC and OPPC acyl chain fragmentation

Though the results of the acyl chain fragmentation of POPC and POPE are repeatable, in isolation it cannot be proved that the difference in relative intensities is due to the position of the chains on the lipid glycerol rather than to the differences in the chains themselves. In order to validate this, 24 MALDI-MSMS spectra of [OPPC + H]$^+$ and [OPPC + Li]$^+$ were collected and the results compared to those for [POPC + H]$^+$ and [POPC + Li]$^+$ (Figure 2.16 and Table 2.11).
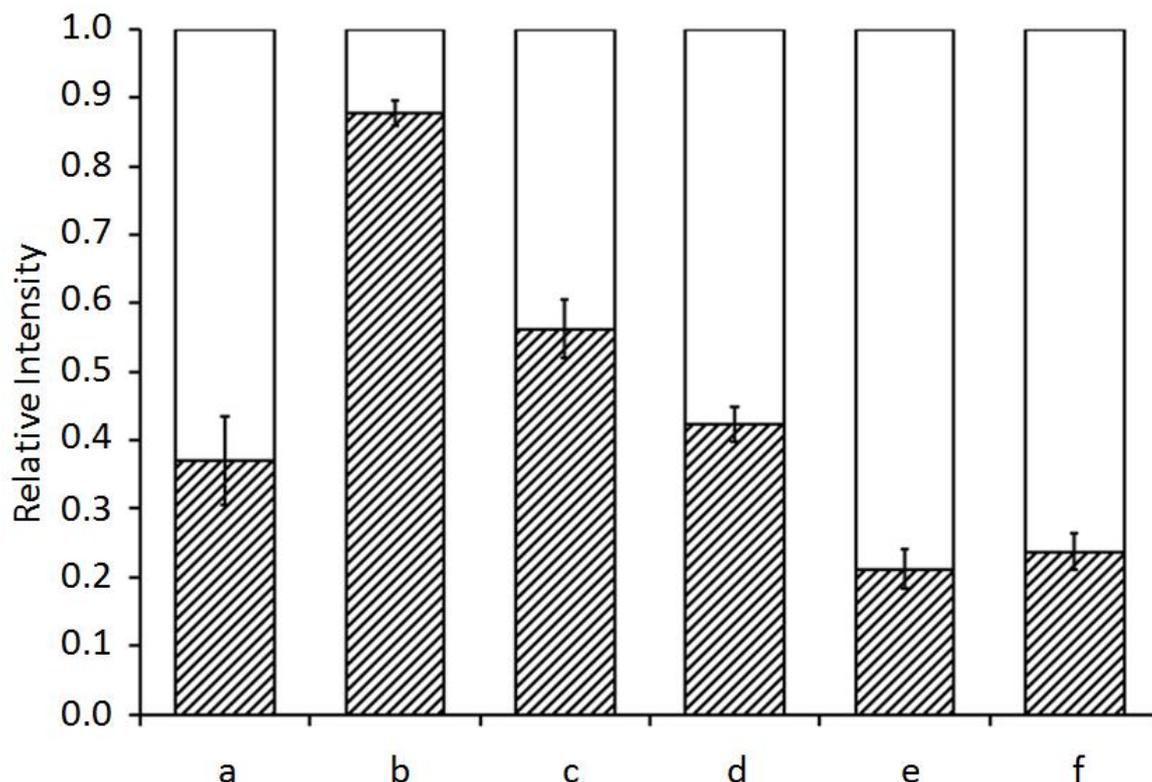
Figure 2.16. The relative intensities of peaks corresponding to loss of the acyl chain from the *sn*-1 and *sn*-2 positions of different types of fragments of OPPC from MALDI-MSMS spectra of [OPPC + H]$^+$ and [OPPC + Li]$^+$. The white sections correspond to a loss from *sn*-1 position, shaded to the *sn*-2 position. Refer to Table 2.11 for identification of a–f. The error bars correspond to two times the standard deviation of the data.

Table 2.11. Product ions corresponding to the loss of the acyl chain from the *sn*-1 or *sn*-2 positions of POPC and OPPC observed in the MALDI-MSMS spectra of [POPC + H]⁺, [OPPC + H]⁺, [POPC + Li]⁺ and [OPPC + Li]⁺. The relative intensities of peaks corresponding to the loss of the acyl chains from the *sn*-1 and *sn*-2 positions have been normalized with respect to one another for each type of fragmentation.

	Parent ion	Fragment[a]	Relative intensity *sn*-1 cleavage[b]	Relative intensity *sn*-2 cleavage
a	[POPC + H]⁺	[M – ii]⁺	55 ± 6	45 ± 6
a	[OPPC + H]⁺	[M – ii]⁺	63 ± 6	37 ± 6
b	[POPC + H]⁺	[M – i + 2H]⁺	28 ± 3	72 ± 3
b	[OPPC + H]⁺	[M – i + 2H]⁺	12 ± 2	88 ± 2
c	[POPC + Li]⁺	[i]⁺	61 ± 4	39 ± 4
c	[OPPC + Li]⁺	[i]⁺	44 ± 4	56 ± 4
d	[POPC + Li]⁺	[M – ii]⁺	53 ± 3	47 ± 3
d	[OPPC + Li]⁺	[M – ii]⁺	58 ± 3	42 ± 3
e	[POPC + Li]⁺	[M – ii – H + Li]⁺	64 ± 4	36 ± 4
e	[OPPC + Li]⁺	[M – ii – H + Li]⁺	79 ± 3	21 ± 3
f	[POPC + Li]⁺	[M – ii – iv – H + Li]⁺	64 ± 3	36 ± 3
f	[OPPC + Li]⁺	[M – ii – iv – H + Li]⁺	76 ± 3	24 ± 3

a) x = 1 and x = 2 correspond to *sn*-1 and *sn*-2 positions of lipid respectively.
b) The error corresponds to two times the standard deviation.

2.2.5.5.1 MALDI-MSMS in the absence of added salt

Two pairs of fragmentations of the protonated POPC and OPPC parents were identified which involved the loss of one or other acyl chain. For the [M – ii]⁺ fragmentation, both lipids showed a greater average loss of the chain from the *sn*-1 position, but for POPC the difference in relative intensity was 0.5:0.5 within an error of 2 times the standard deviation across the 24 repeat analyses. For the [M – i + 2H]⁺ fragmentation, a clear preferential loss of the chain from the *sn*-2 position was observed for both lipids, but the difference in relative intensities between the loss from the *sn*-1 position and that from the *sn*-2 position was greater for OPPC (12 ± 2:88 ± 2 for OPPC compared to 28 ± 3:72 ± 3 for POPC)

2.2.5.5.2 MALDI-MSMS in the presence of LiCl

For the [i]⁺ fragmentation of the lithium adducts of POPC and OPPC, the intensity of the peak corresponding to the palmitoyl chain ($CH_3(CH_2)_{14}CO$) was greater than that corresponding to the oleoyl chain ($CH_3(CH_2)_7CH=CH(CH_2)_7$) whether it was fragmented from the *sn*-1 position (POPC) or the *sn*-2 position (OPPC). For the [M – ii – H + Li]⁺ and [M – ii – iv – H + Li]⁺ fragmentations, a clear preferential loss of the chain from the *sn*-1 position was observed for both lipids. A larger difference between the relative intensity of the peak corresponding to a loss from the *sn*-1 position and that corresponding to a loss from the *sn*-2 position was observed for OPPC in both cases. In the case of the [M – ii]⁺ fragmentation, the average relative intensity over 24 measurements suggested a

preferential loss of the chain from the *sn*-1 position of both lipids, but in the case of POPC the magnitude of the standard deviation across the 24 measurements meant that the relative intensities were 0.5:0.5 within error.

2.2.5.5.3 Discussion

Overall, the results of the OPPC analysis supported the conclusions from the analyses of POPC and POPE. The same preferential losses from the *sn*-1 and *sn*-2 positions were observed in all but one case, though in two cases the magnitude of the standard deviation across the 24 measurements meant that the relative intensities of the fragments of POPC were 0.5:0.5 within error where the difference for the fragments of OPPC was outside error. The $[M - i + 2H]^+$ fragments of the protonated parents and $[M - ii - H + Li]^+$ and $[M - ii - iv - H + Li]^+$ from the lithium adducts allow unambiguous identification of the position of the acyl chain through a preferential loss from the *sn*-2 position of the protonated parent and a preferential loss from the *sn*-1 position of the lithium adduct (Table 2.12). Where a difference in relative intensities was observed, the difference was consistently larger for the fragments of OPPC than POPC.

Table 2.12. Summarised results of the MALDI-MSMS analyses of POPC and OPPC. The relative intensities of peaks corresponding to cleavages of the acyl chains from the *sn*-1 and *sn*-2 positions for different fragment types are shown qualitatively.

Parent ion	Fragment	Preferential cleavage
$[PC + H]^+$	$[M - ii]^+$	=
$[PC + H]^+$	$[M - i + 2H]^+$	*sn*-2>*sn*-1
$[PC + Li]^+$	$[M - ii]^+$	=
$[PC + Li]^+$	$[M - ii - H + Li]^+$	*sn*-1>*sn*-2
$[PC + Li]^+$	$[M - ii - iv - H + Li]^+$	*sn*-1>*sn*-2

2.2.6   The identification of unknown lipids by MALDI-MSMS

Egg and soybean phosphocholines are natural lipid mixtures extracted from hen egg yolks and soya beans respectively. These mixtures were used to test the lipid identification analysis methods developed above, to see how many phosphocholine lipids could be identified and to what degree. The soybean phosphocholine mixture analysed for this work was described by the supplier as containing an average of 55% phosphocholine lipids, 20% phosphoethanolamine lipids and a number of unquantified trace components such as carbohydrates and other lipids. The fatty acid distribution described for soybean PC includes contributions from all lipids present. The egg phosphocholine mixture is described by the supplier as containing 100% phosphocholine lipids. Table 2.13 shows the average contributions of the most common fatty acid

components of the two lipids as analysed by the supplier.[42, 43] Contributions from trace
fatty acids make up the remaining 8% and 3% for egg and soybean phosphocholines
respectively. The trace fatty acids of egg PC include 20:4, 20:5, 22:5 and 22:6.[44]

Table 2.13. Average relative abundances of the main fatty acids of egg phosphocholine and soybean
phosphocholine lipids as analysed by the supplier.[42, 43]

Soybean PC		Egg PC	
Acyl chain	Relative Abundance (%)	Acyl chain	Relative Abundance (%)
16:0	17	16:0	33
18:0	4	18:0	13
18:1	9	18:1	31
18:2	60	18:2	15
18:3	7		

Each lipid mixture was analysed by MALDI-MS and MSMS in the presence of LiCl
and in the absence of added salt. All *m/z* values observed in the MALDI-MS spectra were
compared to theoretical PC (and PE in the case of soybean PC) [M + H]$^+$ and [M + Li]$^+$
ions drawn up from all possible combinations of common and trace acyl chains, to
determine which should be fragmented by MSMS and to give an idea of lipid identities as
a starting point to identify the fragments.

2.2.6.1 Egg PC

Figure 2.17 shows the MALDI-MS spectra of egg PC in A) the absence of added
salt and B) the presence of lithium, centred on the mass region which is likely to include
phosphocholine lipids.
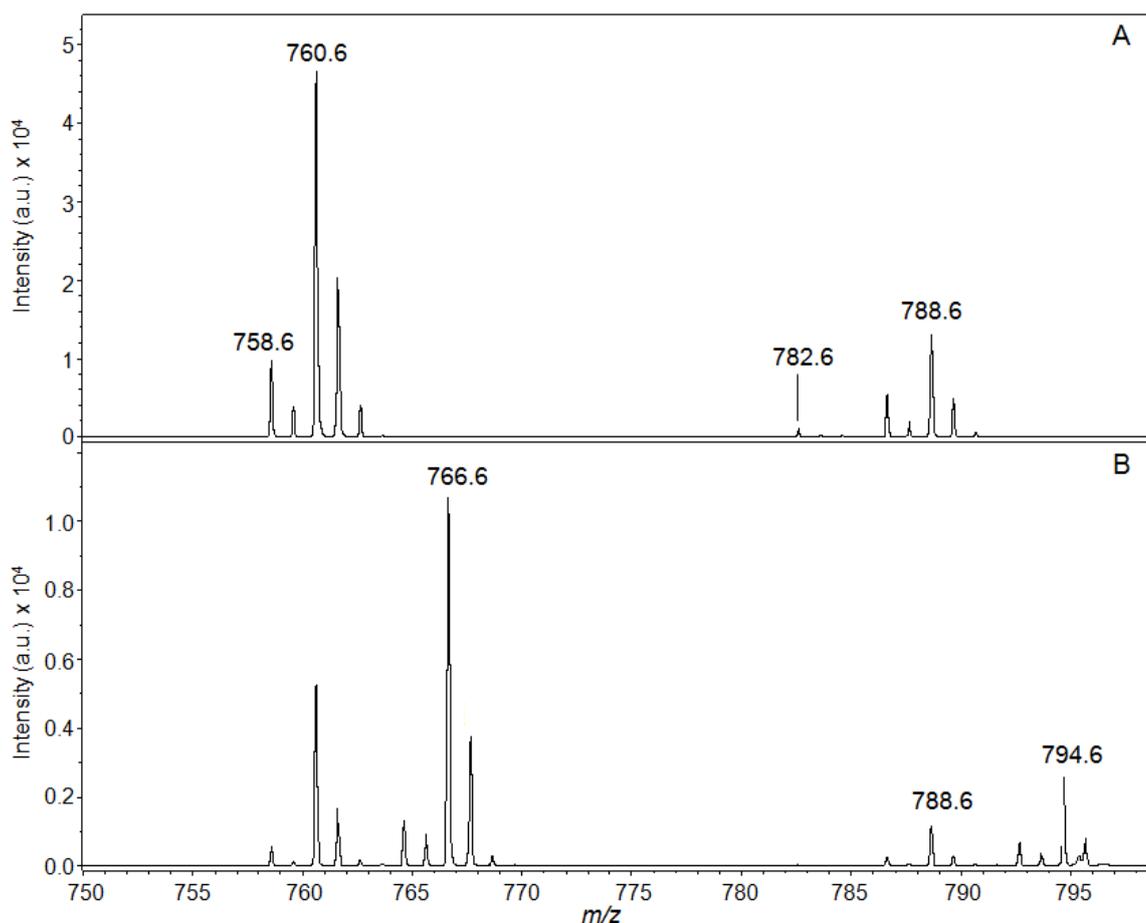
Figure 2.17. MALDI-MS spectra of egg PC A) in the absence of added salt and B) in the presence of lithium, centred on the mass region which is likely to include phosphocholine lipids. The samples were prepared by mixing a solution of the lipid in $CHCl_3$ (1 mg/mL) 2:9 (v/v) with solutions of DHB (30 mg/mL) in $EtOH/H_2O$ ((50:50 (v/v)) or LiCl (100 mM) in $EtOH/H_2O$ (50:50 (v/v)).

2.2.6.1.1 Analyses in the absence of added salt

Table 2.14 shows the *m/z* values of the peaks observed in the MALDI-MS spectrum of egg PC in the absence of added salt which matched possible phosphocholine lipid identities.

Table 2.14. The *m/z* values and possible assignments of peaks observed in the MALDI-MS spectrum of the egg phosphocholine lipid mixture obtained in the absence of added salt.

m/z	Possible acyl chain combinations			
758.6	16:0/18:2 + H			
760.6	16:0/18:1 + H			
782.6	18:1/18:3 + H	18:2/18:2 + H	16:0/20:4 + H	16:0/18:1 + Na
788.6	18:0/18:1 + H			

Of the precursor ions examined by MSMS in the absence of added salt, the product ion spectra of the ions with *m/z* 758.6 ([M + H]$^+$ ion) and *m/z* 788.6 ([M + H]$^+$ ion)

did not provide enough information from which the lipids could be identified. The product ion spectrum of the peak at *m/z* 782.6 ([M + H]$^+$ ion) contained peaks corresponding to fragments of all three of the possible PC lipid species shown in Table 2.14, making complete identification of the individual lipids impossible. The product ion spectrum of the precursor ion with *m/z* 760.6 ([M + H]$^+$ ion) contained enough peaks for identification of the lipid, as shown in Table 2.15 and Figure 2.17. Peaks corresponding to [OP(O)$_2$O(CH$_2$)$_2$NMe$_3$ + 2 H]$^+$ and [M – OP(O)$_2$O(CH$_2$)$_2$NMe$_3$]$^+$ were observed with *m/z* 184.3 and *m/z* 577.6 respectively, which confirmed that the lipid had a PC headgroup . The spectrum showed two pairs of peaks corresponding to fragments involving the loss of an acyl chain, [M – R$_x$COO]$^+$ and [M – R$_x$CO + 2H]$^+$, with the *m/z* values consistent with the identification of the two acyl chains as 16:0 and 18:1. For the [M – R$_x$COO]$^+$ fragments, the ratio of the intensity of the peak corresponding to the loss of the 16:0 chain relative to the peak corresponding to the loss of the 18:1 chain was 0.56:0.44. This ratio was compared to the results for POPC and OPPC summarised in Table 2.12. The ratio of relative intensities of the loss of the chain from the *sn*-1 position to the loss from the *sn*-2 position for this fragmentation was found to be equal within an error of twice the standard deviation. For the other fragment of the unknown lipid, a ratio of 0.11:0.89 was found for the relative intensities of the peaks corresponding to [M – R$_{16:0}$CO + 2H]$^+$ and [M – R$_{18:1}$CO + 2H]$^+$ respectively. This fragmentation was found to preferentially cause cleavage at the *sn*-2 position during the analyses of POPC and OPPC. This suggests that the 16:0 chain is at the *sn*-1 position of the unknown lipid and the 18:1 chain at the *sn*-2 position, making the lipid POPC.
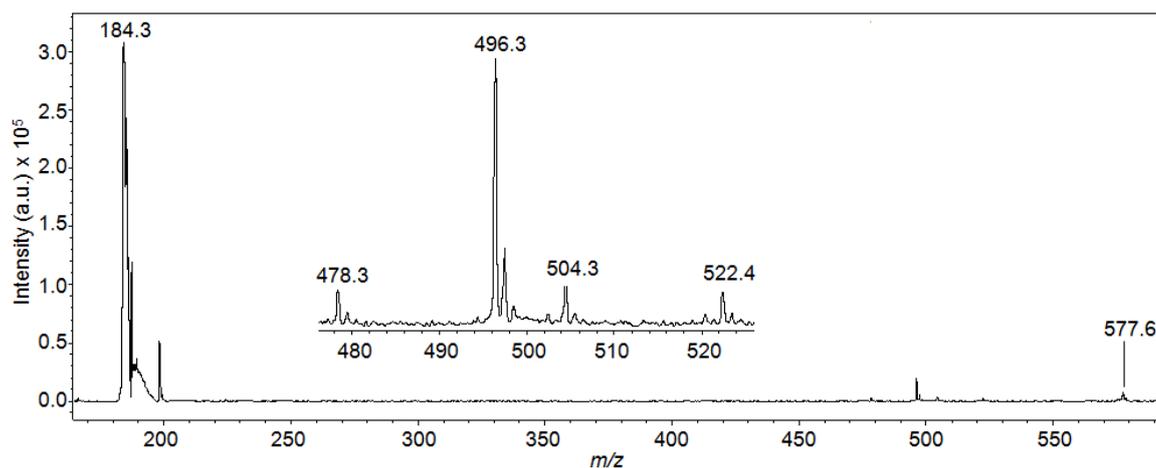
Figure 2.18. MALDI-MSMS spectrum of unknown lipid of egg PC with *m/z* 760.6 ([M + H]$^+$ ion). The samples were prepared by mixing a solution of the lipid in CHCl$_3$ (1 mg/mL) 2:9 (v/v) with a solution of DHB (30 mg/mL) in EtOH/H$_2$O (50:50 (v/v)).

Table 2.15. Product ions corresponding to the loss of an acyl chain observed in the MALDI-MSMS spectrum of the unknown phosphocholine lipid of egg PC with *m/z* 760.6 ([M + H]$^+$ ion). The relative intensities of peaks corresponding to cleavages of the 16:0 and 18:1 chains are shown for each fragment type.

m/z	Assignment	Relative intensities (16:0:18:2)
504.3	[M – R$_{16:0}$COO]$^+$	
478.3	[M – R$_{18:1}$COO]$^+$	0.56:0.44
522.4	[M – R$_{16:0}$CO + 2H]$^+$	
496.3	[M – R$_{18:1}$CO + 2H]$^+$	0.11:0.89

2.2.6.1.2 Analyses in the presence of lithium

Three peaks which could correspond to phosphocholine lipids were identified in the MALDI-MS spectrum of egg PC obtained in the presence of lithium (Table 2.16). The product ion spectrum of the lipid with *m/z* 788.6 ([M + Li]$^+$ ion) showed peaks corresponding to the fragments of a number of lipids, suggesting the presence of both the 18:1/18:3 and 18:2/18:2 acyl chain combinations, and possibly those of a third lipid due to incomplete isolation, so no single lipid could be fully identified. The product ion spectra of the other two lipids did allow identification however, as shown in Tables 2.17 and 2.18 and Figure 2.19.
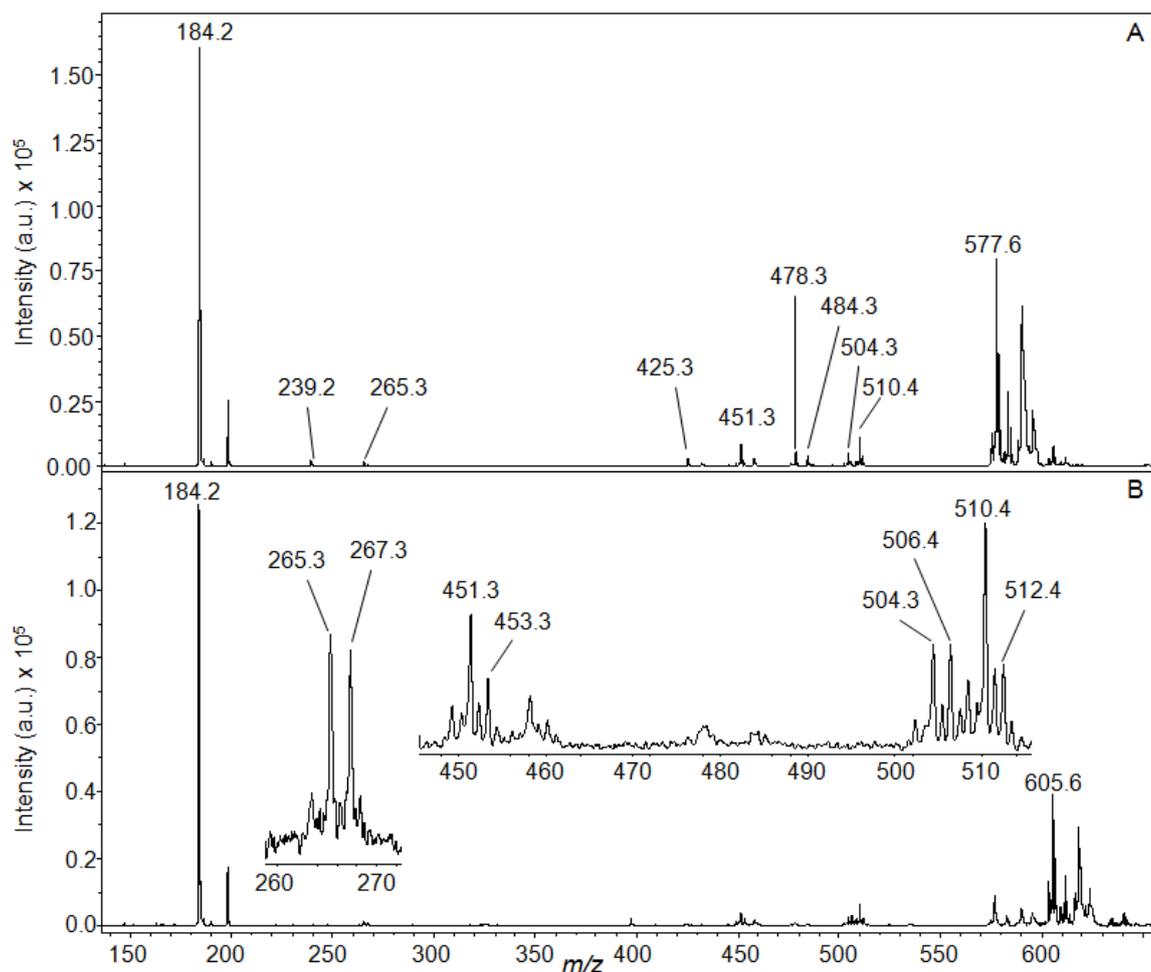
Figure 2.19. MALDI-MSMS spectrum of unknown lipids of egg PC with *m/z* A) 766.6 and B) 794.6 (both [M + Li]$^+$ ions). The samples were prepared by mixing a solution of the lipid in CHCl$_3$ (1 mg/mL) 2:9 (v/v) with a solution of LiCl (100 mM) and DHB (30 mg/mL) in EtOH/H$_2$O (50:50 (v/v)).

Table 2.16. The *m/z* values and possible assignments of peaks observed in the MALDI-MS spectrum of the egg PC lipid mixture obtained in the presence of LiCl.

m/z	Possible acyl chain combinations	
766.6	16:0/18:1 + Li	
788.6	18:1/18:3 + Li	18:2/18:2 + Li
794.6	18:0/18:1 + Li	

The product ion spectrum of the unknown lipid with *m/z* 766.6 ([M + Li]$^+$ ion) (Figure 2.19A) showed peaks with *m/z* 184.2 and *m/z* 577.6, corresponding to [OP(O)$_2$O(CH$_2$)$_2$NMe$_3$ + 2H]$^+$ and [M − OP(O)$_2$O(CH$_2$)$_2$NMe$_3$]$^+$ respectively, confirming that the lipid had a phosphocholine headgroup. Four pairs of peaks were observed in the product ion spectrum which corresponded to fragments involving the loss of an acyl chain (Figure 2.19A and Table 2.17). The relative intensities of the peaks corresponding to [M − R$_{16:0}$COO]$^+$ and [M − R$_{18:1}$COO]$^+$ were found to be 0.5:0.5, so these peaks did not allow

the positions of the chains to be determined, though they did support the chain identities. The other three pairs of peaks ($[M - R_xCOO - H + Li]^+$, $[R_xCO]^+$ and $[M - R_xCOO - NMe_3 - H + Li]^+$) all had significant differences in relative intensity for the loss of each chain, so they were compared to the data obtained for POPC and OPPC in the presence of lithium to identify the chain positions. The relative intensities of the peaks corresponding to $[M - R_{16:0}COO - H + Li]^+$ and $[M - R_{18:1}COO - H + Li]^+$ were found to be 0.74:0.26. For the equivalent fragmentation of $[POPC + Li]^+$ and $[OPPC + Li]^+$ a preferential loss of the chain from the *sn*-1 position was observed. The other two fragmentations of the unknown lipid, $[R_xCO]^+$ and $[M - R_xCOO - NMe_3 - H + Li]^+$, also both showed a preferential loss of the 16:0 chain. The $[M - R_xCOO - NMe_3 - H + Li]^+$ fragmentations of $[POPC + Li]^+$ and $[OPPC + Li]^+$ showed a preferential loss of the chain from the *sn*-1 position. The $[R_xCO]^+$ fragment was found to give inconsistent relative intensity results for POPC and OPPC and therefore could not be used to identify the position of the acyl chains. The relative intensities of the $[M - R_xCOO - H + Li]^+$ and $[M - R_xCOO - NMe_3 - H + Li]^+$ fragments identify the 16:0 chain as being at the *sn*-1 position. This suggests that the unknown lipid is POPC, which supports the conclusion from the analysis in the absence of added salt.

Table 2.17. Product ions corresponding to the loss of an acyl chain observed in the MALDI-MSMS spectrum of the unknown phosphocholine lipid of egg PC with *m/z* 766.6 ($[M + Li]^+$ ion). The relative intensities of peaks corresponding to cleavages of the 16:0 and 18:1 chains are shown for each fragment type.

m/z	Assignment	Relative intensities (16:0:18:1)
504.3	$[M - R_{16:0}COO]^+$	
478.3	$[M - R_{18:1}COO]^+$	0.50:0.50
510.4	$[M - R_{16:0}COO - H + Li]^+$	
484.3	$[M - R_{18:1}COO - H + Li]^+$	0.74:0.26
239.2	$[R_{16:0}CO]^+$	
265.3	$[R_{18:1}CO]^+$	0.60:0.40
451.3	$[M - R_{16:0}COO - NMe_3 - H + Li]^+$	
425.3	$[M - R_{18:1}COO - NMe_3 - H + Li]^+$	0.74:0.26

The product ion spectrum of the unknown lipid with *m/z* 794.6 ($[M + Li]^+$ ion) contained two peaks which confirmed the presence of a phosphocholine headgroup, at *m/z* 184.2 and *m/z* 605.6, corresponding to $[OP(O)_2O(CH_2)_2NMe_3 + 2 H]^+$ and $[M - OP(O)_2O(CH_2)_2NMe_3]^+$ respectively (Figure 2.19B and Table 2.18). Four pair of peaks corresponding to the loss of an acyl chain were observed. No significant difference in relative intensities between the peaks corresponding to losses of the 18:0 and 18:1 chains were observed for the $[M - R_xCOO]^+$ or $[R_xCO]^+$ fragment types. Both the $[M - R_xCOO - H + Li]^+$ and $[M - R_xCOO - NMe_3 - H + Li]^+$ fragmentations showed a preferential loss of

the 18:0 chain. The analogous fragments of [POPC + Li]$^+$ and [OPPC + Li]$^+$ both showed preferential losses of the chain from the *sn*-1 position. This suggests that the 18:0 chain is at the *sn*-1 position and that the unknown lipid is 1-stearoyl-2-oleoyl-*sn*-glycero-3-phosphocholine (SOPC).

Table 2.18. Product ions corresponding to the loss of an acyl chain observed in the MALDI-MSMS spectrum of the unknown phosphocholine lipid of egg PC with *m/z* 794.6 ([M + Li]$^+$ ion). The relative intensities of peaks corresponding to cleavages of the 18:0 and 18:1 chains are shown for each fragment type.

m/z	Assignment	Relative intensities (18:1:18:0)
506.4	[M − R$_{18:1}$COO]$^+$	0.49:0.51
504.3	[M − R$_{18:0}$COO]$^+$	
512.4	[M − R$_{18:1}$COO − H + Li]$^+$	0.27:0.73
510.4	[M − R$_{18:0}$COO − H + Li]$^+$	
265.3	[R$_{18:1}$CO]$^+$	0.52:0.48
267.3	[R$_{18:0}$CO]$^+$	
453.3	[M − R$_{18:1}$COO − NMe$_3$ − H + Li]$^+$	0.34:0.66
451.3	[M − R$_{18:0}$COO − NMe$_3$ − H + Li]$^+$	

Table 2.19 shows the backbone positions of the most common fatty acids of egg PC lipids.[44] This was used to validate the lipid identities. The lipids identified by the MALDI-MSMS analyses were POPC (16:0/18:1) and SOPC (18:0/18:1). The data in the Table 2.19 shows that for the majority of phosphocholine lipids in egg yolk, the 16:0 chain is at the *sn*-1 position if present. This supports the identification of the lipid containing 16:0 and 18:1 chains as POPC. Furthermore, if the 18:1 chain is present in a lipid of egg yolk PC, it is much more likely to be at the *sn*-2 position than the *sn*-1 position, supporting this identification and that of SOPC. A greater mole % of the 18:0 chains of egg PC lipids occur at the *sn*-1 position than the *sn*-2 position. 16:0/18:1 and 18:0/18:1 PC have also been identified as major phosphocholine components of egg yolk.[45]

Table 2.19. Positions of the most common fatty acids of egg phosphocholine lipids.[44]

Chain	*sn*-1 (mol %)	*sn*-2 (mol %)
16:0	68.8	1.8
18:0	25.8	1.2
18:1	4.7	48.9
18:2	0.2	11.1
18:3	0.5	-

2.2.6.2   Soybean PC

Soybean PC was analysed in the same way as egg PC, and Figure 2.20 shows the mass spectra of the lipid mixture in A) the absence of added salt and B) the presence of lithium chloride, centred on the mass region which is likely to include phosphocholine or phosphoethanolamine lipids.
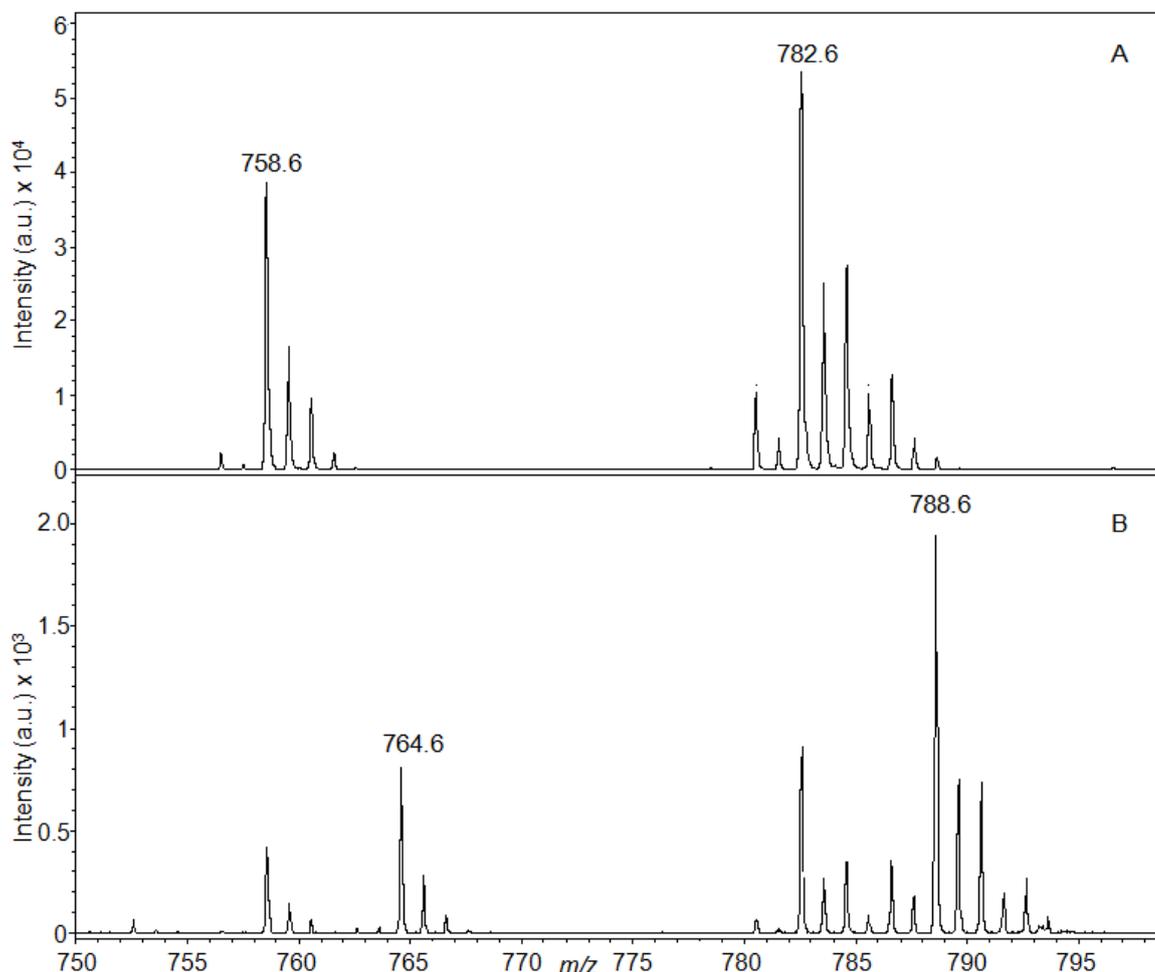
Figure 2.20. MALDI-MS spectra of soy PC A) in the absence of added salt and B) in the presence of lithium, centred on the mass region which is likely to include phosphocholine lipids. The samples were prepared by mixing a solution of the lipid in $CHCl_3$ (1 mg/mL) 2:9 (v/v) with solutions of DHB (30 mg/mL) in $EtOH/H_2O$ (50:50 (v/v)) or LiCl (100 mM) in $EtOH/H_2O$ (50:50 (v/v))).

2.2.6.2.1   Analyses in the absence of added salt

Table 2.20 shows the peaks in the MALDI-MS spectrum of soybean PC analysed in the absence of added salt which were identified as corresponding to possible PC lipid masses. No peaks corresponding to the masses of possible PE lipids were observed.

Table 2.20. The *m/z* values and possible assignments of peaks observed in the MALDI-MS spectrum of the soybean phosphocholine lipid mixture obtained in the absence of added salt.

m/z	Possible acyl chain combinations			
758.6	16:0/18:2 + H			
782.6	18:1/18:3 + H	18:2/18:2 + H	16:0/20:4 + H	16:0/18:1 + Na

The product ion spectrum of the lipid with *m/z* 782.6 ([M + H]$^+$) (Figure 2.21B) showed only peaks corresponding to the loss of 18:2 acyl chains, [M – R$_{18:2}$COO]$^+$ and [M – R$_{18:2}$CO + 2H]$^+$ at *m/z* 502.5 and *m/z* 520.4 respectively, along with peaks from which the PC headgroup could be confirmed at *m/z* 599.4 and *m/z* 184.2 corresponding to [M – OP(O)$_2$O(CH$_2$)$_2$NMe$_3$]$^+$ and [OP(O)$_2$O(CH$_2$)$_2$NMe$_3$]$^+$ respectively. This suggested that the lipid was 1,2-dilinoleoyl-*sn*-glycero-3-phosphocholine (DLPC). The lipid with *m/z* 758.6 was also identified as a phosphocholine lipid, through peaks corresponding to [OP(O)$_2$O(CH$_2$)$_2$NMe$_3$]$^+$ and [M – OP(O)$_2$O(CH$_2$)$_2$NMe$_3$]$^+$ at *m/z* 184.3 and *m/z* 575.5 respectively (Figure 2.21A). The MSMS spectrum of this lipid contained two pairs of peaks corresponding to the loss of an acyl chain, as shown in Table 2.21. No preferential loss was observed for either acyl chain for the [M – R$_x$COO]$^+$ fragments. A much greater loss of the 18:2 chain than the 16:0 chain was observed for the [M – R$_x$CO + 2H]$^+$ fragmentation. The equivalent fragmentation of POPC and OPPC showed preferential cleavage at the *sn*-2 position, suggesting that this lipid has the 18:2 chain at the *sn*-2 position, which would identify it as 1-palmitoyl-2-linoleoyl-*sn*-glycero-3-phosphocholine (PLPC).
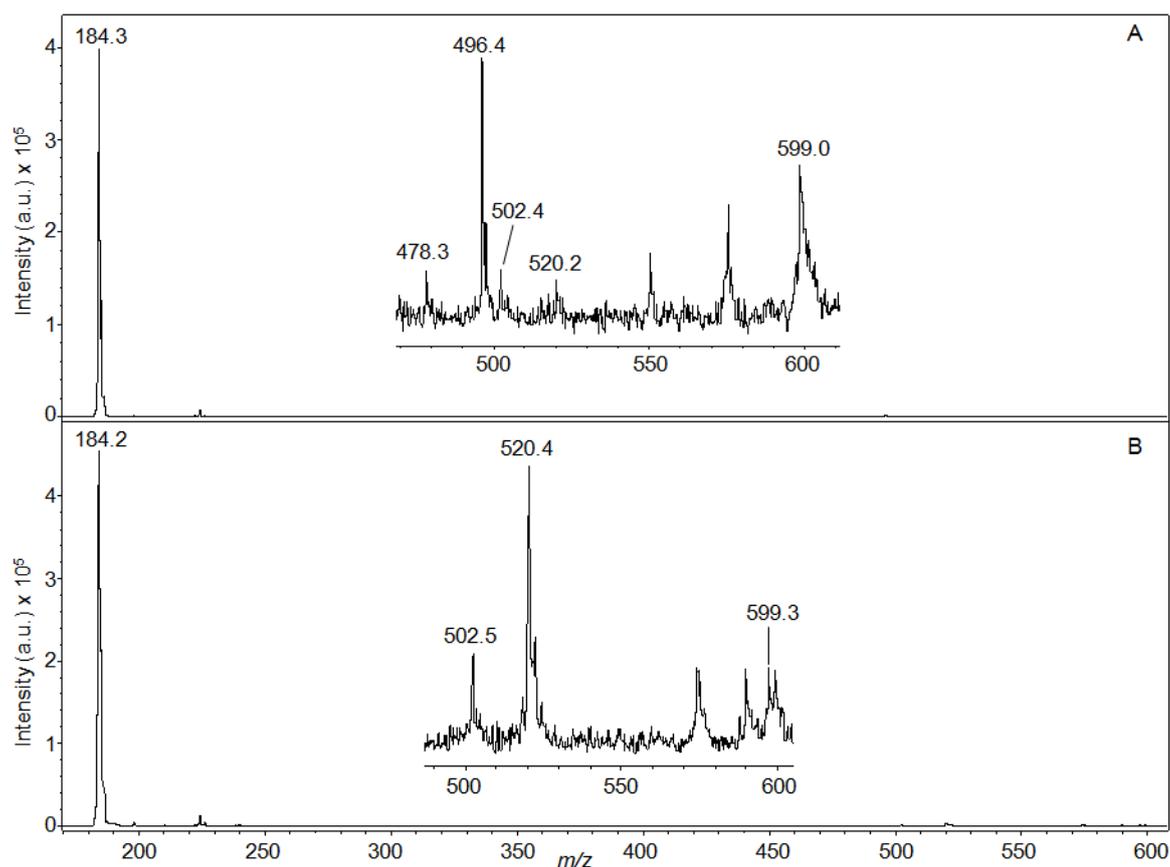
Figure 2.21. MALDI-MSMS spectrum of unknown phosphocholine lipids of soy PC with *m/z* values A) 758.6 and B) 782.6 (both [M + H]$^+$ ions). The samples were prepared by mixing a solution of the lipid in CHCl$_3$ (1 mg/mL) 2:9 (v/v) with a solution of DHB (30 mg/mL) in EtOH/H$_2$O (50:50 (v/v)).

Table 2.21. Product ions corresponding to the loss of an acyl chain observed in the MALDI-MSMS spectrum of the unknown phosphocholine lipid of soy PC with *m/z* 758.6 ([M + H]$^+$ ion). The relative intensities of peaks corresponding to cleavages of the 16:0 and 18:2 chains are shown for each fragment type.

m/z	Assignment	Relative intensities (16:0:18:2)
502.3	[M – R$_{16:0}$COO]$^+$	0.50:0.50
478.3	[M – R$_{18:2}$COO]$^+$	
520.2	[M – R$_{16:0}$CO + 2H]$^+$	0.14:0.86
496.4	[M – R$_{18:2}$CO + 2H]$^+$	

2.2.6.2.2 Analyses in the presence of lithium

Table 2.22 shows the peaks observed in the full-scan spectrum of soybean PC in the presence of lithium which were identified as corresponding to possible PC lipids. No possible PE lipids were identified.

Table 2.22. The *m/z* values and possible assignments of peaks observed in the MALDI-MS spectrum of the soy PC lipid mixture obtained in the presence of LiCl.

m/z	Possible acyl chain combinations	
764.6	16:0/18:2 + H	
788.6	18:1/18:3 + H	18:2/18:2 + H

The spectrum of the lipid with *m/z* 788.6 ($[M + Li]^+$) showed peaks corresponding to the fragments of a number of lipids, suggesting the presence of both the 18:1/18:3 and 18:2/18:2 acyl chain combinations, and possibly those of a third lipid due to incomplete isolation, so no single lipid could be fully identified. Figure 2.22 shows the product ion spectrum of the unknown lipid with *m/z* 764.6 ($[M + Li]^+$ ion), and Table 2.23 lists the *m/z* values and assignments of four pairs of peaks observed which corresponded to the loss of one or other acyl chain. The presence of a phosphocholine headgroup on the lipid was confirmed by the observation of peaks at *m/z* 184.2 and *m/z* 575.5 corresponding to $[OP(O)_2O(CH_2)_2NMe_3]^+$ and $[M - OP(O)_2O(CH_2)_2NMe_3]^+$ respectively. A preferential loss of the 16:0 chain was observed for the $[M - R_xCOO]^+$, $[M - R_xCOO - H + Li]^+$, and $[M - R_xCOO - NMe_3 - H + Li]^+$ fragment types, and the peak corresponding to the $[R_{18:2}CO]^+$ fragment had a greater intensity than that of the $[R_{16:0}CO]^+$ fragment. The analyses of $[POPC + Li]^+$ and $[OPPC + Li]^+$ (Section 2.2.5.5) showed no preferential loss of either chain for the $[M - R_xCOO]^+$ fragmentation within an error of twice the standard deviation. For the $[M - R_xCOO - H + Li]^+$, and $[M - R_xCOO - NMe_3 - H + Li]^+$ fragments, a preferential loss of the chain from the *sn*-1 position was observed, which suggests that the 16:0 chain of the unknown lipid is at the *sn*-1 position. The analyses of POPC and OPPC showed that the relative intensity values of $[R_xCO]^+$ fragments can not be used to identify the positions of the acyl chains. The lipid was therefore identified as 1-palmitoyl-2-linoleoyl-*sn*-glycero-3-phosphocholine (PLPC).

Table 2.23. Product ions corresponding to the loss of an acyl chain observed in the MALDI-MSMS spectrum of the unknown phosphocholine lipid of soy PC with m/z 764.6 ([M + Li]$^+$ ion). The relative intensities of peaks corresponding to cleavages of the 16:0 and 18:2 chains are shown for each fragment type.

m/z	Assignment	Relative intensities (16:0:18:2)
502.3	[M − R$_{16:0}$COO]$^+$	
478.3	[M − R$_{18:2}$COO]$^+$	0.55:0.45
508.3	[M − R$_{16:0}$COO − H + Li]$^+$	
484.3	[M − R$_{18:2}$COO − H + Li]$^+$	0.73:0.27
239.2	[R$_{16:0}$CO]$^+$	
263.2	[R$_{18:2}$CO]$^+$	0.40:0.60
449.3	[M − R$_{16:0}$COO − NMe$_3$ − H + Li]$^+$	
425.3	[M − R$_{18:2}$COO − NMe$_3$ − H + Li]$^+$	0.68:0.32
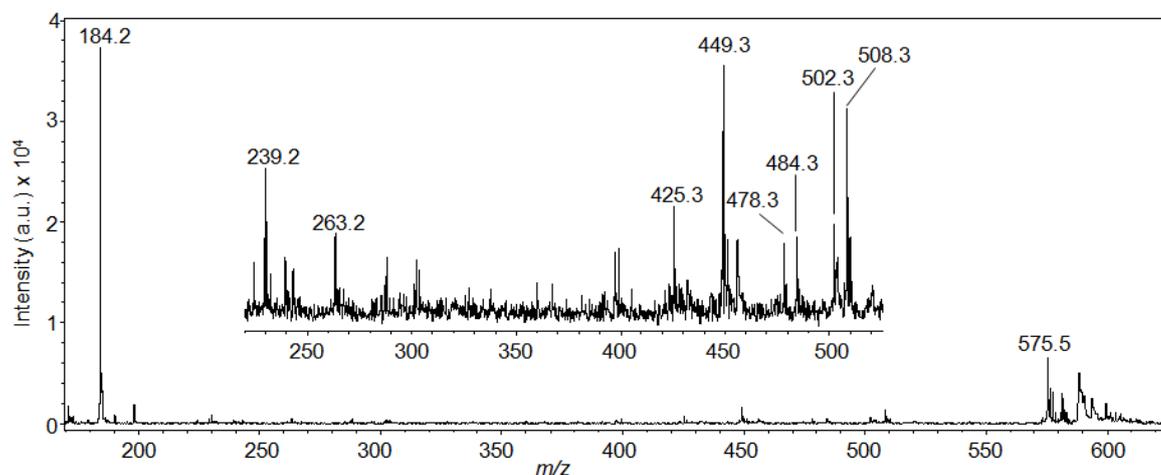
Figure 2.22. MALDI-MSMS spectrum of unknown phosphocholine lipid of soy PC with m/z 764.6 ([M + Li]$^+$ ion). The sample was prepared by mixing a solution of the lipid in CHCl$_3$ (1 mg/mL) 2:9 (v/v) with a solution of LiCl (100 mM) and DHB (30 mg/mL) in EtOH/H$_2$O (50:50 (v/v)).

Table 2.24 shows the backbone positions of the most common fatty acids of the soybean PC lipids.[44] This was used to validate the lipid identities. Two phosphocholine lipids were identified from the MALDI-MS and MSMS spectra of soybean PC, DLPC (18:2/18:2) and PLPC (16:0/18:2). The identification of PLPC is supported by the fact that the 16:0 chain is not observed at the *sn*-2 position of lipids in soybean PC, so this lipid can only be PLPC. DLPC and PLPC have been identified as major components of soybean PC.[46]

Table 2.24. Positions of the most common fatty acids of soybean phosphocholine lipids.[44]

Chain	sn-1 (mol %)	sn-2 (mol %)
16:0	34.4	-
18:0	7.6	-
18:1	30.2	15.8
18:2	23.8	71.8
18:3	4.0	13.1

2.2.6.3 MALDI imaging of TLC plates

The analyses of natural lipid mixtures described in Section 2.2.6 highlight some of the difficulties of analysing lipid mixtures by MALDI-MSMS. Though some of the lipids in egg PC and soybean PC were fully identified, some could not be identified due to incomplete isolation causing fragments from more than just the lipid of interest to be present in the spectrum. In some cases a number of different lipids had the same molecular mass, again causing the fragments of more than one lipid to be present in a spectrum and making positive identification of specific lipids difficult, if not impossible, for example product ions corresponding to both 18:1/18:3 PC and 18:2/18:2 PC were observed in the MSMS spectrum of m/z 788.6 from egg PC. The possible presence of peaks corresponding to fragments of lipids with the same mass also means that measuring the relative intensities of the product ion peaks cannot be relied upon to use to determine the positions of the acyl chains. In the case of PC lipids, the addition of lithium provides the advantage of a number of pairs of peaks corresponding to the loss of one or other acyl chains ($[R_xCO]^+$, $[M - R_xCOO - NMe_3 - H + Li]^+$, $[M - R_xCOO]^+$ and $[M - R_2COO - H + Li]^+$) compared to the two pairs of peaks observed in spectra obtained in the absence of lithium ($[M - R_xCOO]^+$ and $[M - R_2CO + 2H]^+$). This means that if peaks are observed which correspond to fragments of more than one lipid, causing the relative intensities of the peaks corresponding to fragmentations at the sn-1 and sn-2 positions to be affected for one or two pairs of fragments, it may still be possible to rely on the relative intensity data for two or three other pairs of fragments to determine the positions of the acyl chains on the glycerol backbone. These problems could be solved if the individual lipids could be separated out before analysis. One way of doing this is by separating the lipids by thin layer chromatography (TLC) and then analysing the plates by MALDI imaging.

Some method development was required before the analysis of lipids separated on TLC plates could be carried out. Firstly, a method of getting the TLC plate into the instrument was established. This was done using a commercial MALDI target plate

designed to hold surface modified microscope slides. A piece of steel, the same size as a microscope slide, was modified to accommodate an aluminium-backed TLC plate and a strip of conductive double-sided adhesive carbon tape (Figure 2.23). The depth of the channel in which the TLC plate was to be adhered was the same as the combined thickness of the TLC plate and the strip of adhesive, as any discrepancy between the height of the surface of the TLC plate and the normal surface of a target plate would cause loss of mass accuracy.
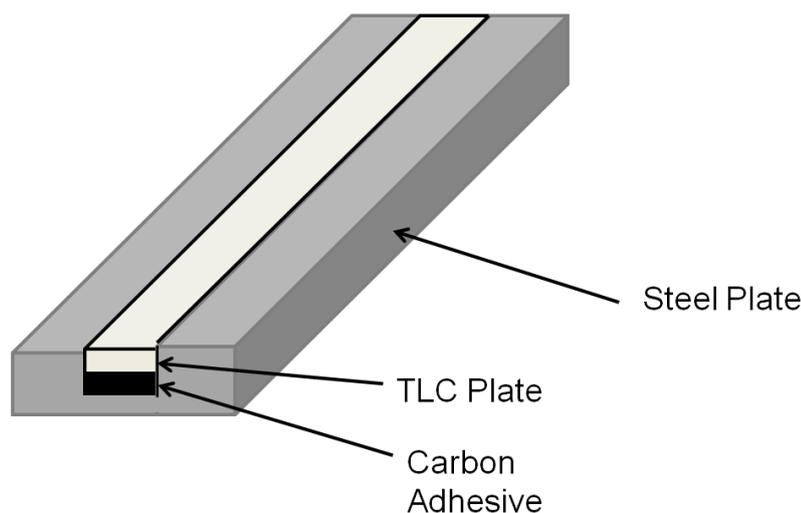
Figure 2.23. Diagram of TLC plate holder.

The next step was to find a way of applying the matrix to the TLC plate which would result in successful ionisation of lipid species on the plate. The MALDI laser cannot penetrate the silica layer of the TLC plate, therefore the addition of the matrix must cause the sample molecules to travel to the surface of the silica. The matrix must also not cause the sample spots to spread laterally within the plate.[47] Three methods were tested to see which gave the most even coverage and the best sample spectrum. A solution of DOPC in chloroform was applied to three pieces of TLC plate, run in 25:25:25:10:9 ethyl acetate, propan-2-ol, $CHCl_3$, MeOH, 0.25% (w/v) KCl and allowed to dry before the application of the matrix as one of three solutions:

a) DHB (100 mg/mL) in 1:1 acetonitrile/$CHCl_3$ (Figure 2.24A)
b) DHB (100 mg/mL) in EtOH (Figure 2.24B)
c) DHB (100 mg/mL) in MeOH (Figure 2.24C)

The application method was adapted from that of Fuchs *et al*, as was the matrix concentration and use of 1:1 acetonitrile/water as one of the solvents tested.[48] A thorough coating of the matrices were applied to the plates by pipette, quickly dried under a stream of argon, then another layer applied. The plates were allowed to dry thoroughly

before analysis. The MALDI images of each TLC plate are shown in Figure 2.24, with the areas where peaks corresponding to [DHB]$^+$ (m/z 154.1) were observed in spectra shown in yellow, and areas where peaks corresponding to [DOPC + H]$^+$ (m/z 786.6) were observed in spectra shown in blue. Very little matrix or DOPC were observed on the plate coated with the matrix in ACN/H$_2$O. Matrix was observed on the plate where it had been applied in MeOH, but very little DOPC was observed. On the plate where the matrix had been applied in EtOH a good coverage of matrix could be observed, along with a clear area of DOPC. This clearly shows that method (b) was the most successful, therefore this method was implemented during further experiments. Soaking the surface of the plate in a solution of DHB in ethanol is not expected to cause lateral spreading of lipid sample spots, as the standard TLC plate staining protocol involves dipping the plate into a solution of phosphomolybdic acid in ethanol, from which no spreading of sample spots is observed.
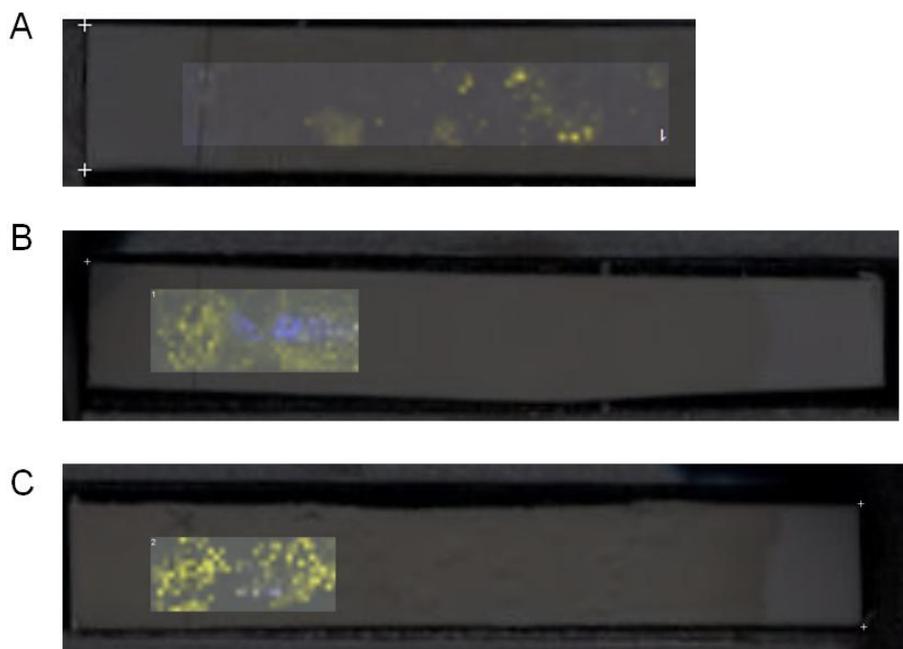
Figure 2.24. Representative image of MALDI imaging analysis of TLC plates to which DOPC had been applied. DOPC (35 µL, 1 mg/mL in CHCl$_3$) was run with 25:25:25:10:9 ethyl acetate, propan-2-ol, CHCl$_3$, MeOH, 0.25% (w/v) KCl, and analysed after the addition of A) DHB (100 mg/mL in ACN/water), B) DHB (100 mg/mL, EtOH) or C) DHB (100 mg/mL, MeOH) matrix solutions. Areas where peaks corresponding to [DHB]$^+$ (m/z 154.1) were observed in spectra are shown in yellow, areas where peaks corresponding to [DOPC + H]$^+$ (m/z 786.6) were observed in spectra are shown in blue.

2.2.6.4 Calibration

Concerns regarding the accuracy of mass measurement across the TLC plate were investigated by calibrating with PEG 600. Poly(ethylene glycol) 600 (PEG 600) (1 mg/mL with 100 mM NaCl in 50:50 (v/v) EtOH/H$_2$O) was spotted onto a piece of TLC

plate, DHB added using method (b) as above and the plate analysed by MALDI imaging, with the aim of calibrating the TLC plate using peaks corresponding to the sodium adducts of PEG molecules. Peaks corresponding to PEG were not observed in the resulting spectrum, but a number of other peaks were observed at regular intervals, which were found to be DHB/Na clusters. Peaks corresponding to DHB/Na clusters were observed in all TLC plate spectra, and therefore be used for internal calibration of the MALDI-MS spectra.

Table 2.25. Monoisotopic masses of DHB clusters used for internal calibration of MALDI-MS spectra obtained from TLC plates.

Mass (monoisotopic)	Cluster
198.9978	$[DHB + 2Na - H]^+$
375.0063	$[2DHB + 3Na - 2H]^+$
551.0149	$[3DHB + 4Na - 3H]^+$
727.0234	$[4DHB + 5Na - 4H]^+$
903.0320	$[5DHB + 6Na - 5H]^+$

The imaging method was then applied to a natural lipid mixtures extracted from mouse lungs and soybean PC.

2.2.6.5 Mouse lung lipids

2.2.6.5.1 Analyses in the absence of added salt

Figure 2.25 shows two TLC plates on which the mouse lipid solution had been run. The plate in Figure 2.25A was stained with phosphomolybdic acid and heat, and that in Figure 2.25B imaged after coating with DHB in EtOH. Though the plates were different sizes, the same areas of interest can be observed on both plates. Any *m/z* values of interest identified from the imaging of the plate were then analysed manually by MALDI-MSMS to try and identify the lipid that they corresponded to. The MS and MSMS spectra obtained were also compared to spectra obtained for the lipid mixture analysed on the standard MALDI target plate without separation.
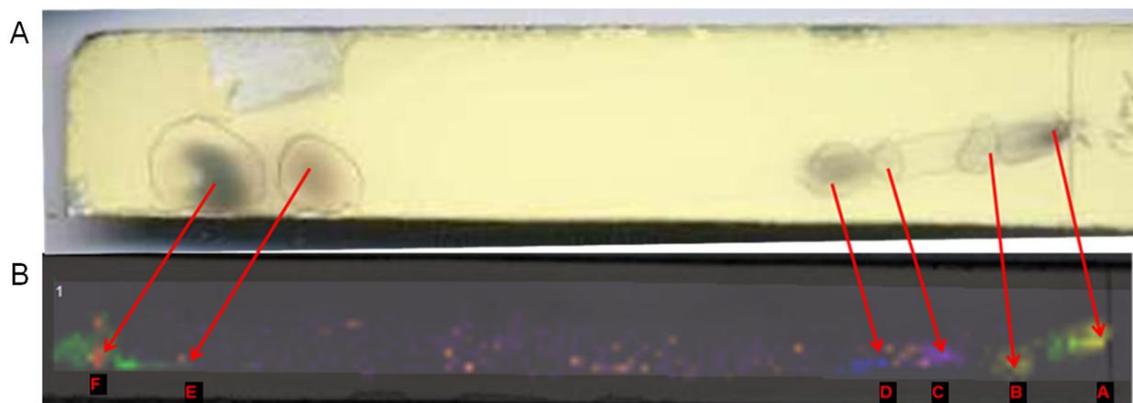
Figure 2.25. A) TLC plate after separation of mouse lipid mixture (45 µL lipid, 2 mg/mL in 50:50 (v/v) MeOH/CHCl₃) with 25:25:25:10:9 ethyl acetate, propan-2-ol, CHCL₃, MeOH, 0.25% (w/v) KCl and staining with PMA (20% w/v in EtOH) and heat. B) Representative image of MALDI imaging analysis of TLC plate after separation of mouse lipid (concentration and running solvents as A), showing areas where peaks not corresponding to [DHB]⁺ or DHB clusters were observed. The MALDI matrix was applied according to Section 2.2.6.3 method 2.

Though MSMS was attempted on a number of species, only one lipid could be tentatively identified in the absence of an added salt. Two product ion spectra were obtained from area A (just above where the lipid was spotted on the plate), from parent ions with m/z 734.5 and m/z 756.5. These were identified as phosphocholine lipids from the presence of peaks at m/z 184.1 corresponding to $[OP(O)_2CH_2CH_2NMe_3]^+$ in each product ion spectrum, but no other structural information could be obtained from the spectra. The lipids appeared to be hydrogen and sodium adducts of the same species, due to a mass difference of 22 Da, giving them possible identities of [16:0/16:0-PC + H]⁺ and [16:0/16:0-PC + Na]⁺, DPPC.

2.2.6.5.2 Analyses in the presence of lithium

100 mM LiCl was added to the DHB matrix solution before addition to another TLC plate on which the mouse lipids had been separated, in an attempt to improve the quality of the MS and MSMS spectra. Overall, the MS spectra produced from the imaging showed much weaker peaks when compared to the spectra obtained in the absence of the salt. A peak was observed at m/z 740.6 in the MS spectra of area A in Figure 2.25B, which was tentatively assigned as the lithium adduct of the PC lipid observed in the spectra obtained in the absence of an added salt. Figure 2.26 shows the MALDI-MSMS spectrum of this lipid, and Table 2.26 describes the identities of the peaks observed. The phosphocholine headgroup can be identified from peaks corresponding to $[OP(O)_2CH_2CH_2NMe_3]^+$ and $[M - OP(O)_2CH_2CH_2NMe_3]^+$, at m/z 184.4 and m/z 551.2, and the palmitoyl chain from peaks corresponding to $[R_{16:0}CO]^+$, $[M - R_{16:0}CO + H]^+$ and $[M - R_{16:0}CO + Li]^+$ at m/z 239.5, m/z 479.0 and m/z 485.0.
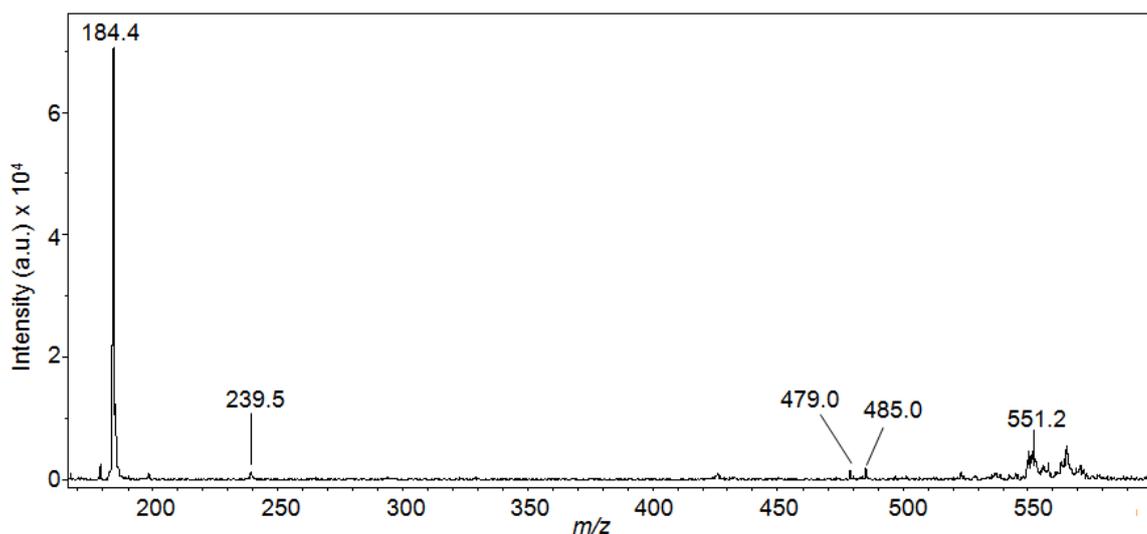
Figure 2.26. MALDI-MSMS spectrum of unknown lipid with *m/z* 740.6, suggested to correspond to [DPPC + Li]⁺. Spectrum recorded from TLC plate after separation of mouse lipid mixture (45 µL lipid, 2 mg/mL in 50:50 (v/v) MeOH/CHCl₃) with 25:25:25:10:9 ethyl acetate, propan-2-ol, CHCl₃, MeOH, 0.25% (w/v) KCl. The MALDI matrix was applied according to Section 2.2.6.3 method 2 with the addition of 100 mM LiCl.

Table 2.26. Product ions observed in the MALDI-MSMS spectrum of the unknown lipid with *m/z* 740.6 ([M + Li]⁺ ion) obtained from a TLC plate on which the mouse lipid mixture had been separated.

m/z	Assignment
184.4	$[OP(O)_2CH_2CH_2NMe_3]^+$
239.5	$[R_{16:0}CO]^+$
479.0	$[M - R_{16:0}COO]^+$
485.0	$[M - R_{16:0}COO - H + Li]^+$
551.2	$[M - OP(O)_2CH_2CH_2NMe_3]^+$

2.2.6.5.3 Discussion

The ability to fully identify DPPC from the MSMS spectrum in the presence of lithium was an improvement on the tentative assignment from the spectra of the hydrogen and sodium adducts. However, it was not possible to isolate and fragment any other species. In the absence of lithium it was possible to carry out MSMS on a number of masses observed in spectra obtained from different regions of the TLC plate, though no lipids could be identified from these MSMS spectra. The signal-to-noise ratio of the MS spectra obtained in the presence of lithium was reduced compared to spectra obtained in the absence of an added salt. The addition of lithium meant that the population of each lipid was split between protonated, sodiated and lithiated ions, therefore reducing the signal-to-noise ratio for each adduct.

The negative ions of a TLC plate on which the mouse lipid mixture had been separated were also analysed by MALDI imaging to see if any different lipids could be

identified, particularly those which might have had the same mass as phosphocholine lipids. Very few non-matrix peaks were observed in the spectra obtained though, and none of these had sufficient intensity to allow MSMS to be carried out.

DPPC was also the only lipid identified by MALDI-MSMS analysis of the mouse lipid mixture on the standard target plate in the presence and absence of Li^+. Table 2.27 shows the fragments from which $[DPPC + H]^+$ (*m/z* 734.6) and $[DPPC + Li]^+$ (*m/z* 740.6) were identified during this analysis. In each case, fragments were identified from which the palmitoyl chain and phosphocholine headgroup could be clearly identified.

Table 2.27. Product ions observed in the MALDI-MSMS spectra of the unknown lipids with *m/z* 734.6 and *m/z* 740.6 obtained from a standard MALDI target plate.

m/z 734.6		*m/z* 740.6	
m/z	**Assignment**	*m/z*	**Assignment**
184.1	$[OP(O)_2CH_2CH_2NMe_3]^+$	184.1	$[OP(O)_2CH_2CH_2NMe_3]^+$
478.2	$[M - R_{16:0}COO]^+$	239.0	$[R_{16:0}CO]^+$
496.2	$[M - R_{16:0}CO + 2H]^+$	425.1	$[M - R_{16:0}COO - NMe_3 - H + Li]^+$
551.2	$[M - OP(O)_2CH_2CH_2NMe_3]^+$	478.2	$[M - R_{16:0}COO]^+$
		484.2	$[M - R_{16:0}COO - H + Li]^+$
		551.4	$[M - OP(O)_2CH_2CH_2NMe_3]^+$

2.2.6.6 Soybean PC

Two TLC plates on which the soybean PC lipid mixture had been separated were analysed in the same way as the mouse lipid TLC plates, one in the absence of added salt and with LiCl added to the matrix solution.

2.2.6.6.1 Analyses in the absence of added salt

Figure 2.27 shows an MS spectrum recorded in the absence of added salt from a position on the TLC plate just above the point at which the lipid solution had been applied. The spectrum shows the same peaks as the spectrum of soybean PC analysed by MALDI-MS on the standard target plate (Figure 2.20A), the only differences being in the relative intensities of the peaks at *m/z* 780.5 and *m/z* 782.5 and the presence of a peak at *m/z* 776.6 in the spectrum recorded from the TLC plate which was not observed in spectrum obtained from the analysis on the target plate. The lipid with *m/z* 758.5 was identified as 1-palmitoyl-2-linoleoyl-*sn*-glycero-3-phosphocholine (PLPC) by MSMS analysis on the standard MALDI target plate. MSMS analysis of the species with the same *m/z* value on the TLC plate produced a spectrum from which only the PC headgroup of PLPC could be identified, from peaks at *m/z* 184.0 and *m/z* 575.1 corresponding to $[OP(O)_2CH_2CH_2NMe_3]^+$ and $[M - OP(O)_2CH_2CH_2NMe_3]^+$ respectively (Figure 2.28). When the lipid mixture was analysed on the standard MALDI target plate it

was also possible to identify the lipid with *m/z* ([M + H]$^+$ ion) 782.6 as 1,2-dilinoleoyl-*sn*-glycero-3-phosphocholine (DLPC). It was not possible to obtain product ion spectra of this or any of the other species observed in the analysis of the TLC plate.
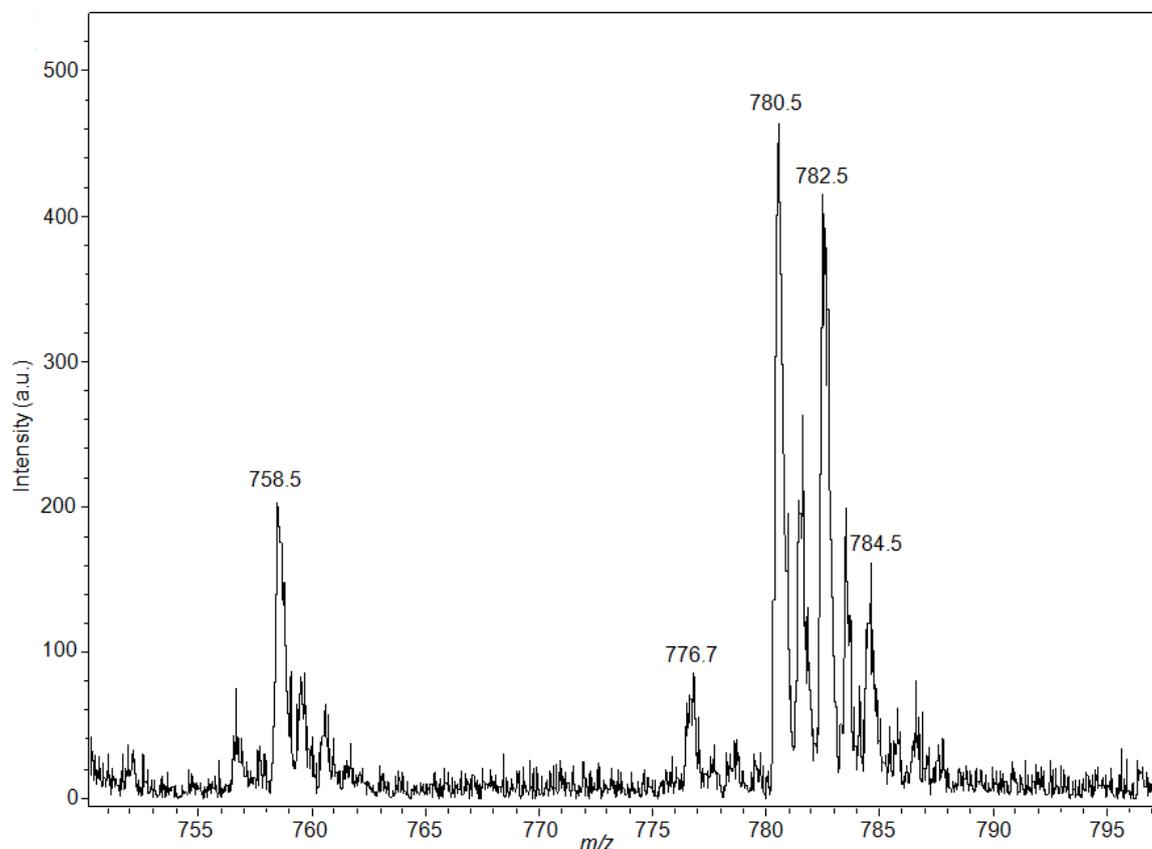
Figure 2.27. MALDI-MS spectrum recorded from TLC plate after separation of soybean PC lipids (45 µL, 2 mg/mL in CHCl$_3$) with 25:25:25:10:9 ethyl acetate, propan-2-ol, CHCL$_3$, MeOH, 0.25% (w/v) KCl. The MALDI matrix was applied according to Section 2.2.6.3 method 2.
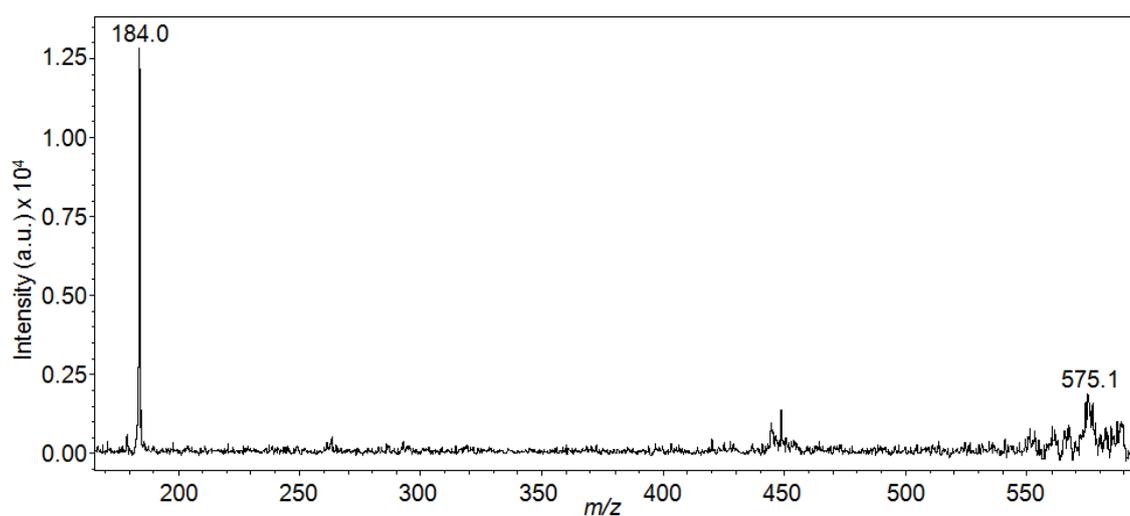
Figure 2.28. MALDI-MSMS spectrum of unknown lipid with *m/z* 758.5, suggested to correspond to [PLPC + H]$^+$. Spectrum recorded from TLC plate after separation of soybean PC (45 µL, 2 mg/mL in CHCl$_3$) with 25:25:25:10:9 ethyl acetate, propan-2-ol, CHCL$_3$, MeOH, 0.25% (w/v) KCl. The MALDI matrix was applied according to Section 2.2.6.3 method 2.

2.2.6.6.2 Analyses in the presence of lithium

An MS spectrum obtained in the presence of lithium from a TLC plate on which soybean PC had been separated is shown in Figure 2.29. The spectrum was recorded from a region of the plate just above the point at which the lipid had been spotted. The spectrum bears a close resemblance to that of soybean PC analysed in the presence of lithium on the standard MALDI target plate (Figure 2.20B). When analysed on the standard MALDI target plate in the presence of LiCl, it was possible to identify the lipid with *m/z* 764.6 as the lithium adduct of 1-palmitoyl-2-linoleoyl-*sn*-glycero-3-phosphocholine (PLPC) from the product ion spectrum. It was not possible to fragment this species when analysis was carried out on the TLC plate. It was not possible to obtain the product ion spectra of any other species on the TLC plate in the presence of lithium.
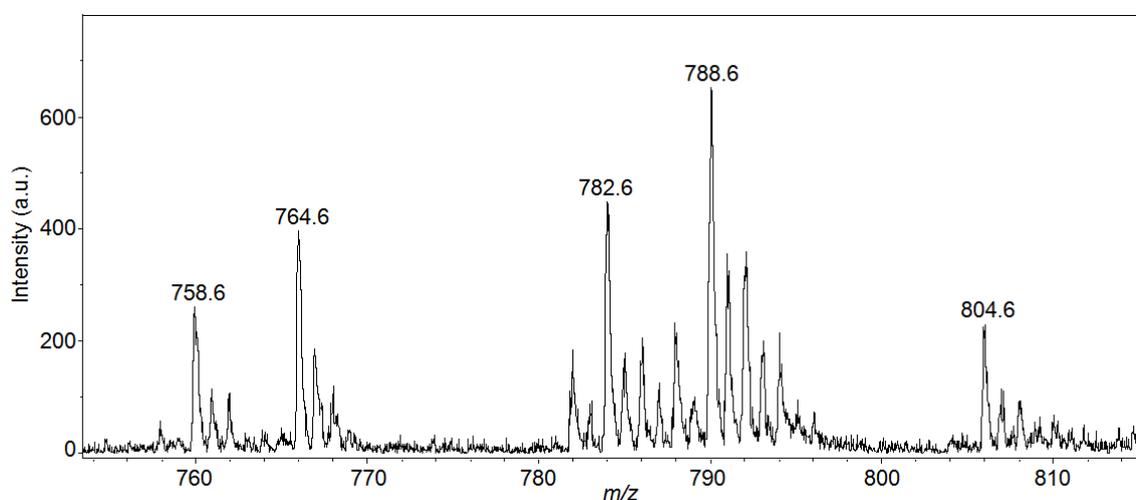
Figure 2.29. MALDI-MS spectrum recorded from TLC plate after separation of soybean PC lipids (45 μL, 2 mg/mL in CHCl$_3$) with 25:25:25:10:9 ethyl acetate, propan-2-ol, CHCL$_3$, MeOH, 0.25% (w/v) KCl. The MALDI matrix was applied according to Section 2.2.6.3 method 2 with the addition of 100 mM LiCl (EtOH).

2.2.6.6.3 Discussion

MALDI imaging of TLC plates on which soybean PC had been separated produced full scan MS spectra which included the same peaks as those observed when the lipid mixture was analysed on the standard MALDI target plate. MSMS analysis on the TLC plate did not prove as informative as the MSMS analyses on the standard MALDI target plate in the presence of lithium or in the absence of added salt. The product ion spectra recorded from the TLC plate in the absence of added salt did not provide information from which the acyl chains of any lipid could be identified, though peaks corresponding to the headgroup and the neutral loss of the headgroup of PLPC were observed. It was not possible to obtain a product ion spectrum of the lithium adduct of the same lipid. Overall less information could be gained from the lipid mixture after separation on the TLC plate than before separation, but the MS spectra which were

recorded suggest that if the method were refined it should be possible to obtain more informative MSMS spectra.

2.3 Discussion

2.3.1 Lipid analysis by MALDI-MS and MSMS

Full scan MALDI-MS analyses of the positive ions of DOPC, DPPC, POPC, DPPE, POPE, DPPA, DOPS and POPG established that the information gained from this technique was insufficient for the identification of all of the lipids. None of the phosphocholine lipids could be ionised in negative mode. Since phosphocholine lipids are major components of mammalian cell membranes, this ruled out both MALDI-MS and MSMS analysis in negative mode for the analysis of unknown lipid mixtures.[2] MALDI-MSMS spectra of the positive ions of DOPC, DPPC, POPC, DPPE, POPE, DPPA, DOPS and POPG provided sufficient information to identify the headgroup and both acyl chains in all cases, though the intensity of some product ion peaks was very low.

2.3.1.1 *The effect of metal salts on the MALDI analysis of phospholipids*

The fragmentation of lithium and sodium adducted lipids was found to produce more useful product ion spectra, in terms of the number of fragmentations and the signal-to-noise ratio, than that of protonated ions or calcium, copper, magnesium or zinc adducts. The Li^+ and Na^+ adducts of POPC dissociated to give analogous product ions (Table 2.7), though the signal-to-noise ratio was better in the spectrum obtained in the presence of Li^+. The fragmentation of $[POPE + Na]^+$ was similar to that of $[POPC + Na]^+$ and $[POPC + Li]^+$, but the product ion spectrum of $[POPE + Li]^+$ gave only 6 peaks from which POPE could be identified, with only two of these corresponding to the neutral loss of an acyl chain (Table 2.6). This may be attributable to the incomplete isolation of $[POPE + Li]^+$, allowing the dissociation products of $[POPE + 2Li – H]^+$ to be visible alongside those of $[POPE + Li]^+$. The product ion spectra of the Na^+ adducts of POPC and POPE provided more information from which the identities of the acyl chains and headgroups could be determined than those of $[POPC + Li]^+$ and $[POPE + Li]^+$; therefore if positioning the acyl chains on the glycerol backbone is not required, the addition of NaCl to PC and PE lipids provides more useful product ion spectra in terms of lipid identification than the addition of LiCl, despite the lower signal-to-noise ratio in the product ion spectrum of the sodium adduct of POPE.

It has been suggested that the different fragmentation of PC lipids observed in the presence of metal ions is due to the different ionic binding of protons and metal ions

(Scheme 2.1). Protons bind tightly to the negatively charged oxygen of the phosphocholine headgroup, while metal cations are more free and can associate with different parts of the molecule, leaving the negatively charged oxygen able to carry out intermolecular attack. This mechanism lends support to the product ion assignments of POPC made in Figure 2.8B, corresponding to $[POPC - R_2COO - NMe_3 - H + Na]^+$ and $[POPC - R_1COO - NMe_3 - H + Na]^+$ in Table 2.7.[11] POPC was observed to dissociate in the same way in the presence of lithium (Figure 2.8C). The mechanism also correlates with the observed fragmentation of $[POPE + Na]^+$, which was analogous to that of $[POPC + Na]^+$ and $[POPC + Li]^+$, as described in Figure 2.6 and Table 2.6. POPE was observed to fragment differently in the presence of Li, with loss of $(CH_2)_2NH_3$ and R_xCOO rather than NH_3 and R_xCOO. This type of fragmentation can not be explained by the mechanism of Al-Saad *et al.* (Scheme 2.1).
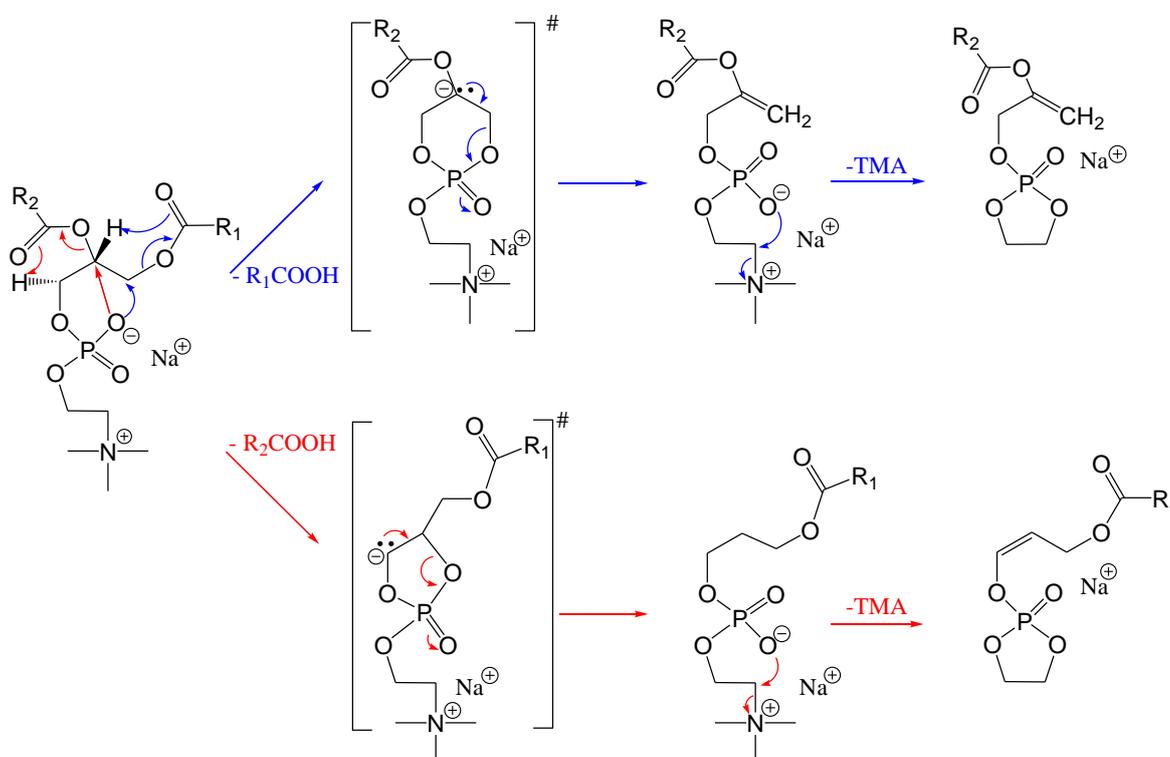
Scheme 2.1. Fragmentation pathway proposed by Al-Saad *et al.* for the neutral loss of R_xCOO and trimethylamine from PC lipids in the presence of Na^+.[11]

2.3.1.2 *Identification of the acyl chain position of phospholipids*

The analysis of 24 samples of each of POPC, POPE and OPPC in the presence and absence of Li^+ and Na^+ has shown that reproducible results can be obtained for the relative intensities of the peaks corresponding to the loss of the acyl chain from the *sn*-1 and *sn*-2 positions. In the absence of added salt, the position of the acyl chains of POPC could only be determined from the $[M - R_xCO + 2H]^+$ fragmentation. The position of the

acyl chains on the glycerol backbone of POPE could be determined from the relative intensities of the $[M - R_xCOO]^+$ and $[M - R_xCO + 2H]^+$ fragmentations in the absence of added salt. In both cases a preferential loss of the acyl chain from the *sn*-2 position was observed.   The $[M - R_xCOO - (CH_2)_2NH_3 + H + Li]^+$ fragmentation of $[POPE + Li]^+$ revealed a clear preference for the cleavage of the chain from the *sn*-1 position, as did the $[M - R_xCO]^+$, $[M - R_xCOO - H + Li]^+$ and $[M - R_xCOO - NMe_3 - H + Li]^+$ fragmentations of $[POPC + Li]^+$.   In the presence of Na^+ a clear difference in relative intensities was observed for the $[M - R_xCOO - NH_3 + 2H]^+$ fragmentation of POPE and a slight difference for the $[M - R_xCOO - H + Na]^+$ fragmentation of POPC. As with the Li^+ adducts, a preferential loss of the acyl chain from the *sn*-1 position of both POPC and POPE was observed in the presence of Na^+.   When the relative intensities of the peaks corresponding to the loss of one or other acyl chain are included in the assessment of the improvement offered by the addition of the metal salts it is clear that the addition of LiCl provides an advantage in terms of lipid identification when compared to analysis in the absence of added salt and analysis in the presence of NaCl. More fragments of $[POPC + Li]^+$ than $[POPC + H]^+$ or $[POPC + Na]^+$ were identified from which the position of the acyl chains on the glycerol backbone could be determined, and the difference in average relative intensities for cleavage at the *sn*-1 and *sn*-2 positions of $[POPC - ii - H + Na]^+$ was only slight. The positions of the acyl chains of POPE could be determined in the presence or absence of Na or Li.

When the dissociation of POPC and OPPC was compared, a greater loss of the acyl chain from the *sn*-2 position of both protonated parents and from the *sn*-1 position of both lithium adducts was observed. The fragments of the lithium adducts corresponding to $[RCO]^+$ were not in keeping with this pattern however. The intensity of the peak corresponding to the palmitoyl chain was greater than that corresponding to the oleoyl chain whether it was fragmented from the *sn*-1 position of POPC or the *sn*-2 position of OPPC. This suggests that the nature of this fragmentation mechanism is dependent on the acyl chain identity rather than the chain's position on the central glycerol.

Different fragmentation mechanisms have been suggested to explain the preferential losses of the acyl chain from the *sn*-1 or *sn*-2 position, and the effects of the addition of alkali metal salts on this. One mechanism was proposed from the results of MALDI-PSD analysis of PC lipids and based on the formation of 5- and 6-membered ring intermediates during the loss of an acyl chain.[11] The authors reported no fragmentations involving the loss of an acyl chain in product ion spectra of protonated lipids, and therefore referred only to the fragmentation of sodium adducts. They proposed that in the formation of $[M - R_xCOO - H + Na]^+$ and $[M - R_xCOO - NMe_3 - H + Na]^+$ product ions,

decomposition goes via 6-membered (loss of R_1COO) or 5-membered (loss of R_2COO) intermediates, where the activation energy of the formation of the 6-membered ring is lower, therefore preferential loss of the chain from the *sn*-1 position is observed (Scheme 2.2). This correlates with the results discussed above for the lithium adducts of POPC and OPPC, but not with all of the results observed for dissociation of the sodium adduct of POPC. In the presence of Na^+, a very slight preference was observed for the cleavage of R_1COO in the $[POPC - R_xCOO - H + Na]^+$ fragmentation, but no preference could be observed for the loss of either chain in the $[POPC - R_xCOO - NMe_3 + Na]^+$ fragmentation.
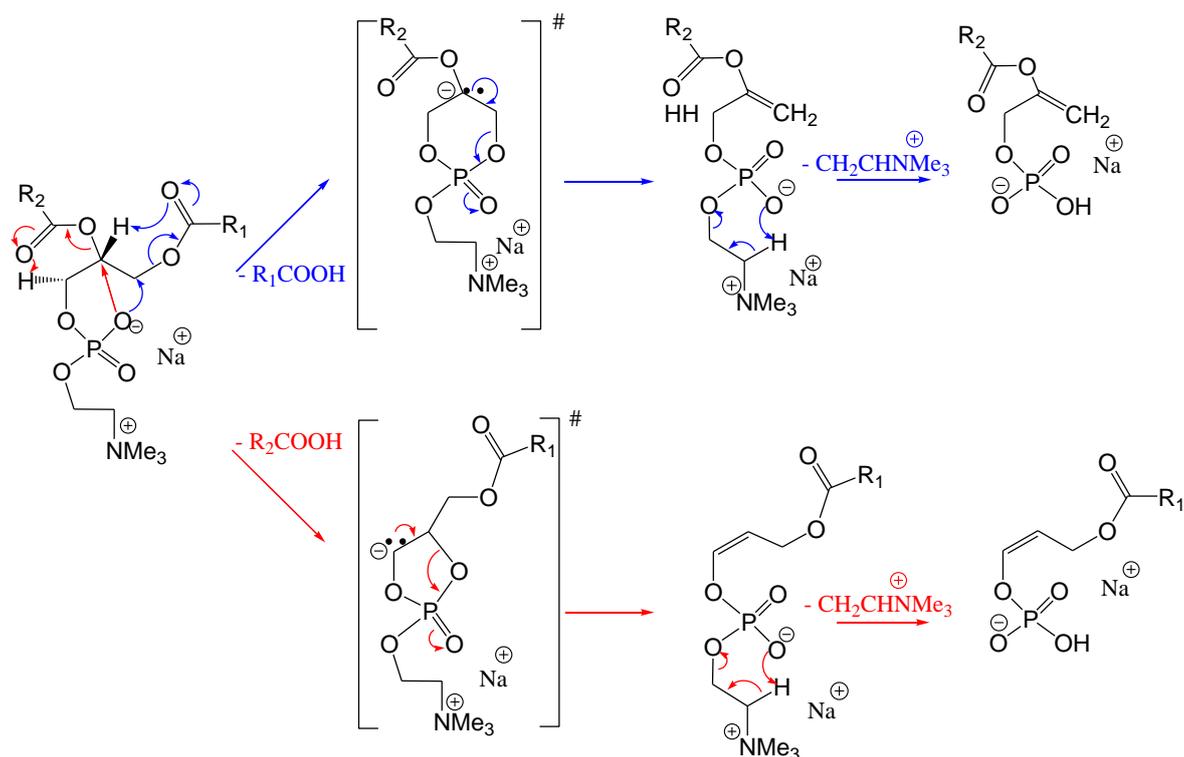
Scheme 2.2. Fragmentation pathway proposed by Al-Saad *et al.* for the neutral loss of R_1COO and R_2COO from $[PC + Na]^+$ via 6- and 5-membered intermediates respectively.[11]

Al-Saad *et al.* also observed that where the metal ion was lost during fragmentation, producing $[M - R_xCOO + H]^+$ fragments, there was no preference for cleavage at the *sn*-1 or *sn*-2 position, which they proposed was based on the equal probability of the Na^+ ion associating with either acyl chain prior to fragmentation. An equal likelihood of cleavage from the *sn*-1 and *sn*-2 positions was observed in the results discussed above for the $[M - R_xCOO + H]^+$ fragmentation of POPC (Table 2.9), but a preferential cleavage of the chain from the *sn*-1 position was observed for this fragmentation of OPPC (Table 2.11). Formation of the $[R_xCO]^+$ fragment was not referred to in the mechanism described.

Another set of proposed mechanisms is based on the suggestion that the α-hydrogen atom on the *sn*-2 acyl chain is more labile than that at the *sn*-1 position.[19, 49] The mechanisms were developed from observation of fragmentation of lipids, some of them deuterium-labelled, by low energy CID after electrospray ionisation. Similarly to Al-Saad *et al.*, Hsu and Turk reported the preferential cleavage of R_1COO and R_1COO + NMe_3 or NH_3 from alkali metal adducts of PC and PE (Scheme 2.3). As described above, this does not fully correlate with the data presented above for POPC, POPE and OPPC. Observation of $[R_xCO]^+$ fragments of the metal ion adducts was reported, but not their relative intensities.
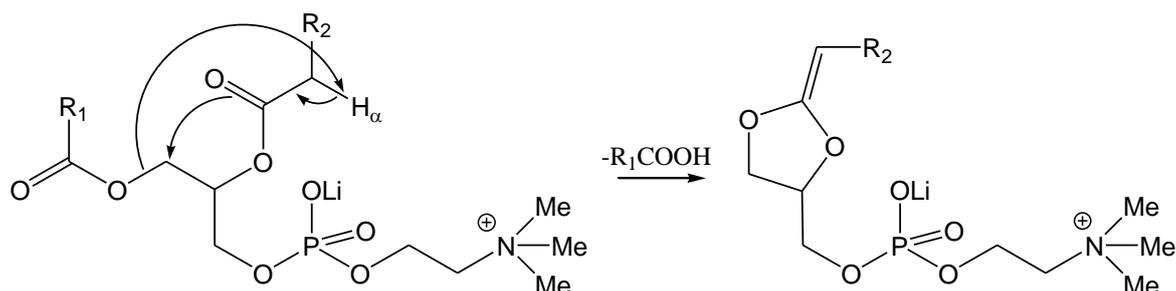
Scheme 2.3. Fragmentation pathway proposed by Hsu and Turk for the neutral loss of R_1COO from [PC + Na]$^+$ due to the α-hydrogen atom on the *sn*-2 acyl chain.[19]

$[M - R_xCO + 2H]^+$ product ions were reported by Hsu and Turk when PC lipids were analysed in the absence of an added salt, with preferential cleavage at the *sn*-2 position. This was again attributed to a more labile α-hydrogen at the *sn*-2 position than the *sn*-1 position (Scheme 2.4). This is supported by the data for POPC and OPPC presented above. The product ion spectra of protonated PE lipids recorded by Hsu and Turk were reported to be too weak for relative peak intensities to be determined.
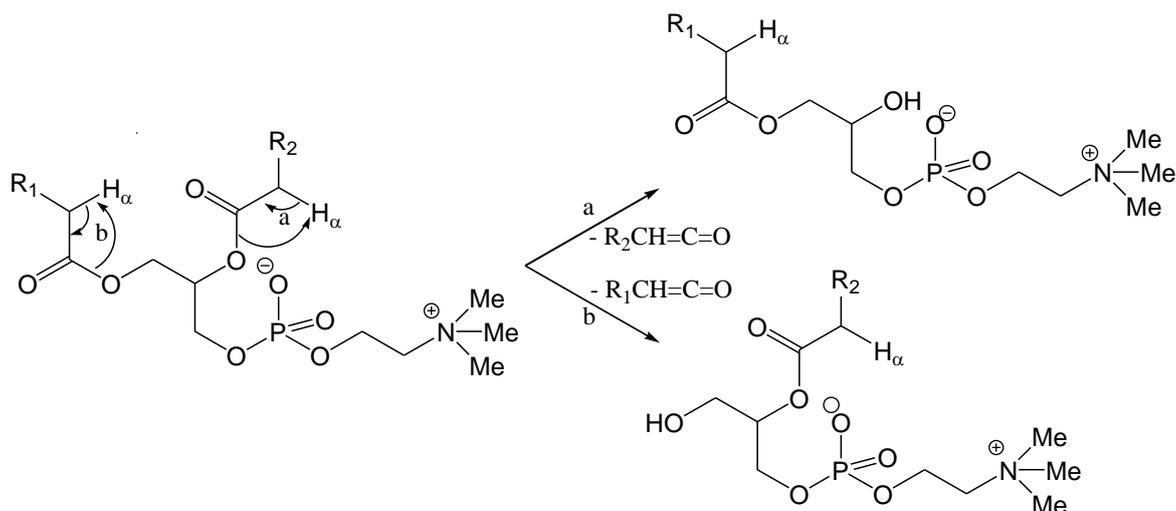
Scheme 2.4. Fragmentation pathway proposed by Hsu and Turk for the neutral loss of R_1CO and R_2CO from [PC + H]$^+$, where preferential cleavage at the *sn*-2 position was attributed to the increased lability of the α-hydrogen atom on the *sn*-2 acyl chain.[19]

101

When LIFT and CID experiments were compared for POPC, some differences were observed in the standard deviations of repeat measurements of the relative intensities of peaks corresponding to fragmentation at the *sn*-1 and *sn*-2 positions. The same product ions involving the acyl chains were observed by each method, with similar average relative intensity values for each method, but the standard deviations of the set of repeat analyses were consistently larger for fragmentation by CID than by LIFT. The average relative intensity of the peaks corresponding to $[RC_1O]^+$ and $[RC_2O]^+$ was 0.61:0.39 for both CID and LIFT. The error value for the 24 repeat analyses was ± 0.04 for the LIFT product ions and ± 0.11 for the CID product ions, indicating a statistically preferential cleavage at the *sn*-1 position only when fragmentation was carried out by LIFT. When $[POPC + H]^+$ was fragmented by CID the position of the acyl chains on the glycerol backbone could only be determined from the $[M - i + 2H]^+$ product ion. When $[POPC + Li]^+$ was fragmented by CID of $[POPC + H]^+$ the acyl chain position could only be determined from the $[M - ii - H + Li]^+$ product ion, and the preferential cleavage at the *sn*-1 position for this product ion was only slight. The greater variation in the CID results may be attributable to the increased fragmentation caused by CID compared to LIFT. As shown in Figure 2.13A and B, a greater number of lower *m/z* product ions were observed in the CID product ion spectrum of $[POPC + H]^+$ compared to LIFT. This is a recognised consequence when comparing these two methods for the tandem mass spectrometry of peptides and proteins.[50] The increased number of product ions in the lower *m/z* range is thought to arise from sequential fragmentation of primary fragments. Secondary fragmentations involving the loss of the acyl chains is a likely cause of the greater standard deviations of the repeat measurements when analyses were carried out by CID compared to those of the LIFT analyses.

2.3.2   The identification of unknown lipids by MALDI-MSMS

One lipid, POPC, was identified from the MALDI-MSMS analysis of egg PC in the absence of an added salt, and a further, SOPC, was identified when LiCl was added to the sample. The identities of the headgroup and both acyl chains, and the positions of the acyl chains of the glycerol backbone, were determined for both lipids. POPC and SOPC are known to be major phosphocholine constituents of hen egg yolk.

Two lipids, DLPC and PLPC, were identified during the analysis of soybean PC in the absence of lithium, and PLPC was identified in the presence of lithium. Again it was possible to fully identify the constituent parts of the lipids and the positions of the acyl chains of PLPC. The palmitoyl chain is known to only occur at the *sn*-1 position of lipids in soybean PC, which supports the identification of PLPC.

The complete identification of some unknown lipids in the soybean and egg PC mixtures has proven that the method of MSMS analysis of positive ions in the presence of lithium determined through the analyses described in Sections 2.2.3–2.2.5 can be applied to the identification of unknown lipids. Figures 2.18 and 2.19 show that the signal-to-noise ratio was better for the product ion spectra obtained in the presence of Li^+ than in the absence of added salt, so in that respect the addition of the salt enhanced the identification. One possible problem was identified with adding lithium salts. In the full scan spectrum of egg PC analysed in the absence of an added salt there are peaks at m/z 782.6 and m/z 788.6. The addition of Li^+ to the sample would create a lithium adduct of the lipid with m/z 782.6 at m/z 788.6, and fragmentation of this mass would give a product ion spectrum containing peaks corresponding to both the lipid with m/z 788.6 for $[M + H]^+$ and the lipid with m/z 788.6 for $[M + Li]^+$, from which it is likely neither could be fully identified. This highlights the need for separation of the lipids before analysis, such as on a TLC plate.

2.3.3   MALDI imaging of TLC plates

A method for analysing lipids on TLC plates was formed for the Autoflex II MALDI-TOF/TOF instrument and was applied to the analysis of soybean PC and an extracted mixture of mouse lung lipids. DPPC was identified from the mouse lung lipid mixture. When MSMS analysis was carried out on this lipid in the absence of added salt, the only identifiable peak in the product ion spectrum corresponded to the PC headgroup. The sodium adduct of DPPC was also tentatively assigned from the full scan analysis and an MSMS spectrum, where again a peak corresponding to the PC headgroup was observed. Though previous analyses have shown that the addition of sodium to samples produced product ion spectra with a number of peaks from which lipids could be identified, in this case the sodium adduct came from just the small quantity of sodium naturally present in the sample and TLC plate, therefore there was only a small quantity of $[DPPC + Na]^+$ present and the signal-to-noise ratio was not sufficient for achievable MSMS. Only MSMS of the lithium adduct provided enough information to fully identify the lipid. DPPC was also the only lipid which could be identified from MS and MSMS analysis of the mouse lung lipid mixture on the standard MALDI target plate in the presence and absence of Li^+, so MALDI imaging of the TLC plate provided no more or less information than analysis of the lipid on the standard MALDI target. In the absence of lithium however, the product ion spectrum obtained from the lipid on the TLC plate was less informative than that obtained on the standard MALDI target.

Soybean PC was also separated by TLC and analysed in the presence and absence of LiCl and the results compared to the analysis of the lipid mixture on the standard target. The full scan MS spectra obtained in the presence and absence of lithium were very similar, but it was not possible to fully identify any species from MSMS spectra recorded from the TLC plates whereas two lipids were identified from the mixture analysed on the standard target plate in the absence of lithium and one in the presence of lithium.

Overall, the lipid mixtures which were separated on TLC plates gave less information than when analysed on the MALDI target plate. The same peaks were observed in the full scan spectra of soybean PC on the standard target plate and on TLC plates, both in the presence and absence of lithium, but the signal was too low for achievable MSMS when analysis was carried out directly on the TLC plate. Fragmentation of the lithium adduct of DPPC on a TLC plate on which the mouse lipids had been separated produced a clear product ion spectrum from which the headgroup and palmitoyl chain could be identified. These results suggest that with refinement of the method more information could be obtained.

2.4 Future work

The analyses of POPE, POPC and OPPC have shown that it is possible to identify the orientation of the acyl chains on the glycerol backbone when the methodology has been completely validated. The correlation between the results reported herein and those reported in the literature is at times tentative however, and there are a number of other factors which may affect the relative intensities of peaks corresponding to cleavages at the sn-1 and sn-2 positions which should be evaluated using the same stringent repeatability experiments performed on POPE, POPC and OPPC. The differences observed between the relative intensity results for POPC and OPPC, where the positions of two chains differing in length and degree of unsaturation are swapped, suggest three areas which could be investigated: The first is the influence of acyl chain length on the relative intensities of the product ions corresponding to the loss of an acyl chain from the sn-1 or sn-2 position. There has been some research in this area reported in the literature which suggests that the preferential cleavage of the chain from one position holds until the chain at the sn-2 position is much shorter ($\geq$ 6 CH$_2$ difference in the paper referenced) than that at the sn-1 position, though the conditions of this analysis (FAB-CAD MSMS in negative mode) were very different from those employed in the present research and, as shown by this work and a review of the literature, the conditions under

which such analyses are carried out have a large effect on the relative intensity values. The second is the influence of unsaturation, both the number of double bonds and their positions. The same researchers reported that when the chain at the *sn*-2 position had more than 3 or 4 double bonds there was no longer preferential cleavage of the chain from the *sn*-2 position. Again, this gives only an insight into the possible results which may be observed under different conditions. The third analysis required would be a more detailed investigation into the influence of acyl chain position on the relative intensities. The results with POPC and OPPC suggest that the influence of chain length or unsaturation differs depending on the position at which the shorter or more unsaturated chain resides. The effect of the headgroup needs to be explored also. The results described herein suggest that the general preferences for the cleavage of a chain from the *sn*-1 or *sn*-2 position are the same for POPC/OPPC and POPE, but in order to fully analyse unknown lipid mixtures it would be necessary to determine if this held for other commonly occurring lipids such as phosphoglycerols.

The idea of identifying lipid mixtures separated on TLC plates by MALDI imaging is fundamentally a good one, and the experiments described above produced encouraging preliminary results but did not reach the full potential of the technique. Adapted MALDI target plates are now commercially available. It was not possible to test whether the apparatus used for the experiments fully allowed high voltage to be conducted across the TLC plate inside the MALDI instrument, although resistance across the apparatus was checked with an ohmmeter to ensure there was some conductance between the metal plate and the TLC plate. The use of the specific adapted target plate designed for the Autoflex would remove any potential problems caused by insufficient conductivity. More conditions could be explored in order to obtain better results, including the use of high performance TLC (HPTLC) plates. These are composed of silica particles which are around half the size of those in standard TLC plates, providing both a smoother surface (which may improve mass accuracy), and reducing the diffusion of samples as the plate is run. This in particular could make a large difference to the analysis of lipid mixtures as the lipids will be concentrated in smaller areas after separation, which should increase the intensity of peaks in MS and MSMS spectra. A TLC solvent solution which gave better separation of the PC lipids would also aid identification of mixtures with a high PC content.

2.5 References

1. M. Zasloff, *Nature*, 2002, **415**, 389–395.

2. J.L. Harwood in *The Lipid Handbook*, ed. F.D. Gunstone, J.L. Harwood and A.J. Dijkstra, CRC Press, Boca Ranton, Fl, USA, 3rd edn., 2007, pp 119–120.

3. A. Wieslander, S. Nordstrom, A. Dahlqvist, L. Rilfors and G. Lindblom, *Eur. J. Biochem.*, 1995, **227**, 734–744.

4. B. A. Lewis and D. M. Engelman, *J. Mol. Biol.*, 1983, **1166**, 211–217.

5. J. R. Silvius in *Lipid Protein Interactions*, ed. P. C. Jost and O. H. Griffth, John Wiley and Sons, New York, USA, 1982, Vol. 2, pp. 240–281.

6. H. Martinez-Seara, T. Rog, M. Pasenkiewicz-Gierula, I. Vattulainen, M. Karttunen and R. Reigada, *J. Phys. Chem. B*, 2007, **111**, 11162–11168.

7. G. Cevc, *Biochemistry*, 1991, **30**, 7186–7193.

8. B.M. Ham, J.T. Jacob and R.B. Cole, *Anal. Chem.*, 2005, **77**, 4439–4447.

9. J. Schiller, R. Süß, B. Fuchs, M. Müller, M. Petković, O. Zschörnig and H. Waschipy, *Eur. Biophys. J.*, 2007, **36**, 517–527.

10. X. Han and R.W. Gross, *J. Am. Soc. Mass Spectrom.*, 1995, **6**, 1202–1210.

11. K.A. Al-Saad, W.F. Siems, H.H. Hill, V. Zabrouskov and N.R. Knowles, *J. Am. Soc. Mass Spectrom.*, 2003, **14**, 373–382.

12. G. Stübinger and O. Belgacem, *Anal. Chem.*, 2007, **79**, 3206–3213.

13. M. Petkovíc, J. Schiller, J. Müller, M. Müller, K. Arnold and J. Arnhold, *Analyst*, 2001, **126**, 1042–1050.

14. S.N. Jackson, H.-Y.J. Wang and A.S. Woods, *J. Am. Soc. Mass Spectrom.*, 2007, **18**, 17–26.

15. G. Stübiger, E. Pittenauer and G. Allmaier, *Anal. Chem.*, 2008, **80**, 1664–1678.

16. S. Chen and K.W. Li, *J. Biochem.*, 1994, **116**, 811–817.

17. F.F. Hsu and J. Turk, *J. Am. Soc. Mass Spectrom.*, 2000, **11**, 892–899.

18. F.F. Hsu and J. Turk, *J. Mass Spectrom.*, 2000, **35**, 596–606.

19. F.F. Hsu and J. Turk, *J. Am. Soc. Mass Spectrom.*, 2003, **14**, 352–363.

20. F.F. Hsu, A. Bohrer and J. Turk, *J. Am. Soc. Mass Spectrom.*, 1998, **9**, 516–526.

21. H. Song, F.F. Hsu, J. Ladenson and J. Turk, *J. Am. Soc. Mass Spectrom.*, 2007, **18**, 1848–1858.

22. S.N. Jackson, H.-Y.J. Wang and A.S. Woods, *J. Am. Soc. Mass Spectrom.*, 2005, **16**, 2052–2056.

23. R.R. Landgraf, T.J. Garrett, N.A. Calcutt, P.W. Stacpoole and R.A. Yost, *Anal. Chem.*, 2007, **79**, 6862–6867.

24. B. Fuchs, C. Schober, G. Richter, R. Süβ and J. Schiller, *J. Biochem. Biophys. Methods*, 2007, **70**, 689–692.

25. Z.-H. Huang, D.A. Gage and C.C. Sweeley, *J. Am. Soc. Mass Spectrom.*, 1992, **3**, 71–78.

26. J.L. Kerwin, A.R. Tuininga and L.H. Ericsson, *J. Lipid Res.*, 1994, **35**, 1102–1114.

27. Y.H. Kim, J.S. Yoo and M.S. Kim, *Bull. Korean Chem. Soc.*, 1997, **18**, 874–880.

28. A. Kayganich and R.C. Murphy, *Anal. Chem.*, 1992, **64**, 2965–2971.

29. S. Ramanadham, F.F. Hsu, S. Zhang, A. Bohrer, Z. Ma and J. Turk, *Biochim. Biophys. Acta*, 2000, **1484**, 251–266.

30. A.M. Hicks, C.J. DeLong, M.J. Thomas, M .Samuel and Z. Cui, *Biochim. Biophys. Acta*, 2006, **1761**, 1022–1029.

31. A. Hayashi, T. Matsubara, M. Morita, T. Kinoshita and T. Nakamura. *J. Biochem.*, 1989, **106**, 264–269.

32. N.J. Jensen and K.B. Tomer, M.L. Gross, *Lipids*, 1986, **21**, 580–588.

33. D. Touboul, H. Piednoël, V. Voisin, S. De La Porte, A. Brunelle, F. Halgand and O. Laprévote, *Eur. J. Mass Spectrum.*, 2004, **10,** 657–664.

34. M. Petković, J. Schiller, M. Müller, S. Benard, S. Reichl, K. Arnold and J. Arnhold, *Anal. Biochem.*, 2001, **289,** 202–216.

35. A.I. Gusev, A. Proctor, Y.I. Rabinovich and D.M. Hercules, *Anal. Chem.*, 1995, **67**, 1805–1814.

36. J.T. Mehl and D.M. Hercules, *Anal. Chem.*, 2000, **72**, 68–73.

37. N. Shenar, N. Sommerer, J. Martineza and C. Enjalbal, *J. Mass Spectrom.*, 2009, **44**, 621–632.

38. D. Suckau, A. Resemann, M. Schuerenberg, P. Hufnagel, J. Franzen, A. Holle, *Anal. Bioanal. Chem.*, 2003, **376**, 952–965.

39. D. Hölscher, R. Shroff, K. Knop, M. Gottschaldt, A. Crecelius, B. Schneider, D.G. Heckel, U.S. Schubert and A. Svatoš, *The Plant Journal*, 2009, **60**, 907–918.

40. P. De Bievre and P.D.P. Taylor, *Int. J. Mass Spectrom. Ion Phys.*, 1993, **123**, 149–166.

41. D. Marsh, *CRC Handbook of Lipid Bilayers*, CRC Press, Florida, USA, 1990.

42. Sigma-Aldrich Product Information Sheet L-α-Phosphocholine Product Numbers P3644/P5638 RLG 8/03.

43. Sigma-Aldrich Product Information Sheet L-α-Phosphocholine Product Numbers P2772/P3556 RLG/SAG 8/03.

44. R.R.C. New, *Liposomes, A Practical Approach*, Vol. 58 of Practical Approach Series, IRL Press, The University of Michigan, US, 1990.

45. A. Kuksis, *Biochim. Biophys. Acta*, 1992, **1124**, 205–222.

46. C.G. Crawford, R.D. Plattner, O.J. Sessa, and J.J. Rackis, *Lipids*, 1980 **15**, 91–94.

47. B. Fuchs, R. Süß, A. Nimptsch and J. Schiller, *Chromatographia*, 2009, **69**, 95–105

48. B. Fuchs, J. Schiller, R. Süß, M. Schürenberg and D. Suckau, *Anal. Bioanal. Chem.*, 2007, **389**, 827–834.

49. F-F. Hsu and J. Turk, *J. Chromatogr. B*, 2009, **877**, 2673–2695.

50. M. Macht, A. Asperger and S.-O. Deininger, *Rapid Commun. Mass Spectrom.*, 2004, **18**, 2093–2105.

3 THE CHEMICAL STABILITY OF PHOSPHOLIPIDS

3.1 Introduction

The stability of liposomes after preparation has significance in two main areas; firstly, any changes in liposomes between their preparation and their use in peptide binding analyses may cause erroneous results, especially if these changes increase over time and the liposomes are not always stored for the same length of time before use. Secondly, liposomes are used as carriers for some drugs. Examples of this include a tumour-targeting drug which is incorporated into liposomes composed of a 2:1 molar ratio of DSPC and cholesterol to improve delivery of the drug to the required area, and an inhaled mixture of the analgesic fentanyl in two forms.[1, 2] The free form is absorbed immediately, while a liposome-encapsulated form is absorbed more slowly to give longer pain relief. The stability of the liposomes has important implications for the shelf-life of these drugs.

3.1.1 Chemical hydrolysis of lipids

Liposomal lipids have been shown to undergo acid- or base-catalysed hydrolysis to lysolipids and free fatty acids under certain conditions. The most stable hydrolysis product is 1-acyl lysophosphocholine (Figure 3.1). Hydrolysis has been observed to occur equally at both the *sn*-1 and *sn*-2 positions of the central lipid glycerol group, but 2-acyl lysophosphocholines are rapidly converted through acyl migration to 1-acyl lysophosphocholines.[3]
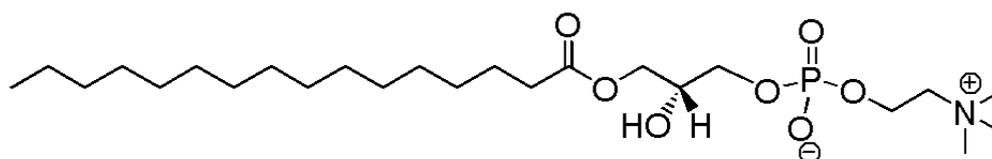
Figure 3.1. Lyso-MPC after hydrolysis of DMPC at the *sn*-2 position or after hydrolysis at the *sn*-1 position followed by acyl migration.

The hydrolysis of liposomal lipids has been shown to be dependent on external factors including pH, temperature, buffer and ionic strength, and on the lipid headgroup and acyl chain length.[3–10]

3.1.1.1 The effect of pH

The slowest rate of hydrolysis of saturated soybean phosphocholine lipids has been shown to occur in liposomes buffered at pH 6.5, with sharp increases above and

below this pH.[4] This is to be expected due to the hydrolysis occurring through acid or base-catalysed reactions. Analysis of the rates of hydrolysis of mostly polyunsaturated phosphocholine and phosphoethanolamine lipids at pH 7.4 and pH 1.5 showed the effect of acidic media on the rate of hydrolysis. After 24 hours at 25 °C and pH 7.4 the percentage by weight of lyso-PC in the sample had increased slightly, from 0.8 to 1.4%, as had the percentage lyso-PE (1.8 to 2.5%). The lyso-PC content of the same lipid mixture at the same temperature at pH 1.5 increased from 0.8% to 3.3% in three hours, with the lyso-PE content increasing from 1.8% to 5.2%.[5]

3.1.1.2 The effect of temperature

When a sample of the same mostly polyunsaturated phosphocholine and phosphoethanolamine lipids was stored at pH 7.4 at 37 °C the lyso-PC content increased from 0.8% to 2.1% and the lyso-PE content increased from 1.8% to 5.5% in 24 hours, compared to increases of 0.6% and 0.7% respectively at 25 °C. At pH 1.5 at 37 °C an even greater increase in the percentages of both lyso-lipids was observed in three hours, with lyso-PC increasing from 0.8% to 8.1% and lyso-PE increasing from 1.8% to 9.2%, compared to increases of 2.5% and 3.4% respectively at 25 °C.[5] Increasing the temperature from 25 °C to 37 °C therefore had a clear effect on the hydrolysis of both the PC and PE lipids, which was stronger under acidic conditions.

A longer-term study of hydrogenated soybean phosphocholines showed that after 6 months storage in the dark at 4 °C only 5.4% of the lipids were lyso-PC (the lyso-PC content at the beginning of the study is not reported), while the same lipids stored at room temperature and in the daylight contained 14.2% lyso-PC after 6 months.[6] It is unclear whether the temperature or UV light was the main factor in this increase in hydrolysis however.

3.1.1.3 The effect of buffers

Increasing buffer ionic strength has been shown to have no effect on the rate of hydrolysis of partially-hydrogenated egg phosphocholine lipids, due to PC lipids having no net charge.[7] Reaction kinetics are only affected by ionic strength if a reaction occurs between two charged species, therefore at pH values where phosphocholine lipids have no net charge increasing the concentration of salts will not affect hydrolysis.[3, 8] Changing the buffer does have an effect on the rate of hydrolysis, but the majority of the catalytic effect appears to still come from H^+ or OH^-.[3]

3.1.1.4 The effect of lipid composition

A slight increase in the rate of hydrolysis has been observed with decreasing chain length of phosphocholine lipids from DPPC to DMPC to DLPC in mixed micelles with Triton X-100. The increase was so small however that it was questioned whether it was meaningful.[9] Marked differences were observed in the hydrolysis rates of egg lipids with phosphocholine and phosphoethanolamine headgroups however, with a rate constant of 14 x 10^3 s^{-1} M^{-1} observed for hydrolysis of phosphocholine in mixed micelles with Triton X-100 and a rate of 4.6 x 10^3 s^{-1} M^{-1} observed for hydrolysis of phosphoethanolamine lipids under the same conditions. The phosphocholine components of mixed PE/PC micelles with Triton X-100 were hydrolysed faster than the phosphoethanolamine components of the same micelles, but the hydrolysis was slower than in pure micelles. This was thought to be caused by the change in surface pH due to the PE lipids, which would be negatively charged due to the alkaline medium used for the experiments (pH 12.7).[3, 9, 10] Hydrolysis of bilayers of PC and PG lipids has also been observed to be slower in alkaline media than in a neutral solution, again due to the surface pH.[10]

3.1.1.5 Physical effects of hydrolysis

The presence of lyso-PC and free fatty acids has a number of effects on liposome dispersions. Liposomes composed of partially hydrogenated egg PC lipids, egg PG lipids and 15% lyso-PC were shown to decrease in size from 0.19 µm to 0.16 µm over 40 days stored at 40 °C. This was attributed to rearrangement due to the release of lyso-PC, which spontaneously forms micelles in aqueous solution.[11] The incorporation of free fatty acids into liposome bilayers has been observed to cause aggregation and fusion during storage below the phase transition temperature of the fatty acid/lipid mixed bilayer. Aggregation occurred rapidly below the phase transition temperature but was reversible if the dispersion was immediately reheated. Fusion occurred by increasing degrees if the dispersion was kept below the phase transition temperature.[12] The presence of lyso-phospholipids in liposome bilayers also increases permeability, allowing small molecules to pass in and out of the liposomes. Greater leak-in of calcein has been reported from liposomes to which lyso-PC has been incorporated into the bilayer compared to those containing lyso-PC and fatty acids that have been formed through hydrolysis however. Bilayers which contained up to 10% hydrolysis products showed less permeability than fresh liposomes, and equal permeability was reported with 15% hydrolysis products. Increased permeability was observed above this point. Leak-in of calcein through lipid bilayers containing exogenous lyso-PC increased with increasing lyso-lipid concentration.[11] Leakage of liposome contents through bilayers containing a proportion of

lyso-lipids was also observed to be temperature-dependant, depending on the fluidity of the bilayer.[13]

3.1.2 Lipid oxidation

Phospholipids are generally oxidised via one of two methods: 1) a free radical chain mechanism (also termed peroxidation or autoxidation); or 2) by ozonolysis.

3.1.2.1 Free radical chain mechanism

The free radical chain oxidation mechanism is composed of three stages: initiation, propagation, and termination (Scheme 3.1). The mechanism is initiated by the loss of a hydrogen radical, which can be caused by heat, light, or the presence of trace metals, and leaves the lipid as a radical.[14] The lipid radical then reacts with dissolved oxygen to form a peroxy radical in the first propagation step. The peroxy radical can then react with more non-radical lipid molecules, removing H· and forming a hydroperoxide, the primary product of lipid peroxidation, and further propagating the reaction.

$$\textbf{Initiation: } RH \rightarrow H\cdot + R\cdot$$
$$\textbf{Propagation}: R\cdot + O_2 \rightarrow ROO\cdot$$
$$ROO\cdot + RH \rightarrow R\cdot + ROOH$$
$$\textbf{Termination: } 2ROO\cdot \rightarrow [ROOOOR] \rightarrow \text{nonradical products and } O_2$$
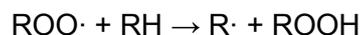
Scheme 3.1. Free radical peroxidation of lipids.[14]

Lipids with polyunsaturated acyl chains are more likely to undergo free radical oxidation, due to the increased stability of the allyl radical through the ability to delocalize an unpaired electron, but lipids with monounsaturated chains also undergo peroxidation. Six hydroperoxide products of methyl oleate have been identified, and a mechanism of competing peroxyl rearrangement and H-atom abstraction proposed for their formation (Scheme 3.2).
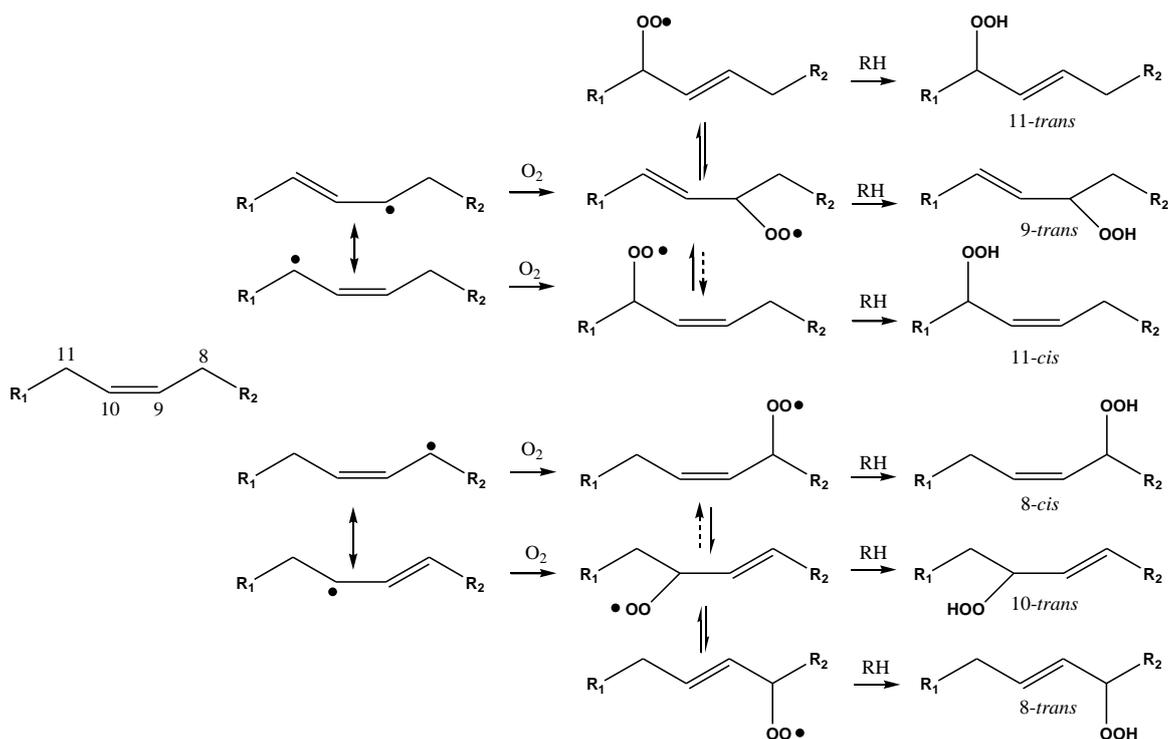
R$_1$ = C$_7$H$_{15}$, R$_2$ = (CH$_2$)$_6$COOCH$_3$, RH = methyl oleate

Scheme 3.2. The primary oxidation products of methyl oleate.

The primary hydroperoxide oxidation products can degrade to secondary products. These include allylic enones, saturated epoxy esters, unsaturated dihydroxy, saturated dihydroxy esters and aldehydes (Scheme 3.3).[15–17]

A

B

R = acyl end of chain; R' = ester end of chain
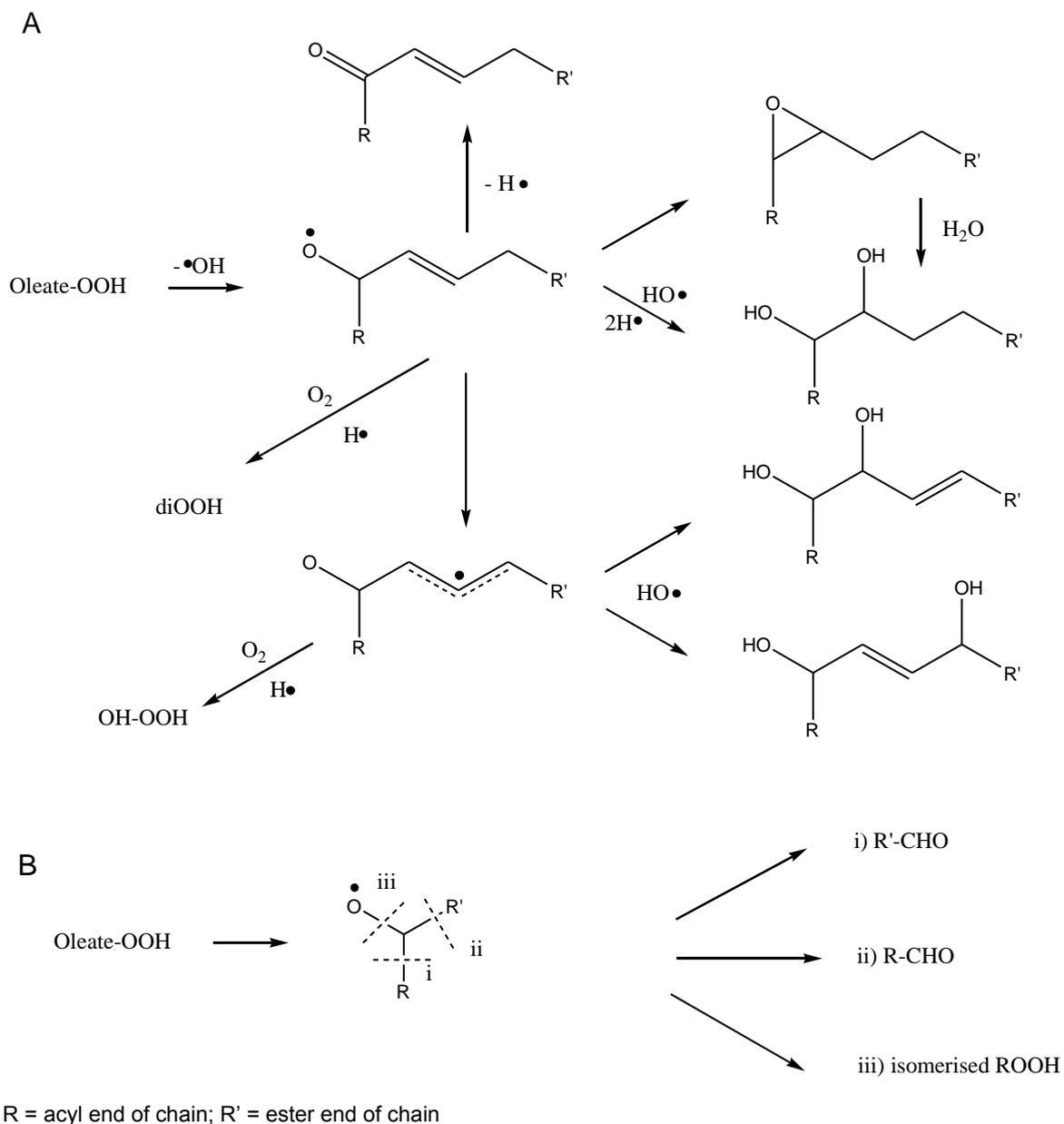
Scheme 3.3. Secondary autoxidation products of methyl oleate. A) Non chain-shortening products; B) chain shortening products. Note from Scheme 3.2 that the initial oxygen radical can be situated on position 8, 9, 10 or 11 of the chain, therefore on the ester or the tail side of the chain relative to the double bond, so different products are possible.

Since peroxidation is initiated by light, heat or the presence of trace metal ions, the elimination of any of these reduces the chance of peroxidation. Reducing the availability of oxygen by the presence of an inert atmosphere also lessens the likelihood of peroxidation occurring.[3]

3.1.2.2 Ozonolysis

Ozonolysis of fatty acid chains has been shown to initially cause formation of an aldehyde and a hydroxyl hydroperoxide. The hydroxyl hydroperoxide then eliminates

H_2O_2, forming a second aldehyde. Further oxidation of the aldehydes can cause formation of carboxylic acids (Scheme 3.4).[18]
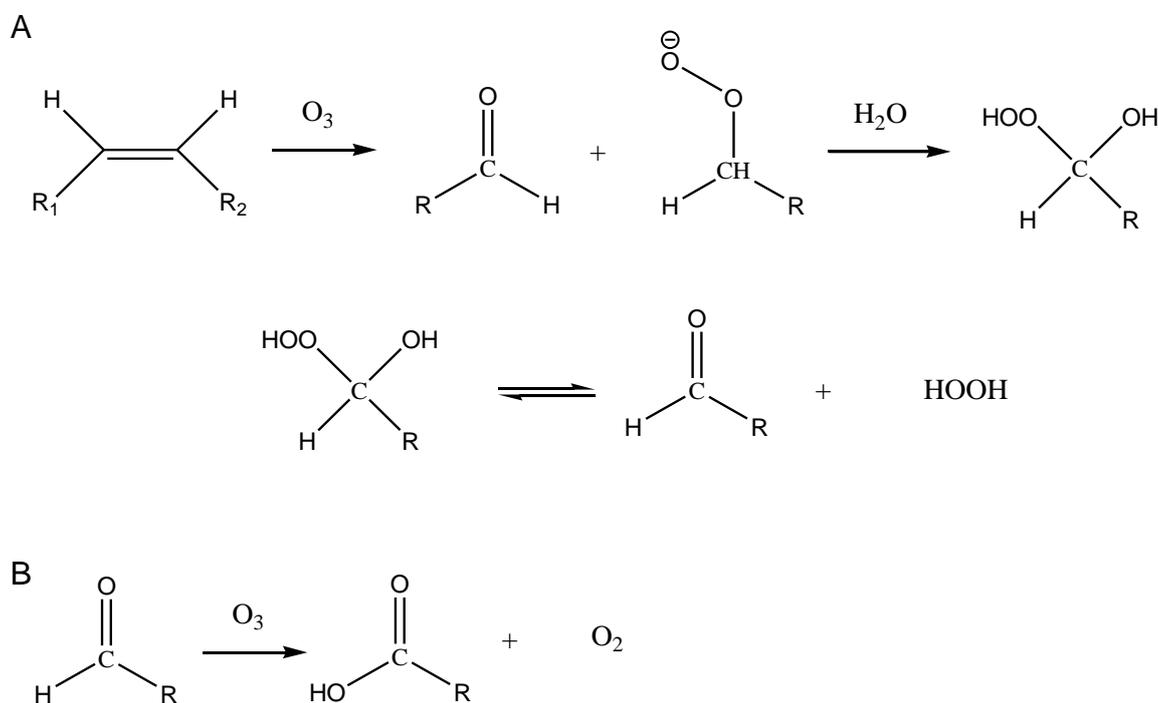
Scheme 3.4. Ozonolysis of double bonds. A) Initial reaction; B) oxidation of aldehyde product with second ozone molecule.

3.1.2.3 Physical effects of oxidation

The oxidation of phospholipids causes a number of chemical changes including the shortening of acyl chains (where aldehydes and carboxylic acids have been formed), a decrease in unsaturation and the addition of polar, and hydrogen-bonding, groups such as carbonyls, hydroxides and peroxides. These have a number of physical effects on bilayer properties. Analysis of mixed monolayers of DPPC with either 1-palmitoyl-2-(9´-oxo-nonanoyl)-*sn*-glycero-3-phosphocholine (PoxnoPC) (Figure 3.2A) or 1-palmitoyl-2-azelaolyl-*sn*-glycero-3-phosphocholine (PazePC) (Figure 3.2B) has shown that the presence of either causes an expansion of lipid monolayers.[19] At high pressures, both are released from the monolayer and form micelles in the aqueous subphase. It has also been proposed that the azelaolyl chain of PazePC bends back through the bilayer to enable the polar group to reside in the membrane-water interface rather than within the hydrophobic region of the bilayer. This was suggested from data showing that bilayers containing PazePC interact with cytochrome *c* in similar way to vesicles composed of acidic lipids such as POPG (Figure 3.3).
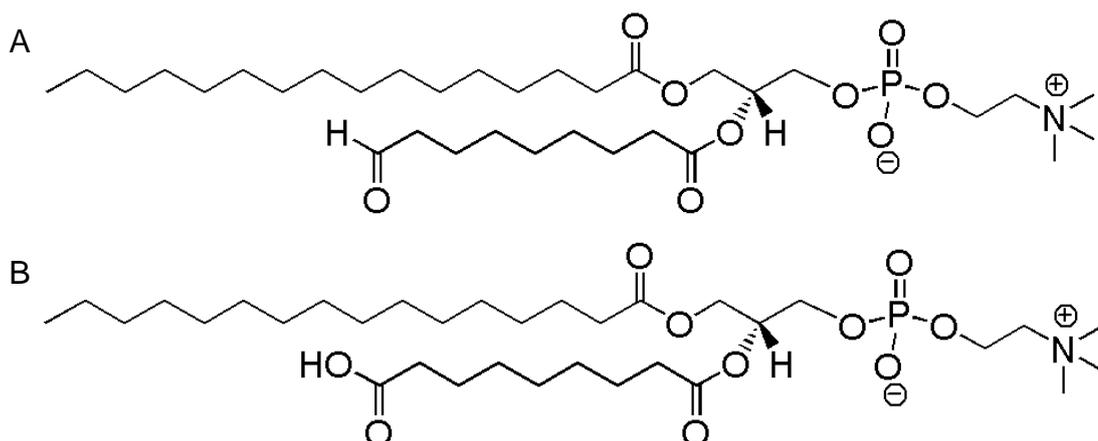
Figure 3.2. A) PoxnoPC, B) PazePC
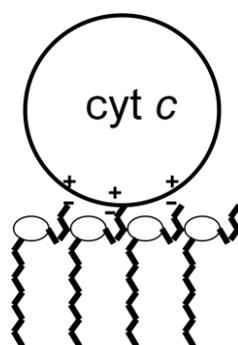
Figure 3.3. Proposed interaction of PazePC with cytochrome *c.*

3.1.3   Melittin

Melittin is an α-helical antimicrobial peptide and is the main protein component of European honey bee (*Apis mellifera*) venom.   It has powerful hemolytic properties, causing the leakage of haemoglobin from erythrocytes at concentrations above 1 µg/mL.[20] Honey bee venom also contains the enzyme phospholipase A_2 (PLA_2). PLA_2 hydrolyses phospholipids at the *sn*-2 position.[21]   This hydrolysis requires catalysis by Ca^{2+}. Commercially-supplied samples of natural melittin contain small amounts of this enzyme, and the observation of lipid hydrolysis in the presence of melittin is attributed to its presence, for example it is reported that the presence of melittin enhances the hydrolysis of lipids by PLA_2 without suggesting that any hydrolysis might be caused by the melittin itself.[22]   The addition of 5 mM EDTA to buffers used for experiments involving natural melittin inhibits the action of PLA_2 through chelation of Ca^{2+}.[20]   It has been proposed that melittin and PLA_2 have a synergistic effect when acting on lipid bilayers.   This has been observed by different methods, including ac impedance analysis of supported bilayers on gold surfaces.[23]   This method allows sensitive detection of changes in conductance and capacitance caused by the formation of defects in lipid membranes.   The effect of natural melittin on a supported POPC bilayer was investigated in the presence and absence of 5

mM EDTA. In the presence of EDTA, low concentrations (1.6 µM) of melittin caused a decrease in capacitance and conductance consistent with adsorption to the surface rather than penetration into the bilayer. The capacitance and conductance were monitored and remained stable for 10 minutes. Higher concentrations of melittin caused an increase in capacitance and conductance correlating to penetration of the peptide into the bilayer and the formation of defects. These effects were small in comparison to those observed in the absence of EDTA however, where the addition of melittin at a low concentration (2 µM) caused an increase in capacitance and conductivity which continued linearly for over 2 hours. Pure PLA_2 applied to the supported bilayer at a concentration comparable to those found in commercial samples (0.03 U mL^{-1}) had only a slight effect on electrical parameters, and addition at a larger concentration (0.1 U mL^{-1}) still had a much smaller effect than that observed for melittin in the absence of EDTA.

3.1.4 Action of small molecules on liposomes

3.1.4.1 Cationic amphiphilic drugs

Cationic amphiphilic drugs have been shown to catalyse the hydrolysis of lipid membranes.[24] Two examples of this class of compounds which have been studied in depth are haloperidol and spiperone (Figure 3.4).[24, 25]
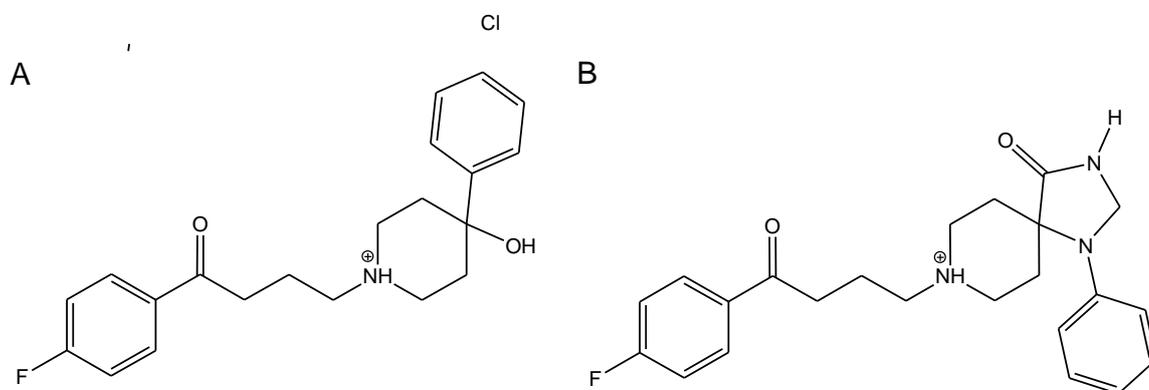
Figure 3.4. A) Haloperidol, B) spiperone.

Casey *et al.* postulated that the weakly acidic quaternary amines act as the source of protons for acid-catalyzed ester hydrolysis.[25] The degradation of lipid bilayers into fatty acids and lyso-lipids is thought to provide a method of translocation and transport for the drug molecules. The lyso-lipids bud off from the bilayer as micelles with drug molecules incorporated inside. The micelles transport the molecules to neighbouring bilayers, bind, and allow the process to be repeated.

3.1.4.2 Alcohols

Small alcohols such as trifluoroethanol (TFE) and 1,1,1,3,3,3-hexafluoroisopropanol (HFIP) have been shown to disrupt lipid bilayers, increasing lateral pressure and causing the leakage of liposome contents.[26] This is thought to be caused by the insertion of the alcohol molecules in between the headgroups in the bilayer, increasing the lateral pressure in this region while decreasing it in the chain region. HFIP was shown to have the greatest effect on bilayers out of methanol, ethanol, isopropanol, propanol, TFE, butanol and HFIP.[26] This supports the theory that the alcohol sits in the headgroup region, as the alcohol hydroxyl groups are thought to hydrogen bond to the phosphate oxygens, and HFIP is the best hydrogen-bond donor of the alcohols tested.[27] Ennaceur and Sanderson studied the effects of HFIP on lipid membranes in aqueous solution, finding a marked decrease in the stability of the bilayer with saturated lipids, which degraded to form mixed HFIP/lipid particles, though this was not observed with unsaturated lipids.[27] They observed physical changes to the lipid membrane using a number of methods including small-angle X-ray scattering (SAXS), differential scanning calorimetry (DSC) and electron microscopy (EM).

3.1.5 The limitations of current research and scope of this research

The work in this section describes studies into the stability of liposomal phospholipids under certain conditions. Having explored the use of MALDI-TOF and TOF/TOF for the identification of phospholipids, the technique was applied to the study of modified phospholipids, partly to complement and assist with the studies of melittin and other antimicrobial peptides by the group of Professor Alison Rodger, and partly to explore current theories as to the actions of certain species on lipids from a different angle. Professor Rodger reported changes in the circular and linear dichroism spectra of antimicrobial peptides depending on the age of the liposomes to which they were binding, and proposed that this may be due to hydrolysis or oxidation of the liposomal lipids during storage.[28] Analyses by MALDI-MS to look for any chemical changes to the lipids under the conditions applied were complemented by DLS and TEM to observe any physical changes such as aggregation, fusion or micellisation.

3.1.5.1 Hydrolysis and oxidation

The hydrolysis and oxidation of lipid acyl chains has been shown to be dependent upon a number of conditions (see Sections 3.1.1 and 3.1.2), making it hard to predict the stability of a specific liposome dispersion and what changes the liposomes may undergo before use in analyses. Following Prof. Rodger's report, a number of experiments were

carried out in an attempt to identify any changes which may have been occurring within the liposomes to affect their stability and permeability.

3.1.5.2 Melittin

The hydrolysis of membrane lipids in the presence of melittin is generally attributed to the presence of PLA$_2$.[22] No reference could be found in the literature which attributed hydrolysis to the effect of melittin itself on liposomal lipids. The research described here aims to determine any chemical effect melittin may have on lipids in the absence of PLA$_2$ and the extent of hydrolysis catalysed by PLA$_2$.

3.1.5.3 Small molecules

The physical effect of HFIP on lipid bilayers has been well reported, but questions remain as to whether any chemical effects accompany them. Since the hydrolysis effects of the cationic amphiphilic drug haloperidol on lipids has already been studied comprehensively, it was deemed to be a good model to support a study of the chemical stability of lipids under different conditions.

3.2 Results and discussion

3.2.1 Liposome stability in different buffers

3.2.1.1 DOPC

3.2.1.1.1 Bis-tris propane

The rate of hydrolysis of DOPC liposomes in water and bis-tris propane buffer (10 mM, pH 7) was compared to determine whether the buffer had an effect on lipid hydrolysis. Both samples were stored at 4 °C. After preparation and after 2, 6, 7, 15, 18 and 20 days a sample of each was removed and analysed by MALDI-MS. Figure 3.5 shows the intensity of the peak corresponding to [DOPC – RCO]$^+$ normalised relative to the combined intensities of the peaks corresponding to [DOPC + H]$^+$ and [DOPC – RCO]$^+$.
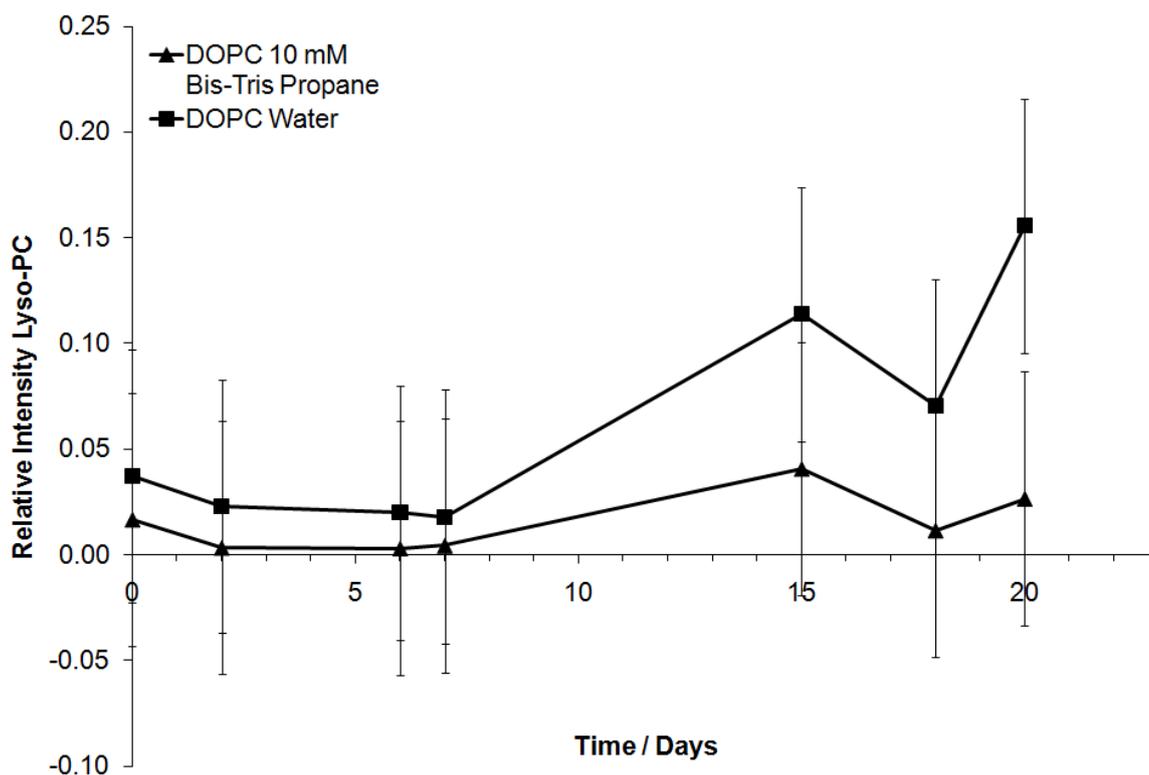
Figure 3.5. MS intensity profile of [DOPC – RCO]$^+$ for DOPC liposomes in 10 mM bis-tris propane or water. Intensity of the peak corresponding to [DOPC – RCO]$^+$ was normalised relative to the combined intensities of the peaks corresponding to [DOPC + H]$^+$ and [DOPC – RCO]$^+$ for DOPC liposomes in 10 mM bis-tris propane or water stored at 4 °C for 20 days. Errors are estimated from the values obtained from repeat measurements.

The DOPC liposomes were not observed to have undergone any hydrolysis, within error, in bis-tris propane or in water over 20 days (Figure 3.5).

3.2.1.1.2 Tris

DOPC was incubated at 4 °C in water and tris buffer (10 mM, pH 7.4) for 12 days with MALDI-MS analyses after preparation and after 2, 5, 7, 9 and 12 days. No overall increase in lyso-PC could be observed over the analysis period in either sample (Figure 3.6).
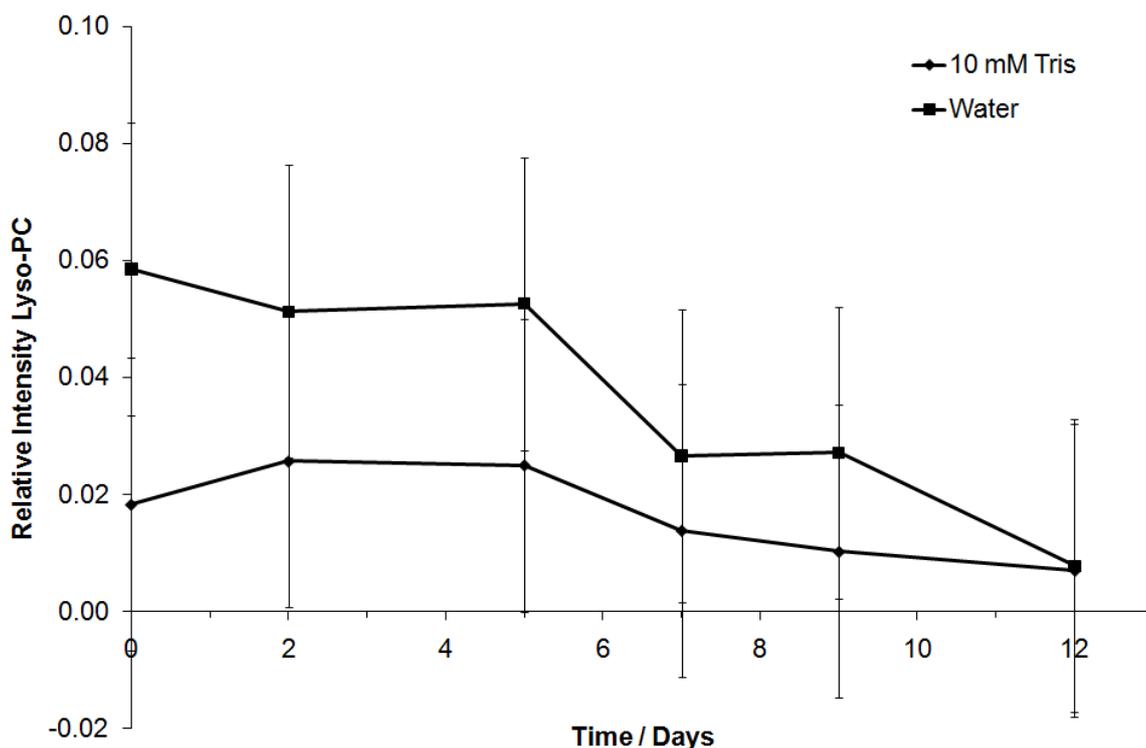
Figure 3.6. MS intensity profile of [DOPC – RCO]$^+$ for DOPC liposomes in 10 mM tris or water. Intensity of the peak corresponding to [DOPC – RCO]$^+$ was normalised relative to the combined intensities of the peaks corresponding to [DOPC + H]$^+$ and [DOPC – RCO]$^+$ for DOPC liposomes in 10 mM tris or water stored at 4 °C for 12 days. Errors are estimated from the values obtained from repeat measurements.

3.2.1.1.3 *Phosphate and NaCl buffer with and without EDTA*

EDTA is added to buffers when natural melittin is analysed in order to chelate Ca^{2+} and prevent the activity of phospholipase A$_2$, which is always present as a contaminant, from masking the actions of the peptide. Figure 3.7 shows the intensity of the peak corresponding to [DOPC – RCO]$^+$ normalised relative to the combined intensities of the peaks corresponding to [DOPC + H]$^+$ and [DOPC – RCO]$^+$ for DOPC liposomes stored at 37 °C in a buffer of 10 mM phosphate and 150 mM NaCl (pH 7) with and without 1 mM EDTA. Although the graph suggests a slight increase in lyso-PC over the first three days in both samples, the overall intensity of lyso-PC compared to DOPC remained very low over the course of the analysis period, and the variation is within an error of ± 1%. There is no suggestion from the data that either the 10 mM phosphate and 150 mM NaCl buffer, the presence of 1 mM EDTA or storage at 37 °C enhances or inhibits lipid hydrolysis.
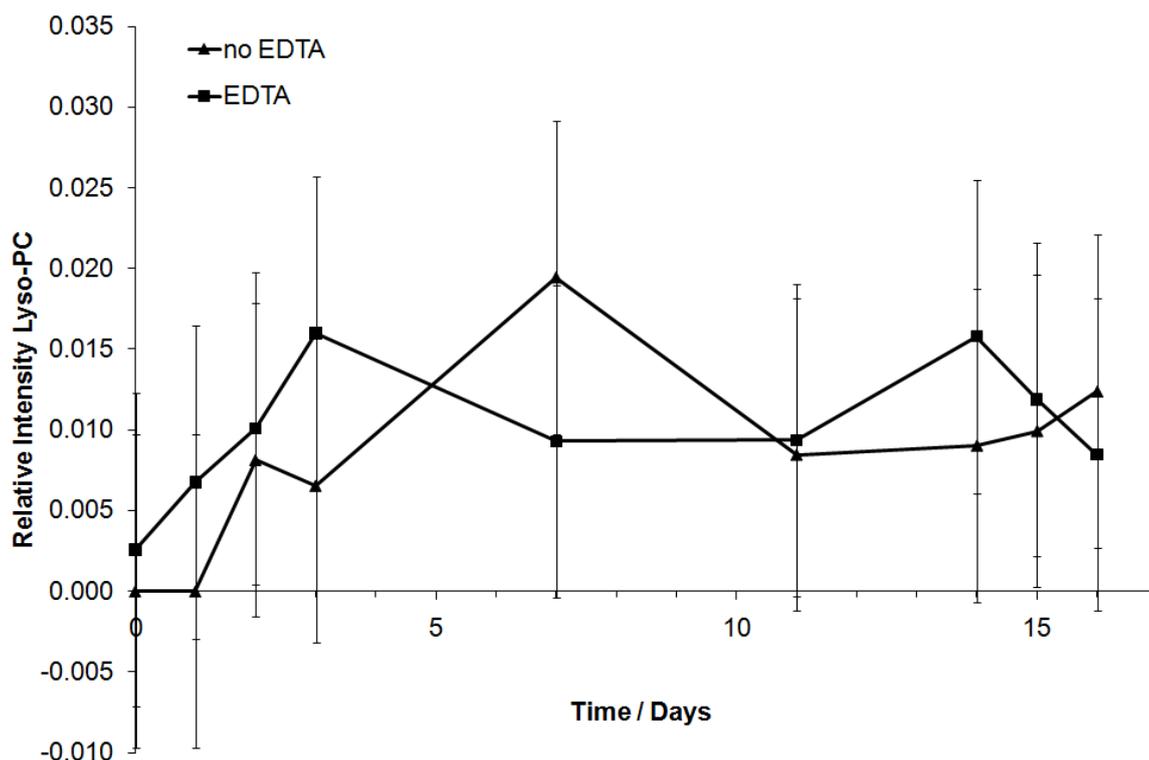
Figure 3.7. MS intensity profile of $[DOPC - RCO]^+$ for DOPC liposomes in 10 mM phosphate and 150 mM NaCl with and without 1 mM EDTA. Intensity of the peak corresponding to $[DOPC - RCO]^+$ was normalised relative to the combined intensities of the peaks corresponding to $[DOPC + H]^+$ and $[DOPC - RCO]^+$ for DOPC liposomes in 10 mM phosphate and 150 mM NaCl with and without 1 mM EDTA stored at 37 °C for 15 days. Errors are estimated from the values obtained from repeat measurements.

3.2.1.2 DPPC

3.2.1.2.1 Bis-tris propane

DPPC and DOPC differ in the length and degree of unsaturation of their acyl chains, and are in different phases at room temperature (T_m DOPC = -20 °C, T_m DPPC = 41 °C).[29] The acyl chains of DOPC are 18 carbon atoms long and contain a double bond, whereas the chains of DPPC are 16 carbons long and fully saturated. DPPC liposomes were made and analysed in the same way as the DOPC liposomes in water and in bis-tris propane buffer (10 mM, pH 7), stored at 4 °C and analysed by MALDI-MS after preparation and 2, 6, 7, 15, 18 and 28 days after extrusion to look for an increase in lyso-PC caused by hydrolysis. As shown in Figure 3.7, no increase in lyso-PC was observed either in water or in bis-tris propane over the analysis period.
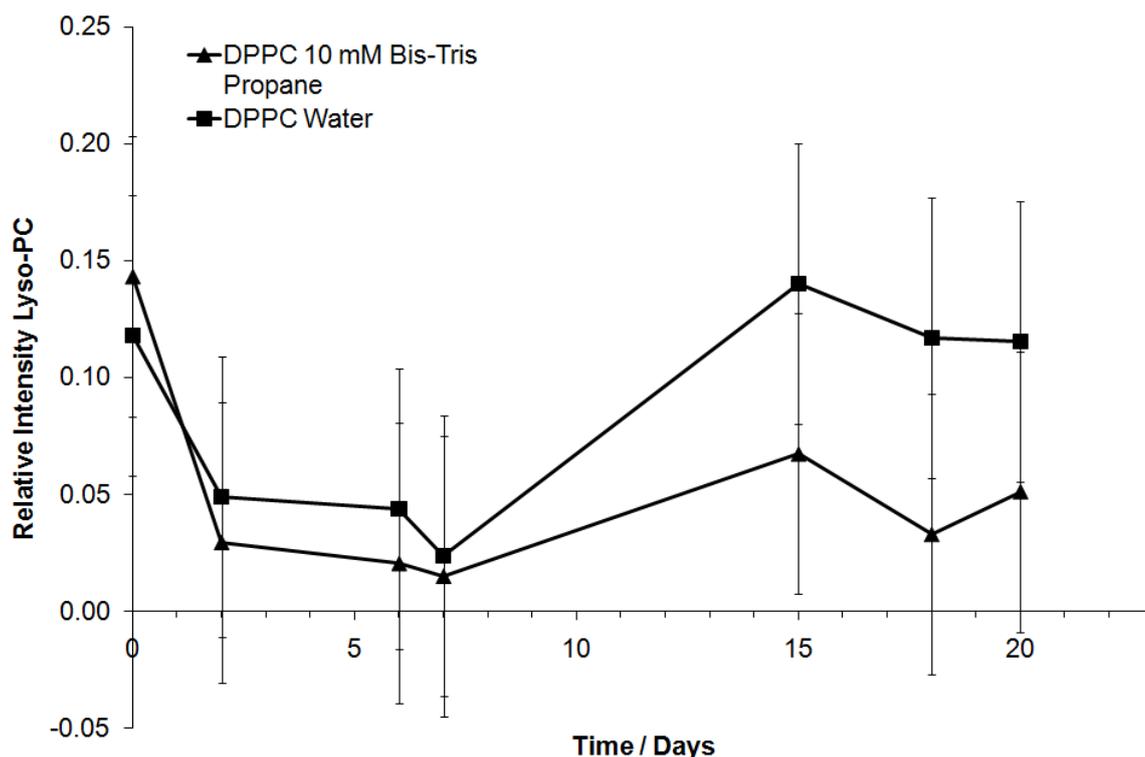
Figure 3.8. MS intensity profile of [DPPC – RCO]$^+$ for DPPC liposomes in10 mM bis-tris propane or water. Intensity of the peak corresponding to [DPPC – RCO]$^+$ was normalised relative to the combined intensities of the peaks corresponding to [DPPC + H]$^+$ and [DPPC – RCO]$^+$ for DPPC liposomes in 10 mM bis-tris propane or water stored at 4 °C for 18 days. Errors are estimated from the values obtained from repeat measurements.

3.2.1.3 Discussion

The results show that DOPC and DPPC are stable with respect to hydrolysis for at least two weeks in water and with a number of commonly used buffers, when stored in the fridge and at 37 °C. This result correlates with literature reports of stability or instability of lipids with respect to hydrolysis. The lipids both have neutral phosphocholine headgroups, which have been shown to make them less susceptible to hydrolysis than those with negatively charged phosphoethanolamine headgroups.[3, 9, 10] The pH was 7 or 7.4 in the buffered samples and 7 in the samples in water, which decreases the chance of acid- or base-catalysed hydrolysis.[30] Storage at 37 °C has been shown to increase the rate of hydrolysis of some lipids,[5] but no increase in hydrolysis was observed in these analyses.

3.2.2 Lipid oxidation

All of the MALDI-MS spectra of the DOPC liposome samples and the DOPC lipid stock solution contained peaks at *m/z* 676.4 (Figure 3.10). The intensity of the peak varied between spectra, with a maximum approximately half that of the protonated

molecular ion. The peak was tentatively assigned as the protonated oxidation product OoxnoPC (Figure 3.9). A weak peak was also observed at *m/z* 566.9 in the spectra of some samples (Figure 3.10), which was thought to correspond to the protonated doubly oxidised species DoxnoPC (Figure 3.9). A peak, again of varying intensity, was observed at *m/z* 650.4 in the MALDI-MS spectra of POPC liposome solutions and lipid stock, which was thought to correspond to protonated PoxnoPC (Figure 3.9).

OoxnoPC[a]
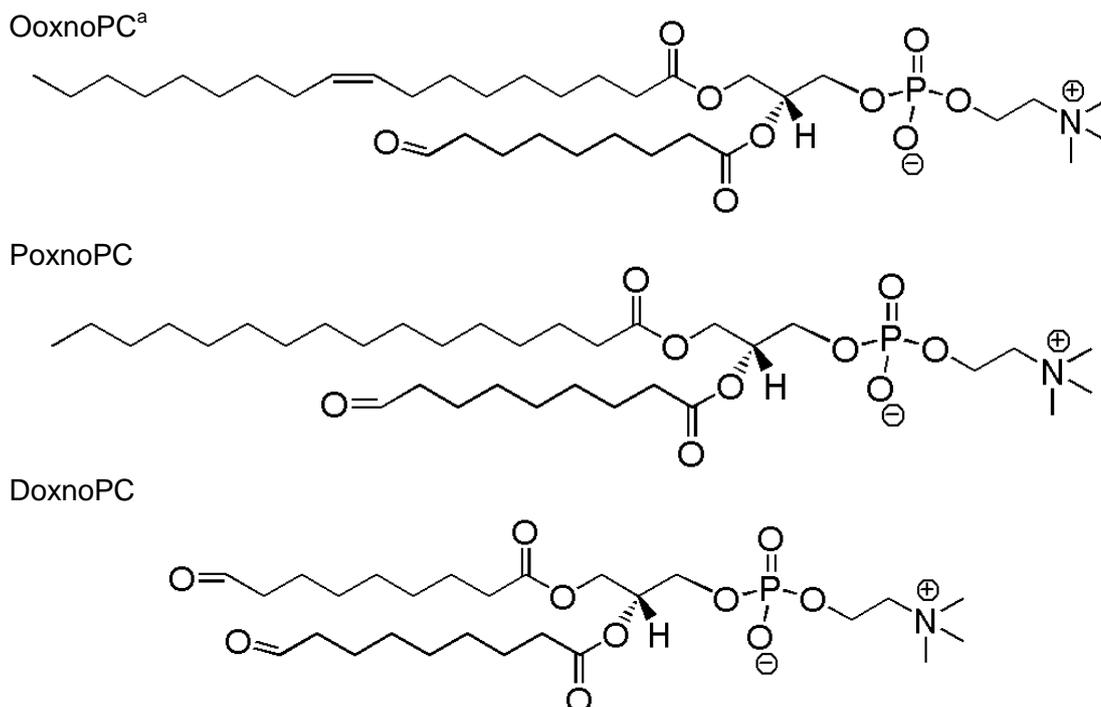
PoxnoPC

DoxnoPC

Figure 3.9. Proposed structures of single oxidation products of DOPC (OoxnoPC), POPC (PoxnoPC); and the double oxidation product of DOPC (DoxnoPC).

    a)   Oxidation of OoxnoPC could occur on either chain
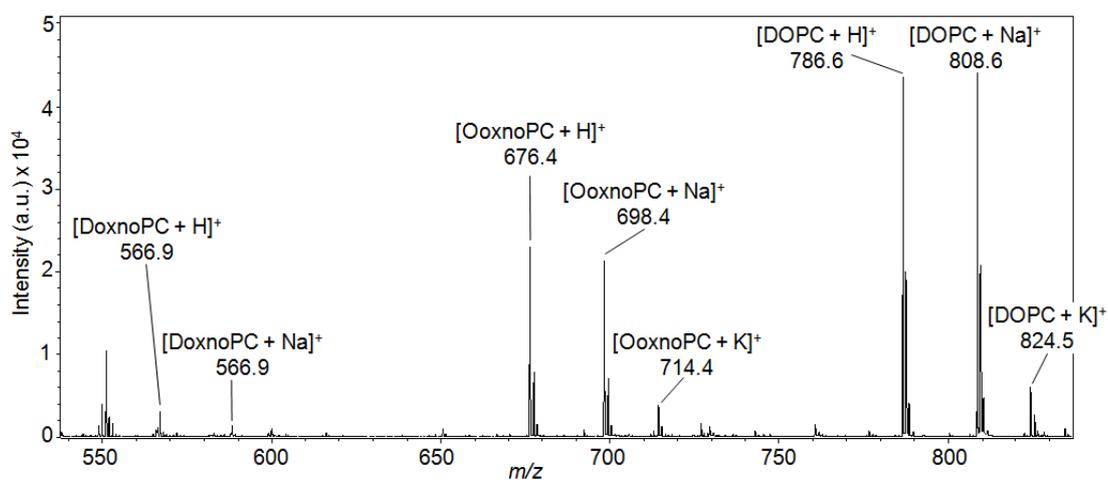
Figure 3.10. MALDI-MS spectrum of DOPC liposomes showing the singly and doubly oxidised lipid (OoxnoPC and DoxnoPC respectively). The sample was prepared by mixing DOPC liposome dispersion (0.5 mg/mL) 2:9 with DHB (30 mg/mL in 50:50 EtOH/water).

3.2.2.1 DOPC oxidation

The proposed DOPC oxidation product was analysed by MALDI-MSMS in the presence of Li^+ and Na^+ and in the absence of added salt in order to determine its structure (Figure 3.11A, B and C respectively and Table 3.1).
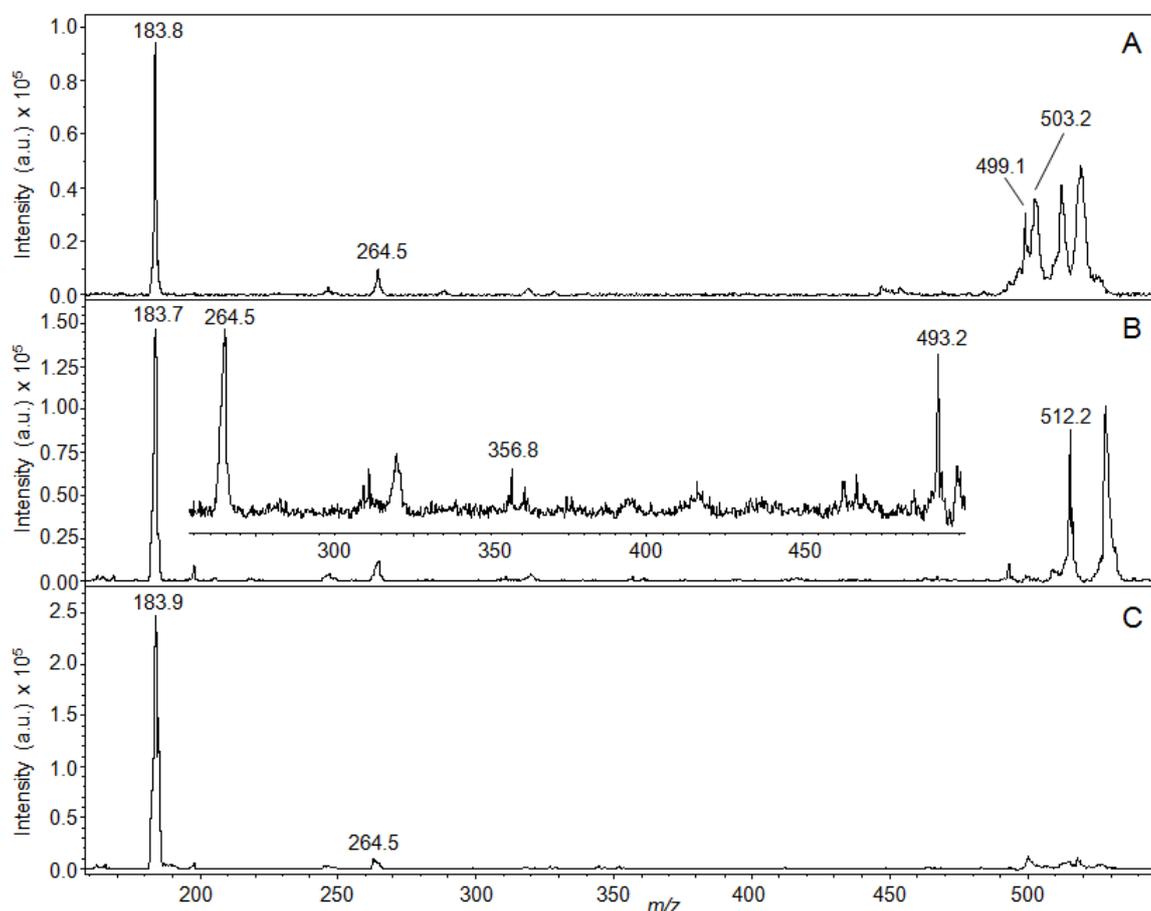
Figure 3.11. MALDI-MSMS spectra of proposed oxidation product of DOPC A) with Li^+, B) with Na^+ and C) in the absence of added salt. The samples were prepared by mixing dispersions of the liposomes in water (0.5 mg/mL) 2:9 (v/v) with solutions of DHB (30 mg/mL) in $EtOH/H_2O$ (50% v/v), for the protonated ion, or LiCl (100 mM) or NaCl (100 mM) and DHB (30 mg/mL) in $EtOH/H_2O$ (50% v/v) for each of the salt adducts respectively.

Table 3.1. Product ions observed in the MALDI-MSMS spectra of the proposed DOPC oxidation product in the presence of Li^+ and Na^+ and in the absence of added salt.

[OoxnoPC + Li][+a]		[OoxnoPC + Na]$^+$	
m/z	Product ion	*m/z*	Product ion
183.8	$[OP(O)_2OCH_2CH_2NMe_3 + 2H]^+$	183.7	$[OP(O)_2OCH_2CH_2NMe_3 + 2H]^+$
264.5	$[RCO]^+$	264.5	$[RCO]^+$
499.1	$[OoxnoPC - OP(O)_2OCH_2CH_2NMe_3 - H + Li]^+$	356.8	$[OoxnoPC - RCOO - NMe_3 - H + Na]^+$
503.2	$[OoxnoPC - HC(O)(CH_2)_7COO]^+$	493.2	$[OoxnoPC - OP(O)_2OCH_2CH_2NMe_3]^+$
		512.2	$[OoxnoPC - OP(O)_2OCH_2CH_2NMe_3 - H + Na]^+$

[OoxnoPC + H]$^+$	
m/z	Product ion
183.9	$[OP(O)_2OCH_2CH_2NMe_3 + 2H]^+$
264.5	$[RCO]^+$

a) R corresponds to the non-oxidised acyl chain

125

The MALDI-MSMS spectrum of [OoxnoPC + Li]$^+$ contained two peaks from which the oxidised and non-oxidised acyl chains could be identified (Figure 3.11A, Table 3.1). These were observed at m/z 264.5 and m/z 503.2, and corresponded to [RCO]$^+$ and [OoxnoPC − HC(O)(CH$_2$)$_7$COO]$^+$ respectively. Two peaks were observed which confirmed the identity of the molecule as a PC lipid, at m/z 183.8, m/z 499.1 corresponding [OP(O)$_2$OCH$_2$CH$_2$NMe$_3$ + 2H]$^+$ and [OoxnoPC − OP(O)$_2$OCH$_2$CH$_2$NMe$_3$ − H + Li]$^+$ respectively. Similar fragments were identified in the fragmentation spectrum of the sodium adduct (Figure 3.11B, Table 3.1). Two peaks were observed which allowed the identification of the oxidised and non-oxidised acyl chains, at m/z 264.5 and m/z 356.8 corresponding to [RCO]$^+$ and [OoxnoPC − RCO − NMe$_3$ − H + Na]$^+$. The PC headgroup was identified from peaks corresponding to [OP(O)$_2$OCH$_2$CH$_2$NMe$_3$ + 2H]$^+$, [OoxnoPC − OP(O)$_2$OCH$_2$CH$_2$NMe$_3$]$^+$ and [OoxnoPC − OP(O)$_2$OCH$_2$CH$_2$NMe$_3$ − H + Na]$^+$ at m/z 183.7, m/z 493.2 and m/z 512.2 respectively. Little information about the structure of the proposed oxidation product could be determined from the MSMS spectrum of [OoxnoPC + H]$^+$ (Figure 3.11C, Table 3.1). Only the PC headgroup and the oleoyl chain could be identified, from peaks at m/z 183.9 and m/z 264.5 corresponding to [OP(O)$_2$OCH$_2$CH$_2$NMe$_3$ + 2H]$^+$ and [RCO]$^+$.

The MALDI-MSMS spectra confirmed the identity of the oxidised species proposed in Figure 3.9. The oxidised chain was identified through the loss of HC(O)(CH$_2$)$_7$COO; the intact acyl chain was identified through different peaks corresponding to the loss of RCOO and through peaks corresponding to [RCO]$^+$. The presence of the phosphocholine headgroup was also confirmed, through fragments involving its neutral loss and to the presence of peaks corresponding to [OP(O)$_2$OCH$_2$CH$_2$NMe$_3$ + 2H]$^+$ in all of the product ion spectra. MALDI-MS analysis was carried out on an unopened batch of DOPC which was dissolved in CHCl$_3$ immediately before analysis as opposed to the old sample which had been stored in the freezer as a solution in CHCl$_3$ for a number of months. Evidence of oxidation was also observed in the new batch (data not shown).

The identification of the oxidised DOPC molecule was further supported by accurate mass MS analysis. A peak corresponding to the oxidised lipid was observed at m/z 676.45540. An elemental composition search on this m/z value produced only one match with the correct P and N composition for a phospholipid, namely C$_{35}$H$_{67}$O$_9$N$_1$P$_1$, with an error of -0.09 mmu. This composition (with 1H subtracted to account for protonation) matches that of the suggested structure of OoxnoPC in Figure 3.9.

The intensity of the peak corresponding to the proposed doubly oxidised species was too low for MALDI-MSMS or accurate mass analysis by FT-MS to be carried out, therefore its structure could not be conclusively identified.

Proton NMR studies were carried out on a DOPC sample which, from MALDI-MS analysis, contained the oxidation product. It was predicted that the oxidised species would cause a peak at 9.5–10 ppm corresponding to the aldehyde proton. The NMR spectrum only showed peaks corresponding to the protons of DOPC however. This suggests that, while the peaks are clearly visible in MALDI-MS spectra, there was very little of the oxidised species present in the lipid and liposome samples. This implies that it is very easily ionised compared to the intact lipid and most of its other decomposition products. It also explains why the intensity of the peak corresponding to the oxidation product is inconsistent from analysis to analysis. If the concentration is extremely low yet a clear peak can be observed, very slight changes in the composition of each sample will have greatly magnified effects on the intensity of this peak.
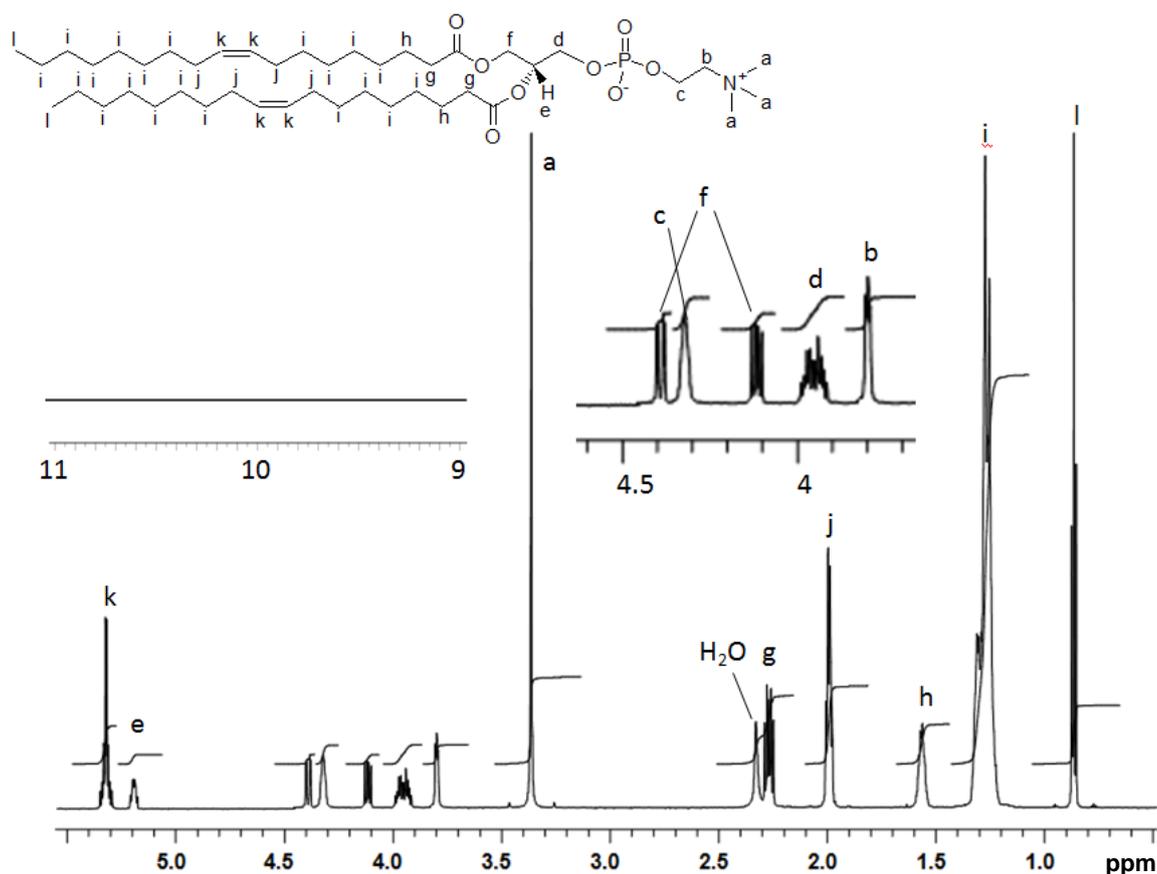
Figure 3.12. The ^{1}H NMR spectrum at 700 MHz in CDCl$_3$ of a sample of DOPC from which OoxnoPC had been observed by MALDI-MS.

3.2.2.2 POPC oxidation

MALDI-MSMS was carried out on the possible analogous POPC oxidation product in the presence of lithium, sodium and in the absence of added salt.
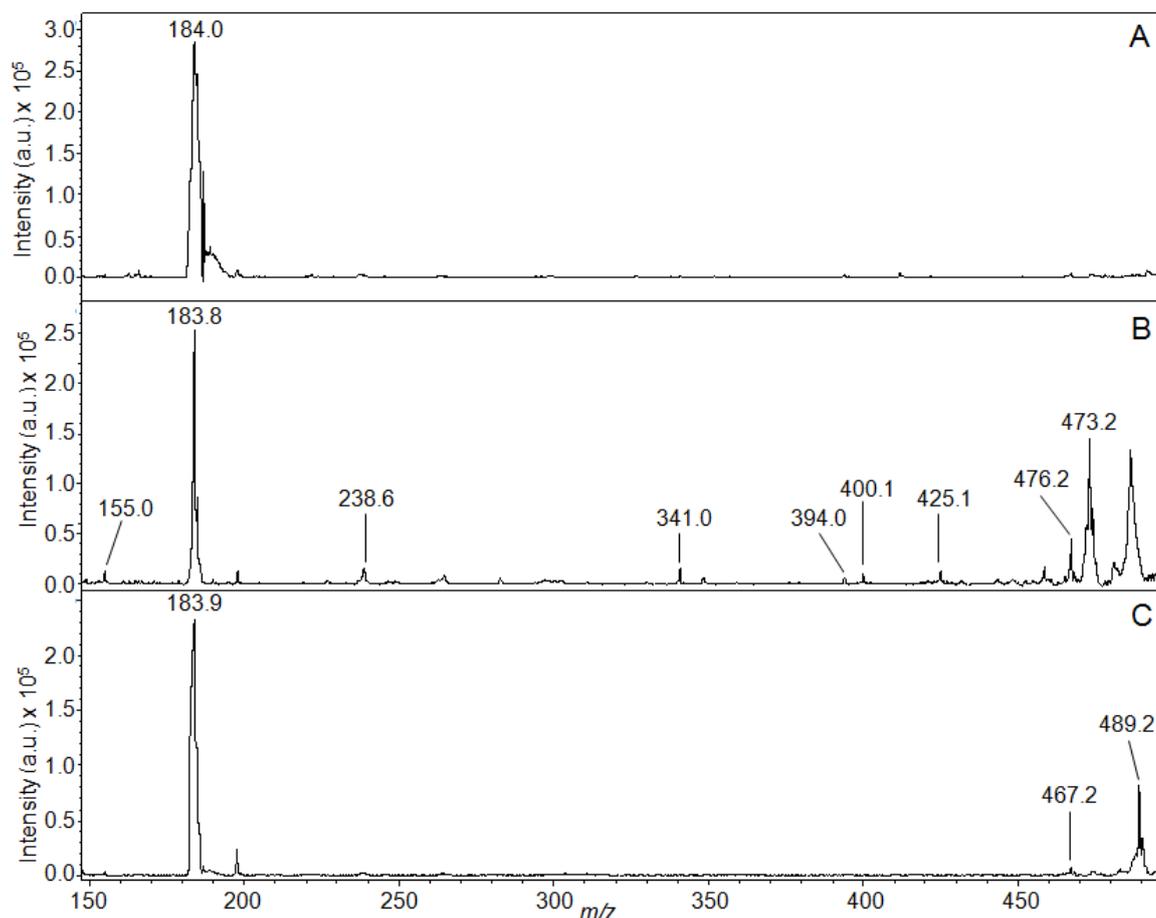
Figure 3.13. MALDI-MSMS spectra of A) [PoxnoPC + H]$^+$, B) [PoxnoPC + Li]$^+$ and C) [PoxnoPC + Na]$^+$. The samples were prepared by mixing solutions of the lipids in CHCl$_3$ (1 mg/mL) 1:9 (v/v) with solutions of DHB (30 mg/mL) in EtOH/H2O (50% v/v), for the protonated ion, or LiCl (100 mM) or NaCl (100 mM) and DHB (30 mg/mL) in EtOH/H2O (50% v/v) for each of the salt adducts respectively.

The MALDI-MSMS spectrum of [PoxnoPC + H]$^+$ (Figure 3.13A) only allowed identification of the headgroup, from a peak corresponding to [OP(O)$_2$OCH$_2$CH$_2$NMe$_3$ + 2H]$^+$ at *m/z* 184.0. Much more information could be gained from the MSMS spectrum of [PoxnoPC + Li]$^+$ (Figure 3.13B, Table 3.2). This spectrum allowed full identification of the oxidised species and confirmed its identity as PoxnoPC (Figure 3.9). The oxidised oleoyl chain could be identified directly from the peak at *m/z* 155.0, corresponding to [HC(O)(CH$_2$)$_7$C(O)H]$^+$, and also from peaks corresponding to its loss (*m/z* 425.1, [PoxnoPC – HC(O)(CH$_2$)$_7$COO – NMe$_3$ – H + Li]$^+$) and to the loss of the palmitoyl chain from the *sn*-1 position at *m/z* 341, *m/z* 394.0 and *m/z* 400.1, corresponding to [PoxnoPC – R$_1$COO – NMe$_3$ – H + Li]$^+$, [PoxnoPC – R$_1$COO]$^+$ and [PoxnoPC – R$_1$COO – H + Li]$^+$

respectively. The peaks corresponding to the loss of the headgroup with and without Li^+, [PoxnoPC – $OP(O)_2OCH_2CH_2NMe_3$]$^+$ and [PoxnoPC – $OP(O)_2OCH_2CH_2NMe_3$ – H + Li]$^+$ with m/z 467.2 and m/z 473.2 respectively, and to its presence ([$OP(O)_2OCH_2CH_2NMe_3$ + 2H]$^+$, m/z 183.8) support this identification. The MSMS spectrum of [PoxnoPC + Na]$^+$ was not as informative as that of [PoxnoPC + Li]$^+$, but did show peaks corresponding to the headgroup and to its loss at m/z 183.9, m/z 467.2 and m/z 489.2 corresponding to [$OP(O)_2OCH_2CH_2NMe_3$ + 2H]$^+$, [PoxnoPC – $OP(O)_2OCH_2CH_2NMe_3$]$^+$ and [PoxnoPC – $OP(O)_2OCH_2CH_2NMe_3$ – H + Na]$^+$.

Table 3.2. Product ions observed in the MALDI-MSMS spectra of the proposed POPC oxidation product in the presence of Li^+ and Na^+.

[PoxnoPC + Li]$^+$		[PoxnoPC + Na]$^+$	
m/z	Fragment[a]	m/z	Fragment
155.0	[$HC(O)(CH_2)_7CO$ + H]$^+$	183.9	[$OP(O)_2OCH_2CH_2NMe_3$ + 2H]$^+$
183.8	[$OP(O)_2OCH_2CH_2NMe_3$ + 2H]$^+$	467.2	[PoxnoPC – $OP(O)_2OCH_2CH_2NMe_3$]$^+$
238.6	[R_1CO]$^+$	489.2	[PoxnoPC – $OP(O)_2OCH_2CH_2NMe_3$ – H + Na]$^+$
341.0	[PoxnoPC – R_1COO – NMe_3 – H + Li]$^+$		
394.0	[PoxnoPC – R_1COO]$^+$		
400.1	[PoxnoPC – R_1COO – H + Li]$^+$		
425.1	[PoxnoPC – $HC(O)(CH_2)_7COO$ – NMe_3 – H + Li]$^+$		
467.2	[PoxnoPC – $OP(O)_2OCH_2CH_2NMe_3$]$^+$		
473.2	[PoxnoPC – $OP(O)_2OCH_2CH_2NMe_3$ – H + Li]$^+$		

    a) R_1 corresponds to the palmitoyl acyl chain at the *sn*-1 position

The structure of the oxidised POPC molecule was confirmed as that in Figure 3.9. Peaks were observed which corresponded to both the presence and the loss of the oxidised chain, such as that at m/z 154.9 corresponding to [$HC(O)(CH_2)_7CO$]$^+$ in the spectrum of [OoxnoPC + Li]$^+$. The intact palmitoyl chain was also identified, both through the fragment [R_1CO]$^+$ and the loss of R_1COO. Finally, the molecule was identified as a PC lipid from the peak corresponding to the headgroup observed in all of the product ion spectra and the peaks corresponding to the loss of the headgroup observed in the spectra of [PoxnoPC + Li]$^+$ and [PoxnoPC + Na]$^+$.

3.2.2.3 Investigation into method of oxidation

The aldehyde oxidation products identified in samples of DOPC and POPC could have been caused by either ozonolysis or peroxidation. In order to investigate the method of oxidation, DOPC and POPC were analysed by MALDI-MS for evidence of any other species which had undergone peroxidation or ozonolysis through which the mechanism of oxidation could be confirmed.

3.2.2.3.1 DOPC

Tables 3.3 and 3.4 show the theoretical products of the peroxidation or ozonolysis of DOPC and whether any evidence of these species were observed in the MALDI-MS spectrum of DOPC.

Table 3.3. Possible peroxidation products of DOPC and peaks observed in MALDI-MS spectrum of DOPC which may correspond to oxidation products. Note the increase in mass of 1 Da for observed peaks compared to molecular weight of possible oxidation products due to protonation.

DOPC peroxidation product[a]	Theoretical molecular weight (Da)	Observed peak *m/z*
Hydroperoxide (DOPC – H + OOH)	817.6	-
Epoxide (DOPC + O)	801.6	-
Saturated dihydroxy lipid (DOPC + 2OH)	819.6	-
Unsaturated dihydroxy lipid (DOPC – 2H + 2OH)	817.6	-
Dihydroperoxide (DOPC – 2H + 2OOH)	849.6	-
Hydroxy hydroperoxide (DOPC – 2H + OH + OOH)	833.6	834.6
Allylic enone (DOPC – 2H + O)	799.6	800.6
Aldehyde (8)	661.4	-
Aldehyde (9)	675.5	676.5
Aldehyde (10) (unsaturated)	687.5	-
Aldehyde (11) (unsaturated)	701.5	-

a) The aldehydes are numbered according to the position of the aldehyde group, and therefore the point of cleavage of the acyl chain. The unsaturated aldehydes incorporate one double bond.

Table 3.4. Possible ozonolysis products of DOPC and peaks observed in MALDI-MS spectrum of DOPC which may correspond to oxidation products. Note the increase in mass of 1 Da for observed peaks compared to molecular weight of possible oxidation products due to protonation.

DOPC ozonolysis product	Theoretical molecular weight (Da)	Observed peak *m/z*
Aldehyde (9)	675.5	676.5
Hydroxy hydroperoxide (9)	709.5	-
Carboxylic acid (9)	691.4	692.5

Three possible peroxidation products of DOPC were observed (Table 3.3) (including OoxnoPC). It was not possible to fully identify these species, as they were not present in sufficient quantities to carry out MALDI-MSMS analysis. No other aldehyde products were observed. The proposed distribution of the hydroperoxide products of methyl oleate shown in (Scheme 3.2) has been suggested to be dependent on the concentration of the oleate if between 0.3 and 3 M. Higher concentrations within this range cause higher quantities of the kinetic products, 8-*cis*, 9-*trans*, 10-*trans* and 11-*cis* hydroperoxides. At lower concentrations the thermodynamic 8-*trans* and 11-*trans*

hydroperoxide products predominate.[14] The lipid analysis was carried out on a solution of 1.3 mM and the stock solution was 13 mM. Though these concentrations are outside those in the work cited, the low concentrations suggest that the thermodynamic products 8-*trans* and 11-*trans* hydroperoxide should predominate, thereby forming aldehydes at the 8 and 11 positions of the oleate chain.

Two possible ozonolysis products were observed, including OoxnoPC (Table 3.4). Again, it was not possible to carry out MALDI-MSMS analysis on the proposed carboxylic acid species to confirm its identity.

Overall, the possible presence of oxidation products which could only be formed by peroxidation or ozonolysis suggests that both processes had occurred in the lipid during storage. The fact that the aldehyde product observed was the only aldehyde which could be produced by ozonolysis and not the most likely aldehyde product of peroxidation, suggests that ozonolysis may be the primary cause of oxidation of the DOPC stock. Oxidation or photooxidation during MALDI analysis can be ruled out due to the vacuum in the sample chamber.

3.2.2.3.2 POPC

Tables 3.5 and 3.6 show the theoretical products of the peroxidation or ozonolysis of DOPC and whether any evidence of these species were observed in the MALDI-MS spectrum of DOPC.

Table 3.5. Possible peroxidation products of POPC and peaks observed in MALDI-MS spectrum of POPC which may correspond to oxidation products. Note the increase in mass of 1 Da for observed peaks compared to molecular weight of possible oxidation products due to protonation.

POPC peroxidation product	Theoretical molecular weight (Da)	Observed peak *m/z*
Hydroperoxide (POPC – H + OOH)	791.6	-
Epoxide (POPC + O)	775.6	-
Saturated dihydroxy lipid (POPC + 2OH)	793.6	-
Unsaturated dihydroxy lipid (POPC – 2H + 2OH)	791.6	-
Dihydroperoxide (POPC – 2H + 2OOH)	823.6	-
Hydroxy hydroperoxide (POPC – 2H + OH + OOH)	807.6	808.5
Allylic enone (POPC – 2H + O)	773.6	-
Aldehyde (8)	635.4	-
Aldehyde (9)	649.4	650.4
Aldehyde (10) (unsaturated)	661.4	-
Aldehyde (11) (unsaturated)	675.5	-

Table 3.6. Possible ozonolysis products of POPC and peaks observed in MALDI-MS spectrum of POPC which may correspond to oxidation products. Note the increase in mass of 1 Da for observed peaks compared to molecular weight of possible oxidation products due to protonation.

POPC ozonolysis product	Theoretical molecular weight (Da)	Observed peak *m/z*
Aldehyde (9)	649.4	650.4
Hydroxy hydroperoxide (9)	683.4	-
Carboxylic acid (9)	665.4	666.4

Not including PoxnoPC, one peak was identified in the spectrum of POPC which may correspond to another peroxidation product (Table 3.5). It was not possible to carry out MSMS analysis on this species, due to it being present at a low concentration. A peak was also identified which may correspond to the carboxylic acid product of ozonolysis of POPC (Table 3.6). The identity could not be confirmed due to its low concentration however. As with DOPC, the results suggest that both peroxidation and ozonolysis have played a part in the oxidation of the POPC stock.

3.2.3 Structural stability of liposomes

3.2.3.1 TEM

Electron microscopy was used to obtain images of the DOPC liposomes stored at 4 °C in water and in bis-tris propane on the day they were prepared and after 9 days to see if any physical changes could be observed. Images of the liposomes in bis-tris propane are shown in Figure 3.14. The images show a range of liposomes of sizes above and below the extrusion membrane pore size of 100 nm, which is to be expected. No aggregation or micellization of any liposome samples could be observed in the micrographs after 9 days compared to those obtained on the day of preparation.
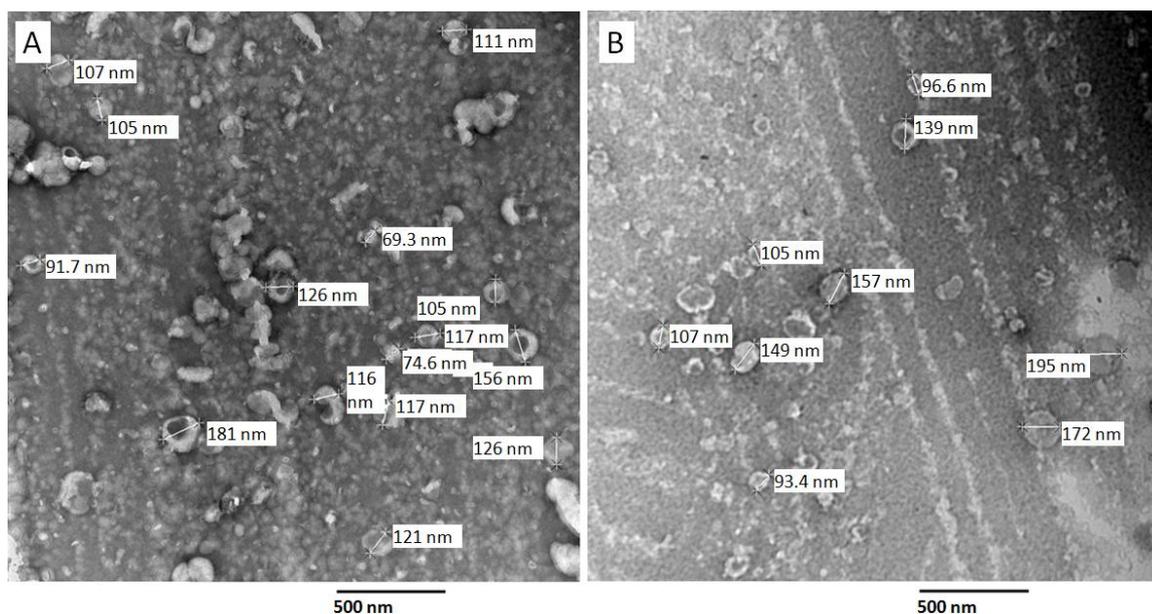
Figure 3.14. TEM images of DOPC liposomes in bis-tris propane A) just after extrusion and B) 9 days after extrusion. Liposomes, 5 mg/mL, diluted to 0.6 mM with water and stained with uranyl acetate.

3.2.3.2 Dynamic light scattering

The DOPC liposomes in water and bis-tris propane (10 mM, pH 7) were analysed by dynamic light scattering (DLS) after preparation and after 2, 5, 7, 9, 12 and 14 days of incubation at 4 °C to look for any size changes. The polydispersity index (PdI) is a measure of the width of the distribution of sizes recorded. The PdI can be used to give the percentage polydispersity (%Pd), where %Pd = $PdI^{1/2}$ x 100, which gives a clearer indication of the width of the distribution. The polydispersity index is in some ways more informative than the average diameter measurement, as the diameter measurement is intensity weighted, and therefore weighted towards the larger liposomes which scatter more, so if the liposomes were breaking down into smaller liposomes or micelles this would be visible more from the polydispersity than from the average diameter measurement. Liposome fusion would have a significant effect on the diameter measurement as well as the polydispersity index. The standard errors of the diameter measurements are also quoted, as these give an indication of the variation of the range of diameter values over 10 measurements.

3.2.3.2.1 DOPC in water

The average diameter of the DOPC liposomes in water did not increase overall during the measurement period (Table 3.7). The final measurement was the highest, but the increase was not great enough to suggest that liposome fusion had occurred, and the measurement after 12 days was the same as the first measurement within error. The

polydispersity index also did not increase during the measurement period, so there was no significant increase in the distribution of the diameter measurements.

Table 3.7. The average diameter, PdI, %Pd and standard error values for DLS measurements of DOPC liposomes in water incubated for 14 days at 4 °C. The diameter, PdI and %Pd values are an average of 10 measurements.

Time (days)	Diameter (nm)	PdI	%Pd	Std Error
0	111.9	0.153	39.1	0.4
2	113.4	0.139	37.3	0.4
5	115.3	0.139	37.3	0.7
7	113.7	0.143	37.8	0.6
9	115.0	0.155	39.4	1.3
12	112.6	0.180	42.4	1.4
14	118.4	0.134	36.6	1.0

3.2.3.2.2 DOPC in bis-tris propane

There was no significant increase in the average diameter measurements of the DOPC liposomes in bis-tris propane buffer, suggesting that no fusion was occurring. The polydispersity index also did not increase significantly over the course of the measurements, suggesting that no micellisation occurred either.

Table 3.8. The average diameter, PdI, %Pd and standard error values for DLS measurements of DOPC liposomes in bis-tris propane buffer (10 mM, pH 7) incubated for 14 days at 4 °C. The diameter, PdI and %Pd values are an average of 10 measurements.

Time (days)	Diameter (nm)	PdI	%Pd	Std Error
0	155.5	0.210	45.8	0.6
2	151.8	0.216	46.5	0.9
5	154.9	0.216	46.5	1.5
7	156.1	0.214	46.3	1.4
9	155.6	0.213	46.2	1.5
12	154.2	0.219	46.8	1.1
14	156.2	0.226	47.5	1.2

3.2.3.3 Discussion

Overall, no evidence of aggregation or micellisation was observed in the DOPC liposomes in water or in buffer over 15 days. This correlates with the observations from the TEM images.

3.2.4 The chemical effects of small molecules

The chemical effects of two small molecules, 1,1,1,3,3,3-hexafluoroisopropanol (HFIP) and haloperidol, on DOPC hydrolysis were explored. HFIP is known to affect the structure of lipid bilayers,[27] and haloperidol has been observed to cause hydrolysis of phospholipid chains to form lyso-PC.[24, 25]

3.2.4.1 HFIP

DOPC liposomes were incubated with 12.5 mM and 125 µM HFIP (10 moles and 0.1 moles HFIP:1 mole DOPC) at 4 °C for 13 days. On the day of preparation and after 2, 5, 7, 9, and 12 days a sample was removed and analysed by MALDI-MS. Figure 3.15 shows the intensity of the peak corresponding to $[M - RCO]^+$ normalised relative to the combined intensities of the peak corresponding to $[DOPC - RCO]^+$ and that corresponding to $[DOPC + H]^+$. The graph shows that the presence of HFIP has no effect on the hydrolysis of the liposomes at either concentration.
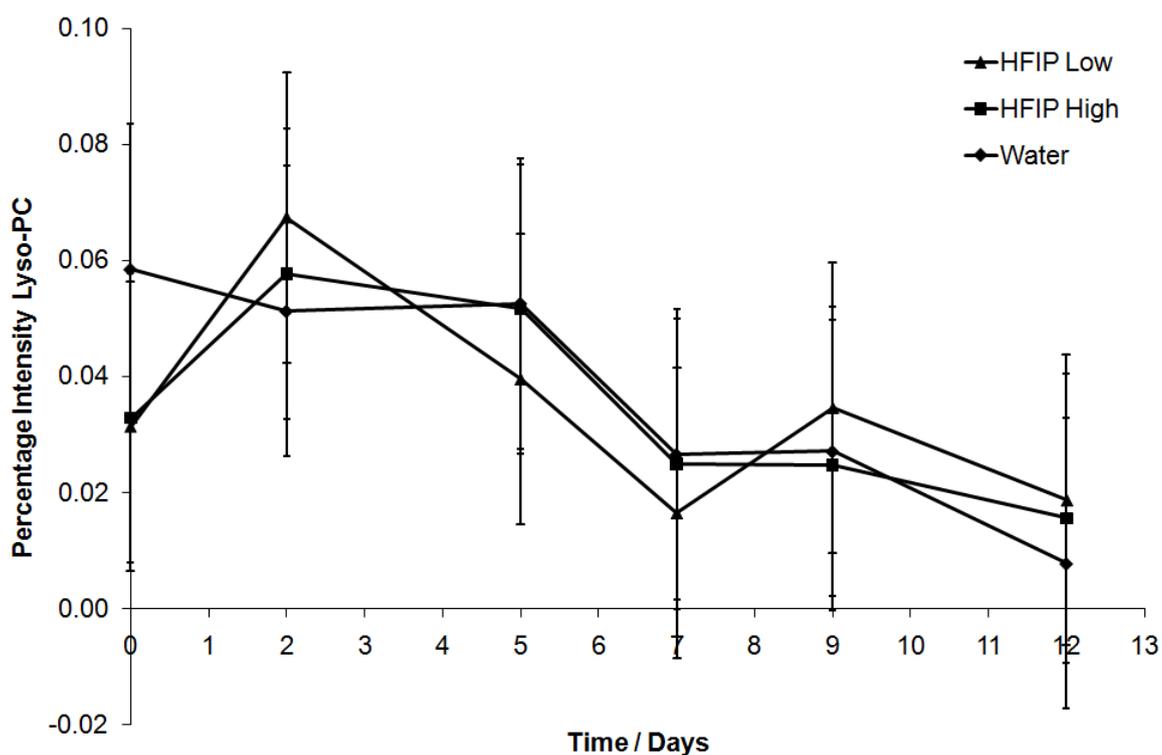
Figure 3.15. MS intensity profile of $[DOPC - RCO]^+$ for DOPC liposomes in water with 12.5 mM and 125 µM HFIP. Intensity of the peak corresponding to $[DOPC - RCO]^+$ was normalised relative to the combined intensities of the peaks corresponding to $[DOPC + H]^+$ and $[DOPC - RCO]^+$ for DOPC liposomes in water with 12.5 mM and 125 µM HFIP stored at 4 °C for 12 days. Errors are estimated from the values obtained from repeat measurements.

3.2.4.2 Haloperidol

A solution of a haloperidol-TFA salt was prepared and added to DOPC liposomes in tris buffer (10 mM pH 7.4) in a 2:1 molar ratio of lipid to haloperidol ions, following the method described by Casey *et al.*[25] The dispersion was stored at 37 °C and analysed regularly over the next 8 days by MALDI-MS. The graph (Figure 3.16) shows that, within an error of ± 0.4%, there was no increase in lyso-PC in the sample.
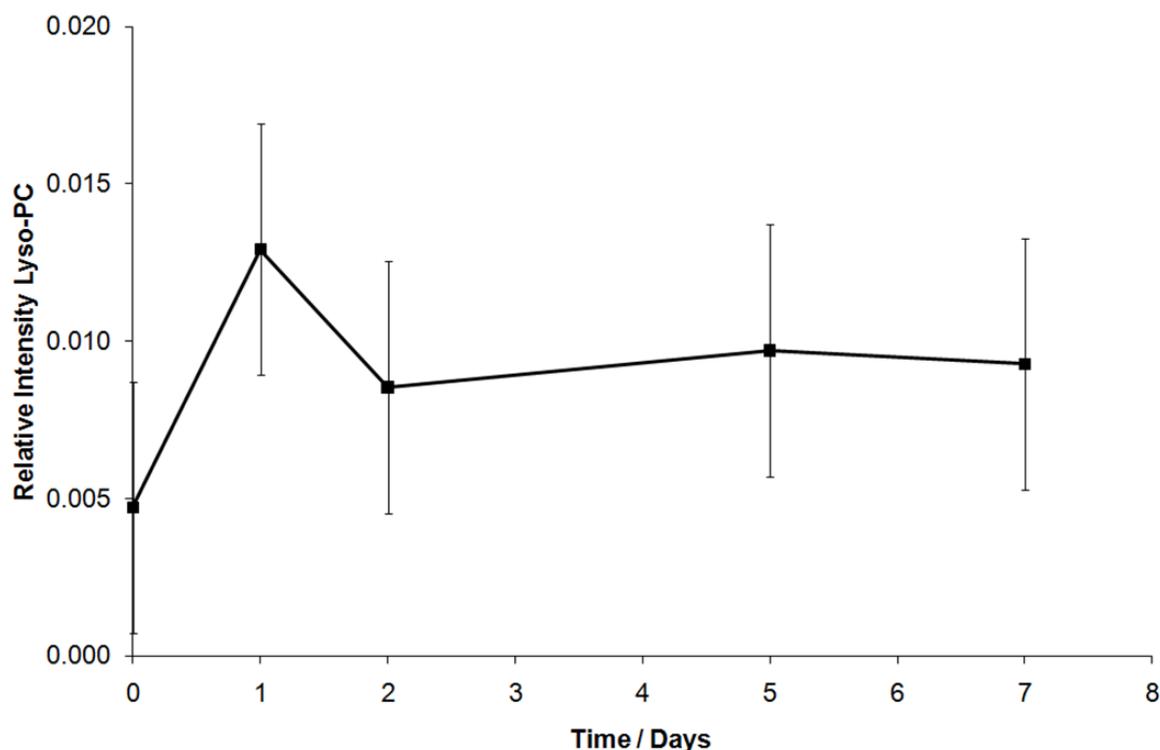
Figure 3.16. MS intensity profile of [DOPC – RCO]$^+$ for DOPC liposomes in tris buffer with haloperidol-TFA. Intensity of the peak corresponding to [DOPC – RCO]$^+$ was normalised relative to the combined intensities of the peaks corresponding to [DOPC + H]$^+$ and [DOPC – RCO]$^+$ for DOPC liposomes in tris buffer (10 mM pH 7.4) with haloperidol-TFA stored at 37 °C for 7 days. Errors are estimated from the values obtained from repeat measurements.

3.2.4.3 Discussion

No DOPC hydrolysis was observed in the presence of HFIP or haloperidol over the 12 and 8 day respective analysis periods. The result of the HFIP experiment suggest that the effect of the alcohol on lipid bilayers is physical as opposed to chemical, as reported in the literature. This was in contrast to literature reports for haloperidol salts however. The most likely reason for this was the need to scale down the experiment compared to the method followed. This meant that to obtain the same ratio and concentration as the literature method followed it was necessary to dissolve the lipid-haloperidol mixture in just 7.5 µL buffer, giving a very small amount of a very concentrated viscous dispersion. It is possible that the haloperidol and lipid could not mix sufficiently under these conditions for the lipids to be hydrolysed.

3.2.5   The effect of melittin on liposomes

Experiments were carried out to study the lysis of the acyl chains of phospholipids in the presence of natural and synthetic melittin under different conditions and over different time-periods.

3.2.5.1   *Short term analysis of lipids in the presence of natural melittin*

Natural melittin was added to DMPC liposomes in 10 mM bis-tris propane in the absence of EDTA, and 1 µL aliquots were removed every 30 seconds and immediately mixed with a solution of DHB matrix. Preliminary experiments had shown that addition to the matrix solution quenched the hydrolysis-catalysing effect of the enzyme PLA_2 (data not shown). MALDI-MS spectra were recorded for each aliquot and the intensity of the peak corresponding to lyso-MPC was normalised relative to the combined intensities of the peaks corresponding to $[DMPC + H]^+$ and $[DMPC - RCO]^+$. Each sample was spotted on the MALDI target plate twice, and data were averaged over 4000 laser shots from each spot. Figure 3.17 shows the relative intensity data. Although the error at two times standard deviation over the two repeats is large, an increase in lyso-PC can clearly be observed over a period of 5 minutes.
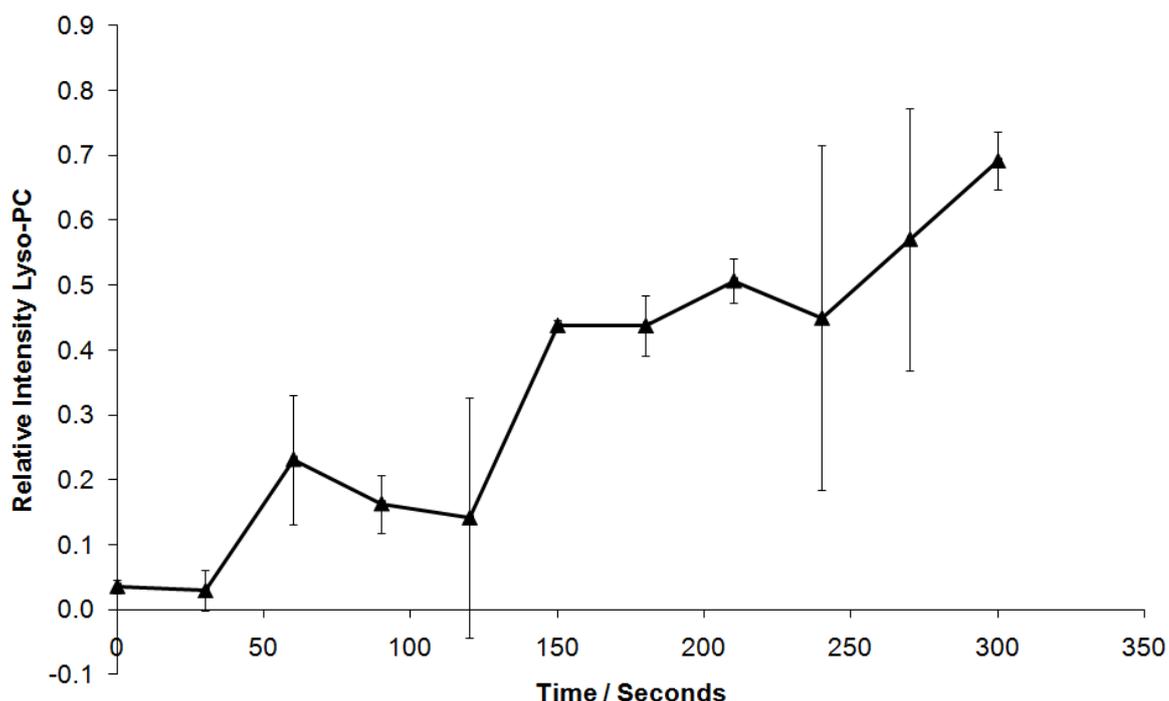
Figure 3.17. MS intensity profile of $[DMPC - RCO]^+$ for DMPC liposomes analysed at 30 s intervals after the addition of natural melittin. Intensity of the peak corresponding to $[DMPC - RCO]^+$ was normalised relative to the combined intensities of the peaks corresponding to $[DMPC + H]^+$ and $[DMPC - RCO]^+$ for MALDI-MS spectra of samples removed from liposome/peptide dispersion at 30 s intervals after the addition of natural melittin. Errors are estimated from the values obtained from repeat experiments.

In the presence of 2 mM EDTA no increase in lyso-PC was observed over 9.5 minutes after the addition of melittin to DMPC liposomes (data not shown). This suggests that the rapid hydrolysis shown in Figure 3.17 is due to the presence of PLA_2 in the sample. The possibility of lipid hydrolysis promoted by melittin in the presence of EDTA or the absence of PLA_2 was addressed in separate experiments with a longer timeframe.

3.2.5.1.1 MALDI-MSMS analysis of lyso-MPC

MALDI-MSMS analysis was carried out on the species identified as lyso-MPC in the MALDI-MS spectra in order to verify its identity. The product ion spectrum produced a number of peaks from which the lyso-lipid could be identified, as shown in Figure 3.18 and Table 3.9. Peaks corresponding to fragments involving the loss of water from the protonated parent correlate with the presence of an OH group on the lyso-lipid due to the hydrolysis ($[Lyso\text{-}MPC - OH - RCO + H]^+$, $[Lyso\text{-}MPC - OH - NMe_3]^+$ and $[Lyso\text{-}MPC - OH]^+$), while peaks corresponding to the loss of RCO confirm the presence of an unhydrolysed acyl chain on the lyso-lipid ($[Lyso\text{-}MPC - OH - RCO + H]^+$, $[Lyso\text{-}MPC - RCO + 2H]^+$). Peaks were also observed which corresponded to the presence and neutral loss of the PC headgroup.
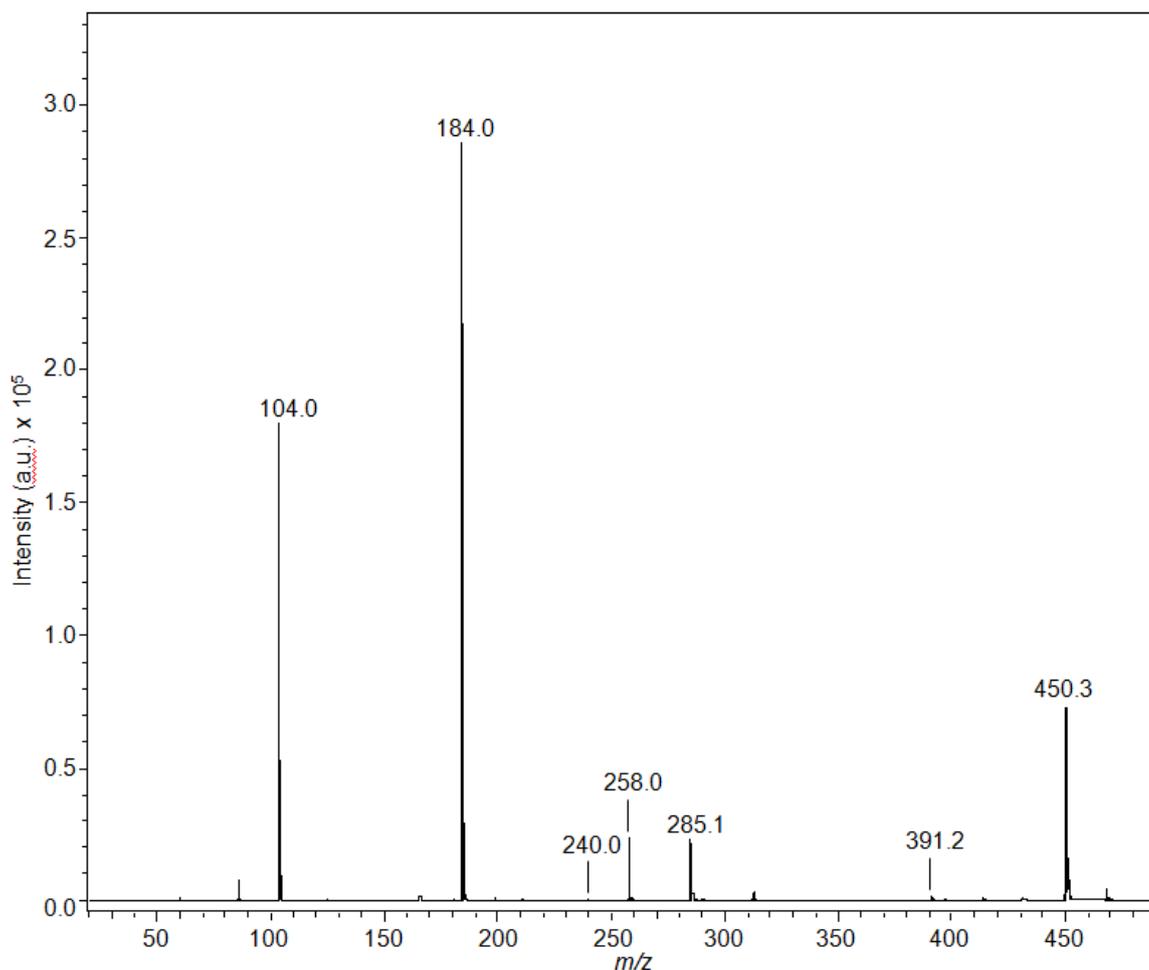
Figure 3.18. MALDI-MSMS spectrum of [Lyso-MPC + H]$^+$. The sample was prepared by mixing the liposome/melittin dispersion (2.5 mg/mL DMPC, 0.1 mg/mL melittin, 10 mM bis-tris propane) 1:9 (v/v) with DHB (30 mg/mL) in EtOH/H$_2$O (50% v/v).

Table 3.9. Product ions observed in the MALDI-MSMS spectrum of Lyso-MPC.

m/z	Fragment[a]
104.0	[OCH$_2$CH$_2$NMe$_3$ + H]$^+$
184.0	[OP(O)$_2$OCH$_2$CH$_2$NMe$_3$ + 2H]$^+$
240.0	[Lyso-MPC – OH – RCO + H]$^+$
258.0	[Lyso-MPC – RCO + 2H]$^+$
285.1	[Lyso-MPC – OP(O)$_2$OCH$_2$CH$_2$NMe$_3$]$^+$
391.2	[Lyso-MPC – OH – NMe$_3$]$^+$
450.3	[Lyso-MPC – OH]$^+$

a) R corresponds to the myristoyl hydrocarbon chain (CH$_3$(CH$_2$)$_{12}$)

3.2.5.2 Long-term analysis of lipids in the presence of natural melittin

3.2.5.2.1 Natural melittin with DOPC liposomes and 1 mM EDTA

DOPC liposomes were incubated at 37 °C in the presence of two concentrations of melittin, with 5:1 and 50:1 lipid:peptide molar ratios, in the presence of 1 mM EDTA,

which was thought to be sufficient to suppress PLA$_2$ activity.[31] After 24 hours, strong peaks corresponding to lyso-OPC were observed in MALDI-MS spectra of both samples, while only a very small peak was observed in the spectrum of the control sample of DOPC without melittin which had also been stored at 37 °C. Repeat analysis 24 hours later did not suggest that any further lyso-PC had been formed. A large formation of Lyso-PC within 24 hours in the presence of EDTA was unexpected.[32] It is now known that 1 mM EDTA is not sufficient to completely suppress the activity of PLA$_2$, and that 5 mM is recommended to ensure no PLA$_2$ activity; [20] therefore this lyso-PC formation was attributed to PLA$_2$ due to incomplete chelation of Ca^{2+}. It was concluded that the optimum way to be certain that PLA$_2$ was having no effect on any hydrolysis observed would be to use synthetic melittin, where there could be no PLA$_2$ contamination.

3.2.5.2.2 *MALDI-MSMS analysis of lyso-OPC*

MALDI-MSMS analysis was carried out on the species identified as lyso-OPC in the MALDI-MS spectra in order to verify its identity. The product ion spectrum (Figure 3.19 and Table 3.10) shows peaks corresponding to choline and phosphocholine and the neutral loss of phosphocholine ([OCH$_2$CH$_2$NMe$_3$ + 2H]$^+$, [OP(O)$_2$OCH$_2$CH$_2$NMe$_3$ + 2H]$^+$ and [Lyso-OPC – OP(O)$_2$OCH$_2$CH$_2$NMe$_3$]$^+$), and to the neutral loss of the oleoyl chain ([Lyso-OPC – RCO + 2H]$^+$).
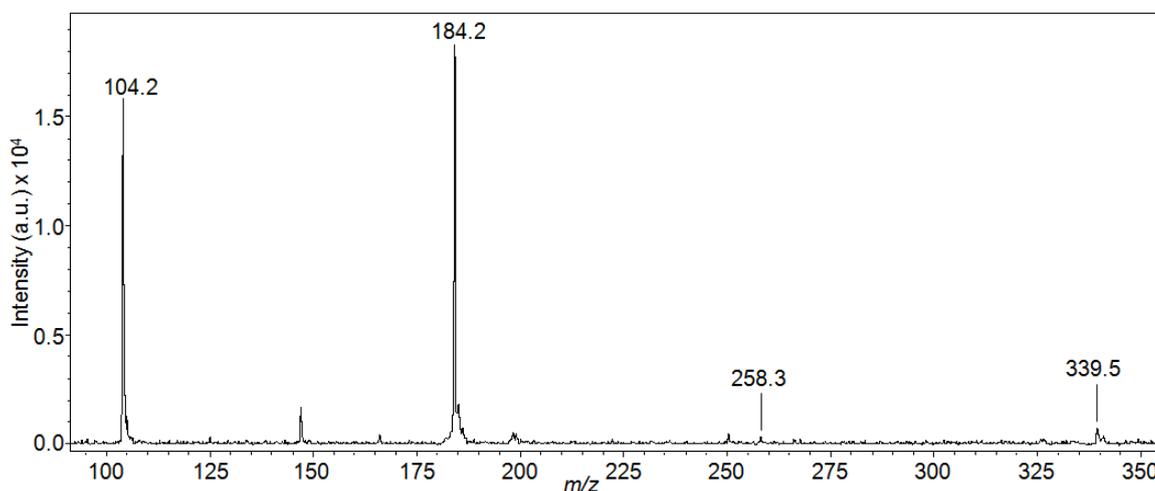
Figure 3.19. MALDI-MSMS spectrum of [Lyso-OPC + H]$^+$. The sample was prepared by mixing the liposome/melittin dispersion (0.27 mg/mL DOPC, 0.16 mg/mL melittin, 8 mM phosphate, 123 mM NaCl) 1:9 (v/v) with DHB (30 mg/mL) in EtOH/H$_2$O (50% v/v).

Table 3.10. Product ions observed in the MALDI-MSMS spectrum of Lyso-OPC.

m/z	Fragment[a]
104.2	$[OCH_2CH_2NMe_3 + H]^+$
184.2	$[OP(O)_2OCH_2CH_2NMe_3 + 2H]^+$
258.3	$[Lyso\text{-}OPC - RCO + 2H]^+$
339.5	$[Lyso\text{-}OPC - OP(O)_2OCH_2CH_2NMe_3]^+$

a) R corresponds to the myristoyl hydrocarbon chain $(CH_3(CH_2)_{12})$

3.2.5.3 Long-term analysis of lipids in the presence of synthetic melittin

CID and ECD MSMS analyses were carried out on the synthetic and natural melittin samples in order to check the structure of the synthetic peptide, as any irregularities in the sequence could affect its interaction with lipids. Figure 3.20 shows the sections of sequence identified from CID and ECD fragmentation spectra of samples of the natural and synthetic peptides.   Data were combined from different charge state deconvolutions and from different CID and ECD energies. Figure 3.21 shows the types of fragmentation undergone by peptides during MSMS analysis. 'a', 'b' and 'c' ions are formed when the charge is retained on the N-terminal fragment, 'x', 'y' and 'z' ions are formed when the charge is retained on the C-terminal fragment.[33]   Low-energy CID generally causes cleavage of the amide bond to give 'b' or 'y' ions,[34] while ECD predominantly causes cleavage of the N – C(R) bond to give 'c' and 'z' fragments.[35]
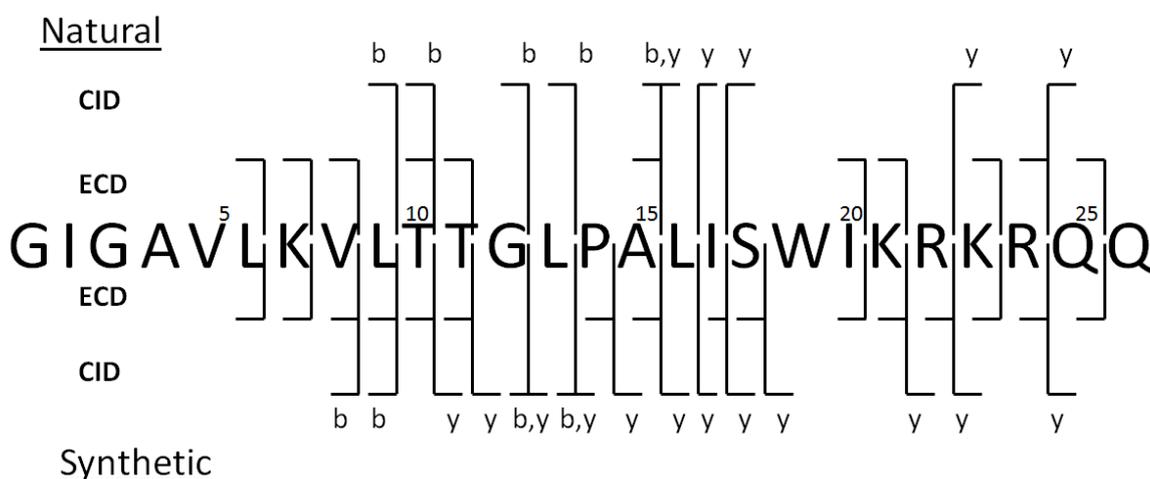
Figure 3.20. Diagram of sequence ions observed during CID and ECD analysis of natural and synthetic melittin. All ECD fragments are c ions. The C-terminal amide has been omitted for clarity.

Figure 3.20 shows that, out of twenty five backbone bonds, only six cleavages were absent when the data from the two fragmentation methods were combined for the synthetic peptide, therefore we could be very confident that the sequence of the synthetic peptide was the same as that of the natural peptide.
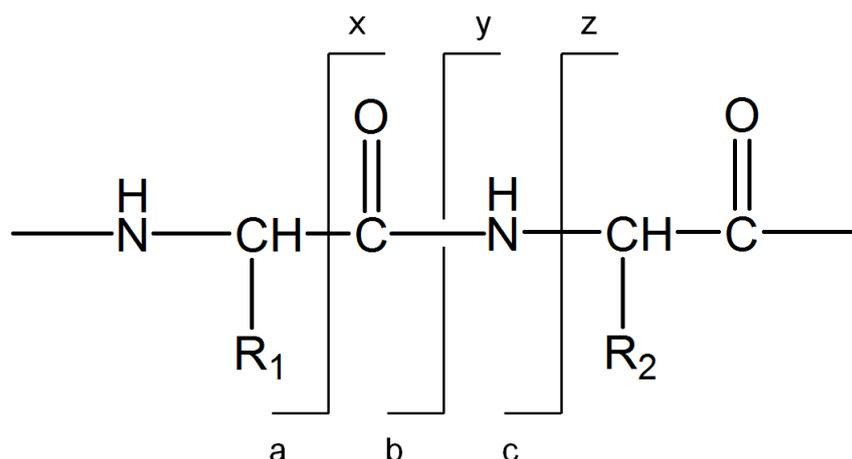
Figure 3.21. Nomenclature for sequence ions produced during MSMS analysis. In a, b and c ions the charge is retained on the N-terminal fragment after cleavage; in x, y and z ions the charge is retained on the C-terminal fragment.

DOPC liposomes were incubated at 37 °C in the presence of two concentrations of synthetic melittin, with 5:1 and 50:1 lipid:peptide molar ratios, for 16 days, along with a liposome sample with no melittin, and analysed regularly by MALDI-MS. The intensity of the peak corresponding to $[DOPC - RCO]^+$ was normalised relative to the combined intensities of the peaks corresponding to $[DOPC + H]^+$ and $[DOPC - RCO]^+$ for each spectrum and the results are shown in Figures 3.22 and 3.23.

3.2.5.3.1 Low concentration melittin

It can be observed from Figure 3.22 that over 15 days no acyl chain lysis of the DOPC lipids occurred in either the control liposomes or in the liposomes incubated with melittin at a 50:1 lipid:peptide molar ratio.
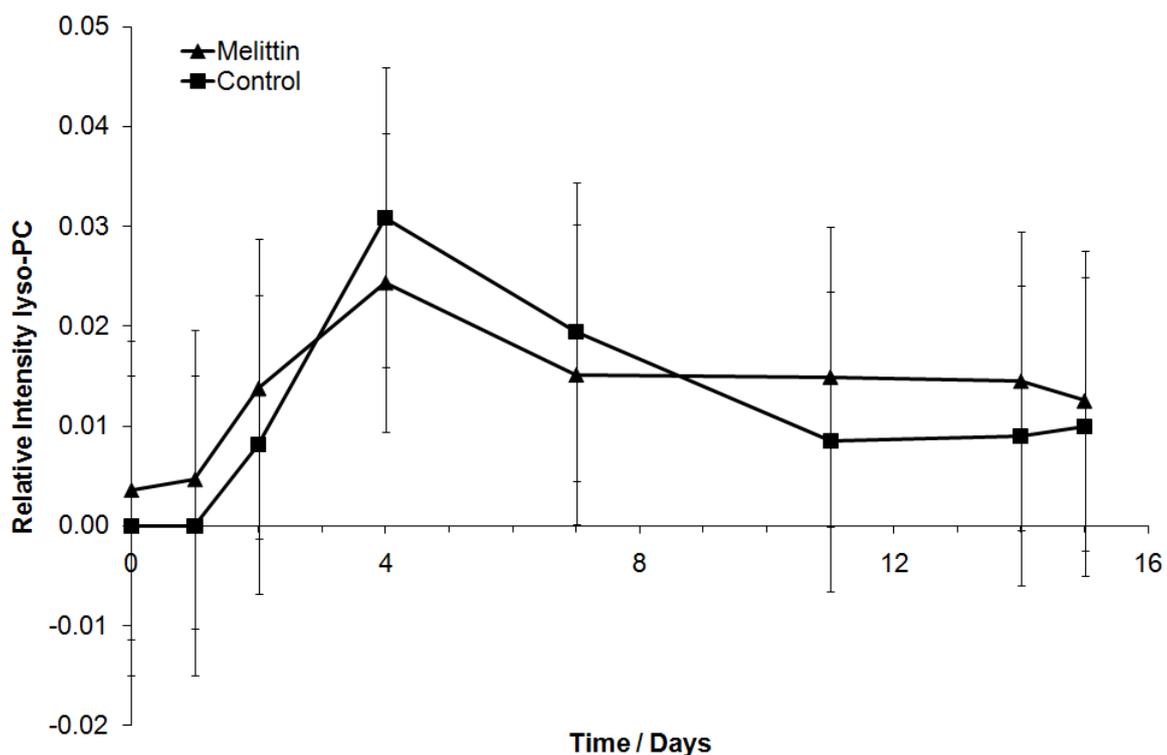
Figure 3.22. MS intensity profile of [DOPC – RCO]$^+$ for DOPC liposomes with synthetic melittin in a 50:1 lipid:peptide molar ratio. Intensity of the peak corresponding to [DOPC – RCO]$^+$ was normalised relative to the combined intensities of the peaks corresponding to [DOPC + H]$^+$ and [DOPC – RCO]$^+$ for DOPC liposomes with synthetic melittin in a 50:1 lipid:peptide molar ratio in 10 mM phosphate and 147 mM NaCl (pH 7) and in the absence of melittin stored at 37 °C for 15 days. Errors are estimated from the values obtained from repeat measurements.

3.2.5.3.2 High concentration melittin

A clear increase in lyso-OPC was observed over 15 days in the sample with a 5:1 lipid:peptide molar ratio (Figure 3.23). Within 24 hours the relative intensity of [DOPC – RCO]$^+$ observed when analysing the sample with melittin was greater than that observed in the control sample. The amount of lyso-PC in the sample continued to increase rapidly over the next 24 hours, then more slowly over the rest of the analysis period. This result suggests that melittin alone promotes the acyl chain lysis of lipids, though on a much slower timescale than catalysis in the presence of PLA$_2$.
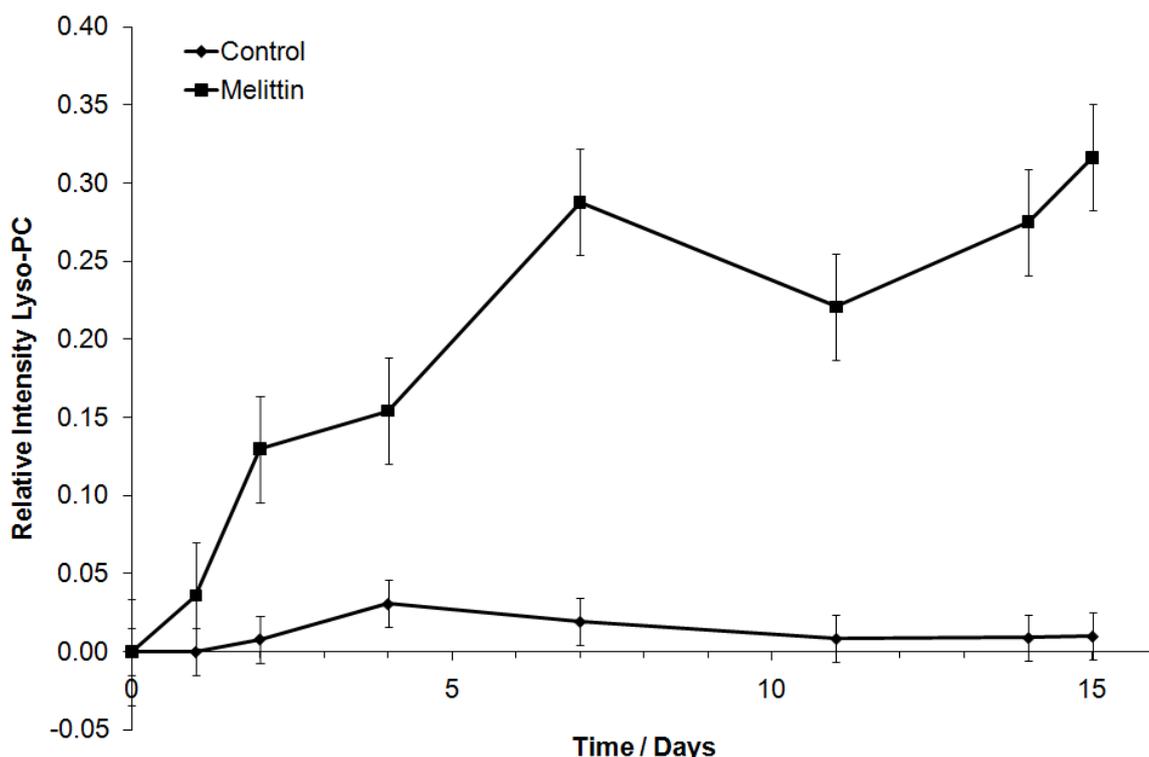
Figure 3.23. MS intensity profile of $[DOPC - RCO]^+$ for DOPC liposomes with synthetic melittin in a 5:1 lipid:peptide molar ratio. Intensity of the peak corresponding to $[DOPC - RCO]^+$ was normalised relative to the combined intensities of the peaks corresponding to $[DOPC + H]^+$ and $[DOPC - RCO]^+$ for DOPC liposomes with synthetic melittin in a 5:1 lipid:peptide molar ratio in 8 mM phosphate and 123 mM NaCl and in the absence of melittin stored at 37 °C for 15 days. Errors are estimated from the values obtained from repeat measurements.

Peaks were also observed at m/z 258.1 in the MALDI-MS spectra of the DOPC liposomes with melittin. These were thought to correspond to the doubly hydrolysed species sn-glycero-3-phosphocholine (glycero-PC). A graph of the intensities of $[DOPC - RCO]^+$ and $[DOPC - 2RCO]^+$ normalised relative to the combined intensities of the peaks corresponding to $[DOPC + H]^+$, $[DOPC - RCO]^+$ and $[DOPC - 2RCO]^+$ (Figure 3.24) shows that the quantity of glycero-PC remained very low during the analysis period. The relative intensity of the glycero-PC remained similar to the relative intensity of lyso-PC in the control sample, and did not increase over the analysis period within an error of ± 1.5%. No glycero-PC was observed in the control liposomes.
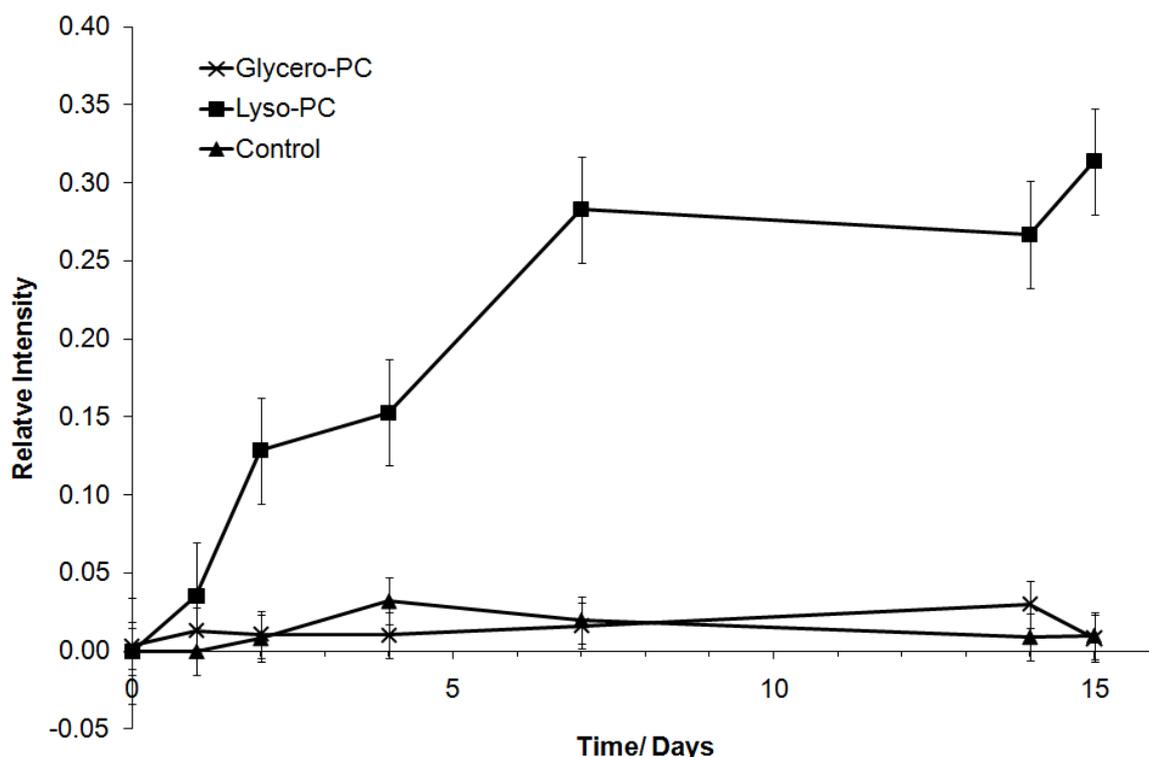
Figure 3.24. MS intensity profiles of [DOPC – RCO]$^+$ and [DOPC – 2RCO]$^+$ for DOPC liposomes with synthetic melittin. Intensities of the peaks corresponding to [DOPC – RCO]$^+$ and [DOPC – 2RCO]$^+$ were normalised relative to the combined intensities of the peaks corresponding to [DOPC + H]$^+$, [DOPC – RCO]$^+$ and [DOPC – 2RCO]$^+$ for DOPC liposomes with synthetic melittin in a 5:1 lipid:peptide molar ratio in 8 mM phosphate and 123 mM NaCl stored at 37 °C for 15 days. Errors are estimated from the values obtained from repeat measurements.

3.2.5.4   *Thin layer chromatography of lipids in the presence of synthetic melittin*

Thin layer chromatography was carried out on a sample of DOPC 17 days after the addition of synthetic melittin in a 5:1 lipid:peptide molar ratio, after the presence of lyso-PC had been confirmed by MALDI analysis. The contents of the sample were compared with DOPC lipid and liposomes in the absence of melittin and a mixture of lyso-PC and oleic acid. The results (Figure 3.25) show clear evidence of lyso-PC in the sample of liposomes with melittin (lane D) and not in the DOPC lipid and liposome samples in the absence of melittin (lanes A and E respectively). No oleic acid can be identified in the sample of DOPC in the presence of melittin, unlike in the mixture of oleic acid and lyso-PC (lane B). The lack of free oleic acid accompanying the formation of lyso-PC suggests that the lysis process may involve the acylation of melittin rather than hydrolysis.
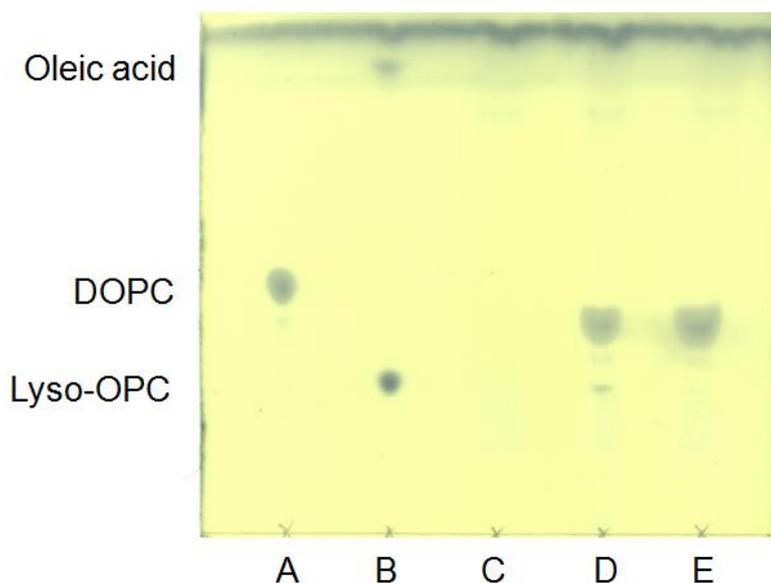
Figure 3.25. TLC plate showing the presence of lyso-PC and absence of oleic acid in DOPC liposomes in the presence of synthetic melittin. Lane A, DOPC spotted from a solution in CHCl$_3$; lane B, lyso-OPC and oleic acid in CHCl$_3$; lane C, 10 mM phosphate and 150 mM NaCl buffer; lane D, DOPC liposomes and melittin (5:1 mol/mol) in 8 mM phosphate and 123 mM NaCl buffer 17 days after addition of; lane E, DOPC liposomes in 10 mM phosphate and 150 mM NaCl buffer. For lanes C, D and E, 30 µL of each sample was lyophilized and re-dissolved in 50:50 (v/v) MeOH/CHCl$_3$ before application to the TLC plate. The TLC plate was developed with 6:4:1 (v/v) CHCl$_3$, MeOH and H$_2$O and stained using phosphomolybdic acid (20 wt. % in EtOH) and heat.

3.2.5.5 Long-term analysis of POPC with synthetic melittin

POPC was incubated at 37 °C with synthetic melittin, with a 5:1 lipid:peptide molar ratio, for 28 days, along with a liposome sample with no melittin, and analysed regularly by MALDI-MS. A graph of the intensities of the peaks corresponding to the lysis of the palmitoyl chain ([POPC – R$_{16:0}$CO]$^+$) and the oleoyl chain ([POPC – R$_{18:1}$CO]$^+$) normalised relative to the combined intensities of the peaks corresponding to [POPC – R$_{16:0}$CO]$^+$, [POPC – R$_{18:1}$CO]$^+$ and [POPC + H]$^+$ is shown in Figure 3.26. An increase in the lysis of each chain was observed over 14 days. This shows that melittin promotes the lysis of both acyl chains, unlike PLA$_2$, which only catalyzes the hydrolysis of acyl chains from the *sn*-2 position of lipids.[21]

Table 3.11 shows that the relative intensity of the peak corresponding to [POPC – R$_{18:1}$CO]$^+$ was approximately twice that of the peak corresponding to [POPC – R$_{16:0}$CO]$^+$ for every measurement. No similar trend could be observed in the control liposomes, where the relative intensities of [POPC – R$_{18:1}$CO]$^+$ and [POPC – R$_{16:0}$CO]$^+$ were the same within error. This suggests that melittin might be preferentially promoting the lysis of the oleoyl chain from the *sn*-2 position of the lipid.
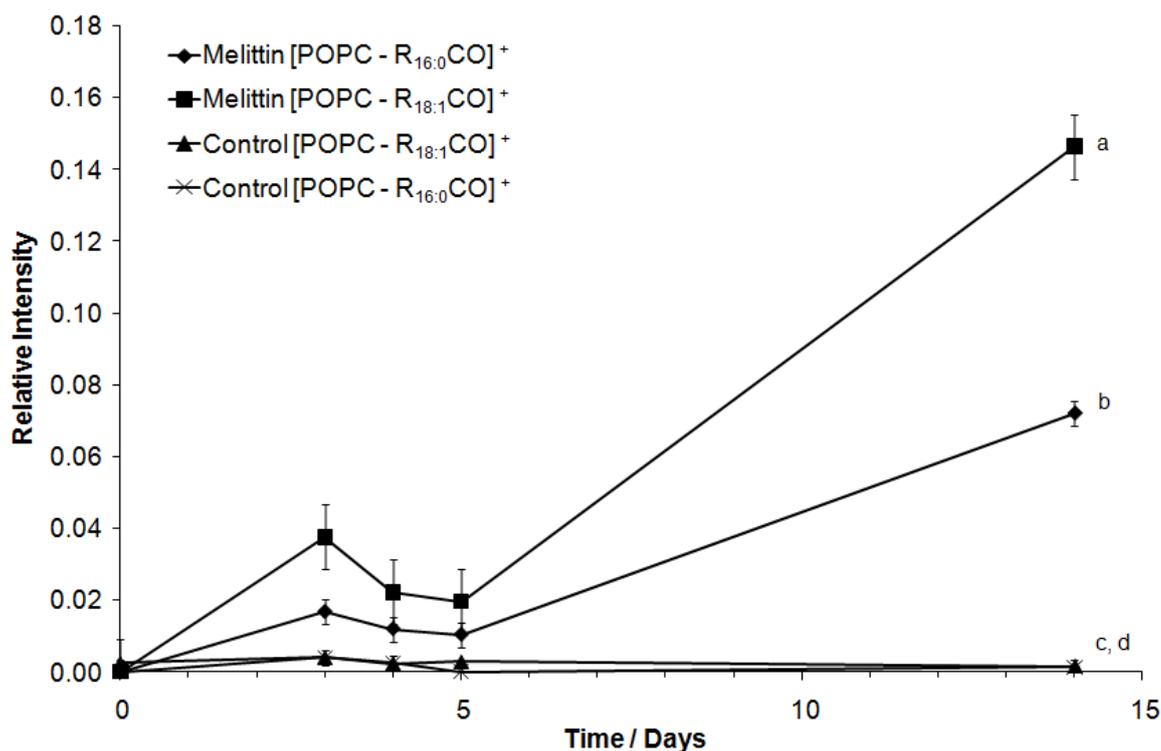
Figure 3.26. MS intensity profiles of $[POPC - R_{18:1}CO]^+$ and $[POPC - R_{16:0}CO]^+$ for POPC liposomes with synthetic melittin. Intensities of the peaks corresponding to $[POPC - R_{18:1}CO]^+$ and $[POPC - R_{16:0}CO]^+$ were normalised relative to the combined intensities of the peaks corresponding to $[POPC + H]^+$, $[POPC - R_{18:1}CO]^+$ and $[POPC - R_{16:0}CO]^+$ for POPC liposomes with synthetic melittin in a 5:1 lipid:peptide molar ratio in 8 mM phosphate and 123 mM NaCl stored at 37 °C for 14 days.

Table 3.11. Intensities of peaks corresponding to $[POPC - R_{18:1}CO]^+$ and $[POPC - R_{16:0}CO]^+$ normalised relative to the combined intensities of the peaks corresponding to $[POPC + H]^+$, $[POPC - R_{18:1}CO]^+$ and $[POPC - R_{16:0}CO]^+$ for POPC liposomes with and without synthetic melittin.

Time / days	Melittin relative intensity $[POPC - R_{16:0}CO]^+$	Melittin relative intensity $[POPC - R_{18:1}CO]^+$	Control relative intensity $[POPC - R_{16:0}CO]^+$	Control relative intensity $[POPC - R_{18:1}CO]^+$
0	0	0	0.0	0.2
3	1.7	3.8	0.4	0.4
4	1.2	2.2	0.2	0.2
5	1.0	2.0	0.0	0.3
14	7.2	14.6	0.1	0.2

3.2.5.6 Discussion

The analyses of the DOPC and POPC liposomes after the addition of synthetic melittin showed a definite formation of lyso-PC. This suggests that melittin itself can promote acyl chain lysis, though on a much slower timescale than in the presence of PLA_2. A small quantity of glycero-PC was also observed in the presence of synthetic melittin. A clear difference was observed in the lysis of the palmitoyl and oleoyl chains of

POPC, with higher intensities of the peaks corresponding to cleavage of the oleoyl chain than those corresponding to the cleavage of the palmitoyl chain.

3.2.6 The effect of metal salts on the lysis of the acyl chains of DOPC promoted by synthetic melittin

A number of analyses were carried out to determine whether the presence of Ca^{2+}, Zn^{2+} or Mg^{2+}, the omission of NaCl from the buffer, or the addition of a haloperidol salt had an effect on the lysis of the acyl chains of DOPC in the presence of synthetic melittin. The concentrations of the metal salts were based on those in Dulbecco's buffer, a balanced salt solution developed for the preparation of cell cultures. Dulbecco's buffer, and similar balanced salt solutions, are designed to perform four functions; 1) to maintain intra- and extracellular osmotic pressure; 2) to provide water and the bulk inorganic ions required for cell metabolism; 3) to provide energy for cell metabolism with the addition of a carbohydrate; 4) to buffer the solution to the medium point in the physiological pH range.[36] Dulbecco's buffer contains 0.133 g/L $CaCl_2$, 0.1 g/L $MgCl_2$, 0.2 g/L KCl, 8 g/L NaCl, 0.2 g/L KH_2PO_4 and 1.15% Na_2HPO_4.[36, 37] 0.133 g/L $CaCl_2$ correlates to 0.9 mM, therefore all salts, and haloperidol-TFA, were included in the buffers at this concentration, with final concentrations of 0.7 mM in each sample after the addition of melittin.

It is clear from the data that quantitative comparisons of relative intensity values can only made between samples which were prepared and analysed on the same days. Less lysis was observed in later experiments than earlier ones, which is attributed to the age of the melittin stock at the time of the preparation of each set of samples. The stock was stored in the freezer and defrosted and vortexed before use. Slight variations in laser power were observed each day. The same percentage of the total laser power was used for each analysis, but the total laser power was slightly variable and the laser was replaced between two sets of experiments. The error bars account for any effect of slight day-to-day laser power variations within sets of analyses.

3.2.6.1 Phosphate buffers containing ZnCl₂ and NaCl, CaCl₂ and NaCl, and no NaCl

Figure 3.27 shows the intensity of the peak corresponding to lyso-PC normalised relative to the combined intensities of the peaks corresponding to the DOPC molecular ion and lyso-PC for DOPC liposomes with and without synthetic melittin under different salt conditions. After 24 hours little acyl chain lysis could be observed in any sample, but from day 3 onwards clear differences could be observed between the levels of lyso-PC in the different samples. In the absence of NaCl and any other added salts (Figure 3.27c), the relative intensity of lyso-PC at each analysis was similar to that observed in the absence of melittin. When NaCl was present, acyl chain lysis was observed in both

samples with divalent metal cations and melittin. The most lysis was observed in the sample with melittin, NaCl and $ZnCl_2$ (Figure 3.27a), where a higher relative intensity of the peak corresponding to lyso-PC could be observed after 2 days, and after 14 days the relative intensity of the peak corresponding to lyso-PC was around twice that observed for the sample with $CaCl_2$. The increase in lyso-PC in the presence of melittin, NaCl and $CaCl_2$ was slower than when $ZnCl_2$ was present (Figure 3.27b), but after 8 days the relative intensity of the peak corresponding to lyso-PC was clearly greater than those of the control samples. No acyl chain lysis, within error, was observed in the control samples (Figure 3.27d–f).
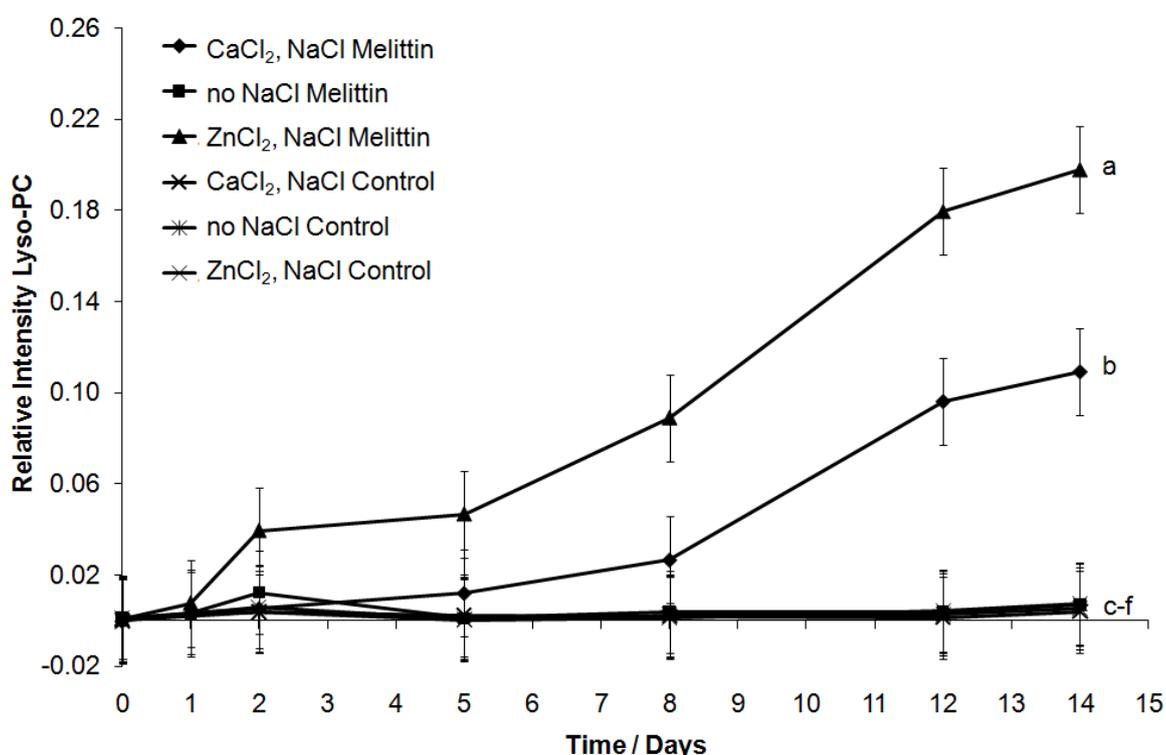
Figure 3.27. MS intensity profiles of $[DOPC - R_{18:1}CO]^+$ for DOPC liposomes with NaCl, $ZnCl_2$ and synthetic melittin; NaCl, $CaCl_2$ and synthetic melittin; synthetic melittin; NaCl and $ZnCl_2$; NaCl, $CaCl_2$; and no additions. Intensities of the peaks corresponding to $[DOPC - RCO]^+$ were normalised relative to the combined intensities of the peaks corresponding to $[DOPC + H]^+$ and $[DOPC - RCO]^+$ for DOPC liposomes in phosphate buffer with a) NaCl, $ZnCl_2$ and synthetic melittin; b) NaCl, $CaCl_2$ and synthetic melittin; c) synthetic melittin; d) NaCl and $ZnCl_2$; e) NaCl, $CaCl_2$ and f) no additions. Errors are estimated from the values obtained from repeat measurements.

Figure 3.28 shows data for DOPC liposomes in phosphate and NaCl buffer in the presence and absence of $ZnCl_2$ and synthetic melittin which were prepared and analysed together. For the first three days the rates of lysis in the presence of melittin were similar with and without Zn^{2+} (Figure 3.28a and b respectively), but lysis in the sample without Zn^{2+} appeared to stop at this stage, while in the presence of Zn^{2+} in continued until for the

next 4 days. No lysis, within error, was observed in the control samples (Figure 3.28c and d).
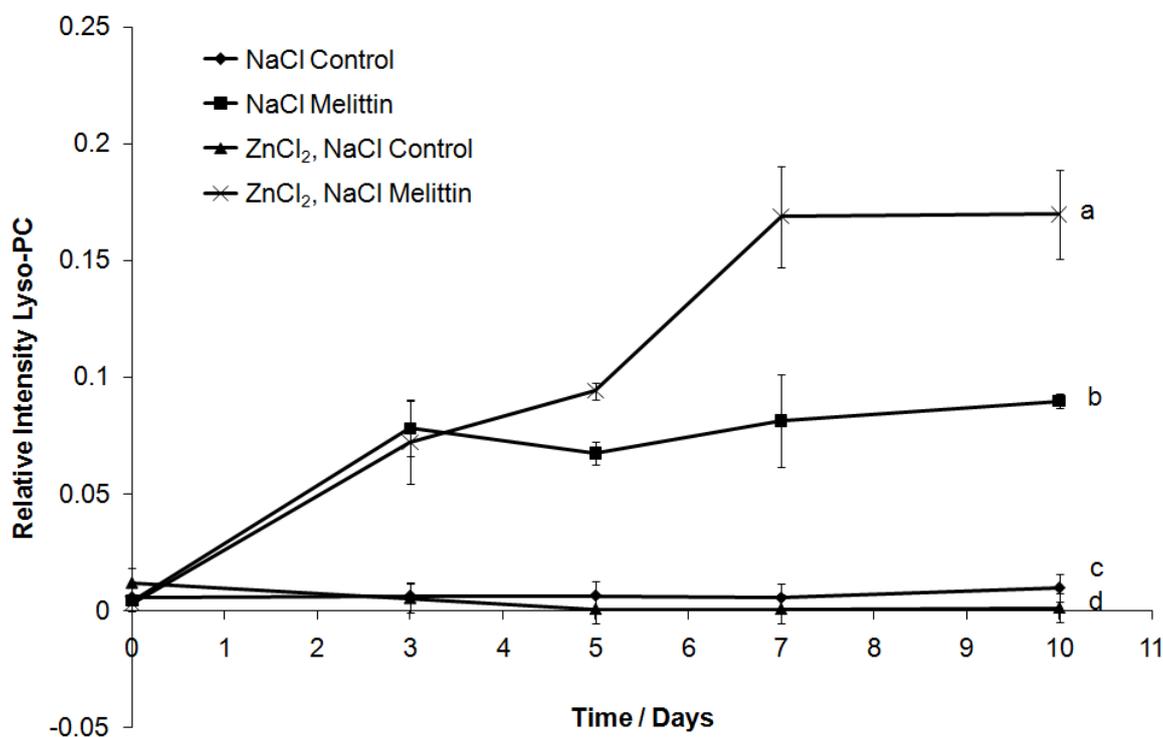
Figure 3.28. MS intensity profiles of [DOPC – $R_{18:1}CO]^+$ for DOPC liposomes with NaCl, ZnCl$_2$ and synthetic melittin; NaCl and synthetic melittin; NaCl; and NaCl and ZnCl$_2$. Intensities of peaks corresponding to lyso-PC were normalised relative to those corresponding to DOPC for DOPC liposomes in phosphate buffer with a) NaCl, ZnCl$_2$ and synthetic melittin; b) NaCl and synthetic melittin; c) NaCl and d) NaCl and ZnCl$_2$. Errors are estimated from the values obtained from repeat measurements.

3.2.6.2 *Phosphate and NaCl buffers containing MgCl$_2$ and Haloperidol*

The formation of lyso-PC in DOPC dispersions in phosphate buffer with melittin was also followed in the presence of NaCl and MgCl$_2$ and in the presence of NaCl and haloperidol. The lyso-PC formation was compared to that in samples with melittin and NaCl and with each buffer without melittin. With melittin, NaCl and either Mg^{2+} or haloperidol the increase in lyso-PC was similar to that observed with melittin and just NaCl for the first 7 days (Figure 3.29c, b and a respectively). After this point there was little more acyl chain lysis in the sample with Mg^{2+}. Continued lysis was observed in the sample with melittin, NaCl and haloperidol after 7 days, but the rate was slower than in the phosphate buffer with just melittin and NaCl. After 15 days the lyso-PC formation in the sample with melittin, NaCl and Mg^{2+} was the same as that in the control samples with NaCl and haloperidol and NaCl and Mg^{2+}, in the absence of melittin. After 3 days, only a weak peak corresponding to melittin was observed when the sample with melittin, NaCl and Mg^{2+} was analysed by MALDI, while when the other samples containing melittin were

analysed over the same mass range clear peaks corresponding to melittin could be observed. When melittin was added to a buffer of phosphate, NaCl and MgCl$_2$ without liposomes and analysed daily by MALDI-MS, a strong peak corresponding to melittin was observed at *m/z* 2845.7, along with one for the sodium adduct of the peptide at *m/z* 2867.7 when the sample was analysed immediately after the addition of melittin. After 24 hours these peaks were weaker, and after 48 hours no peaks corresponding to melittin could be observed (Figure 3.30). The reduction of the intensity of the peaks corresponding to melittin during MALDI analysis of the samples with melittin, NaCl and MgCl$_2$ with and without liposomes is attributed to the precipitation of melittin/Mg complexes. This also accounts for the level of lyso-PC in the sample with DOPC liposomes being similar to that in samples without melittin after 15 days.
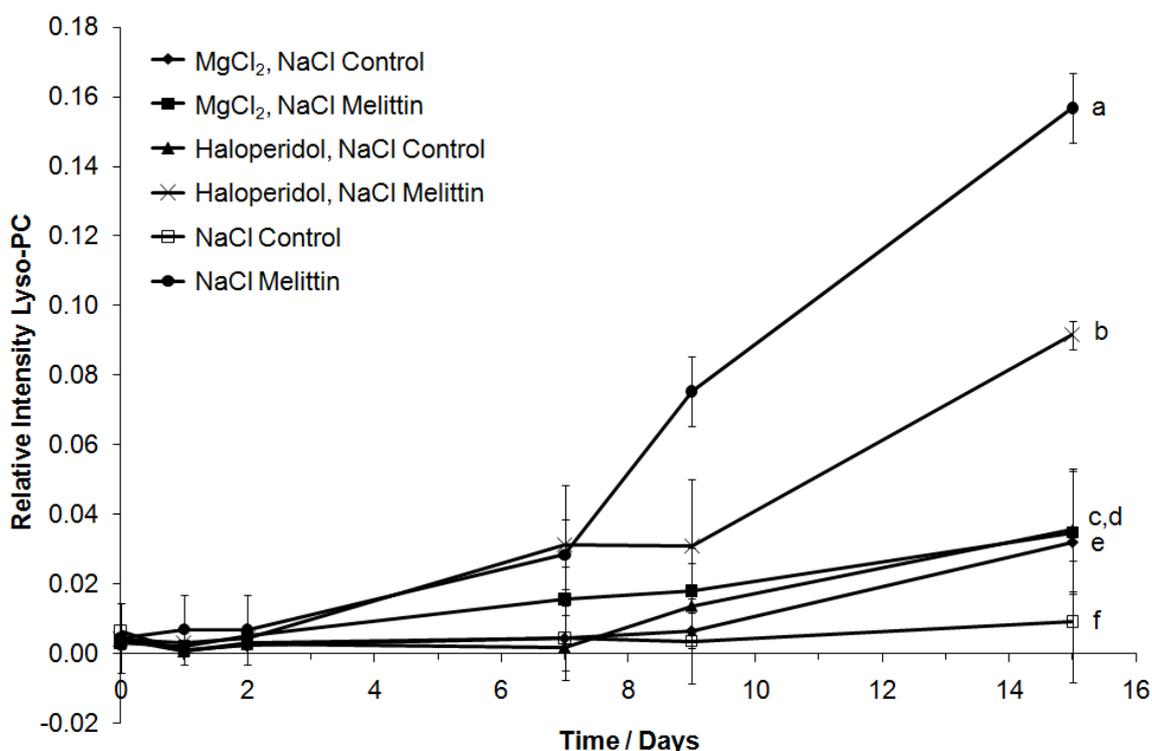
Figure 3.29. MS intensity profiles of [DOPC – R$_{18:1}$CO]$^+$ for DOPC liposomes with NaCl and synthetic melittin; haloperidol, NaCl and synthetic melittin; MgCl$_2$, NaCl and synthetic melittin; haloperidol and NaCl; MgCl$_2$ and NaCl; and NaCl. Intensities of peaks corresponding to lyso-PC were normalised relative to those corresponding to DOPC for DOPC liposomes in phosphate buffer with a) NaCl and synthetic melittin; b) haloperidol, NaCl and synthetic melittin; c) MgCl$_2$, NaCl and synthetic melittin; d) haloperidol and NaCl; e) MgCl$_2$ and NaCl and f) NaCl. Errors are estimated from the values obtained from repeat measurements.
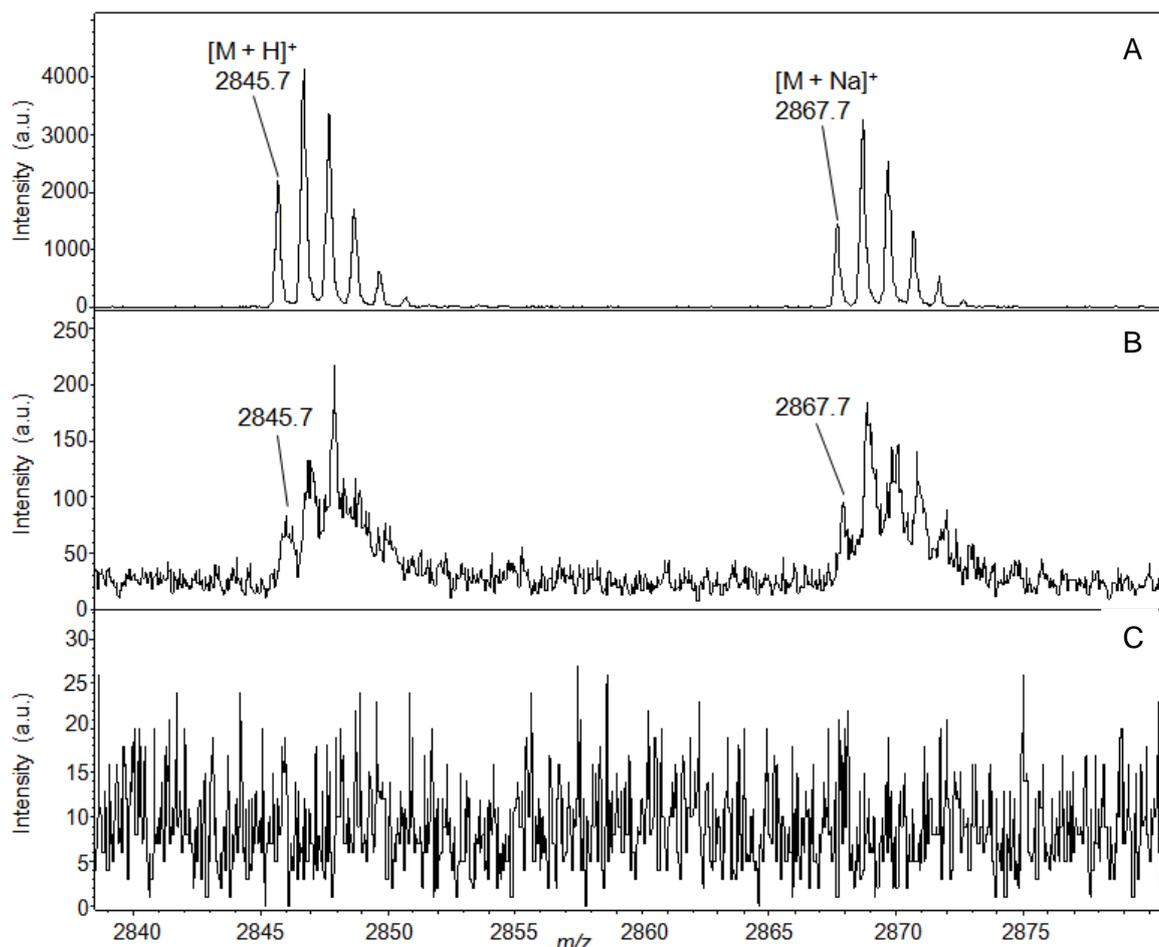
Figure 3.30. MALDI-MS spectrum of synthetic melittin in 10 mM phosphate, 150 mM NaCl and 0.9 mM MgCl$_2$ A) 0, B) 1 and C) 2 days after the addition of melittin. The sample was prepared by mixing the sample 1:9 (v/v) with DHB (30 mg/mL) in EtOH/H$_2$O(50% v/v).

3.2.6.3 Discussion

As discussed in Section 3.2.5.3, the lysis of the acyl chains of DOPC in liposomes was promoted by the presence of synthetic melittin in 8 mM phosphate and 123 mM NaCl. Altering the salt conditions in which synthetic melittin and DOPC liposomes were combined had a number of effects on the lysis. In the absence of NaCl, no lysis was observed in the presence of melittin above that observed in the control samples. The addition of ZnCl$_2$, in the presence of melittin and NaCl, was shown to increase lyso-PC formation compared to that in the absence of ZnCl$_2$. Little lysis was observed in the sample containing melittin, NaCl and MgCl$_2$. The intensity of the peak corresponding to melittin also dropped sharply over 48 hours after preparation in samples with MgCl$_2$ with and without liposomes. This was attributed to the formation of insoluble melittin/MgCl$_2$ complexes.

3.2.7 Acylation of melittin

During the regular MALDI-MS analyses of the liposomes incubated with melittin it became clear that over time peaks were appearing at m/z 3110.0 and m/z 3132.1 in most of the spectra of samples of DOPC and melittin. These corresponded to the molecular weights of [Melittin + $R_{18:1}CO$]$^+$ and [Melittin + $R_{18:1}CO$ – H + Na]$^+$, where $R_{18:1}CO$ is the acyl chain of DOPC. The molecular weight of [Melittin + $R_{18:1}CO$]$^+$ takes into account the loss of H$^+$ from a nucleophile on melittin (e.g. RNH_2) during bonding to the acyl chain and the addition of H$^+$ during ionisation. This proposed identity was supported by the fact that after 28 days strong peaks could be observed at m/z 3084.0, m/z 3105.9, m/z 3110.0 and m/z 3132.0 in the spectrum of melittin with POPC, which corresponded to the molecular weights of [Melittin + $R_{16:0}CO$]$^+$, [Melittin + $R_{16:0}CO$ – H + Na]$^+$, [Melittin + $R_{18:1}CO$]$^+$ and [Melittin + $R_{18:1}CO$ – H + Na]$^+$ respectively (Figure 3.31) where $R_{16:0}CO$ is the palmitoyl chain of POPC and $R_{18:1}CO$ the oleoyl chain. The first sign of the adduct in a sample of melittin and DOPC was observed after 4 days. When analysing the sample with Zn$^+$ in the buffer, and that without NaCl, a peak corresponding to the adduct was observed after 6 days. The first spectrum of the sample with Ca^{2+} which showed the adduct peak was recorded after 7 days. Attempts were made to carry out MSMS on the acylated species in order to positively identify them. It can be noted from Figure 3.32 that the intensities of the peaks corresponding to [Melittin + $R_{18:1}CO$]$^+$ and [Melittin + $R_{18:1}CO$ – H + Na]$^+$ were greater than the intensities of those corresponding to [Melittin + $R_{16:0}CO$]$^+$ and [Melittin + $R_{16:0}CO$ – H + Na]$^+$.
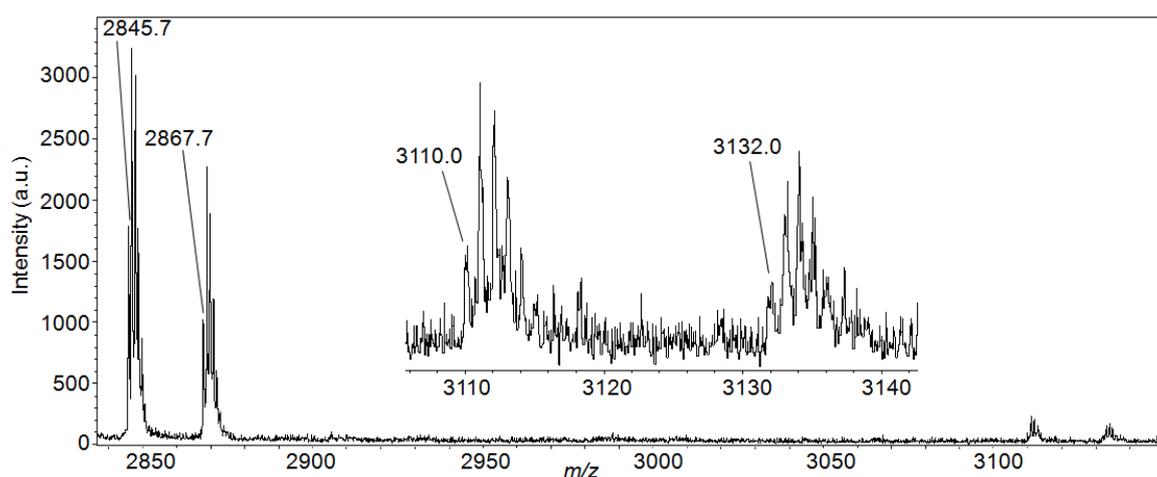
Figure 3.31. MALDI-MS spectrum of synthetic melittin in 8 mM phosphate and 123 mM NaCl 16 days after addition to DOPC liposomes. The peaks at m/z 2845.7, m/z 2867.7, m/z 3110.0 and m/z 3132.0 correspond to [M + H]$^+$, [M + Na]$^+$, [M + $R_{18:1}CO$]$^+$ and [M + $R_{18:1}CO$ – H + Na]$^+$ The sample was prepared by mixing the melittin and liposome dispersion (1:5 peptide: lipid molar ratio) 1:9 (v/v) with DHB (30 mg/mL) in EtOH/H_2O (50% v/v).
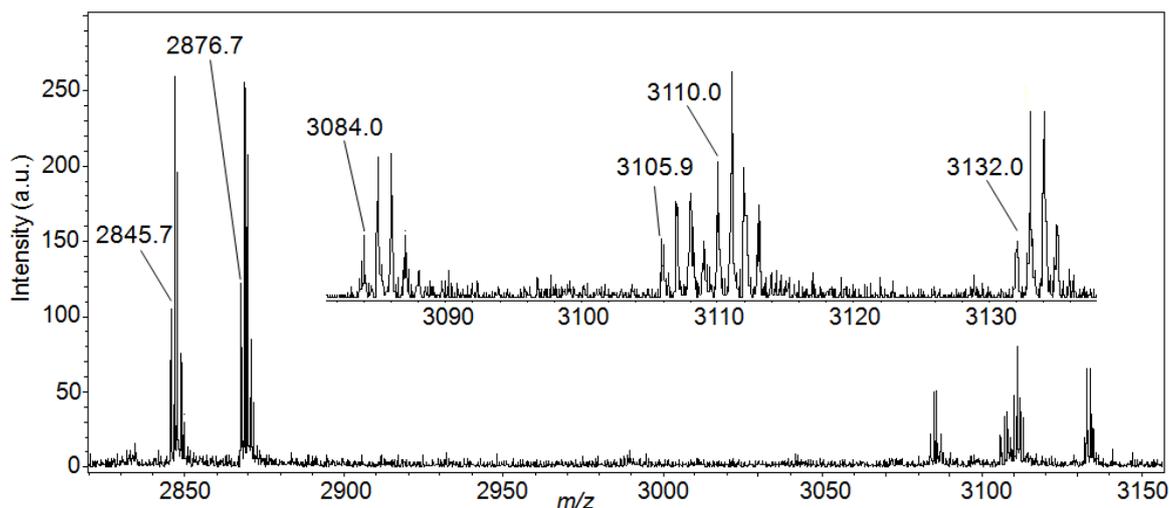
Figure 3.32. MALDI-MS spectrum of synthetic melittin in 8 mM phosphate and 123 mM NaCl 28 days after addition to POPC liposomes. The peaks at m/z 2845.7, m/z 2867.7, m/z 3084.0, m/z 3105.9, m/z 3110.0 and m/z 3132.0 correspond to $[M + H]^+$, $[M + Na]^+$, $[M + R_{16:0}CO]^+$, $[M + R_{16:0}CO - H + Na]^+$, $[M + R_{18:1}CO]^+$ and $[M + R_{18:1}CO - H + Na]^+$. The sample was prepared by mixing the melittin and liposome dispersion (1:5 peptide:lipid molar ratio) 1:9 (v/v) with DHB (30 mg/mL) in EtOH/H$_2$O (50% v/v).

MALDI-MSMS spectra of [melittin + $R_{18:1}CO]^+$ from the sample with DOPC and [melittin + $R_{18:1}CO]^+$ and [melittin + $R_{16:0}CO]^+$ from the sample with POPC were obtained, from which it was possible to identify sections of sequence, including sections which appeared to include an acyl group. Possible positions at which acylation could have occurred are the side chains of lysine, arginine, serine and tryptophan, the N-terminal amino group and the C-terminal amide (Figure 3.33). Although threonine also has a nucleophilic hydroxyl group, acylation at this position was considered to be unlikely compared to acylation of serine, due to the increased steric hindrance caused by the additional methyl group on threonine.
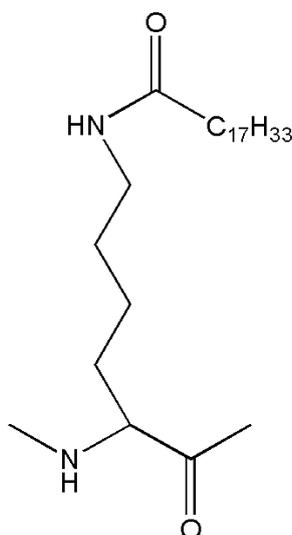
Figure 3.33. Proposed product of addition of the oleoyl chain of DOPC to lysine.

Figure 3.34 shows all of the possible sites of acylation of melittin. The molecular weights of all possible portions of sequence with an acyl group at one of these positions were calculated, including all internal fragments, a, b, c and y sequence ions and y ions where NH_3 was also lost (y-17 ions); a, b, y and y-17 ions are the most likely to be produced under MALDI laser induced fragmentation.[38]

G I G A V L K V L T T G L P A L I S W I K R K R Q Q-NH₂

Figure 3.34. Possible sites of acylation of melittin. The N-terminus, C-terminal amide, lysine, arginine, serine and tryptophan residues are shown in blue.

Only one acylation per section of sequence was accounted for, as the molecular mass of the parent ions only included one acyl group. The *m/z* values of peaks in the product ion spectra of [melittin + $R_{18:1}CO$]$^+$ from the sample with DOPC and [melittin + $R_{18:1}CO$]$^+$ and [melittin + $R_{16:0}CO$]$^+$ from the sample with POPC and were compared with the calculated molecular weights of all possible acylated sequence ions and internal fragments to identify product ions which were within ± 1.5 Da of the molecular weights of acylated sections of sequence. The *m/z* values which corresponded to possible acylated sections of sequence were checked against all possible sequence ions and internal fragments of non-acylated melittin, to rule out misidentification. All *m/z* values within ± 2 Da of the molecular weight of a possible unmodified melittin fragment were ruled out to ensure confidence in the identification of any acylated fragments.

A number of peaks were observed in the product ion spectra of acylated melittin which corresponded to unmodified sequence ions, and comparison between the sequence coverage of modified and unmodified sequence ions provided further information from which the positions of acylation could be determined. Figure 3.35 shows that when non-acylated melittin was fragmented by MALDI-MSMS in the same manner as the acylated species there was virtually full sequence coverage of a, b, or c-ions from the N-terminus and y or y-17 ions from the C-terminus, though a few sequence ions have the same molecular weights as possible internal fragments (shown in green).

Figure 3.35. Sequence ions identified from the product ion spectrum of non-acylated melittin. Amino acids shown in blue are possible sites of acylation; sections of sequence marked in green are those which have the same molecular mass as possible internal fragments. If peaks were observed corresponding to a number of cleavages at the same position, for example a1, b1 and c1, and at least one of these does not have the same molecular mass as a possible internal fragment the section of sequence will be marked in black.

3.2.7.1 DOPC

3.2.7.1.1 Identification of acylated product ions

Table 3.12 and Figure 3.36 show all of the acylated product ions identified in the MALDI-MSMS spectrum of [melittin + $R_{18:1}CO$]$^+$. The spectrum is included as Appendix 1A. Some *m/z* values correspond to two or more possible fragments, as shown by the different colours in Figure 3.36, but others allowed specific sites of acylation to be identified. Sequence ion b2 (*m/z* 435.3) could only have been acylated on the N-terminal amine, and in fragment KVLTT (*m/z* 808.3) acylation could only have occurred on K(7). No other specific sites of acylation could be identified, but all of the *m/z* values correspond to the molecular masses of at least one fragment containing a lysine residue or the N-terminus. Where a number of possible acylation sites could be identified within one fragment or different fragments with the same molecular mass lysine was the most likely point of acylation. The ammonium group of lysine has a lower pKa than the other groups,[39, 40] and though no reference could be found in the literature to non-enzymatic acylation of the epsilon amino group of lysine residues from esters, there are a number of examples of lysine acting as a nucleophile in the addition of reactive acylating agents both *in vitro* and *in vivo*.[41–47] This is supported by the identification of melittin fragments on which acylation could only have occurred on K(7) and no fragments on which acylation had definitely not occurred on a lysine residue or the N-terminus. If the fragments are analysed as if only a lysine residue or the N-terminus could be acylated there are three fragments from which acylation can be narrowed down to the N-terminus (b2, a3 and b4), one where acylation can only have occurred at K(7) (KVLTT), one where acylation can only have occurred at K(21) (WIK) and none where acylation can be isolated to K(23).

Table 3.12. Possible acylated fragments identified from the MALDI-MSMS spectrum of [melittin + R$_{18:1}$CO]$^+$ from melittin with DOPC. Residues on which acylation might have occurred are shown in blue.

Observed *m/z*	Fragment	Peak intensity (a.u.)	Calculated molecular mass (Da)	Possible sites of acylation
435.3	b2	577.3	435.4	N-terminus
464.1	a3	454.1	464.4	N-terminus or S(18)
	IS		465.4	
492.2	KV	4007.6	492.4	N-terminus or K(7)
	b3		492.4	
563.2	b4	1544.6	563.4	N-terminus or W(19)
	WI		564.4	
662.3	b5	274.2	662.5	N-terminus, K(21) or R(22)
	IKR		662.5	
691.5	WIK	109.3	692.5	W(19) or K(21)
808.3	KVLTT	281.2	807.6	K(7) only
977.3	y22	208.1	978.7	C-terminus, K(7), K(21), K(23) or R(22)
	LKVLTTG		977.7	
	KVLTTGL		977.7	
	WIKRK		976.7	
1003.3	b8	215.2	1002.7	N-terminus or K(7)
1076.9	VLKVLTTG	104.7	1076.8	K(7), K(21), S(18) or W(19)
	ALISWIK		1076.7	
1215.5	b10	229.3	1216.9	N-terminus, K(7), S(18) or W(19)
	GLPALISWI		1215.8	
1758.0	LKVLTTGLPALISW	126.4	1758.2	K(7), K(21), S(18) or W(19)
	KVLTTGLPALISWI		1758.2	
	VLTTGLPALISWIK		1758.2	
1941.6	a18	107.5	1941.3	N-terminus, K(7) or S(18)
2835.7	b24	322.4	2836.9	N-terminus, K(7), K(21), K(23), S(18), W(19), R(22), R(24)
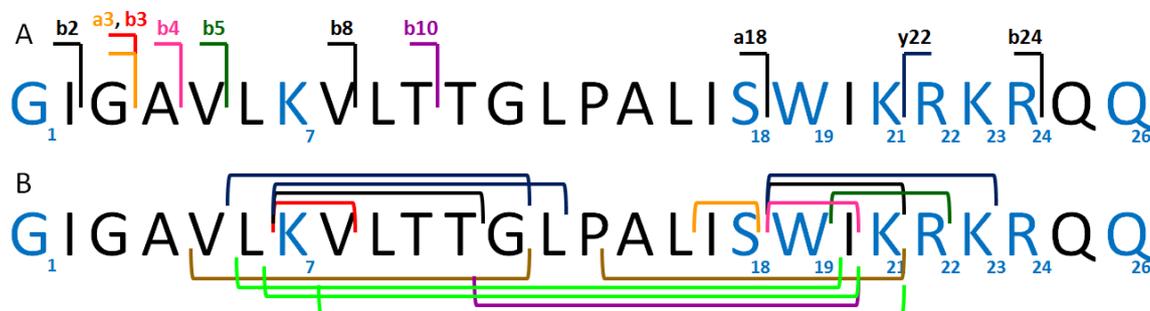
Figure 3.36. Possible acylated fragments identified from the MALDI-MSMS spectrum of [melittin + R$_{18:1}$CO]$^+$ from melittin with DOPC. A) Sequence ions; B) internal fragments. Positions at which acylation might have occurred are shown in blue. Sections marked in the same colour correspond to different fragments with the same molecular mass; sections marked in black are those for which only one type of fragment can be attributed to particular *m/z* value. The C-terminal amide has been omitted for clarity.

3.2.7.1.2   Comparison of sequence coverage of modified and unmodified sequence ions

The product ion spectrum of [melittin + $R_{18:1}CO]^+$ from the sample of melittin with DOPC revealed an unbroken series of non-acylated y or y-17-ions from y26 to y16, only three of which had molecular weights corresponding to possible internal fragments, as well as y14, y12, y11 and y1, (Figure 3.37A and Table 3.13). Only one acylated y-ion, y22, was identified (Figure 3.37B and Table 3.12). Fragment y22 also has the same *m/z* value as a number of possible internal fragments. This suggests that acylation did not occur at the C-terminus. The lack of unmodified y-ions between y11 and y1 suggests that acylation of K(7), the only nucleophilic amino acid in this region, was likely, which correlates with the observation of internal fragment KVLTT, acylated on K(7). A series of acylated and non-acylated a, b, and c-ions were observed up to b5 and a6 respectively from the N-terminus, supporting the conclusion that acylation occurred at the N-terminus and at K(7), though a number of these fragments share the same molecular weight with possible internal fragments. The identification of unmodified fragments c11 and c12 suggests that acylation was not isolated to the N-terminus and K(7), although fragment c11 has the same *m/z* value as two internal fragments. The unmodified fragment b26 is likely to have formed through y-type cleavage of an added acyl chain and b-type cleavage of the C-terminal amide in a similar manner to that of internal fragments rather than b-type fragmentation of melittin with an acylated C-terminus. There is no other evidence of acylation at the C-terminus, and it is an unlikely point of acylation. The peak observed at *m/z* 2844.7 could correspond to c26 or y1 (molecular masses 2844.8 and 2845.7 respectively). Sequence ion y1 could form through y-type cleavage of an added acyl group from the N-terminus; fragment c26 could form through y-type cleavage of the acyl bond and c-type cleavage of the C-terminal amide. Though it is possible that some of the other non-acylated fragments identified have undergone y-type fragmentation of an added acyl chain this is unlikely to have been the main factor in the presence of non-acylated sequence ions as a more even sequence coverage would be expected if this were the case.

Table 3.13. Non-acylated sequence ions identified from the product ion spectrum of [melittin + $R_{18:1}CO$]$^+$ from melittin with DOPC.

Observed m/z	Fragment	Peak intensity (a.u.)	Possible internal fragment?	Calculated molecular mass (Da)
58.6	b1	360.2	No	58.0
74.3	c1	553.8	No	75.1
171.1	b2	647.1	Yes	171.1
200.2	a3	479.9	Yes	200.1
228.2	b3	1305.4	Yes	228.1
299.2	b4	668.7	Yes	299.2
370.0	a5	377.9	Yes	370.2
398.2	b5	436.5	Yes	398.2
482.1	a6	420.1	Yes	483.3
1069.5	c11	262.5	Yes	1070.7
1128.1	c12	376.0	No	1127.7
2826.4	b26	316.1	No	2827.8
2844.7	c26	376.8	No	2844.8
129.1	y-17 26	3687.9	Yes	129.9
256.1	y-17 25	474.5	No	257.1
274.1	y25	812.1	Yes	274.2
413.2	y-17 24	435.8	Yes	413.2
430.1	y24	639.9	No	430.3
541.0	y-17 23	330.0	Yes	541.3
558.2	y23	501.1	No	558.3
697.1	y-17 22	501.1	Yes	697.4
714.1	y22	581.2	Yes	714.4
825.1	y-17 21	401.4	Yes	825.5
842.2	y21	425.9	No	842.5
938.2	y-17 20	304.7	Yes	938.6
955.3	y20	389.6	Yes	955.6
1141.4	y19	428.4	No	1141.7
1228.7	y18	179.1	No	1228.7
1341.5	y17	165.2	No	1341.8
1438.5	y-17 16	173.1	Yes	1437.9
1606.1	y-17 14	217.6	Yes	1606.0
1622.6	y14	287.3	Yes	1623.0
1775.8	y-17 12	127.3	Yes	1776.1
1793.6	y12	210.1	No	1793.1
1877.2	y-17 11	206.5	No	1877.1
2844.7	y1	376.8	No	2845.7

A

$$\text{G}_1 \text{ I G A V L K}_7 \text{ V L T T G L P A L I S}_{18} \text{W}_{19} \text{ I K}_{21} \text{ R}_{22} \text{ K}_{23} \text{ R}_{24} \text{ Q Q}_{26}$$

B

$$\text{G}_1 \text{ I G A V L K}_7 \text{ V L T T G L P A L I S}_{18} \text{W}_{19} \text{ I K}_{21} \text{ R}_{22} \text{ K}_{23} \text{ R}_{24} \text{ Q Q}_{26}$$
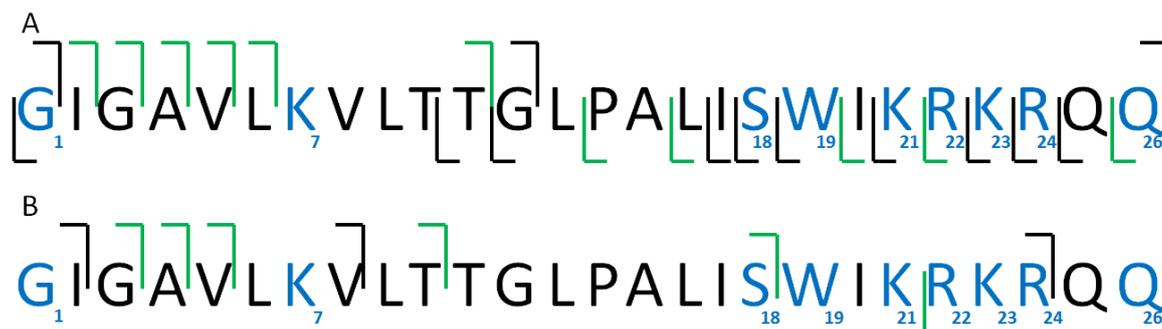
Figure 3.37. Non-acylated and acylated sequence ions identified from the product ion spectrum of [melittin + $R_{18:1}CO]^+$ from melittin with DOPC. A) Non-acylated sequence ions; B) acylated sequence ions. Amino acids shown in blue are possible sites of acylation; sections of sequence marked in green are those which have the same molecular mass as possible internal fragments (non-acylated or acylated for Figures 3.37A and B respectively). If peaks were observed corresponding to a number of cleavages at the same position, for example a1, b1 and c1, and at least one of these does not have the same molecular mass as a possible internal fragment the section of sequence will be marked in black.

3.2.7.2 POPC palmitoyl chain

3.2.7.2.1 Identification of acylated product ions

Similarly to the analysis of [melittin + $R_{18:1}CO]^+$, some peaks observed in the MSMS spectrum of [melittin + $R_{16:0}CO]^+$ from melittin with POPC correspond to two or more possible fragments (Figure 3.38, Table 3.14 and Appendix 1B), but acylation could be isolated to the N-terminal amine, from the fragment with *m/z* 382.1 (a2). No other specific sites of acylation could be identified, but all of the *m/z* values corresponded to at least one fragment containing lysine or the N-terminus. If only acylation of lysine or the N-terminal amine are considered, there is one fragment in which acylation can only have occurred on the N-terminus (a2) and three (two of which have the same molecular mass) for which acylation can only have occurred on K(21) or K(23) (IKRKR and KRKR or RKRQ).

Two peaks corresponding to possible acylated species were observed in the product ion spectra of both [melittin + $R_{16:0}CO]^+$ and [melittin + $R_{18:1}CO]^+$ from the sample of melittin with POPC. These peaks were observed at *m/z* 409.3 and 537.2 in the product ion spectrum of [melittin + $R_{16:0}CO]^+$, with possible identities of b2 and b4 respectively. In the product ion spectrum of [melittin + $R_{18:1}CO]^+$ they were observed at *m/z* 410.0 and 537.1, possibly corresponding to y26 and y25 or SW respectively. They were discounted from the results as it was likely that they were caused by incomplete isolation of one or other acylated melittin parent ions. Peaks were not observed at these *m/z* values in the product ion spectrum of [melittin + $R_{18:1}CO]^+$ from the sample of melittin with DOPC, which suggests that they did not arise from the [melittin + $R_{18:1}CO]^+$ parent from the sample with

POPC. All but one of the other species identified in the product ion spectrum of [melittin + $R_{18:1}CO]^+$ from the sample of melittin with POPC were also observed in the spectrum of melittin with DOPC.

Table 3.14. Possible acylated fragments identified from the MALDI-MSMS spectrum of [melittin + $R_{16:0}CO]^+$ from melittin with POPC. Residues on which acylation might have occurred are shown in blue.

Observed *m/z*	Fragment	Peak intensity (a.u.)	Calculated molecular mass (Da)	Possible sites of acylation
382.1	a2	1439.4	381.3	N-terminus
466.2	b3	13559.6	466.4	N-terminus or K(7)
	KV		466.4	
636.2	b5	1024.3	636.5	N-terminus, K(21), R(22)
	IKR		636.5	
808.2	KRKR	716.7	807.6	K(21), K(23), R(22) or R(24)
	RKRQ		807.6	
	ALISW		809.6	
921.3	IKRKR	511.3	920.7	K(21), K(23), S(18), W(19), R(22) or R(24)
	ALISWI		922.6	
976.2	b8	1081.0	976.7	N-terminus or K(7)
1742.2	b16	403.5	1743.2	N-terminus or K(7)
2840.5	y-17 4	1629.3	2839.9	C-terminus, K(7), K(21), K(23), S(18), W(19), R(22), R(24)
2938.1	b25	494.6	2938.9	N-terminus, K(7), K(21), K(23), S(18), W(19), R(22), R(24)
2957.0	c25	1282.0	2955.9	N-terminus, K(7), K(21), K(23), S(18), W(19), R(22), R(24)
3010.2	y-17 2	6488.1	3010.0	C-terminus, K(7), K(21), K(23), S(18), W(19), R(22), R(24)
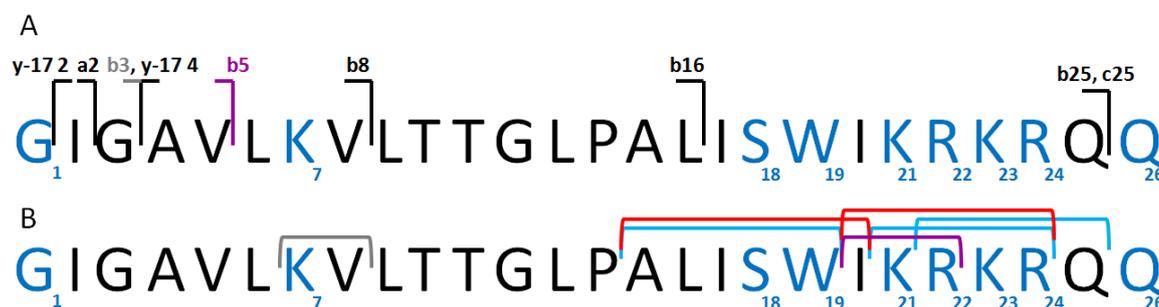
Figure 3.38. Possible acylated fragments identified from the MALDI-MSMS spectrum of [melittin + $R_{16:0}CO]^+$ from melittin with POPC. A) Sequence ions; B) internal fragments. Positions at which acylation might have occurred are shown in blue. Sections marked in the same colour correspond to fragments with the same molecular mass; sections marked in black are those for which only one type of fragment can be attributed to particular molecular mass. The C-terminal amide has been omitted for clarity.

3.2.7.2.2 Comparison of sequence coverage of modified and unmodified sequence ions

A long series of unmodified y and y-17-ions were identified from the product ion spectrum of [melittin + $R_{16:0}CO]^+$ (Figure 3.39A and Table 3.15), with only one missed cleavage between y26 and y11, with three ions which have the same molecular masses as internal fragments, compared with only two modified y or y-17 ions (Figure 3.39B and Table 3.14), both of which were close to the N-terminus. Similarly to the results for [melittin + $R_{18:1}CO]^+$ with DOPC, this suggests that the C-terminal amide was not acylated. The lack of unmodified ions between y11 and y1 suggests acylation of K(7), the only nucleophilic species within this section of sequence. The acylated ions b2, a3 and b5 indicate acylation at the N-terminus, and for ions b8 and b16 acylation could have occurred at the N-terminus or K(7). The unbroken series of non-acylated a, b and c ions from c1 to b6 suggest acylation on K(7), but the presence of non-acylated b7, b8 and c12 ions indicates that acylation was not restricted to the N-terminus and K(7). The peak observed at *m/z* 2828.8 could correspond to sequence ions b26 or y-17 1, and the peak at *m/z* 2846.5 could correspond to ions c26 or y1. As described in section 3.2.7.4.1, the non-acylated fragments b26 and c26 could have formed through an internal-like fragmentation involving y-type cleavage of an acyl chain and b or c-type cleavage at the C-terminus. The y1 and y-17 1 fragments could have occurred from y-type cleavage of an acylated N-terminal amide with or without an additional loss of NH_3.

Table 3.15. Non-acylated sequence ions identified from the product ion spectrum of [melittin + $R_{16:0}CO]^+$ from melittin with POPC.

Observed m/z	Fragment	Peak intensity (a.u.)	Possible internal fragment?	Calculated molecular mass (Da)
74.8	c1	2211.3	No	75.1
143.2	a2	938.8	No	143.1
171.2	b2	4039.7	Yes	171.1
200.2	a3	2266.5	Yes	200.1
228.2	b3	8587.2	Yes	228.1
246.2	c3	1666.4	No	245.2
272.2	a4	2716.0	Yes	271.2
299.1	b4	2407.9	Yes	299.2
369.1	a5	3693.2	Yes	370.2
398.1	b5	2187.1	Yes	398.2
482.1	a6	2478.1	Yes	483.3
511.1	b6	976.1	Yes	511.3
640.1	b7	781.2	No	639.4
737.3	b8	616.8	No	738.5
1128.3	c12	1014.0	No	1127.7
2827.9	b26	1666.7	No	2827.8
2843.9	c26	1473.8	No	2844.8
129.2	y-17 26	29170.8	Yes	129.9
146.2	y26	1066.0	No	146.1
256.2	y-17 25	2169.3	No	257.1
274.1	y25	4925.7	Yes	274.2
413.1	y-17 24	2058.1	Yes	413.2
430.1	y24	1710.0	No	430.3
541.1	y-17 23	1746.9	Yes	541.3
558.1	y23	1620.3	No	558.3
697.1	y-17 22	1711.8	Yes	697.4
714.1	y22	1971.8	Yes	714.4
825.2	y-17 21	1205.7	Yes	825.5
842.3	y21	1124.1	No	842.5
955.1	y20	1908.5	Yes	955.6
1124.7	y-17 19	883.4	No	1124.7
1211.2	y-17 18	466.2	No	1211.7
1228.4	y18	625.7	No	1228.7
1325.0	y-17 17	347.1	No	1324.8
1341.7	y17	350.1	No	1341.8
1438.3	y-17 16	360.1	Yes	1437.9
1454.8	y16	389.8	No	1454.9
1605.9	y-17 14	799.2	Yes	1606.0
1622.5	y14	727.9	Yes	1623.0
1777.1	y-17 12	473.9	Yes	1776.1
1794.1	y12	478.7	No	1793.1
1894.7	y11	513.8	No	1894.2
2827.9	y-17 1	1666.7	No	2828.8
2846.5	y1	507.7	No	2845.8
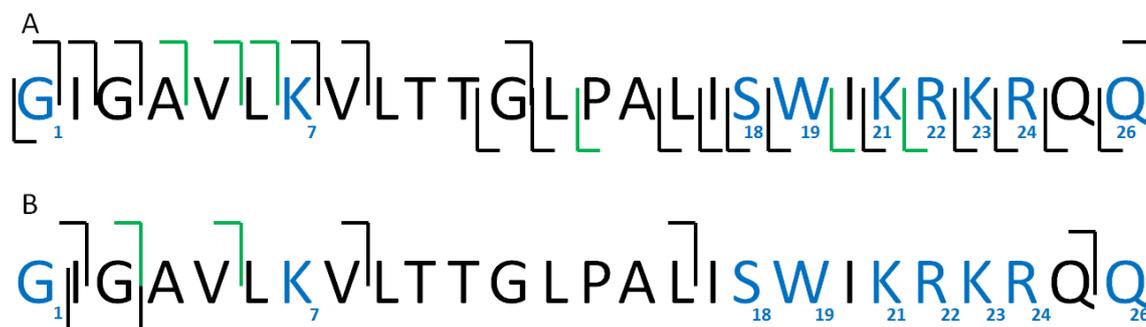
Figure 3.39. Non-acylated and acylated sequence ions identified from the product ion spectrum of [melittin + R$_{16:0}$CO]$^+$ from melittin with POPC. A) Non-acylated sequence ions; B) acylated sequence ions. Amino acids shown in blue are possible sites of acylation; sections of sequence marked in green are those which have the same molecular mass as possible internal fragments (non-acylated or acylated for Figures 3.39A and B respectively). If peaks were observed corresponding to a number of cleavages at the same position, for example a1, b1 and c1, and at least one of these does not have the same molecular mass as a possible internal fragment the section of sequence will be marked in black.

3.2.7.3 POPC oleoyl chain

3.2.7.3.1 Identification of acylated product ions

The MSMS spectrum of [melittin + R$_{18:1}$CO]$^+$ from melittin with POPC revealed a number of acylated product ions (Figure 3.40, Table 3.16 and Appendix 1C). The majority of the *m/z* values correspond to two or more possible acylated fragments, but acylation could be isolated to the N-terminal amine, from the fragment with *m/z* 435.0 (b2). No other specific sites of acylation could be identified, but all of the *m/z* values corresponded to at least one fragment containing a lysine residue or the N-terminus. If only the possibility of lysine of N-terminal acylation is considered, acylation can be isolated to the N-terminus from three fragments (b2, a3 and b4) and to either K(21) or K(23) from one fragment (y-17 13).

Table 3.16. Possible acylated fragments identified from the MALDI-MSMS spectrum of [melittin + R$_{18:1}$CO]$^+$ from melittin with POPC. Residues on which acylation might have occurred are shown in blue.

Observed *m/z*	Fragment	Peak intensity (a.u.)	Calculated molecular mass (Da)	Possible sites of acylation
435.0	b2	324.0	435.4	N-terminus
464.1	a3	428.6	464.4	N-terminus or S(18)
	IS		465.4	
492.2	b3	2294.5	492.4	N terminus or K(7)
	KV		492.4	
563.2	b4	1179.3	563.4	N-terminus or W(19)
	WI		564.4	
663.2	b5	342.8	662.5	N terminus, K(21) or R(22)
	IKR		662.5	

1982.5	y-17 13	176.3	1983.2	C-terminus, K(21), K(23), S(18), W(19), R(22), R(24)
2837.6	b24	262.0	2836.8	N-terminus, K(7), K(21), K(23), S(18), W(19), R(22), R(24)
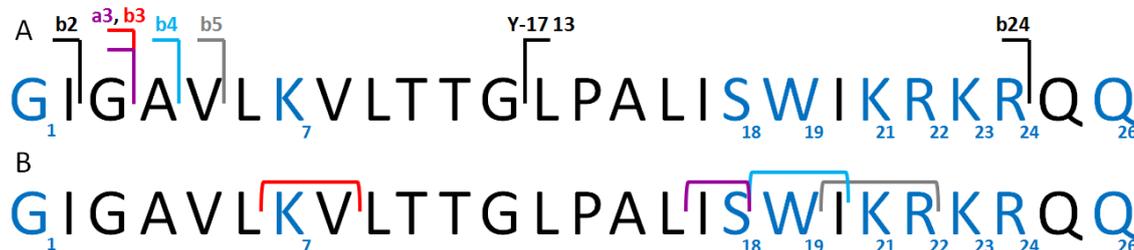
Figure 3.40. Possible acylated fragments identified from the MALDI-MSMS spectrum of [melittin + $R_{18:1}CO$]$^+$ from melittin with POPC. A) Sequence ions; B) internal fragments. Positions at which acylation might have occurred are shown in blue. Sections marked in the same colour correspond to fragments with the same molecular mass; sections marked in black are those for which only one type of fragment can be attributed to particular molecular mass. The C-terminal amide has been omitted for clarity.

3.2.7.3.2 Comparison of sequence coverage of modified and unmodified sequence ions

The product ion spectrum of [melittin + $R_{18:0}CO$]$^+$ revealed a long series of unmodified y or y-17 ions from y-17 26 to y11 with only two missed cleavages and five ions which could also correspond to internal fragments (Figure 3.41 and Table 3.17), suggesting that the C-terminus was not acylated. The lack on unmodified fragments between y11 and y2 suggests acylation of K(7), the only likely site of acylation in this section of sequence. One modified y-ion, y-17 13, was identified (Figure 3.41 and Table 3.16), indicating that there was at least one point of acylation other than the N-terminus or K(7). Acylated and non-acylated a, b and c ions were observed up to b5 and b6 respectively, suggesting that acylation may have occurred on K(7). The next cleavages were b24 and c12 for acylated and non-acylated fragments respectively. The modified and unmodified sequence ions indicate that the N-terminus, K(7) and at least one other position were acylated. Peaks corresponding to unmodified fragments b26 and y-17 1, and c26 and y1 were also observed. As described in sections 3.2.7.4.1 and 3.2.7.4.2, the non-acylated b26 and c26 fragments could have formed through y-type cleavage of an acyl chain and b or c-type cleavage at the C-terminus. The y1 and y-17 1 fragments could have occurred through y-type cleavage of an acylated N-terminal amide with or without an additional loss of NH_3.

Table 3.17. Non-acylated sequence ions identified from the product ion spectrum of [melittin + R$_{18:1}$CO]$^+$ from melittin with POPC.

Observed m/z	Fragment	Peak intensity (a.u.)	Possible internal fragment?	Calculated molecular mass (Da)
74.0	c1	642.9	No	75.1
171.1	b2	631.5	Yes	171.1
200.1	a3	364.0	Yes	200.1
228.1	b3	1670.1	Yes	228.1
272.2	a4	562.4	Yes	271.2
299.1	b4	881.5	Yes	299.2
369.0	a5	780.1	Yes	370.1
398.1	b5	617.3	Yes	398.1
482.1	a6	476.7	Yes	483.3
1128.2	c12	725.9	No	1127.7
1520.5	c16	177.8	Yes	1522.0
2827.5	b26	182.0	No	2827.8
2845.1	c26	442.7	No	2844.8
129.1	y-17 26	3367.7	Yes	129.9
256.1	y-17 25	437.3	No	257.1
274.0	y25	809.0	Yes	274.2
413.0	y-17 24	441.8	Yes	413.2
430.1	y24	705.6	No	430.3
540.9	y-17 23	462.9	Yes	541.3
558.1	y23	627.1	No	558.3
697.2	y-17 22	427.0	Yes	697.4
714.1	y22	897.5	Yes	714.4
825.1	y-17 21	503.6	Yes	825.5
842.2	y21	609.2	No	842.5
938.2	y-17 20	471.5	Yes	938.6
955.3	y20	1016.5	Yes	955.6
1124.5	y-17 19	168.5	No	1124.7
1210.7	y-17 18	191.8	No	1211.7
1229.0	y18	176.4	No	1228.7
1342.5	y17	167.9	No	1341.8
1520.5	y16	177.8	Yes	1454.9
1607.0	y-17 14	169.8	Yes	1606.0
1623.5	y14	258.7	Yes	1623.0
1793.3	y12	211.9	No	1793.1
1893.9	y11	126.5	No	1894.2
2771.5	y-17 2	97.2	No	2771.7
2827.5	y-17 1	182.0	No	2828.8
2845.1	y1	442.7	No	2845.8
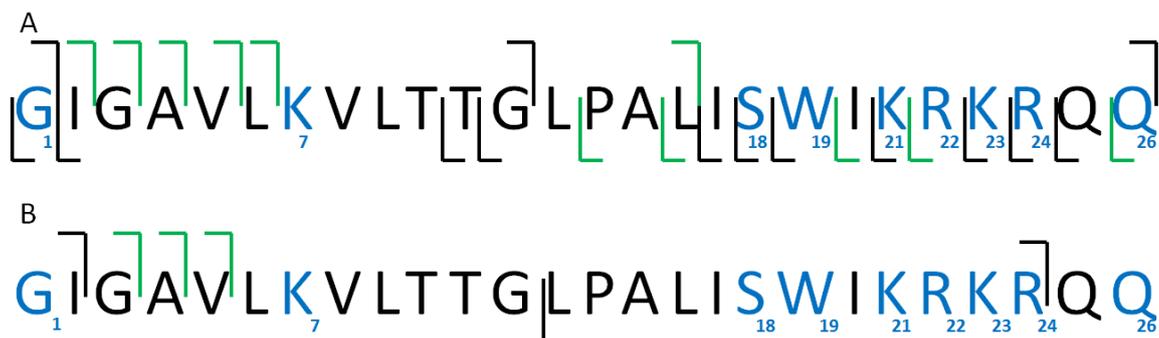
Figure 3.41. Non-acylated and acylated sequence ions identified from the product ion spectrum of [melittin + $R_{18:1}CO]^+$ from melittin with POPC. A) Non-acylated sequence ions; B) acylated sequence ions. Amino acids shown in blue are possible sites of acylation; sections of sequence marked in green are those which have the same molecular mass as possible internal fragments (non-acylated or acylated for Figures 3.41A and B respectively). If peaks were observed corresponding to a number of cleavages at the same position, for example a1, b1 and c1, and at least one of these does not have the same molecular mass as a possible internal fragment the section of sequence will be marked in black.

3.2.7.4   Summary of melittin acylation

The MSMS analyses of [melittin + $R_{18:1}CO]^+$ from the samples of melittin with DOPC and POPC and [melittin + $R_{16:0}CO]^+$ from the sample with POPC all showed that acylation had occurred on the N-terminal amino group. The addition of an oleoyl chain was also identified at K(7) of melittin from the sample with DOPC. There were no cases identified where fragmentation definitely occurred at a position other than the N-terminus or a lysine residue. When the acylated fragments were reviewed in terms of just acylation of the N-terminal amine or a lysine residue, acylation was identified on the N-terminal amine for each acylated parent ion. Acylation could be identified on K(7) and K(21) from the product ion spectrum of [melittin + $R_{18:1}CO]^+$ from melittin with DOPC, and on either K(21) or K(23) for the oleoyl and palmitoyl adducts of melittin with POPC. Comparison between the acylated and non-acylated sequence ions identified from each acylated parent ion showed that C-terminal acylation was unlikely to have occurred and showed that acylation was likely to have occurred at the N-terminus, K(7) and at least one other position.

3.3   Conclusions

3.3.1   Lipid stability

A number of analyses were carried out with the aim of determining the stability of DOPC and DPPC liposomes with respect to hydrolysis and fusion or micellisation. Prof. Rodger reported changes in the binding of antimicrobial peptides to liposomes depending

on how long after preparation the liposomes were used, and hydrolysis, fusion or micellisation had been proposed as possible reasons for this.[28] No changes to any of the liposome samples were observed. These results are encouraging in that they show that the liposomes are stable with respect to hydrolysis over the course of 2–3 weeks, and they showed that hydrolysis, fusion and micellisation were not the cause of the changes noted by Prof. Rodger.

In the course of these analyses it became apparent that a certain amount of oxidised lipids were present in both the DOPC and POPC stocks. Comparison between a new batch of DOPC, which was stored at -20 °C as a powder up until analysis, and a batch which had been stored at -20 °C as a solution in $CHCl_3$ for a number of months showed that storage in $CHCl_3$ was not the cause of the oxidation. It was not possible to observe an increase in oxidation products in the liposome samples analysed, as the peaks corresponding to the oxidation products in the MALDI-MS spectra obtained were variable in intensity. This observation was supported by the fact that no oxidation product of DOPC was observed by ^{1}H NMR analysis of a sample of the same stock solution which gave intense peaks corresponding to the oxidation product in MALDI-MS spectra, suggesting that the actual concentration of the oxidation product was very low, below the detection limit of the 700 MHz NMR spectrometer used, and that it must be very easily ionisable to be observed so strongly in the mass spectra. The presence of a very small concentration of oxidised lipid in the liposomes used in peptide binding experiments is unlikely to have had a significant effect on peptide binding experiments, and any effect will have been consistent due to the presence of the oxidised species in the lipid stocks rather than forming during liposome storage.

3.3.2 The effect of small molecules on DOPC liposomes

The observation that HFIP did not cause the hydrolysis of DOPC liposomes is in keeping with the model proposed in the literature, where the alcohol inserts between lipid headgroups in a bilayer, increasing the lateral pressure in the headgroup region and decreasing it in the chain region, thereby causing permeability through physical disruption of the bilayer rather than chemical disruption.

The results of the analysis of haloperidol with liposomes, intended as a test of the use of MALDI-MS to plot the hydrolysis of liposomes over time, was unexpected, but can most likely be attributed to the very small sample quantity and its sticky consistency limiting the mixing of the drug and the lipid molecules. The sample may also have evaporated partly, due to the very small quantity in a 1 mL sample vial, leaving few water molecules to carry out the hydrolysis. The analysis of the samples of DOPC with melittin

showed that the lyso-lipids could be detected by MALDI-MS however, and that qualitative increases in their concentration could be monitored.

3.3.3 The effect of melittin on lipid bilayers

3.3.3.1 Acyl chain lysis in the presence of melittin

DMPC liposomal lipids were observed to undergo rapid acyl chain lysis over 5 minutes in the presence of natural melittin and the absence of EDTA and no acyl chain lysis over 10 minutes in the presence of 2 mM EDTA. Some hydrolysis of DOPC was observed after 24 hours in the presence of natural melittin and 1 mM EDTA. The lysis in these samples was attributed to hydrolysis by PLA_2 in the sample, due to incomplete chelation of Ca^{2+} when only 1 mM EDTA was used, as a concentration of 5 mM is required for complete chelation of Ca^{2+}.[20] These results were consistent with those reported in the literature.[21, 22] For the first 24 hours after addition, no acyl chain lysis was observed of DOPC liposomes in the presence of synthetic (and therefore PLA_2-free) melittin. After 48 hours however it became clear that with a 5:1 lipid:peptide molar ratio lyso-PC was being formed compared to the control sample to which melittin had not been added. A small amount of sn-glycero-3-phosphocholine was also observed. These results suggest that melittin does promote the lysis of the acyl chains of phospholipids, though over a much slower timescale than in the presence of PLA_2. The two likely explanations for the observed acyl chain lysis are a) hydrolysis, caused by the perturbation of the liposome bilayer by melittin allowing water to access the core of the bilayer, thereby permitting hydrolysis to occur, and/or b) acyl transfer occurring from the lipids to nucleophilic groups of melittin when inserted in the bilayer. TLC analysis of a sample of DOPC 17 days after the addition of synthetic melittin showed the presence of lyso-PC but not oleic acid. This suggests that the mechanism of acyl chain lysis involved acyl chain transfer to melittin rather than hydrolysis.

A clear increase in acyl chain lysis was observed in the presence of melittin and Zn^{2+}. The presence of low concentrations of Zn^{2+} (up to approximately 1 mM) has been found to increase the percentage lysis of liposomes composed of PC or PC/PS (85:15) when compared with liposomes prepared in the absence of Zn^{2+}.[48] This is thought to be due to binding of the metal ions to the surface of the membrane promoting the binding of melittin. This enhancement of liposome lysis in the presence of Zn^{2+} correlates with the results reported herein for acyl chain lysis in the presence of Zn^{2+}. The increased lysis in the presence of Zn^{2+} may reflect increased melittin binding, supporting either the acyl transfer or the melittin-promoted hydrolysis mechanisms, or may be due to the catalysis of ester hydrolysis by Zn^{2+} acting as a Lewis acid.

Melittin did not promote acyl chain lysis when NaCl was excluded from the buffer. This observation is likely to be due to the different conformations of melittin, which are known to be affected by the ionic strength of the buffer. At a neutral or basic pH and in the presence of buffer salts (e.g. 300 mM NaCl), melittin has been shown to form tetrameric aggregates.[49] In lower ionic strength buffers (e.g. 150 mM NaCl), melittin exists as a monomer, but has a rigid α-helical secondary structure. In the absence of added salt, melittin exists as a flexible random coil monomer.[50–52] Red edge excitation shift (REES) analysis of membrane-bound melittin in the presence and absence of NaCl has shown that in the absence of NaCl the water molecules around the tryptophan residue of melittin are rapidly reorienting, giving no REES and suggesting that the residue is not buried in the membrane. In the presence of up to 150 mM NaCl a red-edge shift was reported, suggesting that the tryptophan residue was localised inside the membrane.[53] If melittin does not insert into the membrane in the absence of NaCl, as reported in the literature, this would explain the lack of lysis observed in the absence of NaCl. This supports either model of acyl chain lysis: membrane perturbation by melittin allowing water to access the hydrophobic core of the bilayer for hydrolysis to occur, or acyl transfer to nucleophilic groups of melittin when the peptide is inserted in the membrane.

The MALDI-MS spectrum of POPC to which melittin had been added showed a greater intensity of the peak corresponding to a loss of the oleoyl chain from the *sn*-2 position than that corresponding to the loss of the palmitoyl chain from the *sn*-1 position. Reports of acid and alkali catalysed hydrolysis of POPC in the literature state that equal hydrolysis of the palmitoyl and oleoyl chains was observed, therefore the unequal levels of lysis at the *sn*-1 and *sn*-2 positions must be accounted for by some other mechanism.[9, 54]

3.3.3.2 *Melittin acylation in liposomal membranes*

MALDI-MS analyses of the samples of melittin with DOPC and POPC liposomes showed addition of the oleoyl chain of DOPC and the palmitoyl and oleoyl chains of POPC to the peptide. It was established through MSMS analysis that in each case acyl transfer was occurring on the N-terminal amine of melittin. Fragments were also identified in which oleoyl chain of DOPC had added to K(7). There were no cases where acylation definitely occurred at a position other than the N-terminus or a lysine residue. A number of *m/z* values corresponded to more than one acyated fragment, but in each case there was at least one fragment containing a lysine residue or the N-terminus. In some cases there were a number of possible sites of acylation within one fragment or within fragments

with the same molecular weight. As stated in section 3.2.7.1.1, the N-terminus and lysine residues are the most likely points of acylation. When other acylation sites were discounted, the addition of an acyl chain to the N-terminus and to K(7) could be identified from the product ion spectra of [melittin + $R_{18:1}CO$]$^+$ from DOPC and POPC and from the product ion spectrum of [melittin + $R_{16:0}CO$]$^+$ from POPC. The addition of the oleoyl chain of DOPC to K(21) was identified, along with oleoyl and palmitoyl adducts of melittin with POPC in which acylation had occurred at K(21) or K(23). There was no evidence that acylation had definitely occurred on K(23). When the sequence coverage of acylated and non-acylated sequence ions was compared for each acylated parent ion it was established that acylation was unlikely to have occurred at the C-terminus and in each case was likely to have occurred on the N-terminal amine, K(7) and on at least one other residue. The results of melittin acylation reported herein are consistent with reports of the structure, orientation and location of melittin within lipid membranes. It is assumed that under the conditions in which melittin became acylated the peptide had an α-helical structure, due to the presence of 150 mM NaCl in the buffer.[53] Solid-state NMR analysis has shown that melittin is also helical in the presence of lipid.[55] Hristova *et al.* established from oriented circular dichroism (OCD) analysis that melittin helices bind parallel to DOPC membranes.[56] They followed this with x-ray diffraction, from which the location of a melittin helix within a DOPC bilayer could be determined. The helix was found to be centred close the glycerol groups of the lipids, 17.5 Å from the centre of the bilayer. The edge of the helix extended to the depth of the oleoyl double bonds. This position within the membrane is entirely consistent with membrane acylation. The presence of acylated melittin shows that the formation of lyso-PC is at least partially due to acyl transfer to melittin, and the observed absence of oleic acid in the TLC analysis of DOPC liposomes after the addition of synthetic melittin (Figure 3.25) suggests that acyl transfer is the principle cause of the formation of lyso-PC.

The peak corresponding to [melittin + $R_{18:1}CO$]$^+$ had a greater intensity than that corresponding to [melittin + $R_{16:0}CO$]$^+$ in all of the MALDI analyses of samples of melittin and POPC. This is likely to account for the greater intensity of the peaks corresponding to lyso-PPC compared to those corresponding to lyso-OPC which gave the appearance of increased hydrolysis at the *sn*-2 position of POPC, as more acyl transfer was occurring from the *sn*-2 position than the *sn*-1 position and giving a greater quantity of lyso-PPC than lyso-OPC.

3.4 Future work

The formation of lyso-lipids discussed above has been followed by MALDI-MS using the intensity of the lyso-PC normalised relative to the combined intensities of the peaks corresponding to the lyso-lipid and the molecular ion. Although this method allowed the lyso-lipid formation to be followed qualitatively, the results had a poor signal to noise ratio with a large margin of error. More accurate data could be provided from LCMS analysis of the liposome/melittin dispersion, as the LC trace would provide a quantitative analysis of the lyso-lipid content if compared to standards. The trade-off for this increase in accuracy would be the need to find a different buffer system which was compatible with chromatography, as sodium phosphate buffer is non-volatile and would contaminate the mass spectrometer,[57] and the requirement for a much larger sample volume. The formation of lyso-lipids is likely to be accompanied by the generation of detergent micelles, the formation of which could be monitored by dynamic light scattering to provide a fuller picture of the process and the timescale upon which it was occurring.

The MALDI-MS analysis of the acyl adducts of melittin did not provide a clear indication as to the quantity of adducts formed. Separation of melittin and the adduct by liquid chromatography may allow the adduct to be quantified and therefore give an idea as to the extent of melittin modification occurring.

3.5 References

1. D. K. Kim and J. Dobson, *J. Mater. Chem.*, 2009, **19**, 6294–6307.

2. D.A. Miller, J.C. DiNunzio and R.O. Williams III. *Drug Dev. Ind. Pharm.*, 2008, **34**, 117–133.

3. M. Grit and D.J.A. Crommelin, *Chem. Phys. Lipids*, **64**, 1993, 3–18.

4. M. Grit, W.J. M. Underberg, D.J. A. Crommelin, *J. Pharm. Sci.*, 1993, **82**, 362–366.

5. F. Nacka, M. Cansell and B. Entressangles, *Lipids*, 2001, **36**, 35–42.

6. B. Pietzyk, K. Henschke, *Int. J. Pharm.*, 2000, **196**, 215–218.

7. J. A. Zhanga, J. Pawelchak, *Eur. J. Pharm. Biopharm.*, 2000, **50**, 357–364.

8. M. Grit, N.J. Zuidam, W.J.M. Underberg, D.J.A. Crommelin, *J. Pharm. Pharmacol.*, 1993*, **45**, 490–495.

9. C.R. Kepsil and E.A. Dennis, *Biochemistry*, 1981, **20**, 6079–6085.

10. M. Grit and D.J.A. Crommelin, *Biochim. Biophys. Acta*, 1993, **1167**, 49–55.

11. M. Grit and D.J.A. Crommelin, *Chem. Phys. Lipids,* 1992, **62**, 113–122.

12. J.M.H. Kremer and P.H. Wiersema, *Biochim. Biophys. Acta,* 1977, **471**, 348–360.

13. K. Inoue and T. Kitagawa, *Biochim. Biophys. Acta,* 1974, **363**, 361–372.

14. N.A. Porter, S.E. Caldwell and K.A. Mills, *Lipids*, 1995, **30**, 277–290.

15. E.N. Frankel, *Chem. Phys. Lipids*, 1987, **44**, 73–85.

16. M.D. Guillén and A. Ruiz, *Trends Food Sci. Technol.* 2001, **12**, 328–338.

17. E.N. Frankel, *Prog. Lipid Res.* 1980, **19**. 1–22.

18. J. Santrock, R.A. Gorski and J.F. O'Gara, *Chem. Res. Toxicol.*, 1992, **5**, 134–141.

19. K. Sabatini, J.-P. Mattila, F. M. Megli and P.K.J. Kinnunen, *Biophys. J.*, 2006, **90**, 4488–4499.

20. C.E. Dempsey, *Biochim. Biophys. Acta,* 1990, **1031**, 143–161.

21. M. Murakami and I. Kudo, *J. Biochem.*, 2002, **131**, 285–92.

22. Y. Cajal and M.K. Jain, *Biochemistry*, 1997, **36**, 3882–3893.

23. C. Steinem, H.-J. Galla and A. Janshoff, *Phys. Chem. Chem. Phys.*, 2000, **2**, 4580–4585.

24. M. Baciu, S.C. Sebai, O. Ces, X. Mulet, J.A. Clarke, G.C. Shearman, R.V Law, R.H Templer, C. Plisson, C.A. Parker and A. Gee, *Phil. Trans. R. Soc. A*, 2006, **364**, 2597–2614.

25. D.R. Casey, S.C. Sebai, G.C. Shearman, O. Ces, R.V. Law and R.H. Templer, *Ind. Eng. Chem. Res.* 2008, **47**, 650–655.

26. E. van den Brink-van der Laan, V. Chupin, J.A. Killian, and B. de Kruijff, *Biochemistry*, 2004, **43**, 5937–5942.

27. S.M. Ennaceur and J.M. Sanderson, *Langmuir*, 2005, **21**, 552–561.

28. A. Rodger, personal communication.

29. J.R. Silvius in *Lipid Protein Interactions*, ed. P.C. Jost and O.H. Griffth, John Wiley and Sons, New York, USA, 1982, Vol. 2, pp. 240–281.

30. C. Nora, S. Mabic and D. Darbouret, *Ultrapure Water*, 2002, 56–60.

31. K. Matsuzaki, S. Yoneyama and K. Miyajima, *Biophys. J.*, 1997, **73**, 831–838.

32. C. Dempsey, M. Bitbol and A. Watts, *Biochemistry*, 1989, **28**, 6590–6596.

33. P. Roepstorff, J. Fohlman, *Biomed. Mass Spectrom.*, 1984, **11**, 601–601.

34. A. Schlosser and W.D. Lehmann, *J. Mass Spectrom.*, 2000, **35**, 1382–1390.

35. R.A. Zubarev, K.F. Haselmann, B. Budnik, F. Kjeldson and F. Jensen, *Eur. J. Mass Spectrom.*, 2002, **8**, 337–349.

36. Sigma-Aldrich Product Information Sheet Basel Salt Mixtures, Product D8662.

37. R. Dulbecco, and M. Vogt, *J. Exp. Med.*, 1957, **106**, 167–169.

38. N. Shenar, N. Sommerer, J. Martineza and C. Enjalbal, *J. Mass Spectrom.*, 2009, **44**, 621–632.

39. R. Garrett and C.M. Grisham, *Biochemistry*, Cengage Learning, Boston, USA, 4th edn., 2008.

40. W.A. Remers, *Indoles*, Vol. 25, Part 1, Wiley Interscience, New York, USA, 1979.

41. P.P. Batra, M.A. Roebuck, and D. Uetrecht, *J. Protein Chem.*, 1990, **9**, 37–44.

42. A.E. Jackson and D. Puett, *J. Biol. Chem.*, 1984, **259**, 14985–14992.

43. A.C. Brinegar and J.E. Kinsella, *J. Agric. Food Chem.* 1980, **28**, 818–824.

44. A. Ferjancic-Biagini, T. Giardina and A. Puigserver, *J. Food Biochem.*, 1998, **22**, 331–345.

45. H. Prakash and S. Mazumdar, *Int. J. Mass Spectrom.*, 2009, **281**, 55–62.

46. A. Furuhata, T. Ishii, S. Kumazawa, T. Yamada, T. Nakayama and K. Uchida, *J. Biol. Chem.*, 2003, **278**, 48658–48665.

47. K. Ichihashi, T. Osawa, S. Toyokuni, and K. Uchida, *J. Biol. Chem.*, 2001, **276**, 23903–23913.

48. S.H. Portlock, M.J. Clague and R.J. Cherry, *Biochim. Biophys. Acta*, 1990, **1030**, 1–10.

49. J. F. Faucon, J. Dufourcq and C. Lussan, *FEBS Letts*, 1979, **102**, 187–190.

50. R.C. Dawson, A.F. Drake, J. Helliwell, and R.C. Hider, *Biochim. Biophys. Acta*, 1978, **510**, 75–86.

51. J. Lauterwein, L.R. Brown and K. Wüthrich, *Biochim. Biophys. Acta*, 1980, **622**, 219–230.

52. J. Bello, H.R. Bello and E. Granados, *Biochemistry*, 1982, **21**, 461–465.

53. H. Raghuraman, S. Ganguly and A. Chattopadhyay, *Biophys. Chem.*, 2006, **124**, 115–124.

54. R.J.Y. Ho, M. Schmetz and D.W. Deamer, *Lipids*, 1987, **22**, 156–158.

55. Y.-H. Lam, S. R. Wassall, C. J. Morton, R. Smith and F. Separovic, *Biophys. J.*, 2001, **81**, 2752–2761.

56. K. Hristova, C.E. Dempsey and S.H. White, *Biophys. J.*, 2001, **80**, 801–811.

57. Bruker Daltonics Application Note LCMS-23, *The use of non-volatile Buffers in LC-MS/MS*, 2002.

4 THE MEMBRANE BINDING OF DEFENSIN HNP-2

4.1 Introduction

4.1.1 The defensin family

The defensins are a family of peptides found in plant, invertebrate and vertebrate species. They are small (3–5 kDa), arginine-rich, cationic peptides, with predominately β-sheet structures stabilised by 3–4 disulphide bonds.[1] There are three subtypes of vertebrate defensins: α, β and θ, along with insect and plant subtypes (Table 4.1). The α, β and θ-defensins are categorised by their disulphide bond pairing and distance between cysteine residues.[2] α-Defensins have six cysteine residues, paired Cys 1 – Cys 6, Cys 2 – Cys 4 and Cys 3 – Cys 5.[3] β-Defensins also contain six cysteines, but they are paired Cys 1 – Cys 5, Cys 2 – Cys 4 and Cys 3 – Cys 6.[3] All α and β mammalian defensins identified so far have been shown to have three-stranded antiparallel β-sheet structures, though they differ in the percentage of β-sheet, for example human neutrophil defensin-3 (HNP-3) (an α-defensin) is 53% β-sheet,[4] rabbit kidney defensin-1 (RK-1) (α) is 40% β-sheet and human β defensin-3 (HBD-3) (β) is only 28% β-sheet.[5, 6] There is only one known θ-defensin, rhesus theta defensin-1 (RTD-1), an 18 amino acid cyclic peptide stabilised by three disulphide bonds, found in the leukocytes of rhesus macaques.[7, 8]
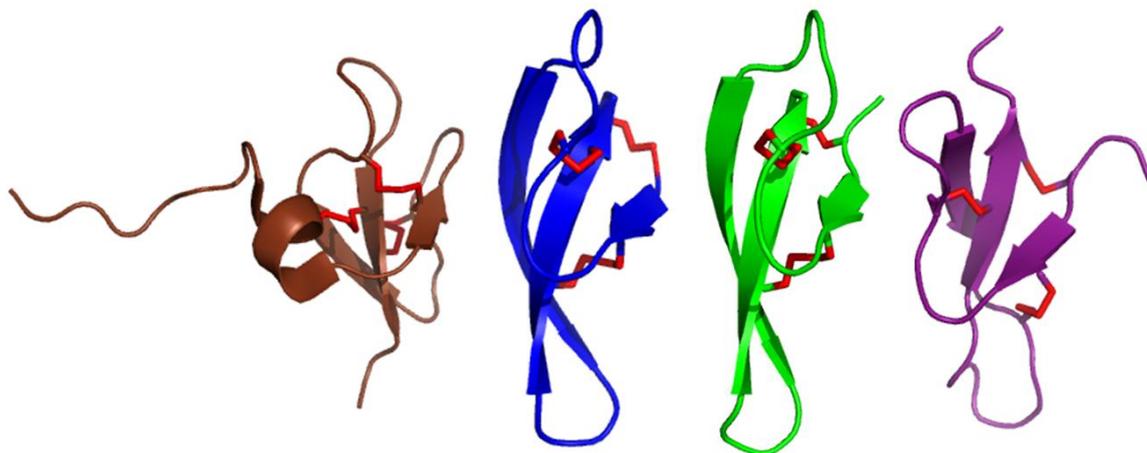
Figure 4.1. The crystal structures of A) HBD-3 (closest to average NMR structure), B) HNP-2 (X-ray; D-Ala(17)-HNP-2), C) HNP-3 (X-ray) and C) RK-1 (lowest energy NMR structure). Entries 1KJ6, 1ZMH, 1DFN and 1EWS respectively in the Protein Data Bank.[5, 9, 4, 6] Disulphide bonds shown in red.

There are six α-defensins, human neutrophil peptides 1-4 (HNP-1-4) and human defensins 4 and 5 (HD-5, HD-6), and eleven β-defensins, human β-defensins 1–6 and 25–29 (HBD-1–6 and 25–29), known to be present in humans, as described in Table 4.2.[10]

4.1.2 Human α-defensin structures

The crystal structures of all six human α-defensins have been determined (HNP-2 was crystallised as D-Ala(17)-HNP-2, with the second Gly residue replaced with D-Ala), along with solid and solution state NMR structures of HNP-1.[4, 9, 11–15] They have very similar triple stranded β-sheet structures connected through tight turns and a β-hairpin. All of the human α-defensins crystallised as dimers, and the solution state NMR analysis of HNP-1 also showed it to have a dimeric structure. HNP-1–3 have primary structures which only differ by one residue (Table 4.2). The secondary structures of HNP-1–3 have been shown to be essentially identical, with three strands of antiparallel β-sheet involving sections 'YCR', 'RYATCIY' and RLWAFC' of the sequence of each peptide, two hydrogen bonded turns involving residues 'AG' and 'QG' and, like all α-defensins, disulphide bonds between Cys 1 and Cys 6, Cys 2 and Cys 4 and Cys 3 and Cys 5 (Figure 4.2). The three dimer crystal structures only show small differences in the sections where no specific secondary structure can be assigned (Figure 4.3).[4, 9, 14] It is therefore possible to combine some structural information which has been gained for each of them individually. The numbering of the amino acids in Section 4.2.1 has been determined by designating the first residue in the peptide referred to at the time as residue 1. This may differ from numbering in the references, where the amino acids have been numbered such that conserved residues have the same number in each peptide, i.e. the first residue of HNP-2 would be labelled C(2) when compared to the other human neutrophil defensins, and C(3) when compared to rabbit neutrophil peptide-2 (NP-2).[9] D-Ala(17)-HNP-2 is modified on the 16th residue if the sequence is numbered in isolation (Figure 4.2).

Figure 4.2. The DSSP secondary structure assignment of D-Ala(17)-HNP-2.[9, 16] ➤ = β strand; ⌒ = hydrogen bonded turn; ▬ = no secondary structure assigned; cysteine residues are circled in green; red, green and blue lines linking cysteines show arrangement of disulphide bonds.
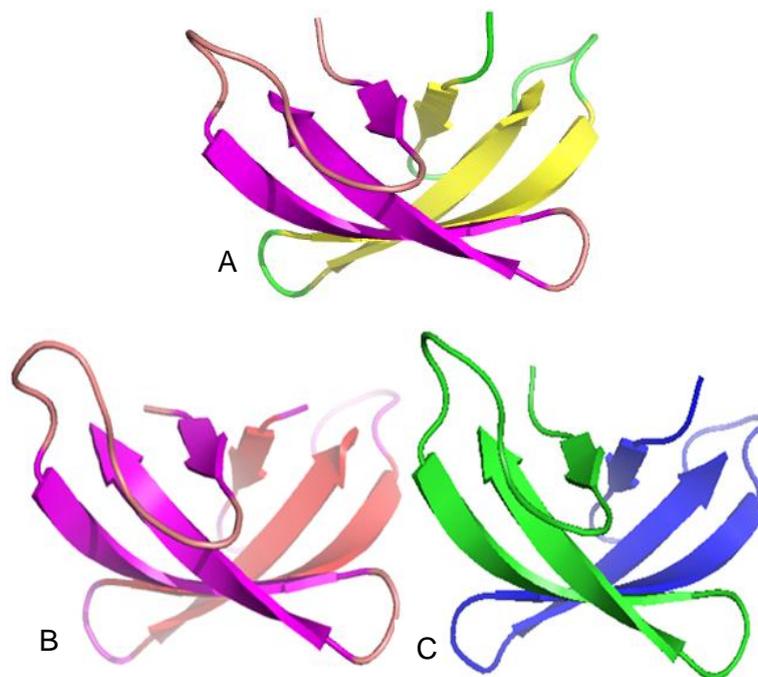
Figure 4.3. The crystal structures of dimers of HNP 1-3 (A–C respectively). Entries 3HJ2, 1ZMH and 1DFN respectively in the RSCB Protein Data Bank.[4, 9, 14]

4.1.2.1   HNP-1

The structure of HNP-1 was initially determined using solution state NMR.[11] Clear evidence was observed for the existence of defensin dimers in solution. Eighteen slowly exchanging protons were observed on the HNP-2 monomers, twice as many as on the homologous rabbit NP-2 peptide (Figure 4.4), which has been shown not to dimerise. The exchange rate of amide protons is slowed when they are not accessible by the solvent, either due to hydrogen-bonding or being buried in the peptide. Some of the protons of interest appeared to be on the surface of the monomer and should have been freely accessible by solvent. This suggests strongly that the peptide was present as either a dimer or an aggregate.

Figure 4.4. The sequences of HNP-1 and NP-2.

The data did not allow the distinction between a symmetrical dimer and an asymmetric dimer where the monomer and aggregate were exchanging fast on the NMR chemical shift timescale. It was also not possible to determine whether the peptide was present as dimers or higher-order aggregates, as the amide proton of residue 26, which was not on the surface thought to lie between the two monomers, was also slowly exchanging, suggesting aggregation. Further evidence which suggested either

dimerisation or aggregation included larger average proton line widths than those in the spectra of monomeric rabbit NP-2, lower signal-to-noise ratios for cross peaks in the COSY spectra and higher signal-to-noise ratios for cross peaks in the 2-dimentional NOE spectra, all consistent with longer rotational correlation times caused by aggregation. The x-ray crystal structure of an HNP-1 dimer has also been determined.

4.1.2.2 HNP-2

Three x-ray crystal structures of D-Ala(17)-HNP-2 (residue Gly(16) replaced with D-Ala) have been determined. The peptide crystallised as a dimer, and a number of interactions between the monomers were identified. Four main-chain N–H---O hydrogen bonds were identified between the Thr(17) and Ile(19) residues of each monomer, along with hydrophobic contacts between Phe(27) and the sulphur atoms of Cys(3) and Cys(18) (which share a disulphide bond) and, in some cases, hydrogen bonds between the Cys(1) residues on each monomer. The monomers participating in dimerisation were shown to have different relative locations, suggesting asymmetry.[9]

4.1.2.3 HNP-3

HNP-3 also crystallised with two monomers in close contact related by a two-fold rotation axis, as shown in Figure 4.5. Four direct hydrogen bonds were identified in the same positions as those observed during the analysis of the HNP-2 crystal (between residues numbered 19 and 21 in Figure 4.5), along with two indirect hydrogen bonds through water molecules (between residues numbered 17 and 23 in Figure 4.5). Hydrophobic interactions were observed between residues Cys(4), Cys(19), Tyr(21), and Phe(28) (labelled 5, 20, 22 and 29 respectively in Figure 4.5) of each monomer.
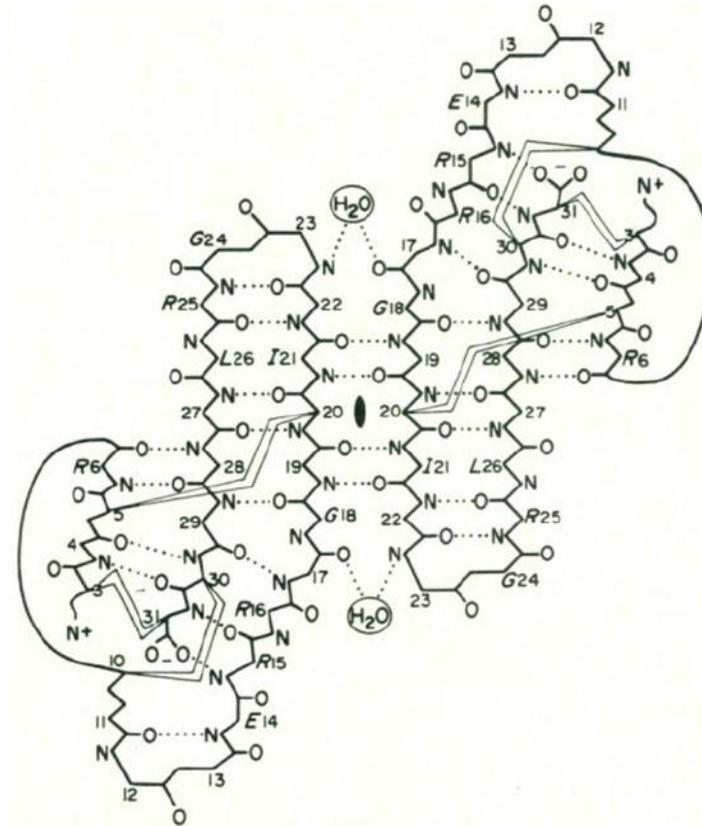
Figure 4.5. Pattern of hydrogen bonding in the HNP-3 dimer.[4] Reproduced with permission from the American Association for the Advancement of Science, license no. 2362010971233.

	Type	Species	Disulphide Bonds	Target	Location	Ref
Human neutrophil peptide (HNP) 1–4	α	Human	Cys 1 – Cys 6, Cys 2 – Cys 4, Cys 3 – Cys 5	Gram +ve and Gram -ve bacteria, fungi, enveloped viruses, yeast	Neutrophils	[1, 13, 17–20]
Human defensin (HD) 5–6	α	Human	Cys 1 – Cys 6, Cys 2 – Cys 4, Cys 3 – Cys 5	Gram +ve and Gram -ve bacteria, fungi, yeast	Small intestine (paneth cells; granulocytes)	[13, 18]
Neutrophil peptide NP 1–5	α	Rabbit	Cys 1 – Cys 6, Cys 2 – Cys 4, Cys 3 – Cys 5	Gram +ve and Gram -ve bacteria, fungi, enveloped viruses	Neutrophils	[21–24]
Macrophage cationic peptide (MCP) 1–2	α	Rabbit	Cys 1 – Cys 6, Cys 2 – Cys 4, Cys 3 – Cys 5	Gram +ve and Gram -ve bacteria, fungi, enveloped viruses	Lung machrophages	[21–24]
Cryptidins	α	Mouse, rat	Cys 1 – Cys 6, Cys 2 – Cys 4, Cys 3 – Cys 5	Gram +ve and Gram -ve bacteria, fungi, protozoans	Small intestine (paneth cells)	[24–27]
Human β defensin (HBD) 1–6, 25–29	β	Human	Cys 1 – Cys 5, Cys 2 – Cys 4, Cys 3 – Cys 6	Gram -ve bacteria	Various	[28–37]
Tracheal antimicrobial peptide (TAP)	β	Cattle	Cys 1 – Cys 5, Cys 2 – Cys 4, Cys 3 – Cys 6	Gram +ve and Gram -ve bacteria, fungi	Tongue	[38]
Rhesus θ defensin (RTD) 1	θ	Rhesus Macaque	Cys 1 – Cys 6, Cys 2 – Cys 5, Cys 3 – Cys 4	Gram +ve and Gram -ve bacteria, fungi	Leukocytes	[7, 8]
4 kDa defensin	Insect	Scorpion	Cys 1 – Cys 4, Cys 2 – Cys 5, Cys 3 – Cys 6	Primarily Gram +ve bacteria	Hemolymph	[39]
Defensin-1	Plant	Garden pea	Cys 1 – Cys 8, Cys 2 – Cys 5, Cys 3 – Cys 6, Cys 4 – Cys 7	Fungi	Epidermis and vascular bundles	[40]

Table 4.1. Examples of defensin peptides.

	Type	Sequence	Target	Location	Ref
HNP-1	α	ACYCRIPACIAGERRYGTCIYQGRLWAFCC	Gram +ve and Gram -ve bacteria, fungi, enveloped viruses, yeast	Neutrophils	[1, 17–19]
HNP-2	α	CYCRIPACIAGERRYGTCIYQGRLWAFCC	Gram +ve and Gram -ve bacteria, fungi, enveloped viruses, yeast	Neutrophils	[1, 18–20]
HNP-3	α	DCYCRIPACIAGERRYGTCIYQGRLWAFCC	Gram +ve and Gram -ve bacteria, fungi, enveloped viruses, yeast	Neutrophils	[18, 19]
HNP-4	α	VCSCRLVFCRRTELRVGNCLIGGVSFTYCCTRV	Gram +ve and Gram -ve bacteria, fungi, yeast	Neutrophils	[13, 17, 18]
HD-5	α	ATCYCRTGRCATRESLSGVCEISGRLYRLCCR	Gram +ve and Gram -ve bacteria, fungi, yeast	Small intestine (paneth cells; granulocytes)	[13, 18]
HD-6	α	AFTCHCRRSCYSTEYSYGTCTVMGINHRFCCL	Very low activity against Gram +ve and Gram -ve bacteria; HIV-1	Small intestine (paneth cells; granulocytes)	[13, 18]
HBD-1	β	DHYNCVSSGGQCLYSACPIFTKIQGTCYRGKAKCCK	Gram -ve bacteria	Various, including plasma and kidney	[28–30]
HBD-2	β	GIGDPVTCLKSGAICHPVFCPRRYKQIGTCGLPGTKCCKKP	Gram +ve and Gram -ve bacteria, yeast	Various, including skin, lung, trachea	[31]
HBD-3	β	GIINTLQKYYCRVRGGRCAVLSCLPKEEQIGKCSTRGRKCCRRKK	Gram +ve and Gram -ve bacteria, yeast	Various, including skin, lung, trachea and kidney	[32]
HBD-4	β	ELDRICGYGTARCRKKCRSQEYRIGRCPNTYACCLRK	Gram +ve and Gram -ve bacteria, yeast	Mainly testis and gastric antrum	[33]
HBD-5	β	GLDFSQPFPSGEFAVCESCKLGRGKCRKECLENEKPDGNCRLNFLCCRQRI	Unknown	Epididymis	[34]
HBD-6	β	FFDEKCNKLKGTCKNNCGKNEELIALCQKSLKCCRTIQPCGSIID	Gram -ve bacteria	Epididymis	[34, 35]
HBD-25	β	SFEPQKCWKNNVGHCRRRCLDTERYILLCRNKLSCCISIISHEYTRR	Unknown	Not trachea or skin	[36]
HBD-26	β	NWYVKKCLNDVGICKKKCKPEEMHVKNGWAMCGKQRDCCVPAD	Unknown	Epididymis	[36, 37]
HBD-27	β	QLKKCWNNYVQGHCRKICRVNEVPEALCENGRYCCLNIKELEAC	Unknown	Not trachea or skin	[36, 37]
HBD-28	β	ARLKKCFNKVTGYCRKKCKVGERYEIGCLSGKLCCANDEEEKKHVSFKKPHQHSGEKLSVLQDYIILPTITIFTV	Unknown	Not trachea or skin	[36]
HBD-29	β	EFIGLRRCLMGLGRCRDHCNVDEKEIQKCKCKMKKCCVGPKVVKLIKNYLQYGTPNVLNEDVQEMLKPAKNSSAVIQRKHILSVLPQIKSTSFFANTNFVIIPNATPMNSATISTMTPGQITYTATSTKSNTKESRDSATASPPPAPPPPNILPTPSLELEEAEEQ	Unknown	Epididymis	[36]

Table 4.2. Human defensin peptides.

4.1.3 Membrane binding and activity

Research to date suggests that defensins act through permeabilization of microbial cell membranes causing leakage of the contents.[19, 41–43]

4.1.3.1 Lipid specificity of HNP-2

HNP-2 has a net charge of +3 at pH 7, making it unsurprising that the peptide will bind to lipid bilayers containing a proportion of negatively charged lipids, due to electrostatic attractions.[44] The extent of binding of HNP-2 (14.5 µM) to vesicles composed of POPG and POPC (10 mM) has been shown to have a sigmoidal dependency on the concentration of POPG. No binding was observed in the absence of POPG (100% POPC). Approximately 20% of HNP-2 was observed to have bound with 10% POPG and approximately 60% of the HNP-2 was bound with 20% POPG. Maximum binding (more than 90% of added HNP-2 bound to the vesicles) did not occur until around 70% of the lipid was negatively charged, though nearly 90% of the peptide was bound at 50% POPG.[45] This suggests that HNP-2 specifically binds to bacterial cells, which contain negatively charged lipids, over erythrocyte cells, which contain mostly neutral lipids. After binding, it has been shown that HNP-2 causes lysis of the membrane. This has been observed with both negatively charged vesicles and with the inner and outer membranes of *Escherichia coli* (*E. coli*) (Gram-negative bacteria) cells.[20, 46] The lack of binding of HNP-2 to neutral membranes is in contrast to the binding of some other antimicrobial peptides, such as melittin. Melittin has a net charge of +5 at pH 7 and binds preferentially to negatively charged lipids, but melittin also binds to neutral liposomes, and causes a greater degree of lysis of neutral liposomes than of those composed of negatively charged lipids.[47]

HNP-2 has been shown to cause fusion and aggregation of vesicles under certain conditions. Wimley *et al.* reported aggregation only with lower concentrations of vesicles (1 mM as opposed to 10 mM) and at least 40% POPG (60% POPC). They observed that with pure POPG liposomes aggregation was rapid as soon as the molar ratio of POPG lipid to HNP-2 dropped below 100:1, which suggests that the aggregation was caused by electrostatic interactions.[20] HNP-1 has also been observed to cause fusion of liposomes containing 25% DOPS in DPPC.[43]

4.1.3.2 Buffer and ionic strength effects

Human neutrophil peptides have been shown to be strongly affected by the ionic strength of buffers.[43] In 5 mM phosphate buffer, HNP-1 caused greater than 50% lysis of 3:1 DPPC/DOPS liposomes and 20–50% fusion of the same liposomes. In 100 mM NaCl

and 25 mM phosphate no lysis was observed and the amount of fusion dropped. The results of a sucrose gradient lipid binding assay showed a higher lipid:peptide molar ratio for HNP-1 bound to DPPC/DOPS liposomes in 100 mM NaCl and 25 mM phosphate than in 5 mM phosphate (20:1 mol/mol and 13:1 mol/mol respectively), showing that the binding was weaker in the presence of NaCl and a higher concentration of phosphate. It has been suggested that the decrease in binding at a high salt concentration is due to ions in solution shielding the charges on the peptide from the charged lipid headgroups. The higher concentration buffer had no effect on the liposome binding of rabbit NP-1, which has a much higher net charge of +9 at pH 7 and therefore may not have been shielded so well.

The antimicrobial activity of HNP-1 against Gram negative (*E. coli*) and Gram positive (*Listeria monocytogenes*) bacteria has been shown to be greatly inhibited by buffers of even medium ionic strength. The minimum inhibitory concentration (MIC) (the lowest peptide concentration at which bacterial cell growth was inhibited) of HNP-1 against *E. coli* in 10 mM phosphate buffer was 1.9 µg/mL. In a 10 mM phosphate buffer with 50 mM or 100 mM NaCl the MIC was over 50 µg/mL. Similarly, with *L. monocytogenes* the MIC in the absence of NaCl was 5.8 µg/mL, and with 50 mM or 100 mM NaCl it was over 50 µg/mL.[48]

4.1.4   Binding models

On publishing the crystal structure of HNP-3, Hill *et al.* proposed three models for the interaction between the peptide and lipid membranes.[4] The structure they found (Figure 4.6) was that of a basket-shaped dimer, with an apolar base and polar top, held together through hydrogen bonds. The centre of the basket was found to contain the hydrophobic amino acids, and a ring of six positively charged arginine side chains was observed around the basket. A mini-channel was observed running through the centre of the dimer (Figure 4.6B). The two strands of β-sheet were found to be linked by hydrogen bonds through ordered solvent molecules in this channel.
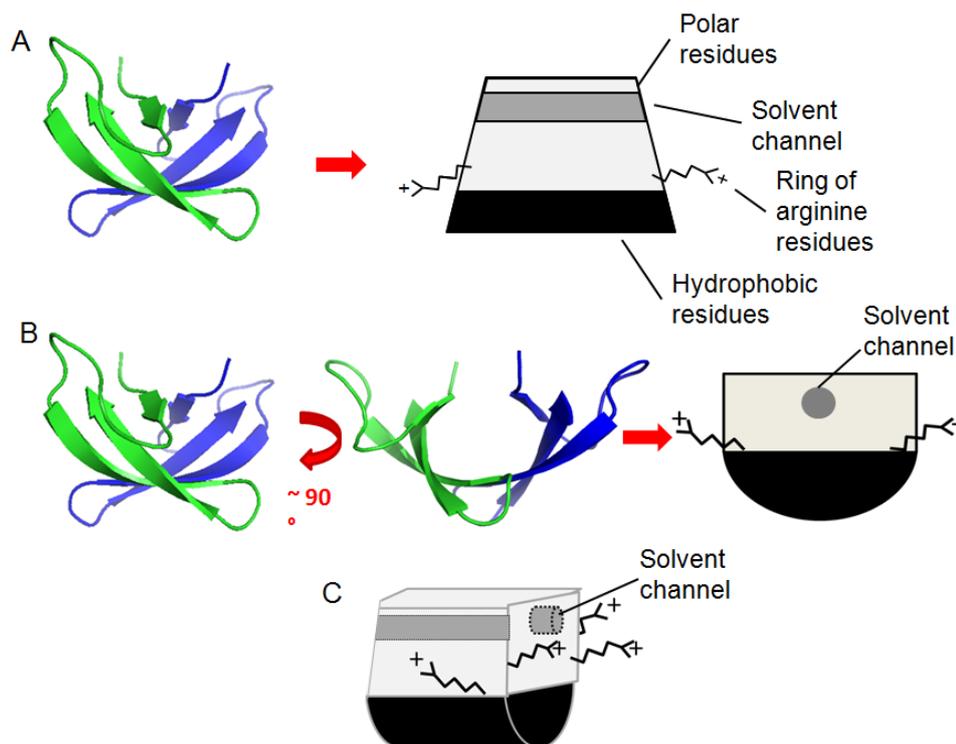
Figure 4.6. Schematic representations of HNP-3 dimer in binding models and how they relate to crystal structure.

The three binding models proposed by Hill *et al*. were:

4.1.4.1 Wedge model

The first model suggested was that of a wedge, with the basket sitting in, and disrupting, the outer leaflet of the membrane.[4] The hydrophobic base of the basket is buried in the hydrophobic centre of the bilayer and the arginine residues are able to interact with the negatively charged lipid headgroups.

4.1.4.2 Multiple dimer pore model

The second model proposed was that of a pore composed of at least four dimers arranged with their polar tops facing into the centre of the pore and their hydrophobic bases facing outwards into the bilayer.[4] The arginine side chains were suggested to be flexible enough to bind the lipid headgroups from this orientation.

4.1.4.3 Two dimer pore model

The final model involved the formation of a two dimer pore within the membrane, with the polar tops of the dimers facing each other at the centre of the pore and the hydrophobic bases facing outwards towards the lipid acyl chains at the centre of the bilayer. The arginine side chains are again able to interact with the lipid headgroups. The

dimers are rotated by 90° compared to the other models to allow the pore to be spanned by the solvent mini channel in the top of the basket.[4]
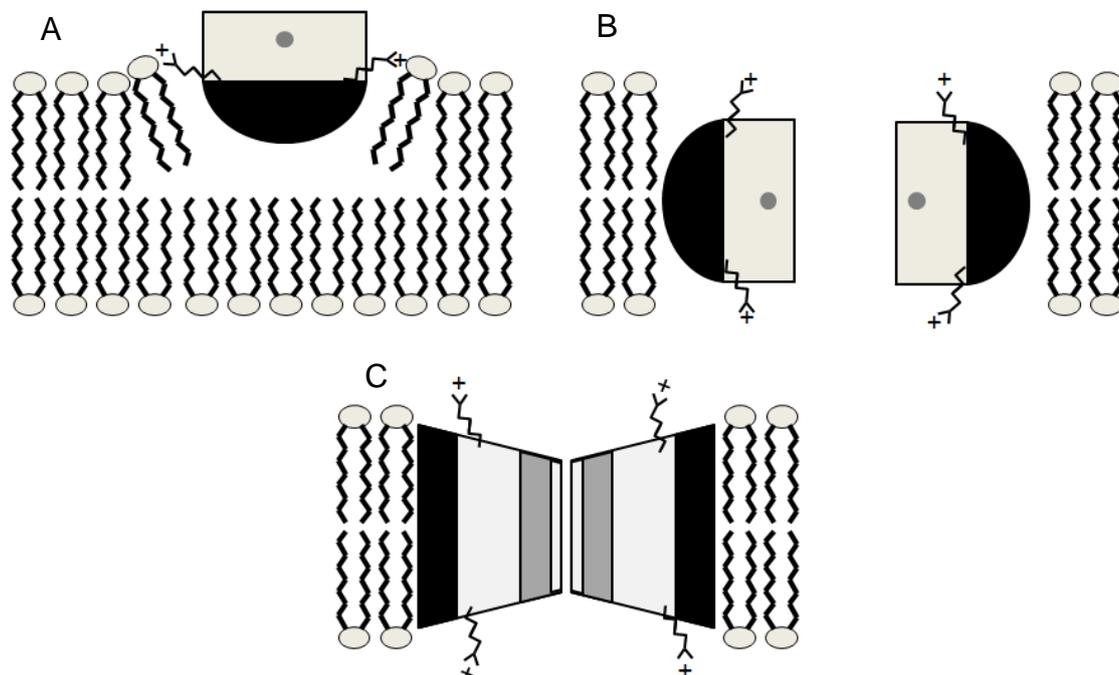
Figure 4.7. HNP-3 binding models proposed by Hill *et al.*[4] A) wedge model; B) multiple dimer pore model; C) two dimer pore model. The relationship between the schematic images of the peptide dimer and the crystal structure is shown in Figure 4.6.

4.1.4.4 Proposed model for HNP-2 membrane binding

Wimley *et al.* used the HNP-3 crystal structure and applied it to experimental data for HNP-2 to develop a proposed model for the membrane binding of the latter peptide.[20] The HNP-3 structure was used because HNP-2 had not been crystallised at that time. They initially studied the effect of the addition of HNP-2 to POPG vesicles containing a mixture of fluorescent 8-aminonaphthalene-1,3,6 trisulfonic acid (ANTS) and the quencher *p*-xylene-bis-pyridinium bromide (DPX) in 50 mM KCl, with the expectation of observing an increase in ANTS fluorescence on lysis of the vesicles due to dilution. On addition of HNP-2 an increase in fluorescence was observed. The release of the vesicle contents appeared to start immediately after addition of the peptide, and then to increase exponentially on a timescale of minutes, with a half time of the leakage being around 2 minutes with 1.45 μM HNP-2.

Further work was then carried out to determine if the fluorophore leakage was due to a graded process where all of the vesicles released some of their fluorophores, or an 'all-or-none' process where a portion of the vesicles released all of their contents and the rest remained intact. The process was found to be all-or-none. An all-or-none leakage

process is caused by either complete destruction of some of the vesicles or the formation of pores. In order to determine the process occurring, HNP-2 was added to vesicles containing a mixture of ANTS/DPX and the fluorescent dextrans FD-4 (fluorescein isothyocyanin-labelled dextran, molecular weight 4,400 Da) and FD-20 (fluorescein isothyocyanin-labelled dextran, molecular weight 18,900 Da). At two different concentrations of HNP-2, 100% of the ANTS/DPX was released, 64% of the FD-4 and 24% of the FD-20. This suggested that pores were being formed, which were large enough to allow ANTS/DPX and FD-4, but too small for FD-20. Through the quantity of defensin added and the proportion of vesicles in which pores were formed, Wimley *et al*. estimated that the pores were composed of 6-8 dimers, and from the size of the dextrans that the maximum pore radius was 25 Å. From all of this, they proposed a pore composed of 6 dimers, with an internal radius of 20 Å (Figure 4.8).[20] This pore model is similar to the second of those proposed by Hill *et al*. for HNP-3, described in Section 4.1.4.3.[4]

Wimley *et al*. proposed that the polar region at the top of the dimer baskets would face into the centre of the pore and the hydrophobic bases would face the hydrophobic lipid chains. The dimers would be oriented such that the arginine residues lay parallel to the bilayer normal in two planes. The furthest distance between the ends of the arginine groups in each plane, and therefore the maximum width of the pore, would then be 25–27 Å, which is approaching the thickness of a fully hydrated bilayer, where the distance between the phosphate groups of a DPPC bilayer is 37 Å.[49] The thickness of the hydrophobic portion of a DPPC bilayer is 26 Å, but the hydrophobic region of the proposed pore would only have a width of 15 Å. The authors suggested that the bilayer might adapt its width to match the width of the pore, as had been proposed for gramicidin A channels.[20]
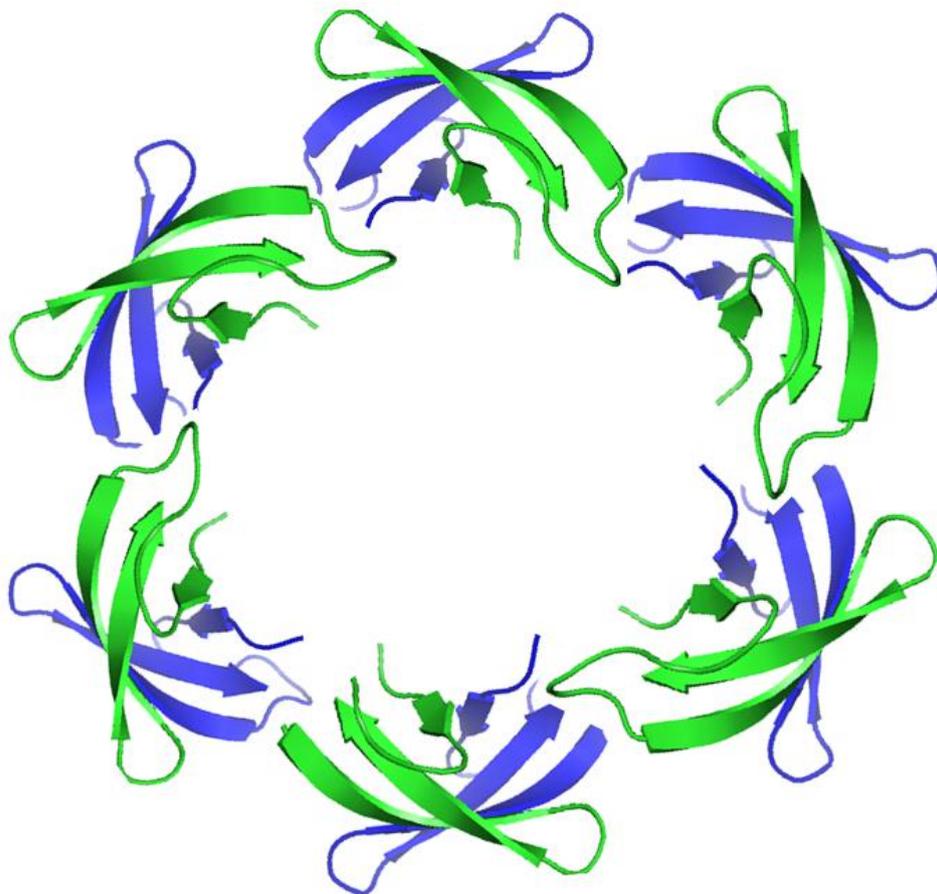
Figure 4.8. A top-down view of the multimeric pore proposed by Wimley *et al.*[20]

4.1.4.5 Proposed model for defensin-induced liposome fusion

Fujii *et al.* used the HNP-3 crystal structure to propose a model for HNP-1-induced liposome fusion.[43]   The fusion was measured using fluorescence resonance energy transfer (FRET) between two types of fluorescent probes.   Liposomes were prepared with a small proportion of each of the donor N-(7-nitro-2,1,3-benzodiazol-4-yl)-phosphatidylethanolamine (NBD-PE) and the acceptor N-(Lissamine Rhodamine B sulfonyl)-phosphatidylethanolamine (Rh-PE).   The addition of HNP-1 caused fusion between labelled and unlabelled liposomes, leading to dilution of the fluorophores and a reduction in fluorescence emission from Rh-PE and increase in fluorescence emission from NBD-PE. Using the HNP-3 crystal structure, they speculated that defensin dimers would associate through the hydrophobic regions at the bases of their 'baskets' and that the three arginine residues on each side of the basket would associate with the negatively charged lipid headgroups on the surface of the membrane, allowing the following process:

A) Two defensin dimers associate with each other through their hydrophobic residues and with the surface of the bilayer through electrostatic interactions.

B) The surface of another liposome is attracted electrostatically and associates with the arginine residues on the other side of the dimer pair.

C) The membranes are destabilised by disruption of the hydration shells surrounding them. The lipids are able to exchange between bilayers due to the lack of hydrophobic shell, initiating fusion. The fused bilayers eventually reform as a larger bilayer.
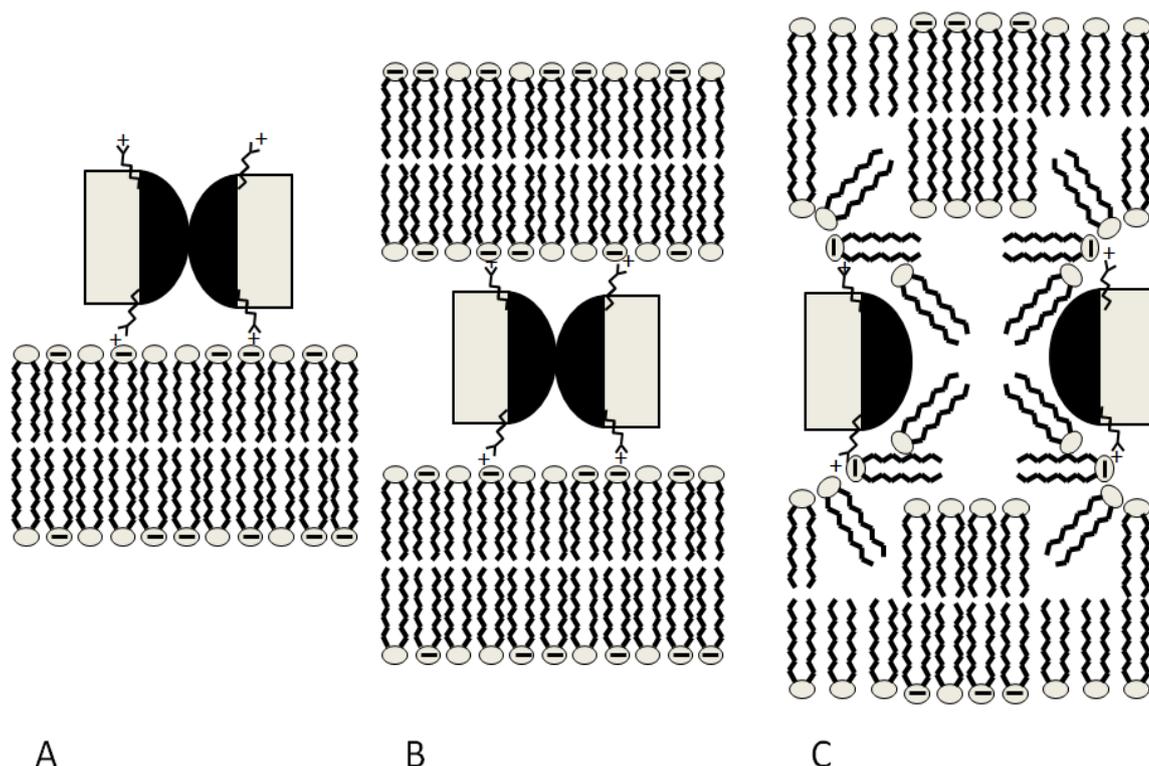
Figure 4.9. The three stages of HNP-1-mediated liposome fusion proposed by Fujii *et al.*[43]

4.1.5 Comparison of human and rabbit α-defensin binding

A number of studies have looked at the action of rabbit α-defensins on liposomes in comparison with the human neutrophil peptides.[42, 43, 50] The solution state NMR structures of rabbit neutrophil defensins NP-2 and NP-5 and the crystal structure of rabbit kidney defensin RK-1 show no evidence of dimerisation or higher order aggregation, even at high peptide concentrations (25 mg/mL).[6, 10, 11, 51] Certain differences have been observed between the binding of the human and rabbit α-defensins, which have been attributed in part to their respective dimer/monomer formation. The effects of six rabbit defensins on leakage from vesicles have been examined and compared to the all-or-none leakage observed for HNP-2.[20, 42] Firstly, it was observed that the rabbit defensins NP-2 and NP-5 only bound to liposomes composed of a proportion of negatively charged lipids,

as was found for HNP-2.[42]   The proportion of POPG required varied with the peptide's charge however, with 100% binding of NP-2 (net charge +8 at pH 7) observed with just 25 mol% POPG in POPC vesicles, and 50 mol% POPG required for 100% binding of NP-5 (net charge +4 and pH 7).   This supports the electrostatic explanation for binding described in Section 4.1.3.1.   Much higher concentrations of the rabbit defensins were required for liposome permeabilization than HNP-2, and the leakage was much slower, although NP-4 did not cause membrane permeabilization at all.   The leakage of vesicle contents was found to be graded rather than all-or-none, suggesting that the rabbit defensins did not form the same stable pores in the bilayer that HNP-2 has been suggested to form.   This difference was attributed to the monomer/dimer difference, and it was suggested that the features which caused HNP-2 dimer assembly were also required for the formation of the larger HNP-2 structures proposed to be responsible for pore formation.

In other experiments, rabbit NP-1 was found cause fusion of 3:1 DPPC:Cholesterol liposomes, though not to permeabilize them.[43]   HNP-1, NP-1 and NP-5 were observed to cause lysis of 3:1 DPPC:DOPS vesicles.   A sucrose density gradient assay was used to study the strength of the binding between the different defensin peptides and DPPC/DOPS liposomes. HNP-1 binding was observed to bind strongly, with a low lipid:peptide ratio (13:1 mol/mol), while the binding of NP-1 and 2 was much weaker (lipid:peptide ratios of 90:1 and 60:1 (mol/mol) respectively).[43]   It was proposed that the higher net charge of NP-1 (+9 at pH 7) made it more stable in aqueous solution, therefore more lipid was required for it to bind.

4.1.6   The scope of this research

A number of important features of the action of defensin HNP-2 on membranes have been determined, as discussed above.   It is known to lyse membranes, but only those with a proportion of negatively charged lipids, and the crystal structure has shown that the peptide exists as a dimer under at least some conditions.

The lysis has been shown to have an all-or-none effect on leakage from vesicles, suggesting that pores are formed rather than more random permeabilization of the bilayer.   It has also been observed that only markers of certain sizes are able to escape through these pores, giving a suggestion of their size.

The proposal that the dimeric form of HNP-2 causes membrane lysis is supported by a comparison with the effects of rabbit NP-2 and NP-5 on membranes.[42]   Structural analysis of the rabbit neutrophil peptides suggests that they only exist as monomers,

despite their sequence similarities with the human neutrophil peptides.[6, 10, 11, 51] These two peptides cause a graded release of vesicle contents during permeabilization rather than the all-or-none effect caused by the human neutrophil peptides, suggesting that they cannot form the same stable pores, which is proposed to be due to their lack of dimerisation.[42] Hill *et al.* proposed that the presence of an invariant Gly residue at position 17 of HNP-3 also suggests that the peptide acts on membranes as a dimer, as replacement of this residue by any other would cause the Cβ atom to overlap with the O atom on residue 19 of the neighbouring monomer (labelled 18 and 20 in Figure 4.5).[4] Again, there is good evidence for the peptide binding as a dimer, though this is inconclusive and does not explain whether the peptide is present as a monomer at lower concentrations and dimerises on the surface of the membrane or during pore formation.

The multimeric pore model for the binding of HNP-2 to membranes is, to quote the authors, "highly speculative... it is only presented to demonstrate that a physically rational structure can be made that is both consistent both with the experimental data and with the known structures of human defensins and phospholipid bilayers".[20] There is no direct evidence for the pore being as proposed, especially concerning the orientation of the dimers. Hill *et al.* propose a pore model where the dimers sit at 90° to those in the Wimley model, also with rational arguments for how the dimers can interact with themselves and the bilayer.

Little is known about the kinetics of the binding of HNP-2, apart from the vesicle leakage half times reported by Wimley *et al.* They observed that the half time increased from around 11 minutes with 0.3 µM HNP-2 to around 2 minutes with 0.9 µM, 1.2 µM and 1.5 µM HNP-2.[20]

There are therefore two main features of the action of HNP-2 which require investigation:

1) The organisation of the peptide after binding to the membrane and whether it correlates with any of the models proposed.
2) The mechanism of this binding.

In order to investigate these two areas, the work described in this chapter was concentrated around determining the kinetics of binding, by recording a series of fluorescence and linear dichroism spectra over 5 hours under different conditions, and studying the orientation of the peptide during and after binding using linear dichroism. By combining these results, a model could be proposed for the mechanism and organisation

of the binding of HNP-2. Analyses were carried out with different lipids and at different temperatures in order to gain wider information as to the nature of binding, and further investigations were carried out to ensure that the data obtained was from HNP-2 binding and not affected by other actions such as liposome fusion.

4.2 Results and discussion

4.2.1 Background to HNP-2 analyses

4.2.1.1 Liposome composition

The liposome mixtures used in the HNP-2 binding analyses were chosen for a number of reasons. As stated previously, HNP-2 is known to only bind to liposomes containing a proportion of negatively charged lipids, with approximately 90% of the peptide reported to bind with 50% POPG (with 50% POPC) at a peptide:lipid ratio of 1.5:1000 (mol/mol). With a peptide:lipid ratio of 1.5:100 (mol/mol) 75% of the peptide was reported to bind to 50:50 (w/w) POPG/POPC membranes.[45] The majority of linear dichroism analyses using the flow cell have been carried out using PC liposomes, often soybean PC, and little research has been carried out into the behaviour of liposomes composed of different lipid types in the flow cell.[52] For initial experiments 50:50 (w/w) negative lipid:PC mixtures were therefore used to minimise the risk of unexpected liposome behaviour affecting the results. Preliminary analyses were carried out using 50% egg or soybean PC lipids, with either POPG or soybean PS but for later analyses DOPC or DMPC lipids were chosen for the PC component and POPG, DMPG or DOPS for the negative component to ensure reproducibility and to remove any possible artifacts from the non-PC lipids known to be present in the natural mixtures, or variation in composition between batches.[53]

The lipid:peptide ratio and overall concentrations used for analyses were selected partly due to analytical factors such as necessary minimum peptide concentrations for signal detection or maximum lipid concentrations, and partly from the work of Wimley *et al.*,[20] who determined the lipid:peptide ratios and concentrations which cause aggregation. Initial LD analyses confirmed that the minimum HNP-2 concentration necessary to obtain a good signal was 15 μM. As discussed previously (Section 4.1.3.1), Wimley *et al.* determined that peptide/lipid aggregates were formed when HNP-2 was added to liposomes containing a minimum of 40% POPG at a concentration of 1 mM lipid, but no aggregation was observed when the lipid concentration was increased to 10 mM, regardless of POPG concentration. They also observed aggregation with pure POPG

liposomes at lipid:peptide ratios below 100:1. A lipid:peptide ratio of approximately 100:1 was therefore used for the experiments described herein, with the understanding that aggregation is thought to be caused by electrostatic forces between the POPG and HNP-2; therefore these forces would be lessened by the presence of only 50% POPG in the liposomes. This gave an overall lipid concentration of approximately 1.4 mM. At 1 mM lipid with 50% POPG in the liposomes some aggregation had been observed by Wimley *et al.*, but with a slightly higher lipid concentration it was hoped that this could be minimised. Wimley *et al.* observed the leakage of fluorescent markers and different sized fluorescent dextran molecules from liposomes with lipid concentrations of 300 µM and peptide concentrations of 1.5 µM or 5.8 µM. A lipid concentration of 300 µM is approximately 20% of the absolute lipid concentration used in the binding experiments described in this chapter, but the lipid to peptide ratios, 200:1 and 52:1 respectively, are either side of the ratio used.

4.2.1.2 The temperature of LD and CD analyses

During the investigation into HNP-2 binding, another user of the LD and CD spectrophotometer discovered that for LD measurements the user-inputted temperature and the actual sample temperature differed, with the difference increasing with distance from room temperature in either direction. This was attributed to the distance between the peltier heating unit and the sample in the LD cell. Little difference between the set and actual temperature was observed for CD, as the heating unit is much closer to the sample cell in the CD cell holder. This means that for some of the analyses the temperatures at which the LD and CD measurements were carried out differ slightly where it was intended that complementary data would be obtained on both instruments under the same conditions. The affected analyses were those using POPG/DOPC and DOPS/DOPC liposome mixtures, both of which have phase transition temperatures well below the analysis temperatures, therefore it was assumed that the small differences between measurement temperatures of the CD and LD spectra would not affect the understanding of the results. Table 4.3 shows the set and actual temperatures for the affected measurements. The CD and LD measurements using the DMPG/DMPC liposome mixture were both carried out at 17 °C and 33 °C.

Table 4.3. Set and actual temperatures of LD analyses.[¤]

Sample	Set temperature (and temperature of CD measurements) (°C)	Sample temperature of LD measurements (°C)
POPG/DOPC 30 DOPS/DOPC 30	30	28.7
POPG/DOPC 40	40	36.8
POPG/DOPC 53	53	47.3

The temperatures of the analyses with DMPG and DMPC liposomes were chosen so as to obtain data above and below the phase transition temperature of the lipids. The temperatures of the other analyses were chosen to determine and compare behaviour over a range, including temperatures above and below 37 °C, which would be presumed to be the optimum temperature for a human peptide.

4.2.1.3 *Phase transition of DMPG/DMPC liposome dispersion*

In order to study the binding of HNP-2 to liposomes composed of a mixture of DMPC and DMPG lipids it was first necessary to establish the gel to liquid crystalline phase transition temperature (T_m) of the mixture. This was required to ensure that binding studies were carried out at temperatures outside the region during which the phase transition was occurring. This analysis was carried out using dynamic light scattering (DLS), following a method developed by N. Michel *et al.* which uses changes in liposome size and shape caused by the lipid phase transition to determine the temperature at which it occurs.[54] This method has the advantage of being carried out on small quantities of the same liposome dispersions that have been prepared for binding analyses, as opposed to differential scanning calorimetry (DSC), the standard technique for determining lipid phase transition temperatures. The liposomes were all prepared by extrusion through polycarbonate membranes with 100 nm diameter pores.

Before the phase transition analyses were carried out, the temperature of the contents of a cuvette was checked over a range of inputted temperatures to ensure the accuracy of the temperature setting. A linear relationship was observed between the inputted and measured temperatures, as shown in Equation 4.1, where T_c is the temperature in the sample cell and T_s is the temperature reported by the DLS instrument.

¤ Sample temperatures were determined using the conversion factor in Equation F1, where T_c is the sample temperature and T_s the temperature set on the instrument. The conversion factor was determined by Emma Gilroy from repeat measurements at a number of set temperatures using a thermocouple probe to record the sample temperatures.

$T_c = (0.907T_s) + 2.2544$ F1

At 25 °C the temperature inside the sample cell was the same as the user-inputted temperature.

$$T_c = (0.907T_s) + 2.2544 \tag{4.1}$$

Table 4.4. Recorded variation between user-inputted temperature and sample temperature for dynamic light scattering measurements.$^{\Diamond}$

Set temperature (°C)	Sample temperature (°C)
10	11.3
15	15.9
20	20.5
25	25.0
30	29.6
35	34.0
40	38.6
45	43.4
50	47.6

Figure 4.10 shows plots of the intensity weighted mean hydrodynamic diameter (z-average diameter) of liposomes composed of DMPG, DMPC and 50:50 (w/w) DMPG/DMPC lipids against temperature. The main transition of DMPG was observed between 20.5 °C and 23 °C (20.8 °C and 23.1 °C after conversion using Equation 4.1). The second transition is attributed to the presence of Na$^+$ in the sample. DMPG was supplied as a sodium salt due to its inherent negative charge, and the presence of Na$^+$ is known from literature on differential scanning calorimetry to split the phase transition of lipids due to the different transition temperatures of the salt adducted and protonated species, with the intensity and position of secondary peaks relative to the transition of the protonated species dependant on the concentration of the Na$^+$.[55] DSC analysis of DMPG produced a plot with two transitions and a shoulder, due to the presence of Na$^+$, the main transition being observed at 22.5 °C (Figure 4.10). DMPC was observed from the DLS analysis shown in Figure 4.10 to undergo the transition between 22 °C and 24 °C (22.2 °C and 24.0 °C after conversion using Equation 4.1). The literature value for the main phase transitions of DMPG and DMPC in the absence of added salt is 23 °C.[56] The liposomes composed of a 50:50 (w/w) mixture of DMPC and DMPG underwent a phase transition between 18 °C and 25 °C (18.6 °C and 25.0 °C after conversion using Equation 4.1), again with a second transition due to the presence of Na$^+$. On the basis of these results,

---

$^{\Diamond}$ Sample temperatures were determined using the conversion factor in Equation 4.1, where T$_c$ is the sample temperature and T$_s$ the temperature set on the instrument. The conversion factor was determined from repeat measurements at a number of set temperatures using a thermometer to record the sample temperatures.

CD and LD analyses of the binding of HNP-2 to 50:50 (w/w) DMPG/DMPC liposomes were carried out at 17 °C and 33 °C, above and below the phase transition temperature the lipid mixture.

Table 4.5. Phase transition temperatures of liposome dispersions identified from DLS analysis.

Liposome composition	Main transition range (°C)[a]	Secondary transition range (°C)[a]
DMPG	20.8–23.1	29.9–34.9
DMPC	22.2–24.0	-
50:50 (w/w) DMPG/DMPC	18.6–25.0	28.1–31.3

a) Temperatures have been converted from observed temperatures to actual temperatures using Equation 4.1.
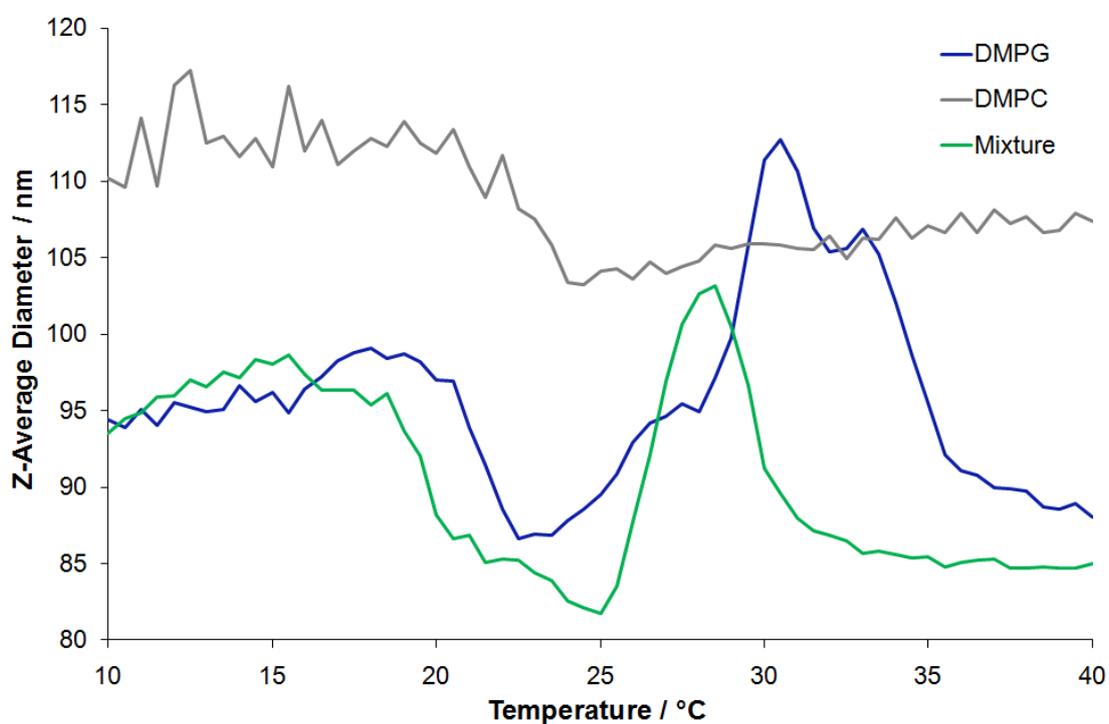
Figure 4.10. Intensity weighted mean hydrodynamic diameter (z-average diameter) measurements of liposomes composed of DMPG (blue), DMPC (red) and 50:50 (w/w) DMPG/DMPC recorded between 10 °C and 40 °C. All liposomes were extruded through polycarbonate membranes with pores of 100 nm diameter during preparation.
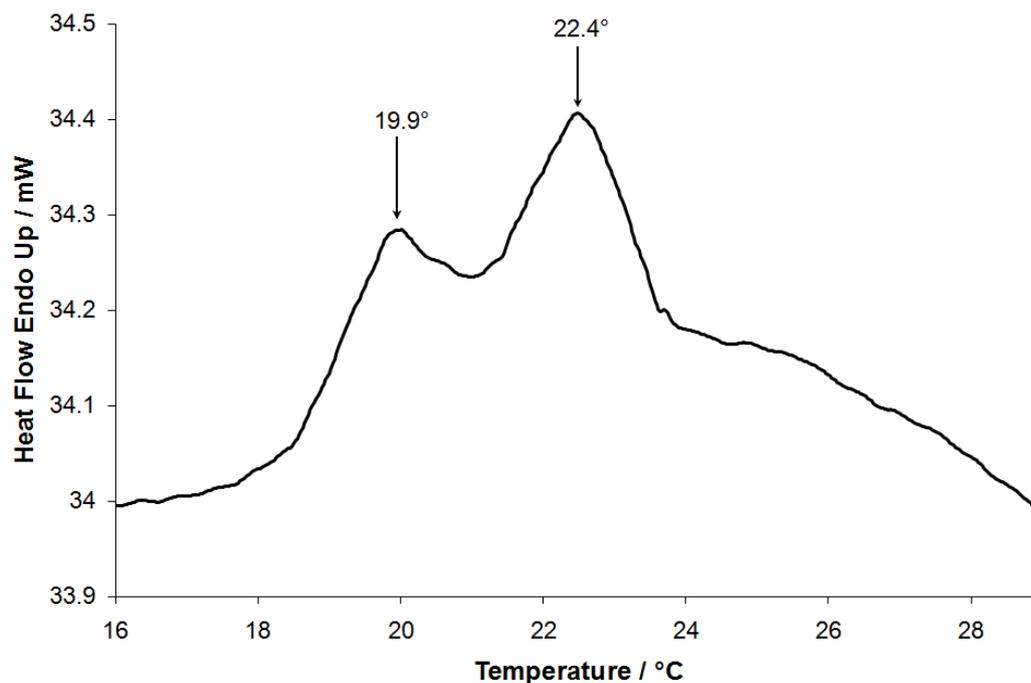
Figure 4.11. Differential scanning calorimetry heating scan of DMPG sodium salt in water. 1.204 mg sample; $\Delta H = 14.2$ kJmol^{-1}.

For comparison, liposomes composed of 50:50 (w/w) POPG/DOPC were also analysed by DLS between 10 °C and 60 °C to determine whether they underwent any size changes. It was not expected that any phase transitions would be observed, as POPG and DOPC have phase transition temperatures of -20 °C and -2 °C respectively.[56] As shown in Figure 4.12, the POPG/DOPC liposomes underwent only a gradual increase in diameter of approximately 6 nm between 10 °C and 35 °C, unlike the DMPG, DMPC and DMPG/DMPC liposomes, which decreased in size by 6–15 nm over temperature ranges of 2 °C to 7 °C during phase transition. The slight increase in size of the DOPC liposomes is likely to have been caused by thermal fluctuations.
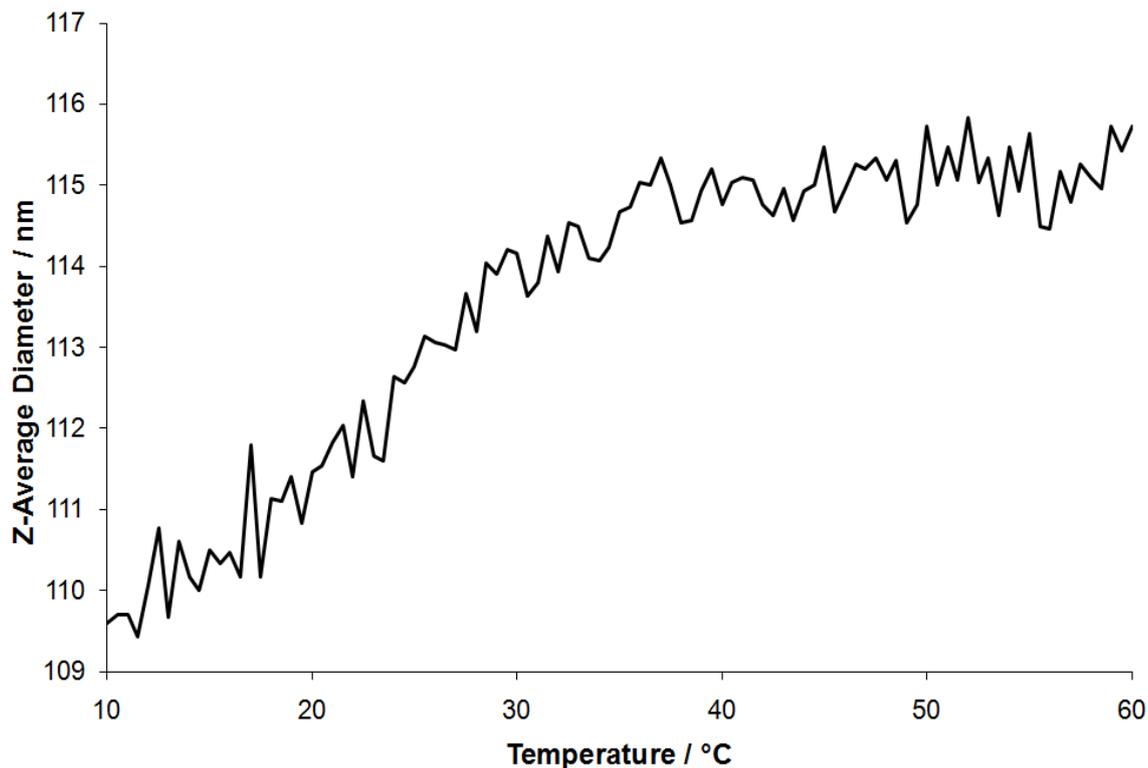
Figure 4.12. Intensity weighted mean hydrodynamic diameter (z-average diameter) measurements of liposomes composed of 50:50 (w/w) POPG/DOPC recorded between 10 °C and 40 °C. All liposomes were extruded through polycarbonate membranes with pores of 100 nm diameter during preparation.

4.2.2 Analysis of HNP-2 by fluorescence spectroscopy

4.2.2.1 Binding constant for dimerisation of HNP-2

The crystal and NMR structures described in the literature for the HNP1–3 have shown them all to have dimeric structures. These structures were generally obtained from analysis of solutions at much higher concentrations than those suitable for membrane binding studies however, for example HNP-2 was crystallised from a 15 mg/mL solution and the solution state NMR structure of HNP-2 determined from a 2 mg/mL solution.[9, 10] Although HNP-1–3 are reported to have dimeric structures in literature discussing their action on membranes, no measurements of dimer binding constants have been reported; therefore it cannot be stated with certainty that HNP-2 is predominately in the dimeric form at the concentrations at which binding studies are carried out.[20, 57]

Fluorescence spectroscopy can be used to study the insertion of antimicrobial peptides into a lipid bilayer. The three aromatic amino acids tryptophan, tyrosine and phenylalanine contribute to the fluorescence of proteins (Table 4.6).

Table 4.6. The spectral properties of tryptophan, tyrosine and phenylalanine in proteins in aqueous solution at pH 7.[58]

	Emission maximum (nm)	Quantum yield[a]
Tryptophan	350	0.13
Tyrosine	303	0.14
Phenylalanine	282	0.03

a)　λ_{ex} tryptophan = 280 nm; λ_{ex} tyrosine = 275 nm; λ_{ex} phenylalanine = 260 nm

The emission spectra of peptides and proteins are often recorded after excitation at 280 nm, at which wavelength tryptophan and tyrosine are both excited but phenylalanine is not. Tryptophan fluorescence generally dominates the fluorescence spectra of peptides and proteins regardless of the number of other fluorescent amino acids they contain, due to its relatively high extinction coefficient and the fact that it often absorbs energy from phenylalanine and tyrosine residues by fluorescence resonance energy transfer (FRET).[58] Tryptophan fluorescence is very sensitive to its environment. In peptides and proteins the quantum yield varies above and below the figure for the free amino acid due to factors such as quenching by proton or electron transfer from neighbouring amines, amides or carboxyl groups or disulphide bonds, or resonance energy transfer between tryptophan and tyrosine residues, depending on the structure of the peptide or protein.[58] The emission wavelength is very sensitive to the hydrophobicity of the tryptophan environment, due to both the location of the residue on the structure and the environment around the peptide or protein. This makes tryptophan fluorescence in bulk solvent a useful probe for the location of the tryptophan residues, whether they are solvated or embedded in the hydrophobic environment at the centre of the lipid bilayer.

A series of fluorescence measurements were obtained from solutions of increasing (1 μM – 39 μM) and decreasing (1.5 μM – 0.013 pM) HNP-2 concentration in order to study the self-association of the peptide. The tryptophan fluorescence spectrum of HNP-2 shows two emission maxima (Figure 4.13) at all concentrations down to 0.046 μM, where no more signal could be observed. This suggests two populations of tryptophan within the HNP-2 solution. A cross section was plotted of the average of the fluorescence intensities at 324 nm, 324.5 nm, 325 nm, 325.5 nm and 326 nm, the wavelength of the emission maximum. This plot shows that the intensity began to decrease sharply at around 2 μM (Figure 4.14), which was attributed to dissociation of the defensin dimers.
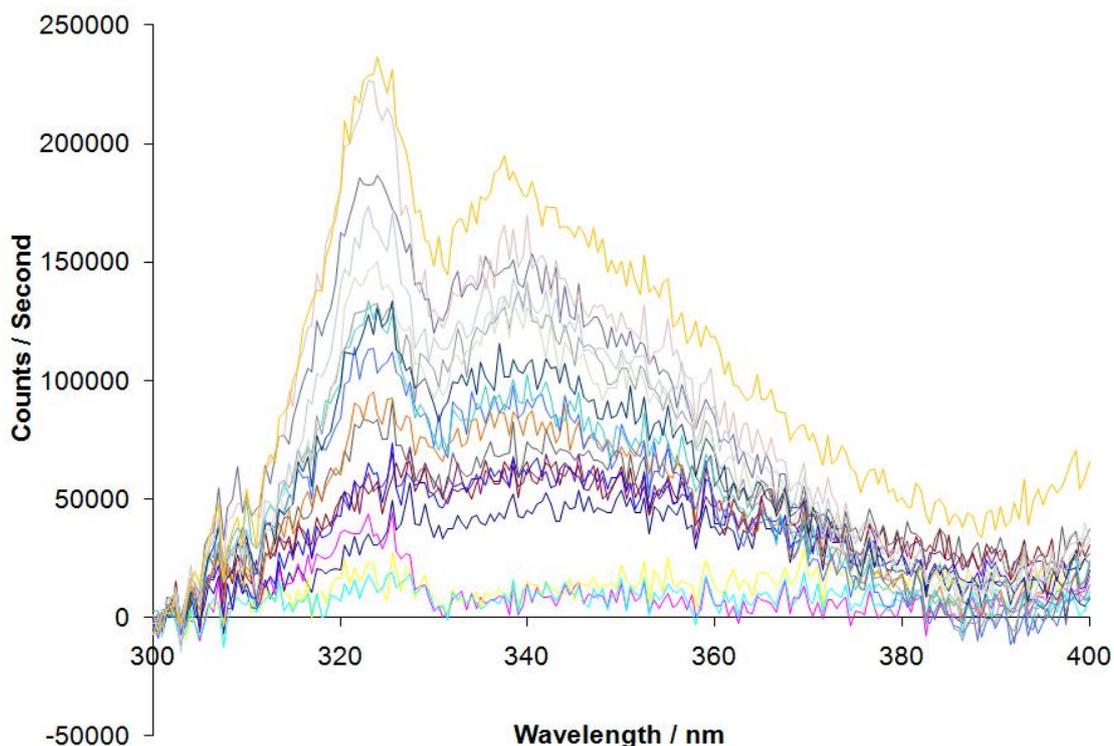
Figure 4.13. Fluorescence emission spectrum of HNP-2 in water at concentrations of 0.4 μM – 39 μM. λ_{ex} = 280 nm.

Least squares fitting was used to determine the binding constant, K_a (Equation 4.3), for the equilibrium between the monomer (P) and dimer (D) from the data obtained over the range of 0.012 μM to 6.2 μM.

$$2P \rightleftharpoons D \tag{4.2}$$

$$K_a = \frac{[D]}{[P]^2} \tag{4.3}$$

An equation was determined for the concentration of the dimer ($[D]$) in terms of K_a and the total peptide concentration ($[P]_t$) (Equation 4.9) by substituting Equation 4.3 for the concentration of the monomeric peptide ($[P]$) in Equation 4.5 and rearranging to give Equation 4.6.

$$[P]_t = [P] + 2[D] \tag{4.4}$$

$$[P] = [P]_t - 2[D] \tag{4.5}$$

$$[D] = K_a([P]_t - 2[D])^2 \tag{4.6}$$

Equation 4.6 was then rearranged to give Equation 4.7

$$[D] = 4K_a[D]^2 - 4K_a[P]_t[D] + K_a[P]_t^2 \tag{4.7}$$

and formed into a quadratic equation:

$$0 = 4K_a[D]^2 - (4K_a[P]_t[D] + K_a[P]_t^2$$

(4.8)

and solved using the quadratic formula to give Equation 4.9.

$$[D] = \frac{1 + 4K_a[P]_t - \sqrt{(1 + 4K_a[P]_t{}^2 - 16K_a{}^2[P]_t^2}}{8K_a}$$

(4.9)

At any time, the observed fluorescence emission signal, S_{obs} is a combination of the emission from tryptophan residues in the monomers and the emission from tryptophan residues in the dimers:

$$S_{obs} = (S_m F_m) + (S_d F_d)$$

(4.10)

where S_x is the fluorescence emission per monomer or dimer and F_x is the fraction of peptide in either a monomeric or a dimeric state, were $F_m + F_d = 1$. Equation 4.11 was gained from substituting Equation 4.5 into Equation 4.10.

$$S_{obs} = S_m \left(\frac{[P]_t - 2[D]}{[P]_t} \right) + S_d \left(\frac{2[D]}{[P]_t} \right)$$

(4.11)

Substitution with Equation 4.12 gave Equations 4.13 and 4.14.

$$2D = 2K_a[P]^2$$

(4.12)

$$S_{obs} = S_m \left(\frac{[P]_t - 2K_a[P]^2}{[P]_t} \right) + S_d \left(\frac{2K_a[P]^2}{[P]_t} \right)$$

(4.13)

$$S_{obs} = \frac{S_m[P]_t}{[P]_t} + \left(\frac{2K_a[P]^2 - (S_d - S_m)}{[P]_t} \right)$$

(4.14)

Equation 4.14 was then rearranged to give:

$$S_{obs} = \frac{2K_a[P]^2(S_d - S_m)}{[P]_t} + S_m$$

(4.15)

Least squares fitting was carried out on Equation 4.15 to give calculated fluorescence values at each $[P]_t$, changing the parameters S_m, S_d and K_a. $[P]$ and $[D]$ were calculated for each $[P]_t$ using Equations 4.5 and 4.9 respectively. The best fit was produced with S_m = 1778 ±178, S_d = 114256 ± 11426 and K_d = 3.8 x 10^{-6} ± 4 x 10^{-7} M^{-1}. This suggests that at the peptide concentration used in the binding analyses (15 µM) the majority of the peptide will be present as dimers. The fit between the experimental and calculated fluorescence (Figure 4.14) is moderate, but this is understandable due to the

weak fluorescence emission at the HNP-2 concentrations over which the analysis was carried out.
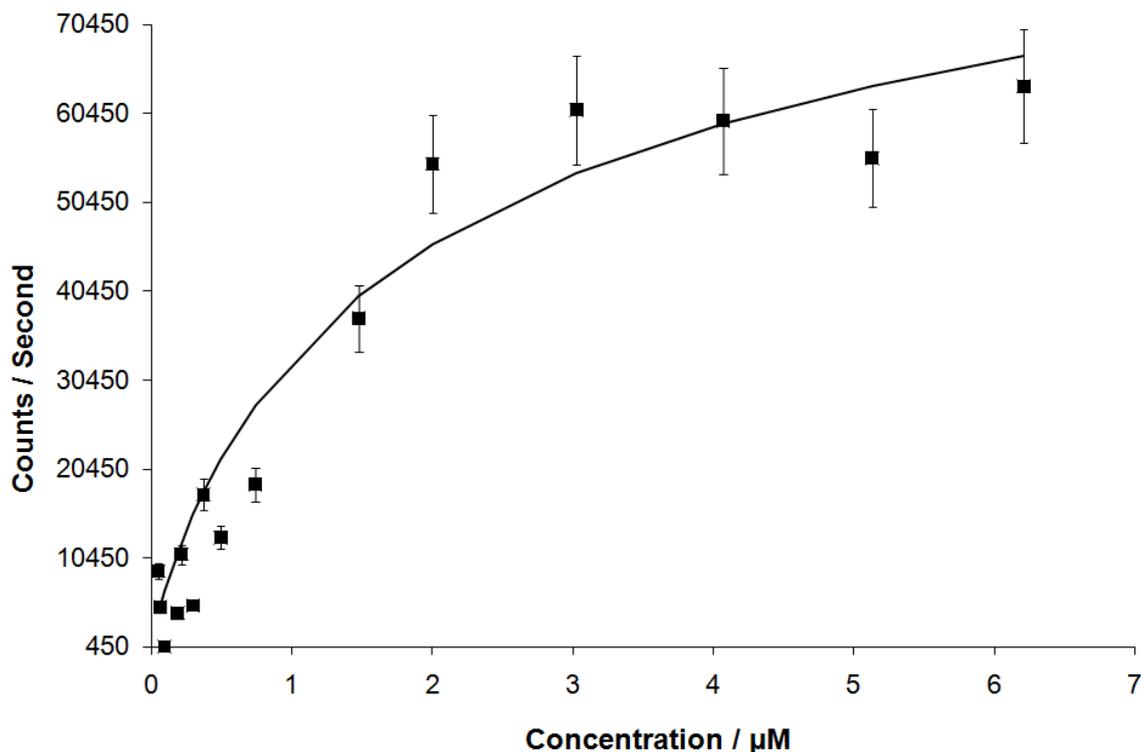
Figure 4.14. Experimental and calculated fluorescence emission of HNP-2 in water at 325 nm. Experimental data are presented as points and the profile calculated from non-linear regression as a line. λ_{ex} = 280 nm.

The magnitude of S_d was more than two times that of S_m. This can be explained by studying the crystal structure of an HNP-2 dimer (Figure 4.15), which shows that the distances between Trp(26) on one monomer and Tyr(16), Tyr(3) and Tyr(21) on the other monomer are 10.6, 12.2 and 14.4 Å respectively. These distances are close enough for fluorescence resonance energy transfer (FRET) to occur from the tyrosine residues to the tryptophan residue across the dimer.[59] The same effect has been observed for Human Recombinant Interferon γ, a peptide which exists as a dimer in its biologically active form. Each monomer contains one tryptophan and four tyrosine residues. On dissociation of the dimer the quantum yield of tryptophan drops significantly due to the loss of FRET from tyrosine residues on one monomer to tryptophan on the other.[60]
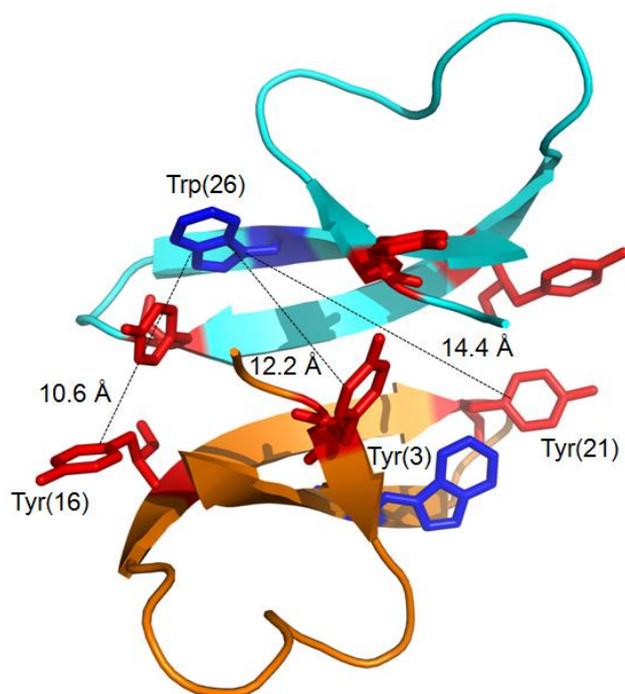
Figure 4.15. Crystal structure of HNP-2 showing distances between tryptophan and tyrosine residues on neighbouring subunits of the dimer. Distances measured and structures displayed using The PyMOL Molecular Graphics System, Version 1.2r1, Schrödinger, LLC (www.pymol.org).

4.2.2.2   *Fluorescence in water and MeOH*

The fluorescence spectrum of HNP-2 in water (Figure 4.13) shows two emission maxima, both of which appear to be blue-shifted relative to the expected emission wavelength of tryptophan in water (350 nm).[58]   This suggests that there are two populations of tryptophan residues. A fluorescence spectrum was recorded in 75% (v/v) MeOH/H_2O, a more hydrophobic environment than water, to mimic the hydrophobic region of the lipid bilayer to see if a further blue-shift would be observed (Figure 4.16).[61] The change from water to MeOH had no effect on the position of either emission maximum. The two emission maxima were less resolved in the spectrum in MeOH. This is attributed to the fact that the instrument used to obtain the spectra of the peptide in water used an array photon multiplier tube (PMT), which gives more sensitive detection than the mesh PMT in the instrument used to record the spectrum in 75% MeOH.
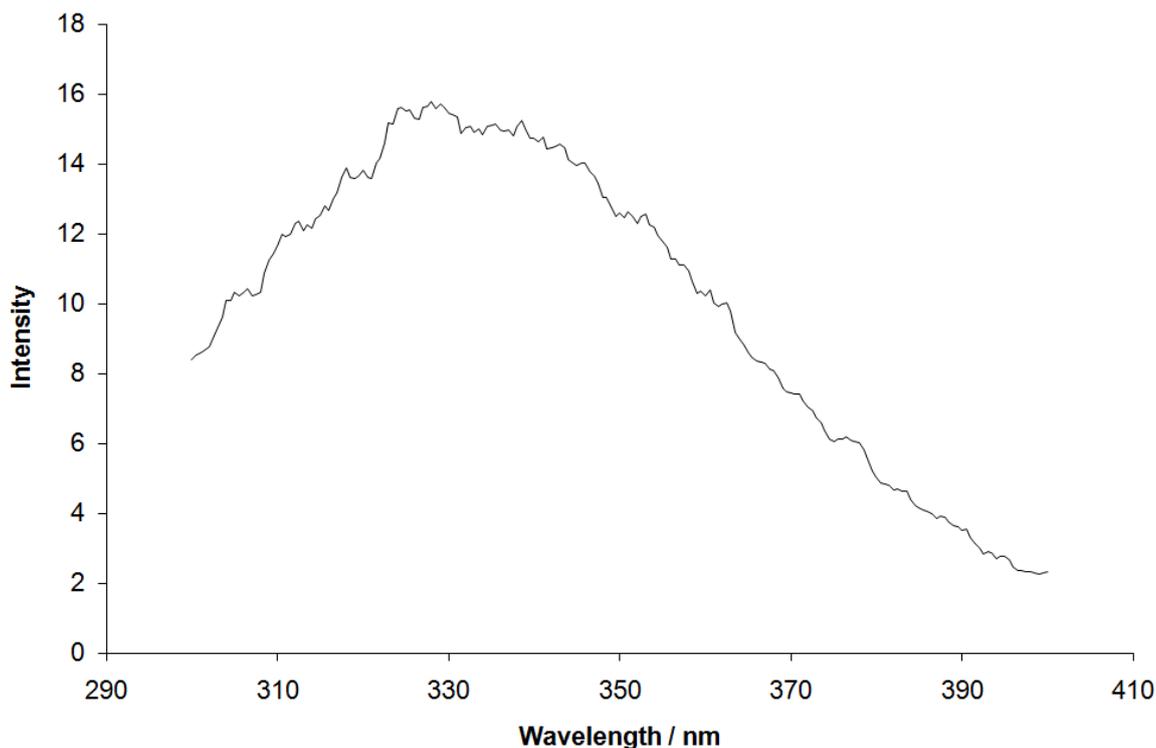
Figure 4.16. Fluorescence emission spectrum of HNP-2 (15 µM) in 75% (v/v) MeOH/H$_2$O. λ_{ex} = 280 nm.

The two populations of tryptophan observed in the fluorescence spectra can be explained by studying the crystal structure of HNP-2 and the solid state NMR (SSNMR) structures of HNP-1.[15] Each HNP-2 monomer contributes one tryptophan residue, three tyrosine residues and one phenylalanine residue to the dimer. The crystal structure of an HNP-2 dimer reveals that, although the backbone of the dimer is symmetrical, the two tryptophan side chains are not in equivalent environments relative to nearby tyrosine side chains, and that the tryptophan and tyrosine residues are close enough for excimer coupling to occur (Figure 4.17). This suggests that there are at least two low energy interactions between tryptophan and neighbouring tyrosine residues which can contribute to the tyrosine emission.
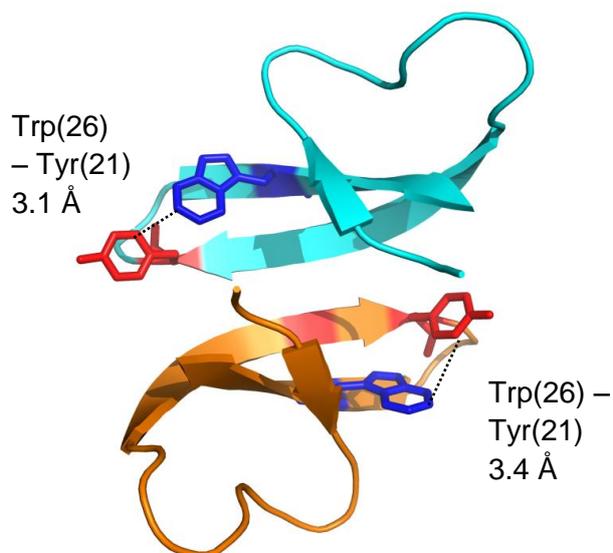
Figure 4.17. Structure of HNP-2 dimer showing different orientations of tryptophan relative to neighbouring tyrosine residues and the closest C–C contact distances. Distances measured and structures displayed using The PyMOL Molecular Graphics System, Version 1.2r1, Schrödinger, LLC (www.pymol.org).

The published SSNMR analysis of HNP-1 produced 10 minimum energy structures of peptide monomers within dimers in which there was little variation in the orientations of the backbone or tyrosine residues but a large degree of variation in the orientation of the tryptophan residue. Two main tryptophan rotamers can be distinguished, as shown in Figure 4.18A and B. In Figure 4.18A the closest C–C contact distance between Trp(26) and Tyr(21) is 4.1 Å, and in Figure 4.18B the closest C–C distance between Trp(26) and Tyr(21) is also 4.1 Å. This is close enough for aromatic–aromatic interactions to occur.[62, 63]
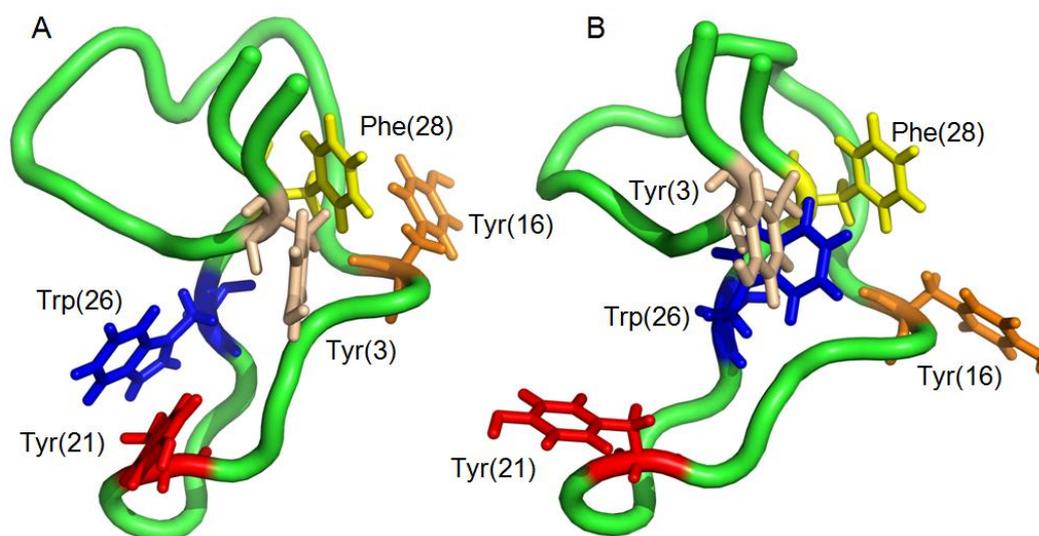
Figure 4.18. Interactions between A) Trp(26) and Tyr(21) and B) Trp(26) and Tyr(3) in HNP-1 showing the two main rotamers of Trp(26). Residues are labelled according the sequence of HNP-1 and correspond to Tyr(2), Tyr(15), Tyr(20), Trp(26) and Phe(27) of HNP-2. Structures displayed using The PyMOL Molecular Graphics System, Version 1.2r1, Schrödinger, LLC (www.pymol.org).

4.2.2.3 HNP-2 fluorescence in a liposome dispersion

Figure 4.19 shows a time series spectrum of HNP-2 in 50:50 (w/w) POPG/DOPC liposomes recorded at 2.5 minute intervals for five hours, with just the first, 60th, and final spectra shown together in Figure 4.20. Two pieces of information can be drawn from the shapes of the spectra in Figure 4.20. Firstly, there is no evidence of blue-shifting during binding compared to the spectra of the peptide in water and in MeOH, though the tryptophan fluorescence emission is blue-shifted in water, MeOH and in liposomes relative to the expected emission wavelength of tryptophan in water. Secondly, the two emission maxima became more resolved during the course of the analysis, as shown by their clarity in spectra B and C in Figure 4.20 compared to spectrum A. This suggests that the peptide was binding to the membrane and that when the peptide is bound the tryptophan residues exchange more slowly between the two main conformations. Cross sections of the time series spectra at 330 nm and 340 nm (Figure 4.21) show changes in fluorescence intensity, from which the binding kinetics of HNP-2 can be studied (Section 4.2.6).
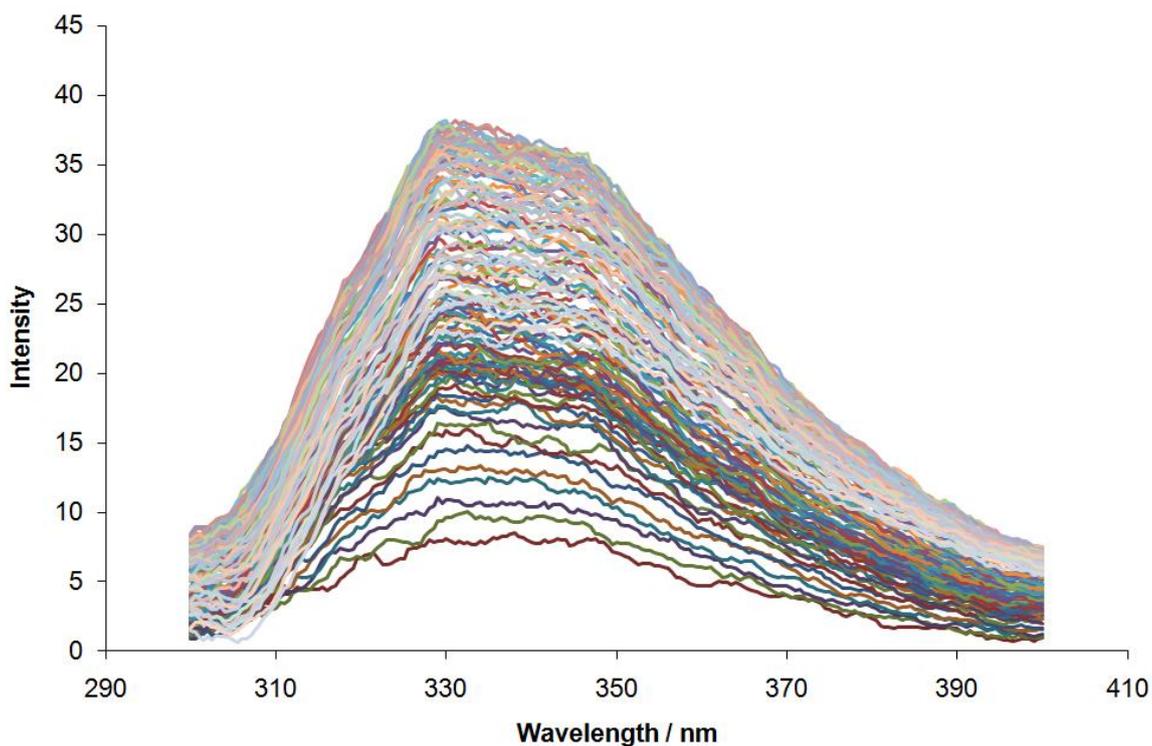
Figure 4.19. Time series fluorescence emission spectrum of HNP-2 (15 µM) in 50:50 (w/w) POPG/DOPC liposomes (1.4 mM) acquired over a 5 hour period. Spectra were recorded at 2.5 minute intervals. λ_{ex} = 280 nm.
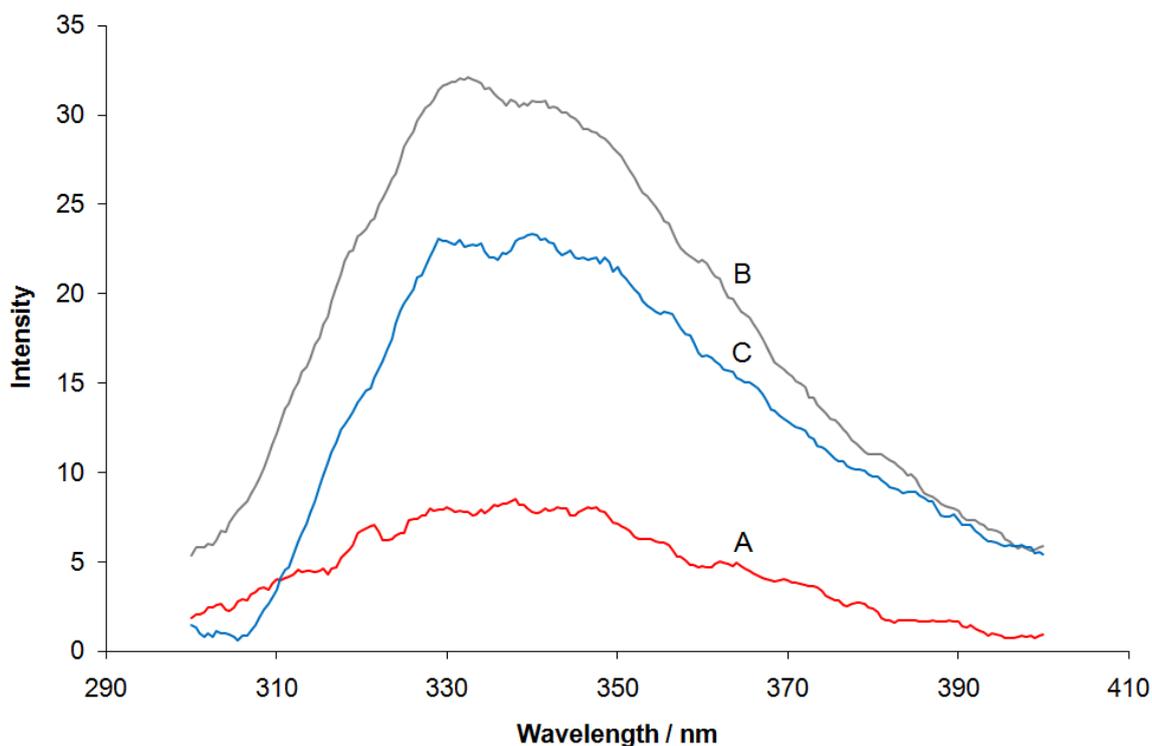
Figure 4.20. Spectra A, B and C recorded after 0, 147.5 and 297.5 minutes respectively from combined fluorescence emission spectrum of HNP-2 (15 µM) in 50:50 (w/w) POPG/DOPC liposomes (1.4 mM). Spectra recorded every 2.5 minutes for 5 hours. λ_{ex} = 280 nm.
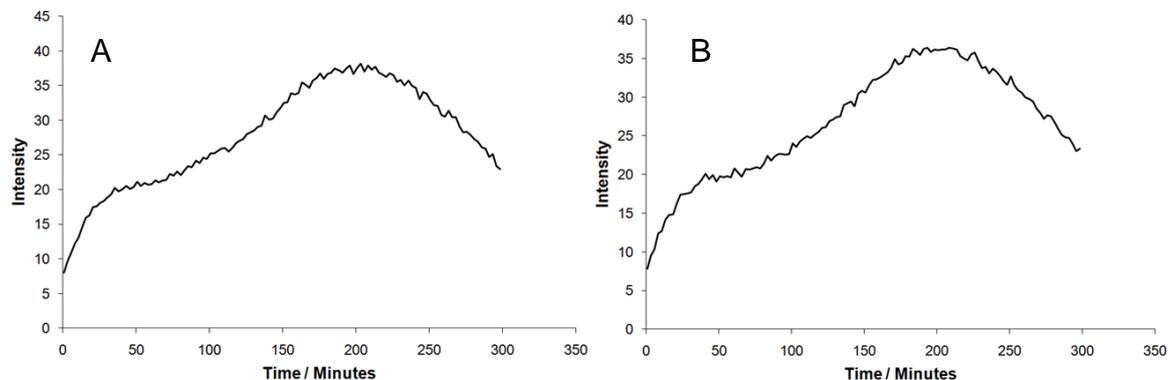
Figure 4.21. Evolution of the fluorescence emission intensity of HNP-2 (15 µM) in 50:50 (w/w) POPG/DOPC liposomes (1.4 mM) at A) 330 nm and B) 340 nm. Spectra were recorded at 2.5 minute intervals for 5 hours. λ_{ex} = 280 nm.

There was no real change in the wavelength of the tryptophan emission maxima between water, 75% MeOH and the liposome dispersions. If the tryptophan residues in the dimer were exposed to the solvent or liposomes a blue-shift would be expected in less polar, more hydrophobic, environments. The fact that this was not observed suggests that the tryptophan residues are not exposed to the environment surrounding the peptide dimer. This was confirmed by examining space-filling models of the two main HNP-1 rotamers identified in Figure 4.18 (Figure 4.22), which show that in both conformations the

tryptophan residue is not freely solvated. The blue-shift of the tryptophan emission in all of the spectra is due to the interactions between tryptophan and tyrosine.
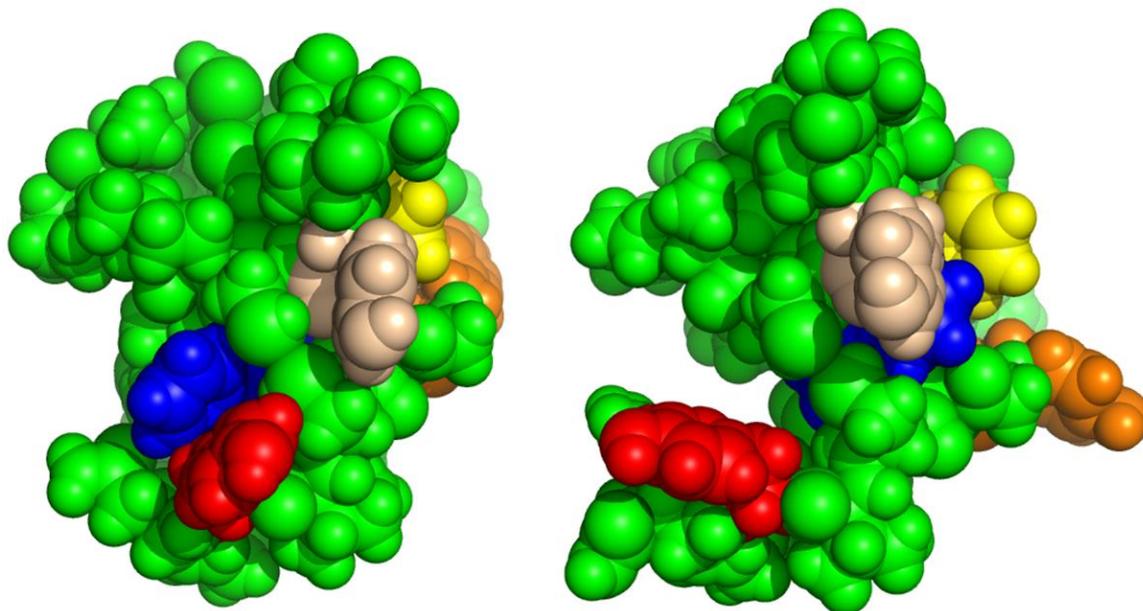
Figure 4.22. Space-filling models of HNP-1 showing the two main rotamers of tryptophan. Residues shown in white, orange, red, blue and yellow correspond to residues Tyr(2), Tyr(15), Tyr(20), Trp(25) and Phe(27) of HNP-2. Structures displayed using The PyMOL Molecular Graphics System, Version 1.2r1, Schrödinger, LLC (www.pymol.org).

4.2.3 Linear dichroism analyses

A series of LD spectra were obtained in order to determine the peptide orientation with relation to the lipid bilayer during binding and the kinetics of binding (Figure 4.23). Sixty scans were recorded at 5 minute intervals for each of the analyses to produce time series spectra.
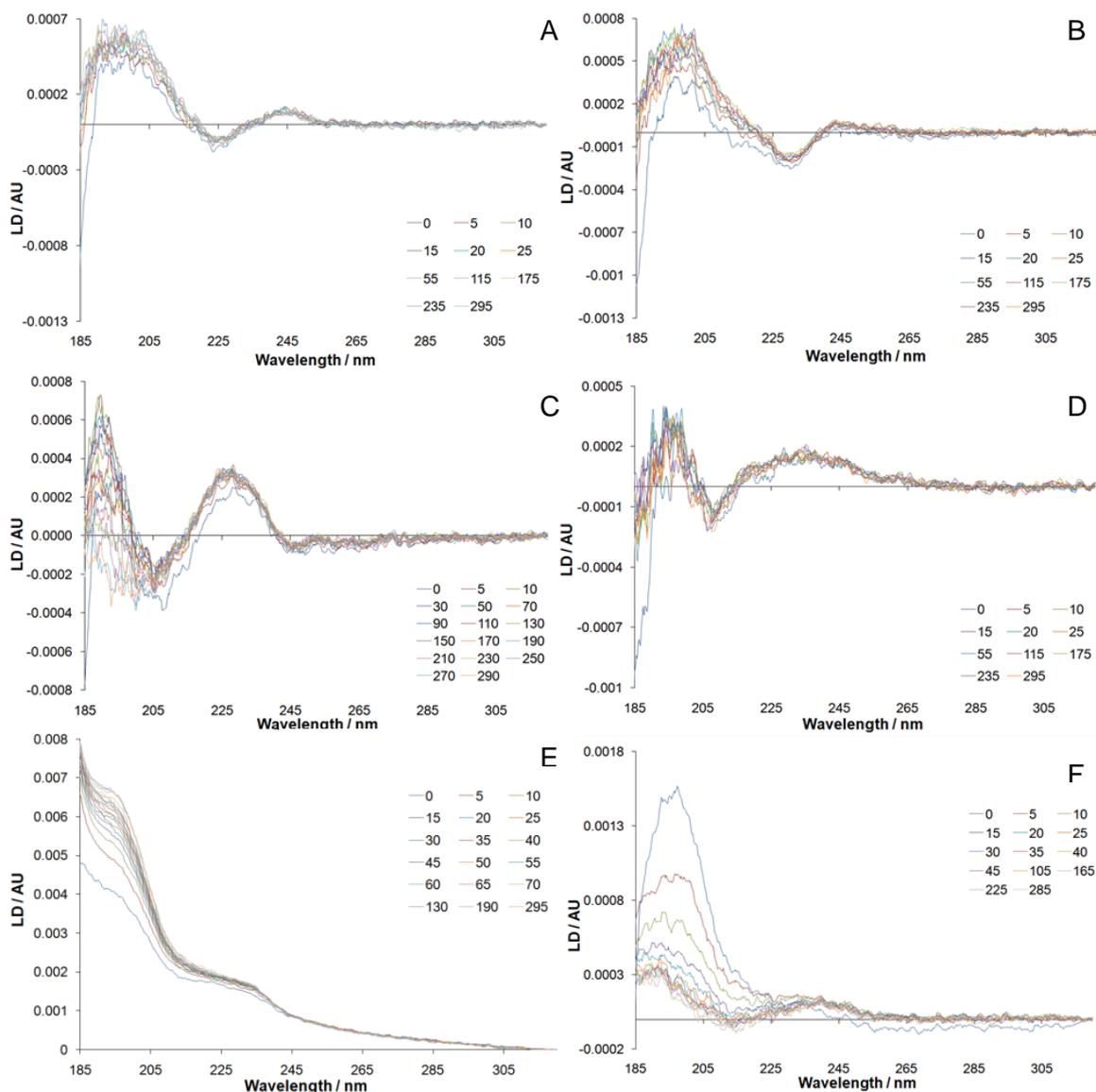
Figure 4.23. Selected linear dichroism spectra of HNP-2 with POPG/DOPC, DOPS/DOPC or DMPG/DMPC liposomes. HNP-2 (15 µM) was added to A) 50:50 (w/w) POPG/DOPC (1.4 mM) at 30 °C; B) 50:50 (w/w) POPG/DOPC (1.4 mM) at 40 °C; C) 50:50 (w/w) POPG/DOPC (1.4 mM) at 53 °C; D) 50:50 (w/w) DOPS/DOPC (1.05 mM) at 30 °C; E) 50:50 (w/w) DMPG/DMPC (1.4 mM) at 17 °C; F) 50:50 (w/w) DMPG/DMPC (1.4 mM) at 33 °C. Sixty scans were recorded at 5 minute intervals, the legends show the starting times of the included spectra in minutes.

The LD spectra show clear changes in intensity over time, suggesting changes in orientation which allow the binding kinetics to be followed (Section 4.2.6). Figure 4.24 shows the cross section at 200 nm of the spectra obtained with POPG/DOPC at 30 °C.
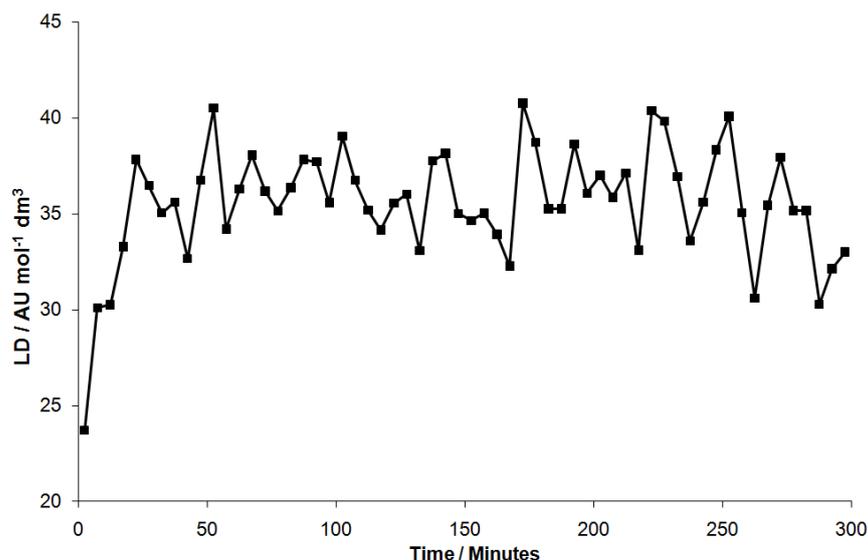
Figure 4.24. Evolution of the LD signal at 200 nm over 5 hours after the addition of HNP-2 (3 μM) to 50:50 (w/w) POPG/DOPC (280 μM) at 30 °C.

4.2.4 The effect of HNP-2 on liposomes and liposome stability

4.2.4.1 Fluorescence resonance energy transfer studies of liposome fusion

Fluorescence resonance energy transfer (FRET) was used to determine whether HNP-2 was causing liposome fusion under the conditions employed for the other analyses. The FRET experiment was carried out using POPG/DOPC liposomes with 0.5 mol% of each of the donor N-(7-nitro-2,1,3-benzodiazol-4-yl)-phosphatidylethanolamine (NBD-PE) and the acceptor N-(Lissamine Rhodamine B sulfonyl)-phosphatidylethanolamine (Rh-PE). If liposomes composed of these two species are excited at around 460 nm (the excitation wavelength of NBD-PE), emission is observed from both species (λ_{em} NBD-PE = 540 nm, λ_{em} Rh-PE = 590 nm). If these liposomes are mixed with unlabelled liposomes and a species added which causes fusion or exchange between the labelled and unlabelled liposomes, an increase in the NBD-PE emission and decrease in the Rh-PE emission will be observed due to dilution.[64]

HNP-2 was added to a 3:1 mixture of unlabelled 50:50 (w/w) POPG/DOPC liposomes and NBD-PE/Rh-PE labelled POPG/DOPC liposomes to give the same peptide:lipid ratio as in the peptide binding experiments, and 60 fluorescence spectra recorded at 5 minute intervals (λ_{ex} 450 nm, λ_{em} 470–650 nm) (Figure 4.25) over 5 hours. A spectrum was also recorded of the same ratio of liposomes to which a 0.1% solution of Triton X-100 had been added. Triton X-100 is a detergent which causes lysis and aggregation of liposomes.[65] No Rh-PE emission was observed after the addition of Triton X-100, showing that the liposomes had been broken up and the donor NBD-PE and

acceptor Rh-PE lipids separated. A baseline spectrum of non-labelled liposomes in the absence of HNP-2 and triton X-100 was subtracted from all spectra.
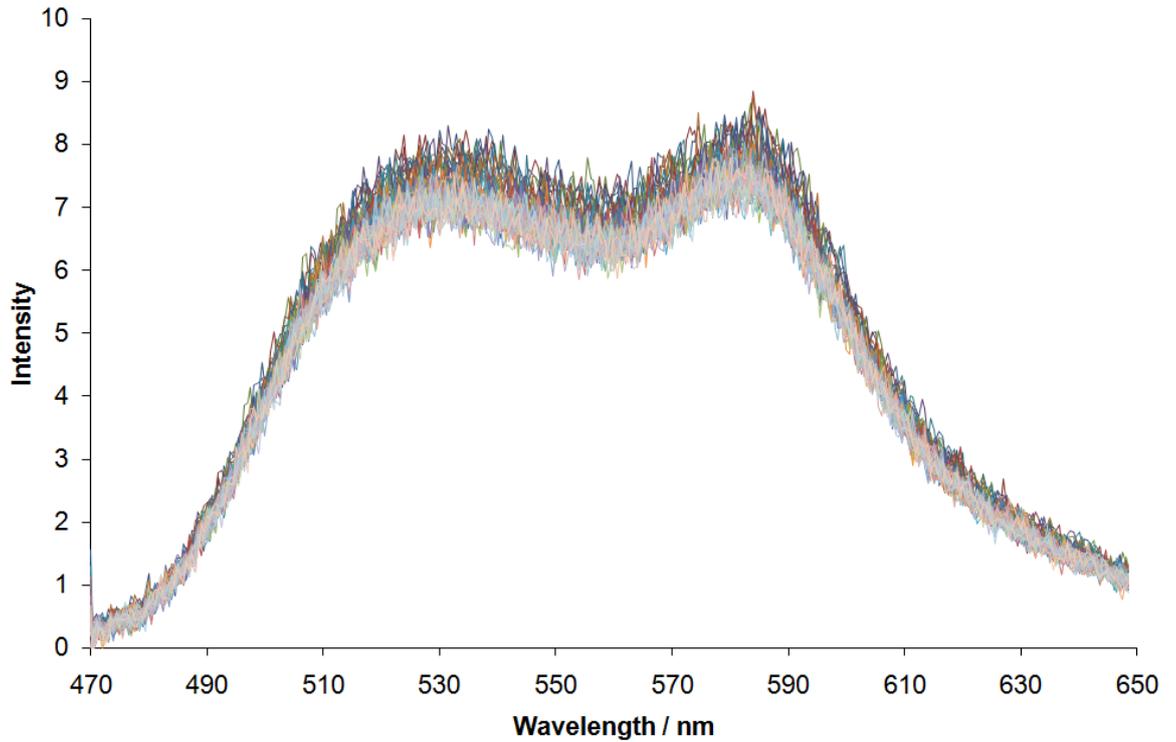
Figure 4.25. Time series FRET spectrum of HNP-2 with unlabelled and labelled POPG/DOPC liposomes. HNP-2 (15 μM) was added to 3:1 (v/v) unlabelled 50:50 (w/w) POPG/DOPC liposomes and 50:50 (w/w) POPG/DOPC liposomes with 0.5 mol% of each of Rh-PE and NBD-PE (1.4 mM total lipid concentration) and fluorescence analyses recorded over 5 hours at 5 minute intervals. λ_{ex} = 450 nm.

The ratio of NBD-PE fluorescence to Rh-PE fluorescence was calculated to see if it was changing over time using Equation 4.16.

$$\frac{(F_1-F_2)_t}{(F_1-F_2)_0}/t \tag{4.16}$$

F_x, λ_1 and λ_2 are described in Equations 4.17 and 4.18, where $(F_1)_0$ data were obtained from the spectrum of 3:1 (v/v) labelled:unlabelled liposomes recorded in the absence of HNP-2; $(F_1)_t$ data were taken from the spectra with obtained with 3:1 (v/v) labelled:unlabelled liposomes and HNP-2; and $(F_2)_0$ and $(F_2)_t$ data were taken from the spectra obtained with Triton X-100 without and with HNP-2 respectively.

$$F_\chi = \frac{Counts\ \lambda_2}{Counts\ \lambda_1} \tag{4.17}$$

$$\lambda_1 = \lambda_{em\ obs\ NBD-PE} = 531\ nm$$
$$\lambda_2 = \lambda_{em\ obs\ Rh-PE} = 580\ nm \tag{4.18}$$

$(F_1 - F_2)_t$ was calculated for each of the 60 spectra, and then a graph of Equation 4.16 produced (Figure 4.26). The time t of each scan at a given wavelength (λ_t) was calculated using Equation 4.19, where λ_s is the starting wavelength of each scan, n corresponds to the number of completed scans and s corresponds to the scan rate (nm/minute). The scan rate is multiplied by 2.5 due the interval between scans.

$$t = \frac{(\lambda_t - \lambda_s)}{s} + 2.5n \qquad\qquad (4.19)$$
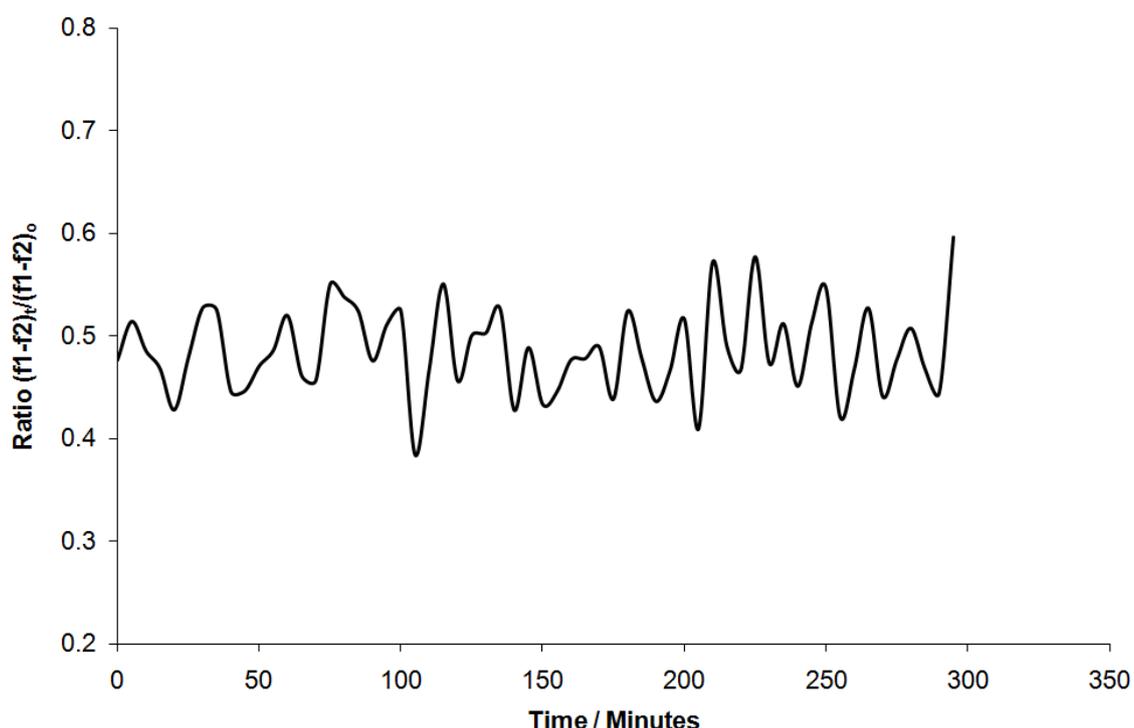
Figure 4.26. Ratio of NBD-PE fluorescence to Rh-PE fluorescence against time, calculated using Equation 4.16 from time series fluorescence analysis of HNP-2 (15 µM) with 3:1 (v/v) unlabelled 50:50 (w/w) POPG/DOPC liposomes and 50:50 (w/w) POPG/DOPC liposomes with 0.5 mol% of each of Rh-PE and NBD-PE (1.4 mM total lipid concentration) recorded over 5 hours at 5 minute intervals. λ_{ex} = 450 nm.

No change can be observed in the plot of the ratio of NBD-PE fluorescence to Rh-PE fluorescence over five hours after the addition of HNP-2 to the liposomes (Figure 4.26), confirming that there was no exchange of lipids between the labelled and unlabelled liposomes and therefore no fusion occurring.

4.2.4.2 Dynamic light scattering

Dynamic light scattering (DLS) was used to determine of the average size of the liposomes before and after the addition of HNP-2, which would show the effects of any fusion, aggregation, micellization or increase in size due to the addition of peptide.

Liposome dispersions were analysed in the absence of HNP-2, diluted to the same concentration as those in the presence of HNP-2, and in the presence of HNP-2 after each 5-hour LD analysis. All DLS measurements were recorded at 21 °C regardless of the temperature of the LD analysis.   The diameter was averaged over 74 measurements.   The diameter measurement used was the 'z-average', the intensity weighted average of the distribution of liposome sizes. The polydispersity index (PdI) is a measure of the width of the distribution of sizes recorded. The PdI can be used to give the % polydispersity (%Pd) (Equation 4.20), which gives a clearer indication of the width of the distribution.

$$\%\mathrm{Pd}=100\sqrt{\mathrm{PdI}}$$

(4.20)

The data (Table 4.7) show that there was no real change in the diameter of the liposomes before and after the addition of HNP-2.

Table 4.7. Diameter and polydispersity measurements of liposomes before and after the addition of HNP-2.

Name	Diameter (nm)[a]	Average PdI	%Pd
POPG/DOPC Blank	119	0.067	26
POPG/DOPC HNP-2 30 °C	110	0.078	28
POPG/DOPC HNP-2 40 °C	113	0.071	27
POPG/DOPC HNP-2 53 °C	111	0.082	29
DMPG/DMPC Blank	83	0.193	44
DMPG/DMPC HNP-2 17 °C	92	0.258	51
DMPG/DMPC HNP-2 33 °C	82	0.188	43
DOPS/DOPC Blank	122	0.077	28
DOPS/DOPC HNP-2 30 °C	115	0.070	27

a)   Each value is an average of 74 individual measurements

4.2.5 Binding kinetics

The results of the fluorescence and linear dichroism analyses both showed changes in signal over time, which enabled the binding kinetics of HNP-2 to be determined. The combined data from the two techniques were analysed using different binding models in order to determine which best described the binding of HNP-2.

4.2.5.1 Two-state model

4.2.5.1.1 Fluorescence data

Cross sections of the time series fluorescence spectra at 330 nm and 340 nm (Figure 4.27) suggest an initial binding stage during the first 50 minutes, followed by either

a second, slower, binding stage or an increase in scattering due to the settling and grouping of the liposomes due to the lack of stirring, and then a drop-off in signal which is attributed to photobleaching of the samples.
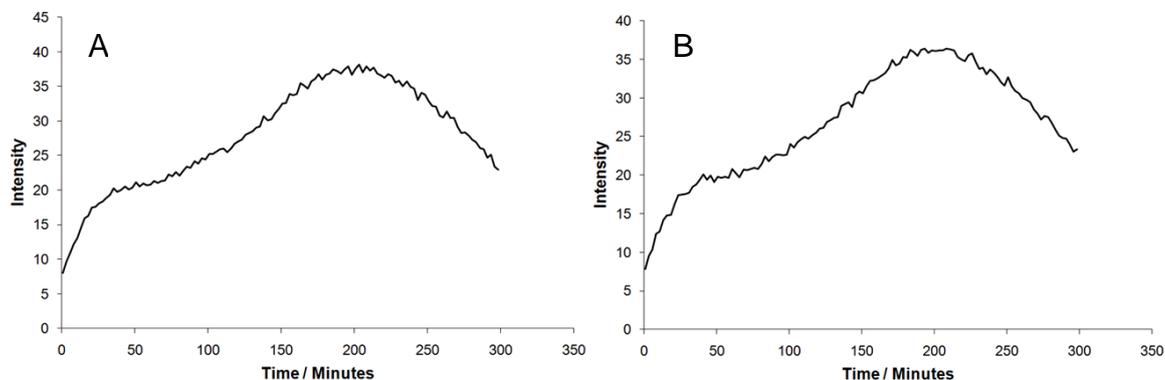
Figure 4.27. Evolution of the fluorescence emission intensity of HNP-2 (15 µM) in 50:50 (w/w) POPG/DOPC liposomes (1.4 mM) at A) 330 nm and B) 340 nm. Spectra were recorded at 2.5 minute intervals for 5 hours. λ_{ex} = 280 nm.
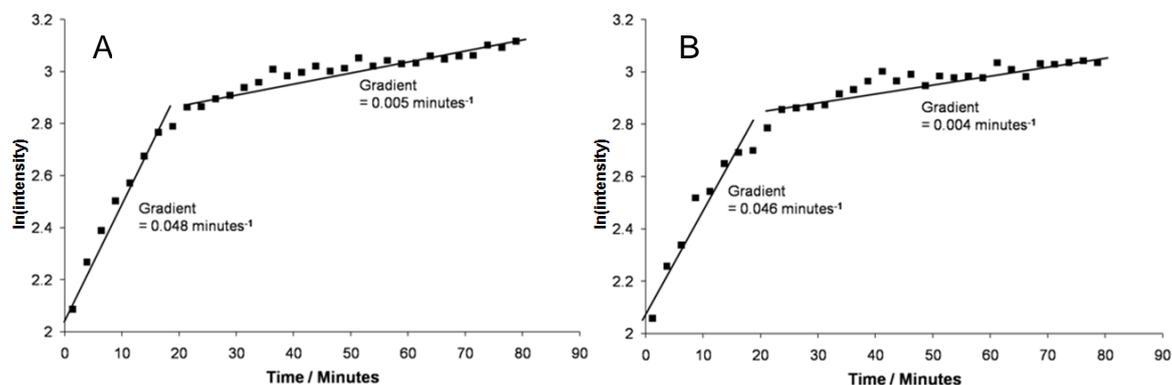
Figure 4.28. Semi-log plots of the evolution of the fluorescence emission intensity of HNP-2 (15 µM) in 50:50 (w/w) POPG/DOPC liposomes (1.4 mM) at A) 330 nm and B) 340 nm. Spectra were recorded at 2.5 minute intervals for 5 hours. λ_{ex} = 280 nm.

Semi-log plots of the evolution of the fluorescence intensity at 330 and 340 nm over the first 80 minutes (Figure 4.28A and B respectively) suggest that the binding was pseudo-first order with respect to HNP-2. Pseudo-first order kinetics are reasonable given the large excess of lipid, but they also suggest that the mechanism being followed did not involve multimer formation. Plots of fluorescence intensity against time and the reciprocal of fluorescence intensity against time (data not shown) ruled out zero and second order binding, as they were not linear. It was not possible to study the kinetics after 80 minutes due to the drop in signal at around 200 nm, which meant that the end of the process could not be modelled. The gradient of the semi-log plots can be used to approximate the reaction rate. From Figure 4.28A and B, the gradients of the semi-log

plots are initially 0.048 minutes⁻¹ and 0.046 minutes⁻¹ at 330 nm and 340 nm respectively, corresponding to half lives of approximately 15 minutes. This initial process was followed by one with a much slower rate, with gradients of 0.005 minutes⁻¹ and 0.004 minutes⁻¹ at 330 nm and 340 nm respectively, corresponding to half lives of 173 minutes. Due to the very shallow gradient of this stage, the binding was initially just fitted to a two state model, treating the slight increase in signal after 20 minutes as negligible. It was assumed that the majority of the peptide was present, and binding, in the dimeric form, due to the binding constant established in Section 4.2.2.1. The two-state model described the binding of free peptide dimers to give one bound peptide state, as shown in Figure 4.29, where P_f and P_m correspond to free and bound peptides dimers respectively.
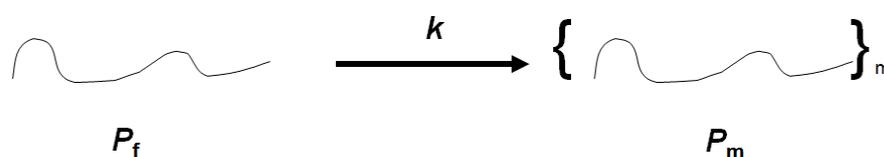
Figure 4.29. The two state kinetic model used for analysis of the LD and fluorescence data.

At any time, the observed fluorescence intensity, F_{obs} was a combination of the fluorescence from the peptides in state P_f and those in state P_m (Equation 4.21).

$$F_{obs} = \left([P]_f \frac{F_f}{[P]_t}\right) + \left([P]_m \frac{F_m}{[P]_t}\right)$$

(4.21)

$[P]_f$ and $[P]_m$ correspond to the concentrations of the peptides in states P_f and P_m respectively, $[P]_t$ corresponds to the total peptide concentration and F_f and F_m correspond to the fluorescence from each peptide in state P_f and P_m respectively.

The time series data from each experiment were analysed using weighted least squares fitting to determine the rate constant, k. The time t of each scan at a given wavelength (λ_t) could be calculated using Equation 4.22, where λ_s is the starting wavelength of each scan; n corresponds to the number of completed scans and is multiplied by 2.5 due to the 2.5 minute interval between scans. The scan rate, in nm/minute, is represented by s.

$$t = \frac{(\lambda_t - \lambda_s)}{s} + 2.5n$$

(4.22)

The concentrations $[P]_f$ and $[P]_m$ were calculated at each time t using equations 4.23 and 4.24.

$$[P]_f = [P]_t e^{-kt}$$

(4.23)

$$[P]_{\mathrm{m}} = [P]_{\mathrm{t}} - [P]_{\mathrm{f}} \qquad\qquad (4.24)$$

The fluorescence intensity corresponding to these values, F_{calc}, was then calculated at each time point (Equation 4.25).

$$F_{\mathrm{calc}} = \left(F_{\mathrm{f}}\frac{[P]_{\mathrm{f}}}{[P]_{\mathrm{t}}}\right) + \left(F_{\mathrm{m}}\frac{[P]_{\mathrm{m}}}{[P]_{\mathrm{t}}}\right) \qquad\qquad (4.25)$$

Weighted non-linear least squares fitting was performed simultaneously on data at 330 nm and 340 nm. The least squares values were weighted by multiplication by $\frac{1}{t^2}$ to give a better fit over the whole data range. As shown in Table 4.8, the rate constant correlated closely with the gradients of the semi-log plots at 330 nm and 340 nm.

Table 4.8. Rate constant and half-life calculated from fitting of fluorescence analysis of HNP-2 binding to 50:50 (w/w) POPG/DOPC liposomes.

Liposomes	Temperature (°C)	k (minute^{-1})	$t_{1/2}$ (minutes)
POPG/DOPC	30	0.043 ± 0.004	16.3 ± 1.6

4.2.5.1.2 LD data

Semi-log plots of the cross sections of the linear dichroism data at major peaks and negative bands also suggested a 1st order binding model, with a fast binding stage followed by a levelling off of the signal (Figure 4.30). The gradients of these semi-log plots suggested rate constants of around 0.150 minutes^{-1}, corresponding to half lives of around 5 minutes. Plots of intensity against time and the reciprocal of intensity against time were not linear, which ruled out zero or second order binding models (data not shown).
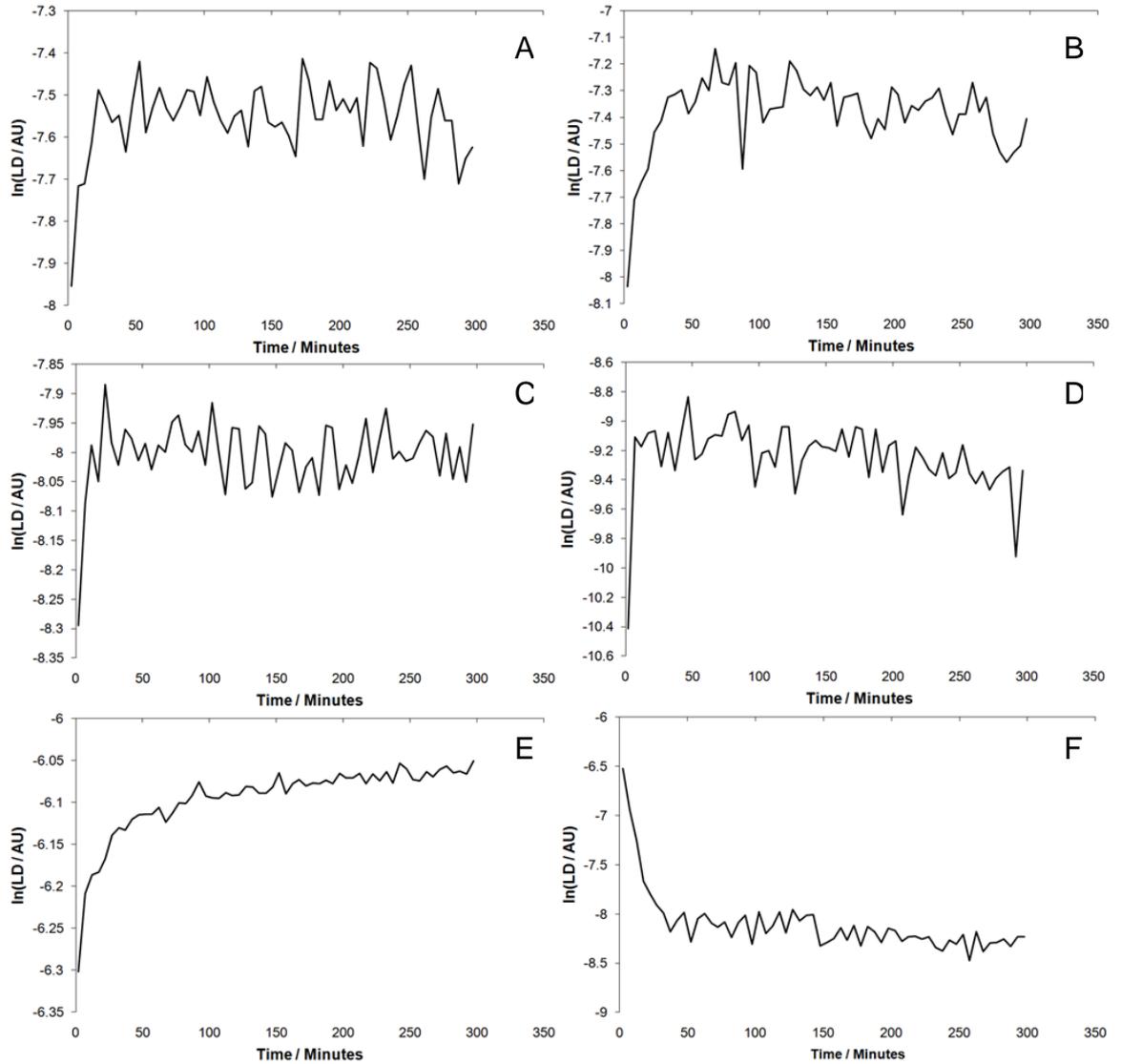
Figure 4.30. Semi-log plots of the evolution of the LD signal over 5 hours after the addition of HNP-2 to POPG/DOPC, DOPS/DOPC or DMPG/DMPC liposomes. HNP-2 (14 µM) was added to A) 50:50 (w/w) POPG/DOPC (1.4 mM) at 30 °C (200 nm); B) 50:50 (w/w) POPG/DOPC (1.4 mM) at 40 °C (198 nm); C) 50:50 (w/w) POPG/DOPC (1.4 mM) at 53 °C (228 nm); D) 50:50 (w/w) DOPS/DOPC (1.05 mM) at 30 °C (225 nm); E) 50:50 (w/w) DMPG/DMPC (1.4 mM) at 17 °C (215 nm) and F) 50:50 (w/w) DMPG/DMPC (1.4 mM) at 33 °C (194 nm). Sixty scans were recorded at 5 minute intervals.

An LD signal is only observed when the peptides in the sample are oriented, therefore the LD signal, LD_{obs}, will only include LD signals from peptides which are bound to the oriented liposomes, in state P_m (Equation 4.26).

$$LD_{obs} = \left([P]_m \frac{LD_m}{[P]_t} \right) \qquad (4.26)$$

The LD data were fitted to the same 2-state binding model as the fluorescence data (Figure 4.29), and the equations for the concentrations of free and bound peptide ($[P]_f$ and $[P]_m$ respectively) were the same as those used to analyse the fluorescence data

(Equations 4.23 and 4.24). The time t of each scan at a given wavelength (λ_t) could be calculated using Equation 4.27, where λ_s and λ_e are the starting and final wavelengths of each scan respectively; n corresponds to the number of completed scans and is multiplied by 5 due to the 5 minute interval between scans. The scan rate, in nm/minute, is represented by s.

$$t = \frac{(\lambda_s - \lambda_t)}{s} + 5n \tag{4.27}$$

The LD signal corresponding to the bound peptide, LD_{calc} was calculated at each time using Equation 4.28.

$$LD_{calc} = \left([P]_m \frac{LD_m}{[P]_t}\right) \tag{4.28}$$

Weighted non-linear least squares fitting was performed. Global fitting was carried out on each set of data using data from 2–5 wavelengths simultaneously. Each set of experimental data was truncated at scan 21 ($t \approx 100$ mins) or scan 31 ($t \approx 150$ mins) depending on the time when the binding process which was being fitted could be observed to have completely finished and the curve had levelled out.

It was not possible to obtain a good fit between the experimental and calculated LD data from this model. The calculated plots gave a very poor match to the experimental plots. Though it was possible to fit the two-state model to the fluorescence data, since it did not fit the LD data it was clear that it did not correctly describe the binding of HNP-2. More models were applied to the data to seek one which would describe the binding correctly. Three-state binding models were initially applied to the fluorescence and LD data for binding to 50:50 (w/w) POPG/DOPC liposomes at 30 °C to find a model which fitted both sets of data.

4.2.5.2 Three-state binding models

4.2.5.2.1 Three-state binding model: Treatment one

The three-state binding model explored involved three states, free peptide and two bound states (Figure 4.31).
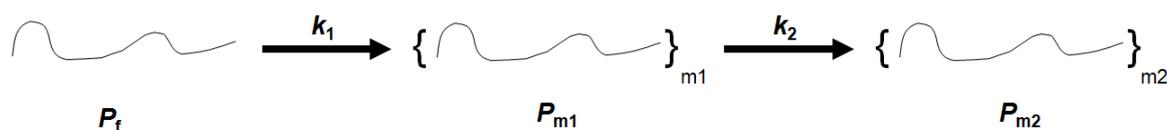
Figure 4.31. The three state kinetic model used for analysis of the LD and fluorescence data.

The LD signal at any time was calculated using Equation 4.29.

$$LD_{\text{calc}} = \left(LD_{\text{m1}} \frac{[P]_{\text{m1}}}{[P]_{\text{t}}}\right) + \left(LD_{\text{m2}} \frac{[P]_{\text{m2}}}{[P]_{\text{t}}}\right) \tag{4.29}$$

As described in Section 4.2.6.1.2, only bound peptide dimers would be oriented and contribute to the observed LD signal but it was necessary to take the concentration of free peptide (Equation 4.23) into account when determining the concentration of peptide in the two bound states ($[P]_{\text{m1}}$ and $[P]_{\text{m2}}$ in Equation's 4.31 and 4.32).

$$[P]_{\text{t}} = [P]_{\text{f}} + [P]_{\text{m1}} + [P]_{\text{m2}} \tag{4.30}$$

$$[P]_{\text{m1}} = \frac{[P]_{\text{t}} k_1 \left(e^{-k_1 t} - e^{-k_2 t}\right)}{k_2 - k_1} \tag{4.31}$$

$$[P]_{\text{m2}} = [P]_{\text{t}} \left(1 + \left(\frac{k_1 e^{-k_2 t} - k_2 e^{-k_1 t}}{k_2 - k_1}\right)\right) \tag{4.32}$$

Equation 4.33 was fitted to the fluorescence data, as the fluorescence emission from the free peptide contributes to the total fluorescence intensity. The concentration of free peptide and of peptide in the two bound states was determined using Equations 4.23, 4.31 and 4.32 respectively. The least squares values were weighted by multiplication by $\frac{1}{t^2}$ to give a better fit over the whole data range.

$$F_{\text{calc}} = \left(F_{\text{f}} \frac{[P]_{\text{f}}}{[P]_{\text{t}}}\right) + \left(F_{\text{m1}} \frac{[P]_{\text{m1}}}{[P]_{\text{t}}}\right) + \left(F_{\text{m2}} \frac{[P]_{\text{m2}}}{[P]_{\text{t}}}\right) \tag{4.33}$$

The calculated rate constants and half lives from this fit are shown in Table 4.9.

Table 4.9. Parameters calculated from non-linear least squares fitting of fluorescence and LD analyses of HNP-2 binding to 50:50 (w/w) POPG/DOPC liposomes using 3-state binding model described by Equations 4.29–4.32 or 4.30–4.32 and 4.33 for LD and fluorescence data respectively.

	k_1 (minute^{-1})	$t_{1/2}$ (minutes)	k_2 (minute^{-1})	$t_{1/2}$ (minutes)
Fluorescence	2.57 ± 0.26	0.27 ± 0.03	0.080 ± 0.008	8.6 ± 0.9
LD	3.74 ± 0.37	0.19 ± 0.02	0.128 ± 0.013	5.4 ± 0.5

4.2.5.2.2 Three-state binding model: Treatment two

The scan speed for the fluorescence analysis was four times that of the LD analyses (200 nm/minute and 50 nm/minute respectively), and fluorescence spectra were recorded every 2.5 minutes and LD data recorded every 5 minutes. The value for k_1 calculated from the fluorescence data using the second 3-state binding model is therefore likely to be more accurate due improved sampling of the initial stages of binding. The LD data were therefore refitted using the second 3-state binding model using Equations

4.29–4.32 but with k_1 fixed at the value calculated from analysis of the fluorescence data (Table 4.9). The rate constant for the second binding step, k_2, was calculated as 0.137 minutes^{-1}, corresponding to a half life of 5.1 minutes. There was a good match between the experimental and calculated data (Figure 4.32) and the calculated LD_{m1} and LD_{m2} values, shown as plots in Figure 4.33, were within a sensible range.
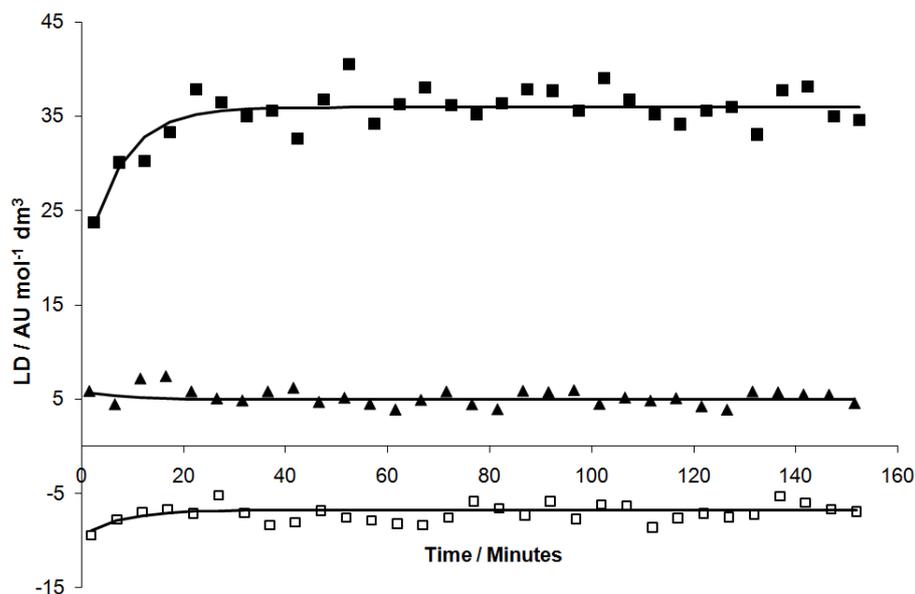
Figure 4.32. Experimental and calculated LD signal for HNP-2 in 50:50 POPG/DOPC liposomes at 200 nm (■), 225 nm (□) and 245 nm (▲). Experimental data are presented as points and the profiles calculated from fitting Equation 4.29 to the experimental data by non-linear regression as lines.
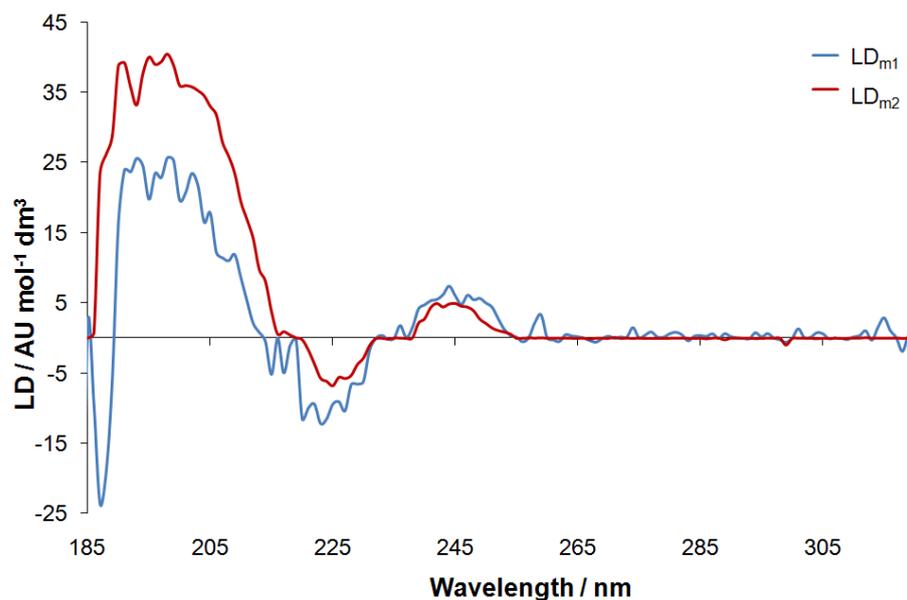
Figure 4.33. LD spectra of the P_{m1} and P_{m2} states of HNP-2 (15 μM) binding to 50:50 (w/w) POPG/DOPC (1.4 mM) at 30 °C described by Equation 4.29.

4.2.5.3 Analysis of all LD data using the 3-state model

The three-state model described by Equations 4.29–4.32 was fitted to the data from each of the other LD analyses using weighted least squares fitting to find LD_{m1}, LD_{m2}, k_1 and k_2. Global fitting was carried out on each set of data using data from 2–5 wavelengths simultaneously. Each set of experimental data was truncated at scan 21 ($t \approx$ 100 mins) or scan 31 ($t \approx$ 150 mins) depending on the time when the binding process which was being fitted could be observed to have completely finished and the curve had levelled out. The calculated rate constants are shown in Table 4.10, and examples of the correlation between the experimental and calculated data for each experiment are shown in Figure 4.34. The concentration of the free peptide, $[P]_f$, 100 minutes after mixing the peptide and liposomes was negligible in each case.

Table 4.10. Parameters calculated from non-linear least squares fitting of LD analyses of HNP-2 binding to 50:50 (w/w) POPG/DOPC, DOPS/DOPC and DMPG/DMPC liposomes using 3-state binding model described by Equations 4.29–4.32.

	T (°C)	k_1 (minute^{-1})	$t_{1/2}$ (minutes)	k_2 (minute^{-1})	$t_{1/2}$ (minutes)
POPG/DOPC	30	2.57 ± 0.26	0.27 ± 0.03	0.137 ± 0.014	5.06 ± 0.51
POPG/DOPC	40	2.60 ± 0.26	0.27 ± 0.03	0.222 ± 0.022	3.11 ± 0.31
POPG/DOPC	53	3.43 ± 0.34	0.20 ± 0.02	0.194 ± 0.019	3.57 ± 0.36
DOPS/DOPC	30	0.727 ± 0.07	0.95 ± 0.10	0.231 ± 0.023	3.00 ± 0.30
DMPG/DMPC	17	1.40 ± 0.14	0.50 ± 0.05	0.047 ± 0.005	14.9 ± 1.49
DMPG/DMPC	33	1.03 ± 0.10	0.67 ± 0.07	0.117 ± 0.012	5.93 ± 0.59
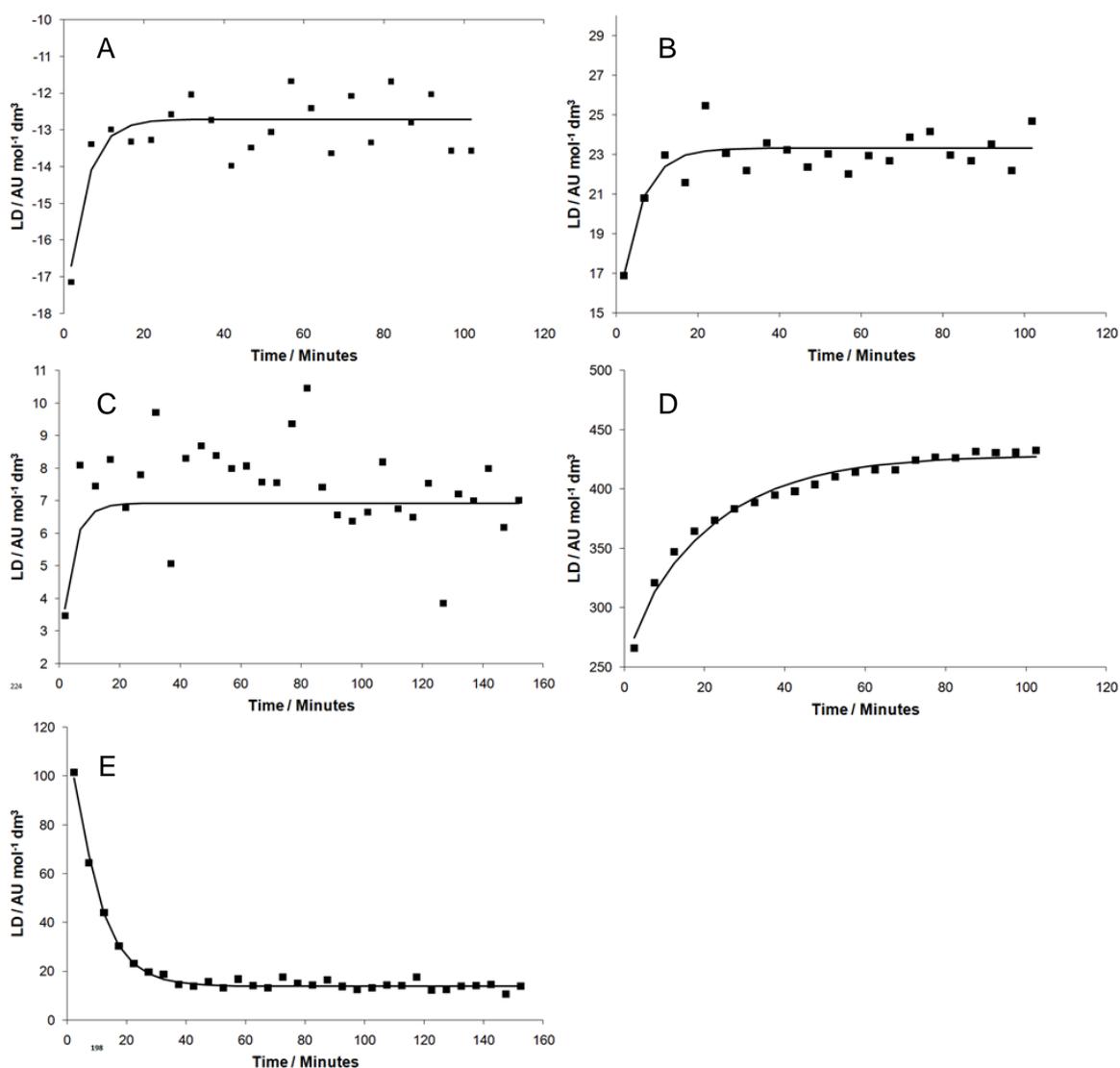
Figure 4.34. Experimental and calculated LD signal for HNP-2 binding to A) 50:50 (w/w) POPG/DOPC liposomes at 40 °C at 230 nm; B) 50:50 (w/w) POPG/DOPC liposomes at 53 °C at 228 nm; C) 50:50 (w/w) DOPS/DOPC liposomes at 30 °C at 224 nm; D) 50:50 (w/w) DMPG/DMPC liposomes at 17 °C at 196 nm and E) 50:50 (w/w) DMPG/DMPC liposomes at 33 °C at 198 nm. Experimental data are presented as points and the profiles calculated from non-linear regression as lines.

The quality of the fits of the 3-state model to the LD and fluorescence data were determined by plotting the residual (ε) (Equation 4.34) against time at each of the wavelengths used for the fits. The plots of the residuals showed some noise, but were all linear or close to linear across the time period analysed, showing a good fit across the range of the data (Appendix 2).

$$\varepsilon = LD_{calc} - LD_{obs} \qquad \textbf{(4.34)}$$

4.2.5.4   Binding model revealed by kinetics

All of the sets of LD data fitted to a 3-state model with a fast first binding stage followed by a slower reorientation (Table 4.10). Due to the fast rate of the first binding stage compared to the interval between LD scans it is likely that the error in the value for k_1 is greater than 10%.

4.2.5.4.1   Binding to 50:50 POPG/DOPC liposomes

k_1 was essentially the same for the three analyses of HNP-2 binding to the POPG/DOPC liposomes at different temperatures. The second stage of the binding to the POPG/DOPC liposomes was slowest at 30 °C. At 40 °C and 53 °C the rates of the second stage of the binding were almost the same within an error of 10%.

4.2.5.4.2   Binding to 50:50 DOPS/DOPC liposomes

The first stage of the binding of the DOPS/DOPC liposomes was slower than binding to the POPG/DOPC liposomes, but the second stage of the binding had essentially the same rate as the binding to the POPG/DOPC liposomes at 40 °C.

4.2.5.4.3   Binding to 50:50 DMPG/DMPC liposomes

The rate of the first stage of binding to the DMPG/DMPC liposomes was essentially the same at 17 °C and 33 °C. The clearest difference was observed when comparing the rates of the second stage of the binding however. At 33 °C, above the phase transition temperature of DMPG and DMPC, k_2 was only slightly lower than for binding to the POPG/DOPC liposomes. When binding occurred at 17 °C, below the phase transition of the lipids, the second stage of binding was much slower. This is to be expected given the increased order of the lipids in the membrane below the phase transition temperature; insect defensin and colicin A have been shown to not insert at all into lipid membranes below the phase transition temperature.[66, 67]

Figure 4.35A–F shows the calculated LD spectra corresponding to HNP-2 in the first and second membrane bound states, P_{m1} and P_{m2} respectively. All of the spectra except those for the binding of HNP-2 to DOPS/DOPC at 30 C show some changes in the spectral shape between the two membrane bound states consistent with a change in the orientation of the peptides. The faster kinetics of the first stage of binding and slower second stage suggests that the peptide dimers initially bind rapidly and weakly to the lipid bilayer, then more slowly reorient and insert into the membrane. This mechanism is supported by the very similar k_1 values for binding to DMPG/DMPC above and below the phase transition temperature of the lipids, where the state of the lipids did not affect the rate, followed by a much smaller k_2 value for the second stage of binding to the liposomes

below the phase transition temperature than above it, consistent with a difficulty in insertion when the lipids were ordered. The pseudo 1st order kinetics observed for these stages suggest that multimeric pores are not formed during the two binding stages identified here, as the formation of multimeric pores is likely to involve higher order rate constants.   The binding model which has been fitted to the data implies irreversible binding of HNP-2 to the membrane. Similar irreversible kinetic models have been applied successfully to other peptides, and in others where a reversible model has been used the backwards rate constants have been found to be negligible for all stages of binding.[68, 69]
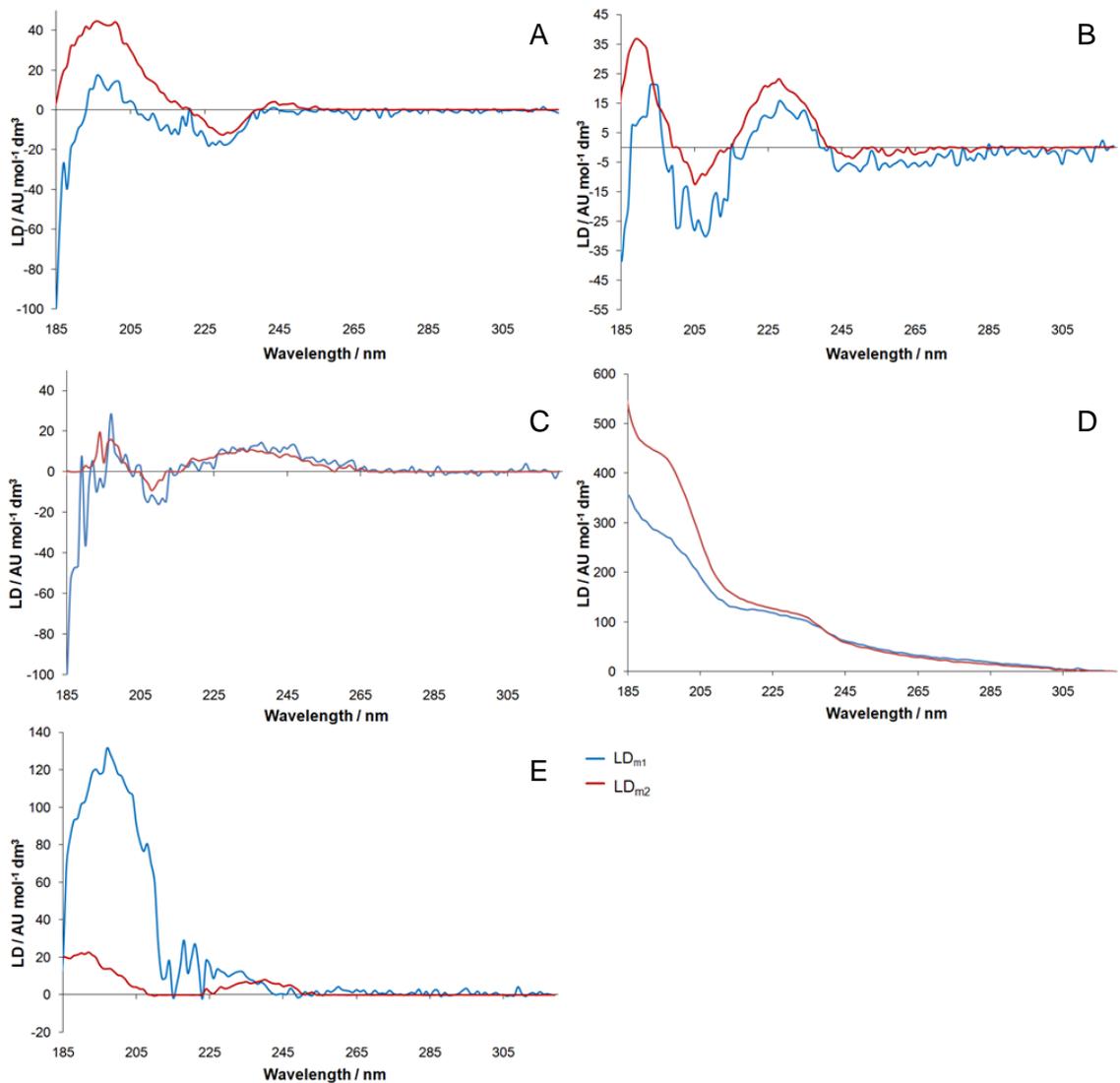
Figure 4.35. LD spectra of the P_{m1} and P_{m2} states of HNP-2 as described by Equation 4.29. Spectra calculated for HNP-2 (15 μM) binding to A) 50:50 (w/w) POPG/DOPC (1.4 mM) at 40 °C; B) 50:50 (w/w) POPG/DOPC (1.4 mM) at 53 °C; C) 50:50 (w/w) DOPS/DOPC (1.05 mM) at 30 °C; D) 50:50 (w/w) DMPG/DMPC (1.4 mM) at 17.4 °C; E) 50:50 (w/w) DMPG/DMPC (1.4 mM) at 33 °C.

4.2.6 Entropy and enthalpy of HNP-2 binding to POPG/DOPC liposomes

The rate constants determined for binding to POPG/DOPC liposomes at 30, 40 and 53 °C allowed a semi-quantitative assessment of the entropic and enthalpic contributions to the binding to be made. The Eyring equation and its linear form are shown as Equations 4.35 and 4.36. An Eyring plot of $\ln(k/T)$ against $1/T$ produces a straight line of the form $y = mx + c$, where the gradient gives $\Delta H^{\ddagger}/R$ and the y-intercept gives $\ln(k_B/h) + \Delta S^{\ddagger}/R$ (Figure 4.36).

$$k = \frac{k_B T}{h} e^{-\frac{\Delta H^{\ddagger}}{RT}} e^{\frac{\Delta S^{\ddagger}}{R}} \tag{4.35}$$

$$\frac{\ln k}{T} = -\frac{\Delta H^{\ddagger}}{R} \cdot \frac{1}{T} + \ln\frac{k_B}{h} + \frac{\Delta S^{\ddagger}}{R} \tag{4.36}$$

The free energy of activation, $\Delta G^{\ddagger}$, was calculated using Equation 4.37. The enthalpy and entropy of activation are represented by $\Delta H^{\ddagger}$ and $\Delta S^{\ddagger}$ respectively, R is the universal gas constant and k_b the Boltzmann constant. The activation parameters for the binding of HNP-2 to POPG/DOPC (50:50 (w/w) liposomes are shown in Table 4.11.

$$\Delta G^{\ddagger} = \Delta H^{\ddagger} - T\Delta S^{\ddagger} \tag{4.37}$$
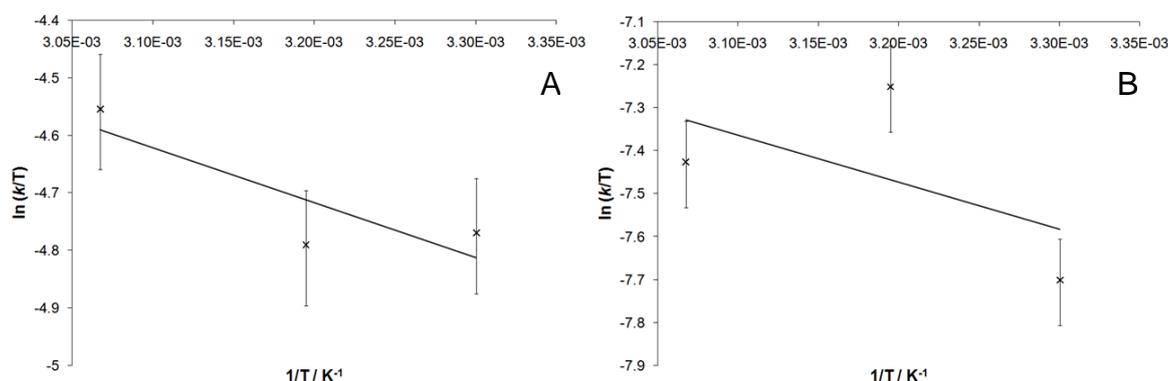
Figure 4.36. Temperature dependence of A) the first rate constant and B) the second rate constant for the binding of HNP-2 to 50:50 (w/w) POPG/DOPC liposomes shown as an Eyring plot. The error bars were propagated from an error of $\pm$ 10% in the value of *k*.

Table 4.11. Activation parameters for HNP-2 binding to POPG/DOPC (50:50 (w/w)) liposomes.

	$\Delta H^{\ddagger}$ (kJmol^{-1})	$\Delta S^{\ddagger}$ (kJK^{-1}mol^{-1})	$\Delta G^{\ddagger}$ (kJmol^{-1})[a]
k_1	8.0 ± 5.0	-0.20 ± 0.01	68.3 ± 5.9

a) $\Delta G^{\ddagger}$ was calculated at 303 K

b) Errors were propagated from the uncertainties in the gradient and y-intercept determined from linear regression analysis

The activation parameters were determined from the gradient and y-intercept of a line of best fit through only three data points. The line of best fit in the Eyring plot of the first rate constants is within the error bars, calculated from propagating an error of 10% in the value of k_1, and therefore though the errors in the values calculated for the enthalpy and entropy are high, the results can be used to determine whether the entropy and enthalpy changes are favourable or not. The line of best fit through the Eyring plot of the second rate constants is outside the error bars for two of the points and just inside error for the third. Activation parameters calculated using the gradient and intercept of this line are unlikely to be meaningful. The positive $\Delta H^{\ddagger}$ value for the first binding step suggests an electrostatic energy barrier, due to factors such as the desolvation of the peptide before binding and breaking van der Waals forces between the lipids during insertion into the membrane. Positive $\Delta H^{\ddagger}$ values are to be expected for elementary reaction steps due to the energy required to partially break bonds to give the activated intermediate complex.[70] The negative, unfavourable, entropy is due to a decrease in rotational, translational and possibly vibrational degrees of freedom of the peptide and lipids when the peptide binds. For some protein folding reactions the Eyring plots can be curved rather than linear, as the rate constant increases with increasing temperature until a maximum, where it then decreases. The initial increase in rate with increasing temperature gives a positive enthalpy value, as expected for the majority of chemical reactions. The decrease in rate with increasing temperature after this point can be due to different factors such as temperature-induced changes of the peptide in the ground state and changes in the heat capacity in the activated complex, or a temperature-induced change in the rate limiting step.

4.2.7   Orientation

4.2.7.1   Qualitative analysis of orientation

As described in Section 1.3.4.2, linear dichroism probes the orientation of transition moments relative to an axis system by measuring the difference in absorbance of parallel and perpendicular linearly polarised light by an oriented sample. As shown in Figure 4.37, in this analysis we define the long axis of the liposome as the x-axis, which is parallel to the surface of the membrane. The z-axis is perpendicular to the membrane and to the incident light. If a transition moment is aligned with the x-axis a peak will be observed in the LD spectrum. If a transition is aligned with the z-axis a negative band will be observed.
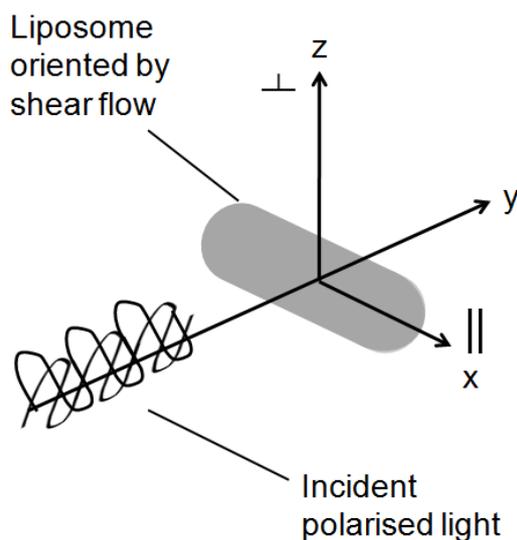
Figure 4.37. Orientation of the LD experiment.[¥]

The LD spectrum of HNP-2 is expected to show contributions from the transitions of β-sheets, tryptophan, tyrosine and phenylalanine, and possibly from the disulphide bonds. As shown in Figure 4.38, a signal from the π–π* transition of the backbone amide bonds is expected at around 195 nm (see Figure 1.10 for amide bond transitions). The opposing polarisations of the amide n–π* transition at 219 nm and 221 nm usually cancel each other out in LD spectra of β-sheet peptides.[73] Tryptophan has three transitions in the region between 200 and 320 nm: B_b at 220 nm, L_a at 270 nm and L_b at 280 nm. Tyrosine has two transitions in this region: L_a at 230 nm and L_b at 275 nm. Of the two transitions of phenylalanine in this region, the L_b transition at 260 nm is not expected to be observed due to its very low extinction coefficient compared to the other transitions. The phenylalanine L_a transition at 210 nm is expected to contribute to the LD spectrum.[74] Any band from the disulphide bonds is also likely to be weak.[75] The wavelength at which signals corresponding to the side chains are observed is strongly dependant on their environment, for example the L_b transition of tyrosine has been observed to be shifted to lower wavelengths in the LD spectra of peptides with high aromatic content.[76] The crystal structure of HNP-2 (Figure 4.17) shows that the two tryptophan residues are both close

---

[¥] The axis system in Figure 4.37 differs from the standard axis system commonly referred to when discussing LD experiments, where the z-axis is the long axis of the liposome and the x-axis normal to membrane surface.[71] This is due to the fact that Dichrocalc uses the standard LD equation (Equation F2) where β is the angle between the transition polarization direction and the flow direction For analyses of binding to liposomes the equation required is Equation F3, where α is the angle between the membrane normal and the polarization direction.[72] The molecule's orienting force is the membrane, which is perpendicular to the flow direction. In order to interpret the Dichrocalc results correctly it was necessary to describe the results in term of the axis system in Figure 4.41 and invert the spectra produced by the Dichrocalc calculations.

$$LD^r = \frac{3}{2}S(3\cos^2\beta - 1) \hspace{6cm} \text{F2}$$

$$LD^r = \frac{3}{4}S(1 - 3\cos^2\alpha) \hspace{6cm} \text{F3}$$

enough to tyrosine residues for excimer coupling to occur. This would cause a tryptophan or tyrosine transition to be split to give an in phase and an out of phase contribution, which would be observed as a peak and negative band centred on the wavelength of the transition.[77]
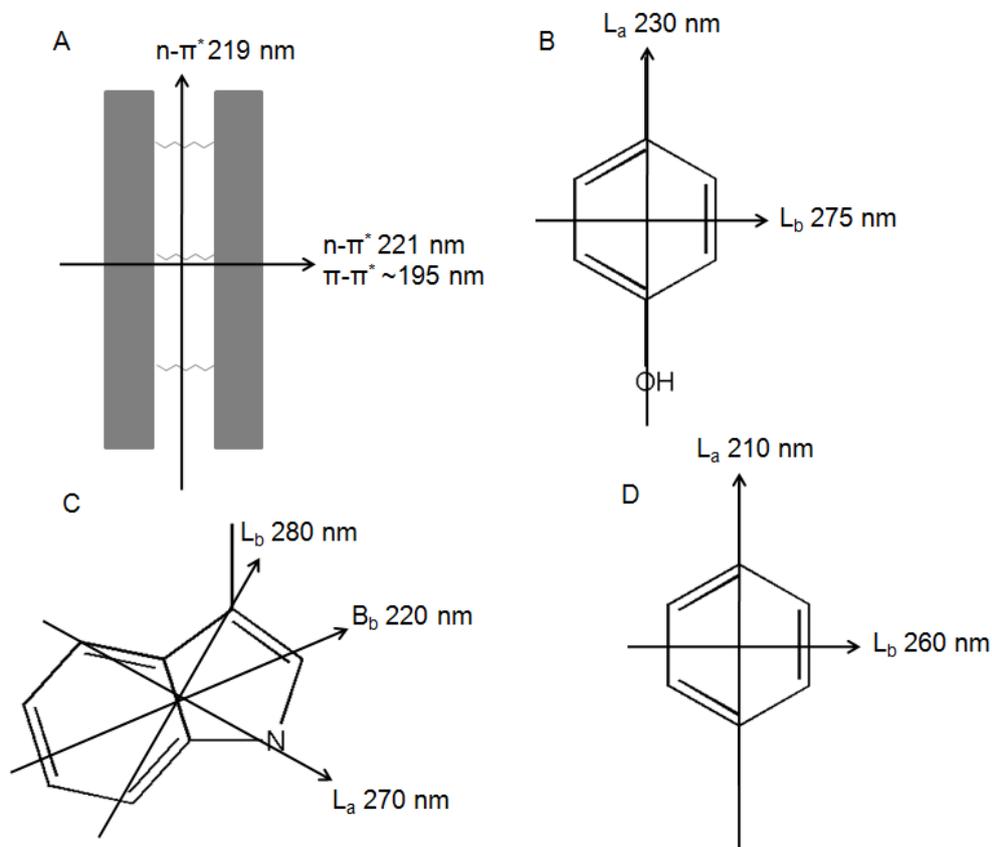
Figure 4.38. The transition moments of A) amide bonds in β-sheets; B) tyrosine C) tryptophan and D) phenylalanine.
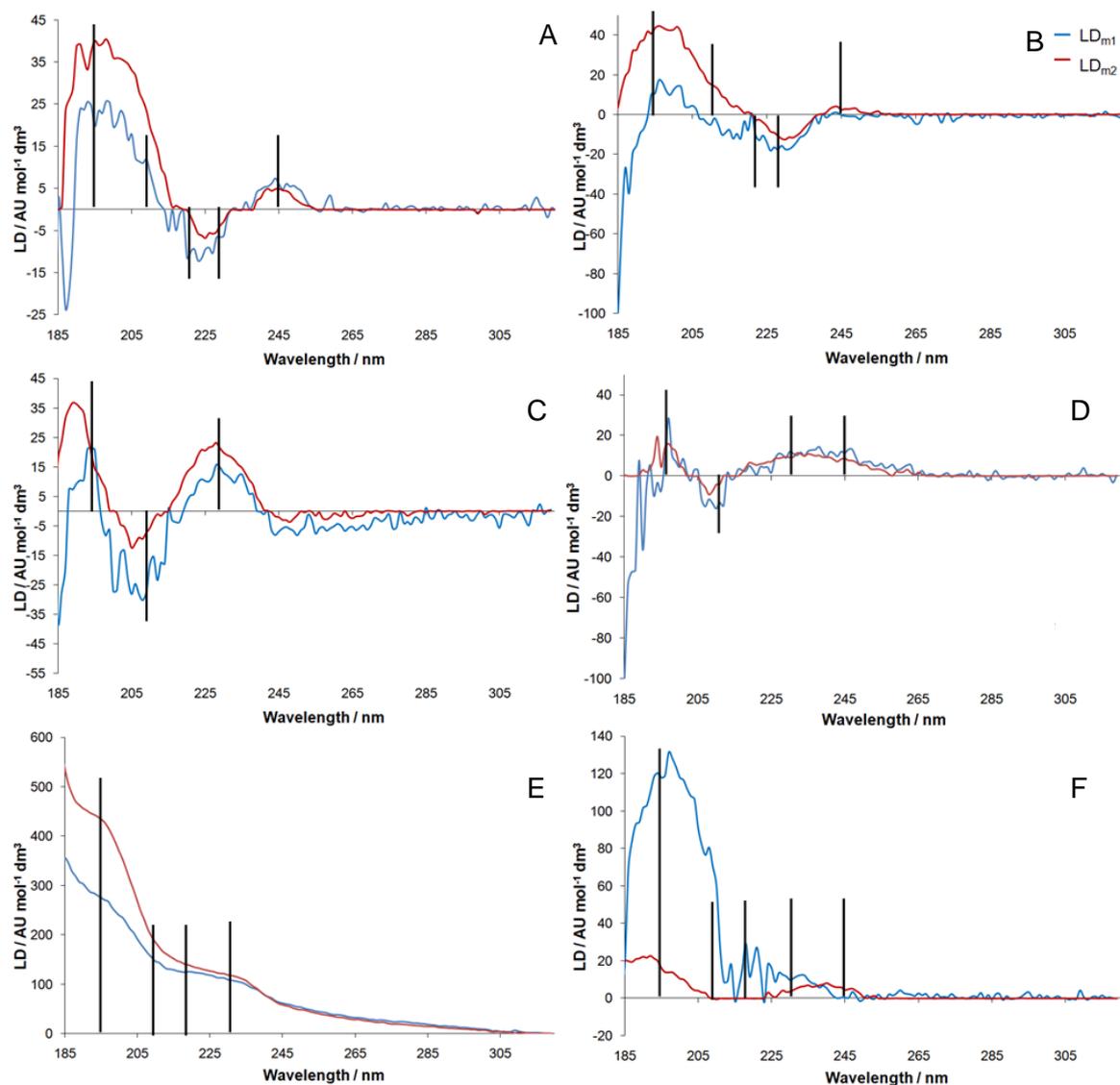
Figure 4.39. LD spectra of the P_{m1} and P_{m2} states of HNP-2 (15 µM) binding to A) 50:50 (w/w) POPG/DOPC (1.4 mM) at 30 °C; B) 50:50 (w/w) POPG/DOPC (1.4 mM) at 40 °C; C) 50:50 (w/w) POPG/DOPC (1.4 mM) at 53 °C; D) 50:50 (w/w) DOPS/DOPC (1.05 mM) at 30 °C; E) 50:50 (w/w) DMPG/DMPC (1.4 mM) at 17.4 °C; F) 50:50 (w/w) DMPG/DMPC (1.4 mM) at 33 °C. The black lines show the positions of transitions discussed in Section 4.2.8.

4.2.7.1.1   *Backbone amide transitions*

All of the LD spectra of the two bound states of HNP-2 (Figure 4.39) show peaks at 195 nm, regardless of membrane composition or temperature. The $\pi-\pi^*$ transitions of the backbone amide bonds are therefore parallel to the surface of the membrane.

4.2.7.1.2   *Exciton coupling*

The spectra of the first and second bound states of HNP-2 with POPG/DOPC liposomes at 53 °C and DOPS/DOPC liposomes at 30 °C (Figure 4.39C and D) both show splitting of the B_b transition of tryptophan due to exciton coupling. The B_b band, expected at 220 nm, has been split to give a peak at 230 nm and a negative band at 205 nm.

4.2.7.1.3 Transitions of tyrosine

The peaks attributed to exciton coupling in the spectra of the first and second bound states of HNP-2 with POPG/DOPC liposomes at 53 °C and DOPS/DOPC liposomes at 30 °C (Figure 4.39C and D) at 230 nm may also incorporate a peak corresponding to the L_a transition of tyrosine oriented parallel to the membrane. A peak or shoulder at 230 nm corresponding to the L_a band of tyrosine is also observed in the spectra of HNP-2 binding to DMPG/DMPC liposomes at 17 °C and at 33 °C (Figure 4.39E and F). Negative bands can be observed at the same wavelengths in the spectra of HNP-2 with POPG/DOPC liposomes at 30 °C and 40 °C (Figure 4.39A and B). The spectra of both membrane bound states of HNP-2 binding to POPG/DOPC and DOPS/DOPC liposomes at 30 °C (Figure 4.39A and D) show peaks at 245 nm. These are attributed to the tyrosine L_b transition, which has been observed to be shifted to lower wavelengths in the spectra of peptides with a high aromatic content, oriented parallel to the membrane.[83] The first membrane bound state of HNP-2 binding to POPG/DOPC liposomes at 40 °C (Figure 4.39B) shows no signal at 245 nm, suggesting that the tyrosine L_b transition is oriented close to 54.7°. The spectrum of the second membrane bound state shows a weak peak at 245 nm, suggesting that the transition reoriented towards being parallel with the surface of the membrane. In the case of binding to DMPG/DMPC liposomes at 33 °C (Figure 4.39F) a weak peak is observed in the spectrum of the second membrane bound state and no signal in the first membrane bound state. Neither of the spectra of HNP-2 binding to POPG/DOPC liposomes at 53 °C (Figure 4.39C) show a signal at 245 nm, and no clear peak or shoulder can be observed at 245 nm in the spectra of binding to DMPG/DMPC liposomes at 17 °C (Figure 4.39E), though a signal may be masked by scattering.

4.2.7.1.4 Transitions of tryptophan

In the spectrum of the first membrane bound state of HNP-2 binding to DMPG/DMPC liposomes at 33 °C a peak can be observed at 220 nm corresponding to the B_b transition of tryptophan oriented parallel to the surface of the membrane. In the spectrum of the second membrane bound state of HNP-2 with DMPG/DMPC liposomes at 33 °C (Figure 4.39F), and in both membrane bound states when binding to POPG/DOPC liposomes at 30 °C and 40 °C (Figure 4.39A and B), the signal at 220 nm is zero, suggesting that the B_b transition is oriented close to 54.7° relative to the membrane normal. When the transition is oriented at 54.7° relative to the membrane normal the LD signal is zero. This can be explained by referring to the LD equation (Equation 4.38), where α is the angle between the transition moment and the membrane normal, μ is the transition moment and S is the scaling factor.

$$LD = \frac{S\mu^2(1-3\cos^2\alpha)}{4} = \frac{S\mu^2(1-(3\times0.334))}{4} = 0 \qquad \textbf{(4.38)}$$

No clear shoulder or negative band corresponding to the B_b band can be observed in the spectra of either bound state of HNP-2 with DMPG/DMPC liposomes at 17 °C (Figure 4.39E). It is likely that there is no signal in these spectra at this wavelength, with the transition oriented close to 54.7° relative to the membrane normal, and that this is masked by the large amount of scattering. The scattering in the spectrum is attributed to the lipids being in the gel phase. The intensity of light scattered from liposomes drops sharply when they are heated above the phase transition temperature.[78]

4.2.7.1.5 Transitions of phenylalanine

The negative band of the split tryptophan B_b band at 205 nm in the spectra of HNP-2 with POPG/DOPC liposomes at 53 °C and DOPS/DOPC liposomes at 30 °C (Figure 4.39C and E) may incorporate a negative band at around 210 nm from the L_a band of phenylalanine oriented perpendicular to the membrane. In the spectra of HNP-2 with POPG/DOPC liposomes at 30 °C (Figure 4.39A) and in the spectrum of the first membrane bound state of HNP-2 binding to DMPG/DMPC liposomes at 33 °C (Figure 4.39F) the LD signal is positive at 210 nm which may be due to the L_a band of phenylalanine being oriented parallel to the membrane, or the phenylalanine transition may be masked by the π–π* transition of the backbone amide bonds. No signal can be observed at the same wavelength in the spectrum of the second membrane bound state of HNP-2 binding to DMPG/DMPC liposomes at 33 °C, suggesting that the L_a transition is oriented close to 54.7°. A negative band can be observed at 210 nm in the spectrum of the first membrane bound state of HNP-2 binding to POPG/DOPC liposomes at 40 °C (Figure 4.39B), and a positive band in the spectrum of the second membrane bound state, suggesting that the transition reorients from parallel to the membrane to perpendicular to it when changing between the two states. No clear shoulder or negative band corresponding to the L_a band can be observed in the spectra of either bound state of HNP-2 with DMPG/DMPC liposomes at 17 °C (Figure 4.39E).

4.2.7.1.6 Other transitions

No signal can be observed from the L_a or L_b transitions of tryptophan in any of the spectra. This could be due to the transitions being oriented close to 54.7°. No clear band can be observed at 260 nm corresponding the disulphide bonds or to the L_b band of phenylalanine, but this was expected due to the weak nature of these absorptions.

4.2.7.1.7 Comparison between spectra of first and second membrane bound states

The spectra of HNP-2 binding to POPG/DOPC membranes at all temperatures and DMPG/DMPC membranes at 17 °C (Figure 4.39A–C and E) increase in intensity

between the first and second membrane bound states. The signal strength of a transition gets weaker as the transition moment is oriented further away from being oriented parallel or perpendicular to the membrane, with no signal being observed when it is oriented at 54.7° to the membrane normal. This suggests that the backbone in the second membrane bound state is oriented so that the π–π* transition of the backbone amide bonds are oriented closer to parallel to the membrane surface in the second membrane bound state than in the first. There is no real change in intensity between the spectra of the first and second membrane bound states of HNP-2 when binding to DOPS/DOPC liposomes at 30 °C (Figure 4.39D), suggesting that there is little change in orientation between the two membrane bound states. The spectrum of the second membrane bound state of HNP-2 binding to DMPG/DMPC liposomes at 33 °C (Figure 4.39F) is much weaker than the first membrane bound state, suggesting that the backbone is oriented closer to 54.7° in the second membrane bound state than in the first.

4.2.7.2 Discussion of qualitative analysis of LD spectra

All of the spectra discussed in Section 4.2.8.1 suggest that the π–π* transitions of the backbone amide bonds are parallel to the surface of the membrane. When the HNP-2 dimer is examined it is clear that the β-sheet portions are twisted and therefore the orientations of the dimer in which the β-sheets are oriented with the π–π* transitions mostly parallel to the membrane cannot be determined by eye. In order to determine the true orientation of the peptide it was necessary to analyse the spectra quantitatively through fitting spectra of HNP-2 in known orientations to them.

A qualitative analysis of the spectra provides more information on the orientation of the phenylalanine, tryptophan and tyrosine side chains. In Section 4.2.2.2 it was noted that the fluorescence spectrum of HNP-2 reveals that the tryptophan residues within the dimer occupy two distinct environments due to their proximity to and interaction with tyrosine residues. Furthermore, the distance between the tryptophan and tyrosine residues was close enough for coupling to occur. The LD spectra of HNP-2 binding to POPG/DOPC at 53 °C and to DOPS/DOPC at 30 °C (Figure 4.39C and D) show evidence of excimer coupling between at least one of the tryptophan residues and a neighbouring tyrosine residue, causing a peak and a negative band to be observed centred on the wavelength of the tryptophan B_b transition. In most of the other spectra no signal can be observed from this transition, although a peak was observed at 220 nm in the spectrum of the first membrane bound state of HNP-2 binding to DMPG/DMPC at 33 °C (Figure 4.39F) suggesting that the tryptophan residues are oriented with the B_b transition parallel to the membrane surface. The orientations of the other side chain transitions appeared to

vary for binding to the different liposomes at different temperatures. The variation observed in the orientation of the side chains shows the rotational freedom of these residues and suggests that the orientation of the aromatic side chains may be independent of the backbone orientation.

4.2.7.3 Quantitative analysis of orientation

The orientation of the β-sheet backbone in the two membrane bound states was determined using a set of model spectra. These were obtained using Dichrocalc, a program which calculates the linear dichroism spectra of peptides and proteins from oriented PDB files.[79–82] The software has an "orientation search" function, which takes the inputted oriented peptide through a series of rotations about two axes, calculating a spectrum at each new orientation. One of these axes is defined as the tilt axis and one as the rotation axis (Figure 4.40). The interval and total rotation about each axis can be specified. The peptide is initially taken through the specified rotation about the rotation axis. The peptide and the rotation axis are then both tilted about the tilt axis by a specified angle, before the rotation is repeated around the tilted rotation axis.
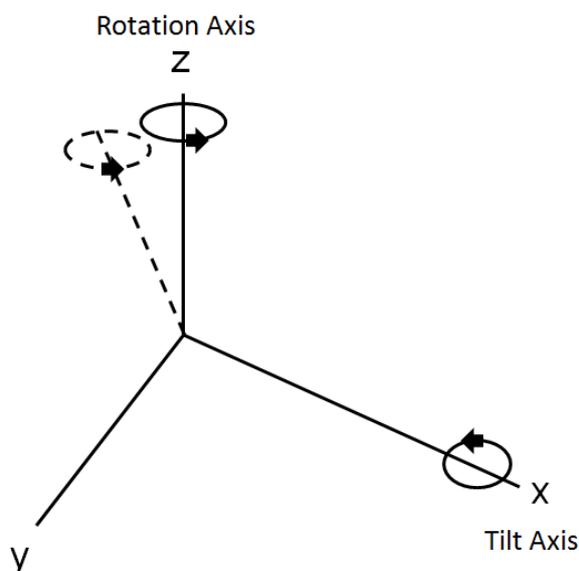
Figure 4.40. Explanation of the "orientation search" feature of the Dichrocalc program.

The aim of the quantitative analysis was to determine the orientation of the peptide in relation to rotation around the x and y-axes. A reference peptide orientation was established, as shown in Figure 4.41.
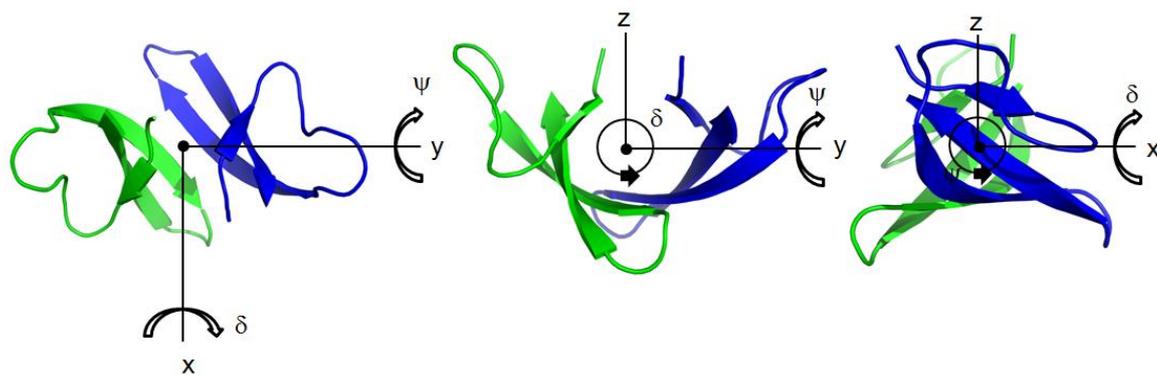
Figure 4.41. The orientation of the peptide dimer in the reference state.

LD spectra were calculated for the peptide dimer oriented as in Figure 4.41 and from starting structures rotated by increments of 9° around either the x or y-axis (δ or ψ = 0, 9, 18, 27, 36, 45, 54, 63, 72, 81 and 90) relative to the reference state. In order to take account of the fact that the peptide could bind in any orientation relative to rotation about the z-axis, and could be at any position around the cylindrical surface of the shear-deformed liposome a series of spectra obtained at 30° rotations about the z-axis and 30° tilt angles about the x-axis were averaged for each starting structure (Figure 4.40). The reference orientation was chosen due to the C_2 symmetry around the z-axis, and spectra were calculated for rotations of up to 90° around the x- and y-axes due to symmetry; a calculated spectrum of the peptide rotated by 170° around the x-axis would be the same as that of the peptide rotated by 10°, for example.

The peptide dimer incorporates a number of different transitions, as discussed in Section 4.2.8.1, with transition dipoles polarized in different directions. As shown in Figure 4.42, rotation about the y-axis keeps the transition moments, μ_y, polarized along the y-axis constant (where μ_y is the sum of the vectors aligned along the y-axis), but varies the rest of the transition moments as a function of ψ (and α). Similarly, rotation about the x-axis keeps the transition moments polarized along the x-axis, μ_x, constant, but varies the other transition moments as a function of δ (and α).
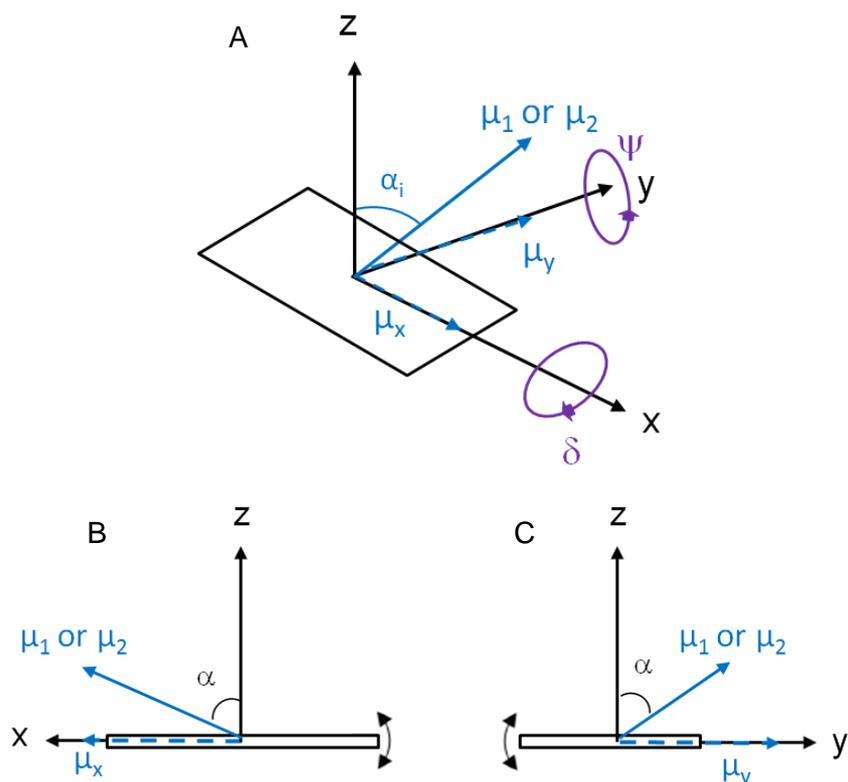
Figure 4.42. Specific geometrical parameters for the determination of the orientation of a peptide in relation to rotation about the x and y-axes. μ_x and μ_y are the sum of the vectors aligned along the x and y-axes respectively and μ_1 and μ_2 are the transition moment vectors, with the subscripts 1 and 2 relating to analysis of the orientation in relation to rotation about the x and y-axes respectively.

The angle of μ about the z-axis is α. In the reference state we can define $\alpha = \alpha_{i0}$, therefore Equations 4.39 and 4.40 apply (Figure 4.42B and C). In the reference state δ and $\psi = 0°$.

$$\alpha = \alpha_{i0} + \varphi \tag{4.39}$$

$$\alpha = \alpha_{i0} + \delta \tag{4.40}$$

As described in Section 1.3.4.2, LD is the difference in absorbance of light oriented parallel and perpendicular to an oriented sample. This can also be written in terms of the x and y components of the transition dipole, μ_x and μ_y, as described in Equation 4.41, where S is a scaling factor.

$$LD = A_{\parallel} - A_{\perp} = S\left(\mu_x^2 - \mu_y^2\right) \tag{4.41}$$

Two axis systems can be used to describe the LD experiment.[71] The {x, y, z} axis system defines the coordinates in relation to the long axis of the liposome, where the z/y plane is perpendicular to this (the axis system in Figure 4.37). The {X, Y, Z} system defines the

coordinates in relation to the bilayer and the analyte, where the analyte can be at any position around the surface of the liposome and Z is the normal to the cylinder surface that passes through the origin of the analyte. The long axis of the liposome is the same in both axis systems, x = X. Equation 4.41 can be rewritten as Equation 4.43, which describes the LD signal in terms of rotation about the x-axis. For rotation about the x-axis, μ_x is constant. μ_y is calculated as the dot product of the transition moment vector, μ_1, with the y-axis vector in the {X, Y, Z} system (Equation 4.41), and changes with rotation about the x-axis.

$$\mu_y = \mu_1 \cdot y = \mu_1(\cos\alpha, \sin\beta_v \sin\alpha, \cos\beta_v \sin\alpha) \cdot (\sin\gamma, \cos\gamma, 0)$$

$$= \mu_1(\cos\alpha \sin\gamma + \sin\beta_v \sin\alpha \cos\gamma) \tag{4.42}$$

The angle between the projection of μ onto the X/Y plane and the Z-axis is represented by β_v (Figure 4.43) and γ can take any value between 0 and 2π. The scaling factor has been omitted for clarity.
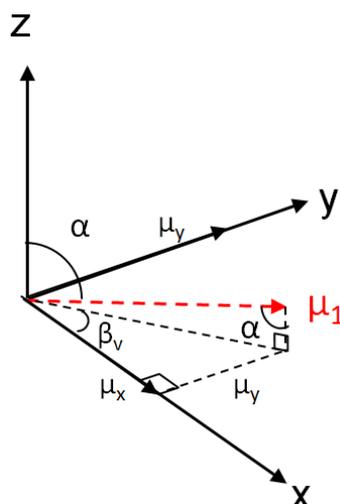
Figure 4.43. Geometrical parameters relating the transition dipole μ_1 to the {x, y, z} axis system.

$$LD_1 = (\mu_x^2 - \mu_y^2) = \mu_x^2 - \mu_1(\cos\alpha \sin\gamma + \sin\beta_v \sin\alpha \cos\gamma)^2 \tag{4.43}$$

$$LD_1 = \mu_x^2 - \mu_1^2(\cos^2\alpha \sin^2\gamma + \sin^2\beta_v \sin^2\alpha \cos^2\gamma + 2\cos\alpha \sin\gamma \sin\beta_v \sin\alpha \cos\gamma) \tag{4.44}$$

Equation 4.44 can be developed to give Equation 4.44 be averaging γ and β over 0 to 2π radians.

$$LD_1 = \mu_x^2 - \mu_1^2(0.5\cos^2\alpha + 0.25\sin^2\alpha) \tag{4.45}$$

Equation 4.45 is developed through Equations 4.46 and 4.47 to give Equation 4.48.

$$LD_1 = \mu_x^2 - 0.25\mu_1^2(2\cos^2\alpha + \sin^2\alpha) \tag{4.46}$$

$$LD_1 = \mu_x^2 - 0.25\mu_1^2(2\cos^2\alpha + 1 - \cos^2\alpha) \tag{4.47}$$

$$LD_1 = \mu_x^2 - 0.25\mu_1^2(1 + \cos^2\alpha) \tag{4.48}$$

Rotation about the y-axis is treated in a similar fashion, starting with Equation 4.49, where μ_y is treated as a constant.

$$LD_2 = \left(\mu_x^2 - \mu_y^2\right) = \mu_2^2(\cos\beta_v \sin\alpha)^2 - \mu_y^2 \tag{4.49}$$

β_v in Equation 4.49 is averaged over 0 to 2π radians to give Equations 4.50.

$$LD_2 = 0.5\mu_2^2 \sin^2\alpha - \mu_y^2 \tag{4.50}$$

This is developed to give:

$$LD_2 = 0.5\mu_2^2(1 - \cos^2\alpha) - \mu_y^2 \tag{4.51}$$

Equations 4.45 and 4.51 are then modified to take into account the transition moment dipole in the reference state and the scaling factor reintroduced, producing Equations 4.52 and 4.53.

$$LD_1 = S\left(\mu_x^2 - 0.25\mu_1^2(1 + \cos^2(\alpha_{i0} + \delta))\right) \tag{4.52}$$

$$LD_2 = S\left(0.5\mu_2^2(1 - \cos^2(\alpha_{i0} + \varphi)) - \mu_y^2\right) \tag{4.53}$$

For each starting orientation the values of μ_x or μ_y, α_{io} and μ_1 or μ_2 would be the same at each wavelength regardless of the angle of ψ and δ, allowing non-linear least squares fitting to be performed simultaneously on the calculated data at each wavelength to determine these parameters by fitting Equations 4.52 and 4.53 to the data from the Dichrocalc calculations.

Equations 4.52 and 4.53 were then fitted to the LD data calculated for HNP-2 in the first and second membrane bound states (P_{m1} and P_{m2} in Figure 4.31) in Section 4.2.6.3, using the values of μ_x or μ_y, α_{io} and μ_1 or μ_2 calculated from fitting the Dichrocalc data, in order to determine the values of δ or ψ for which the best fit could be obtained between the calculated and experimental data. It is likely that a number of possible orientations could be fitted to the data, including individual rotations involving just δ or ψ, and combinations of rotations around both axes. The experimental and fitted spectra are included as Appendix 3, and an example is shown in Figure 4.44. None of the fits

between the experimental and calculated data matched well above approximately 220 nm. This can be explained by the fact that the orientation of the aromatic transition moments in the bound state will differ more significantly than those of the amide backbone from the x-ray structure. It also appears that the coupling between the tryptophan and tyrosine residues, which caused splitting in some of the LD spectra as discussed in Section 4.2.8.1, has not been accounted for in the calculated spectra.
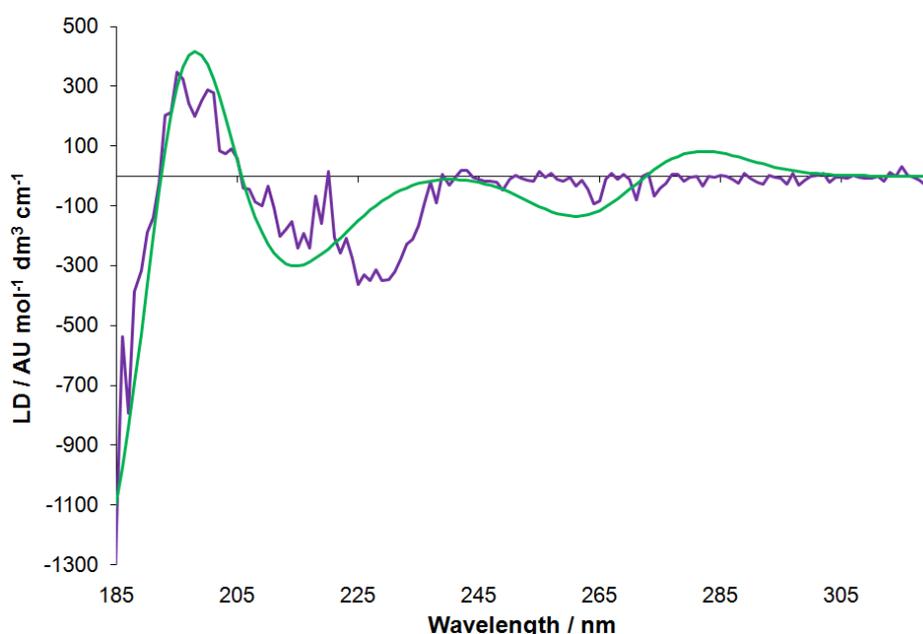
Figure 4.44. LD spectrum of the P_{m1} state of HNP-2 binding to 50:50 (w/w) POPG/DOPC at 40 °C (purple) and closest-fit calculated spectrum determined through least squares fitting using Equation 4.53 (green).

The scaling factors and rotations about δ and ψ determined from fitting the calculated data to the data from the first and second membrane bound states of HNP-2 are listed in Table 4.12. It was not possible to fit the spectra of HNP-2 binding to DMPG/DMPC liposomes below the phase transition temperature due to the high degree of scattering in the spectra. The calculated rotation angles in Table 4.12 are likely to be the maximum extents of the peptide tilt, and a large degree of error will be present for each angle due both to the mathematical error inherent in least squares fitting (10%) and due to modelling dynamic systems using a static structure.

Table 4.12. Parameters obtained from fitting Equations 4.52 and 4.53 to data for the first and second membrane bound states (P_{m1} and P_{m2} (Figure 4.31)) of HNP-2 binding to POPG/DOPC, DMPG/DMPC and DOPS/DOPC liposomes at different temperatures.

		S	δ(°)	ψ(°)
POPG/DOPC 30 °C	P_{m1}	1.1	10	
		0.9		8
	P_{m2}	0.6	-18	
		0.8		19
POPG/DOPC 40 °C	P_{m1}	0.9	16	
		0.6		0
	P_{m2}	0.6	-16	
		0.9		22
POPG/DOPC 53 °C	P_{m1}	0.8	17	
		0.5		0
	P_{m2}	0.6	-2	
		0.8		28
DOPS/DOPC 30 °C	P_{m1}	1.6	18	
		1.0		0
	P_{m2}	0.2	-33	
		0.2		2
DMPG/DMPC 33 °C	P_{m1}	2.2	-21	
		2.1		0
	P_{m2}	0.2	-16	
		0.4		28

4.2.7.4 Discussion of results of quantitative analysis of binding

The data in Table 4.12 suggest that the peptide sits on or partially inserted into the surface of the liposome with a tilt of up to 33° around the x or y-axes as defined in Figure 4.41. Figures 4.45A–I show the furthest extent of the tilts around the y and x-axes in first and second membrane bound states.
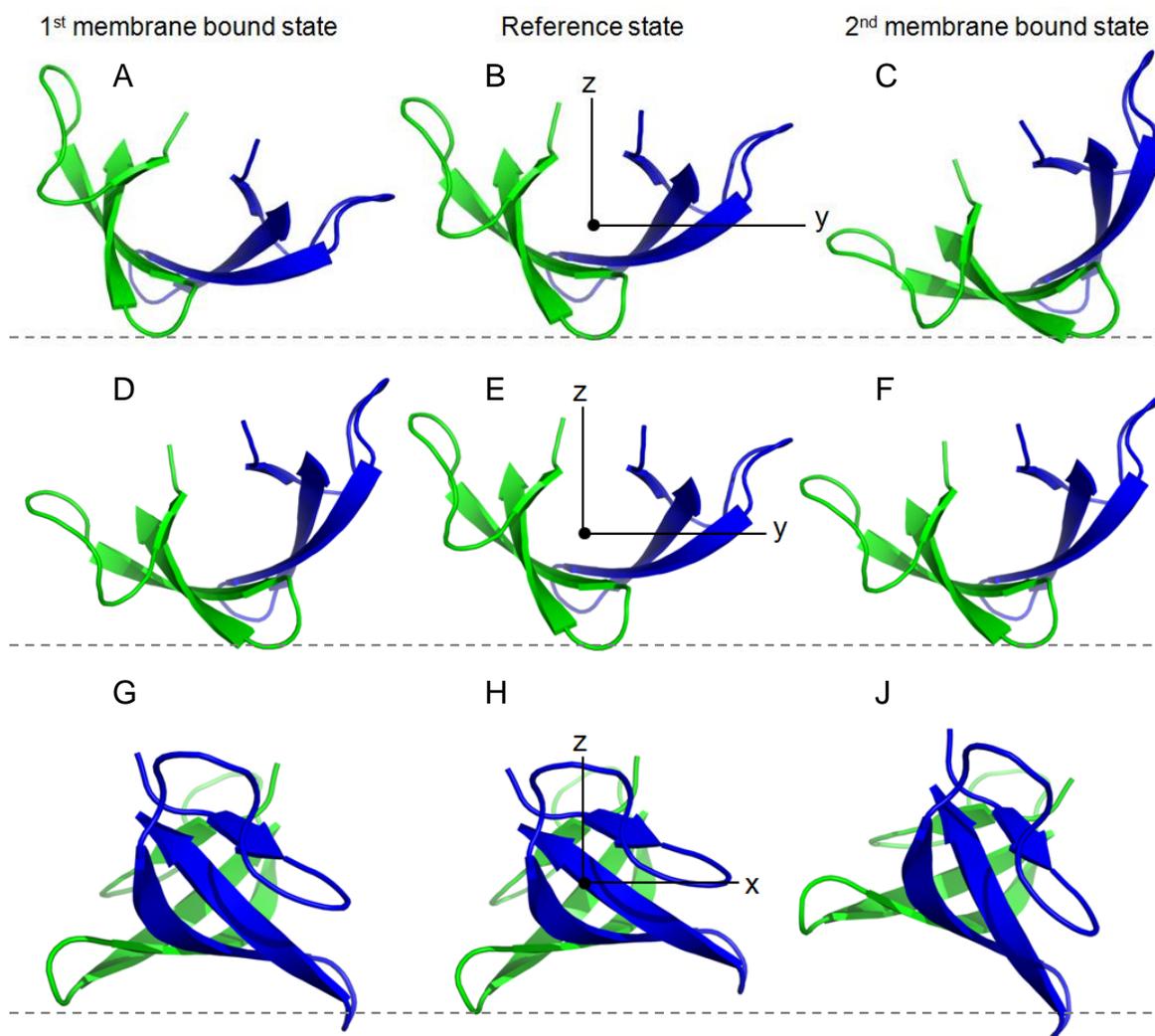
Figure 4.45. Orientations of HNP-2 in the first and second membrane bound states. A–C) The furthest extent of the tilts around the x-axis in the first and second membrane bound states of HNP-2 binding to 50:50 (w/w) POPG/DOPC at any temperature or to 50:50 (w/w) DOPS/DOPC at 30 °C compared to the peptide in the reference state ($\delta = 18°$, 0° and -33° respectively); D–F) the furthest extent of the tilts around the x-axis in the first and second membrane bound states of HNP-2 binding to 50:50 (w/w) DMPG/DMPC at 33 °C compared to the peptide in the reference state ($\delta = -21°$, 0° and -16° respectively); G–I) the furthest extent of the tilts around the y-axis in the first and second membrane bound states of HNP-2 binding to any of the liposomes under any conditions compared to the peptide in the reference state ($\delta = 8°$, 0° and 28° respectively). The plane of the membrane, though not necessarily the position of the surface of the membrane relative to the peptide dimers, is indicated by hashed line.

4.2.7.4.1 Binding to 50:50 (w/w) POPG/DOPC liposomes

When binding to POPG/DOPC liposomes in the first membrane bound state the peptide as shown in Figure 4.45B is tilted between 10° and 17° clockwise around the x-axis and/or between 0° and 8° clockwise around the y-axis looking towards the origin in Figure 4.45H. In the second membrane bound state the peptide is tilted between 2° and 33° clockwise around the x-axis and/or between 19° and 28° around the y-axis. The tilts

around the x-axis in the first membrane bound states are very similar, essentially the same within error, while the tilts around the y-axis are the same within 10% when binding to POPG/DOPC at 40 °C and 53 °C, but lower at 30 °C. In the second membrane bound state the extent of the tilt around the x-axis decreases with temperature, while the tilt around the y-axis increases with increasing temperature.

4.2.7.4.2   Binding to 50:50 (w/w) DOPS/DOPC liposomes

The angles at which the peptide inserts into DOPS/DOPC membranes at 30 °C, and the changes between the peptide in the two membrane bound states are similar to those for binding to POPG/DOPC membranes.   The angles of HNP-2 in the first membrane bound state are within 10% of those of the peptide in the first membrane bound state when binding to POPG/DOPC liposomes at 53 °C. The tilt around the x-axis in the second membrane bound state is greater than for binding to POPG/DOPC membranes at any temperature, while the tilt around the y-axis is lower than observed for binding to the POPG/DOPC liposomes. Rotation about both axes increases between the two membrane bound states.

4.2.7.4.3   Binding to 50:50 (w/w) DMPG/DMPC liposomes

When binding to DMPG/DMPC liposomes above the phase transition temperature a rotation of 21° anticlockwise around the x-axis, looking towards the origin, compared to Figure 4.45E was calculated for HNP-2 in the first membrane bound state, which is different from the orientation observed in the first membrane bound state when binding to the other liposomes at any temperature. In the second membrane bound state this tilt is reduced to 16°, which is the same as calculated for binding to POPG/DOPC liposomes at 40 °C. In the first membrane bound state there is no tilt around the y-axis, as observed for POPG/DOPC at 40 °C and 53 °C and DOPS/DOPC at 30 °C, and in the second membrane bound state a tilt of 28° clockwise around the y-axis, looking towards the origin, compared to Figure 4.45H is observed, which correlates with that observed for POPG/DOPC at 53 °C.

4.2.8   Binding model for defensin HNP-2

Combining the information gained from determining the kinetics and orientation of HNP-2 binding to membranes allows us to propose a model for the nature of the binding of this peptide to membranes. The first stage of the binding has a very fast rate constant, and leaves the peptide in an orientation where it is generally tilted only slightly away from being normal to the membrane surface. This is consistent with the peptide initially binding rapidly to the surface of the membrane. The initial tilt of 10–18° around the x-axis in the

first membrane bound state when binding to POPG/DOPC or DOPS/DOPC membranes (Figure 4.45A), or 21° when binding to DMPC/DMPC membranes (Figure 4.45D) can be explained by the presence of 6 arginine residues around the middle of the dimer (Figure 4.46). In Figure 4.46A and B it is clear that a tilt around the x-axis would allow at least one of these positively charged residues to interact with the negatively charged lipid headgroups in the membrane. Figure 4.46C shows that the arginine residues are mainly located on two sides of the membrane, and that rotation about the y-axis would not allow the arginine residues to interact with the membrane, which may explain why initially little or no rotation around this axis is observed in the first membrane bound state. The $\Delta H^{\ddagger}$ value determined for the first binding step (Section 4.2.7) was found to be positive, which is consistent with partial desolvation of the peptide and lipids and breaking van der Waals forces between the lipids in the transition state during insertion. The entropy of activation for the first stage of binding, $\Delta S^{\ddagger}$, was found to be unfavourable, due to the decrease in rotational freedom of the peptide and the freezing out of motion of the lipids, which correlates with a binding processing occurring.
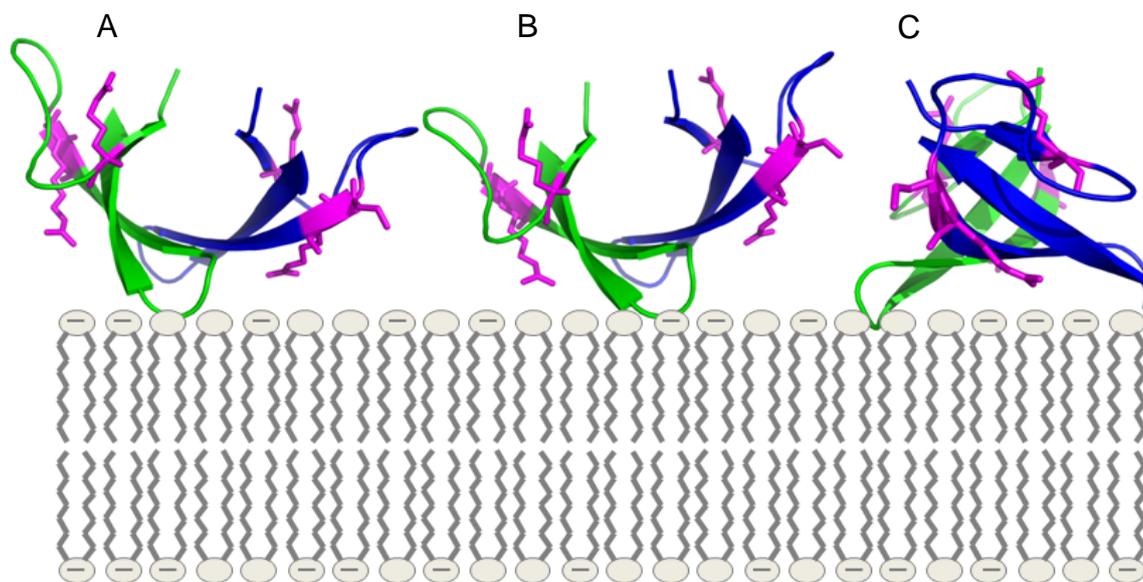
Figure 4.46. Orientation of HNP-2 dimers in first membrane bound state. A) $\delta = 10°$; B) $\delta = -21°$ and C) $\psi = 0°$. Arginine residues are shown in purple.

The second membrane bound state is formed more slowly and involves a tilt around both the x- and y-axes of between 2° and 33°. In this orientation it is unlikely that the dimer is completely buried in the membrane, but it is likely to have inserted slightly into the membrane. This is consistent with the much slower rate for the second stage of binding to the DMPG/DMPC liposomes below the phase transition temperature compared

to above the phase transition temperature, in contrast to the first stage, where it is likely that only an interaction with the surface was occurring, where the rates were similar. There are four hydrophobic residues at the base of the HNP-2 dimer, two glycine and two leucine residues, which create a hydrophobic region of 344 $Å^2$ on the base of the dimer (Figure 4.47). This is likely to be positioned inside the hydrophobic core of the membrane if the dimer is bound in a stable position. The slight tilts around the x and y-axes may occur to allow more arginine residues to interact with the PG headgroups than if the dimer inserted vertically. The distance between the hydrophobic base of an HNP-2 dimer to the backbone carbon of an arginine residue is approximately 9 Å and the distance longest between the base of the peptide dimer and the guanidinium group of an extended arginine residue is approximately 18 Å. When this is compared to the thickness of one leaflet of a DOPC bilayer, where the hydrophobic portion is 16 Å thick and the interface region, incorporating the rest of the lipid and the waters of hydration, 15 Å,[83] it is clear that a dimer could partially insert into one leaflet with the base within the hydrophobic region and the guanidinium groups able to interact with the lipid headgroups.
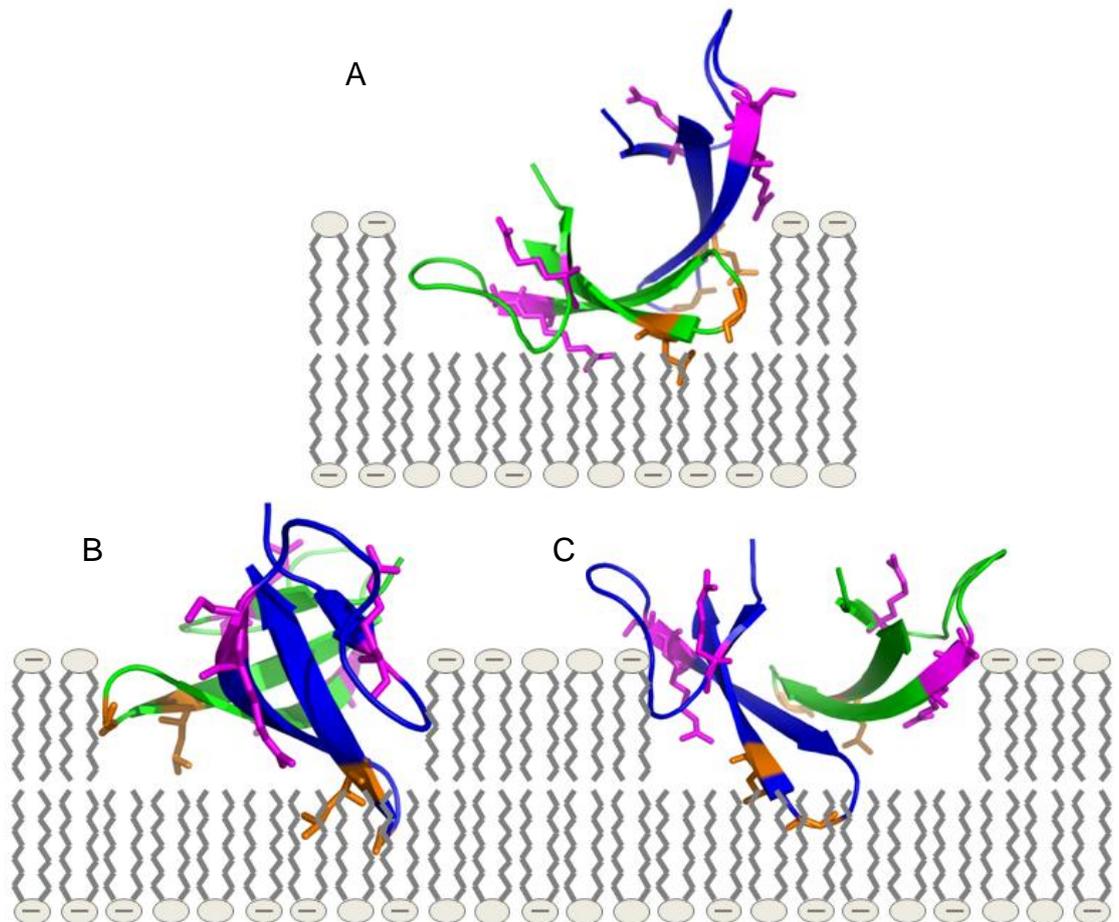
Figure 4.47. Proposed orientation of HNP-2 in second membrane bound state showing maximum rotations about the x and y-axes where A) δ = -33°, and where ψ = 28 viewed along B) the y-axis and C) the x-axis. Arginine residues are shown in purple; glycine and leucine residues are shown in orange.

4.2.8.1　Comparison between results and proposed literature models

As described in Section 4.1.4, three models were proposed for the binding of HNP-2 to lipid membranes by Hill *et al.* in their paper describing the crystal structure of HNP-3: the wedge model, the multiple dimer pore (or multimeric pore) model and the two dimer pore model, and Wimley *et al.* carried out binding experiments using HNP-2 from which they proposed that the multiple dimer pore model best fitted to their results.[4, 20] The binding of HNP-2 in the analyses reported herein displayed first-order kinetics, ruling out the formation of multimeric pores during the time period of the analyses. Nevertheless, models of the two dimer pore and multiple dimer pore were analysed using Dichrocalc to determine what their calculated LD spectra would be and to see how they differed from the experimental spectra and the fitted spectra. In each case a series of calculated spectra obtained at 30° rotations about the z-axis and 30° tilt angles about the x-axis were averaged to account for the possibility of the pores being situated at any position on a shear-deformed liposome and to have any orientation with relation to rotation about the z-axis. The resulting spectra are compared with the spectrum of the second membrane bound state of HNP-2 binding to POPG/DOPC membranes at 30° and to the spectra where $\delta = 198$ and $\psi = 19$ (Figure 4.48), which were found to correlate most closely with the spectrum of HNP-2 in the second membrane bound state. It is clear from Figure 4.48 that the spectra of the two pore models are very different from the spectrum of the second membrane bound state and from the spectra fitted to spectrum of HNP-2 in the second membrane bound state. This is not surprising, but reinforces the orientation which we propose for the second membrane bound state.
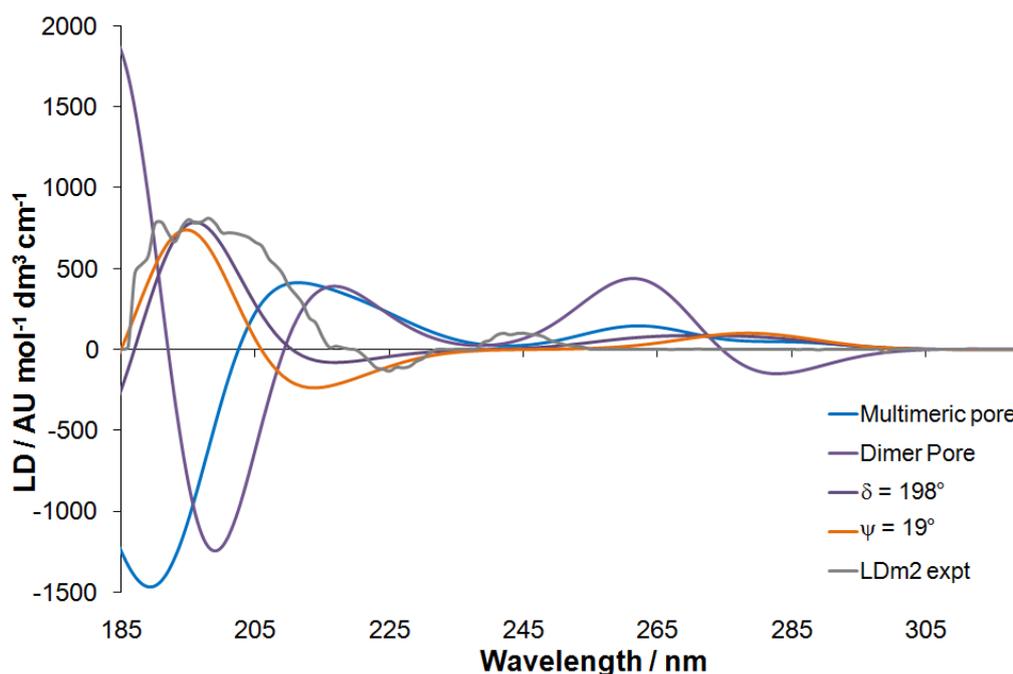
Figure 4.48. Calculated LD spectra of a multimeric pore (blue), a two dimer pore (purple) and HNP-2 dimers oriented as in Figure 4.41 where δ = 198 (grey) and ψ = 19 (orange). These are compared to the spectrum of the second membrane bound state of HNP-2 binding to 50:50 (w/w) POPG/DOPC at 30.

The orientation of HNP-2 in the second membrane bound state resembles the 'wedge model' proposed by Hill *et al* and shown in Figure 4.7A, and suggests that the peptide acts on membranes through a carpet-type mechanism, when a large number of peptides bind to the membrane surface and cause it to weaken and become permeable through a detergent-like action, rather than through the formation of pores. Hill *et al.* suggested that the wedge model would disrupt the bilayer by distorting interactions between the lipids through burying the dimer into the outer leaflet of the membrane and allowing the arginine residues to interact with the negatively charged PG or PS headgroups.[4] In proposing the multimeric pore model Wimley *et al.* studied the release of fluorescent markers from liposomes after the addition of HNP-2 and determined that it occurred through an all-or-none mechanism which was indicative of the presence of pores in the membrane.[20] It is possible for artifacts to be observed which suggest all-or-none release but are actually due to inefficient mixing immediately after the addition of the peptide to the liposomes causing transient high local peptide concentrations. The data Wimley *et al.* used to propose all-or-none release of fluorescent markers was also re-analysed by some of the authors of the original paper at a later date using an extended model for analysing the data. They determined from this more comprehensive data analysis that the original data could be interpreted as all-or-none or as graded release with a very high preference of ANTS leakage over DPX, though they argued that the latter

was unlikely due to the observation of the release of large dextrans after the addition of HNP-2.[84] Peptides which have been suggested to act through carpet-type mechanisms have been shown to cause the release of large markers however.[85, 86] It is also possible that HNP-2 acts in a 2-state model which has been used to describe the some antimicrobial peptides, including the helical antimicrobial peptide magainin, where below a certain peptide-to-lipid ratio the peptides adsorb to the surface and above this ratio they insert into the membrane to form toroidal pores.[87, 88] Wimley *et al.* carried out analyses at peptide:lipid ratios half and twice those used for the experiments reported in this chapter, with little difference between the results for the two concentrations, and observed the release of large markers within two hours of the addition of HNP-2 to liposomes, so it is unlikely that they observed a different binding process to that observed in these experiments. The degree of binding of HNP-2 to liposomes composed of 50:50 (w/w) POPG/DOPC reported by Wimley *et al.* (75% with 14.5 µM HNP-2 and 1 mM lipid) is also inconsistent with the results of the experiments reported herein, where the concentration of free peptide 100 minutes after mixing HNP-2 (15 µM) with 50:50 (w/w) POPG/DOPC, DOPS/DOPC or DMPG/DMPC liposomes (1.4 or 1.05 mM) was found to be negligible.[45]

4.3   Future and other work

Preliminary experiments were carried out using a cross-linking method and neutron reflectivity to further explore the membrane binding of HNP-2. Neither were taken to completion, but the experiments and the information they were designed to provide are outlined.

4.3.1   Cross-linking

The photo-induced cross-linking of unmodified proteins (PICUP) method, developed by Fancy and Kodadek,[89] involves photolysis of ruthenium(II) tris-bipyridyl dication ($Ru(II)bpy_3^{2+}$) to give an excited state of ruthenium, which donates an electron to a persulphate ion (present as ammonium persulphate), causing the O–O bond to break. This leaves $Ru(III)bpy_3^{3+}$ and a sulphate radical, which cause cross-linking between the tyrosine side chains of neighbouring peptides. The exact cross-linking method is not known, but the two mechanisms proposed by Fancy and Kodadek, on which the method was designed, are shown in Scheme 4.1.
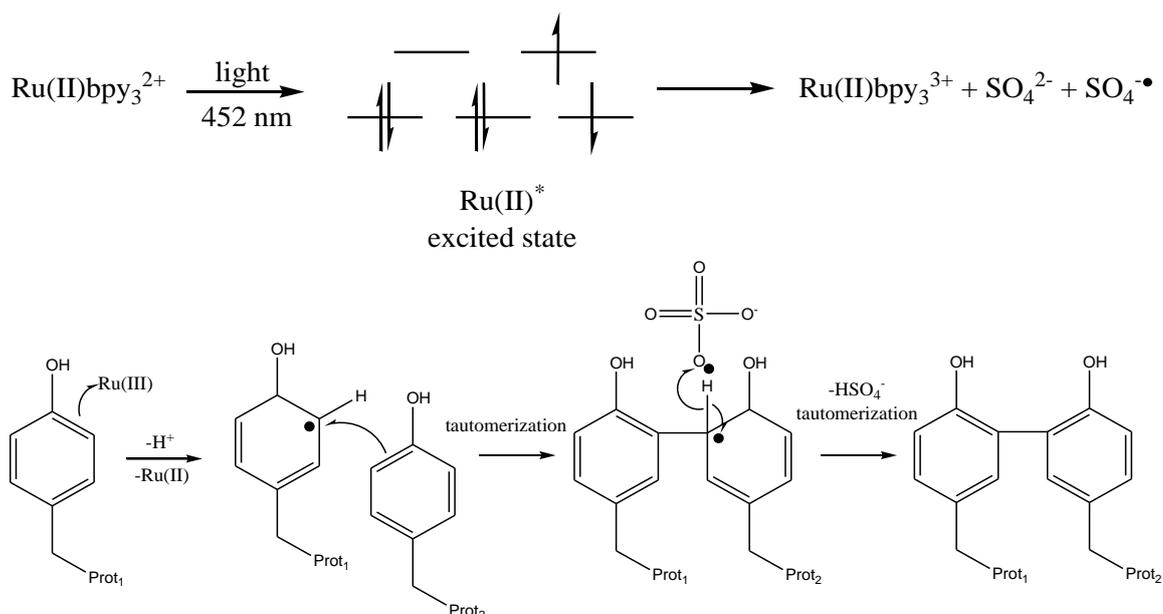
Scheme 4.1. Mechanisms proposed by Kodadek and Fancy for the PICUP process.

Experiments were carried out with the aim of using this method to cross-link HNP-2 peptides at different times during their insertion into POPG liposomes, to give a 'snap-shot' of the insertion process and to hopefully identify the arrangement of the peptides during and after binding. Analyses were carried out using MALDI-MS and sodium dodecyl sulfate polyacrylamide gel electrophoresis (SDS-PAGE) with the aim of observing the size of any groups of peptides linked together, where small groups would support the proposed multimeric pore binding method while larger aggregates would suggest something more like the carpet mechanism.

It was not possible to observe defensin multimers by any analysis method. Different ratios of reagents were tested, with different peptide:lipid ratios and cross-linking at different times after the addition of the cross-linking reagent. The initial experiments were thought to be unsuccessful due to the use of a buffer containing 150 mM NaCl, a known inhibitor of defensin binding, but even in the absence of added salt and just 5 mM phosphate buffer it was not possible to observe any cross-linking.

Two main theories were proposed for the lack of observation of multimers. The first was the low concentration of peptide used in the experiments. It was proposed that if the peptide formed oligomers these would each be present at too low a concentration to observe. It was hoped that an antibody could be obtained to enhance detection of the peptide. With antibodies, Western Blotting could be carried out, as this is more sensitive than silver or Coomassie blue staining, due to the 10-fold increase in peptide mass when it is bound by an antibody causing a 10-fold increase in sensitivity towards amino acid

detection. The antibodies could also be labelled, for example with colloidal gold, which can be viewed by TEM without staining, facilitating identification of the resulting pictures as only the antibody (attached to the peptide) would be visible. The other likely cause of the lack of observed oligomers is the position of the tyrosine residues within the peptide dimer. Tyr(20) sits in the centre of the HNP-2 dimer and has been said to participate in the binding through hydrophobic interactions. The other two tyrosine residues sit at the top and side of the dimer, and may not be in suitable positions for cross-linking after the formation of a multimeric pore or carpet-like aggregation.

4.3.2 Neutron reflectivity

Neutron reflectivity (NR) allows the study of nature of peptide binding through analysing changes in lipid bilayers after the addition of peptides. Features which can be studied include the depth of bilayer penetration, the orientation of the bound peptide and the nature of any pore formed. Deuterium labelled lipids are deposited on silicon crystals via the adsorption and rupture of liposomes. The peptide is then added and the nature of the disruption of the bilayer studied.[90] Washing with H_2O and D_2O can be used to reveal pores in the bilayer.[91] Preliminary experiments explored methods of obtaining a bilayer with a high enough percentage of negatively charged DMPG lipid for HNP-2 to bind. The binding of lipids to hydrophobic surfaces is strongly affected by the lipid charge, but this can be overcome by varying the ratio of neutral and negative lipid and by the addition of Ca^{2+} salts.[92] A bilayer was formed when 80:20 (w/w) dDOPC/DMPG in 10 mM $CaCl_2$ was left for 2 hours to adsorb onto the surface. It is hoped that further neutron reflectivity experiments would reveal more information about the depth and orientation of HNP-2 in membranes to compliment the results of the linear dichroism experiments.

4.3.3 Future work

The results of the analyses of HNP-2 have suggested that the peptide acts on membranes via a carpet mechanism under the conditions used, rather than the pore model which has been proposed to explain the action of HNP-2. Further LD analyses of the binding at different peptide:lipid ratios would establish whether the peptide reorients to form toroidal pores through the membrane at higher concentrations in a similar way to the model which has been proposed for magainin. Further information about the binding process could be obtained by measuring the enthalpy, through measuring the heat released after the addition of HNP-2 to liposomes.

4.4 References

1. H. Chen, Z. Xu, L. Peng, X. Fang, X. Yin, N. Xu and P. Cen, *Peptides*, 2006, **27**, 931–940.

2. T. Ganz, *Nat. Rev. Immunol.*, 2003, **3**, 710–720.

3. A. van Dijk, E.J.A. Veldhuizen and H.P. Haagsman, *Vet. Immunol. Immunop.*, 2008, **124**, 1–18.

4. PDB ID: 1DFN, C.P. Hill, J. Yee, M.E. Selsted and D. Eisenberg, *Science*, 1991, **251**, 1481–1485.

5. PDB ID: 1KJ6, D.J. Schibli, H.N. Hunter, V. Aseyev, T.D. Starner, J.M. Wiencek, P.B. McCray Jr., B.F. Tack and H.J. Vogel, *J. Biol. Chem.*, 2002, **277**, 8279–8289.

6. PDB ID: 1EWS, A.M. McManus, N.F. Dawson, J.D. Wade, L.E. Carrington, D.J. Winzor and D.J. Craik, *Biochemistry*, 2000, **39**, 15757–15764.

7. Y-Q. Tang, J. Yuan, G. Ösapay, K. Ösapay, D. Tran, C.J. Miller, A.J. Ouellette and M.E. Selsted, *Science*, 1999, **286**, 498–502.

8. M. Trabi, H.J. Schirra and D.J. Craik, *Biochemistry*, 2001, **40**, 4211–4221.

9. PBD ID: 1ZMH, C. Xie, A. Prahl, B. Ericksen, Z. Wu, P. Zeng, X. Li, W-Y. Lu, J. Lubkowski and W. Lu, *J. Biol. Chem.*, 2005, **280**, 32921–32929.

10. J.J. Schneider, A. Unholzer, M. Schaller, M. Schäfer-Korting and H.C. Korting, *J. Mol. Med.*, 2005, **83**, 587–595.

11. X-L. Zhang, M. E. Selsted and A. Pardi, *Biochemistry*, 1992, **31**, 11348–11356.

12. A. Pardi, X-L Zhang, M.E. Selsted, J.J. Skalicky and P.F. Yip, *Biochemistry*, 1992, **31**, 11357–11364.

13. A. Szyk, Z. Wu, K. Tucker, D. Yang, W. Lu and J. Lubkowski, *Protein Sci.*, 2006, **15**, 2749–2760.

14. PDB ID: 3HJ2, G. Wei, E. de Leeuw, M. Pazgier, M. Rajabi, J. Li, G. Zou, B. Ericksen, Z. Wu, W. Yuan, H. Szmacinski, W.-Y. Lu, J. Lubkowski, R.L. Lehrer and W. Lu, to be published.

15. Y. Zhang, T. Doherty, J. Li, W. Lu, C. Barinka, J. Lubkowski and M. Hong, *J. Mol. Biol.*, 2010, **397**, 408–422.

16. W. Kabsch and C. Sander, *Biopolymers*, 1983, **22**, 2577–637.

17. C.G. Wilde, J.E. Griffith, M.N. Marra, J.L. Snable and R.W. Scott, *J. Biol. Chem.*, 1989, **264**, 11200–11203.

18. B. Ericksen, Z. Wu, W. Lu and R.I. Lehrer, *Antimicrob. Agents Chemother.*, 2005, **49**, 269–275.

19. M.E. Selsted, S.S.L. Harwig, T. Ganz, J.W. Schilling and R.I. Lehrer, *J. Clin. Invest.*, **76**, 1436–1439.

20. W.C. Wimley, M.E. Selsted and S.H. White, *Protein Sci.*, 1994, **3**, 1362–1373.

21. R.I. Lehrer, A.K. Lichtenstein and T. Canz, *Annu. Rev. Immunol.*, 1993, **11**, 105–128.

22. B.L. Kagan, T. Canz and R.I. Lehrer, *Toxicology*, 1994, **87**, 131–149.

23. T. Canz and R.I. Lehrer, *Curr. Opin. Immunol.*, 1994, **6**, 584–589.

24. M.E. Selsted and A. Ouellette, *Trends Cell. Biol.*, 1995, **5**, 114–119.

25. M.E. Selsted, S.I. Miller, A.H. Henschen and A. Ouellette, *J. Cell Biol.*, 1992, **118**, 929–936.

26. A. Ouellette, M.M. Hsieh, M.T. Nosek, D.F. Cano-Gauci, K.M. Huttner, R.N. Buick and M.E. Selsted, *Infect. Immun.*,1994, **62**, 5040–5047.

27. S.B. Aley, M. Zimmerman, M. Hetsko, M.E. Selsted and F.D. Giliin, *Infect. Immun.*, 1994, **62**, 5397–5403.

28. E.V. Valore, C.H. Park, A.J. Quayle, K.R. Wiles, P.B. McCray Jr and T. Ganz, *J. Clin. Invest.*, 1998, **101**, 1633–1642.

29. R. Bals, X. Wang, Z. Wu, T. Freeman, V. Bafna and M. Zasloff, *J. Clin. Invest.*, 1998, **102**, 874–880.

30. J.M. Schröder, *Biochem. Pharmacol.*, 1999, **57**, 121–34.

31. J. Harder, J. Bartels, E. Christophers and J.M. Schroder, *Nature,* 1997, **387**, 861–861.

32. J. Harder, J. Bartels, E. Christophers and J.M. Schroder, *J. Biol. Chem.*, 2001, **276**, 5707–5713.

33. J.R. García, A. Krause, S. Schulz, F.J. Rodríguez-Jiménez, E. Klüver, K. Adermann, U. Forssmann, A. Frimpong-Boateng, R. Bals and W-G. Forssmann, *FASEB J.*, 2001, **15**, 1819–1821.

34. Y. Yamaguchi, T. Nagase, R. Makita, S. Fukuhara,T. Tomita, T. Tominaga, H. Kurihara and Y. Ouchi, *J. Immunol.*, 2002, **169**, 2516–2523.

35. C. Y. Kao, Y. Chen, Y. H. Zhao and R. Wu, *Am. J. Respir. Cell Mol. Biol.*, 2003, **29**, 71–80.

36. L. Huang, S.S.J. Leong and R. Jiang, *Appl. Microbiol. Biotechnol.*, 2009, **84**, 301–308.

37. F.J. Rodríguez-Jiménez, A. Krause, S. Schulz, W.-G. Forssmann, J.-R. Conejo-Garcia, R. Schreeb and D. Motzkus, *Genomics*, 2003, **81**, 175–183.

38. G. Diamond, M. Zasloff, H. Eck, M. Brasseur, W.L. Malay and C.L. Bevins, *Proc. Natl. Acad. Sci. USA*, 1991, **88**, 3952–3956.

39. S. Cociancich, M. Goyffon, F. Bontems, P. Bulet, F. Bouet, A. Menez and J. Hoffman, *Biochem. Biophys. Res. Commun.*, 1993, **194**, 17–22.

40. M.S. Almeida, K.M. Cabral, R.B. Zingali and E. Kurtenbach, *Arch. Biochem. Biophys.*, 2000, **378**, 278–286.

41. S. Cociancich, A. Ghazi, C. Hetru, J.A. Hoffman and L. Letellier, *J. Biol. Chem.*, 1993, **268**, 19239–19245.

42. K. Hristova, M.E. Selsted and S.H. White, *Biochemistry*, 1996, **35**, 11888–11894.

43. G. Fujii, M.E. Selsted and D. Eisenberg, *Protein Sci.*, 1993, **2**, 1301–1312.

44. J. Kim, M. Mosior, L.A. Chung, H. Wu and S. McLaughlin, *Biophys. J.*, 1991, **60** 135–148.

45. W.C. Wimley and S.H. White. *Anal. Biochem.*, 1993, **213**, 213–217.

46. R.I. Lehrer, A. Barton, K.A. Daher, S.S. L. Harwig, T. Ganz and M.E. Selsted, *J. Clin. Invest.*, 1989, **84**, 553–561.

47. S. Ohki, E. Marcus, D.K. Sukumaran and K. Arnold, *Biochim. Biophys. Acta*, 1994, **1194**, 223–232.

48. A. M. Cole, T. Ganz, A.M. Liese, M.D. Burdick, L. Liu and R.M. Strieter, *J. Immunol.*, 2001, **167**, 623–627.

49. B.A. Lewis and D.M. Engelman, *J. Mol. Biol.*, 1983, **166**, 211–217.

50. K. Hristova, M.E. Selsted and S.H. White, *J. Biol. Chem.*, 1997, **272**, 24224–24233.

51. A. Pardi, D.R. Hare, M.E. Selsted, R.D. Morrison, D.A. Bassolino and A.C. Bach, J*. Mol. Biol.* 1988, **201**, 625–636.

52. A. Rodger, personal communication.

53. Sigma-Aldrich Product Information Sheet L-α-Phosphocholine Product Numbers P3644/P5638 RLG 8/03.

54. N. Michel, A.-S. Fabiano, A. Polidori, R. Jack and B. Pucci, *Chem. Phys. Lipids*, 2006, **139**, 11–19.

55. I.S. Salonen, K.K. Eklund, J.A. Virtanen and P.K.J. Kinnunen, *Biochim. Biophys. Acta,* 1989, **982**, 205–215.

56. J.R. Silvius in *Lipid Protein Interactions*, ed. P. C. Jost and O. H. Griffth, John Wiley and Sons, New York, USA, 1982, Vol. 2, pp. 240–281.

57. S.H. White, W.C. Wimley and M. Selsted, *Curr. Opin. Struc. Biol.*, 1995, **5**, 521–527.

58. J.R. Lakowicz, *Principles of Fluorescence Spectroscopy*, Kluwer Academic/Plenum, New York, 2nd edn., 1999, pp 63–64.

59. E. Haas, M. Wilchek, E. Katchalski-Katzir and I.Z. Steinberg, *Proc. Nat. Acad. Sci. USA*, 1975, **72**, 1807–1811.

60. R. Boteva, T. Zlateva, V. Dorovska-Taran, A.J.W.G. Visser, R. Tsanev and B. Salvat, *Biochemistry*, 1996**, 35**, 14825–14830.

61. S.-C. Li, N.K. Goto, K.A. Williams, and C.M. Deber, *Proc. Natl. Acad. Sci. USA*, 1996, **93**, 6676–6681.

62. G.B. McGaughey, M. Gagne and A.K. Rappe, *J. Biol. Chem.*, 1998, **273**, 15458–15463.

63. C.A. Hunter, J. Singh and J.M. Thornton, *J. Mol. Biol.* 1991, **218**, 837–846.

64. V. Marchi-Artzner, T. Gulik-Krzywicki, M.-A. Guedeau-Boudeville, C. Gosse, J.M. Sanderson, J.-C. Dedieu and J.-M. Lehn, *ChemPhysChem*, 2001, **2**, 367–376.

65. M.-A. Urbaneja, F.M. Gori and A. Alonso, *Eur. J. Biochem.* 1988, **173**, 585–588.

66. S. Cociancich, A. Ghazi, C. Hetru, J.A. Hoffmann and L. Letellier, *J. Biol. Chem.*, 1993, **268**, 19239–19245.

67. J.P. Bourdineaud, P. Boulanger, C. Lazdunski and L. Letellier, *Proc. Natl. Acad. Sci. USA*, 1990, **87**, 1037–1041.

68. J. Tang, H. Yin, J. Qiu, M.J. Tucker, W.F. DeGrado and F. Ga, *J. Am. Chem. Soc.* 2009, **131**, 3816–3817**.**

69. S.M. Ennaceur, M.R. Hicks, C.J. Pridmore, T.R. Dafforn, A. Rodger and J.M. Sanderson, *Biophys. J.*, 2009, **96**, 1399–1407.

70. M. Oliveberg, Y.-J. Tan and A.R. Fersht, *Proc. Natl. Acad. Sci. USA*, 1995, **92**, 8926–8929.

71. A. Rodger, J. Rajendra, R. Marrington, M. Ardhammar, B. Nordén, J.D. Hirst, A.T.B. Gilbert, T.R. Dafforn, D.J. Halsall, C.A. Woolhead, C. Robinson, T.J. T. Pinheiro, J. Kazlauskaite, M. Seymour, N. Perez and M.J. Hannon, *Phys. Chem. Chem. Phys.*, 2002, **4**, 4051–4057.

72. B.M. Bulheller, A. Rodger and J.D. Hirst, *Phys. Chem. Chem. Phys.*, 2007, **9**, 2020–2035.

73. T.R Dafforn and Al. Rodger, *Curr. Opin. Struc. Biol.*, 2004, **14**, 541–546.

74. R.W. Woody in *Luminescence Spectroscopy & Circular Dichroism : Methods in Protein Structure & Stability*, ed. V.N. Uversky and E.A. Permyakov, Nova Science Publishers, Inc., New York, USA., 2007, pp 291–344.

75. G.D. Fasman, *Circular Dichroism and the Conformational Analysis of Biomolecules*, Plenum Press, New York, USA., 1996.

76. L.H. Greene, E. D. Chrysina, L.I. Irons, A.C. Papageorgiou, K.R. Acharya and K. Brew, *Protein Sci.*, 2001, **10**, 2301–2316.

77. E.K. Esbjörner, C.E.B. Caesar, B. Albinsson, P. Lincoln and B. Nordén, *Biochem. Biophys. Res. Co.*, 2007, **361**, 645–650.

78. P.N. YI and R.C. Macdonald, *Chem. Phys. Lipids*, 1973, **11**, 114–134.

79. B.M. Bulheller and J.D. Hirst, *Bioinformatics*, 2009, **25**, 539–540.

80. N.A. Besley and J.D. Hirst, *J. Am. Chem. Soc.*, 1999, **121**, 9636–9644.

81. D.M. Rogers and J.D. Hirst, *J. Phys. Chem. A*, 2003, **107**, 11191–11200.

82. M.T. Oakley and J.D. Hirst, *J. Am. Chem. Soc*, **128**, 2006, 12414–12415.

83. M.C. Wiener and S.H. White, *Biophys. J.*, 1992, **61**, 434–447.

84. A.S. Ladokhin, W.C. Wimley and S.H. White, *Biophys. J.*, 1995, **69**, 1964–1971.

85. P. Butko, F. Huang, M. Pusztai-Carey and W.K. Surewicz, *Biochemistry*, 1996, **35**, 11355–11360.

86. P. Butko, *Appl. Environ. Microb.*, 2003, **69**, 2415–2422.

87. S.J. Ludtke, K. He, W.T. Heller, T.A. Harroun, L. Yang and H.W. Huang, *Biochemistry*, 1996, **35***, 13723–13728.

88. S.J. Ludtke, K. He, Y. Wu and H.W. Huang, *Biochim. Biophys. Acta*, 1994, **1190**, 181–184.

89. D.A. Fancy and T. Kodadek, *Proc. Natl. Acad. Sci. USA*, 1999, **96**, 6020.

90. H.P. Wacklin, F. Tiberg, G. Fragneto and R.K. Thomas, *Biochim. Biophys. Acta*, 2007, **1768**, 1036–1049.

91. D. Constantin, G. Brotons, A. Jarre, C. Li and T. Salditt, *Biophys. J.* 2007, **92**, 3978–3987.

92. R. Richter, A. Mukhopadhyay and A. Brisson, *Biophys. J.*, 2003, **85**, 3035–3047.

5 CONCLUSIONS

5.1 The identification of phospholipids by mass spectrometry

The objective of the study of phospholipids was to establish a validated protocol for identifying unknown phospholipids in mixtures, which could ultimately be applied to the analysis of lipid bilayers and lipid mixtures separated on TLC plates.

After analyzing the positive and negative ions of a number of different lipids by MALDI-MS and MSMS it was established that only MSMS analysis of the positive ions could provide enough information to identify the acyl chains and headgroups of all of the lipids studied. The addition of Li^+ or Na^+ was shown to improve the MSMS spectra of POPC and POPE in terms of signal to noise ratio and number of useful product ions, with the product ion spectra in the presence of Na^+ providing the most information from which the identities of the acyl chains and headgroups could be determined. Repeat MSMS analyses of POPE, POPC and OPPC in the presence of Li^+ or Na^+ and in the absence of added salt found clear preferences for the loss of the acyl chain from the *sn*-2 position in some product ions of POPE, POPC and OPPC in the absence of added salt, and from the *sn*-1 position in the presence of Li^+ or Na^+. Analysis of POPC in the presence of Li^+ was shown to give a greater difference in relative intensity of peaks corresponding to the loss of the acyl chain from the *sn*-1 and *sn*-2 positions compared to analysis in the presence of Na^+ or in the absence of added salt, while analysis of POPE in the presence of Na^+ or Li^+ and in the absence of added salt gave information from which the position of the acyl chains could be clearly determined. Comparison between the analyses of POPC and OPPC validated the method of identifying the position of acyl chains on the glycerol backbone through the relative ease with which they are cleaved during MSMS analysis through showing that for all but one fragment the position of the acyl chain and not its identity controlled the ease with which it was fragmented. The standard deviations of repeat measurements of the relative intensities of peaks corresponding to fragmentation at the *sn*-1 and *sn*-2 positions were consistently larger for fragmentation by CID than by LIFT, which was attributed to secondary fragmentations of the primary fragments from which the relative intensities were determined.

The protocol established for lipid analysis was applied to the analysis of unknown PC lipids and enabled some to be completely identified including the position of the acyl chain on the glycerol backbone. Preliminary MALDI imaging of TLC plates on which lipid mixtures had been separated produced full-scan MALDI spectra but in most cases the

signal was too low for achievable MSMS. It was possible to identify DPPC on a TLC plate on which mouse lung lipids had been separated from a clear product ion spectrum produced in the presence of Li$^+$. With refinement of the method it is likely that much more information could be obtained from MALDI imaging of TLC plates on which lipid mixtures have been separated.

5.2   The chemical stability of phospholipids

The techniques identified from the analyses of phospholipids were applied to the study and identification of lipids modified by actions such as hydrolysis and oxidation, both under normal conditions for membrane binding experiments and after the addition of melittin or small molecules.

Professor Alison Rodger reported changes in the CD and LD spectra of antimicrobial peptides depending on the age of the liposomes with which they were mixed. MALDI-MS analyses of liposomes composed of DOPC or DPPC under a number of conditions, including different buffers and temperatures, revealed no hydrolysis over at least 2 weeks after liposome preparation. Electron microscopy and dynamic light scattering analyses showed that the liposomes were not undergoing any physical changes consistent with aggregation or micellization. Evidence of oxidation was found in all stocks of DOPC and POPC lipid, whether stored as a solid or as a solution in CHCl$_3$. The results of MS and MSMS analyses of these lipids suggested that both peroxidation and ozonolysis were contributing to this oxidation. The concentration of oxidized DOPC in the stock was found to be very low, below the detection limit when the lipid was analysed by ^{1}H NMR, and was therefore unlikely to have had a significant effect on peptide binding experiments. The presence of oxidized lipid in the stock solutions rather than its formation during liposome storage would mean that any effects on peptide binding should be consistent regardless of the age of the liposomes.

HFIP was not shown to cause hydrolysis of DOPC liposomes, which correlated with proposals in the literature that HFIP causes membranes to become permeable through physical disruption rather than through causing chemical changes to the membrane lipids.

Lysis of the acyl chains of liposomal lipids was observed in the presence of both natural and synthetic melittin. Hydrolysis in the presence of natural melittin is well-documented and attributed to contamination with phospholipase A$_2$, which is present in all

natural melittin. No reference could be found in the literature to the lysis of the acyl chains of liposomal lipids in the presence of synthetic melittin, i.e. when there could be no possible PLA_2 contamination. The rate of lysis in the presence of synthetic melittin was much slower than with natural melittin, but was found to be enhanced by the presence of Zn^{2+} and to be inhibited when NaCl was excluded.

The addition of acyl chains to melittin from both POPC and DOPC was observed a few days after mixing the peptide and liposomes. MALDI-MSMS analysis identified the N-terminus as a site of acylation by the oleoyl chains of DOPC and POPC and the palmitoyl chain of POPC, and acylation was observed on K(7) from the oleoyl chain of DOPC. Acylation was likely to have occurred on K(21) and possibly also on K(23). There was no case in which acylation could be confirmed at a position other than the N-terminus or a lysine residue. When samples where melittin had been added to POPC liposomes were analysed, a greater transfer of the oleoyl chain from the *sn*-2 position of the lipid was observed, which is consistent with the observation of higher intensities of lyso-PPC than lyso-OPC. The observation of acylated melittin, along with the lack of free oleic acid after acyl chain lysis suggests that the formation of lyso-PC in the presence was primarily due to acyl transfer to melittin.

5.3 The membrane binding of defensin HNP-2

Fluorescence analyses were carried out on HNP-2 over a range of concentrations in order to determine the dimer binding constant and confirm whether the peptide would be predominately in a monomeric or dimeric form during the liposome binding analyses. The binding constant was found to be 3.8 μM^{-1}. All of the binding analyses were carried out using 15 μM HNP-2, therefore the observed results could be attributed to the actions of HNP-2 dimers. Comparison between fluorescence analyses of HNP-2 in water, 75:25 (v/v) MeOH/water and in 50:50 (w/w) POPG/DOPC liposomes showed that no blue shift occurred in the emission wavelengths of the tryptophan residues when the peptide was in a more hydrophobic environment, suggesting that these residues were shielded from the solvent. Two peaks were observed in all of the fluorescence spectra, which was indicative of the presence of two tryptophan environments within the dimer. This was confirmed through reference to the solid state NMR structures of HNP-1, which showed two main tryptophan rotamers, each interacting with a different tyrosine residue. When fluorescence spectra of HNP-2 in 50:50 (w/w) POPG/DOPC liposomes were recorded every 2.5 minutes for 5 hours changes in shape and fluorescence intensity were observed over time which suggested that the peptide was binding to the membrane.

Linear dichroism analyses of HNP-2 with POPG/DOPC, DMPG/DMPC or DOPS/DOPC at different temperatures showed that HNP-2 was changing orientation over 5 hours after its addition to liposome dispersions.

Fluorescence resonance energy transfer and dynamic light scattering analyses were carried out to study the effects of HNP-2 on the liposomes following binding. Fluorescence analysis of labelled liposomes over 5 hours after the addition of HNP-2 showed that no mixing of lipids between liposomes was occurring, and that therefore HNP-2 was not causing aggregation or fusion. Liposome samples were analysed by DLS before the addition of HNP-2 and after each 5-hour LD analysis to look for any changes in size which would indicate that HNP-2 was causing aggregation, fusion or micellization. No changes consistent with any of these processes were observed.

The fluorescence and LD data were found to fit to a 1st order 3-state binding model with the binding mechanism involving free peptide and two membrane-bound states. The first stage of binding was found to be fast, with the rate constants varying a little for binding to the different liposomes but similar for binding to the same liposomes at different temperature. This was consistent with an interaction with the surface of the membrane but no insertion. The second stage of the binding was slower and had some dependence on the temperature at with the binding took place, particularly the binding to 50:50 (w/w) DMPG/DMPC, where the second stage of binding was much slower below the phase transition temperature of DMPG and DMPC than above it. This suggests that the peptide dimer was inserting into the membrane to some extent during the second stage of binding. The orientation of the dimer in the second membrane bound state and the 1st order binding kinetics were consistent with a carpet-type binding mechanism with partial insertion of the peptide dimer into the bilayer, and not the formation of multimeric pores.

6 Materials and methods

6.1 Materials

Unless otherwise stated, all chemicals were used as received. 1,1,1,3,3,3-hexafluoroisopropanol was obtained from Apollo Scientific Ltd., Stockport, UK and distilled before use. All other reagents were reagent grade and obtained from Fisher Scientific, Loughborough, UK, and used without further purification. Water was purified using a Milli-Q Direct Q system from Millipore (UK) Ltd., Watford, UK, with a resistivity of 18.2 MΩ/cm. 2,5-dihydroxybenzoic acid (DHB) and α-cyano-4-hydroxycinnamic acid (α-CHCA) were purchased from Sigma-Aldrich, Dorset, UK.

All metal salts and buffer salts were obtained from Sigma-Aldrich. Buffer solutions were prepared in Milli-Q water and the pH adjusted with concentrated aqueous HCl.

1,2-Dioleoyl-*sn*-glycero-3-phosphocholine (DOPC), 1,2-dioleoyl-*sn*-glycero-3-phosphoserine (DOPS), 1-oleoyl-2-palmitolyl-*sn*-glycero-3-phosphocholine (OPPC), egg phosphocholine from hen egg yolk (egg PC, product P2772, ≥ 99% purity) and soybean phosphocholine (soybean PC, product P3644, ≥ 30% purity) were Fluka brand, obtained from Sigma-Aldrich. 1,2-dimyristoyl-*sn*-glycero-3-phosphocholine (DMPC), 1,2-dipalmitoyl-*sn*-glycero-3-phosphocholine (DPPC), 1,2-dipalmitoyl-*sn*-glycero-3-phosphoethanolamine (DPPE) and 1,2-dioleoyl-*sn*-glycero-3-phosphoethanolamine (DOPE) were purchased from Bachem (UK) Ltd., St. Helens, UK. 1-palmitolyl-2-oleoyl-*sn*-glycero-3-phosphoethanolamine (POPE), 1-palmitolyl-2-oleoyl-*sn*-glycero-3-phosphocholine (POPC) and 1-palmitolyl-2-oleoyl-*sn*-glycero-3-phosphoglycerol (POPG) were obtained from Avanti Polar Lipids through Instruchemie B.V., The Netherlands. DMPG was Alexis brand, obtained from Enzo Life Sciences (UK) Ltd., Exeter, UK. N-(Lissamine Rhodamine B sulfonyl)-phosphatidylethanolamine (Rh-PE) and N-(7-nitro-2,1,3-benzoxadiazol-4-yl)-phosphatidylethanolamine (NBD-PE) were Molecular Probes brand, from Invitrogen, Paisley, UK. All lipids except POPG, soybean PC and egg PC were obtained as lyophilised solids. POPG and egg PC were obtained as solutions in CHCl$_3$ and soybean PC was obtained as a waxy solid. The mouse lipids were extracted from the lung tissue of freshly culled CD-1 mice by Helen McPhee. The tissue was frozen in liquid nitrogen and homogenized with a 2:1 (v/v) solution of CHCl$_3$/MeOH using a pestle and mortar, before filtering (Whatman grade no. 1 paper). The biphasic mixture was washed with 1–2 ml distilled water and the organic phase separated off. The interfacial liquid was washed again with water and a small quantity of CHCl$_3$/MeOH, which was separated off and added to the original organic phase.[1] All lipids were stored at -20 °C as

solids (DPPC, DPPE, DOPE, soybean PC) or solutions in $CHCl_3$ (POPG, POPC, DOPC, egg PC, mouse lipids, Rh-PE, NBD-PE) or $CHCl_3$/MeOH (10:2 (v/v)) (DMPG).

Defensin human neutrophil peptide-2 (HNP-2) was obtained from Bachem. Natural melittin was from Sigma-Aldrich and synthetic melittin Alexis brand from Enzo Life Sciences. All were obtained as lyophilised solids. HNP-2 was stored as a solid at -20 °C or as a solution in water at 4 °C. Melittin was stored as a solid or a solution in water at -20 °C. Haloperidol was obtained from Sigma-Aldrich and stored as a solid at -20 °C.

6.2   General methods

Unless otherwise stated, the following standard protocols were used.

6.2.1.1 MALDI-MS and MSMS analyses

MALDI-TOF-MS and MSMS analyses were carried out using an Autoflex II MALDI-TOF/TOF spectrometer with 337 nm nitrogen laser (Bruker Daltonics Ltd., Coventry, UK). The instrument was calibrated for MS analysis with the sodium adducts of poly(ethylene glycol) 600. A ground steel target plate was used, and cleaned with methanol and acetone before use. Positive and negative ion MS analyses were made using the reflectron. Positive ion MSMS experiments were made using the LIFT capability in the absence of a collision gas and at a source pressure of around 2.5×10^{-7} mBar. Data were analysed with Flex Analysis version 3.0 (Bruker Daltonics Ltd). DHB was used as a matrix for all MALDI experiments unless otherwise stated. In the absence of added salt DHB was prepared at 30 mg/mL in EtOH/H_2O (50:50 v/v). For experiments in the presence of lithium or sodium, DHB was prepared at 30 mg/mL in solutions of 100 mM LiCl or NaCl in EtOH/H_2O (50% (v/v)). Matrix solutions were mixed 9:1 (v/v) with lipid samples and 9:2 (v/v) with liposome samples, and 1 µL applied to a ground steel target plate and allowed to air dry. In order to achieve a thicker sample layer, for automated runs 2 x 0.5 µL were spotted on top of each other and allowed to air dry between applications.

6.2.1.2   Liposome preparation

Liposomes were prepared by evaporation of a solution of the lipid in $CHCl_3$ or $CHCl_3$/MeOH (10:2 (v/v)) to a thin film inside a round bottomed flask in vacuo. Lipid films were placed in a vacuum desiccator for a minimum of 2 hours before the addition of water or buffer. The flask was then vortexed and 5 freeze-thaw cycles carried out using liquid nitrogen and warm water. The lipid suspensions were extruded 10 times through laser-etched polycarbonate membranes (Whatman) with 100 nm pores using a LIPEX

thermobarrel extruder (Northern Lipids Inc., BC, Canada). The extruder was warmed to a temperature above the phase transition temperature of the lipids being prepared.

6.2.1.3 Least squares fitting

Non-linear least squares curve fitting was performed using the Solver function in Excel (Office 2007, Microsoft Corp.). Where weighted fitting is stated, the least squares value was weighted by multiplication by $\frac{1}{t^2}$, where t is the time of each scan at a given wavelength.

6.2.1.4 Preparation of images and manipulation of pdb files

Images of peptides were prepared using Pymol (DeLano Scientific, Palo Alto, CA, USA., (http://www.pymol.org/) and the orientation of HNP-2 dimers was manipulated using Pymol and Swiss-PdbViewer for use in Dichrocalc calculations.[2]

6.3 The identification of phospholipids by mass spectrometry

6.3.1 MSMS analyses

MSMS analyses using the collision-induced decay (CID) capability were carried out using argon as collision gas at a source pressure of approximately 8.5×10^{-7} mBar. MSMS experiments were carried out using the LIFT capability unless otherwise stated. Isolation of the protonated and sodium adduct parents was sufficient with instrument default settings. For LIFT of the lithium adducts of POPC and POPE, the isolation windows were set to exclude the protonated ion, and in the case of POPE the [POPE – H + 2Li]$^+$ ion also. For the automated LIFT analysis of [POPE + Li]$^+$ it was necessary to widen the window slightly to ensure fragmentation of the parent. For CID and for the LIFT analyses of OPPC the precursor ion isolation window could not be altered from the default setting of ± 1% of the parent m/z value due to constraints included in an upgrade of the software. The isolation windows are summarised in Table 5.1.

Table 5.1. Summary of precursor ion isolation windows for automated MSMS analyses.

	[POPC + H]$^+$ (Da)	[POPC + Na]$^+$ (Da)	[POPC + Li]$^+$ (Da)	[OPPC + H]$^+$ (Da)
LIFT	± 15	± 15	+ 9, − 5	± 8
CID	± 8	n/a	± 8	n/a
	[OPPC + Li]$^+$ (Da)	[POPE + H]$^+$ (Da)	[POPE + Na]$^+$ (Da)	[POPE + Li]$^+$ (Da)
LIFT	± 8	± 14	± 14	+ 6, − 7
CID	n/a	n/a	n/a	n/a

For experiments in the presence of lithium, DHB was prepared at 30 mg/mL in solutions of LiCl (5 to 100 mM in EtOH/H$_2$O (50% v/v)). Where added, LiCl was used at a concentration of 100 mM unless otherwise stated. For experiments in the presence of other salts, DHB was prepared at 30 mg/mL in solutions of NaCl (100 mM), CaCl$_2$ (4.5 mM), CuCl$_2$ (100 mM), MgCl$_2$ (100 mM) or ZnCl$_2$ (100 mM) in EtOH/H$_2$O (50% (v/v)).

6.3.2 MALDI imaging

For the MALDI imaging of thin layer chromatography (TLC) plates, 35 µL DOPC (1 mg/mL in CHCl$_3$) or 45 µL extracted mouse lung lipid (2 mg/mL in 50:50 MeOH/CHCl$_3$ (v/v)) or soybean PC (2 mg/mL in CHCl$_3$) were spotted onto aluminium-backed silica TLC plates (Merck brand from Sigma-Aldrich) and run in 25:25:25:10:9 (v/v) ethyl acetate/propan-2-ol/CHCL$_3$/MeOH/0.25% (w/v) KCl. A channel was ground out of a microscope-sized slice of steel to the combined depth of the TLC plate and double-sided adhesive carbon sheets (Agar Scientific, Essex, UK). TLC plates were allowed to dry for at least 30 minutes before cutting to size and sticking into the channel of the steel plate with a strip of adhesive tape. DHB matrix was dissolved at 100 mg/mL in ACN/H$_2$O (50% v/v), 100% EtOH, 100% MeOH or 100 mM LiCl in 100% EtOH. The matrices were generously applied to the plates by pipette, ensuring thorough coverage, quickly dried under a stream of argon, then another layer applied. The plates were allowed to dry thoroughly before MALDI analysis. TLC plates not analysed by MALDI were visualised by dipping in phosphomolybdic acid (20 wt. % in EtOH), allowing to air dry and heating until the appearance of spots.

6.4 The chemical stability of phospholipids

6.4.1 Preparation

DOPC and DPPC liposomes were prepared as in Section 5.2.1.2 in 10 mM bis-tris propane (pH 7), 10 mM tris (pH 7.4), Milli-Q water or 10 mM phosphate and 150 mM NaCl with and without 1 mM EDTA. Liposomes in 10 mM bis-tris propane (pH 7) or 10 mM tris (pH 7.4) were stored at 4 °C; liposomes in 10 mM phosphate and 150 mM NaCl with and without EDTA were stored 37 °C.

6.4.2 MS and MSMS analyses

MALDI-MS analyses of liposomes in the absence of melittin were carried out as described in Section 6.2.1.1.

The MALDI-MS analysis of the short-term action of natural melittin was carried out on an Ultraflex II MALDI-TOF/TOF spectrometer with 337 nm nitrogen laser (Bruker Daltonics Ltd.). The target plate and calibration were as in Section 6.2.1.1. 1 µL aliquots of a solution of DMPC liposomes (2.5 mg/mL in 10 mM bis-tris propane pH 7) with melittin concentration (0.1 mg/ml) were removed at 30 second intervals after the addition of the melittin and were immediately mixed with a solution of DHB (30 mg/mL in EtOH/H_2O (50% v/v)) to quench the hydrolysis. 1 µL aliquots of each sample/matrix solution were then spotted on the target plate and allowed to air dry. The information from 4000 laser shots was averaged for each sample spot.

For the long-term analyses of the effects of natural melittin on liposomes, melittin was mixed with DOPC liposomes (5:1 and 50:1 lipid:peptide (mol/mol)) in 10 mM phosphate and 150 mM NaCl (pH 7) with 1 mM EDTA to give final concentrations of 8 mM phosphate, 123 mM NaCl, 1 mM EDTA, 0.27 mg/mL DOPC and 0.16 mg/mL melittin with a 5:1 lipid:peptide molar ratio, and 10 mM phosphate, 147 mM NaCl, 1 mM EDTA, 0.32 mg/mL DOPC and 0.02 mg/mL melittin with a 50:1 lipid:peptide molar ratio. The samples were incubated at 37 °C and analysed as described in Section 6.2.1.1. A control sample was prepared in the absence of melittin and stored and analysed in the same way as the samples containing melittin.

For initial long-term analyses of the effects of synthetic melittin on liposomes, melittin was mixed with DOPC liposomes (5:1 and 50:1 lipid:peptide mol/mol) in 10 mM phosphate and 150 mM NaCl (pH 7) to give final concentrations of 8 mM phosphate, 123 mM NaCl, 0.27 mg/mL DOPC and 0.16 mg/mL melittin with a 5:1 lipid:peptide molar ratio, and 10 mM phosphate, 147 mM NaCl, 0.32 mg/mL DOPC and 0.02 mg/mL melittin with a 50:1 lipid:peptide molar ratio. The samples were incubated at 37 °C. Further analyses were carried out using 5:1 lipid:peptide (mol/mol) with DOPC or POPC liposomes in 8 mM phosphate and 123 mM NaCl (pH 7), 8 mM phosphate, 123 mM NaCl and 0.7 mM $CaCl_2$, $ZnCl_2$ or $MgCl_2$, or 10 mM phosphate (pH 7). In the presence of haloperidol-TFA (0.7 mM, pH 7), the buffer was 7 mM phosphate and 113 mM NaCl. Control samples were prepared in the absence of melittin. All samples were stored at 37 °C and analysed as described in Section 6.2.1.1.

For the MSMS analyses of melittin and modified melittin, samples were mixed 1:9 (v/v) with solutions of α-CHCA (20 mg/mL in 30:70 (v/v) ACN/H_2O (0.1% TFA)). MS analyses in the mass region of melittin were calibrated with the sodium adducts of poly(propylene glycol) 3000. All other details of the MALDI analyses were as described in Section 6.2.1.1.

The normalised intensity of the peak corresponding to lyso-PC was calculated using Equation 6.1 for DOPC

$$I_{nOPC} = I_{OPC} \div (I_{lipid} + I_{OPC})$$ **6.1**

and Equations 6.2 and 6.3 for POPC

$$I_{nOPC} = I_{OPC} \div (I_{lipid} + I_{OPC} + I_{PPC})$$ **6.2**

$$I_{nPPC} = I_{PPC} \div (I_{lipid} + I_{OPC} + I_{PPC})$$ **6.3**

where I_{lipid}, I_{OPC} and I_{PPC} are the absolute intensities of the peaks corresponding to the lipid molecular ion, lyso-OPC and lyso-PPC respectively and I_{nOPC} and I_{nPPC} are the normalised intensities of lyso-OPC and lyso-PPC respectively.

6.4.3 ^{1}H NMR

The ^{1}H NMR spectrum of DOPC was recorded at 700 MHz on a 10 mg sample dissolved in CDCl$_3$ using a Varian 700 NMR spectrometer (Varian, Inc., Palo Alto, USA).

6.4.4 Electron microscopy

Transmission electron microscopy (TEM) analysis was carried out using a Hitachi TEMH7600 transmission electron microscope in high resolution mode with an accelerating voltage of 80–100 kV. Liposome solutions were diluted to 0.5 mg/mL with Milli-Q water then 5 μL deposited on 400 mesh carbon film coated copper grids (Agar Scientific). After approximately 1 minute, the droplet was soaked up with filter paper from the edge of the grid. The process was repeated with 5 μL 1% uranyl acetate negative stain solution.

6.4.5 Dynamic light scattering

Dynamic light scattering (DLS) analyses were carried out using a ZetaPlus Zeta Potential Analyzer (Brookhaven Instruments Corporation, Holtsville, USA) in a 10 mm

pathlength cell. The liposome solutions were analysed without dilution and the diameter value is an average of the results of ten one minute runs.

6.4.6 Haloperidol-trifluoroacetic acid preparation and analysis with lipid

Haloperidol-trifluoroacetic acid was prepared according to the method of Casey *et al.*[3] Haloperidol (40 mg) was dissolved in TFA/DCM (4 mL) and stirred at room temperature for 1 hour. The solvents were removed under vacuum. DOPC (2.5 mg in $CHCl_3$) was dried to a thin film in vacuo in a round bottomed flask then placed in a vacuum desiccator overnight. Haloperidol-TFA (0.8 mg) was dissolved in 50:50 (v/v) MeOH/$CHCl_3$ (513 µL) and 50 µL of this solution (0.16 µmoles) used to dissolve the DOPC film. The solution was diluted with 150 µL 50:50 (v/v) MeOH/$CHCl_3$ and transferred to a 1 mL sample vial before drying to a film under vacuum and storing in a vacuum desiccator overnight. The film was rehydrated with 7.5 µL tris buffer (10 mM pH 7.4) and vortexed for 5 x 30 seconds to homogenise.

6.4.7 Thin layer chromatgraphy

For the TLC analysis of DOPC liposomes 17 days after the addition of melittin, DOPC liposomes with melittin (30 µL, 5:1 lipid:melittin molar ratio in 10 mM phosphate and 150 mM NaCl buffer), DOPC liposomes (30 µL, 0.33 mg/mL in 10 mM phosphate and 150 mM NaCl buffer), prepared and stored with melittin sample, and an aliquot of phosphate buffer (30 µL, 10 mM with 150 mM NaCl) were lyophilized and each redissolved in 15 µL MeOH/$CHCl_3$ (50:50 (v/v)). All of each redissolved sample was applied drop-wise to an aluminium-backed silica TLC plate (Merck brand from Sigma-Aldrich). DOPC lipid (5 µL, 0.5 mg/mL in $CHCl_3$) and a mixture of lyso-PC and oleic acid were also applied to the TLC plate in separate lanes. The TLC plate was run in 6:4:1 (v/v) $CHCl_3$, MeOH and H_2O and stained with phosphomolybdic acid (20 wt. % in EtOH) and heat.

6.5 The membrane binding of defensin HNP-2

6.5.1 Protein concentration determination

The concentration of HNP-2 was determined before each set of experiments using UV analysis. A blank spectrum was recorded of 3 mL water in a quartz cuvette from 200-350 nm. Four additions of 5 mL HNP-2 were made to the 3 mL water and a spectrum recorded after each addition. The concentration of the peptide was then calculated using

the absorbance at 280 nm using the following equations, where A is the observed absorbance at 280 nm and A_{corr} is the corrected absorbance allowing for the change in volume after each addition of peptide solution. V_0 is the initial volume of water in the cuvette and V is the volume of peptide solution added.

$$A_{corr} = A\left(\frac{V_0 + V}{V_0}\right)$$
(6.4)

The concentration of the peptide solution, x, is then given by Equation 6.5, where c is the overall concentration in the cuvette.

$$x = c \times \frac{V}{V_0}$$
(6.5)

Equation 6.5 can be rearranged to give Equation 6.6.

$$c = \frac{xV}{V_0}$$
(6.6)

This can then be combined with the Beer–Lambert law to give Equation 6.7, where ε is the extinction coefficient of the peptide.

$$A_{corr} = \frac{\varepsilon x V}{V_0}$$
(6.7)

A plot of A_{corr} against V has a gradient of $\varepsilon x / V_0$. This allows x to be calculated, provided ε and V_0 are known. The extinction coefficient of HNP-2 was calculated using the ProtParam tool from the ExPASy Proteomics Server.[4] The ProtParam tool calculates extinction coefficients using the equation

$$\varepsilon(prot) = N(Tyr) \cdot \varepsilon(Tyr) + N(Trp) \cdot \varepsilon(Trp) + N(Cystine) \cdot \varepsilon(Cystine)$$

(6.8)

where $\varepsilon(Tyr) = 1490$, $\varepsilon(Trp) = 5500$ and $\varepsilon(cystine) = 125$ M^{-1} cm^{-1}, noting that in HNP-2 all cysteine residues are involved in disulphide bonds and are therefore present as half cystines, and N corresponds to the number of each residue. The extinction coefficient of HNP-2 was calculated as 10345 M^{-1} cm^{-1}.

6.5.2   Dynamic light scattering

DLS experiments were carried out using a Zetasizer Nano ZS (Malvern Instruments Ltd., Malvern, UK) with a 3 mm pathlength cell. For the determination of the phase transition temperature, 50 µL aliquots of liposome solutions (2 mg/ml, H_2O) were heated from 10 °C to 40 °C or 60 °C at 0.5 °C intervals. The samples were equilibrated

for 5 minutes before the start of the analyses, then for 1 minute at each temperature. The attenuator, sample position and number of repeat analyses (within a range of 15–17) were automatically optimised at each temperature. A fresh aliquot of liposome solution was used for each set of measurements. Diameter measurements before and after the addition of defensin were averaged from 71 individual measurements at 21 °C on the same instrument.

6.5.3   Differential scanning calorimetry

DSC analysis of DMPG was carried out using a PerkinElmer Pyrus 1 calorimeter (PerkinElmer, Cambridge, UK). Solid DMPG (1.204 mg) was sealed in an aluminium pan with a drop of water and taken through three heating and cooling cycles between 0 and 60 °C, heating at 4 °C/minute.

6.5.4   Dimer binding analysis

The dimer binding equilibrium was calculated from data obtained on an ISA Jobin-Yvon Spex Fluorolog-3 luminescent spectrometer (Horiba Jobin Yvon Ltd., Middlesex, UK) with an array photon multiplier tube using DataMax v2.20 software. The data for 1–39 μM HNP-2 was collected by adding 30 aliquots of 2 μL HNP-2 to 60 μL H_2O Two spectra were recorded after each addition with the results averaged. For the lower concentration range, a solution of 1.5 μM HNP-2 was increasingly diluted by the addition of H_2O and the data from two spectra averaged at each concentration. All analyses were carried out with an excitation wavelength of 280 nm, 3 nm excitation and emission bandwidths and a 3 mm pathlength.

6.5.5   Fluorescence resonance energy transfer

The FRET experiment was carried out using an LS 55 fluorimeter (Perkin Elmer, Cambridge, UK) with a mesh photomultiplier tube with FL Winlab 95 software. The excitation and emission bandwidths were 2.5 nm and the pathlength was 3 mm. 50:50 (w/w) POPG/DOPC liposomes and 50:50 (w/w) POPG/DOPC liposomes with 0.5 mol % each of Rh-PE and NBD-PE were prepared at 4 mg/mL in H_2O as in Section 6.2.1.2. Labelled and unlabelled liposomes were mixed 3:1 (v/v) for analyses and used at a final concentration of 1.4 mM. 60 measurements were made at 5 minute intervals in the presence and absence of 15 μM HNP-2. 45 μL of a 0.1% solution of Triton X-100 was added to 1.4 mM liposomes with and without 15 μM HNP-2 to give a final concentration of 1.2 mM Triton X-100 for the spectra of lysed liposomes. A baseline spectrum of unlabelled liposomes was recorded and subtracted from all other measurements.

6.5.6 Fluorescence analysis in MeOH and kinetic analysis

HNP-2 (15 µM) in 75% MeOH was analysed on a Jasco FP-6500 fluorimeter (Jasco UK, Great Dunmow, UK) with 2.5 nm excitation and emission bandwidths and a 3 mm pathlength. The kinetic analysis was also performed using the FP-6500 fluorimeter. HNP-2 (15 µM) and 50:50 (w/w) POPG/DOPC liposomes (1.4 mM) were analysed at 2.5 minute intervals for 5 hours with a scan speed of 200 nm/min with excitation at 280 nm and a 3 mm pathlength.

6.5.7 Linear dichroism

Linear dichroism (LD) measurements were performed using a Jasco J-815 spectropolarimeter (Jasco UK) using Jasco Spectra Manager version 1.53.01 software, in a microvolume Couette flow cell (Crystal Precision Optics, Rugby, UK; now available from Kromatek Ltd., Great Dunmow, UK).[5] The Couette cell was rotated at ~3000 rpm (3.0 V). Analyses were carried out with 15 µM HNP-2 and 1.4 mM (50:50 (w/w) POPG/DOPC and DMPG/DMPC) or 1.05 mM (50:50 (w/w) DOPS/DOPC) liposomes. Spectra were recorded at 5 minute intervals over 5 hours at a scan speed of 50 nm/minute with a response time of 2 seconds and a data pitch of 0.2 nm.

Model LD spectra of HNP-2 were obtained using Dichrocalc v3.3 software through the web interface (http://comp.chem.nottingham.ac.uk/dichrocalc/).[6–9] All model spectra were inverted before comparison with measured spectra as explained in Section 4.2.8.1.

6.6 References

1. H.K. McPhee, Ph.D. Thesis, Durham University, 2009.

2. N. Guex and M.C. Peitsch, *Electrophoresis*, 1997, **18**, 2714–2723, (http://www.expasy.org/spdbv/).

3. D.R. Casey, S.C. Sebai, G.C. Shearman, O. Ces, R.V. Law and R.H. Templer, *Ind. Eng. Chem. Res.*, 2008, **47**, 650–655.

4. E. Gasteiger, C. Hoogland, A. Gattiker, S. Duvaud, M.R. Wilkins, R.D. Appel, A. Bairoch in *The Proteomics Protocols Handbook*, ed. John M. Walker, Humana Press,New York, USA, 2005, pp. 571-607.

5. R. Marrington, T.R. Dafforn, D.J. Halsall, J.I. MacDonald, M. Hicks and A. Rodger. *Analyst*, 2005, **130**, 1608–1616.

6. B.M. Bulheller & J.D. Hirst, *Bioinformatics*, 2009, **25**, 539–540.

7. N.A. Besley & J.D. Hirst, *J. Am. Chem. Soc.*, 1999, **121**, 9636–9644.

8. D.M. Rogers & J.D. Hirst, *J. Phys. Chem. A*, 2003, **107**, 11191–11200.

9. M.T. Oakley & J.D. Hirst, *J. Am. Chem. Soc*, 2006, **128**, 12414–12415.

Appendix 1: MALDI-MSMS spectra of acylated melittin
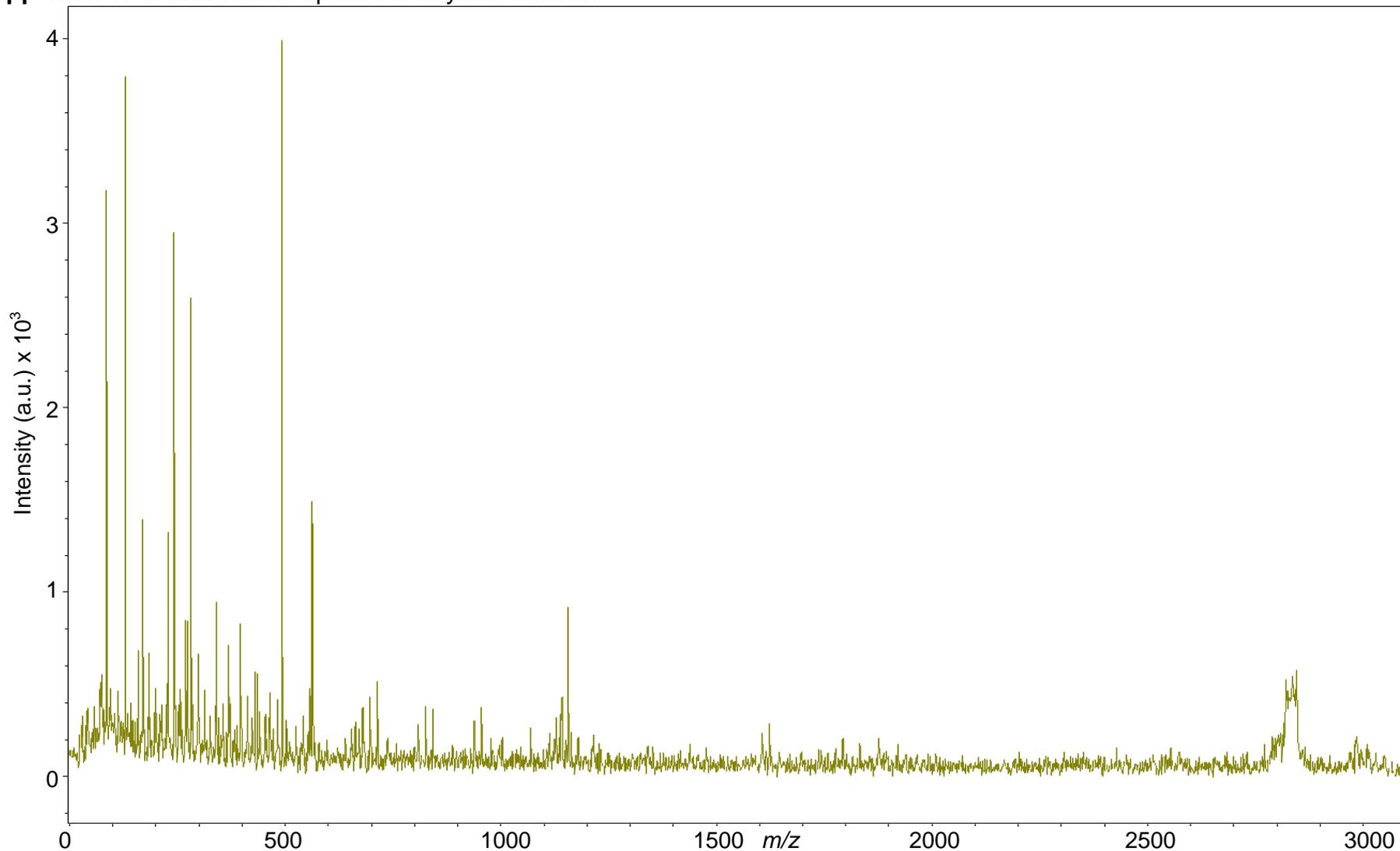
A) MALDI-MSMS spectrum of [melittin + $R_{18:0}CO$]$^+$ from melittin with DOPC. The sample was prepared by mixing the melittin and liposome dispersion (1:5 peptide:lipid molar ratio) 1:9 (v/v) with solutions of α-CHCA (20 mg/mL in 30:70 (v/v) ACN/H2O (0.1% TFA)).
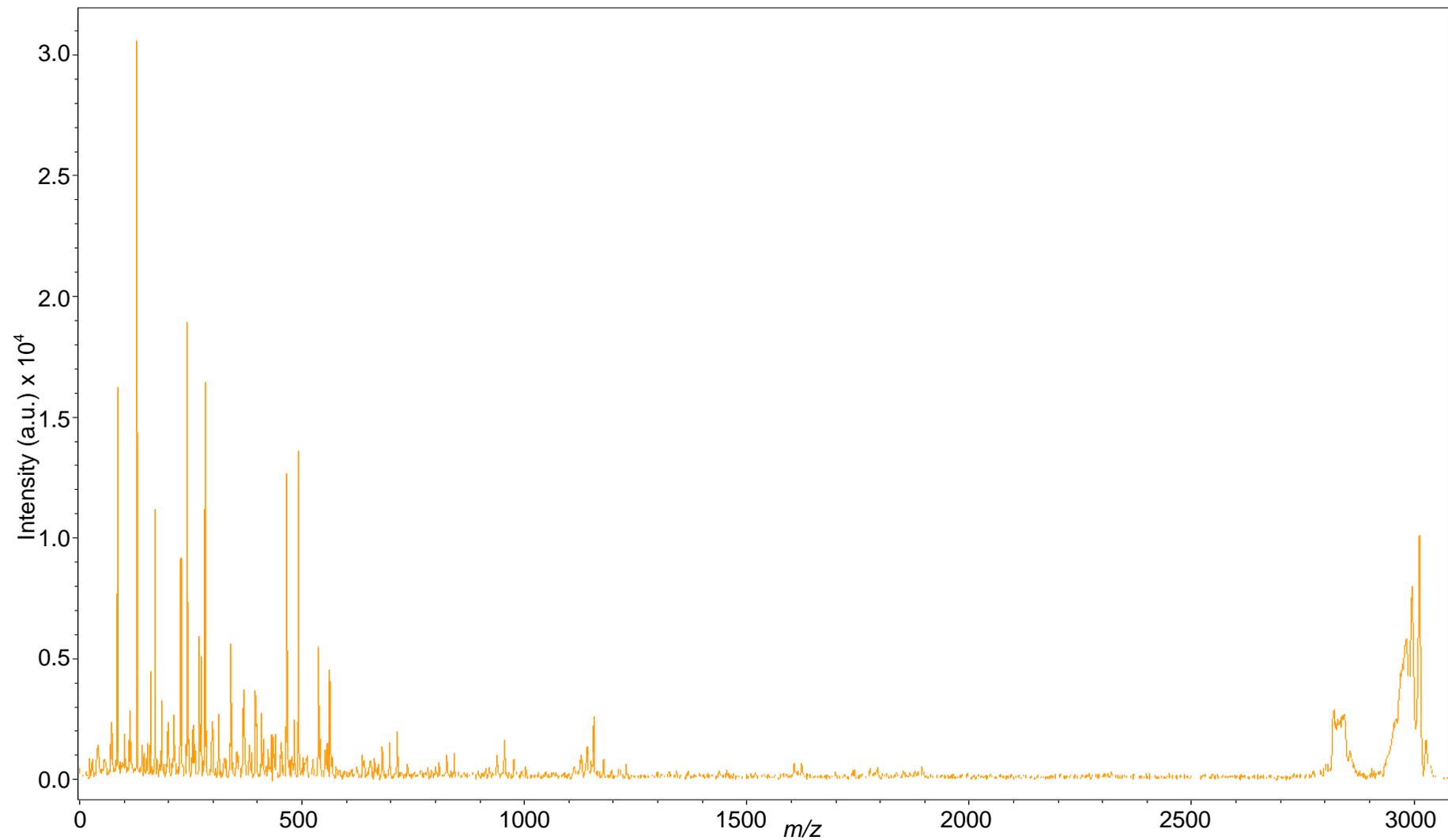
B) MALDI-MSMS spectrum of [melittin + R$_{16:1}$CO]$^+$ from melittin with POPC. The sample was prepared by mixing the melittin and liposome dispersion (1:5 peptide:lipid molar ratio) 1:9 (v/v) with solutions of α-CHCA (20 mg/mL in 30:70 (v/v) ACN/H2O (0.1% TFA)).
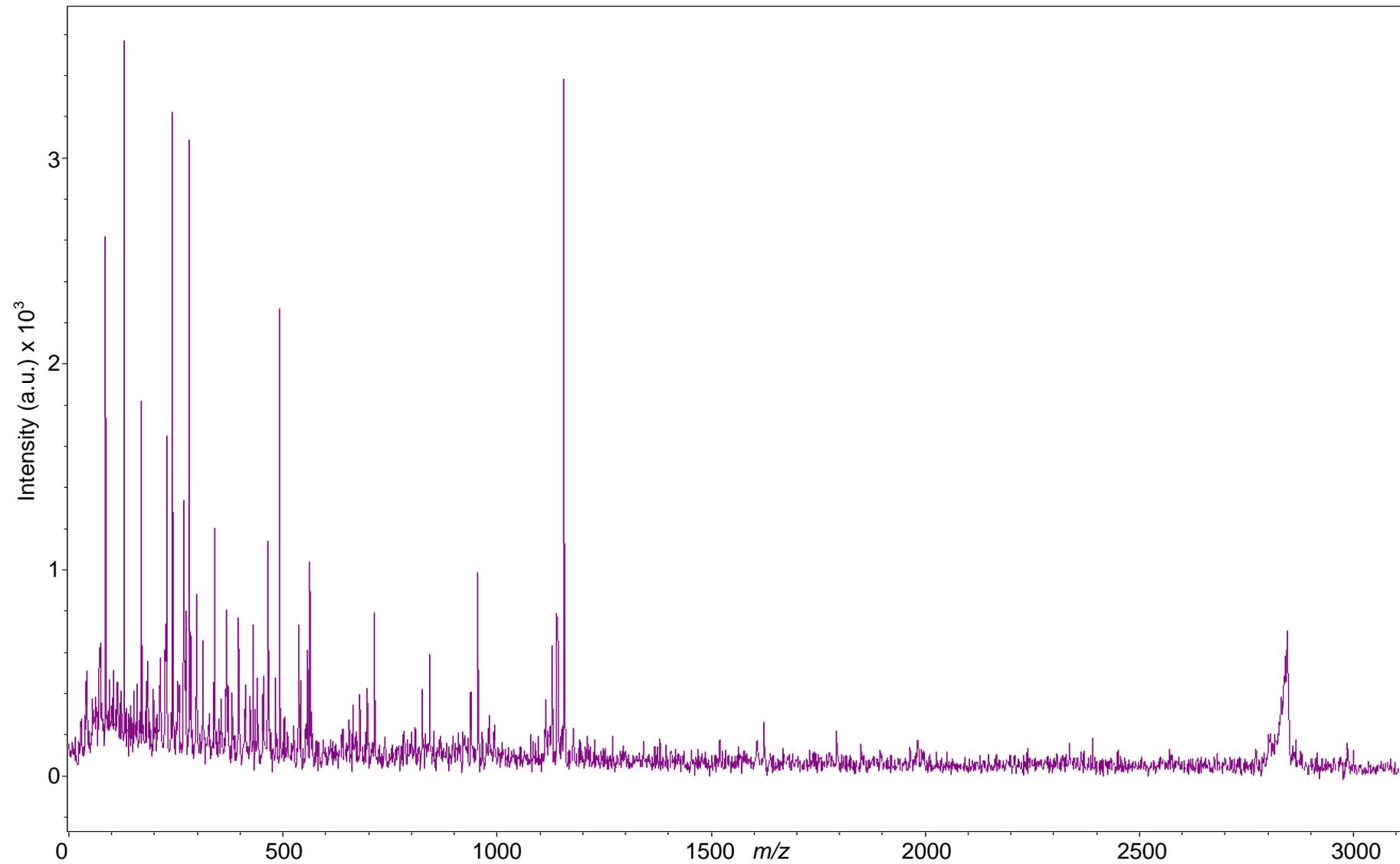
C) MALDI-MSMS spectrum of [melittin + R$_{18:0}$CO]$^+$ from melittin with POPC. The sample was prepared by mixing the melittin and liposome dispersion (1:5 peptide:lipid molar ratio) 1:9 (v/v) with solutions of α-CHCA (20 mg/mL in 30:70 (v/v) ACN/H2O (0.1% TFA)).

271

Appendix 2: Residuals of the least-squares fitting of LD data to the 3-state kinetic model
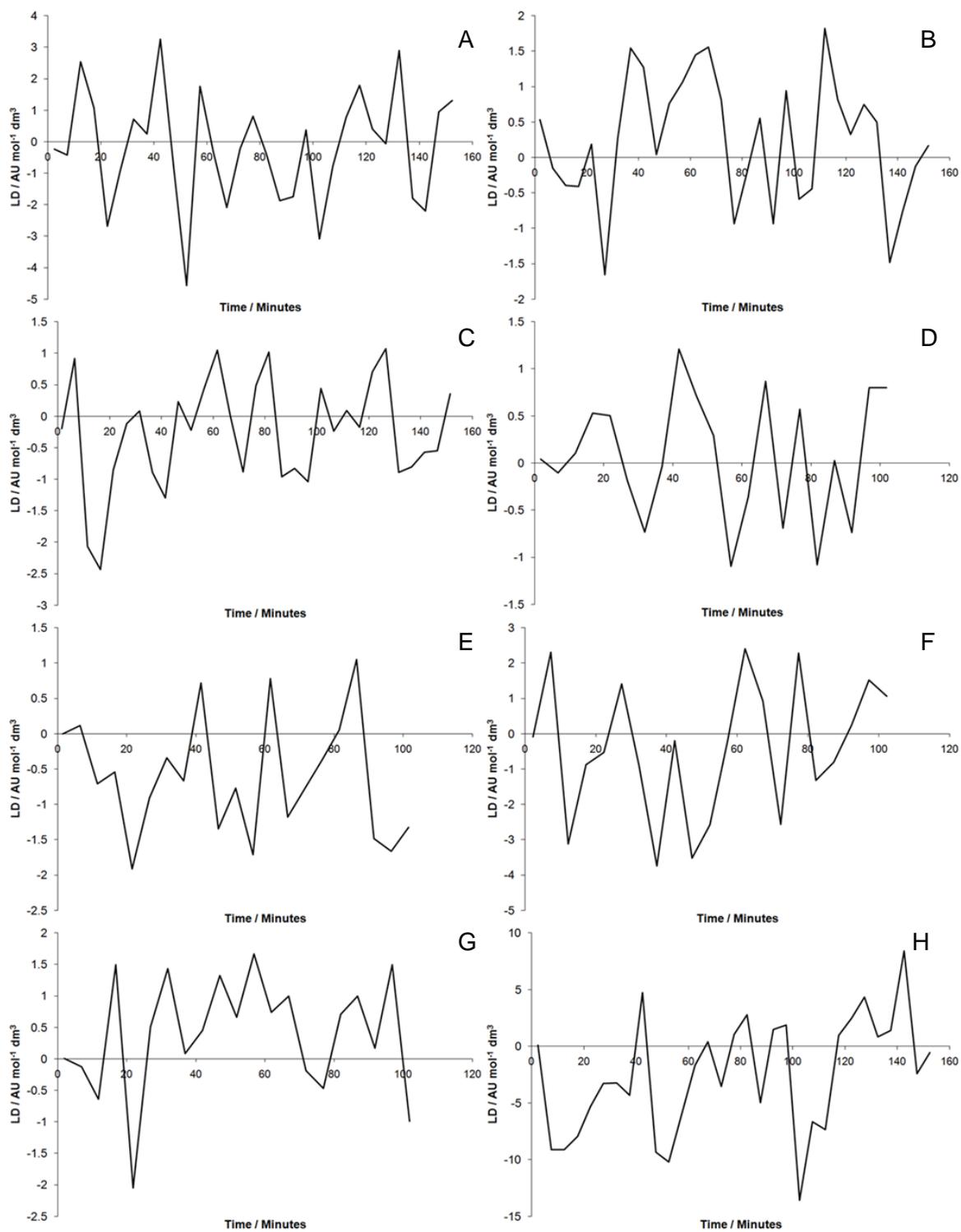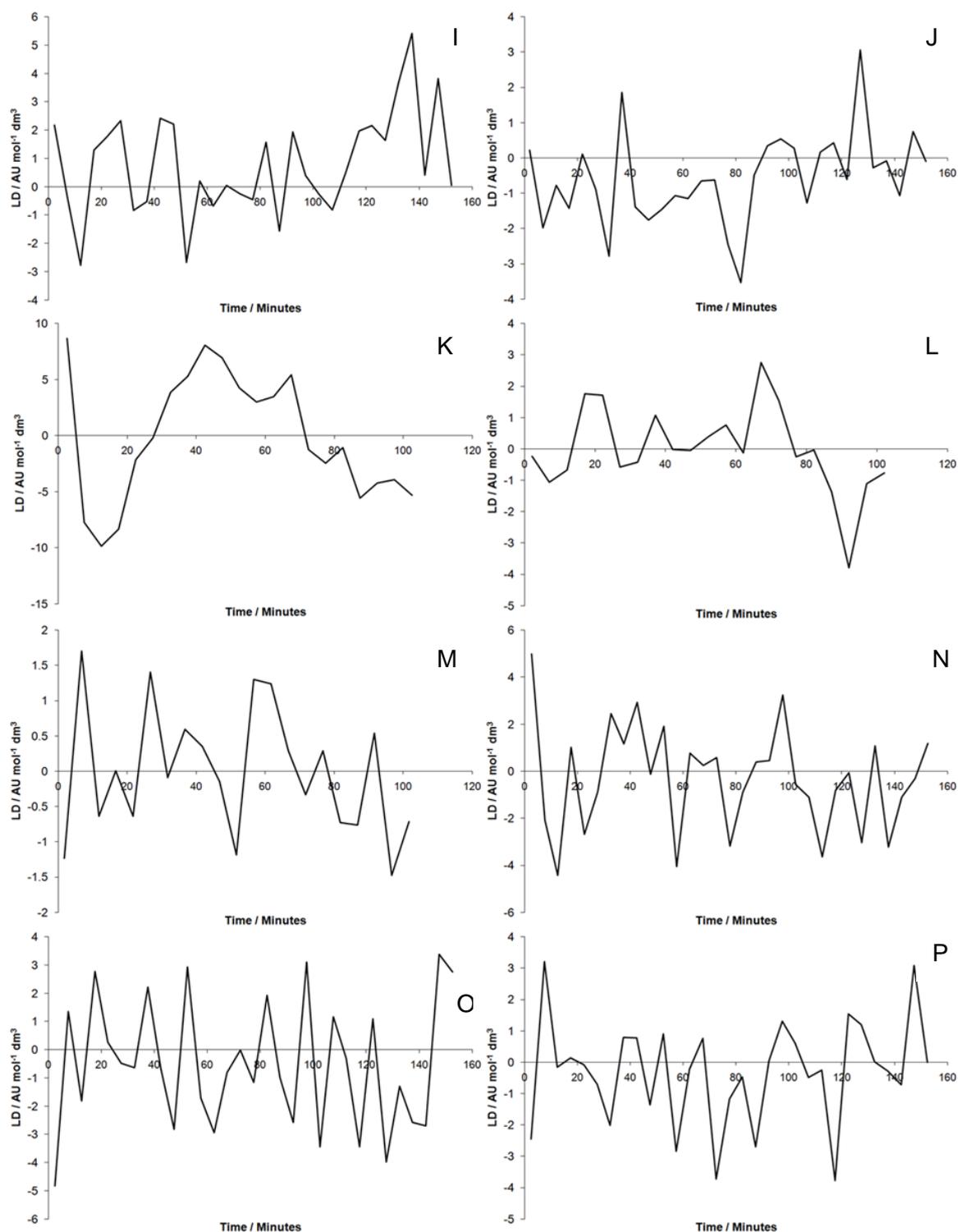
Appendix 2. Residuals of the least-squares fitting of LD data to the 3-state kinetic model described in Section 4.2.6.2. A–C) 50:50 (w/w) POPG/DOPC 30 °C at 200, 225 and 245 nm; D–E) 50:50 (w/w) POPG/DOPC 40 °C at 230 and 245 nm; F–G) 50:50 (w/w) POPG/DOPC 53 °C at 206 and 228 nm; H–J) 50:50 (w/w) DOPS/DOPC 30 °C at 194, 209 and 224 nm; K–M) 50:50 (w/w) DMPG/DMPC 17 °C at 196, 215 and 235 nm and N–P) 50:50 (w/w) DMPG/DMPC 33 °C at 188, 194 and 198 nm.

Appendix 3: LD spectra of the P_{m1} and P_{m2} states of HNP-2 with closest-fit calculated spectra
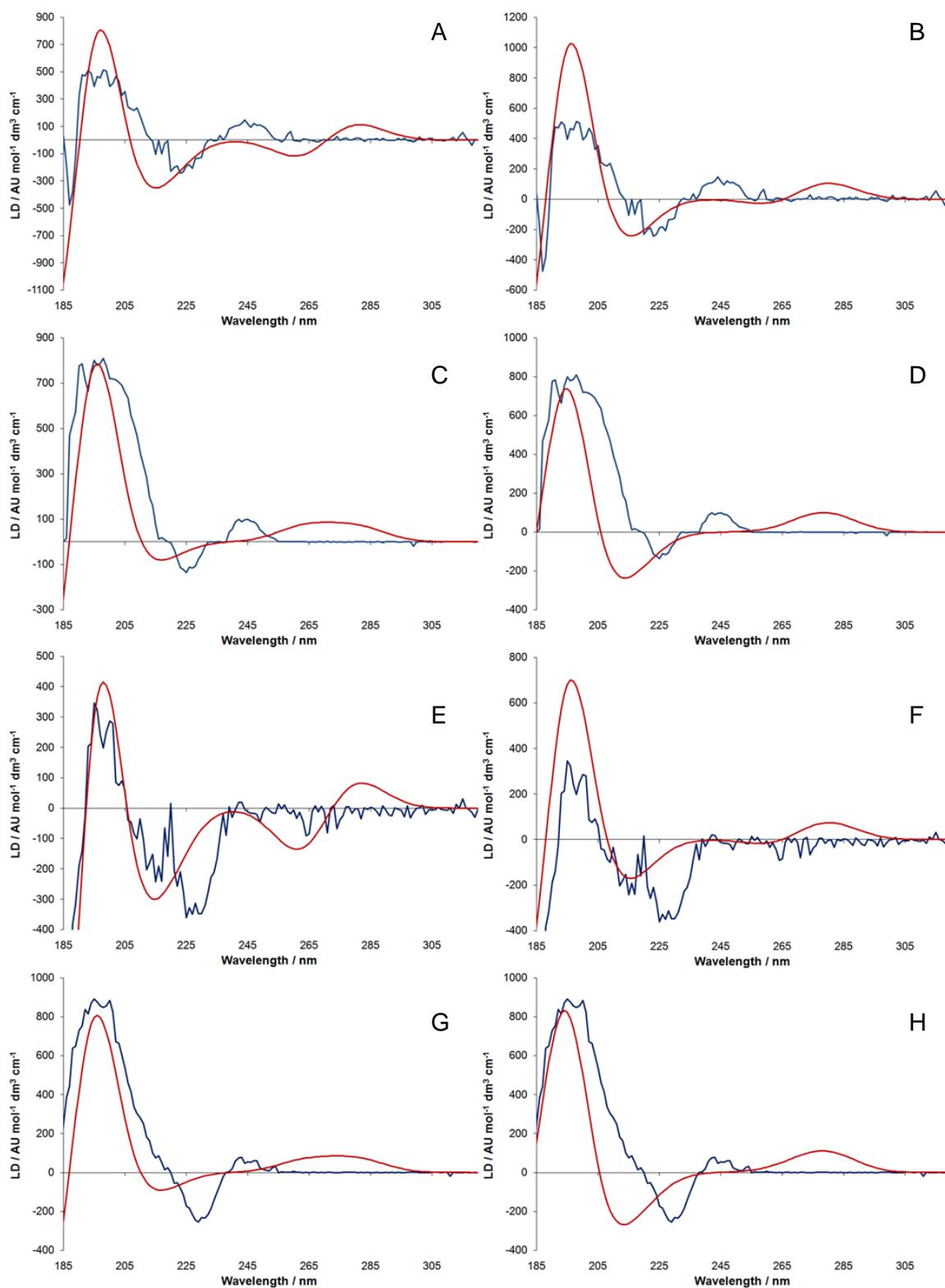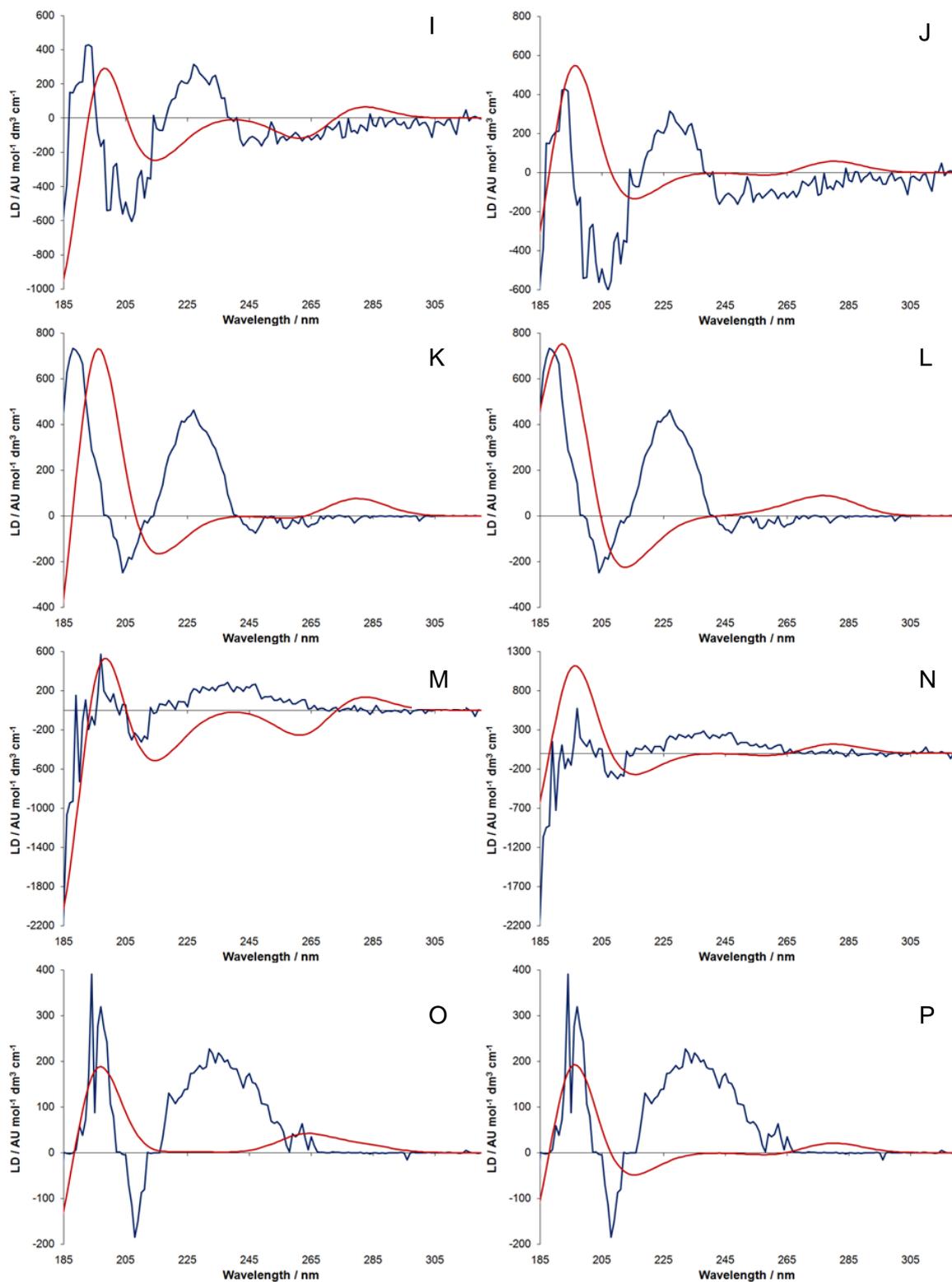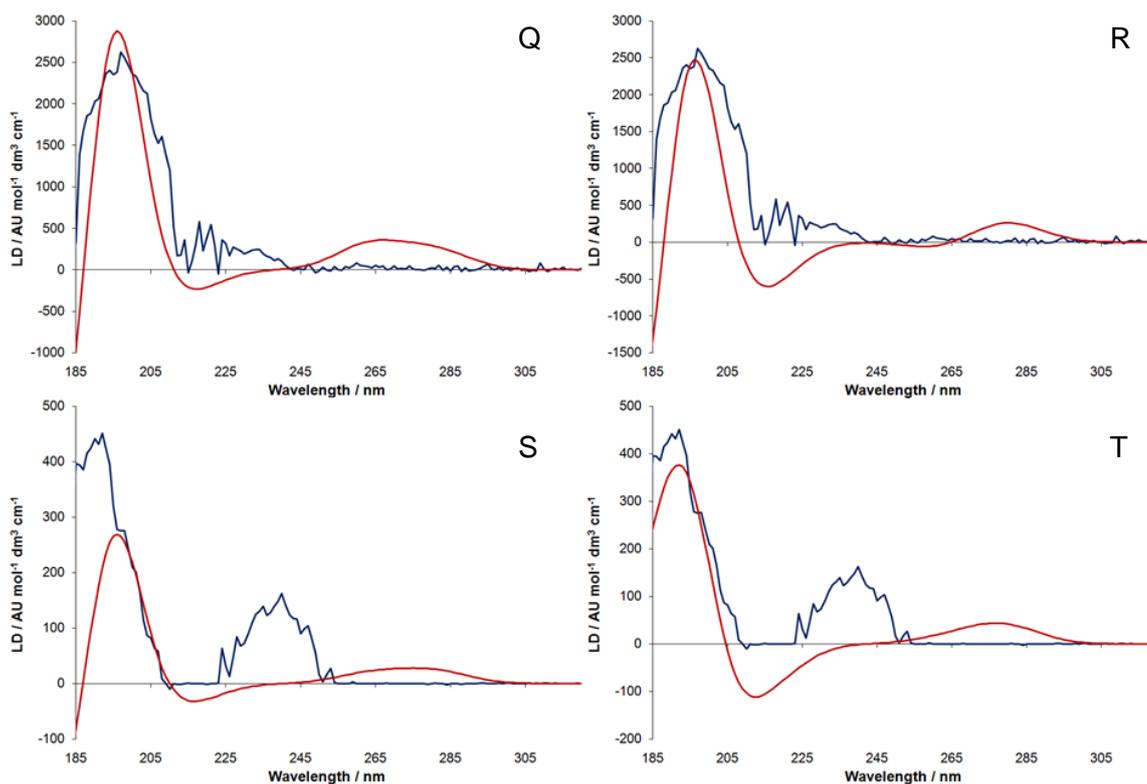
Appendix 3. LD spectra of the P_{m1} and P_{m2} states of HNP-2 (blue) with closest-fit calculated spectra determined through least squares fitting using Equation 4.52 (red). A–D) Spectra of P_{m1} with best fit spectra for rotation around δ and ψ and spectra of P_{m2} with best fit spectra for rotation around δ and ψ respectively for binding to 50:50 (w/w) POPG/DOPC at 30 °C; E–H) Spectra of P_{m1} with best fit spectra for rotation around δ and ψ and spectra of LD_{m2} with best fit spectra for rotation around δ and ψ respectively for binding to 50:50 (w/w) POPG/DOPC at 40 °C; I–L) Spectra of LD_{m1} with best fit spectra for rotation around δ and ψ and spectra of P_{m2} with best fit spectra for rotation around δ and ψ respectively for binding to 50:50 (w/w) POPG/DOPC at 53 °C; M–P) Spectra of P_{m1} with best fit spectra for rotation around δ and ψ and spectra of P_{m2} with best fit spectra for rotation around δ and ψ respectively for binding to 50:50 (w/w) DOPS/DOPC at 30 °C and Q–T) Spectra of P_{m1} with best fit spectra for rotation around δ and ψ and spectra of P_{m2} with best fit spectra for rotation around δ and ψ respectively for binding to 50:50 (w/w) DMPG/DMPC at 33 °C.

Appendix 4: Published papers

S. M. Ennaceur, M. R. Hicks, C. J. Pridmore, T. R. Dafforn, A. Rodger and J. M. Sanderson, *Biophys. J.*, 2009, **96**, 1399–1407.

A. Damianoglou, A. Rodger, C. Pridmore, T. R. Dafforn, J. A. Mosely, J. M. Sanderson and M. R. Hicks, *Protein Pept. Lett.,* 2010, **17**, 1351–1362.

C. J. Pridmore, J. A. Mosely, A. Rodger and J. M. Sanderson, *Chem. Commun.,* 2011, **47**, 1422–1424.

C. J. Pridmore, J. A. Mosely and J. M. Sanderson, *Analyst*, DOI: 10.1039/C0AN00436G.

Peptide Adsorption to Lipid Bilayers: Slow Processes Revealed by Linear Dichroism Spectroscopy

Sue M. Ennaceur,[†] Matthew R. Hicks,[‡] Catherine J. Pridmore,[†] Tim R. Dafforn,[§] Alison Rodger,[‡] and John M. Sanderson[†]*

[†]Department of Chemistry, University Science Laboratories, Durham, DH1 3LE, United Kingdom; [‡]Department of Chemistry, University of Warwick, Coventry, CV4 7AL, United Kingdom; and [§]School of Biosciences, University of Birmingham, Edgbaston, Birmingham, B15 2TT, United Kingdom

ABSTRACT   The adsorption and insertion kinetics for the association of two 34-residue cyclic peptides with phosphocholine membranes have been studied using circular and linear dichroism approaches. The two peptides studied are identical with the exception of two residues, which are both tyrosine in one of the peptides and tryptophan in the other. Both peptides adopt random coil conformations in solution in the absence of membranes and do not aggregate at concentrations below 20 μM. After addition to liposome dispersions, circular dichroism spectroscopy indicated that both peptides undergo an extremely rapid transformation to a β-conformation that remains unchanged throughout the remainder of the experiment. Linear dichroism (LD) spectroscopy was used to study the kinetics of membrane adsorption and insertion. The data were analyzed by nonlinear least squares approaches, leading to identification of a number of bound states and their corresponding LD spectra. Two pseudo-first order processes could be identified that were common to both peptides. The first occurred with a time constant of the order of 1 min and led to a bound state characterized by weak LD signals, with significant bands corresponding to the transitions of aromatic side chains. The second process occurred with an unusually long time constant of between 75 and 100 min, forming a state with considerably stronger positive LD absorbance in the far-ultraviolet region of the spectrum. For the tyrosine-substituted peptide, a third slow process with a long time constant (76 min) could also be delineated and was attributed to rearrangements of the peptide within the membrane.

INTRODUCTION

There has been much speculation in recent years concerning the roles of aromatic amino acids in the interactions of proteins and peptides with lipid bilayers (1–4). Recent studies have suggested that tryptophan in particular, has significant interactions with lipids, using the hydrogen bonding donor potential of the indole ring combined with a possible role for cation-π interactions of the large aromatic ring system (5,6). Tyrosine has also been found to have significant interactions with phospholipid headgroups (5,1,2).

From data produced by studies on model transmembrane peptides (7,8) it is clear that tryptophan plays a key role in membrane anchoring, with NMR evidence suggesting that the indole group of the tryptophan side chain interacts with lipid acyl carbonyl groups (9); recent experiments with ether lipids have shown similar peptide behaviors to those observed with acyl lipids (10). These experiments, however, have been generally restricted to transmembrane species that are helical in nature. Systematic studies on model transmembrane β-peptides have been conducted less frequently, despite the relative abundance of stable membrane proteins and antimicrobial peptides rich in β-structure. Experiments on short tryptophan- and leucine-rich β-sheet peptides have highlighted the particular importance of hydrogen bond

formation in the low dielectric membrane environment (11,12), and shown that significant changes in behavior can occur in response to single amino acid changes, particularly concerning substitutions for tryptophan. Similar modifications to the membrane activities of β-sheet peptides after single amino acid substitutions for tryptophan have been shown elsewhere (13), raising questions with regard to the mechanisms that control the membrane insertion and stability of peptides.

To obtain mechanistic information, it is desirable to have access to both kinetic and structural information during the insertion process itself. Circular dichroism (CD) spectroscopy has proved to be a useful tool for monitoring the conformations of peptides in membrane-associated and free forms, but does not show information concerning the location of the peptide within the membrane. Oriented CD (14–18) and linear dichroism (LD) approaches have been used to address this concern. LD shows the orientation of electronic transitions with respect to the experimental frame of reference and can therefore furnish information on the orientation of peptides with respect to membranes, provided that the latter can be aligned. The development of a low volume Couette cell (19,20) has allowed facile measurement of LD spectra from membrane-bound species in shear-aligned liposomes (21,22). This has been used to study the alignments of cell-penetrating peptides and was able to correlate reduced membrane penetrating ability with α-helix alignment in the plane of the membrane (23). Combined CD

and LD studies on gramicidin have enabled probing of the tryptophan side chains in the $\beta 6.3$ conformation of the peptide, with the axis of the peptide found to align along the bilayer normal and the tryptophan side chains to adopt orientations away from the plane of the membrane (21). This approach therefore has the potential to allow both peptide structure and membrane alignment to be probed as a function of time, enabling insertion kinetics to be determined with greater certainty.

In previous work (24), we described a cyclic peptide system that was able to porate liposomal membranes with high efficacy. In this study, we describe spectroscopic experiments concerning this and a related peptide (Fig. 1) that show that these peptides undergo a range of kinetic processes after binding to membranes, some of which exhibit much slower kinetics than anticipated. The data further highlight the differential effects of tyrosine and tryptophan in relation to membrane anchoring and shows the potential for deconvoluting LD data to reveal details of intermediate states in the insertion process.

MATERIALS AND METHODS

Materials

All amino acids, benzotriazole-1-yl-oxy-tris-pyrrolidino-phosphonium hexafluorophosphate (PyBOP) and the solid support (Novasyn TGR) were purchased from Novabiochem (Nottingham, UK). 1,1,1,3,3,3-Hexafluoroisopropanol (HFIP) and 2,2,2-trifluoroethanol (TFE) were purchased from Fluorochem (Glossop, UK) and distilled before use. All other solvents and reagents, including N,N-dimethylformamide (DMF), 1-hydroxybenzotriazole (HOBt), N,N-diisopropylethylamine (DIEA), N-methylmorpholine (NMM), N,N-diethyldithiocarbamate, sodium salt (DEDC), trifluoroacetic acid (TFA), 1,2-ethanedithiol (EDT), triisopropylsilane (TIS) and 2-(4-hydroxyphenylazo)benzoic acid (HABA) were purchased from Aldrich (Gillingham, UK), Fisher Scientific (Loughborough, UK), or Lancaster Synthesis (Heysham, UK) and used without further purification.

For liposome preparation, egg phosphatidylcholine (EPC; 100 mg/mL in chloroform) was purchased from Sigma (Gillingham, UK) and 100 nm laser-etched polycarbonate membranes from Whatman (Maidstone, UK).

Peptide chain assembly

Peptides **1** and **2** were synthesized by batch solid-phase peptide synthesis under a nitrogen atmosphere at room temperature on an Advanced Chemtech 348Ω synthesizer using a Novasyn TGR solid support (0.29 mmol/g; 0.10 g, 0.03 mmol) and Fmoc protection strategies. Coupling of amino acids was carried out for 1 h in DMF (2.5 mL) using PyBOP (5 eq) in the presence of HOBt (5 eq) and DIEA (10 eq). Deprotection between cycles was con-

ducted with 20% v/v piperidine in DMF (2×2 mL). The solid support was washed with DMF after each coupling and Fmoc-deprotection step (2×2.5 mL and 4×2.5 mL respectively). In the first cycle, N-α-Fmoc-L-aspartic acid α-allyl ester (Fmoc-Asp-OAll) was double-coupled to the solid support. Valine, leucine, tryptophan, and tyrosine residues were added as pseudoproline dipeptides (Fmoc-Val-Ser($\psi^{Me,Me}$Pro)-OH, Fmoc-Leu-Ser($\psi^{Me,Me}$Pro)-OH, Fmoc-Trp(Boc)-Ser($\psi^{Me,Me}$Pro)-OH, Fmoc-Tyr(^{t}Bu)-Ser($\psi^{Me,Me}$Pro)-OH) (25). After peptide assembly, a small portion (~5 mg) of the resin was removed for analysis.

Peptide cyclization

The resin was washed with CH_2Cl_2 (3×2 mL) and then treated with CH_2Cl_2 (2 mL) and a freshly prepared solution of tetrakis(triphenylphosphine)palladium(0) in $CHCl_3$/AcOH/NMM (37:2:1; 30 mM, 1.5 mL) (26). The mixture was agitated for 2 h at room temperature before being washed successively with DIEA (0.5 M in DMF, 3.3 mL), DEDC (0.3 M in DMF, 2.5 mL), and DMF (2×3 mL). The resin was then treated with a solution of DIEA (0.026 g, 0.15 mmol), HOBt (0.023 g, 0.15 mmol), and PyBOP (0.078 g, 0.15 mmol) in DMF (3 mL) for 5 h at room temperature before being washed successively with DMF (4×1.5 mL), MeOH (5×2 mL), and CH_2Cl_2 (5×2 mL) and dried under a stream of nitrogen for 30 min. This yielded 0.19 g and 0.18 g of peptide-bound resin for peptides **1** and **2** respectively.

Cleavage of peptides from the solid support

Cleavage of the peptide was conducted when necessary by treating portions of the resin (50 mg) with a mixture of TFA/water/EDT/TIS (9.5:0.25:0.25:0.1; 1 mL) for 4 h at room temperature. The mixture was then filtered and the resin washed with TFA (3×0.5 mL). The combined filtrants were treated with dry diethyl ether (20 mL) and cooled to 0°C. The precipitate was pelleted by centrifugation at $14,000 \times g$ for 10 min and triturated with diethyl ether (20 mL) before repeating the centrifugation/trituration process a further two times and drying the pellet in vacuo to give the crude product.

Peptide purification and analysis

The crude product was dissolved in TFE (1.5 mL) for purification. Three eluants were used for HPLC purification: 80% HFIP/TFE (10% v/v; eluant A), TFA/MeCN (0.1% v/v; eluant B), and 20% TFA/water (0.1% v/v; eluant C). HFIP and TFE were obtained from Fluorochem and distilled before use. Other solvents were of HPLC grade from Fisher Scientific. Chromatography was carried out on a Supelcosil LC-8 (C_8) column (Supelco; 25 cm $\times$ 1 cm) using isocratic elution between 0 and 6 min with an eluant composition of 80% A and 20% C, followed by a linear gradient between 6–9 min of 80%–50% A, 0%–50% B, and 20%–0% C. The flow rate was 2 mL/min throughout. Retention times were 7.23 min (**1**) and 6.56 min (**2**). Fractions corresponding to the top of peaks in the elution profile were collected manually, pooled and concentrated in vacuo before being rechromatographed. Fractions from the base of peaks were pooled separately and subjected to a further two rounds of chromatography, producing final yields of 0.6 μmol (19%) for **1** and 0.2 μmol (12%) for **2**, (based on the maximum
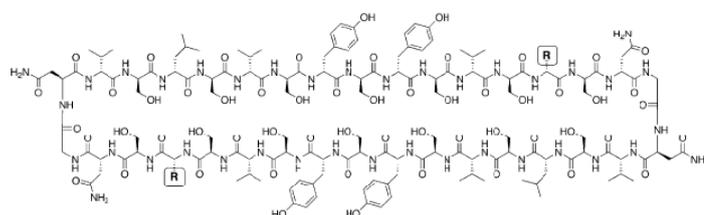
FIGURE 1   Structures of the cyclic peptides described in this study.

1 R = -CH$_2$C$_6$H$_4$OH; **2** R = 3-indole

theoretical yield for 50 mg of resin). Peptides were analyzed by MALDI mass spectrometry on a Voyager-DE STR apparatus using a stainless steel target. Peptides and matrix (HABA) were codissolved in HFIP at a molar ratio of 1:1400 to 1:3000 and 1 μL of the solution spotted on to the MALDI target. Calculated for linear allyl ester of **1**: $C_{161}H_{236}N_{38}O_{59}Na$ requires m/z 3670.81; found 3670.54, $[M + Na]^+$. Calculated for linear allyl ester of **2**: $C_{165}H_{238}N_{40}O_{57}Na$ requires m/z 3716.88; found 3716.35, $[M + Na]^+$. Calculated for **1**: $C_{158}H_{228}N_{38}O_{58}Na_3$ requires m/z 3656.69; found 3656.73, $[M + 3Na - 2H]^+$. Calculated for **2**: $C_{162}H_{230}N_{40}O_{56}Na_3$ requires m/z 3702.76; found 3702.77, $[M + 3Na - 2H]^+$.

Stock solutions of the peptides were prepared in TFE and their concentrations determined through absorbance measurements at 280 nm after dilution of small aliquots into water (extinction coefficients were calculated as $\varepsilon = 8940$ mol^{-1} cm^{-1} and $\varepsilon = 16,960$ mol^{-1} cm^{-1} at 280 nm for peptides **1** and **2** respectively) (27).

Liposome preparation

A solution of egg phosphatidylcholine (100 μL, 10 mg) was concentrated in vacuo in a 25 mL round bottomed flask to form a thin film that was dried in vacuo overnight. The lipid film was hydrated with 1 mL of aqueous medium containing 150 mM NaCl buffered with 10 mM tris at pH 7.4 and mixed thoroughly before being subjected to five freeze thaw cycles and extruded 10 times through 100 nm laser-etched polycarbonate membranes at 30°C using a thermobarrel extruder (Northern Lipids, Burnaby, Canada).

Circular and LD spectroscopy

Experiments were carried out on Jasco J-810 (CD) or Jasco J-715 (LD) spectropolarimeters and processed using the Spectra Analysis program (version 1.50, Jasco, Great Dunmow, UK). All experiments were carried out in 10 mM tris buffer at pH 7.4 containing 150 mM NaCl using a 1 cm quartz cell (CD) or a purpose made 50 μL quartz Couette cell (LD) (19) at 25°C. A portion of the stock solution of the peptide in TFE was added to the aqueous medium containing liposomes at concentrations in the range 1.5–1.82 mg/mL (~2 mM) and mixed by gentle shaking, producing peptide concentrations in the range 0.34–10.1 μM. Volumes were selected such that the proportion of TFE was never >10% v/v. Time series spectra were acquired between 350–190 nm at a scan rate of 10 nm/min, with a response time of 16 s and a bandwidth of 2 nm. Blank spectra were recorded after the addition of identical quantities of pure TFE to the aqueous medium and subtracted from the raw time series spectra. LD spectra were further processed using 15-point binomial smoothing, before analysis. Data from time series acquisitions were fitted to two- or three-state models (Fig. 2) using Eq. 1 ($[P]_3$ and $LD_3 = 0$ for the 2-state model).

$$LD_{calc} = \frac{([P]_1 LD_1) + ([P]_2 LD_2) + ([P]_3 LD_3)}{[P]_T}, \quad (1)$$

where $[P]_1$, $[P]_2$, and $[P]_3$ are the concentrations of peptide in states 1, 2, and 3 respectively, and LD_1, LD_2, and LD_3 are the LD signals corresponding to these states. $[P]_T$ is the total concentration of peptide. LD_{calc} is the calculated LD signal.

Concentrations of the peptides in each state were calculated according to Eqs. 2–4:

$$[P]_1 = \frac{[P]_T k_1 (e^{-k_1 t} - e^{-k_2 t})}{k_2 - k_1} \quad (2)$$

$$P \xrightleftharpoons{k_1} P_1 \xrightarrow{k_2} P_2 \xrightarrow{k_3} P_3$$

FIGURE 2 The kinetics model used for analysis of LD data.

$$[P]_2 = [P]_T k_1 k_2 \left\{ \frac{e^{-k_1 t}}{(k_2 - k_1)(k_3 - k_1)} + \frac{e^{-k_2 t}}{(k_1 - k_2)(k_3 - k_2)} + \frac{e^{-k_3 t}}{(k_1 - k_3)(k_2 - k_3)} \right\} \quad (3)$$

$$[P]_3 = [P]_T \left\{ 1 - \frac{(k_2 k_3 e^{-k_1 t})}{(k_2 - k_1)(k_3 - k_1)} - \frac{(k_1 k_3 e^{-k_2 t})}{(k_1 - k_2)(k_3 - k_2)} - \frac{(k_1 k_2 e^{-k_3 t})}{(k_1 - k_3)(k_2 - k_3)} \right\}, \quad (4)$$

where k_1, k_2, and k_3 are the rate constants for the formation of states 1–3 and t is time. With $k_3 = 0$, Eqs. 3 and 4 revert to those for a 2-state model.

For the purposes of these calculations, time t at which the instrument was at a given wavelength (λ_t) on each independently collected scan could be related to the scan rate using Eq. 5:

$$t = \frac{\lambda_s - \lambda_t + n(\lambda_s - \lambda_e)}{s}, \quad (5)$$

where λ_s is the starting wavelength of each scan, λ_e is the end wavelength of the scan, λ_t is the wavelength of the monochromator at time t, s is the scan rate in nm/min, and n is an integer corresponding to the number of completed scans ($n = 0, 1, 2…$). Global least squares fitting to shared rate constants (k_1, k_2, and k_3) was carried out using the data from four wavelengths (193 nm, 228 nm, 245 nm, and 254 nm) to calculate LD evolution profiles (LD_{calc}). Nonlinear least squares curve fitting procedures were carried out using the Solver function in the program Excel (Microsoft, Redmond, WA). The rate constants determined from the above process were then used to evaluate the LD parameters at all wavelengths by nonlinear least squares fitting, to generate the full LD spectrum for each of the bound states.

RESULTS

Peptide synthesis

Peptides **1** and **2** were synthesized in moderate yield using an approach based on coupling the majority of the amino acids as pseudoproline dipeptides. This approach was expected to enable assembly of the peptide chains while minimizing the formation of nonproductive conformations and favor the final cyclization process. To further facilitate cyclization, the syntheses were carried out on a solid support with a polyethylene glycol spacer to ensure that the reaction occurred in more solution-like conditions. The use of an allyl group as orthogonal protection for the first amino acid proved successful, although it was necessary to prepare fresh Pd(PPh$_3$)$_4$ in-house (see Supporting Material) for the deprotection to proceed to completion. Analysis of small portions of cleaved resin by mass spectrometry before cyclization indicated that the chain had been assembled successfully. Minor peaks at lower mass than the target peptide were consistent with small amounts of peptide for which coupling of Fmoc-Val-Ser($\psi^{Me,Me}$Pro)-OH had not gone to completion, but at levels that were not detrimental to isolation of the target peptides. Cyclization and cleavage proceeded without difficulties, to yield the crude peptides. As anticipated, these were not trivial to manipulate due to the lack of charged residues and high amphiphilicity. Nevertheless,

successful purification to $\geq 90\%$ was reproducibly achieved through the use of fluorinated alcohols as the principal solvents. Once solubilized, peptide solutions could be diluted in to aqueous media at solvent compositions $\leq 10\%$ alcohol by volume and remained stable over several hours.

Liposome binding experiments

Both peptides exhibited CD spectra in solution in the absence of membranes that were consistent with random coil conformations (see Supporting Material). Furthermore, at the concentrations used for these experiments there was no evidence of aggregation. After addition to liposomes, CD spectra were produced that were consistent with rapid association to the liposomal membranes (Fig. 3, A and B). Single minima at 213 nm and 216 nm were observed for **1** and **2** respectively, similar to those observed for β-barrel membrane proteins (28) and consistent with the adoption of β-structure. Due to the high salt conditions and path lengths used for CD experiments, data could not be recorded at wavelengths <210 nm. The profiles of the CD spectra exhibited by both peptides did not change significantly during the course of the experiments. LD measurements over the same time period (Fig. 3, C and D) yielded spectra indicative of changes in membrane alignment occurring on a timescale of minutes to hours. During these measurements, the LD signal remained positive at all wavelengths, with notable

shoulders observed in the regions of 190–195 nm and 245–250 nm for both peptides and additional shoulders at 227 nm and 291 nm for peptide **2**.

Least squares fitting of the experimental data

LD data were analyzed using kinetic models that assumed pseudo-first order kinetics for consecutive processes. This was reasonable, given the combination of the excess lipid used in the experiments and the likelihood that the early phases in the binding of peptides to membranes do not involve aggregates. Examination of semi-log plots for the evolution of the LD signal (Fig. 4, A and B) support these models, particularly for peptide **2**, where it is evident that the semi-log plot consists of two processes with strikingly linear rate profiles. For peptide **1**, the data could be modeled adequately using a triple exponential model (Eqs. 1–5). Applying a double exponential model for peptide **1** yielded inferior fits to the experimental data. Data from four wavelengths corresponding to regions with the major shoulders in the LD spectra were used for the analysis of both peptides. Global least-squares fitting to shared rate constant values yielded good fits to the experimental data for both peptides (Table 1).

The binding of peptide **1** (Fig. 4 C) was characterized by three processes, with $k_1 > k_2 \approx k_3$. The calculated LD values for each of the bound states are indicative of an initially
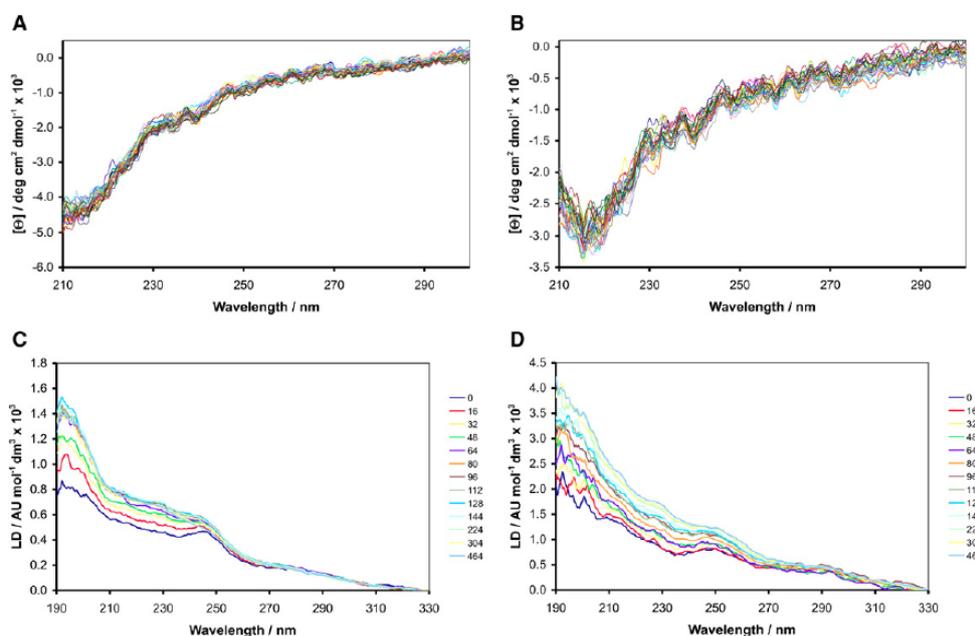
FIGURE 3   Time series spectra acquired at 20°C over an 8-h period after the addition of peptides to 100 nm EPC liposomes in 10 mM tris/150 mM NaCl at pH 7.4. CD spectra for **1** (A) and **2** (B) at respective peptide concentrations of 10.1 μM and 3.23 μM and an EPC concentration of 1.82 mg/mL (2 mM); LD spectra for **1** (C) and **2** (D) at respective peptide concentrations of 1.05 μM and 0.34 μM and an EPC concentration of 1.5 mg/mL (2 mM). The legend associated with each LD spectrum indicates the time (min) after which acquisition of the corresponding spectrum commenced.
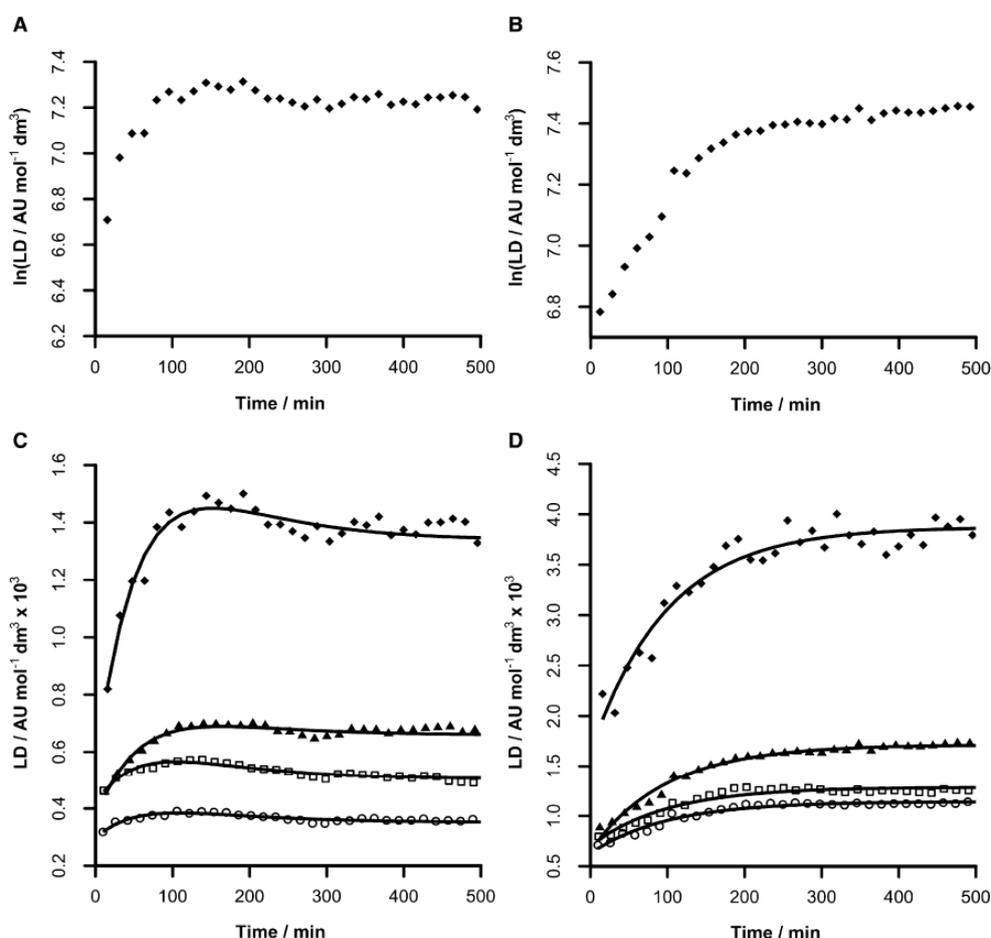
FIGURE 4   The evolution of LD signals after the addition of peptides **1** and **2** at respective concentrations of 1.05 μM and 0.34 μM to EPC liposomes (1.5 mg/mL; 2 mM) in 10 mM tris/150 mM NaCl at pH 7.4: semi-log plots for peptide **1** at 193 nm (*A*) and **2** at 228 nm (*B*); experimental and calculated profiles for peptides **1** (*C*) and **2** (*D*) at 193 nm (■), 228 nm (▲), 245 nm (□) and 254 nm (○). Experimental data are presented as points and the calculated profiles from nonlinear regression as lines.

weakly-oriented state (P_1, formed with rate constant k_1) with low LD. The peptide then converts to a considerably more oriented state (P_2, formed with rate constant k_2) before relaxing to a state with intermediate LD values (LD_3, formed with rate constant k_3). For peptide **2** (Fig. 4 *D*), two processes were characterized, with $k_1 > k_2$. As with peptide **1**, a state with low orientation forms with rapid kinetics before converting to a state that is considerably more ordered.

Calculation of the LD parameters at all wavelengths using the kinetic parameters in Table 1 enabled the LD spectra corresponding to each of the bound states to be determined (Fig. 5). In the case of peptide **1** (Fig. 5 *A*), the initial bound state (P_1) is characterized by an LD spectrum (LD_1) that is relatively weak across the whole spectrum, but has a pronounced maximum at 246 nm and a shoulder at ~275 nm. This gives way to spectra (LD_2 and LD_3,

Fig. 5 *A*) exhibiting significantly higher LD values in the far-ultraviolet (UV) range, with a significant maximum at 193 nm. Interestingly, changes in the near-UV spectrum are considerably smaller than those of the far-UV for both of these bound states. The spectrum of the initial bound state of peptide **2** (LD_1, Fig. 5 *B*) shares similar features with that of peptide **1**, with a maximum at 249 nm and a shoulder at 292 nm. This also gives way to a spectrum (LD_2, Fig. 5 *B*) with higher LD values in the far-UV range and smaller changes in the near-UV, but with a shoulder at 228 nm in addition to the maximum at 192 nm.

One feature enabled by the nonlinear regression using this model is the ability to calculate the concentration of all intermediates throughout the experiment. This gives rise to the concentration profiles in Fig. 6. For both peptides, the initially formed state (P_1) forms rapidly and then decays

TABLE 1 Parameters obtained from nonlinear least squares fitting of the model described by Eqs. 1-5 to the experimental data for the binding of peptides 1 and 2 at respective concentrations of 1.05 μM and 0.34 μM to EPC liposomes (1.5 mg/mL; 2 mM) in 10 mM tris/150 mM NaCl at pH 7.4

Parameter	Peptide	
	1*	2*
k_1/min^{-1}	1.01 $\pm$ 0.20	1.62 $\pm$ 0.47
k_2/min^{-1}	0.013 $\pm$ 0.001	0.010 $\pm$ 0.001
k_3/min^{-1}	0.013 $\pm$ 0.001	—
τ_1/min	0.99 $\pm$ 0.19	0.62 $\pm$ 0.18
τ_2/min	76.3 $\pm$ 5.9	98.6 $\pm$ 9.7
τ_3/min	76.4 $\pm$ 5.9	
LD/AU mol^{-1} dm^3		
193 nm		
LD_1	570 $\pm$ 13	1649 $\pm$ 9
LD_2	2130 $\pm$ 79	3874 $\pm$ 4
LD_3	1340 $\pm$ 20	—
228 nm		
LD_1	377 $\pm$ 2	706 $\pm$ 7
LD_2	909 $\pm$ 37	1286 $\pm$ 5
LD_3	659 $\pm$ 10	—
245 nm		
LD_1	423 $\pm$ 9	662 $\pm$ 2
LD_2	739 $\pm$ 12	1715 $\pm$ 1
LD_3	505 $\pm$ 4	—
254 nm		
LD_1	300 $\pm$ 3	631 $\pm$ 4
LD_2	482 $\pm$ 7	1142 $\pm$ 2
LD_3	352 + 4	—

*Errors are reported to 95% confidence limits and were estimated by repeating the nonlinear regression ten times from random estimates of the variables.

FIGURE 5 LD spectra for each binding state described by Eq. 1, calculated by regression analysis of the binding profiles for the association of peptides **1** (A) and **2** (B) with EPC liposomes in 10 mM tris/150 mM NaCl at pH 7.4. The identity of the binding state is indicated by the text associated with each spectrum.

exponentially to zero during the period of the experiments. In the case of peptide **2**, the final state (P_2) forms completely during the same period. With peptide **1**, this state exists as a transient intermediate, decaying to zero and being replaced by the final state (P_3).

DISCUSSION

Peptides **1** and **2** were designed following bioinformatics exercises on β-barrel membrane proteins on the basis that, due to their hydrophobicity and amphiphilicity, membrane association would be favored (24). Their cyclic nature was intended to promote the formation of secondary structure after membrane binding and render analysis of insertion processes more straightforward, as the issue of which end of the peptide inserts into the membrane first would not be a consideration.

Both peptides adopt random coil conformations in aqueous solution at concentrations <20 μM in the absence of membranes. However, after addition to membranes, secondary structure forms rapidly and once formed, remains unchanged for the duration of the experiment. As a consequence, LD data can be interpreted with the certainty that they reflect only changes in alignment with respect to the experimental frame of reference and do not contain contribu-

tions from secondary structure changes. It further enables LD profiles at all wavelengths to be simultaneously fitted to the same kinetics parameters, improving the reliability of data analysis. The purpose of this study was to explore the possibilities for using LD to probe the membrane-association kinetics of two peptides designed to undergo insertion, by assaying relative changes in alignment. As such, it was not necessary to use an internal reference to define the experimental frame of reference, as has been described elsewhere (29). For this work, the semiquantitative assessment made here enables us to extract the mechanistic information required.

Nonlinear fitting of the model described by Eqs. 1–5 produced good fits to the experimental data for both peptides. Two processes are common to both peptides. The first (k_1) is a rapid process that leads to a bound state (P_1) characterized by a weak positive LD spectrum with distinct maxima and shoulders in the near-UV that correspond closest to the L_a and L_b transitions of tyrosine and tryptophan (20). The L_b transition of tyrosine is oriented normal to the C_β-C_1-C_4-O axis and is usually found in the region of 260 nm, although transitions in the region of 250 nm have been reported for β-rich proteins with a high aromatic amino acid content, such as retinol binding protein (30). Tryptophan has an L_a transition occurring at ~265 nm that lies on an axis that bisects the indole N_1-C_4 atoms and an L_b
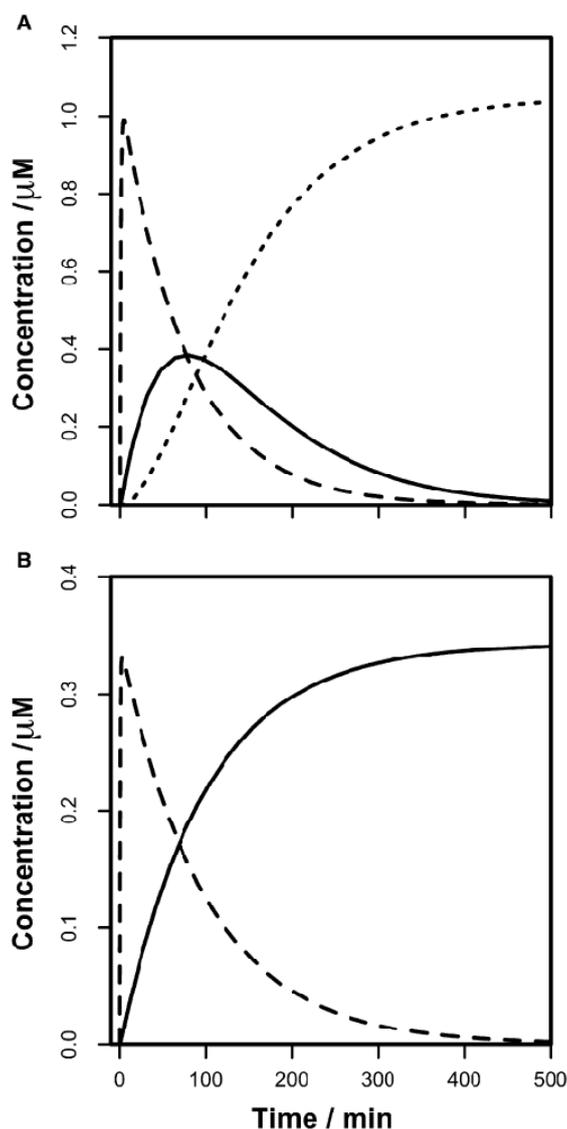
FIGURE 6 Concentrations of each of the liposome-bound states after addition of peptides **1** (*A*) and **2** (*B*) at respective concentrations of 1.05 μM and 0.34 μM to EPC liposomes (1.5 mg/mL; 2 mM) in 10 mM tris/150 mM NaCl at pH 7.4, calculated by fitting of Eq. 1 to the experimental data by nonlinear regression. (*Dashed line*) $[P]_1$; (*solid line*) $[P]_2$; (*dotted line*) $[P]_3$.

transition at 287 nm oriented orthogonally to the L_a transition. The deconvoluted LD spectrum for P_1 is consistent with a state that is weakly bound to the membrane through the side chains of aromatic residues, leading to alignment of these side chains, with the peptide backbone either poorly aligned or aligned close to 54.7° with respect to the membrane normal (that would also give a weak signal)

(22). As the wavelengths corresponding to these bands are red-shifted by ~5 nm in peptide **2** with respect to the corresponding bands of peptide **1**, indicating that they arise from the tryptophan residues of the former, it would seem that the residues near the ends of the peptides as depicted in Fig. 1 are those that are primarily participating in interactions, although it does not rule out contributions from the others. Positive LD bands for both L_a and L_b of tryptophan have been observed in other systems (23) and are indicative of the indole side chain being oriented perpendicular to the membrane normal. In these studies, the same rationale can be applied to the phenolic side chain of tyrosine. The observation of a spectrum that is positive across the wavelength range suggests that the alignment of the peptide as a whole is nearer to the membrane normal than the plane of the membrane, as the main amide transitions in β-hairpins that contribute to the far-UV region have a cross strand orientation. Taken together, these observations are consistent with an anchoring interaction of a small number of residues with the membrane surface. It is noteworthy that the signals corresponding to the L_b transitions of tyrosine and tryptophan do not change significantly throughout the duration of the experiment, which suggests that some of the side chain interactions are relatively strong and implies that changes in alignment of the peptide backbone are accommodated by changes in the side chain torsional angles.

The second process (k_2) is characterized by surprisingly slow kinetics, which was not anticipated at the outset of this work. The spectrum of the bound state (P_2) has significantly more positive LD values across the spectrum, particularly for the 190 nm region (corresponding to the π-π^* transition of the backbone), indicative of an alignment that is closer to the membrane normal than P_1. Accounts of kinetic processes for the binding of peptides to membranes with half-lives of the order of ~1 h are rare. White et al. (16) reported conditions under which a designed helical peptide underwent slow membrane insertion kinetics, on a timescale of hours, although this phenomenon was only observed at nonphysiological pH values ($\leq$pH 5.3). It will be of interest to determine whether peptide rearrangements on these timescales are a general phenomenon or a property particular to these peptides. Earlier studies on marker release by peptide **1** indicated that apparent poration of EPC membranes occurs on a timescale of seconds to minutes (24), which is more consistent with the kinetics of k_1 than k_2, raising the possibility that membrane disruption occurs primarily during the initial binding process, rather than by specific poration. An explanation for the slow kinetics lies in the lack of charge complementarity between the peptides and the membrane, both of which are neutral in the physiological pH range. Given the low molar peptide/lipid ratios (typically 1:1000) and that the peptides do not promote significant changes in lipid morphology at higher ratios (24), the changes in LD can be assigned to changes in peptide orientation.
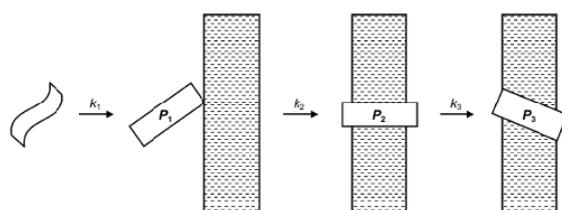
FIGURE 7 Peptide binding conformations consistent with the calculated LD spectra for binding states of peptides **1** and **2**. The membrane is represented by the hatched boxes and the peptide by open rectangles.

A third kinetic process is observed for peptide **1**, but not peptide **2**. This also occurs on a slow timescale, and leads to a diminution of positive LD values, consistent with the adoption of a conformation that lies further away from the membrane normal. One possibility is that this represents a realignment of peptide **1** to minimize the effects of mismatch (31,32) between the peptide and the membrane or promote peptide aggregation, whereas peptide **2** does not realign due to the known anchoring effects of tryptophan in the interfacial region of lipid membranes (9), which would favor lipid redistribution as a means of overcoming mismatch.

One study of the refolding of a β-barrel outer membrane protein reported three processes with kinetics on a similar timescale to those reported here (33). Of these, a moderately slow process with a timescale of minutes was attributed to the formation of a partially folded state within the membrane, with the slower process on a timescale of hours attributed to adoption of the folded state. These are broadly similar to the processes observed here, indicating that these peptides may prove to be good models for transmembrane β-barrels. A model for the behavior of these peptides is shown schematically in Fig. 7.

The peptides form secondary structure on a timescale that is more rapid than k_1. The full description of binding therefore requires at least one additional rate constant to be included in the process depicted in Fig. 7. An advantage of the rapid adoption of secondary structure, however, is that changes in LD relate only to changes in peptide orientation, enabling us to interpret the LD data more definitively than if folding and insertion were coupled. The data illustrate that the LD methodology is a useful tool for probing membrane adorbtion kinetics that is of general applicability to systems where confomational changes during adsorbtion can be assayed.

SUPPORTING MATERIAL

Additional figures and data are available at http://www.biophysj.org/biophysj/supplemental/S0006-3495(08)00127-6.

REFERENCES

1. Ulmschneider, M. B., and M. S. Sansom. 2001. Amino acid distributions in integral membrane protein structures. *Biochim. Biophys. Acta.* 1512:1–14.

2. Landolt-Marticorena, C., K. A. Williams, C. M. Deber, and R. A. Reithmeier. 1993. Non-random distribution of amino acids in the transmembrane segments of human type I single span membrane proteins. *J. Mol. Biol.* 229:602–608.

3. Liu, W., and M. Caffrey. 2006. Interactions of tryptophan, tryptophan peptides, and tryptophan alkyl esters at curved membrane interfaces. *Biochemistry.* 45:11713–11726.

4. Sanderson, J. M. 2005. Peptide-lipid interactions: insights and perspectives. *Org. Biomol. Chem.* 3:201–212.

5. Sanderson, J. M., and E. J. Whelan. 2004. Characterization of the interactions of aromatic amino acids with diacetyl phosphatidylcholine. *Phys. Chem. Chem. Phys.* 6:1012–1017.

6. Sanderson, J. M. 2007. Refined models for the preferential interactions of tryptophan with phosphocholines. *Org. Biomol. Chem.* 5:3276–3286.

7. Killian, J. A. 2003. Synthetic peptides as models for intrinsic membrane proteins. *FEBS Lett.* 555:134–138.

8. Wimley, W. C., and S. H. White. 2000. Designing transmembrane alpha-helices that insert spontaneously. *Biochemistry.* 39:4432–4442.

9. de Planque, M. R. R., B. B. Bonev, J. A. A. Demmers, D. V. Greathouse, R. E. Koeppe, et al. 2003. Interfacial anchor properties of tryptophan residues in transmembrane peptides can dominate over hydrophobic matching effects in peptide-lipid interactions. *Biochemistry.* 42:5341–5348.

10. van der Wel, P. C. A., N. D. Reed, D. V. Greathouse, and R. E. Koeppe II. 2007. Orientation and motion of tryptophan interfacial anchors in membrane-spanning peptides. *Biochemistry.* 46:7514–7524.

11. Wimley, W. C., K. Hristova, A. S. Ladokhin, L. Silvestro, P. H. Axelsen, et al. 1998. Folding of beta-sheet membrane proteins: A hydrophobic hexapeptide model. *J. Mol. Biol.* 277:1091–1110.

12. Wimley, W. C., and S. H. White. 2004. Reversible unfolding of beta-sheets in membranes: a calorimetric study. *J. Mol. Biol.* 342:703–711.

13. Jin, Y., H. Mozsolits, J. Hammer, E. Zmuda, F. Zhu, et al. 2003. Influence of tryptophan on lipid binding of linear amphipathic cationic antimicrobial peptides. *Biochemistry.* 42:9395–9405.

14. Pan, Y. -L., J. T. -J. Cheng, J. Hale, J. Pan, R. E. W. Hancock, et al. 2007. Characterization of the structure and membrane interaction of the antimicrobial peptides aurein 2.2 and 2.3 from Australian southern bell frogs. *Biophys. J.* 92:2854–2864.

15. Clayton, A. H. A., and W. H. Sawyer. 2000. Oriented circular dichroism of a class a amphipathic helix in aligned phospholipid multilayers. *Biochim. Biophys. Acta.* 1467:124–130.

16. Ladokhin, A. S., and S. H. White. 2004. Interfacial folding and membrane insertion of a designed helical peptide. *Biochemistry.* 43:5782–5791.

17. Wu, Y., H. W. Huang, and G. A. Olah. 1990. Method of oriented circular dichroism. *Biophys. J.* 57:797–806.

18. Chen, F. -Y., M. -T. Lee, and H. W. Huang. 2003. Evidence for membrane thinning effect as the mechanism for peptide-induced pore formation. *Biophys. J.* 84:3751–3758.

19. Marrington, R., T. R. Dafforn, D. J. Halsall, J. I. MacDonald, M. Hicks, et al. 2005. Validation of new microvolume Couette flow linear dichroism cells. *Analyst.* 130:1608–1616.

20. Dafforn, T. R., J. Rajendra, D. J. Halsall, L. C. Serpell, and A. Rodger. 2004. Protein fiber linear dichroism for structure determination and kinetics in a low-volume, low-wavelength Couette flow cell. *Biophys. J.* 86:404–410.

21. Rodger, A., J. Rajendra, R. Marrington, M. Ardhammar, B. Nordén, et al. 2002. Flow oriented linear dichroism to probe protein orientation in membrane environments. *Phys. Chem. Chem. Phys.* 4:4051–4057.

22. Rodger, A., R. Marrington, M. A. Geeves, M. Hicks, L. de Alwis, et al. 2006. Looking at long molecules in solution: what happens when they are subjected to Couette flow? Phys. Chem. Chem. Phys. 8:3161–3171.

23. Caesar, C. E. B., E. K. Esbjörner, P. Lincoln, and B. Nordén. 2006. Membrane interactions of cell-penetrating peptides probed by tryptophan fluorescence and dichroism techniques: correlations of structure to cellular uptake. Biochemistry. 45:7682–7692.

24. Sanderson, J. M., and S. Yazdani. 2002. The design, synthesis and characterization of channel-forming peptides. Chem. Commun. 1154–1155.

25. Wohr, T., F. Wahl, A. Nefzi, B. Rohwedder, T. Sato, et al. 1996. Pseudo-prolines as a solubilizing, structure-disrupting protection technique in peptide synthesis. J. Am. Chem. Soc. 118:9218–9227.

26. Kates, S. A., N. A. Sole, C. R. Johnson, D. Hudson, G. Barany, et al. 1993. A novel, convenient, three-dimensional orthogonal strategy for solid-phase synthesis of cyclic peptides. Tetrahedron Lett. 34:1549–1552.

27. Pace, C. N., F. Vajdos, L. Fee, G. Grimsley, and T. Gray. 1995. How to measure and predict the molar absorbtion coefficient of a protein. Protein Sci. 4:2411–2423.

28. Tamm, L. K., H. Hong, and B. Liang. 2004. Folding and assembly of beta-barrel membrane proteins. Biochim. Biophys. Acta. 1666:250–263.

29. Ardhammar, M., P. Lincoln, and B. Nordén. 2001. Ligand substituents of ruthenium dipyridophenazine complexes sensitively determine orientation in liposome membrane. J. Phys. Chem. B. 105:11363–11368.

30. Greene, L. H., E. D. Chrysina, L. I. Irons, A. C. Papageorgiou, K. R. Acharya, et al. 2001. Role of conserved residues in structure and stability: tryptophans of human serum retinol-binding protein, a model for the lipocalin superfamily. Protein Sci. 10:2301–2316.

31. Harzer, U., and B. Bechinger. 2000. Alignment of lysine-anchored membrane peptides under conditions of hydrophobic mismatch: a CD, ^{15}N and ^{31}P solid-state NMR spectroscopy investigation. Biochemistry. 39:13106–13114.

32. de Planque, M. R. R., J. -W. P. Boots, D. T. S. Rijkers, R. M. J. Liskamp, D. V. Greathouse, et al. 2002. The effects of hydrophobic mismatch between phosphatidylcholine bilayers and transmembrane alpha-helical peptides depend on the nature of interfacially exposed aromatic and charged residues. Biochemistry. 41:8396–8404.

33. Surrey, T., and F. Jähnig. 1995. Kinetics of folding and membrane insertion of a beta-barrel membrane protein. J. Biol. Chem. 270: 28199–28203.

The Synergistic Action of Melittin and Phospholipase A2 with Lipid Membranes: Development of Linear Dichroism for Membrane-Insertion Kinetics

Angeliki Damianoglou[1], Alison Rodger[1], Catherine Pridmore[2], Timothy R. Dafforn[3], Jackie A. Mosely[2], John M. Sanderson[2] and Matthew R. Hicks[1,*]

[1]*Department of Chemistry, University of Warwick, Coventry, CV4 7AL, UK;* [2]*Department of Chemistry, Centre for Bioactive Chemistry, University Science Laboratories, Durham, DH1 3LE, UK;* [3]*Department of Biological Sciences, University of Birmingham, Birmingham B15 2TT, UK*

Abstract: Here we present data on the kinetics of insertion of melittin, a peptide from bee venom, into lipid membranes of different composition. Another component of bee venom is the enzyme phospholipase A2 (PLA$_2$). We have examined the interaction of melittin and PLA$_2$ with liposomes both separately and combined and demonstrate that they work synergistically to disrupt the membranes. A dramatic difference in the action of melittin and PLA$_2$ is observed when the composition of the membrane is altered. Temperature also has a large effect on the kinetics of insertion and membrane disruption. We use a combination of techniques to measure liposome size (dynamic light scattering), peptide secondary structure (circular dichroism spectroscopy), peptide orientation relative to the membrane (linear dichroism spectroscopy) and enzymatic digestion of the lipids (mass spectrometry).

Keywords: Amphipathic, peptide, antimicrobial, membrane protein, linear dichroism, liposome, dynamic light scattering.

INTRODUCTION

Membrane proteins make up to 30% of all proteins coded for by most genomes [1] and they facilitate a wide range of cellular functions for the cell and are a means by which the cell communicates with its environment. They are popular drug targets for the pharmaceutical industry [2]. There is also an increasing family of antimicrobial peptides that bind to lipid membranes [3]. The mechanism by which such antimicrobial peptides act has become a complex issue. It is widely accepted that it is important to understand how the peptides act in order to fully exploit the use of peptides as antimicrobial agents [4]. However, the techniques that have been so successfully applied to understand structural questions for globular proteins, including crystallography and NMR, are not as readily applied for the study of membrane proteins. Membrane proteins and peptides are not easy to crystallize and they usually require lipid or detergent environments to remain soluble and folded. Although progress is being made with solution and solid-state NMR the size of the membrane protein-detergent complexes usually results in slow tumbling rates and poor resolution spectra with broad peaks. The other side of the membrane protein-membrane interaction system is the lipid bilayer itself. We currently know very little about how membrane-binding drugs interact with cell membrane lipids. The aim of this work is to explore both sides of this question for the bee venom peptide melittin. By using flow linear dichroism of liposomes, a perspective on membrane

peptide-membrane interactions becomes available that is not available from any other technique.

Linear dichroism (LD), although not an atomic-level resolution technique, has been found to be ideally suited to membrane environments. Linear dichroism is the differential absorbance of light polarized parallel and perpendicular to an orientation axis. A non-zero signal requires an oriented sample to have absorbance bands in a given region of the spectrum. Following the discovery by Ardhammar *et al* [5], that model membranes, known as liposomes, become sufficiently distorted in shear flow to become aligned, together with any molecules bound to the lipid, we showed that membrane peptides and proteins could be flow aligned when bound to liposomes [6-7]. As has been illustrated in subsequent work, one can qualitatively and quantitatively identify the orientation of membrane guest molecules, provided that the molecules of interest have significant absorption in the UV-Visible region. One can also measure insertion kinetics in real time to give insight into peptide folding and insertion in membranes [8-12]. In solution, LD has the advantage over other biophysical techniques of being insensitive to off-membrane events—unbound ligands or peptides are invisible as they do not orient.

LD is the ideal technique for probing insertion / binding (or not) into / onto membranes in real time since the signal is zero unless the analyte (for example a peptide) binds to the membrane, and an α-helical peptide on the surface has opposite signed LD signals to when it is inserted as summarized in Fig. (**1**).

The peptide of interest in this work, melittin, is an amphiphilic and cationic peptide. It is a 26 amino acid residue

*Address correspondence to this author at the Department of Chemistry, University of Warwick, Coventry, CV4 7AL, UK; Tel: +44(0)24 765 23293; Fax: +44(0)765 24112;
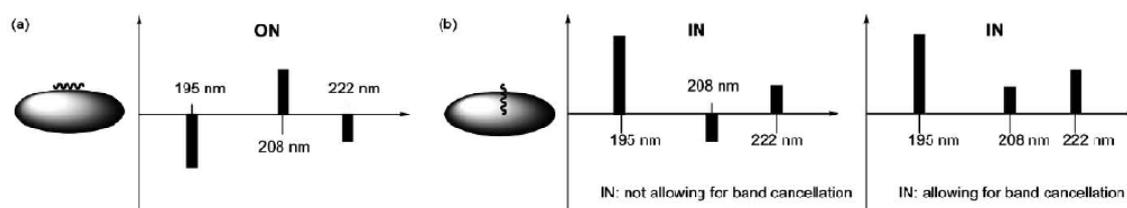E mail: matthew.hicks@warwick.ac.uk

Figure 1. Schematic illustration of expected *LD* signals for an α-helix (**a**) on the surface of or (**b**) inserted in a membrane. The right hand part of (**b**) is what is expected in a spectrum given the reality of overlap between bands and net cancellation.

peptide with a positively charged C-terminus and a proline residue at position 14 that allows it to form kinked helices in non-polar environments [13]. Its secondary structure changes from random coil in aqueous solutions to helical in membranes [14]. At low concentration is in a monomeric conformation, whereas at higher concentrations it forms tetramers in aqueous solution [14-15].

Melittin Fig. (**2a**) is an interesting peptide in its own right, being a main component of bee venom and also having anti-microbial properties [16]. In addition it is a popular model peptide for studying cytolytic activities on both eukaryotic and prokaryotic cell membranes. Melittin is known to bind to membranes to form pores, although the mechanism by which it disrupts the membranes is still a matter of debate. Papo and Shai concluded that melittin binds on surface of a membrane or in a transmembrane manner *via* a carpet-like or barrel-stave mechanism depending on whether it is driven by a combination of hydrophobic or electrostatic effects [17]. Van den Bogaart *et al.* have studied the mechanism of pore formation of melittin in membranes made from the lipids 1,2-dioleoyl-sn-glycero-3-phosphocholine (DOPC) and 1,2-dioleoyl-sn-glycero-3-[phospho-rac-(1-glycerol)] (DOPG). They concluded that melittin caused pore formation in DOPC membranes but not those made of DOPG [18]. Most recently Manna *et al.* concluded from modeling that in 1-palmitoyl-2-oleoyl-sn-glycero-3-phosphocholine (POPC) membranes melittin forms pores in the membrane by the toroidal mechanism [19]. The peptide's behaviour in membranes depends on many variables such as the concentration of the peptide, the composition and phase of the lipid membrane or even the solvents and buffers used to carry out the experiments.

In bee venom, melittin is always accompanied by the enzyme phospholipase A2 (PA2). Melittin and PA2 are known to act synergistically on cell membranes: melittin enhances the movement of anions in membranes and lyses cells at high concentration, this is facilitated by the lipolytic activity of PA2 which catalyses the hydrolysis of the *sn*-2 ester bond of lipids in the presence of Ca^{2+} [20]. Conversely, melittin enhances the rate of hydrolysis by perturbing the lipid bilayer and reorienting the *sn*-2 ester bond. Of particular relevance to this work, PA2 is known to hydrolyse the lipid 1,2-dimyristoyl-sn-glycero-3-phosphocholine DMPC, Fig. (**1**) to form lyso MPC and myristic acid [21].

In this work we have used LD, complemented by other spectroscopic techniques as well as dynamic light scattering (DLS) and MALDI mass spectrometry, to probe the behaviour of melittin inserting into different membrane-mimicking lipid environments and to consider the effect of the enzyme PA2 on that process. The lipids vary in their acyl chain length, degree of unsaturation and charge. By complementing LD with a range of other biophysical techniques including circular dichroism (CD), MALDI-MS, thin layer chromatography (TLC), DLS and oriented CD (OCD) we have been able to follow the folding and insertion process of melittin into membranes in real time and to understand key aspects of the process. Most of the work has been undertaken with melittin co-purified with trace amounts of PA2 present (<0.05 U/mg), denoted melittin[PA2]. However control experiments on isolated melittin (melittin[pure]), phospholipase A2, and a controlled mixture of the two have also been undertaken.

MATERIALS AND METHODS

Materials

Melittin from bee venom was purchased from Sigma-Aldrich (Dorset, UK). This melittin is co-purified with PA2 (<0.5 U/mg). Bis-tris propane (B6755) CH_2 [$CH_2NHC(CH_2OH)_3$]$_2$ was purchased from Sigma-Aldrich. Its pH was adjusted with diluted hydrochloric acid. DMPC, 1-palmitoyl-2-oleoyl-sn-glycero-3-phosphocholine (POPC), 1,2-dioleoyl-sn-glycero-3-phosphocholine (DOPC), 1,2-dipalmitoyl-sn-glycero-3-phospho-(1'-rac-glycerol) (DPPG), 1,2-dipalmitoyl-*sn*-glycero-3-phosphocholine (DPPC) and 1-palmitoyl-2-docosahexaenoyl-*sn*-glycero-3-phosphocholine (PDPC) were purchased from Avanti polar Lipids, Alabama, USA. All other chemicals were obtained from Sigma-Aldrich.

Methods

Liposome Preparation

A stock solution of 2.5 mg/mL small unilamellar vesicles (SUVs) was prepared by dissolving the lipid (or lipids) in either 2,2,2-trifluoroethanol (DMPC) or chloroform (the remainder). The sample was then dried under nitrogen flow and placed under vacuum overnight to remove residual organic solvent resulting in a lipid film on the inner surface of the container. The lipid film was then suspended in 10 mM bis-tris propane (BTP, 10 mM, pH 7) and freeze/thawed five times using dry ice/ethanol and room temperature (RT) for DMPC, DOPC, POPC and PDPC and dry ice/ethanol and 37 °C for DPPC, DPPG, POPC/DPPG. The lipid samples were then extruded 11 times through a 100 nm polycarbonate membrane at temperatures similar to those used during the thawing process to create nominal 100 nm liposomes (the actual size of the liposomes is larger once they relax following extrusion as discussed below).

(a)   NH$_2$-GIGAVLK$^+$VLTTGLPALISWIK$^+$R$^+$K$^+$R$^+$QQ-CONH$_2$
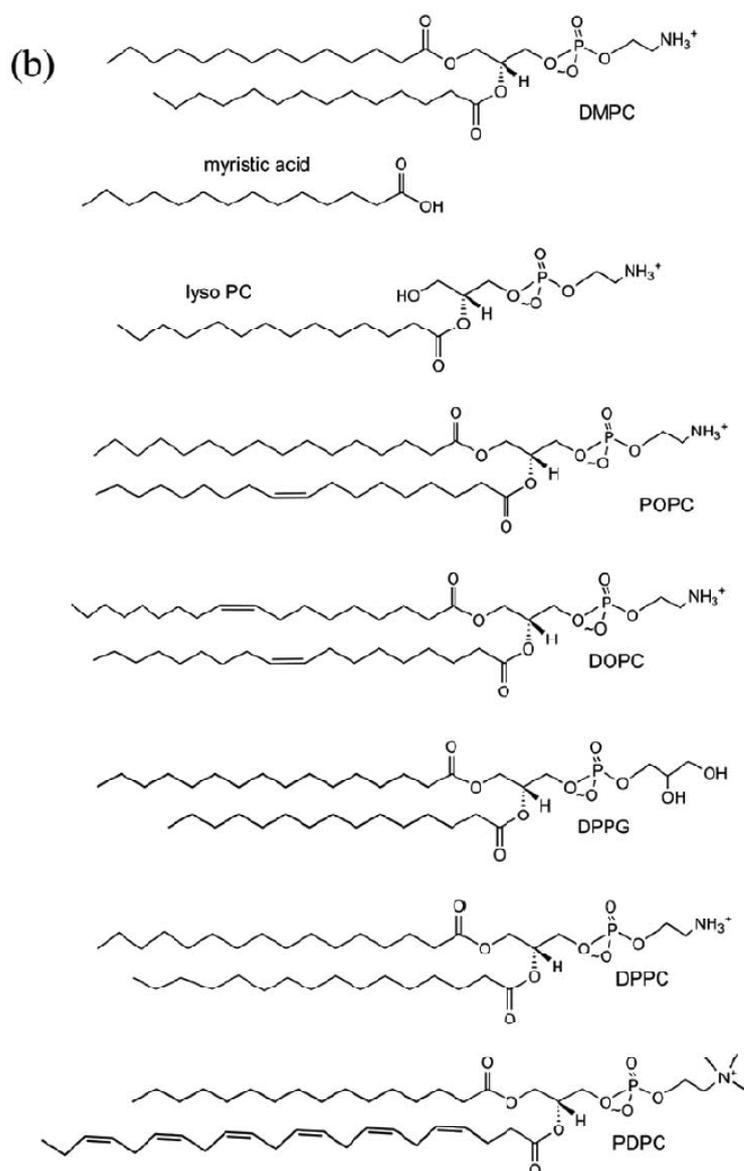
Figure 2. (a) Sequence of melittin. **(b)** Structures of lipids of relevance to this work: DMPC, myristic acid, lyso PC, 1-palmitoyl-2-oleoyl-sn-glycero-3-phosphocholine (POPC), 1,2-dioleoyl-sn-glycero-3-phosphocholine (DOPC), 1,2-dipalmitoyl-sn-glycero-3-phospho-(1'-rac-glycerol) (DPPG), 1,2-dipalmitoyl-sn-glycero-3-phosphocholine (DPPC), 1-palmitoyl-2-docosahexaenoyl-*sn*-glycero-3-phosphocholine (PDPC).

Peptide Solutions

The peptide was dissolved in water to produce stock solutions of 5 mg/ml. Experiments were all undertaken at lipid:peptide molar ratio of 100:1 and peptide concentration of 0.1 mg/mL. Samples were prepared by adding the appropriate volume of the peptide stock solution to a buffered solution of liposomes.

Spectroscopy

CD spectra were collected in a range of different path length quartz cells in a Jasco (Great Dunmow, UK) J-815 CD spectropolarimeter. LD spectra were collected using a Jasco J-815 spectropolarimeter adapted for LD measurements in a microvolume Couette flow cell manufactured by Crystal Precision Optics, Rugby, UK and now available via Kromatek Ltd., (Great Dunmow, UK). [7, 8, 11, 12, 22-26] Far UV CD and LD spectra (190–320 nm) were collected using a data pitch of 0.2 nm, continuous scanning mode, scanning speed of 100 nm/min, response of 1 s, band width of 1 or 2 nm. Fluorescence spectra were collected using a Jasco FP-6500 fluorimeter using excitation wavelength 280 nm, with 3 nm bandwidth for excitation and emission, and 3 mm path length microvolume cuvettes (Starna Hainalt, UK). DLS data were collected using a Malvern Zetasizer Nano S (Malvern Instruments, Malvern, UK) and the 3 mm path length microvolume fluorescence cuvette. DLS data was analysed using the Dispersion Technology Software (version 5.10) from Malvern Instruments. The sizes reported are from an intensity distribution analysis (note that this is not the same as the Z-average from the cumulants analysis which should not be used for polydisperse samples with a broad size distribution). Samples for OCD were deposited on a flat cylindrical quartz cuvette and allowed to dry overnight before being inserted into the light beam with the light beam incident perpendicular to the plane of the quartz.

MALDI

Melittin[PA2] was added to DMPC liposomes in 10 mM bis-tris propane (pH 7) in the absence of EDTA, and 1 μl aliquots were removed every 30 seconds and immediately mixed with a solution of 2,5-dihydroxybenzoic acid (DHB) matrix (9 μl, 10 mg/ml, water/0.1% TFA). The addition to the matrix solution was found, in preliminary experiments, to quench the hydrolysis-catalysing effect of the enzyme PA2. Two aliquots of 0.6 μl of each sample were spotted on separate positions on the MALDI target plate. MALDI-MS spectra were recorded, using a Ultraflex II MALDI-TOF/TOF spectrometer with 337 nm nitrogen laser (Bruker Daltonics Ltd., Coventry, UK) for each aliquot the intensity of the peak corresponding to lyso-MPC was normalized relative to that of the sum of the peaks corresponding to lyso-MPC and the $[DMPC + H]^+$ molecular ion. Data were averaged over 4000 laser shots from each spot. The error bars correspond to two times the standard deviation of the data from the two spots.

Results

We first consider the secondary structure of melittin in a range of lipids. An analysis of data collected during the binding of melittin with DMPC liposomes is then followed by an overview of its behaviour with a range of other lipids. The key properties of the lipids used in this work are summarized in Table **1**. The variables include charge and unsaturation as well as chain length.

Secondary Structure of Melittin

Melittin is known to be unfolded in aqueous solution and to be folded into an α-helix when in the presence of any lipids for which the CD has been measured [27-32]. Melittin's CD spectra in water and in lipid (DMPC) are illustrated in Fig. (**3a**). The secondary structure of melittin in DMPC is established within the dead-time of loading the cuvette and remains unchanged thereafter Fig. (**3b**).

In this work, for the first time, the effect of lipid unsaturation and lipid charge on the CD spectra of melittin has

Table 1. Properties of Lipids Used in This Work, the Orientation of Melittin on or in the Liposome, and the Ratios of the Melittin CD Signals at 222 nm and 208 nm. The Notation 18:2 Denotes a Lipid Tail Length of 18 Carbons with 2 Unsaturated Bonds. DMPC at 25° C is very Close to its Phase Transition Temperature (23° C for Pure DMPC) as Indicated by Labelling the Phase 'Transition' Rather than 'Liquid' or 'Gel'

Lipid	Lipid Charge and Phase	Degree of Unsaturation	Melittin	Orientation on or in Membrane	CD_{222}/CD_{208}	Fluorescence Maximum
DOPC	+/– (liquid)	18:1_18:1	Melittin[PA2]	In	1.4	336
POPC	+/– (liquid)	18:1_16:0	Melittin[PA2]	In	1.2	335
80POPC:20DPPG	– (liquid)	18:1_16:0/16:0	Melittin[PA2]	In	1.2	336
DPPG	– (gel)	16:0	Melittin[PA2]	In	0.96	333
80DPPC:20DPPG	– (gel)	16:0/ 16:0	Melittin[PA2]	In	1.04	335
DPPC 37 °C	+/– (liquid)	16:0	Melittin[PA2]	-	0.92	339
DMPC 37 °C	+/– (liquid)	14:0	Melittin[PA2]	In	1.05	338
DMPC 25 °C LUV	+/– (transition)	14:0	Melittin[PA2]	In	1.05	335
DMPC 25 °C SUV	+/– (transition)	14:0	Melittin[PA2]	In	0.99	335
DMPC 37 °C	+/– (liquid)	14:0	Melittin[pure]	In	0.87	341
DMPC 37 °C	+/– (liquid)	14:0	Melittin[pure]+ PA2	In	0.96	342
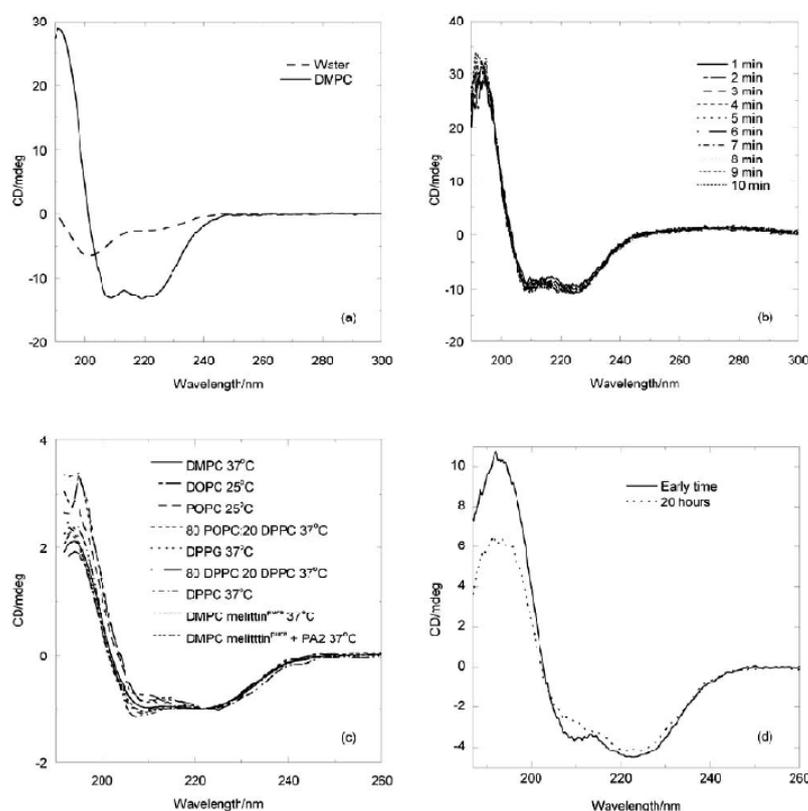
Figure 3. CD spectra of melittin (0.1 mg/mL) as a function of lipid environment (lipid:melittin molecular ratio 100:1). (**a**) Melittin[PA2] in DMPC and water at 25°C. Path length = 2 mm. (**b**) Melittin[PA2] in buffered DMPC at 25°C as a function of time. Path length = 2 mm. (**c**) Melittin in different lipids and temperatures (as indicated in the figure). Melittin is melittin[PA2] unless otherwise indicated. Pathlength = 0.2 mm. (**d**) Melittin[pure] in PDPC . Path length = 1 mm.

been investigated. The concentration of PA2 in all samples was so low that it makes no direct contribution to the CD spectra. As shown in Fig. (**3c**) the melittin CD spectra are all indicative of it having a helical conformation and they are very similar in magnitude, but vary slightly in shape as a function of lipid composition of the membrane. The intensity of the CD spectra of melittin at 222 nm are larger than those at 208 nm when melittin is inserted (see below for proof of insertion by LD) in membranes made of unsaturated lipids and conversely for saturated lipids, as summarized in Table 1. The CD_{222}/CD_{208} ratio is associated in the literature with the hydrophobicity of the environment of a helical peptide (originally methanol versus lipid) [33] as well as its oligomeric state (oligomerisation presumably also providing a more hydrophobic environment). For example, larger CD_{222}/CD_{208} ratios have been deemed to indicate membrane insertion or oligomerisation [34, 35]. Although this has not been proven, the idea is sufficiently widely used in the literature that we can conclude it is consistent with most data that have been collected. It should be noted that although a contribution from a random coil spectrum would decrease the CD_{222}/CD_{208} it would also decrease the average magnitude, which does not happen.

Our results therefore imply that the unsaturated lipids provide a more hydrophobic environment for melittin. In support of this, the fluorescence maximum of melittin's tryptophan shifts to lower wavelength (which also implies a more hydrophobic environment) with increasing lipid unsaturation (Table 1). It therefore follows that increasing unsaturation enables the lipids to pack about the helix more effectively. We attribute this effect to membrane flexibility and packing. Consistent with this, melittin with PA2 and melittin with mixed lipids (all where the membrane is more flexible) have higher CD_{222}/CD_{208} ratios. We return to this issue below.

There is one report in the literature of melittin becoming a β-sheet in a lipid with 6 double bonds, 1-palmitoyl-2-docosahexaenoyl-*sn*-glycero-3-phosphocholine (PDPC). The observed loss of the CD signal at 208 nm that has been attributed to a β-sheet structure [36] is almost certainly a spectral artifact. The published spectrum at longer wavelength is actually close to that expected for an α-helix (24) and that at lower wavelength consistent with the artifacts that arise from the saturation of the photomultiplier tube [37]. To confirm this is actually the case, we measured the *CD* spectrum of melittin when first added to PDPC liposomes and after 20

hours Fig. (**3d**). Both spectra are clearly α-helical. They also have a higher 222 nm/208 nm ratio than the spectra of Fig. (**3c**) which supports the above conclusion about the hydrophobic environment provided by unsaturated lipids. Infra red data (not shown) confirm the lack of β structure for melittin with this lipid.

Interaction of Melittin^pa2 and Melittin^pure with DMPC

Our aim was to probe, for the first time, the insertion of melittin into lipid biplayers in aqueous solution in real time. As shown in Fig. (**5**) at time zero (when the melittin is already helical as shown by CD, Fig. (**3a**) at both 25°C and 37°C, for melittin[PA2] and DMPC liposomes, LD~0. After a few minutes at both temperatures a positive LD signal is apparent in the region of 224 nm and 192 nm. The minimum at 210 nm is in fact the negative signal from the long wavelength component of the π-π* transition Fig. (**1**). Since α-helix transitions at 222 nm and 192 nm are polarized perpendicular to the helix axis and that at 210 nm is polarized parallel to the helix axis, [26] and since for liposome-bound chromophores [5, 26]

$$LD = \frac{3}{4} S (1 - 3\cos^2 \beta) A_{iso}$$

where S is the orientation parameter, β is the angle between a transition moment and the normal to the bilayer surface and A_{iso} is the isotropic absorbance of the sample (*i.e.* the unaligned sample), it follows that the melittin is inserting into the bilayer after the first few minutes with either (i) its orientation becoming more parallel to the membrane normal as time goes on or (ii) more melittin inserts.

Given that the α-helical CD signature of melittin with DMPC tells us that it is membrane associated (see above) from the beginning of the LD experiment, it is intriguing that the initial LD is zero. Some of this could be due to melittin being bound to lipid particles too small to orient. However, that does not completely resolve the issue. If the melittin α-helix is lying flat on the surface then its LD sign pattern should simply be approximately opposite from that observed at later time as illustrated in Fig. (**1**). The only other option for having LD=0 but the peptide membrane associated (and folded) is that the dominant 222 nm and 192 nm bands are oriented with transition moments having average orientation close to the magic angle β=54.7°. Since melittin is known to kink at its central proline, the LD therefore suggests that the kink angle is ~110° as illustrated in Fig. (**4**).

The insertion kinetics of melittin with DMPC liposomes are much faster at 25°C than at 37°C Fig. (**5**). Further, by *t*=6 minutes the 25°C melittin LD is back to zero, whereas the 37°C signal begins to decrease only after hours. The reason for the LD at 25 °C having vanished by *t*=6 minutes is apparent from the DLS data Fig. (**6a**): the average vesicle size increases from its initial value of about 180 nm to 240 nm at 3 minutes and then dramatically drops to 25–35 nm These particles are too small or too rigid to orient in the Couette flow. The 37°C data, by way of contrast, shows a gradual increase in LD and no micellisation. The DMPC liposomes alone remain the same size over time, measured using DLS (data not shown). The oriented CD spectra of Fig. (**6b**) measured on a 25°C sample collected at the conclusion of its

kinetic process and then dried onto a flat surface, show that the melittin is still inserted into the bilayer in a trans-membrane orientation (the 208 nm band is attenuated compared with the spectra of Fig. (**3**) and the 192 nm band shifts to longer wavelength) [37].
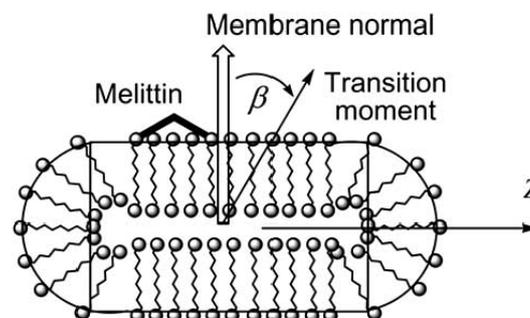
Figure 4. Schematic illustration of melittin (bold lines) bound on the surface of the liposome with the backbone lying at the magic angle to the membrane normal.

Performing the LD/DLS experiment at other temperatures (21° C, 25° C, 29° C, 35° C and 37° C, data not shown) indicated that at the lower temperatures rapid fusion of liposomes followed by lipid micellisation occurs, yet at 35° C and 37° C only gradual fusion of the liposomes occurs. The DMPC phase transition is at 23° C so near the phase transition is where we observe micellisation to occur. It is somewhat counter-intuitive that the insertion is faster in the more rigid lower temperature environment. We return to this below.

The Role of PA2 in Melittin Insertion Kinetics

Since it is known that PA2 hydrolyses lipids and since we see a change (albeit small) in the CD spectrum of melittin with and without catalytic amounts of PA2, we were interested to see how PA2 affected the insertion kinetics of melittin. The data of Fig. (**5**) and Fig. (**7**) show that the same kind of insertion and liposome growth occurs for both melittin[PA2] and melittin[pure], however, it is all noticeably slower and smaller for melittin[pure] at 25°C. At 37°C the kinetics are comparable for both melittin[PA2] and melittin[pure] though melittin[PA2] achieves a higher magnitude *LD* signal. There is no evidence of micellisation on an hours to days timescale at either 25°C or 37°C with melittin[pure]. When we added PA2 (at the upper bound of that present in melittin[PA2] from Sigma) to melittin[pure], then the rates/intensities observed with melittin[PA2] were recovered (or indeed exceeded).

We also investigated the effect of PA2 on DMPC liposomes. The DLS data of Fig. (**7c**) show that PA2 alone does disrupt the liposomes at 25°C, however, the time takes about twenty times longer than that of the combined melittin/PA2 preparation. There was no PA2 LD or CD evident in this sample due to the low protein concentration of PA2.

To determine how the PA2-catalysed DMPC hydrolysis affected melittin interaction with DMPC liposomes we adapted a TLC method taken from the Avanti web site and
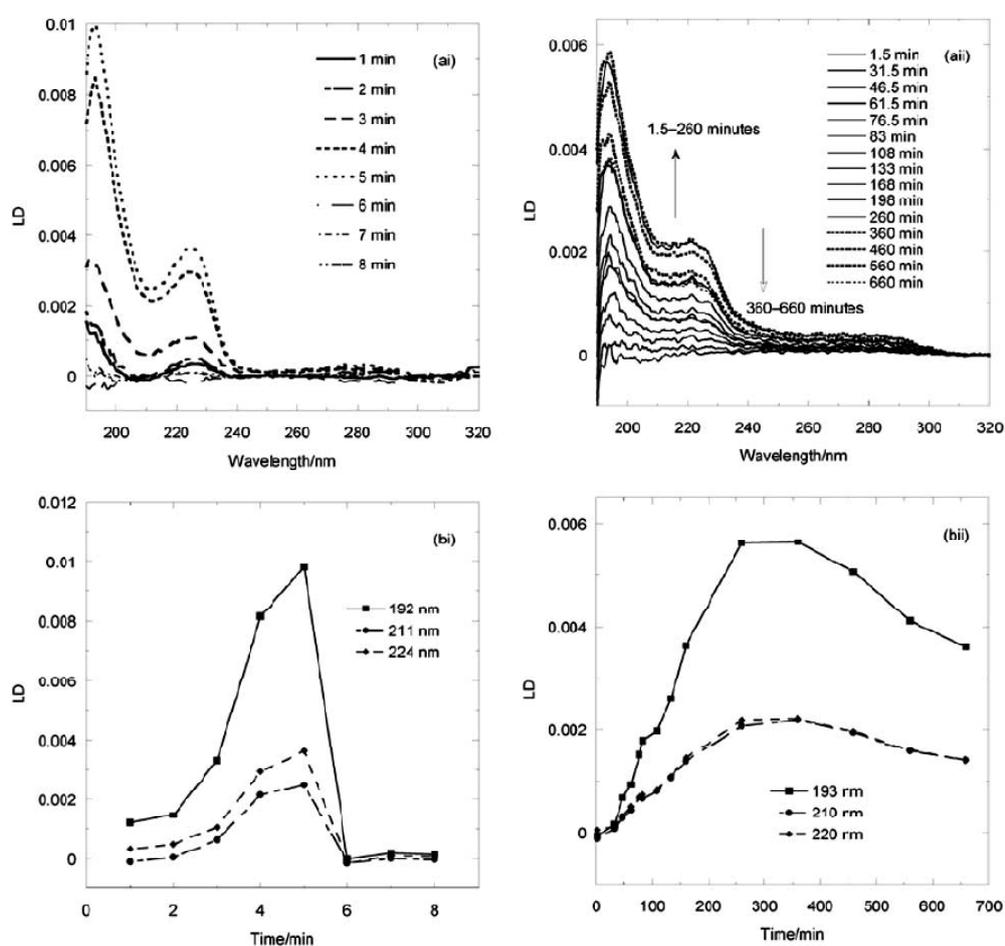
Figure 5. LD of melittin[PA2] (0.1 mg/mL) when added to DMPC liposomes (at molar ratio of lipid: peptide of 100:1) at (i) 25 °C and (ii) 37°C. (**a**) Wavelength scans. (**b**) Data plotted as a function of time at selected wavelengths.
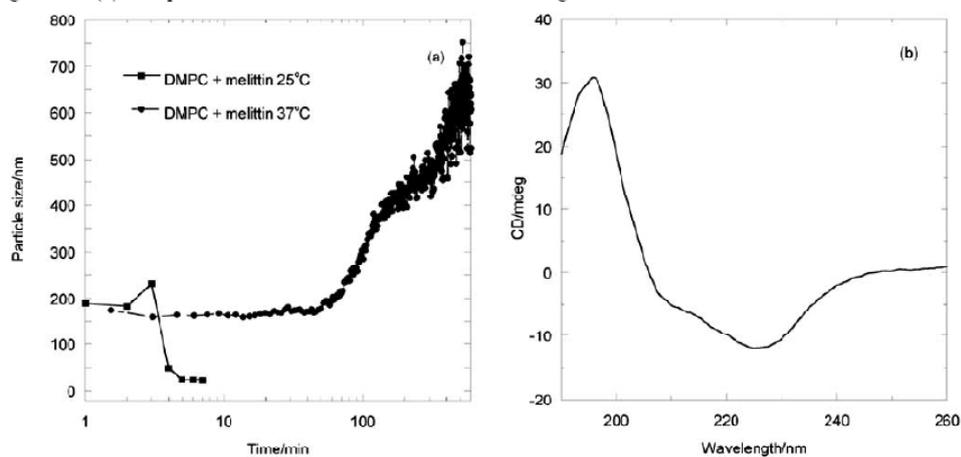
Figure 6. (**a**) DLS of DMPC liposomes after addition of melittin[PA2] (0.1 mg/mL) (at molar ratio of lipid: peptide of 100:1) at 25 °C and 37°C. (Note log scale on *x*-axis.) (**b**) OCD of the 25°C sample at the end of the kinetics after the water has been evaporated.
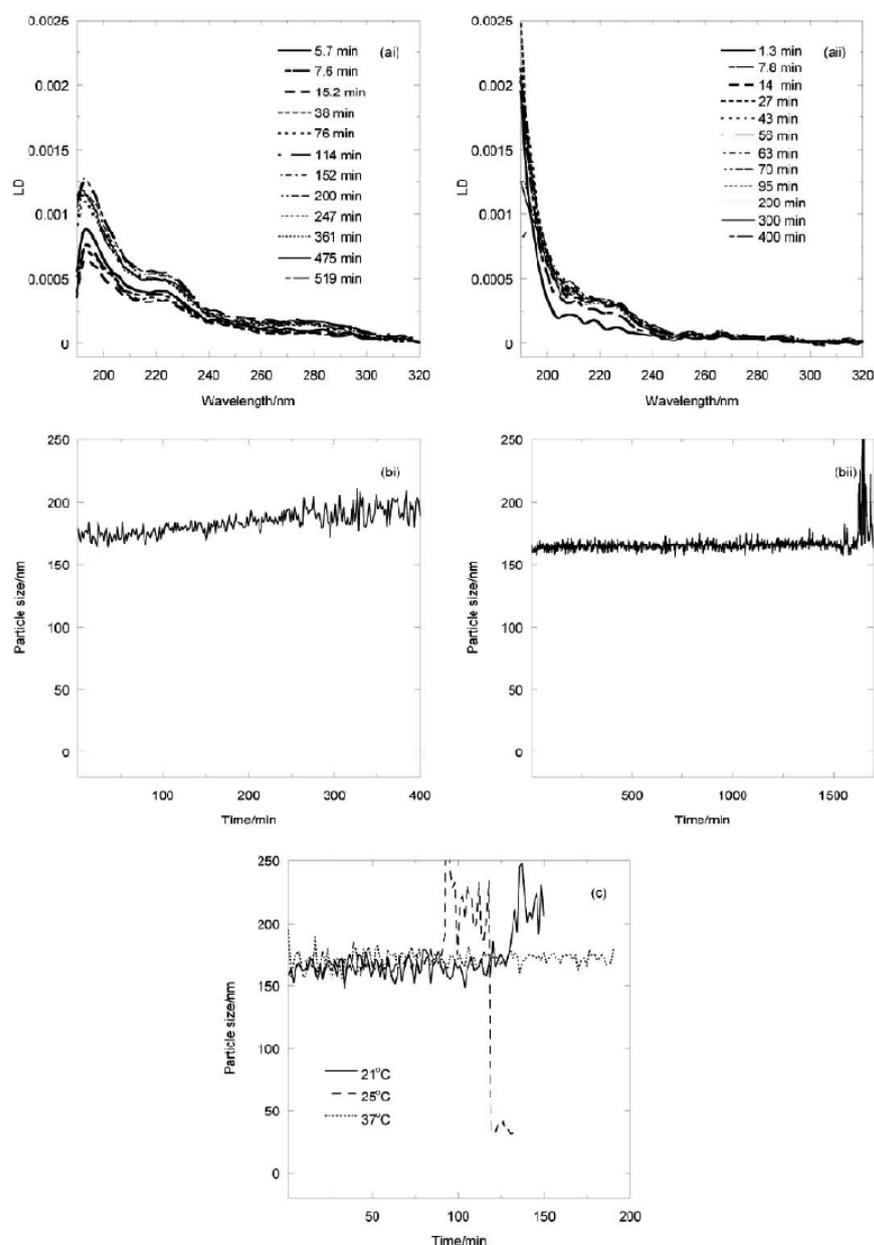
Figure 7. (**a**) LD and (**b**) DLS of melittin^pure (0.1 mg/mL) in DMPC (at molar ratio of lipid: peptide of 100:1) at (i) 25°C and (ii) 37°C. (**c**) DLS of DMPC liposomes with PA2 (0.05 Units) as a function of temperature.

developed a MALDI methodology to follow any changes in the lipids during the insertion reaction. We first established that both the TLC plate and the MALDI matrix (DHB) quenched the enzyme-catalyzed hydrolysis of DMPC, so it was a straightforward matter to sample a reaction at different time-points and measure the lipid content. As shown in Fig. (**8**) the intensity of the DMPC signal reduces and that of lys-

oPC increases at a compensating rate. The TLC results (data not shown) confirm the MALDI data. At about *t*=6 minutes (where the intensities of the DMPC and lysoPC peaks are comparable) the liposomes fragment into smaller particles. Not surprisingly, the *LD* signal is maximum just before this time point
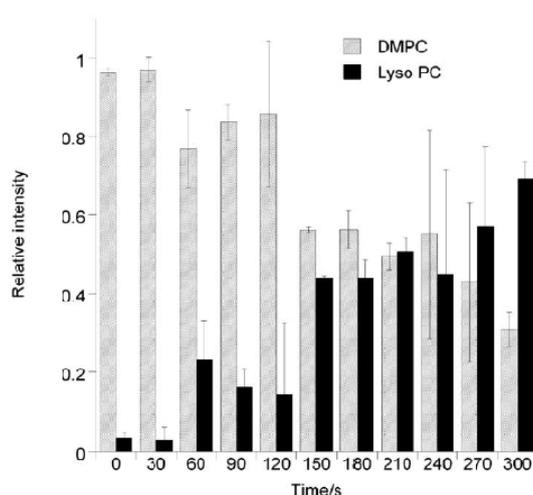
Figure 8. MALDI analysis of the lipids present after melittin[PA2] was added to DMPC liposomes. Experimental details are as for Fig. (**5**). Timepoints are indicated on the figure.

EDTA is known to suppress the activity of PA2 [21]. Addition of EDTA (2 mM) to the DMPC/melittin[PA2] reaction mixture slowed down the whole process (insertion and membrane disruption) to a timescale of tens of hours.

There is evidence in the literature that PA2 activity increases when there are more defects present in the membrane, such as at temperatures near the gel-to-liquid crystalline transition temperature, [38-41] following adsorption of disruptive molecules such as peptides (particularly in the gel phase), [42-47] or electrical disruption. [48] It has been suggested that the activities of melittin and PA2 are synergistic, [49, 50] a notion that is supported by the data presented in this paper. It is somewhat counter-intuitive that the insertion is faster in the more rigid lower temperature environment, but this may be the underlying reason.

Melittin Insertion as a Function of Lipid Composition

Biological membranes are made predominately of *sn*-1 saturated, *sn*-2 unsaturated acyl chains or even of phospholipids with two polyunsaturated acyl chains. Phospholipids with polyunsaturated acyl chains are known to influence membrane dynamics [51, 52]. Further, it has been shown that the degree of unsaturation of a membrane modulates the membrane-disruption action of melittin (lytic power and bilayer micellisation) [36]. This has been claimed to be at least in part due to the secondary structure of melittin changing with the membrane. However, as discussed above, their observed increase in the 222 nm CD band is more likely to be due to better packing of the hydrophobic phase. We therefore chose to consider the effect of melittin[PA2] on a range of lipids formed into liposomes.

DLS showed us a first difference between the lipids, namely that the vesicles made from unsaturated lipids by extruding through a 100 nm polycarbonate membrane were approximately twice the size of those made from saturated vesicles (which were ~110 nm). This reflects the greater flexibility of the unsaturated lipid vesicles operating during the extrusion process.

The maximum LD signals, obtained after the time indicated in the figure, are shown in Fig. (**9**). From the data it can be concluded that the orientation of melittin is similar in all the systems studied. Although the unsaturated lipids have slightly larger signals, as their lipids are of higher molecular weight and the sample viscosity is somewhat higher we cannot ascribe any significance to this. Another key parameter is how quickly that maximum signal is obtained. The peptide adopts its maximum LD signal in the order indicated in Table 2. Somewhat surprisingly the slightly higher temperature but still less flexible saturated gel-phase membranes obtain maximum transmembrane orientation (LD maximum) more quickly than the unsaturated more flexible ones. Addition of negative lipids speeds the process up for the saturated lipids whereas it slows it down further for the unsaturated one. Pure DPPC Table 2, Fig. (**9**) shows no LD signal. Overall, the LD data suggest that flexibility of the membrane slows down the insertion process but the end product is better oriented.

Table 2. Summary of Kinetic Data for Melittin as a Function of Lipid Properties. Ranking is as Follows: 0 Denotes None; 1 Denotes Least Flexible/Rate of Insertion / Micellisation / Fusion; 2 Denotes Slightly More /etc./

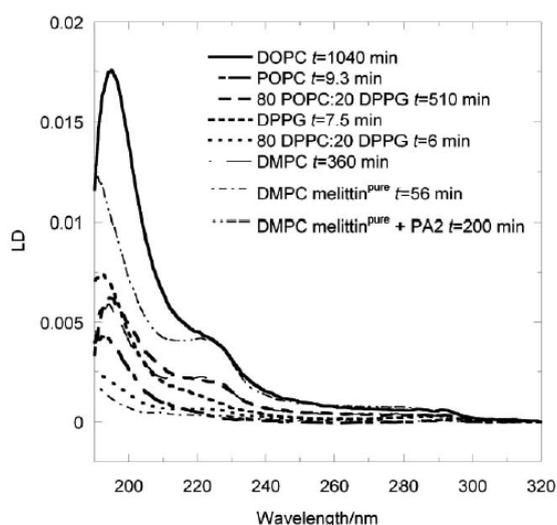|	DOPC	POPC/DPPG	DMPC 37°	POPC	DPPG	DMPC 25°C	DPPC/DPPG	DPPC
	18:1_18:1	18:1_16:0/16:0	14:0	18:1_16:0	16:0	14:0	16:0/16:0	16:0
Estimate of membrane flexibility	8	7	5	5	1	2	2	2
Negative charge	0	1	0	0	2	0	1	0
LD intensity	7	3	4	2	5	6	1	0
Rate of insertion	1	2	3	4	5	6	7	0 (no LD)
Micellisation	0	0	0	1	0	3	2	4
Fusion	3	4	4	2	0	1	0	5

Figure 9. Maximum LD spectra obtained for melittin^PA2 (0.1 mg/mL) added to liposomes at lipid:peptide ratio of 100:1. Times and lipids are indicated on the figure.

Not only does the membrane provide an environment for the peptide, it is also affected by the peptide as summarized in Table **2**. Two competing perturbations to the membranes occur: fusion and micellisation. Negative charge and unsaturation increase the tendency for the liposomes to grow (presumably by fusion) in size whereas saturation (or more rigid membranes, *e.g.* the gel phase of DMPC) favours membrane micellisation. However, this conclusion is over simplistic since POPC with one double bond is dominated by micellisation.

CONCLUSION

For the first time, in this work, flow aligned linear dichroism has been applied to study the orientation of melittin in the membrane-mimicking environment of a liposome. It is the ideal technique for such real-time measurements. Overall, the pattern is a very complicated molecular process even for a simple peptide such as melittin, however, LD helps one clearly identify when insertion is happening which improves our ability to analyse peptide/membrane interactions. However, LD does not stand on its own and needs to be complemented by a range of other biophysical techniques.

Melittin is co-purified from bee venom with phospholipase A2. They were known to affect each other's behaviour. We developed TLC and MALDI methods from those available in the literature to follow the lipid kinetics in parallel with the LD experiments. We found that PA2 speeded up the insertion of melittin (as measured by the increase of the LD signal) and also speeded up any membrane disruption that melittin induces. Similarly, melittin speeds up the phospholipase action of PA2. However, by comparing melittin co-purified with phospholipase A2, pure melittin and pure melittin doped with phospholipase A2 we concluded there was no other difference in behaviour. We therefore focused our

analysis on melittin with catalytic amounts of the enzyme as a more representative sample of the action of native melittin.

For the first time we have surveyed the behaviour of melittin with a range of lipids. Overall our conclusions about melittin are that melittin is helical with all the lipids studied, though random coil in aqueous solution. When added to liposomes it rapidly folds and then inserts more or less parallel to the membrane normal. The membrane insertion behaviour of melittin varies with lipid and membrane phase. In general terms, the insertion is faster with more rigid lipids but generally reaches a higher level (as indicated by LD magnitude) with less rigid lipids. Inclusion of 20% negatively-charged lipids affects the insertion, speeding the process up for the saturated lipids but slowing it down further for the unsaturated one. We detected no insertion with the liposomes made from 100% of the long chain saturated lipid DPPC. Any assessment of insertion effectiveness is affected by how the melittin is perturbing the membrane: it can induce both fusion and micellisation—the latter leading to no LD while retaining insertion into the membrane. Saturated lipids are more prone to micellisation.

The mechanistic conclusions to be deduced from this work relate to the insertion/fusion/micellation properties of melittin with a range of lipids, which suggest a mechanism whereby melittin in collaboration with phospholipaseA2 acts on membranes to insert and then degrade the lipids to facilitate micellisation. This will enable the melittin to be recycled to affect more membranes than the initial target. These observations are consistent with the recent realization that the way many cationic amphiphilic drugs work is by catalysing the chemical degradation of the phospholipid fabric of plasma membranes. Melittin as with other peptides thus does not simply interact passively with cellular membranes as postulated by current drug translocation mechanisms, rather it is an active physical and chemical process [20, 53-54].

ACKNOWLEDGEMENTS

REFERENCES

[1] Wallin, E.; von Heijne, G. Genome-wide analysis of integral membrane proteins from eubacterial, archaean, and eukaryotic organisms. *Protein Sci.,* **1998**, *7*, 1029-1038.
[2] Terstappen, G. C.; Reggiani, A. In silico research in drug discovery. *Trends Pharmacol. Sci.,* **2001**, *22*, 23-26.
[3] Vaara, M. New approaches in peptide antibiotics. *Curr. Opin. Pharmacol.,* **2009**, *9*, 571-576.
[4] Hancock, R. E. W.; Chappel, D. S. Peptide antibiotics. *Antimicrob. Agents Chemother.,* **1999**, *43*(6), 1317-1323.
[5] Ardhammar, M.; Mikati, N.; Nordén, B. Chromophore orientation in liposome membranes probed with flow linear dichroism. *J. Am. Chem. Soc.,* **1998**, *120*, 9957-9958.
[6] Rajendra, J.; Baxendale, M.; Dit Rap, L. G.; Rodger, A. Flow linear dichroism to probe binding of aromatic molecules and DNA to single walled carbon nanotubes. *J. Am. Chem. Soc.,* **2004**, *126*, 11182-11188.
[7] Rajendra, J.; Damianoglou, A.; Hicks, M.; Booth, P.; Rodger, P. M.; Rodger, A. Quantitation of protein orientation in flow-oriented unilamellar liposomes by linear dichroism. *Chem. Phys.,* **2006**, *326*(1), 210-220.
[8] Ennaceur, S. M.; Hicks, M. R.; Pridmore, C. J.; Dafforn, T. R.; Rodger, A.; Sanderson, J. M. Peptide adsorption to lipid bilayers:

Slow rearrangement processes revealed by linear dichroism spectroscopy. *Biophys. J.*, 2009, *96*(4), 1399-1407.

[9] Esbjörner, E. K.; Caesar, C. E. B.; Albinsson, B.; Lincoln, P.; Nordén, B. Tryptophan orientation in model lipid membranes. *Biochem. Biophys. Res. Commun.*, 2007, *361*, 645-650.

[10] Esbjörner, E. K.; Oglcka, K.; Lincoln, P.; Gräslund, A.; Nordén, B. Membrane binding of ph-sensitive influenza fusion peptides. Positioning, configuration, and induced leakage in a lipid vesicle model. *Biochemistry*, 2007, *46*, 13490-13504.

[11] Hicks, M. R.; Dafforn, T.; Damianoglou, A.; Wormell, P.; Rodger, A.; Hoffmann, S. V. Synchrotron radiation linear dichroism spectroscopy of the antibiotic peptide gramicidin in lipid membranes. *Analyst*, 2009, *134*, 1623-1628.

[12] Hicks, M. R.; Damianoglou, A.; Rodger, A.; Dafforn, T. R. Folding and membrane insertion of the pore-forming peptide gramicidin occur as a concerted process. *J. Mol. Biol.*, 2008, *383*(2), 358-66.

[13] Raghuraman, H.; Chattopadhyay, A. Melittin: a membrane-active peptide with diverse functions. *Biosci. Rep.*, 2007, *27*, 189-223.

[14] Talbot, J. C. Conformational change and self association of monomeric melittin. *FEBS Lett.*, 1979, *102*, 191-193.

[15] Dempsey, C. E. The actions of melittin on membranes. *Biochim. Biophys. Acta*, 1990, *1031*, 143-161.

[16] Shai, Y. Molecular recognition between membrane–spanning polypeptides. *Trends Biochem. Sci.*, 1995, *20*, 460-464.

[17] Papo, N.; Shai, Y. Exploring peptide membrane interaction using surface plasmon resonance: Differentiation between pore formation versus membrane disruption by lytic peptides. *Biochemistry*, 2003, *42*, 458-466.

[18] Bogaart, G. v. d.; Guzmán, J. V.; Mika, J. T.; Poolman, B. On the mechanism of pore formation by melittin. *J. Biol. Chem.*, 2008, *283*, 33854-33857.

[19] Manna, M.; Mukhopadhyay, C. Cause and effect of melittin-induced pore formation: A computational approach. *Langmuir*, 2009, *25*, 12235-12242.

[20] Casey, D. R.; Sebai, S. C.; Shearman, G. C.; Ces, O.; Law, R. V.; Gee, A. D.; Templer, R. H. Formulation affects the rate of membrane degradation catalyzed by cationic amphiphilic drugs. *Ind. Eng. Chem. Res.*, 2008, *47*, 650-665.

[21] Dempsey, C. E.; Watts, A. A. Deuterium and phosphorus-31 nuclear magnetic resonance study of the interaction of melittin with dmpc bilayers and the effects of contaminating phospholipase a2. *Biochemistry*, 1987, *26*, 5803-5811.

[22] Marrington, R.; Dafforn, T. R.; Halsall, D. J.; Hicks, M.; Rodger, A. Validation of new microvolume couette flow linear dichroism cells. *Analyst*, 2005, *130*, 1608-1616.

[23] Marrington, R.; Dafforn, T. R.; Halsall, D. J.; Rodger, A. Micro volume couette flow sample orientation for absorbance and fluorescence linear dichroism. *Biophys. J.*, 2004, *87*, 2002-2012.

[24] Rodger, A.; Marrington, R.; Geeves, M. A.; Hicks, M.; de Alwis, L.; Halsall, D. J.; Dafforn, T. R. Looking at long molecules in solution: What happens when they are subjected to couette flow? *Phys. Chem. Chem. Phys.*, 2006, *8*(27), 3161-3171.

[25] Rodger, A.; Patel, K. K.; Sanders, K. J.; Datt, M.; Sacht, C.; Hannon, M. J. Anti-tumour platinum acylthiourea complexes and their interactions with DNA. *Dalton*, 2002, 3656-3663.

[26] Rodger, A.; Rajendra, J.; Marrington, R.; Ardhammar, M.; Nordén, B.; Hirst, J. D.; Gilbert, A. T. B.; Dafforn, T. R.; Halsall, D. J.; Woolhead, C. A.; Robinson, C.; Pinheiro, T. J.; Kazlauskaite, J.; Seymour, M.; Perez, N.; Hannon, M. J. Flow oriented linear dichroism to probe protein orientation in membrane environments. *Phys. Chem. Chem. Phys.*, 2002, *4*, 4051-4057.

[27] Andersson, A.; Biverståhl, H.; Nordin, J.; Lindahl, E.; Maler, L. The membrane induced structure of melittin is correlated with the fluidity of the lipids. *Biochim. Biophys. Acta*, 2007, *1768*, 115-121.

[28] Constantinescu, I.; Lafleur, M. Influence of the lipid composition on the kinetics of concertedinsertion and folding of melittin in bilayers. *Biochim. Biophys. Acta*, 2004, *1667*, 26-37.

[29] Ghosh, A. K.; Rukmini, R.; Chattopadhyay, A. Modulation of tryptophan environment in membrane-bound melittin by negatively charged phospholipids: Implications in membrane organization and function, . *Biochemistry*, 1997, *36*, 14291-14305.

[30] Raghuraman, H.; Chattopadhyay, A. Interactions of melittin with membrane cholesterol: A fluorescence approach. *Biophys. J.*, 2004, *87*, 2419-2432.

[31] Sui, S. Conformational changes of melittin upon insertion into phospholipid monolayer and vesicle. *J. Biochem.*, 1994, *116*, 482-487.

[32] Veen, M. V.; Georgiou, G. N.; Drake, A. F.; Cherry, R. J. Circular-dichroism and fluorescence studies on melittin: Effects of c-terminal modifications on tetramer formation and binding to phospholipid vesicles. *Biochem. J.*, 1995, *305*, 785-790.

[33] Ladokhin, A. S.; White, S. H. Folding of amphipathic alpha-helices on membranes: Energetics of helix formation by melittin. *J. Mol. Biol.*, 1999, *285*, 1363-1369.

[34] Lazarova, T.; Brewin, K. A.; Stoeber, K.; Robinson, C. R. Characterization of peptides corresponding to the seven transmembrane domains of human adenosine a_{2a} receptor. *Biochemistry*, 2004, *43*, 12945-12954.

[35] Thevenin, D.; Lazarova, T.; Roberts, M. F.; Robinson, C. R. Oligomerization of the fifth transmembrane domain from the adenosine a_{2a} receptor. *Protein Sci.*, 2005, *14*, 2177-2186.

[36] Raghuraman, H.; Chattopadhyay, A. Influence of lipid chain unsaturation on membrane bound melittin : a fluorescence approach. *Biochim. Biophys. Acta*, 2004, *1665*, 29-39.

[37] Nordén, B.; Rodger, A.; Dafforn, T. Linear dichroism and circular dichroism: A textbook on polarized-light spectroscopy. Royal Society of Chemistry: Cambridge, 2010.

[38] Apitz-Castro, R.; Jain, M. K.; De Haas, G. H. Origin of the latency phase during the action of phospholipase a2 on unmodified phosphatidylcholine vesicles. *Biochim. Biophys. Acta*, 1982, *688*(2), 349-56.

[39] Bell, J. D.; Burnside, M.; Owen, J. A.; Royall, M. L.; Baker, M. L. Relationships between bilayer structure and phospholipase a2 activity: Interactions among temperature, diacylglycerol, lysolecithin, palmitic acid, and dipalmitoylphosphatidylcholine. *Biochemistry*, 1996, *35*(15), 4945-55.

[40] Op den Kamp, J. A.; Kauerz, M. T.; van Deenen, L. L. Action of pancreatic phospholipase a2 on phosphatidylcholine bilayers in different physical states. *Biochim. Biophys. Acta*, 1975, *406*(2), 169-77.

[41] Wells, M. A. Mechanism of interfacial activation of phospholipase a2. *Biochemistry*, 1974, *13*(11), 2248-2257.

[42] Code, C.; Domanov, Y. A.; Kilhan, J. A.; Kinnunen, P. K. Activation of phospholipase a2 by temporin b: Formation of antimicrobial peptide-enzyme amyloid-type cofibrils. *Biochim. Biophys. Acta*, 2009, *1788*(5), 1064-72.

[43] Koumanov, K.; Momchilova, A.; Wolf, C. Bimodal regulatory effect of melittin and phospholipase a2-activating protein on human type ii secretory phospholipase a2. *Cell Biol. Int.*, 2003, *27*(10), 871-7.

[44] Mingarro, I.; Perez-Paya, E.; Pinilla, C.; Appel, J. R.; Houghten, R. A.; Blondelle, S. E. Activation of bee venom phospholipase a2 through a peptide-enzyme complex. *FEBS Lett.*, 1995, *372*(1), 131-4.

[45] Pochet, S.; Tandel, S.; Querriere, S.; Tre-Hardy, M.; Garcia-Marcos, M.; De Lorenzi, M.; Vandenbranden, M.; Marino, A.; Devleeschouwer, M.; Dehaye, J. P. Modulation by ll-37 of the responses of salivary glands to purinergic agonists. *Mol. Pharmacol.*, 2006, *69*(6), 2037-46.

[46] Signor, G.; Mammi, S.; Peggion, E.; Ringsdorf, H.; Wagenknecht, A. Interaction of bombolitin iii with phospholipid monolayers and liposomes and effect on the activity of phospholipase a2. *Biochemistry*, 1994, *33*(21), 6659-70.

[47] Zhao, H.; Kinnunen, P. K. Modulation of the activity of secretory phospholipase a2 by antimicrobial peptides. *Antimicrob. Agents Chemother.*, 2003, *47*(3), 965-71.

[48] Thuren, T.; Tulkki, A. P.; Virtanen, J. A.; Kinnunen, P. K. Triggering of the activity of phospholipase a2 by an electric field. *Biochemistry*, 1987, *26*(16), 4907-10.

[49] Dufton, M. J.; Hider, R. C.; Cherry, R. J. The influence of melittin on the rotation of band 3 protein in the human erythrocyte membrane. *Eur. Biophys. J.*, 1984, *11*(1), 17-24.

[50] Rudenko, S. V.; Nipot, E. E. Protection by chlorpromazine, albumin and bivalent cations against haemolysis induced by melittin, [ala-14]melittin and whole bee venom. *Biochem. J.*, 1996, *317 (Pt 3)*, 747-54.

[51] Mitchell, D. C. Molecular order and dynamics in bilayers consisting of highly polyunsaturated phospholipids. *Biophys. J.*, 1998, *74*, 879-891.

[52]   Saiz, L. Computer simulation studies of model biological membranes. *Acc. Chem. Res.*, 2002, *35*, 482-489.

[53]   Baciu, M.; Sebai, S. C.; Ces, O.; Mulet, X.; Clarke, J. A.; Shearman, G. C.; Law, R. V.; Templer, R. II.; Plisson, C.; Parker, C. A.; Gee, A. Degradative transport of cationic amphiphilic drugs

across phospholipid bilayers. *Philos. Trans. R. Soc., A*, 2006, *364*, 2597-2614.

[54]   Shearman, G. C.; Attard, G. S.; Hunt, A. N.; Jackowski, S.; Baciu, M.; Sebai, S. C.; Mulet, X.; Clarke, J. A.; Law, R. V.; Plisson, C.; Parker, C. A.; Gee, A.; Ces, O.; Templer, R. H. Using membrane stress to our advantage. *Biochem. Soc. Trans.*, 2007, *35*, 498-501.

298

Acyl transfer from phosphocholine lipids to melittin†

Catherine J. Pridmore,[a] Jackie A. Mosely,[a] Alison Rodger[b] and John M. Sanderson[*a]

Transfer of fatty acyl groups from membrane phospholipids to melittin, a commonly studied membrane-active peptide, has been observed to occur over extended time periods. Transfer can be detected after 1–2 days and selectively targets amino groups at the N-terminal end of the peptide.

Chemical modifications to peptides and proteins, most notably the addition of acyl groups such as myristoyl or palmitoyl, are known to produce profound changes to the membrane behaviour of these molecules, with effects including increased membrane affinity and modified partitioning behaviour.[1–3] Acyl groups are usually added enzymatically *in vivo* (both translationally and post-translationally).[3] In the absence of enzyme catalysis, the membrane itself is generally seen as an inert medium. Despite the large number of membrane-active peptides that are studied for their intrinsic membrane behaviour, or as models for proteins, the chemical purity and identity of peptide–lipid systems is seldom examined upon the completion of binding experiments. Most biological membranes have a significant protein content (typically between 20% and 80% by weight)[4] and proteins may be in contact with the membrane for a considerable period of time before recycling, with half-lifes ranging from minutes to days.[5,6] As a consequence, studying the longer term behaviour of peptide– and protein–lipid systems is of fundamental interest, particularly with regard to examining the reactivity of these systems towards reactions such as acyl transfer from the lipids to the protein.

Melittin (H-GIGAVLKVLTTGLPALISWIKRKRQQ-NH₂) is a widely studied membrane active peptide, with well-documented pore-forming properties.[7] During the course of experiments to examine the effects of melittin on lipid stability,[8] we undertook control experiments using synthetic melittin in order to circumvent the possibility of complications due to any activity of the enzyme phospholipase A₂ (PLA₂), which is usually co-purified with melittin prepared from bee venom.[9] Addition of synthetic melittin to liposomes composed of 1,2-dioleoyl-*sn*-glycero-3-phosphocholine (DOPC) in phosphate buffered saline (PBS) at 37 °C and pH 7 led to the formation of new species, detectable in the mass spectrum of the sample (Fig. 1A) after a period of 1–2 days. These new species are identified as melittin plus the addition of an oleoyl chain, observed as protonated and sodiated adducts. When incubated under similar conditions with liposomes prepared using
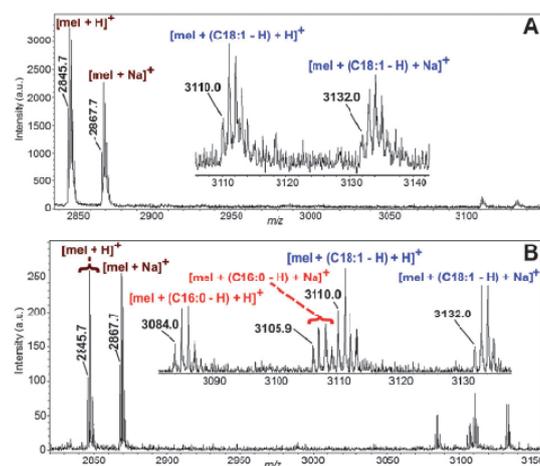
[a] *Department of Chemistry, Durham University, South Road, Durham, DH1 3LE, UK. E-mail: j.m.sanderson@durham.ac.uk; Tel: +44 (0)191 3342107*
[b] *University of Warwick, Department of Chemistry, Coventry, CV4 7AL, UK. E-mail: A.Rodger@warwick.ac.uk; Tel: +44 (0)24 7652 3234*

Fig. 1 Mass spectrum of melittin following mixing with DOPC (A) and POPC liposomes (B) at 37 °C in PBS (8 mM phosphate, 123 mM NaCl) at pH 7. Melittin and lipid concentrations were 71 μM and 0.35 mM, respectively. Mass spectra were obtained after 14 days (A) or 28 days (B) using matrix-assisted laser desorption ionisation (MALDI) with α-cyano-4-hydroxycinnamic acid (CHA) as matrix. Ions at *m/z* 3110.0 and 3132.0 are assigned as [melittin + (oleoyl − H) + H]⁺ and [melittin + (oleoyl − H) + Na]⁺, respectively (calculated monoisotopic *m/z* 3110.0 and 3132.0); ions at *m/z* 3084.0 and 3105.9 are assigned as [melittin + (palmitoyl − H) + H]⁺ and [melittin + (palmitoyl − H) + Na]⁺, respectively (calculated monoisotopic *m/z* 3084.0 and 3106.0).

1-palmitoyl-2-oleoyl-*sn*-glycero-3-phosphocholine (POPC), species were observed after 2 days corresponding to the transfer of either an oleoyl or a palmitoyl group from the lipid to the peptide (Fig. 1B), again as protonated and sodiated adducts.

Further analysis by TLC and mass spectrometry revealed the presence of *lyso*-phosphatidylcholine (*lyso*-PC) in the mixtures, indicating that the reaction to produce the acylated melittin species was likely to involve attack of a reactive nucleophile on the peptide with the carbonyl groups of the lipid esters. In order to monitor the progress of the reaction, the experiments were repeated and the formation of *lyso*-PC was followed by mass spectrometry as an indicator of the extent of reaction. Experiments were conducted at a molar peptide : lipid ratio of 1 : 5. Although this ratio is at the upper end of the range typically used for membrane binding experiments, at lower peptide concentrations it proved challenging to detect the formation of small quantities of the reaction products in the presence of a large excess of lipid.

Even at a molar peptide : lipid ratio of 1 : 5, due to the excess of lipid it was necessary to remove and concentrate (by lyophilisation) a significant volume of the sample in order
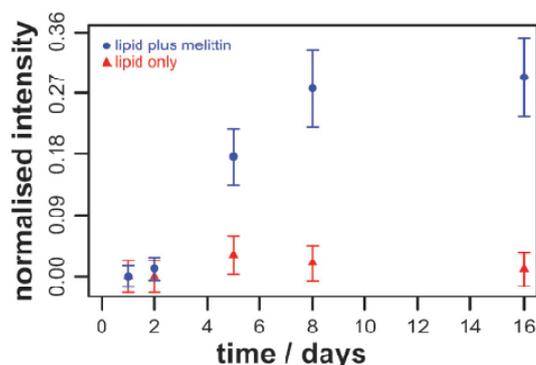
Fig. 2 The formation of *lyso*-PC monitored by MALDI-MS following mixing of melittin (71 μM) with DOPC liposomes (0.35 mM) in PBS at 37 °C and pH 7. MALDI-MS was performed using 2,5-dihydroxybenzoic acid as matrix. Normalised peak intensities for *lyso*-PC are calculated as the sum of the intensities of the protonated and sodiated *lyso*-PC peaks divided by the sum of the intensities of the protonated and sodiated *lyso*-PC and DOPC peaks. Errors are estimated from repeat experiments.

to detect the *lyso*-PC by TLC. With DOPC, in the initial stages (Fig. 2) the reaction was slow, with the first statistically significant detection of *lyso*-PC after 2 days. The intensity of the *lyso*-PC peaks increased steadily over the next 14 days and then increased slowly thereafter. No formation of *lyso*-PC was observed in control experiments without melittin and oleic acid was not detected in any of the samples (with or without melittin), indicating that the level of background lipid hydrolysis was negligible. Due to absence of either competing hydrolysis or multiple acylation products, the formation of *lyso*-PC was therefore taken to be a reliable indicator of the extent of melittin acylation.

After 16 days, the relative intensity of the *lyso*-PC peaks was 0.3 ± 0.05. By comparison with a 1-oleoyl-*sn-glycero*-3-phosphocholine/DOPC calibration curve, this corresponded to a mole fraction of *lyso*-PC in the sample of 0.1 ± 0.02 and a corresponding extent of conversion of the melittin to acylated product of 50 ± 10%. This compared favourably with estimation of the extent of *lyso*-PC formation by TLC, which also indicated an extent of conversion of 50 + 10% after 17 days (see the ESI[1]). In experiments with POPC, similar kinetic profiles were obtained, with relative *lyso*-PC peak intensities of 0.15 for palmitoyl-*sn-glycero*-3-phosphocholine (corresponding to oleoyl transfer) and 0.07 for oleoyl-*sn-glycero*-3-phosphocholine (corresponding to palmitoyl transfer) after 14 days, and corresponding values of 0.18 and 0.10 after 28 days (see the ESI†). These data indicated that acyl transfer from POPC was slower than from DOPC, and transfer of the oleoyl group was favoured over the palmitoyl group.

The most favourable positions of melittin for nucleophilic attack could reasonably be proposed as the N-terminal amino group and the ε-amino groups of the three lysines (K7, K21 and K23). Tandem mass spectrometry (MS/MS) was therefore performed on unmodified melittin and acylated melittin precursor ions in order to generate fragments that would permit the site of acylation to be localised. Performing all of these MS/MS analyses on the same sample, under identical conditions, enabled direct comparisons to be made between them. MS/MS of peptides generally induces cleavage along the backbone. Products of such cleavages are labelled as a-, b- or c-type should the fragment retain the N-terminus, and x-, y- or z-type should it retain the C-terminus.[10] In our case, a key requirement for confirming acylation at a particular site was the ability to identify unique product ions that only matched modification at that site and were therefore absent from the spectrum of the unmodified peptide. Furthermore, for reaction at a melittin amino group leading to amide formation, it was to be expected that cleavage of the acyl group would occur under MS/MS conditions, resulting in the formation of ions with similar or identical masses to the unmodified peptide. This was confirmed in the product ion spectra of both modified forms of melittin (*m/z* 3083 and 3110), in which an ion corresponding to loss of the acyl group was observed at *m/z* 2845. As a consequence, ladders of unmodified ions at the N-terminus or C-terminus of the peptide were unreliable as a means of identifying sites of modification.

In the product ion spectrum of oleoyl–melittin (*m/z* 3110), a ladder of b-type product ions can be identified that corresponds to N-terminal modification (Fig. 3a), although the first ion in this series (corresponding to the oleoylated N-terminal Gly) is absent. Nevertheless, the ions with *m/z* 435.3, 492.2 and 563.2 are unique to this spectrum and can be assigned as oleoylated fragments with confidence. These N-terminal fragment ions are consistent with the addition of an oleoyl group to the N-terminus of the peptide. A weak fragment with *m/z* 758.4 is also unique to this spectrum and matches a b-type fragment that has lost ammonia (oleoyl-GIGAVL, b-17-type). An additional b-type fragment is found at *m/z* 1000.3 (oleoyl-GIGAVLKV) and a fragment assigned as an a-18-type at *m/z* 1069.5 (oleoyl-GIGAVLKVL). These latter two product ions are again consistent with N-terminal modification, but may also arise through modification of K7. Interestingly, the high-intensity ion with *m/z* 492.2 is also a match for an internal fragment with K7 oleoylation (oleoyl-KV, formed *via* b/y-type cleavage). A corresponding ion at *m/z* 464.1 matches both an a-type fragment (oleoyl-GIG) and an internal fragment (oleoyl-KV, formed *via* a/y-type cleavage). Weak ions at *m/z* 888.7 and 808.3 match internal fragments that include only K7 (oleoyl-AVLKVL and oleoyl-KVLTT), although the latter of these is also present in the spectrum of the unmodified melittin (Fig. 3c). None of the higher mass fragments enabled the position of modification to be identified with certainty. Taken together, it is clear that the N-terminal amino group is a significant site of modification, with likely additional modification of the side chain of K7. No evidence could be found for the addition of oleoyl groups to the remaining two lysines (K21 and K23).

Fragmentation of the palmitoylated melittin ion at *m/z* 3083 yields an N-terminal ladder of b-type ions at *m/z* 296.1, 409.2, 466.2, 537.2 and 636.3 (Fig. 3b). Of these, the ions at *m/z* 409.2, 466.2 and 537.2 are unique to this spectrum. As with the product ion spectrum of oleoylated melittin, the peak at 466.2 can also be assigned as a palmitoylated internal fragment (palmitoyl-KV in this case). An additional fragment unique to this spectrum at *m/z* 782.1 is assigned as an internal fragment involving modification of the side chain of
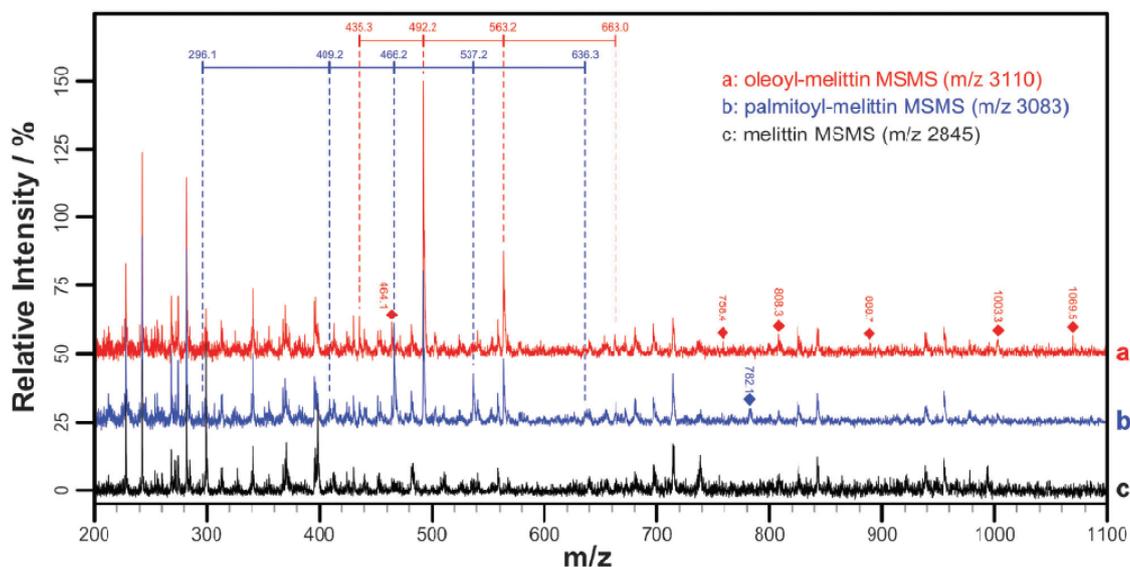
Fig. 3 A section of the MALDI-MS/MS spectra of (a) oleoyl–melittin (m/z 3110, offset on the y-axis by 50%), (b) palmitoyl–melittin (m/z 3083, offset on the y-axis by 25%) and (c) melittin (m/z 2845) from a sample of melittin incubated with POPC in PBS for 28 days at 37 °C, pH 7. Ladders corresponding to modified b-type fragments are indicated by dashed vertical lines. Key ions corresponding to modified (or potentially modified) fragments are indicated by diamonds. Spectra were obtained using CHA as matrix and are base peak normalised. See the ESI† for full spectra and assignments.

K7 (palmitoyl-KVLTT formed *via* b/y-type cleavage). A number of product ions in this spectrum correspond to oleoylated products (*e.g.* the ion at m/z 492.2), which indicates that isolation of the parent ion was not complete. Nevertheless, these ions do not prohibit the identification of unique palmitoylated fragments. It may therefore be concluded that palmitoyl modification occurs at the N-terminal amino group, with the side chain of K7 likely to be an additional site of modification. No acyl melittin could be detected when peptide : lipid ratios were lowered to 1 : 50, although this may be more a consequence of a lack of relative sensitivity of the analytical methods than a lack of reaction. A number of other experiments were conducted in order to examine the effects of salts and metal ions on the acylation process. Repeating the experiments with DOPC in the presence of zinc or calcium salts gave data comparable to the PBS/NaCl data. Conducting the experiments with DOPC in phosphate buffer alone (*i.e.* without NaCl or any other metal salts) yielded no detectable oleoylated products. This latter result may reflect either a change in reactivity, or salt-related effects on melittin conformation.[11]

Overall, it is apparent that the amino groups of a prototypical membrane-active peptide are able to react with the ester groups of phosphocholines to yield product amides with an acyl group appended to the peptide. In the case of melittin at least, this process is selective for amino groups near the N-terminus of the peptide. The rate of acylation, although slow, is nevertheless relevant for membrane proteins that exhibit low rates of turnover in biological membranes. The ratio of peptide to lipid used, although higher than normal for many peptide binding experiments, is still within the range found for proteins in biological membranes, and as a consequence raises the possibility that similar processes may occur *in vivo*. It should be noted that it is unclear whether this reactivity of melittin is typical of all membrane peptides (and proteins), or the result of a particular chemical or structural feature of the peptide that favours reaction. It is perfectly feasible that this reaction will be promoted by the presence of particular amino acids near the sites of acylation and the scope of this reaction therefore merits further scrutiny.

Notes and references

1 J. E. Smotrys and M. E. Linder, *Annu. Rev. Biochem.*, 2004, **73**, 559; M. J. Nadolski and M. E. Linder, *FEBS J.*, 2007, **274**, 5202.
2 N. Hayashi and K. Titani, *Proc. Jpn. Acad., Ser. B*, 2010, **86**, 494; T. A. Farazi, G. Waksman and J. I. Gordon, *J. Biol. Chem.*, 2001, **276**, 39501.
3 A. N. Hannoush and J. Sun, *Nat. Chem. Biol.*, 2010, **6**, 498.
4 P. J. Quinn, in *The Lipid Handbook*, ed. F. D. Gunstone, J. L. Harwood and A. J. Dijkstra, CRC Press, Boca Raton, 2007, 3rd edn, p. 512.
5 Y. Ohsumi, *IUBMB Life*, 2006, **58**, 363.
6 J. Hare and R. Hodges, *J. Biol. Chem.*, 1982, **257**, 3575; S. M. Russell, J. S. Amenta and R. J. Mayer, *Biochem. J.*, 1984, **220**, 489.
7 H. Raghuraman and A. Chattopadhyay, *Biosci. Rep.*, 2007, **27**, 189.
8 A. Damianoglou, A. Rodger, C. Pridmore, T. R. Dafforn, J. A. Mosely, J. M. Sanderson and M. R. Hicks, *Protein Pept. Lett.*, 2010, **17**, 1351.
9 C. Code, Y. A. Domanov, J. A. Killian and P. K. J. Kinnunen, *Biochim. Biophys. Acta, Biomembr.*, 2009, **1788**, 1064; L. Vernon and J. Bell, *Pharmacol. Ther.*, 1992, **54**, 269.
10 P. Roepstorff and J. Fohlman, *Biol. Mass Spectrom.*, 1984, **11**, 601.
11 H. Raghuraman, S. Ganguly and A. Chattopadhyay, *Biophys. Chem.*, 2006, **124**, 115.

Analyst

PAPER

The reproducibility of phospholipid analyses by MALDI-MSMS†

Catherine J. Pridmore, Jackie A. Mosely* and John M. Sanderson*

The identification of phosphocholine and phosphoethanolamine lipids by MALDI TOF/TOF, including characterisation of the headgroup and delineation of the acyl chain at each position of the glycerol backbone, has been explored using lipids representative of each type. The relative intensities of fragments involving the neutral loss of one or other of the acyl chains from ion adducts of 1-palmitoyl-2-oleoyl-*sn-glycero*-3-phosphoethanolamine (POPE), 1-palmitoyl-2-oleoyl-*sn-glycero*-3-phosphocholine (POPC) and 1-oleoyl-2-palmitoyl-*sn-glycero*-3-phosphocholine (OPPC) were compared. For POPC and POPE, a statistical preference for the loss of the chain from the *sn*-1 position was observed in the presence of lithium. For OPPC this selectivity was reversed for one of the fragments. In the absence of lithium, fragmentation was favoured at the *sn*-2 position for all lipids. In all cases, spectra obtained in the presence of lithium yielded more intense product ion peaks. Although Collision Induced Dissociation (CID) could be used for complete lipid characterisation, LIFT™ was found to be a better method due to the presence of a greater number of distinguishing product ion peaks and a better shot-to-shot reproducibility of peak intensities.

Introduction

Glycerophospholipids are the most abundant type of lipid found in cell membranes. The characteristics of membranes from different types of cell are defined by the chemical identities of their constituent phospholipids. Factors such as headgroup charge, degree of unsaturation and acyl chain length influence the fundamental physical parameters of the membrane, such as bilayer thickness, phase-transition temperature and mixing behaviour.[1] All of these factors highlight the importance of being able to fully identify phospholipids, including the chemical identity of both acyl chains (together with the number, position and geometry of all double bonds) and the nature of the headgroup. Mass spectrometry (MS) has the potential to fulfil this need through the identification of suitable fragments corresponding to each of these key functional groups. The most commonly used soft-ionisation methods for characterising lipids are electrospray ionisation (ESI) and matrix-assisted laser desorption/ionisation (MALDI). More recent methods such as ozone-induced dissociation (OzID), desorption electrospray ionisation (DESI) and rapid evaporative ionisation mass spectrometry (REIMS) are gaining popularity, offering alternative methods for generating ions in mild conditions and gleaning structural information.[2] Tandem ESI-MS offers very high sensitivity, as well as the ability to provide a great deal of

structural information. Tandem MALDI-MS, on the other hand, is the most readily applicable method able to provide the spatial resolution required for imaging techniques, alongside structural information, and is therefore enjoying increasing use for the analysis of biological materials. The LIFT™ technique is of particular note as it permits the analysis of product ions that are produced as a consequence of increased laser power. The LIFT device accelerates product ions to a high potential energy that is sufficient to allow the product ions passage through the reflectron, resulting in improved sensitivity, resolution and mass accuracy.[3]

MALDI-time of flight MS (MALDI-TOF MS) analysis of lipids has been conducted using matrices such as isomers of 2,5-dihydroxybenzoic and 2,4,6-trihydroxyacetophenone,[4,5] as well as more novel species such as ionic liquids.[6] The identification of product ion peaks following fragmentation of lipids by MSMS in the presence of metal cations has proved to be a useful method for lipid analysis. Fragmentation of phosphocholine (PC) molecular ions by post-source decay (PSD) MALDI-TOF MSMS typically yields only one strong product ion peak for the headgroup at *m/z* 184 from the parent proton adduct, whereas the parent sodium adduct produces a number of product ions, including those corresponding to the loss of one or other of the acyl chains.[7] Stübiger and Belgacem have studied lipids from several classes,[5] comparing the MALDI-MSMS product ion spectra from the proton, lithium and sodium adduct molecular ions. The product ion spectra of the parent lithium adduct were found to give more intense product ion peaks than those of the parent sodium adduct and produced protonated and lithiated product ions separated by 6 Da. Both of these features are

Department of Chemistry, Durham University, Durham, DH1 3LE, UK.
E-mail: j.m.sanderson@durham.ac.uk; jackie.mosely@durham.ac.uk;
Fax: +44 (0)191 3844737; Tel: +44 (0)191 3342107

Analyst

advantageous for lipid identification and have been put to good use for techniques such as MALDI imaging.[8]

In order to fully identify a phospholipid, it is necessary to identify the acyl chain at each position of the glycerol backbone, termed the *sn*-1 and *sn*-2 positions (Fig. 1). The relative intensities of peaks corresponding to the loss of the chains from the *sn*-1 and *sn*-2 positions in tandem mass spectra are a potential method of determining this, although published data for PC and phosphoethanolamine (PE) lipids reveal a number of inconsistencies. This is manifested both in terms of the ability to observe peaks corresponding to the loss of both of the acyl chains, and in their relative intensities if they are observed.[5,7–27] Evidence for the loss of the acyl chains from each of the *sn*-1 and *sn*-2 positions has been reported where fragmentation has been carried out using Collision Induced Dissociation (CID) in either a sector instrument,[10,11,20,22,26,27] a linear ion trap,[16,18] or a MALDI-TOF/TOF.[5,8,17] In approximately 50% of cases involving fragmentation by Post Source Decay (PSD) or seamless Post Source Decay (sPSD),[7,10,19] it was reported that fragments corresponding to the release of the acyl chains were not present.[10,19] Fragmentation by CID in a triple quadrupole has led to a range of outcomes. These include: no evidence for cleavage of the acyl chains;[13] evidence of the loss of the acyl chain from each position with a statistical difference in their intensities;[12,13,15,24] evidence of the loss of the acyl chain from each position with no statistical difference in their intensities;[21] and evidence of the loss of each chain as different types of fragments, with differences in the relative intensities of losses from the *sn*-1 and *sn*-2 positions depending on fragment type.[14] A clear example of the range of outcomes is presented by [PC + Na]$^+$, where a lack of observable fragments corresponding to the loss of the acyl chains was reported when this ion underwent sPSD.[10] Al-Saad *et al.* and Landgraf *et al.* have reported the appearance of fragments corresponding to the loss of the acyl chains from both the *sn*-1 and *sn*-2 positions, with a higher intensity of the peaks corresponding to the loss of the chain from the *sn*-1 position when fragmenting [PC + Na]$^+$ by PSD or by CID in a linear ion trap.[7,18] Kim *et al.* fragmented the same ion by high energy CID in a sector instrument and reported the direct opposite, with a higher intensity of the peaks corresponding to the loss of the acyl chain from the *sn*-2 positions.[22] These data highlight the need for a systematic study of the effects of different MSMS methods on the relative cleavage of the acyl chains.

The work reported herein describes a systematic study by MALDI-TOF/TOF of two phosphocholines and a phosphoethanolamine using LIFT™ technology in the absence of a collision gas,[28] and using Collision Induced Dissociation (CID) in the presence of argon. The benefits of the addition of a lithium salt during the MALDI TOF/TOF analysis of lipids are reported, along with the relative intensities of the product ions corresponding to the loss of the acyl chains from the *sn*-1 and *sn*-2 positions of the lithiated and protonated molecular ions, determined from a number of automated analyses.

Experimental

Reagents

1-Palmitoyl-2-oleoyl-*sn*-*glycero*-3-phosphoethanolamine (POPE), and 1-oleoyl-2-palmitoyl-*sn*-*glycero*-3-phosphocholine (OPPC) were purchased from Avanti Polar Lipids (Alabama, USA). 1-Palmitoyl-2-oleoyl-*sn*-*glycero*-3-phosphocholine (POPC), 2,5-dihydroxybenzoic acid (DHB), lithium chloride, poly(ethylene glycol) 600 and ethanol (HPLC grade) were purchased from Sigma-Aldrich, UK. Chloroform (reagent-grade) was purchased from Fisher Scientific, UK. Water with resistivity >18 MΩ cm^{-1} was purified using a Milli-Q Direct Q system from Millipore (Millipore (UK) Ltd.).

Sample preparation

The matrix, DHB, was prepared at a concentration of 30 mg mL^{-1} in EtOH/H$_2$O (50%, v/v) for analyses in the absence of lithium. For experiments in the presence of lithium, DHB was prepared at a concentration of 30 mg mL^{-1} in solutions of 5 mM to 100 mM LiCl in EtOH/H$_2$O (50%, v/v) (a concentration of 100 mM LiCl was used unless otherwise stated). These solutions were mixed at a ratio of 9 : 1, v/v with lipid solutions (each 1 mg mL^{-1} in CHCl$_3$). For manual experiments, 1 μL of the matrix/lipid solution was spotted onto the target and allowed to air dry. For automated runs, 2 × 0.5 μL aliquots were spotted on top of each other and allowed to dry between applications.

Mass spectrometry

MS and MSMS experiments were carried out using an Autoflex II MALDI-TOF/TOF spectrometer with a 337 nm nitrogen laser (Bruker Daltonics Ltd., Coventry, UK). This was calibrated for MS experiments with the sodium adducts of poly(ethylene glycol) 600. A ground steel target plate was cleaned with methanol and acetone prior to use. Positive ion MS experiments were conducted using the reflectron for enhanced performance. Positive ion MSMS experiments were conducted using the LIFT capability in the absence of a collision gas at a source pressure of approximately 2.5 × 10^{-7} mbar unless otherwise stated. For CID experiments, argon was used as the collision gas at a source pressure of approximately 8.5 × 10^{-7} mbar. Isolation of the protonated ion was sufficient with instrument defaults. The isolation windows for LIFT of the lithium adduct ions were set in order to exclude the [POPC + H]$^+$ ion from fragmentation of [POPC + Li]$^+$, and both [POPE + H]$^+$ and [POPE + 2Li − H]$^+$ from the fragmentation of [POPE + Li]$^+$. For MS, data were acquired from 25 laser pulses per location with 20 individual
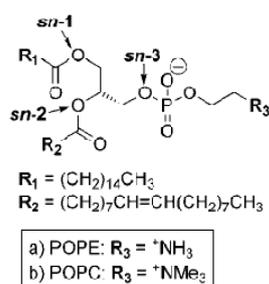

Fig. 1 The structures of (a) POPE and (b) POPC. The *sn*-1, *sn*-2 and *sn*-3 positions on the glycerol backbone of POPE are labelled, along with sections of the acyl chains which are referred to as R$_1$ and R$_2$ in the main text.

$R_1 = (CH_2)_{14}CH_3$
$R_2 = (CH_2)_7CH=CH(CH_2)_7CH_3$

a) POPE: $R_3 = {}^+NH_3$
b) POPC: $R_3 = {}^+NMe_3$

locations sampled per spot preparation totalling 500 shots. For MSMS, data were acquired for the precursor ion from 25 shot steps for a total of 150 shots, and for the product ions in 50 shot steps for a total of 450 shots. Laser power was set at the lower threshold for peak detection, with the upper limit fixed at the laser power where saturation was known to occur during validation experiments. For the automated LIFT analysis of [POPE + Li]$^+$ the figures represent the narrowest window from which results could successfully be produced. For CID the precursor ion isolation window could not be altered from the default setting of ±1% due to software constraints. A summary of the isolation windows for all precursor ions is given in Table S1 (ESI†). Lithium exists as two isotopes, ^{6}Li and ^{7}Li, with isotopic abundances of 7.5 and 92.5 respectively.[29] It was not possible to separate the isotopes when selecting [M + Li]$^+$ precursor ions, but the ^{7}Li adduct is referred to in all the discussion of fragments. Data were analysed using Flex Analysis version from 3.0 Bruker Daltonics Ltd. (Coventry, UK).

Results and discussion

MALDI-MS analysis

The lipids POPE (Fig. 1a) and POPC (Fig. 1b) were studied by MALDI-MS.

The appearance in the mass spectra of these lipids of peaks separated by 6 Da (corresponding to [M + H]$^+$ and [M + ^{7}Li]$^+$ in the case of POPC; [M + H]$^+$, [M + ^{7}Li]$^+$ and [M + 2^{7}Li − H]$^+$ in the case of POPE) provided a visual aid for the identification of lipid molecular ions, as exemplified in the spectra of POPE (Fig. 2) and POPC (Fig. 3).

For POPE, [M + H]$^+$ was observed at the lowest intensity, with [M + 2^{7}Li − H]$^+$ and [M + ^{7}Li]$^+$ observed at progressively higher intensities. [M + ^{6}Li]$^+$ and [M + ^{6}Li + ^{7}Li − H]$^+$ were present as minor peaks. The additional doubly lithiated ions observed in spectra of POPE are accounted for by the ability of the ethanolamine ammonium group (pK_a = 9.8) to exist in a neutral form (unattainable with the choline 4° ammonium group). In the case of POPC, [M + H]$^+$ and [M + ^{7}Li]$^+$ were observed as major peaks with [M + ^{6}Li]$^+$ as a minor peak.

The full scan mass spectra showed evidence that the lipids fragment readily (ESI†, Fig. S1). Direct comparison with matrix-

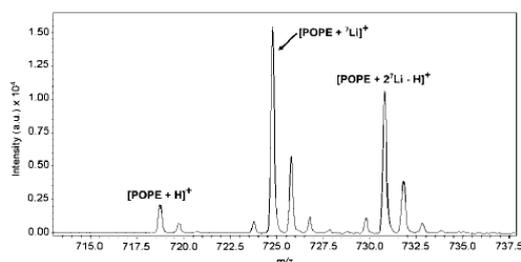**Fig. 3** MALDI-MS spectrum of POPC in the presence of LiCl showing the molecular ions [POPC + H]$^+$ (m/z 760.7) and [POPC + Li]$^+$ (m/z 766.7). The sample was prepared by mixing a solution of the lipid in CHCl$_3$ (1 mg mL^{-1}) 1 : 9 (v/v) with a solution of LiCl (100 mM) and DHB (30 mg mL^{-1}) in EtOH/H$_2$O (50%, v/v).
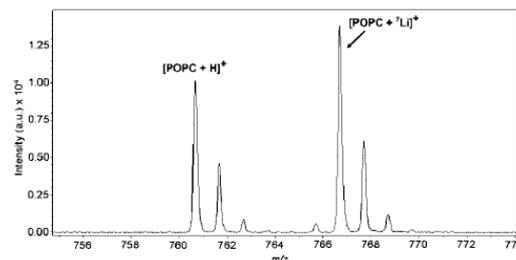
only spectra showed ions corresponding to the headgroup in the spectra of the proton and lithium adduct ions of POPC, and to the loss of a headgroup fragment from the proton and lithium adduct ions of POPE. No evidence for the acyl chains themselves, or for their loss, was observed in any of the four spectra.

MALDI-MSMS analysis

MALDI-MSMS analysis was initially conducted using the proton adducts, alongside samples prepared in the presence of either sodium or lithium. Although fragmentation of parent sodium adducts yielded product ion spectra that could potentially have facilitated headgroup and acyl chain identification[30] (ESI†, Fig. S2), these spectra had a lower signal to noise ratio than the corresponding spectra obtained in the presence of lithium. Subsequent work therefore focused on the lithium adduct ions.

POPE molecular ions. MALDI-MSMS spectra of both the proton and lithium adduct ions of POPE showed evidence of product ions at m/z 577, resulting from the loss of a headgroup fragment, as the dominant species (Fig. 4).

Both of the product ion spectra exhibited peaks that could be assigned to fragments of one or other of the acyl chains, or to the headgroup, as well as products arising from their neutral loss. The product ion spectrum of the proton adduct ion (Fig. 4a and Table 1) showed two pairs of peaks corresponding to the acyl chain loss from the sn-1 or sn-2 positions, at m/z 436/462 and m/z 454/480. Fragmentation of the lithium adduct ion (Fig. 4b and Table 1) yielded only one pair of peaks at m/z 399/425 from which both acyl chains could be identified. These peaks, corresponding to [M + ^{7}Li − (R$_2$CO$_2$H + H$_2$C=CHNH$_2$)]$^+$ and [M + ^{7}Li − (R$_1$CO$_2$H + H$_2$C=CHNH$_2$)]$^+$, had much greater intensities, relative to the dominant peak at m/z 577, than any of the peaks corresponding to the loss of an acyl chain observed in the product ion spectrum of the proton adduct. As a consequence, the product ion spectra of the lithium adducts were clearer and allowed easier identification of the lipid. Less intense peaks could be observed in the product ion spectrum of the lithium adduct ion at m/z 405 and m/z 431 (Fig. 4b). These are assigned to [POPE + 2^{7}Li − R$_2$CO$_2$H]$^+$ and [POPE + 2^{7}Li − R$_1$CO$_2$H]$^+$ respectively and have arisen from incomplete isolation of the

Fig. 2 MALDI-MS spectrum of POPE in the presence of lithium showing the molecular ions [POPE + H]$^+$ (m/z 718.6), [POPE + ^{7}Li]$^+$ (m/z 724.6) and [POPE + 2^{7}Li − H]$^+$ (m/z 730.7). The sample was prepared by mixing a solution of the lipid in CHCl$_3$ (1 mg mL^{-1}) 1 : 9 (v/v) with a solution of LiCl (100 mM) and DHB (30 mg mL^{-1}) in EtOH/H$_2$O (50%, v/v).
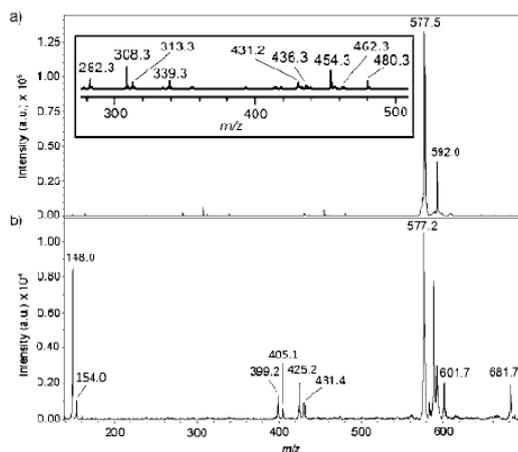
Fig. 4 MALDI-MSMS spectra of (a) [POPE + H]⁺ and (b) [POPE + Li]⁺.

Fig. 5 MALDI-MSMS spectra of (a) [POPC + H]⁺ and (b) [POPC + Li]⁺.

[POPE + Li]⁺ parent, with an isolation window of ±5 Da, allowing some dissociation products from the doubly lithiated precursor to be observed.

POPC molecular ions. In a similar manner to POPE, the product ion spectra of both the proton and lithium adduct ions of POPC exhibited a strong peak at m/z 577, corresponding to the loss of a headgroup fragment (Fig. 5), although the headgroup fragment itself at m/z 184 was the dominant product ion in this case. Both spectra, however, contained other fragments that permitted identification of each of the acyl chains. The product ion spectrum of proton adduct (Fig. 5a and Table 2) showed two pairs of peaks corresponding to the loss of the acyl chains, whereas the spectrum of the lithium adduct (Fig. 5b and Table 2) contained four pairs.

Most of the peaks corresponding to the neutral loss of the acyl chains in the product ion spectrum of [POPC + Li]⁺ had a greater relative intensity relative to the corresponding peaks in the
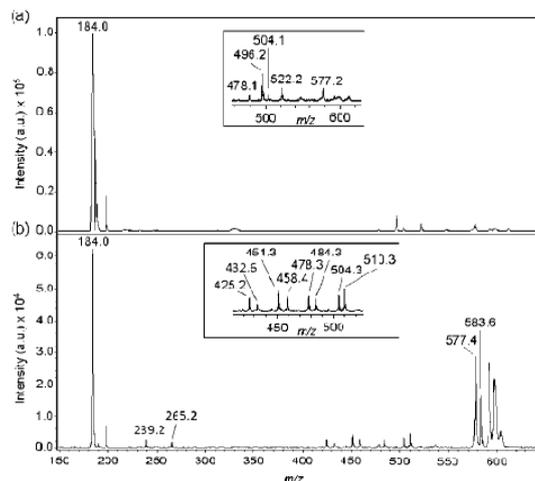
spectrum of [POPC + H]⁺. This higher relative intensity for products of lithium adduct fragmentation should be useful in cases where the sensitivity is an issue. Peaks at m/z 432 and m/z 458 in the [POPC + Li]⁺ product ion spectrum (Fig. 5b) could not be assigned, although the difference in their mass would suggest a level of similarity between them, with the principle difference being the identity of the acyl chain.

As with the molecular ions in the MS spectra of both lipids, characteristic peaks in the product ion spectrum of the lithium adduct (Fig. 5b) occurred as pairs of protonated and lithium adduct ions separated by 6 Da. These are exemplified by the peaks at m/z 478 and m/z 484, corresponding respectively to [POPC + ⁷Li − R₂CO₂⁷Li]⁺ and [POPC + ⁷Li − R₂CO₂H]⁺.

The influence of lithium levels on ion fragmentation. Having found that MALDI-MSMS of lithium adducts enabled the unambiguous identification of the lipid headgroup and both acyl chains, the range of lithium levels suitable for MALDI-MSMS

Table 1 Product ions observed in MALDI-MSMS spectra of the proton and lithium adduct ions of POPE

[POPE + H]⁺		[POPE + Li]⁺	
m/z	Product ion[abc]	m/z	Product ion[abd]
282.3	[R₂CO₂H]⁺	148.0	[(HO)₂PO₂Etn + ⁷Li]⁺
308.3	[R₂CO₂CHCH₂]⁺	399.2	[M + ⁷Li − (R₂CO₂H + H₂CCHNH₂)]⁺
313.3	[R₁CO₂C₃H₅O + H]⁺	425.2	[M + ⁷Li − (R₁CO₂H + H₂CCHNH₂)]⁺
339.3	[R₂CO₂C₃H₅O + H]⁺	577.2	[M + ⁷Li − (⁷LiO)(HO)PO₂Etn]⁺
431.2	[R₂CO₂CHCHPO₂C₂H₄ + H]⁺	601.7	[M + ⁷Li − (HPO₃ + H₂CCHNH₂)]⁺
436.3	[M + H − R₂CO₂H]⁺	681.7	[M + ⁷Li − H₂CCHNH₂]⁺
454.3	[M + H − R₂=C=O]⁺		
462.3	[M + H − R₁CO₂H]⁺		
480.3	[M + H − R₁=C=O]⁺		
577.5	[M + H − (HO)₂PO₂Etn]⁺		
592.0	[M + H − H(HO)PO₂Etn]⁺		

[a] R₁ and R₂ are defined in Fig. 1. [b] Etn = (CH₂)₂NH₂. [c] Assignments involving glycerol fragments (m/z 313.3, 339.3 and 431.2) or the neutral loss of ketenes (m/z 454.3 and 480.3) are based on literature precedents.[7,19] [d] Assignments involving the loss of carboxyl and enamine groups (m/z 399.2, 425.2, 601.7 and 681.7) are based on literature precedents.[14]

Table 2 Product ions observed in MALDI-MSMS spectra of the proton and lithium adduct ions of POPC

[POPC + H]$^+$		[POPC + Li]$^+$	
m/z	Product ion^{ab}	m/z	Product ion^{ab}
184.0	$[(HO)_2PO_2Chn]^+$	184.0	$[(HO)_2PO_2Chn]^+$
478.1	$[M + H − R_2CO_2H]^−$	239.2	$[R_1CO]^+$
496.2	$[M + H − R_2—C=O]^+$	265.2	$[R_2CO]^+$
504.1	$[M + H − R_1CO_2H]^−$	425.2	$[M + ^7Li − (R_2CO_2H + NMe_3)]^+$
522.2	$[M + H − R_1=C=O]^+$	432.6	$[R_1CO_2C_3H_4PO_4C_2H_4 + 2Li − H]^+$
577.2	$[M + H − HOPO_3Chn]^+$	451.3	$[M + ^7Li − (R_1CO_2H + NMe_3)]^+$
		458.4	$[R_2CO_2C_3H_4PO_4C_2H_4 + 2Li − H]^+$
		478.3	$[M + ^7Li − R_2CO_2^7Li]^−$
		484.3	$[M + ^7Li − R_2CO_2H]^+$
		504.3	$[M + ^7Li − R_1CO_2^7Li]^−$
		510.3	$[M + ^7Li − R_1CO_2H]^+$
		577.4	$[M + ^7Li − ^7LiOPO_3Chn]^+$
		583.6	$[M + ^7Li − HOPO_3Chn]^−$

^{a} R_1 and R_2 are defined in Fig. 1. ^{b} Chn = $(CH_2)_2NMe_3$.

analysis was investigated. For POPE, the normalised intensities of the fragments corresponding to the headgroup at m/z 148, the loss of the acyl chains from either the sn-1 or sn-2 position together with aminoethane (m/z 425.2 and 399.2 respectively) and the loss of the headgroup (m/z 577.2) were averaged for eight repeats of six target applications with varying lithium levels. Lithium chloride quantities were varied in the range 4.5 nmol to 90 nmol per spot, with fixed amounts of lipid and matrix. No statistical differences were observed between the normalised intensities of the fragments obtained at different mole ratios of lithium, regardless of whether the fragments contained lithium or not, as shown in Fig. 6. Similar results were obtained for POPC, where the normalised intensities of the fragments corresponding to the headgroup (m/z 184), the loss of the acyl chain from either the sn-1 or sn-2 position together with the trimethylamine group (m/z 451.3 and 425.2 respectively), the loss of the acyl chains from either the sn-1 or sn-2 position with and without lithium (m/z 510.3, 504.3, 484.3 and 478.3) and the loss of the headgroup with and without lithium (m/z 583.6 and 577.4
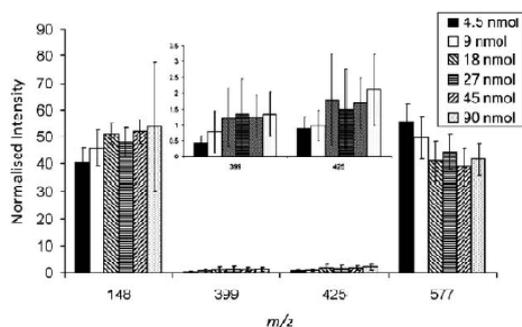
respectively), showed no statistical difference over a similar range of lithium levels (ESI†, Fig. S3).

Acyl chain identification by LIFT

Fragmentation of POPE ions. Successful identification of the acyl chain present at each position of a lipid requires that product ions can be identified in MSMS spectra that have arisen by fragmentation processes at each of the sn-1 and sn-2 positions. Furthermore, in order for assignments to be unambiguous, there should be a difference in the relative intensity that is statistically significant for the loss of equivalent fragments from each position. In order to examine whether these criteria applied to fragmentation of POPE ions, twenty four MSMS spectra for each of the protonated and lithiated adducts were collected using an automated method to minimise experimental errors. Table 3 shows the different types of fragment observed which involved the neutral loss of fragments from one or other of the acyl chains. For each of these types, the intensities of peaks corresponding to equivalent neutral losses from the sn-1 and sn-2 positions were normalised relative to each other. Two types of fragment from the parent proton adduct were identified that showed a preferential loss of a neutral acyl chain fragment from the sn-2 position (Fig. 7 and Table 3, entries a and b). A further type of fragmentation of the parent lithium adduct involving the neutral loss of an acyl chain was noted (Fig. 7 and Table 3, entry c), although in this case the acyl chain fragment was preferentially lost from the sn-1 position.

Three points can be made from these results. Firstly, as shown previously, the parent proton and lithium adducts fragmented to give different product ions. Secondly, there were differences in the relative abundance of ions corresponding to the neutral loss of acyl fragments from the sn-1 and sn-2 positions for the three different types of product ions (Table 3, a–c).

Thirdly, the preference for the neutral loss from the sn-2 over the sn-1 position for the proton adduct was reversed for the lithium adduct.

Overall, the greatest difference in the relative intensity corresponding to the loss from sn-1 $vs.$ sn-2 was found for the neutral

Fig. 6 Normalised intensities of [POPE + Li]$^+$ fragment peaks with varying amounts of lithium chloride per target spot (4.5, 9, 18, 27, 45, 90 nmol) and fixed amounts of DHB (0.2 μmol) and lipid (0.2 nmol). Ion identities for m/z 148.0, 399.2, 425.2 and 577.2 are given in Table 1. Error bars represent 2× the standard deviation from 8 repeat scans in each case.

Table 3 Product ions corresponding to the loss of the acyl chain from the *sn*-1 or *sn*-2 positions of POPE observed in the MSMS spectra of [POPE + H]⁺ and [POPE + Li]⁺. The relative intensities of peaks corresponding to the loss of the acyl chains from the *sn*-1 and *sn*-2 positions have been normalised with respect to one another for each type of fragment

Entries	Parent ion	Fragment[a]	RI, $x = 1$[bc]	RI, $x = 2$[bc]
a	[M + H]⁺	[M + H R_xCO₂H]⁺	0.43 ± 0.05	0.57 ± 0.05
b	[M + H]⁺	[M + H − R_x=C=O]⁺	0.28 ± 0.03	0.72 ± 0.03
c	[M + Li]⁺	[M + Li − (R_xCO₂H + H₂CCHNH₂)]⁺	0.60 ± 0.05	0.40 ± 0.05

[a] $x = 1$ and $x = 2$ correspond to chains at the *sn*-1 and *sn*-2 positions of the lipid respectively. [b] RI = relative intensity. [c] The error is calculated as 2× the standard deviation of the data from 24 spectra.
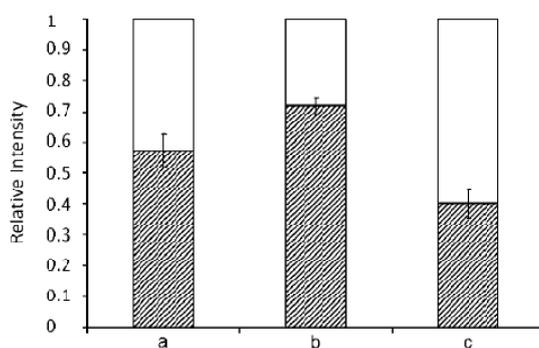

Fig. 7 The relative intensities of peaks corresponding to the loss of the acyl chain from the *sn*-1 and *sn*-2 positions of different types of fragments of POPE from MSMS spectra of [POPE + H]⁺ and [POPE + Li]⁺. The white sections correspond to a loss from *sn*-1 position, shaded to the *sn*-2 position. Refer to Table 3 for identification of a–c. The error bars correspond to 2× the standard deviation of the data from 24 repeat scans.

loss of ketene from the proton adduct ion (Table 3, entry *b*). The position of the acyl chains of POPE can therefore be identified from the product ions of fragmentation, whether or not lithium is added.

Fragmentation of POPC ions. Twenty four MSMS spectra for each of the parent proton and lithium adducts of POPC were collected using an automated method and analysed in the same way as those of POPE. As for POPE, fragmentation of the parent lithium and proton adducts gave a range of product ions differing in their propensity for fragmentation at the *sn*-1 *versus* the *sn*-2 position (Table 4). More types of POPC fragment involving the neutral loss of an acyl chain were observed than for POPE. However, in this case there were two types of fragment, one of the parent proton adduct and one of the lithium adduct, for which peak intensities corresponding to the loss from the *sn*-1 and *sn*-2 positions were not significantly different (Fig. 8 and Table 4, entries *a* and *d*). In similar control experiments with OPPC, it was notable that formation of the equivalent product ions by the loss of fragments from the *sn*-1 position was clearly favoured (ESI†, Fig. S4 and Table S2, entries *a* and *d*).

For the proton adduct, the ratio of the product ion intensities corresponding to the neutral loss of a ketene fragment from either the *sn*-1 or the *sn*-2 position lay outside a value of 0.5 : 0.5, within error, favouring the loss from the *sn*-2 position (Fig. 8 and Table 4, entry *b*).

Three of the four types of fragment produced from the parent lithium adduct had statistically significant differences between the normalised peak intensities for fragmentation at the *sn*-1 position *versus* the *sn*-2 position (Fig. 8 and Table 4, entries *c*, *e*, and *f* respectively). Again, there was a difference in the acyl chain preferentially lost from each of the two parent ions, favouring the loss from the *sn*-2 position of the proton adduct and the *sn*-1 position of the lithium adduct. It was notable, however, that in one case with OPPC, formation of the [R_xCO]⁺ fragment from the parent lithium adduct occurred preferentially through fragmentation at the *sn*-2 position (ESI†, Fig. S4 and Table S2, entry *c*), in stark contrast to POPC. This would preclude using this fragment as a reliable means of determining the identity of the chains at each position.

Overall, the positions of the acyl chains can be determined from the product ion spectra of the proton and lithium adduct ions, with the product ion spectrum of the lithium adduct providing more usable fragments (Table 4, entries *e* and *f*) and the product ion spectrum of the parent proton adduct providing the statistically most reliable fragment (Table 4, entry *b*).

Comparison of POPE and POPC ion fragmentation by LIFT. A number of comparisons can be made between the results for POPE and POPC. The fragments of the protonated parents are the same, involving the loss of a carboxylic acid (R_xCO₂H) or a ketene (R_xCO), and the relative intensities of the peaks corresponding to $x = 1$ and $x = 2$ are very similar for these fragments in both cases. Whilst there are more fragments of lithiated POPC than lithiated POPE that involve a loss of one or other of the acyl chains, there are nevertheless fragments, such as those involving the loss of the headgroup ([POPE + Li − (R_xCO₂H + H₂C=CHNH₂)]⁺ and [POPC + Li − (R_xCO₂H + NMe₃)]⁺), for which the relative intensities between the two lipids for $x = 1$ and $x = 2$ are similar. Where the selective loss from the *sn*-1 or *sn*-2 chains was evident, it was notable that for both POPC and POPE the parent proton adducts showed a preferential loss of the acyl chain from the *sn*-2 position, whilst the lithium adducts of both lipids preferentially lost the acyl chain from the *sn*-1 position. The finding that similar experiments with OPPC yield the reverse preference for the fragmentation position in one case demonstrates that the acyl chain plays a role in the formation of some fragments and obligates careful calibration of the instrument for each fragment type.

Comparison of LIFT and CID

Twenty five CID spectra of the proton and lithium adducts of POPC were collected, using an automated method to minimise

Table 4 Product ions corresponding to the loss of the acyl chain from the *sn*-1 or *sn*-2 positions of POPC observed in the MSMS spectra of [POPC + H]⁺ and [POPC + Li]⁺. The relative intensities of peaks corresponding to the loss of the acyl chains from the *sn*-1 and *sn*-2 positions have been normalised with respect to one another for each type of fragmentation

Entries	Parent ion	Fragment[a]	RI, $x = 1^{bc}$	RI, $x = 2^{bc}$
a	[M + H]⁺	[M + H − R_xCO_2H]⁺	0.55 ± 0.06	0.45 ± 0.06
b	[M + H]⁺	[M + H − R_x=C=O]⁺	0.28 ± 0.03	0.72 ± 0.03
c	[M + Li]⁺	[R_xCO]⁺	0.61 ± 0.04	0.39 ± 0.04
d	[M + Li]⁺	[M + Li − R_xCO_2Li]⁺	0.53 ± 0.03	0.47 ± 0.03
e	[M + Li]⁺	[M + Li − R_xCO_2H]⁺	0.64 ± 0.04	0.36 ± 0.04
f	[M + Li]⁺	[M + Li − (R_xCO_2H + NMe_3)]⁺	0.64 ± 0.03	0.36 ± 0.03

[a] $x = 1$ and $x = 2$ correspond to chains at the *sn*-1 and *sn*-2 positions of the lipid respectively. [b] R I = relative intensity. [c] The error is calculated as 2× the standard deviation of the data from 24 spectra.
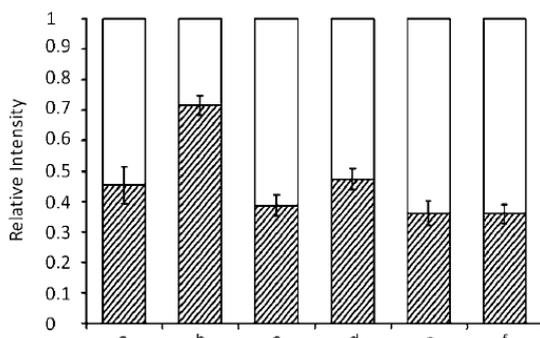

Fig. 8 The relative intensities of peaks corresponding to the loss of the acyl chain from the *sn*-1 and *sn*-2 positions of different types of fragments of POPC from MSMS spectra of [POPC + H]⁺ and [POPC + Li]⁺. The white sections correspond to a loss from *sn*-1 position, shaded to the *sn*-2 position. Refer to Table 4 for identification of a–f. The error bars correspond to 2× the standard deviation of the data from 24 repeat scans.

experimental errors. Table 5 shows the different types of fragments observed which involve the loss of one or other of the acyl chains, along with the average percentage intensity of the peak corresponding to a loss from the *sn*-1 position relative to the peak corresponding to a loss from the *sn*-2 position for each fragment. Three main points can be identified from a comparison of the LIFT and CID data. Firstly, both fragmentation methods produce the same fragments involving the loss of one or other of the acyl chains, for both the parent proton and the parent lithium adducts. Secondly, the relative intensities of $x = 1$ and $x = 2$ for the different fragments are the same between the LIFT data

(Table 4) and the CID data (Table 5) in all but one case. For the fragments of the proton adduct of POPC, the higher intensity of [POPC + H − R_2=C=O]⁺ relative to [POPC + H − R_1=C=O]⁺ was particularly notable (ESI†, Fig. S5 and S6). The only fragment of the parent lithium adduct to show any difference from the LIFT data in terms of the relative intensities of the loss from the *sn*-1 and *sn*-2 positions was the [M + Li − (R_xCO_2H + NMe_3)]⁺ peak. In this case, CID produced no difference in the peak intensities following the loss from the *sn*-1 and *sn*-2 positions, contrasting the case for LIFT, where a preferential loss from *sn*-1 occurred. Thirdly, the CID data were less reproducible than the LIFT data, with larger standard deviations for all of the peak intensities.

Differences in the product ratios between CID and LIFT, and the comparison of product ratios for OPPC and POPC, are a reflection of the ion internal energies involved in each process. CID, as a higher energy method, will favour pathways with higher activation energies, whereas LIFT will select neutral loss pathways with lower activation energy barriers. Comparison of POPC with OPPC highlights that for some processes, the differences in energy barrier are extremely small and have some dependence not only on structural features relating to the position itself, but also on the identity of the acyl chain attached at that position. LIFT, as a lower energy technique, is more sensitive to these differences.

Conclusions

The objectives of this study were to examine the reproducibility of lipid fragmentation patterns in MSMS and determine the optimum conditions for characterisation of glycerophospholipids by this method. Under the conditions employed,

Table 5 Product ions corresponding to the loss of the acyl chain from the *sn*-1 or *sn*-2 positions of POPC observed in CID spectra of [POPC + H]⁺ and [POPC + Li]⁺. The relative intensities of peaks corresponding to the loss of the acyl chains from the *sn*-1 and *sn*-2 positions have been normalised with respect to one another for each type of fragmentation

Parent ion	Fragment[a]	RI, $x = 1^{bc}$	RI, $x = 2^{bc}$
[M + H]⁺	[M + H − R_xCO_2H]⁺	0.45 ± 0.16	0.55 ± 0.16
[M + H]⁺	[M + H − R_x=C=O]⁺	0.29 ± 0.08	0.71 ± 0.08
[M + Li]⁺	[R_xCO]⁺	0.61 ± 0.11	0.39 ± 0.11
[M + Li]⁺	[M + Li − R_xCO_2Li]⁺	0.53 ± 0.06	0.47 ± 0.06
[M + Li]⁺	[M + Li − R_xCO_2H]⁺	0.59 ± 0.08	0.41 ± 0.08
[M + Li]⁺	[M + Li − (R_xCO_2H + NMe_3)]⁺	0.50 ± 0.08	0.50 ± 0.08

[a] $x = 1$ and $x = 2$ correspond to chains at the *sn*-1 and *sn*-2 positions of the lipid respectively. [b] R I = relative intensity. [c] The error is calculated as 2× the standard deviation of the data from 25 spectra.

repeat MSMS analyses of POPE and POPC with and without the addition of lithium have shown that there is a statistical preference for the cleavage of one of the acyl chains for the generation of a number of different fragments, with opposite preferences for the parent proton and lithium adducts.

Three main advantages of analysis using LIFT in the presence of lithium can be described: (i) more intense product ion peaks, facilitating lipid identification; (ii) the frequent appearance of pairs of protonated and lithiated ions of 6 mass units apart in both MS and product ion spectra that facilitate peak identification; and (iii) the presence of a greater number of product ion peaks that enable lipid characterisation. However, the differences in fragmentation between POPC and OPPC indicate that each fragment type needs to be carefully assessed using appropriate standards. The most reliable peak for lipid identification in these experiments, both in terms of applicability to all of the lipids studied and the ratio of sn-1 to sn-2 fragmentation products, resulted from fragmentation of the protonated species. Fragmentation of POPC using CID was shown to be less specific, although preferential cleavage was observed in some cases. The presence of more useful fragment peaks and the better reproducibility of peak intensities when using LIFT make this a better method for analysis of lipids than CID. Variations in the relative peak intensity following cleavage at the sn-1 and sn-2 positions, observed here for lithium adducts and elsewhere for sodium adducts,[7,18,22] highlight the need to rigorously validate each instrument for each method used for lipid analysis.

References

1 A. Wieslander, S. Nordstrom, A. Dahlqvist, L. Rilfors and G. Lindblom, *Eur. J. Biochem.*, 1995, **227**, 734.
2 S. J. Blanksby and T. W. Mitchell, *Annu. Rev. Anal. Chem.*, 2010, 3, 433.
3 D. Suckau, A. Resemann, M. Schuerenberg, P. Hufnagel, J. Franzen and A. Holle, *Anal. Bioanal. Chem.*, 2003, 376, 952.
4 J. Schiller, R. Süβ, B. Fuchs, M. Müller, M. Petković, O. Zschörnig and H. Waschipy, *Eur. Biophys. J.*, 2007, 36, 517.
5 G. Stubinger and O. Belgacem, *Anal. Chem.*, 2007, 79, 3206.
6 M. Mank, B. Stahl and G. Boehm, *Anal. Chem.*, 2004, 76, 2938.
7 K. A. Al-Saad, W. F. Siems, H. H. Hill, V. Zabrouskov and N. R. Knowles, *J. Am. Soc. Mass Spectrom.*, 2003, **14**, 373.
8 S. N. Jackson, H.-Y. J. Wang and A. S. Woods, *J. Am. Soc. Mass Spectrom.*, 2007, **18**, 17.
9 X. Han and R. W. Gross, *J. Am. Soc. Mass Spectrom.*, 1995, 6, 1202.
10 G. Stübiger, E. Pittenauer and G. Allmaier, *Anal. Chem.*, 2008, **80**, 1664.
11 S. Chen and K. W. Li, *J. Biochem.*, 1994, **116**, 811.
12 F. F. Hsu and J. Turk, *J. Am. Soc. Mass Spectrom.*, 2000, **11**, 892.
13 F. F. Hsu and J. Turk, *J. Mass Spectrom.*, 2000, 35, 596.
14 F. F. Hsu and J. Turk, *J. Am. Soc. Mass Spectrom.*, 2003, **14**, 352.
15 F. F. Hsu, A. Bohrer and J. Turk, *J. Am. Soc. Mass Spectrom.*, 1998, **9**, 516.
16 H. Song, F. F. Hsu, J. Ladenson and J. Turk, *J. Am. Soc. Mass Spectrom.*, 2007, **18**, 1848.
17 S. N. Jackson, H.-Y. J. Wang and A. S. Woods, *J. Am. Soc. Mass Spectrom.*, 2005, **16**, 2052.
18 R. R. Landgraf, T. J. Garrett, N. A. Calcutt, P. W. Stacpoole and R. A. Yost, *Anal. Chem.*, 2007, 79, 6862.
19 B. Fuchs, C. Schober, G. Richter, R. Süβ and J. Schiller, *J. Biochem. Biophys. Methods*, 2007, 70, 689.
20 Z.-H. Huang, D. A. Gage and C. C. Sweeley, *J. Am. Soc. Mass Spectrom.*, 1992, 3, 71.
21 J. L. Kerwin, A. R. Tuininga and L. H. Ericsson, *J. Lipid Res.*, 1994, 35, 1102.
22 Y. H. Kim, J. S. Yoo and M. S. Kim, *Bull. Korean Chem. Soc.*, 1997, **18**, 874.
23 A. Kayganich and R. C. Murphy, *Anal. Chem.*, 1992, 64, 2965.
24 S. Ramanadham, F. F. Hsu, S. Zhang, A. Bohrer, Z. Ma and J. Turk, *Biochim. Biophys. Acta Gen. Subj.*, 2000, **1484**, 251.
25 A. M. Hicks, C. J. DeLong, M. J. Thomas, M. Samuel and Z. Cui, *Biochim. Biophys. Acta, Gen. Subj.*, 2006, **1761**, 1022.
26 A. Hayashi, T. Matsubara, M. Morita, T. Kinoshita and T. J. Nakamura, *Biochemistry*, 1989, **106**, 264.
27 N. J. Jensen, K. B. Tomer and M. L. Gross, *Lipids*, 1986, **21**, 580.
28 D. Suckau, A. Resemann, M. Schuerenburg, P. Hufnagel, J. Franzen and A. Holle, *Anal. Bioanal. Chem.*, 2003, 367, 952.
29 P. De Bievre and P. D. P. Taylor, *Int. J. Mass Spectrom. Ion Processes*, 1993, **123**, 149.
30 K. A. Al-Saad, V. Zabrouskov, W. F. Siems, N. R. Knowles, R. M. Hannan and H. H. Hill, Jr, *Rapid Commun. Mass Spectrom.*, 2003, **17**, 87.